SPECIAL COLLECTIONS

UNIVERSITY OF ALBERTA LIBRARY

REQUEST FOR DUPLICATION

I wish a photocopy of the thesis by

Dusseault M.B. (author)

entitled The Geotechnical Characteristics of Oil Sands.

The copy is for the sole purpose of private scholarly or scientific study and research. I will not reproduce, sell or distribute the copy I request, and I will not copy any substantial part of it in my own work without permission of the copyright owner. I understand that the Library performs the service of copying at my request, and I assume all copyright responsibility for the item requested.

Date	Name and address	Pages copied	Signature
09.1984	M.G. Kurowski	136-145	
	#132 Pembina Hall	150-172	
	U. of A.	246-261	
		291.	
86 12 18	JOHN McKay	140	John McKay.
	#307-10515-99 St Edm		
28th Sept 90	A.A. OLAGOKE	1, 4-9, 11	
May 6/93	Syncrude Res. - Paula MacGillivray 10120 - 17 St. Edmonton, Alta. T6P 1V8 449-2801	all	P. MacGillivray

THE UNIVERSITY OF ALBERTA

THE GEOTECHNICAL CHARACTERISTICS OF THE ATHABASCA OIL SANDS

MAURICE B. DUSSEAULT

A THESIS

SUBMITTED TO THE FACULTY OF GRADUATE STUDIES AND RESEARCH
IN PARTIAL FULFILMENT OF THE REQUIREMENTS FOR THE DEGREE
OF DOCTOR OF PHILOSOPHY

DEPARTMENT OF CIVIL ENGINEERING

EDMONTON, ALBERTA

SPRING, 1977

THE UNIVERSITY OF ALBERTA

FACULTY OF GRADUATE STUDIES AND RESEARCH

The undersigned certify that they have read, and recommend to the Faculty of Graduate Studies and Research, for acceptance, a thesis entitled "THE GEOTECHNICAL CHARACTERISTICS OF THE ATHABASCA OIL SANDS" submitted by Maurice Bernard Dusseault in partial fulfilment of the requirements for the degree of Doctor of Philosophy in Civil Engineering.

....
N.R. Morgenstern, Supervisor

....
[illegible], External Examiner

....
D.M. Cruden

....
S. Thomson

....
F.W. Schwartz

February 2, 1977

ABSTRACT

This thesis investigates the geomorphology of natural oil sand slopes, the geotechnical properties of the Athabasca Oil Sands, and several similar friable quartzose sandstones, the behaviour of high steep pit walls upon excavation, and the mineralogy and index properties of the basal clays of the McMurray Formation.

Natural oil sand slopes are high (>70 m), steep (55°), and stable. The presence of slope base erosion results in slopes steeper than 33°; the absence of debris-removal agents results in slopes at angles of less than 34°. Basal strata, bitumen saturation, overlying strata, and exposure to solar radiation are the dominant variables affecting the morphology of exposed oil sand slopes. Detailed examination indicates that bitumen, cementation, and pore pressures do not contribute significantly to long-term natural slope stability. Slopes recede as a result of sloughing along stress-relief exfoliation fractures sub-parallel to the slope face. These fractures, and several other features, indicate high values of in situ horizontal stresses.

The Athabasca Oil Sands display high shear strengths as a result of a characteristic interpenetrative granular fabric. Mohr-Coulomb failure envelopes consequently show a significant curvature, and, since the oil sands have no cohesion, the envelopes can be usefully approximated by a power-law relationship. The curvature is a result of dilatancy at low stresses and increasing grain shear at higher stresses. Two other friable quartzose sandstones, St. Peter Sandstone and Swan River Sandstone, are shown to behave in a similar manner.

The dilatant behaviour at low stresses is the consequence of interlock arising from diagenetic alteration of these geologically old, quartzose sands: artificial dense sands and natural, geologically young sands do not display similarly high shear strengths. Optical and scanning electron microscope studies show the diagenetic surface textures characteristic of these locked sands, and reveal the diagenetic intergranular fabric. The specific processes responsible for the fabric are crystal overgrowth and solution: a consequent and diagnostic property is reduced porosity (increased density).

Wedge stability analysis indicates probable high factors of safety for excavated pit walls, and finite element stress analysis indicates tension zones at the slope top, tension zones or high stress ratios in the slope face, and stress concentrations in the slope toe.

The basal clays of the McMurray Formation, which directly underlie the oil sands, are illite-kaolinite-vermiculite clays, often of high plasticity. They are slickensided when exposed at slope bases, and are therefore at a residual strength state.

ACKNOWLEDGEMENTS

The research reported in this thesis was carried out at the University of Alberta in Edmonton under the auspices of the Civil Engineering Department. Professor N.R. Morgenstern supervised the research, and provided invaluable inspiration and direction.

Many professors in the Department of Civil Engineering contributed to this thesis with advice and moral support. I would particularly like to thank Professors Z. Eisenstein, D.W. Murray, and S. Thomson.

Discussions with fellow students have been an excellent source of information and constructive criticism. Messrs. W.D. Roggensack, P. Kaiser, and M. Milligan in particular have donated their time willingly.

The staff of the Alberta Research Council have made equipment available, and Dr. D. Scafe participated in a portion of the research as well as performing numerous X-ray analyses. Drs. J.D. Godfrey, G. Mossop, and E.A. Babcock were generous in contributing their time for discussions.

Technical expertise has been provided by Mr. G. Braybrook, with the scanning electron microscope; Mr. C. Sullivan, in the preparation of thin sections; and Mr. O. Wood and the other technical staff members of the Department of Civil Engineering for equipment operation and numerous analyses. Mr. R. Howells contributed computer consulting services; and Mr. A. Muir built the specimen trimming lathe, modified all test equipment, and contributed valuable practical advice on

equipment operation.

Mr. J. Root contributed editing and organizational skills, and Mrs. J. Root contributed many hours of valuable time in compilation and proof-reading.

Mrs. B.A. Dusseault spent hundreds of hours in manuscript preparation, editing, and typing, as well as providing four years of moral support.

Syncrude Canada Limited supplied camp facilities and drilling rig time, and Mrs. P. Lulman and Mr. L. Nichols have participated in many hours of discussion.

Funding for the research was provided by the Government of Canada through the agencies of the National Research Council and the Department of Energy, Mines and Resources.

The National Research Council and the International Nickel Company of Canada Limited each provided two years of financial support through postgraduate scholarships. Bursaries and partial teaching assistantships were provided by the University of Alberta and the Department of Civil Engineering.

The writer wishes to express his sincere appreciation for all of the help received throughout his years of work at the University of Alberta.

TABLE OF CONTENTS

CHAPTER PAGE

II. (continued)

CHAPTER PAGE

V. (continued)

CHAPTER PAGE

VI. (continued)

CHAPTER PAGE

VII. (continued)

CHAPTER PAGE

IX. (continued)

APPENDIX

LIST OF TABLES

Table Page

Appendices

LIST OF FIGURES

Figure Page

Appendices

Figure Page

Appendices (continued)

LIST OF PHOTOGRAPHIC PLATES

CHAPTER I

INTRODUCTION

1.1 The Oil Sands of Alberta

The most conservative estimates of population growth and technological expansion indicate an increasing world demand for energy continuing well into the next century (Hubbert, 1971). At present, fossil fuels provide most of the world's energy, and it is estimated that they will continue to do so beyond the year 2000 (Starr, 1971). Rapidly increasing prices for energy have accompanied the increase in demand, and these trends are expected to continue for at least the next 50 years. For these reasons, there has been a dramatic increase in the search for, and development of, sources of energy by the petroleum industry. Alberta's oil sand deposits (Figure 1.1) represent a major source of oil for the future.

The depth of burial of the oil-bearing strata varies from 0 to 650 m. At present, those portions of the deposits covered by up to 50 m of overburden (Figure 1.2) can be recovered profitably by surface mining methods. Deposits covered by more than 200 m of overburden can be recovered through *in situ* extraction techniques presently under development. No economically feasible extraction technology has yet been developed for oil sand deposits overlain by 50 to 200 m of overburden. Because oil recovery by surface mining methods is more efficient than oil recovery by *in situ* methods, as much of the Athabasca deposit as possible will be recovered by surface

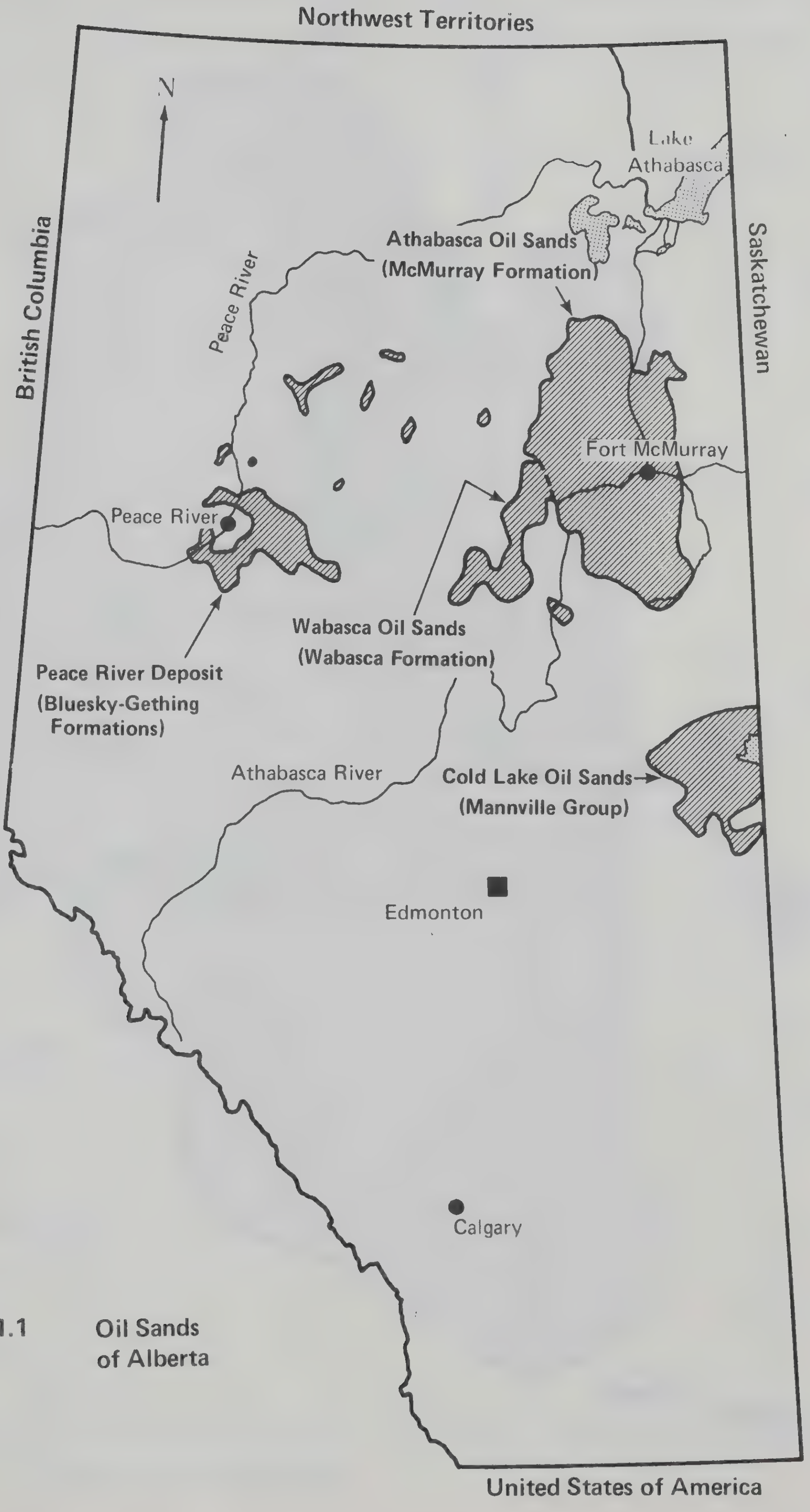

Figure 1.1 Oil Sands of Alberta

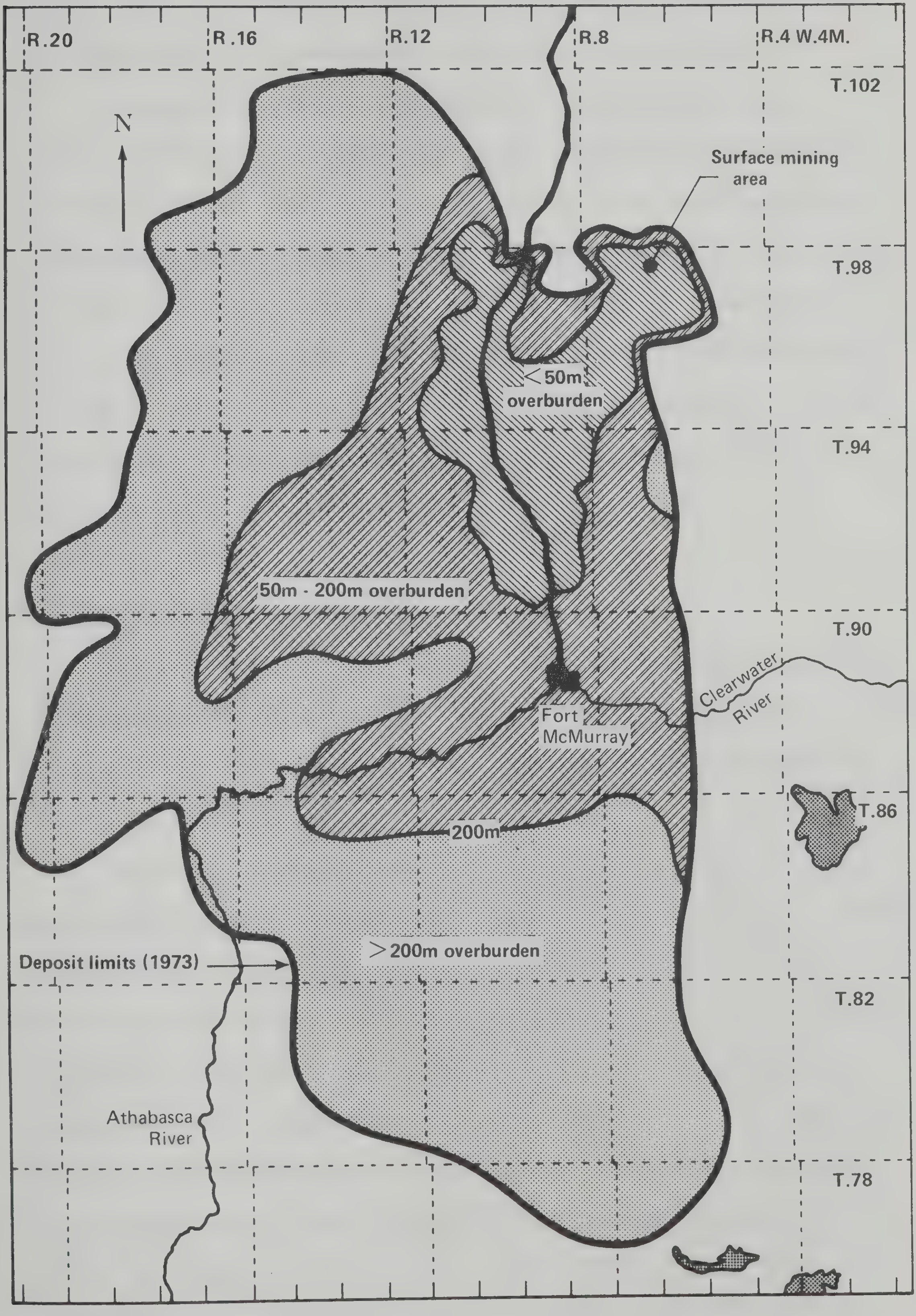

Figure 1.2 Athabasca Oil Sands Deposit

mining. Oil sand deposits outside the Athabasca Oil Sands area are too deeply buried for the use of surface mining techniques.

The existence of the Athabasca Oil Sands has been known to Canadian industry for over 100 years, but large-scale exploitation has been attempted only in the last 10 years. The future will bring further development, likely at a rapidly increasing rate, for the next 20 to 30 years. This development will require large investments of capital and research time from government and private industry alike. After this period, development will proceed at a slower rate as this huge resource is systematically utilized during the next several hundred years.

1.2 Estimates of Alberta's Heavy Oil Reserves

The Athabasca Oil Sands and other similar but smaller deposits underlie about 50,000 km^2 of northern Alberta. The Athabasca Oil Sands alone have been estimated to contain a minimum of 600 BB (billion barrels) of heavy oil (Govier, 1973).

About 14% of the oil-containing sands of the Athabasca deposit can be mined through surface mining methods: this constitutes a reserve of over 80 BB of heavy oil (Table 1.1). The recoverable reserves accessible by surface mining methods are estimated at 38 BB. This estimate is based on rejection of material containing less than five percent bitumen by weight, overburden to oil sand ratios of 1.0 or less, and an extraction recovery factor of about 90%. Conversion of the heavy oil to conventional lighter oil products (i.e. synthetic crude oil) reduces the figure to 27 BB (Govier, 1973). Energy requirements for surface mining are relatively low, so a further reserve reduction

TABLE 1.1

ALBERTA'S HEAVY BITUMEN RESOURCES

DEPOSIT	OVERBURDEN (METERS)	BITUMEN IN PLACE (MMSTB) (4)	RECOVERABLE CRUDE BITUMEN (1) (MMSTB) (4)	RECOVERABLE SYNTHETIC CRUDE OIL (2) (MMSTB) (4)
Athabasca Oil Sands	0 - 50 50 - 600	74,000 551,900	38,000 (3) 166,000	26,500 (3) 93,000
Wabasca Deposit	100 - 750	53,800	16,000	9,000
Cold Lake Oil Sands	300 - 600	164,100	49,000	28,000
Peace River Oil Sands	300 - 750	50,400	15,000	8,500
Other Deposits	150 - 750	2,000	------	------
Totals	---	896,200	284,000	165,000

(Adapted from Govier, 1973.)

(1) Assuming a recovery ratio of 0.30 by *in situ* methods.

(2) Assuming: a) Conversion ratio to synthetic crude of 0.80 and,
b) Energy consumption of 30% for processing.

(3) ERCB: Proven reserves, surface mining methods.

(4) Millions of standard oil field barrels.

factor is unnecessary. The synthetic crude oil, a partially refined product, requires little further refining and is a most desirable refinery feedstock. At present, the synthetic crude oil price is set to match that of conventional crude oil; therefore, at the 1976 export price of $13 per barrel, the portion of the Athabasca Oil Sands to be surface mined represents a gross resource value of approximately $350 billion.

Approximately 60% of the oil sands of the Athabasca deposit, and all of the other oil sands in Alberta, eventually may be exploited through *in situ* recovery methods. This portion of Alberta's oil sands contains a gross reserve of about 600 BB of bitumen. Applying a recovery factor of 40% and a separation factor of 70%, this reserve could yield 170 BB of synthetic crude oil. The large energy requirements of *in situ* extraction methods (perhaps as high as 50% of the BTU value of the recovered bitumen) would result in a significant further decrease of this yield.

The total dollar value of the oil sand reserves is immense; if present economic assessments continue to apply, the Athabasca Oil Sands and similar deposits represent Alberta's single most valuable resource reserve.

1.3 History of Commercial Development of the Athabasca Deposit

Recovery of the bitumen from the oil sands has been attempted sporadically since the beginning of the century. These small-scale attempts at exploitation used surface mining methods and various extraction techniques. The most ambitious pilot project was a surface mine and hot water extraction plant at Bitumount, begun by the Alberta

government in 1948. The extraction technology perfected in this project led to the opening of the first commercial oil sands mine in 1967: Great Canadian Oil Sands Limited, a subsidiary of Sun Oil Company. It has been operating for nine years, mining the sands with bucket-wheel excavators and extracting the bitumen by a hot-water separation technique. A second, larger, oil sands mine is presently under construction by Syncrude Canada Limited. Several other plants are in the planning stages.

1.4 Future of the Athabasca Oil Sands

1.4.1 Surface Mining Methods

The total amount of synthetic crude oil presently considered recoverable by conventional surface mining methods is estimated at 27 BB. Economies of scale indicate that a daily production of 125,000 to 250,000 barrels per extraction plant would be desirable. Since the estimated life of each oil sands plant would be about 30 years, ultimately 10 to 20 surface mining and extraction operations may be built. Each of these sites would require an initial capital investment of over two billion 1976 dollars, and each would directly employ over 2000 persons. Operating costs in the future would remain high, despite the development of new extraction and mining techniques, but the long-term reliability of crude oil production would balance the high costs.

1.4.2 Other Recovery Methods

No commercially viable underground mining method or *in situ* extraction method has yet been perfected to recover oil from oil sands.

Imperial Oil of Canada Limited is conducting the largest pilot project to date in the Cold Lake deposit (Figure 1.1), but economic evaluations and energy consumption data are not yet available. Previous pilot projects conducted by several other oil companies have indicated high energy consumptions, relatively poor recovery ratios, and operating costs considerably higher than those of surface mining methods. In the future, as the output of synthetic crude oil from conventional surface mining methods reaches a maximum and then begins to decline, underground methods will be used to maintain Canadian crude oil output. Most researchers are presently considering _in situ_ extraction in some form, but new underground mining technologies may be developed to overcome some of the present deficiencies of _in situ_ methods.

1.5 Geotechnical Contribution to Oil Sands Development

Development of the Athabasca Oil Sands requires geotechnical expertise from the initial conceptual stages, throughout the project life, to the termination of the project, when the land is reclaimed for other uses.

With surface mining methods, geotechnical data and assessment are required in foundation design, pit wall design, mine layout, material storage, process water storage, and, finally, reclamation. _In situ_ extraction methods require less geotechnical expertise; nevertheless geotechnical contributions will be valuable in process design, process management, and surface facility design. Secondary development resulting directly from resource exploitation also creates a large demand for geotechnical services: new townsites, commercial development, access roads, recreational facilities, railways, air strips, and

many other ancillary facilities must be built. If underground mining methods are employed, the role of the geotechnical sciences will be as significant as in the present open pit mining methods. In total, the demands for the expertise of earth sciences technology probably will be second only to the demands for the services of the petrochemical sciences.

1.6 The Basic Characteristics of Oil Sand

The majority of the oil-rich (i.e. greater than 10% bitumen) oil sands are fine- to medium-grained dense sands with small quantities of silt- and clay-sized material. The finest-grained mineral fractions consist mainly of clay minerals; specifically, kaolinite and illite (Carrigy, 1973). The quartz grains are at least 99% water-wet (Bowman, 1967); the other minerals (generally finer-grained) are hydrophilic and are concentrated in the water layer (Figure 1.3). Bitumen and gas occupy the remainder of the pore space. Appreciable quantities of gas, predominantly nitrogen and methane (Hardy and Hemstock, 1963), are dissolved in both bitumen and water phases. The mean bitumen content of the oil-bearing strata is 10% by total weight, but bitumen content varies from 0% to 18%. The bitumen falls into the heavy oil category, with a specific gravity slightly higher than one, and *in situ* viscosities ranging from 6000 to several million poises (Ward and Clark, 1950). In summary, the Athabasca Oil Sands are fine to coarse grained, water-wet, and orthoquartzitic, with significant volumes of viscous interstitial bitumen.

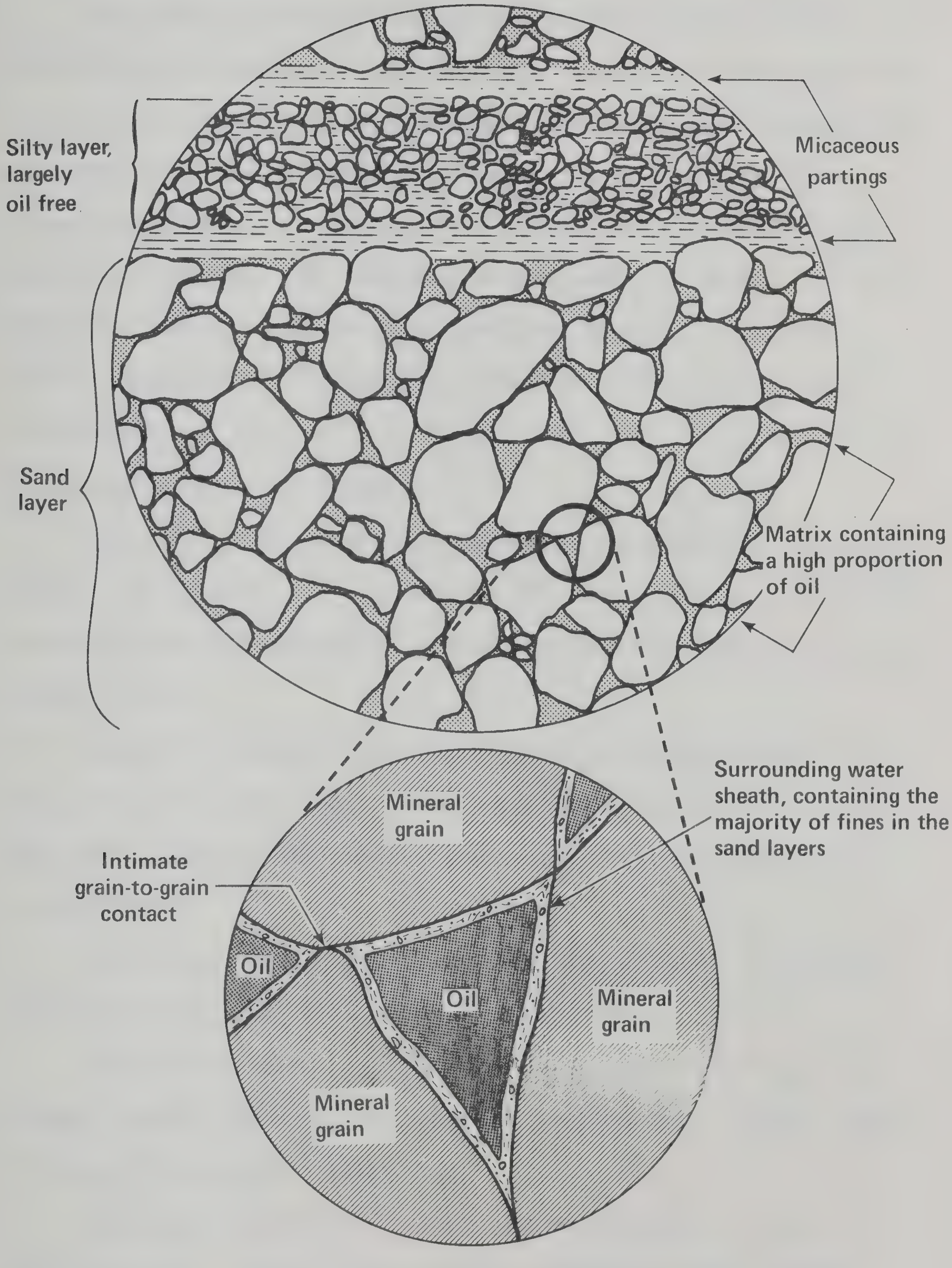

Figure 1.3 *In Situ* Structure of Oil-Rich Quartzose Oil Sand

1.7 Scope of the Thesis

The task of this thesis is to investigate the geotechnical properties of the Athabasca Oil Sands with emphasis on those properties of concern in surface mining operations. The major topics explored in this thesis are the stress-strain-strength characteristics of the Athabasca Oil Sands, natural slope morphology, microstructure of the sands, and computer stress analysis of high steep pit walls. The mineralogy and index properties of the McMurray Formation basal clay deposits, sampling techniques, and geophysical methods are discussed in the appendices.

1.8 Organization of the Thesis

Chapter II consists of descriptions of the geography, climate, geology, and lithology of the Athabasca Oil Sands area. The information discussed is obtained from publications and from study of outcrops and borehole cores.

Chapter III reports the conclusions of a geomorphological investigation of natural slopes in oil sands and discusses the geotechnical implications of the observed high strengths with respect to pit wall stability.

Published strength data on oil sands are limited. These data and their limitations are discussed in Chapter IV.

Chapter V presents the results of an extensive laboratory shear strength testing program on oil sands and on densified quartzose sands. The source of strength is identified.

Chapter VI extends the strength source hypothesis to other similar materials. Two friable quartzose sandstones and a natural dense sand were tested.

In Chapter VII the microfabric of the tested natural materials is studied. Grain textures as a diagnostic tool are discussed; porosity reduction mechanisms are evaluated.

Chapter VIII first presents a method of evaluating the factor of safety of high steep slopes in oil sand, then assesses the likelihood of progressive failure and tension crack generation by a finite element technique.

Chapter IX summarizes the previous seven chapters and presents the conclusions drawn from the thesis.

A series of appendices (A through H) reports extensive supplementary data.

CHAPTER II

ATHABASCA OIL SANDS: GEOGRAPHICAL SETTING, CLIMATE, GEOLOGY, AND LITHOLOGY

2.1 Introduction

The initial research on the geotechnical characteristics of the Athabasca Oil Sands consisted of a synthesis of pertinent published data. In this chapter, the geographical setting of the oil sands and the area's climate are described briefly; the geology and lithology of the oil sands are discussed in more detail.

2.2 Geographical Setting

The Athabasca Oil Sands region lies at the northeastern rim of the Interior Plains, and is almost entirely within the drainage basin of the Athabasca River. The area underlain by oil sands deposits suitable for surface mining is in the Clearwater Lowlands and is flanked to the east, west, and south by highlands (Figure 2.1). The dominant physiographic features of the area are the deep east-west valleys of the Clearwater and Athabasca rivers and the wide north-south basin occupied by the Athabasca River north of Fort McMurray.

After the recession of the continental glacier, the valley of the Clearwater, and that of the Athabasca north of Fort McMurray, formed a major meltwater system, which drained the glacier when its front lay to the northeast of the oil sands area. The Clearwater valley (Figures 2.2 and 2.3) is relatively straight, broad (3000 to

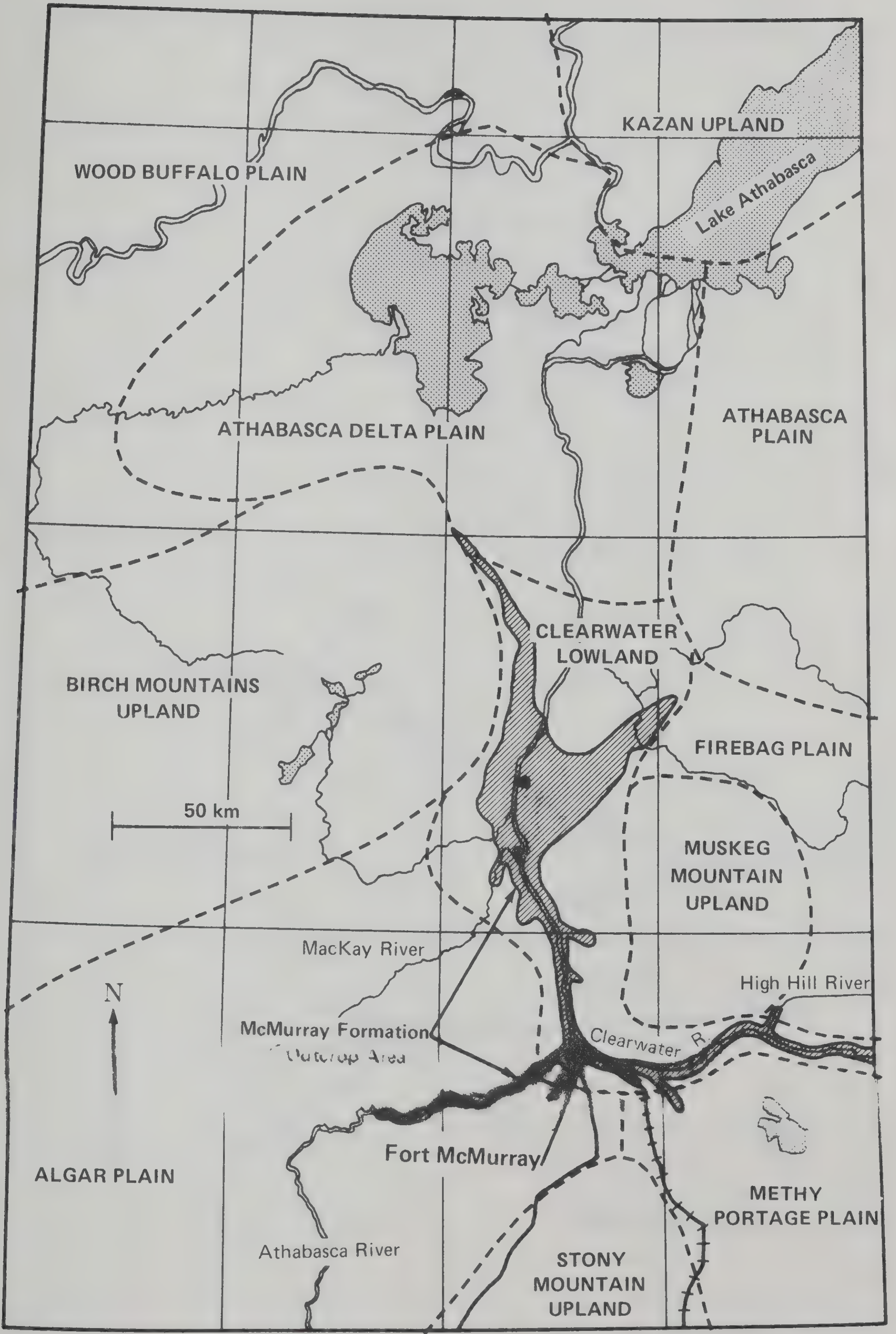

Figure 2.1 Physiography of the Athabasca Oil Sands

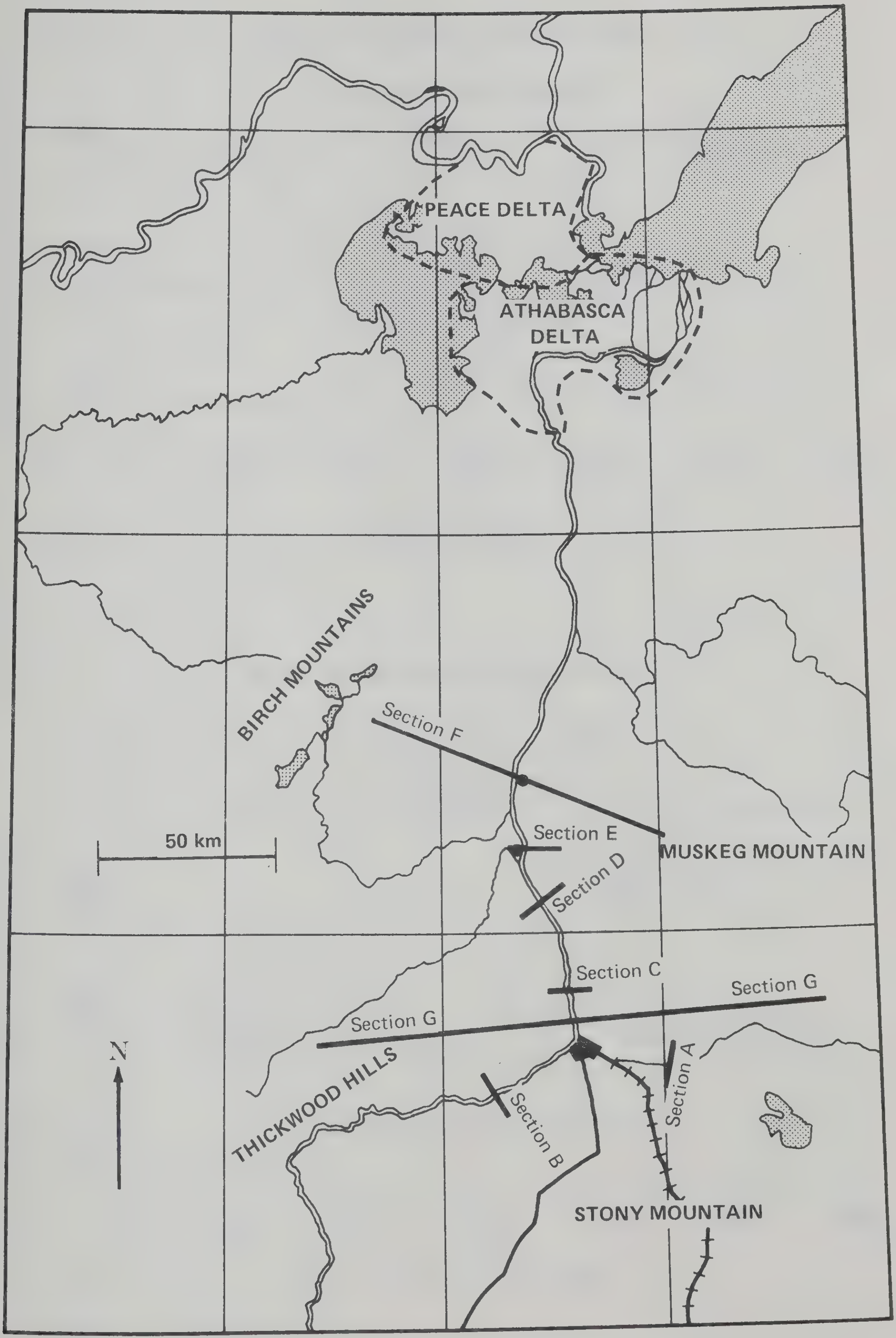

Figure 2.2 Cross-Section Locations

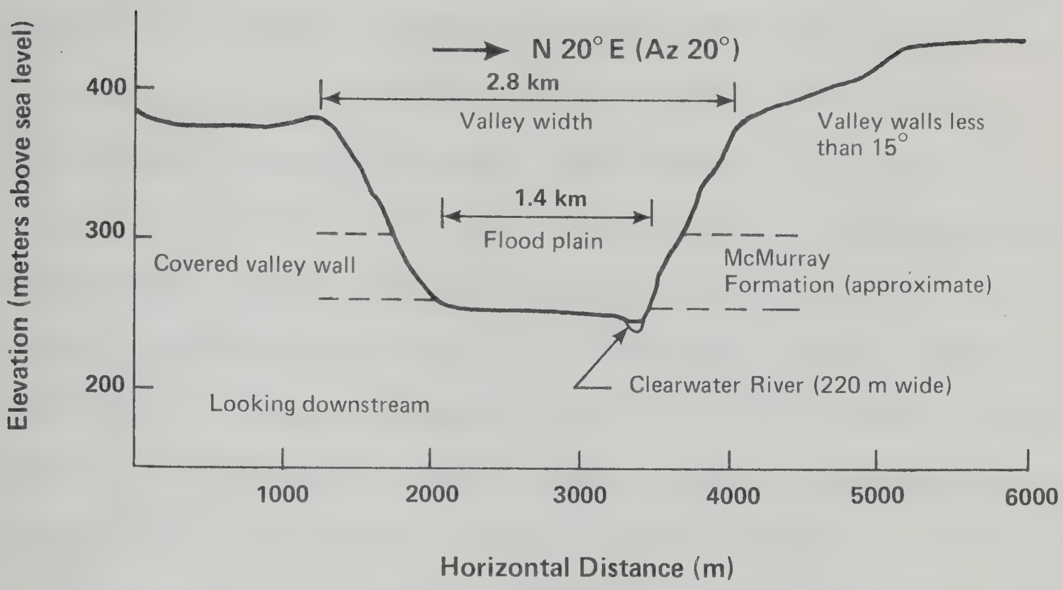
Section A: NW corner, TWP 88, R7W4

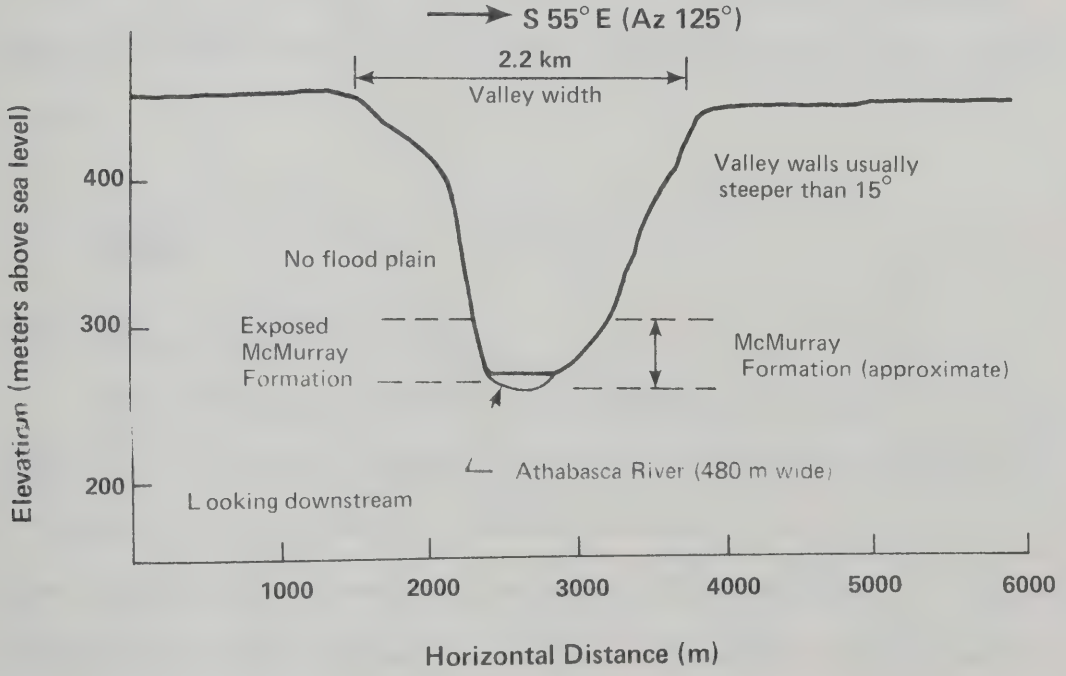
Section B: SE corner, TWP 88, R12W4

Figure 2.3 Valley Profiles, Clearwater and Athabasca Rivers

7500 m), and deep (100 to 220 m); and the valley walls display gentle slopes (less than 15°). The Athabasca River west of Fort McMurray (Figure 2.3) occupies a steep-walled (over 15°), narrow (less than 3200 m), deep (110 to 210 m) postglacial valley. The absence of a flood plain, the numerous rapids, and the steep incision into the surrounding plain are evidence of the postglacial development of the river valley. North of Fort McMurray, the Athabasca River valley changes significantly (Figure 2.4). Valley wall heights decrease gradually to the north, dropping from 110 m in the vicinity of Fort McMurray to five meters or less in the levees of the Athabasca Delta (Figure 2.5). There are no rapids along this reach of the river, and the valley is wide, with a well-developed flood plain in most places. The northern section of the Athabasca River lies in the approximate center of a large, gently sloping basin (Figure 2.6). No evidence exists for a preglacial river course of any consequence, although surface drainage must have occupied approximately the present river course.

2.3 Climate

2.3.1 General Climatic Setting

Fort McMurray, situated at the northwestern edge of the Great Plains, has a typical subarctic, continental climate, characterized by short hot summers and long cold dry winters. Selected climatic data, recorded at the weather station near Fort McMurray, are reported in Figure 2.7 and in Tables 2.1 and 2.2. These data are typical of the Athabasca Oil Sands region. Although the mining area lies at a

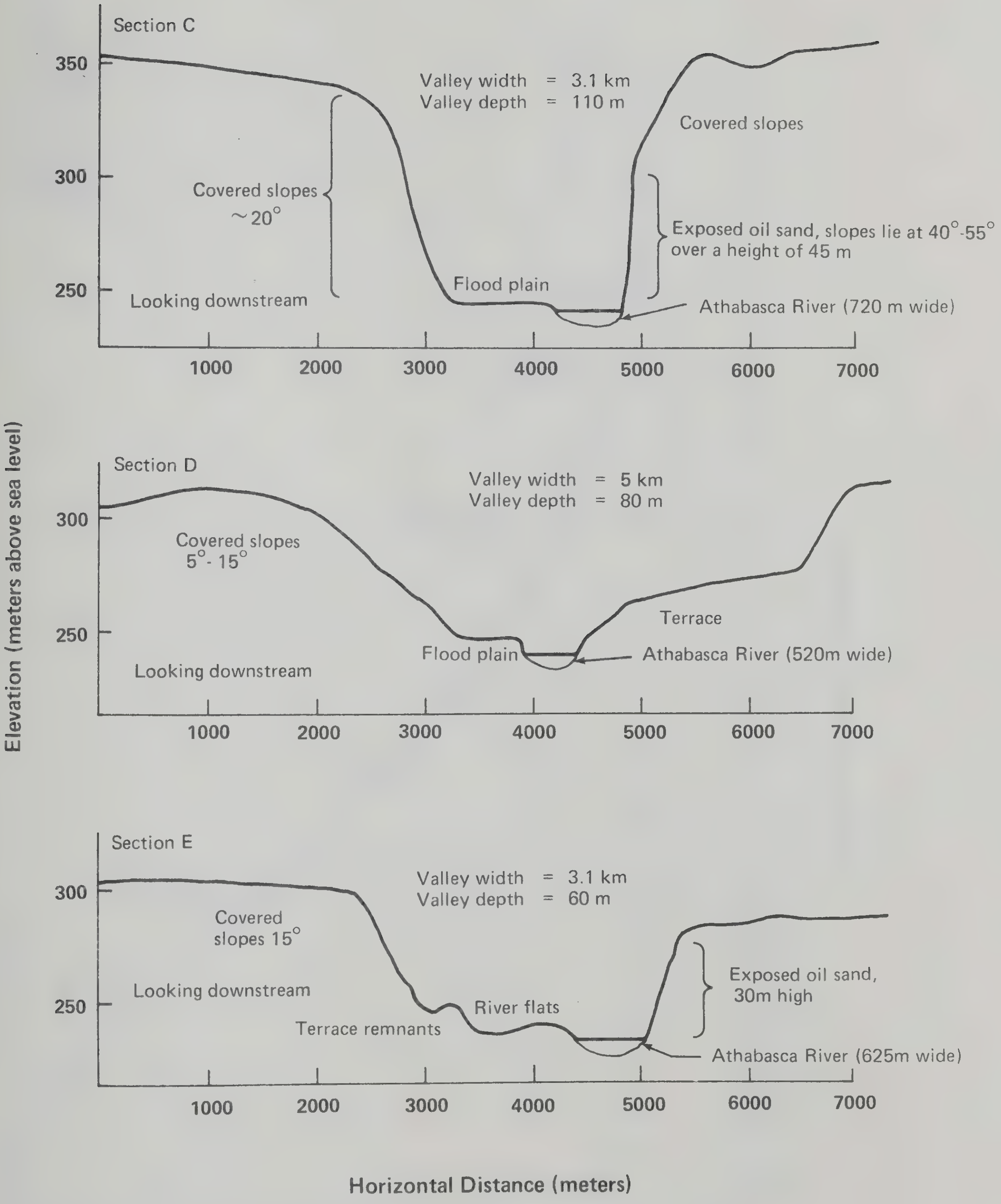

Figure 2.4 Profiles of the Athabasca River Valley North of Fort McMurray

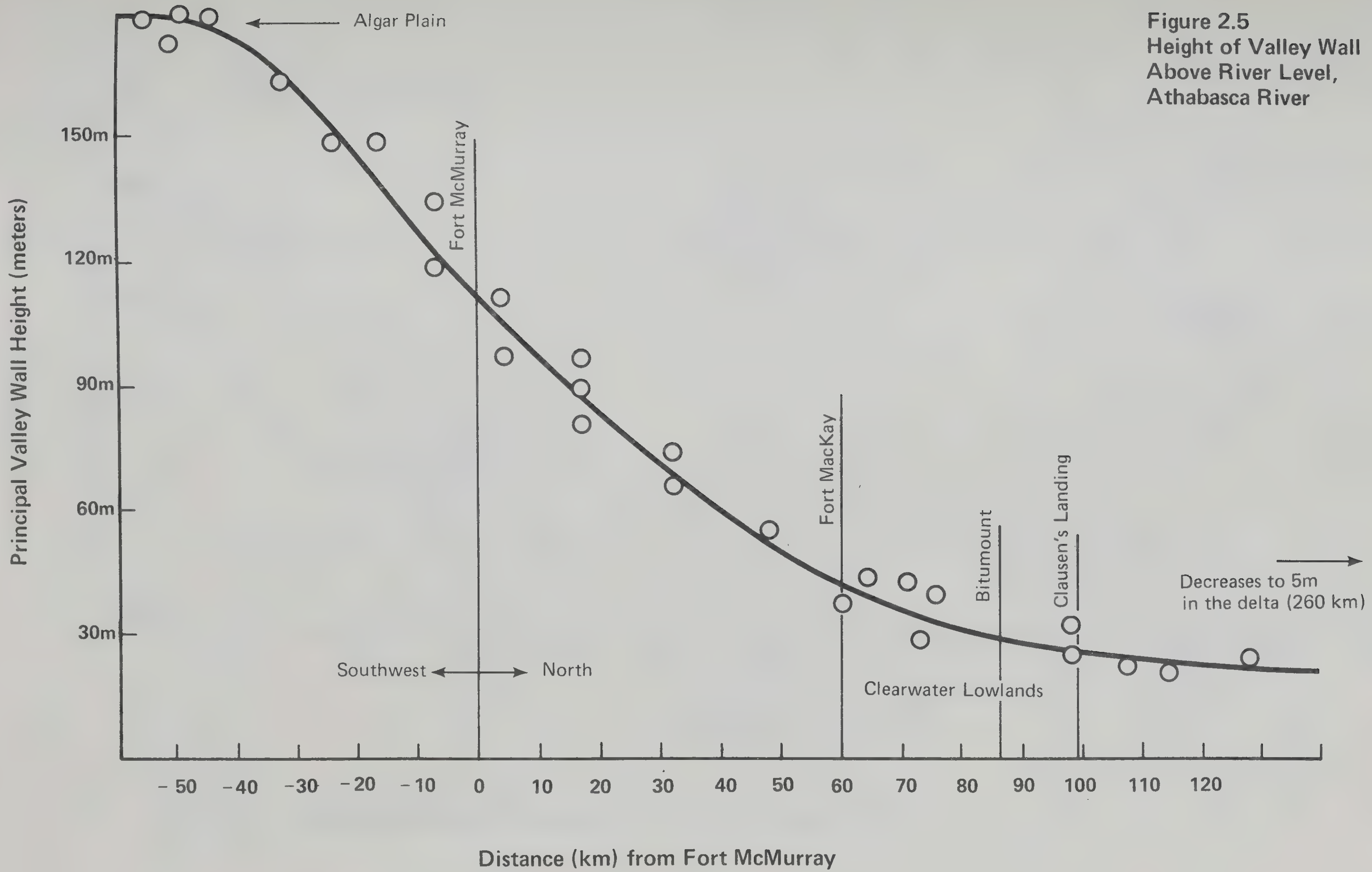

Figure 2.5
Height of Valley Wall
Above River Level,
Athabasca River

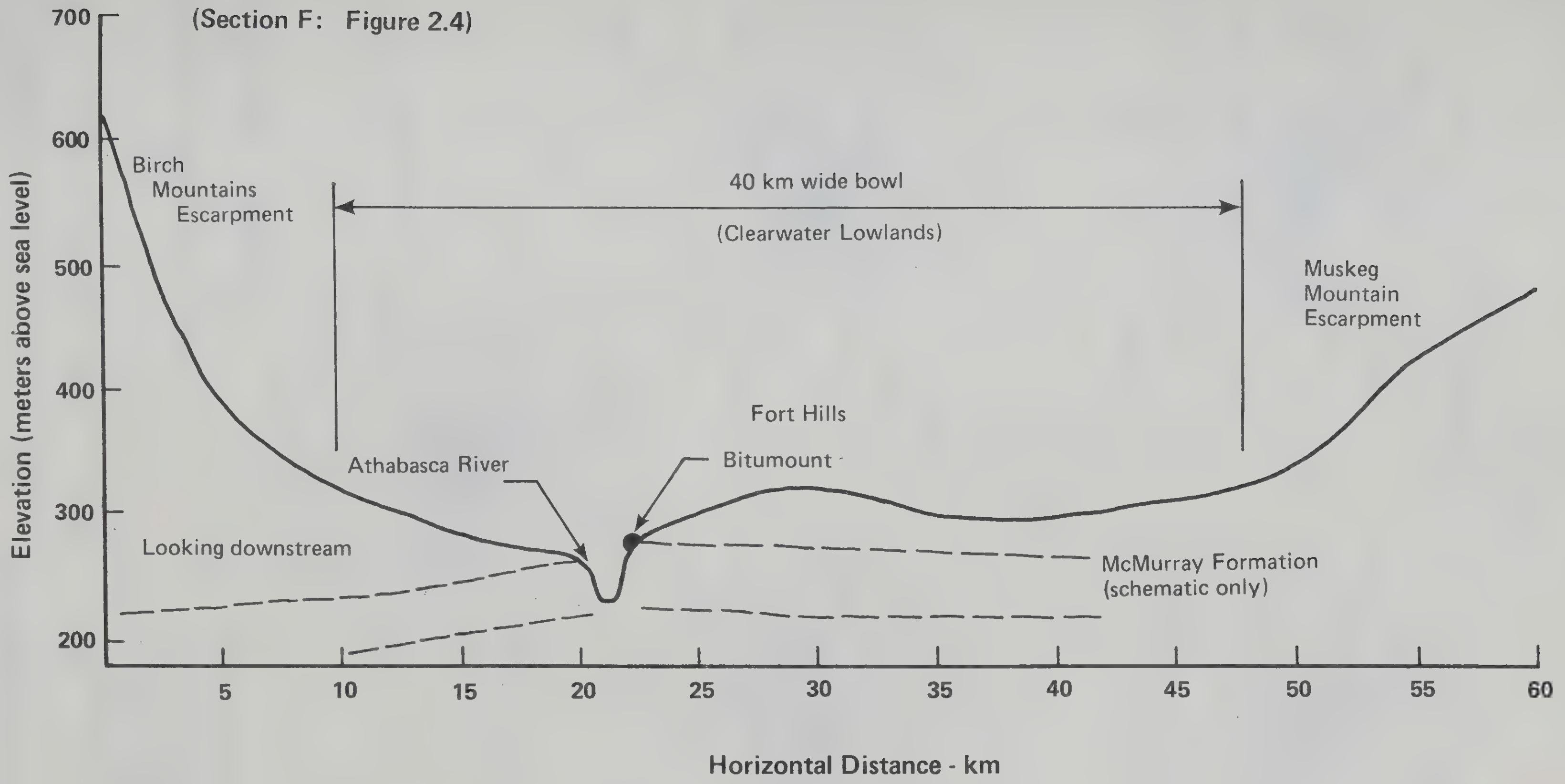

Figure 2.6 Athabasca River Cross-Section - 80 km North of Fort McMurray

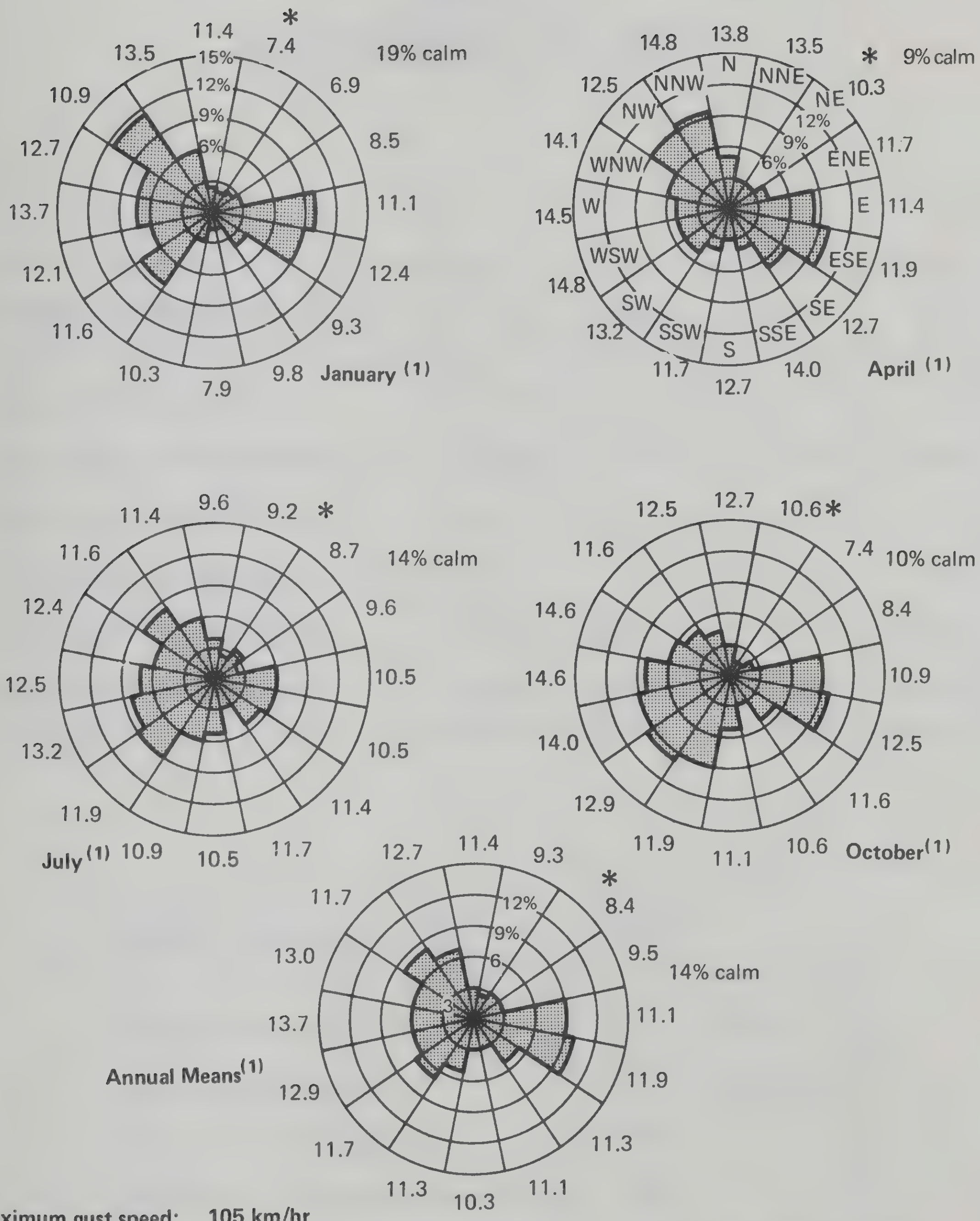

Maximum gust speed: 105 km/hr

Maximum observed hourly speed: 72 km/hr

1) The rose diagrams represent a frequency distribution of wind directions. Peripheral values are mean velocities for a particular direction (in km/hr).

Figure 2.7
Wind Direction and
Mean Velocities,
Fort McMurray, Alberta

Atmospheric Environment Service of Canada

TABLE 2.1

TEMPERATURE DATA: FORT McMURRAY

MONTHLY TEMPERATURE DATA	Jan.	April	July	Oct.
Mean Daily Temperature	-21.5°C	1.2°C	16.3°C	3.0°C
Mean Daily Maximum Temp.	-16.0°C	7.8°C	23.4°C	8.5°C
Mean Daily Minimum Temp.	-26.9°C	-5.4°C	9.1°C	2.4°C
Mean No. of Days with Frost	31	25	0	22
Maximum Recorded Temp.	10.0°C	26.1°C	35.6°C	26.7°C
Minimum Recorded Temp.	-50.0°C	-35.0°C	-3.3°C	-22.8°C

ANNUAL TEMPERATURE DATA (1973 RECORDS)	
Maximum Temperature	36.1°C (June)
Minimum Temperature	-50.6°C (February)
Mean Daily Temperature	-0.5°C
Mean Daily Maximum Temperature	6.9°C
Mean Daily Minimum Temperature	-6.8°C
Mean Frost-Free Period	69 days
Longest Frost-Free Period	115 days
Shortest Frost-Free Period (including July 15th)	8 days

TABLE 2.2

PRECIPITATION DATA: FORT McMURRAY

MONTHLY DATA	January	April	July	October
Mean Rainfall (mm of water)	0.5	7.1	73.7	13.0
Mean Snowfall (mm of snow)	221.0	127.0	0.0	111.8
Mean Equivalent Precipitation	21.1*	20.3*	73.7*	24.1*
Days with Measurable Rainfall (Mean)	0	4	13	6
Days with Measurable Snowfall (Mean)	14	5	0	5
Maximum 24 Hour Rainfall	6.4	10.9	51.6	21.8
Maximum 24 Hour Snowfall	154.9	208.3	0	109.0

ANNUAL DATA	
Number of Days with Measurable Precipitation	131 days
Greatest 24 Hour Rainfall	60.4 mm (September)
Greatest 24 Hour Snowfall	297.2 mm (March)
Mean Annual Precipitation (in mm of water)	435.4 mm
Greatest Annual Snowfall	2966.7 mm (1971-2)
Least Annual Snowfall	459.7 mm (1948-9)
Mean Annual Snowfall	1397.0 mm

* One mm of snow is approximately equal to 0.1 mm of equivalent precipitation.

somewhat lower elevation than the observing station and about 50 km to the north, climatic differences are probably minor.

2.3.2 Climate-Related Mining Difficulties

The wide range of temperatures in the oil sands area presents special difficulties in continuous mining operations and great demands on men and machinery. The long cold winters result in cold-indurated bitumen; this causes an increase in the abrasiveness of the oil sand, greater penetration resistance to digging equipment, and a reduction in machinery efficiency. Frost penetration on north-facing pit walls is rapid and deep, because of the absence of snow cover on the steep slopes. Conversely, in the hot sunny summer months, south-facing pit walls experience high temperatures because of high radiation absorption by the black bitumen in the oil sand, and rapid pit face raveling is a common result.

2.4 Geology of the Athabasca Oil Sands

2.4.1 Introduction

Early explorers (Bell, 1884, 1908; McConnell, 1891) noted the existence and the major features of the oil sands and speculated on their origins, but detailed study of the deposits with exploitation in mind did not begin until the early part of this century with the mining engineering work of Ells (e.g. 1914, 1915b, 1922, 1926). Since that time, numerous scientists have written about the oil sands. The majority of the articles are arguments concerning the origin of the bitumen (e.g. Ball, 1935; Corbett, 1955; Gussow, 1956; Hume, 1947, 1951; Link, 1951; Sproule, 1938, 1951). Other studies have concentrated on

lithological and structural data (e.g. Falconer, 1951; Kidd, 1951; Mellon, 1956; Mellon and Wall, 1956). In recent years, most of the work on the geological and lithological features of the McMurray Formation has been done by Carrigy (e.g. 1959, 1962, 1963a, 1963b, 1966, 1967, 1973). Other important contributions have been made, but only a few are of direct geological interest (e.g. Alberta Oil and Gas Conservation Board, 1963; Hitchon, 1963; Ansley and Bierlmeir, 1963; Vigrass, 1966; Energy Resources Conservation Board, 1973).

The following discussion of the geology of the Athabasca Oil Sands is a synthesis of published information, the writer's field observations of the natural slopes (Plate 2.1), examination of core specimens, laboratory investigations, and discussions with those involved in oil sands research.

2.4.2 Geological Definition of the Oil Sands

The Athabasca Oil Sands are defined as the oil-bearing portion of two geological formations (Carrigy, 1959): the McMurray Formation, which contains well over 95% of the oil reserves; and the lower, arenaceous portion of the Clearwater Formation. The McMurray Formation is often considered a continuous massive oil-bearing body. In actuality, various portions of the formation contain little or no oil: the argillaceous basal deposits, portions of the coarse-grained basal sands, large intraformational lenses of silty clay and silt, and occasional thick beds of clean fine-grained sand occur as oil-free strata. The entire McMurray Formation becomes oil free east of Range 6 west of the Fourth Meridian (Carrigy, 1959). The formation pinches out westwards against a paleotopographic high (Figure 2.8), and grades into

PLATE 2.1 Outcrop of Athabasca Oil Sands 3km North of Fort McMurray. Note the gullied nature of the outcrop. The lower portion of the outcrop above the limestone is oil-free sand and lies at a repose angle of 33°. The outcrop is about 72m high.

PLATE 2.2 Karst Features, Christina River. Karst dome visible in background, geologist's left foot rests on a 15cm paleocaliche immediately overlying limestone. Coarse-grained, oil-free striped sand is draped over the sides of the karst domes.

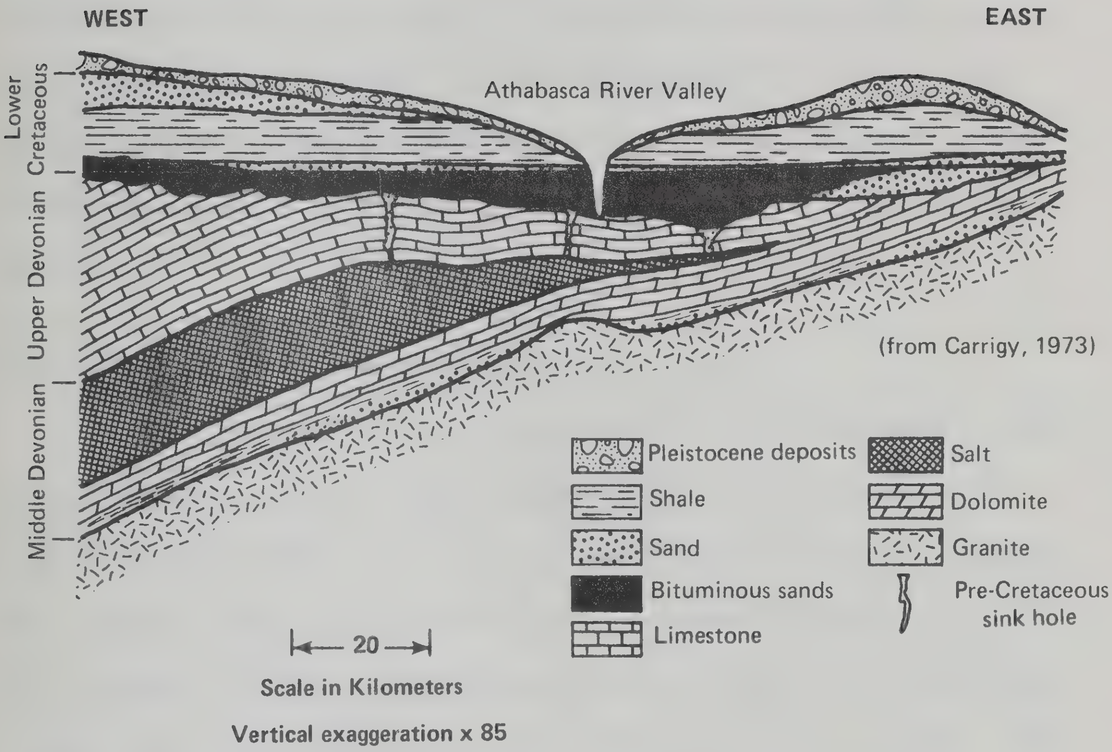

Formations	Age (millions of years) 1)	Period	Rock Type
Unnamed Laurentide drift and postglacial sediments	0	Quaternary (Pleistocene)	Glacial till, proglacial lake sediments, aeolian sand
Joli Fou Fmn.	~1.5 ~100	(Post-Cretaceous erosion surface)	Shale
Grand Rapids Fmn.			Sandstone
		Lower Cretaceous	Shale to fine-grained sand at base
Clearwater Fmn.			
Wabiskaw Mem. McMurray Fmn.			Sand to basal pebble conglomerate, largely uncemented
	~106 ~360	(Pre-Cretaceous erosion surface) Upper Devonian	
Waterways			Limestones and dolomites
Elk Point		Middle Devonian	Shale, anhydrite salt, dolomite
	~370 ~1800?	(Pre-Devonian erosion surface) Aphebian (Pre-Cambrian)	Granites, gneisses, Granites, gneisses, schists
Unnamed Plutonic rocks			

1) From: Geology and Economic Minerals of Canada, 1970.

Figure 2.8 Stratigraphy of the Athabasca Oil Sands

marine shales to the northwest. To the south and southeast, an oil-water contact forms the boundary of the Athabasca Oil Sands. The northern and northeastern boundaries represent the southward limit of Pleistocene glacial erosion of materials from the McMurray Formation.

2.4.3 Predepositional Geological History

Faunal studies have shown that the McMurray Formation is Lower Cretaceous in age (Bell, 1884; McLearn, 1932, 1945; Russell, 1932; Mellon and Wall, 1956). The deposit rests unconformably on an extensive erosion surface of argillaceous limestones, calcareous shales, and limestones of Upper Devonian age (Norris, 1973). The basal unconformity represents a hiatus of about 250 million years. During this time, extensive cycles of subaerial erosion, alternating with minor depositional periods, produced gentle overall relief of about 50 m, characterized by numerous karst features (Plate 2.2). Well-developed drainage systems existed, all with a gentle regional dip to the north and northeast (Martin and Jamin, 1963; Carrigy, 1973). The McMurray Formation contains few readily weathered materials. This indicates that the materials which now form the McMurray Formation were extensively weathered before final deposition (Mellon, 1956). Salt solution in the underlying Prairie Evaporites (Elk Point Group equivalent) in pre-McMurray times (Figure 2.8), possibly in conjunction with differential settlements, has resulted in a series of structural domes and basins being superimposed upon the Devonian strata (Carrigy, 1959; and others). These structural features show local relief of less than 25 m, regional relief of perhaps 100 m, wave lengths from

100 to 1000 m, and flank dips from 2° to 10° with minor local exceptions having dips to 20° (Kidd, 1951). These structures, as well as the differing resistances of the calcareous materials of the Devonian sequences, have influenced the paleodrainage patterns and paleotopography. Drainage channels cutting through the sedimentary structure are visible on the Muskeg River in several locations, and have been delineated by drilling in other locations (Carrigy, 1959).

The general subsidence (or rise in sea level) before and during McMurray times resulted in extensive scour and removal of large quantities of the continental residual and sedimentary materials. Nevertheless, two types of continental pre-McMurray deposits have been identified: coarse channel deposits and fossilized remnants of soil horizons (paleosols and paleocaliches).

2.4.4 Pre-McMurray Sedimentation

Evidence of pre-McMurray sediments of continental origin is found in the paleosols, paleocaliches, and minor continental deposits found directly above the Devonian sequence at the base of the McMurray Formation.

Paleosols and paleocaliches have been identified at many river outcrops: in a 2 to 3 m thick bed south of Slope 7 (Appendix A), in a 1.7 m bed in Slope 51 (Appendix A), and overlying many of the karst features on the Christina River (Plate 2.2). Furthermore, they have been identified tentatively in borehole cores, although there they do not display the oxidized red colour which is diagnostic in the outcrop. The ironstone bed reported at the base of the McMurray Formation (Carrigy, 1959) may actually be a paleocaliche. To date, the observed

occurrences have been on paleotopographic high points, directly upon limestone. Furthermore, the presence of paleosol seems to preclude significant overlying argillaceous deposits. This relationship (Figure 2.9) suggests contemporaneous development of the continental clastic deposits and the adjacent sequences of basal clays. This subject is discussed in greater detail in Appendix H.

In several localities, large deposits of oil-free coarse-grained sands and conglomerates can be observed. The stratigraphic position of these sands is uncertain. They display some characteristics indicating a greater age than the McMurray Formation, but the absence of fossil remains has hampered identification (Carrigy, 1973). They are definitely channel deposits: they show strong current features such as scour channels, and they contain extensive lithoclastic conglomerates, with the lithoclasts largely altered to siderite.

2.4.5 McMurray Formation: Depositional Environment and Geologically Equivalent Formations

Early Cretaceous time was marked by a gradual but continual subsidence of the Interior Plains in North America. This subsidence permitted the encroachment of shallow seas from the northwest and south (Rudkin, 1966). Sedimentary deposits on the regional unconformity are therefore characterized by a distinct basal sequence of transgressive deposits (Figure 2.10). The lower member of this sequence is usually a relatively coarse-grained fluviodeltaic quartzose deposit referred to as an unconformity sand or a blanket sand (Krumbein and Sloss, 1963). Several lithologically and stratigraphically equivalent, although not necessarily time equivalent, unconformity sands exist in the Western

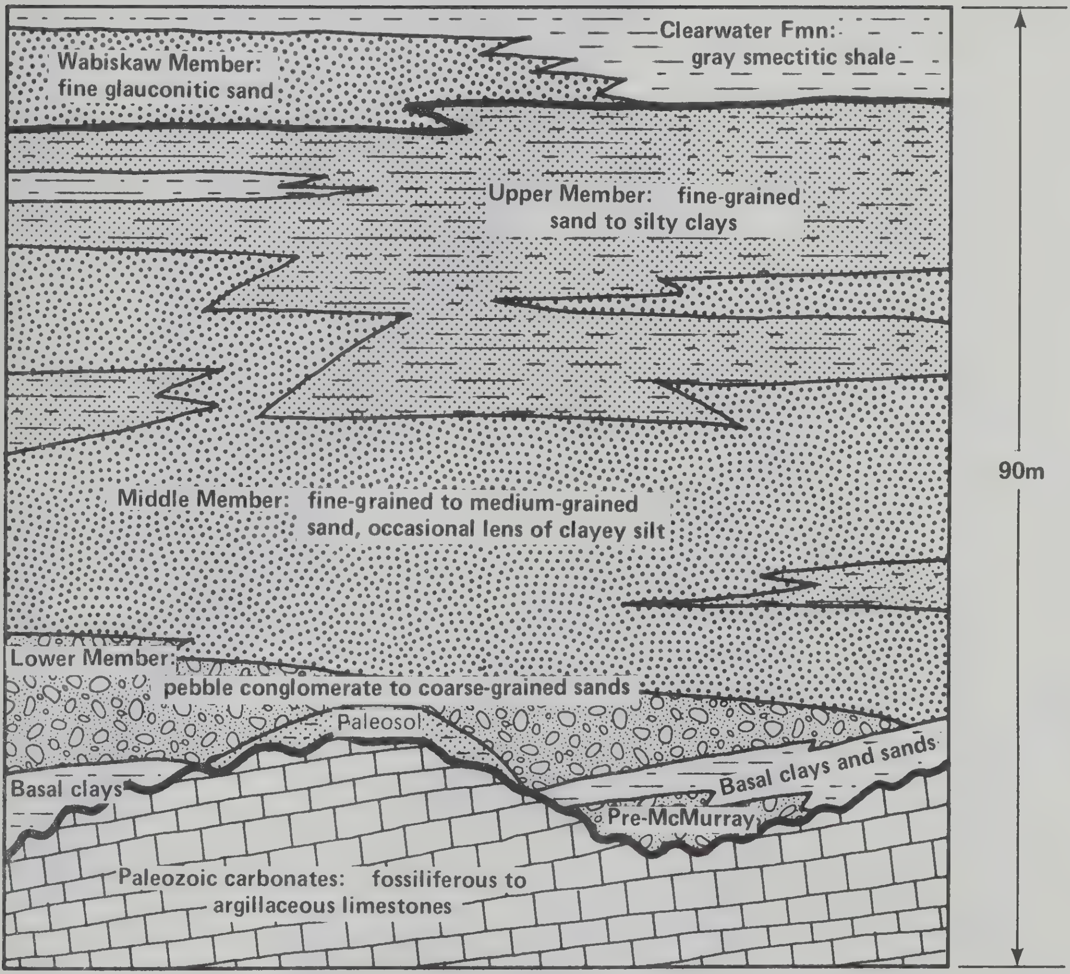

Figure 2.9 Hypothetical McMurray Formation Cross-Section

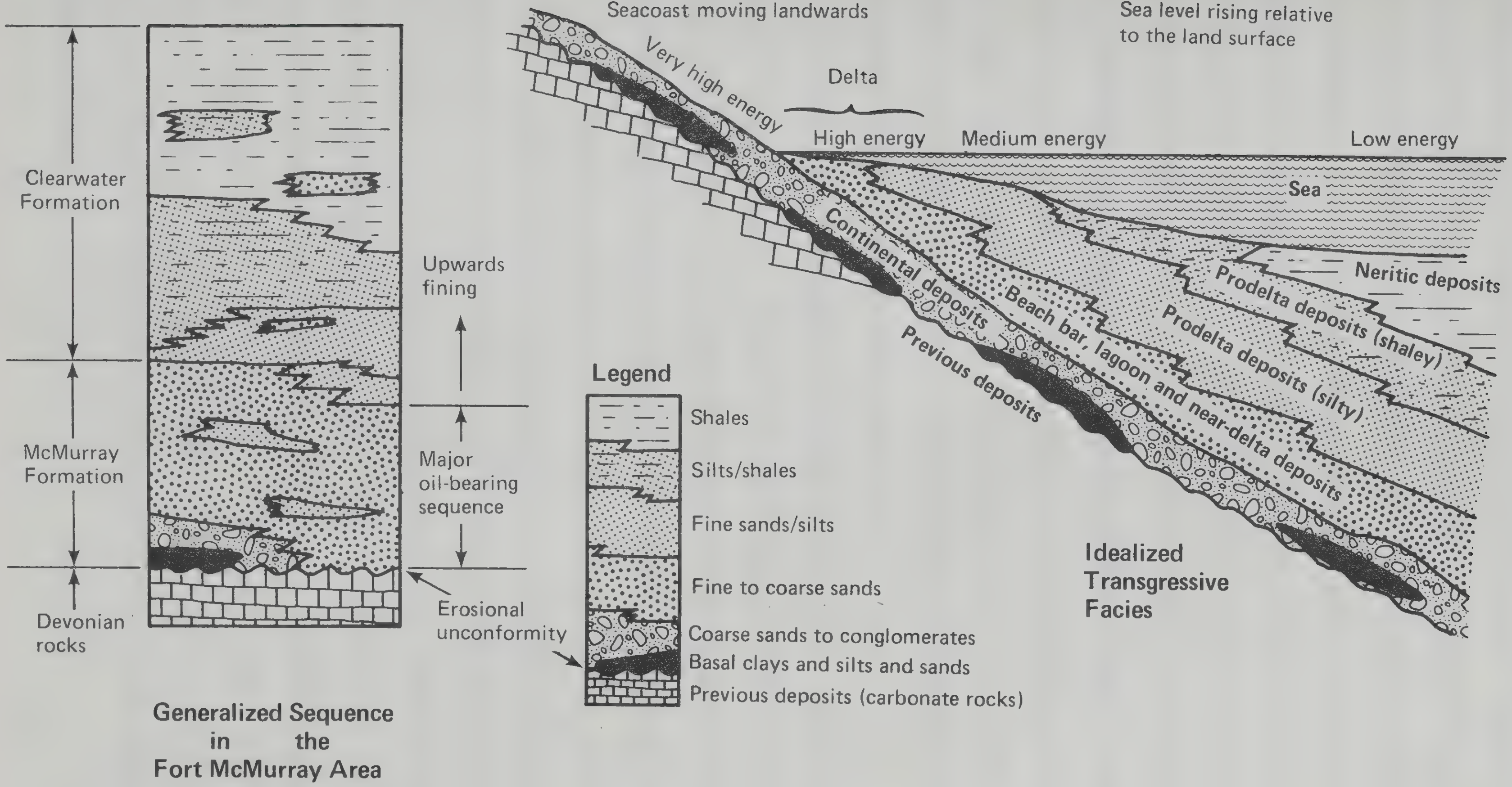

Figure 2.10 Transgressive Deposition

Canadian Sedimentary Basin. These are the Cadomin Formation in the Alberta foothills; the Lower Manville Group in Saskatchewan and eastern and central Alberta; the somewhat more argillaceous Gething Formation in northwestern Alberta and northeastern British Columbia; the Cutbank and Sunburst Formations in southern Alberta, Montana, and North Dakota; the Swan River Sandstone in Manitoba; and of course the McMurray Formation in northeastern Alberta. All these basal sands may represent one lithosome, but intervening paleotopographic highs in some cases may have resulted in discontinuities in the basal blanket sand. In any case, their petrographic characteristics, without considering cement, are similar, and their stratigraphic relationships also are distinctly similar (Wickenden, 1951).

These basal Cretaceous blanket sands, which underlie very large areas of North America, display several characteristics in common. These characteristics are sand-to-shale ratios greater than 1.0, basal conglomerate beds, upwards-fining of arenaceous material, and common but minor lignite or coal occurrences (Rudkin, 1966). Their transgressive nature reflects the gradually diminishing hydraulic energy available as the midcontinental region slowly subsided. As a group, these formations are the continental and marine deltaic deposits formed along and at the mouths of the rivers which drained the Canadian Shield to the east and the Cordillera to the west. The Lower Cretaceous dividing line between the two sources of sediment on the regional unconformity is thought to be a paleotopographic high (a buried ridge) running approximately northwest to southeast about 80 km east of Edmonton (Rudkin, 1966).

2.4.6 Geology of the McMurray Formation

The division of McMurray Formation geology into Lower, Middle, and Upper Members was formalized by Carrigy in 1959. The separations are not characterized by distinct geological horizons, but by gradual changes in lithological characteristics.

The Lower Member of the McMurray Formation includes argillaceous deposits and very coarse-grained clastics. The change from underlying clayey beds to overlying arenaceous beds is so abrupt that the inclusion of both sequences in the Lower Member tends to grossly oversimplify the geological relationships. The coarse-grained sands are fluvial deposits: lithoclastic and conglomeratic lag deposits and cross-bedded point bar and subaqueous dune deposits are diagnostic. Bedding features may be obscured by the coarseness of the materials.

The Lower Member is absent over large areas of the McMurray Formation, and nowhere has its thickness been reported as greater than 25 m. Appendix H contains further data on the argillaceous portions of the Lower Member.

The Middle Member of the McMurray Formation was deposited in a fluviodeltaic environment (Carrigy, 1973). The monomineralic nature and the high degree of sorting displayed by many of the fine- and medium-grained sands indicate extensive sorting in a river bar or beach regime. The lower portion of the Middle Member is characterized by high angle (10^o to 35^o) cross-bedded units ranging in thickness from 10 to 300 cm. These cross-bedded units become progressively thinner and display gentler angles (5^o to 15^o) higher in the sequence. Oil impregnation is generally uniform and oil content is high. These cross-bedded, oil-impregnated sands are the "typical" sands of the

Athabasca Oil Sand deposit. They occur in any complete McMurray sequence in thicknesses up to 40 m. Bedding features observed by the writer include high and low angle cross-bedding, festoon cross-bedding, subaqueous slump deposits, and minor lithoclastic deposits with large quantities of clay clasts (up to 30% by volume).

Progressive southeastwards movement of the sea coast resulted in further decrease of depositional energy as sediment accumulation rates lagged behind the rate of sea level rise. The Upper Member of the McMurray Formation is relatively flat lying (0^{o} to 6^{o}) and consists of silts to very fine-grained sands and occasional intraformational clays. These strata are characteristic of shallow brackish-water deposition (probably lagoonal) and shallow deltaic environments (Dickinson _et_ _al_., 1972). Bioturbic features are common in these fine-grained sands, bedding units are thin (laminae to 20 cm thick), and small-scale reverse cross-beds, indicative of tidal deposition, are common. Oil saturation is variable: the most fine-grained portions are completely oil free. The Upper Member of the McMurray Formation has a maximum thickness of 30 m.

2.4.7 Post-McMurray Geology

The upper boundary of the McMurray Formation is defined by the glauconitic fine-grained sand of the Wabiskaw Member of the overlying Clearwater Formation. The glauconite is indicative of marine (neritic) conditions (Heckel, 1972). The increased montmorillonite and decreased quartz contents indicate a gradual westward shift of sediment source. The Wabiskaw Member is occasionally oil-impregnated, and where it is, it is included as part of the Athabasca Oil Sands (Carrigy and Zamora,

1960).

Sedimentation continued until the Late Cretaceous period, and ultimately 760 m (Corbett, 1955) to 1220 m (Sproule, 1955) of sediments were deposited over the McMurray Formation. As a result of the depth of burial, the maximum temperatures and sedimentary effective pressures experienced by the McMurray Formation were about 40°C and 140 kg/cm^2. The present lithological characteristics of the McMurray Formation are a result of the physical and chemical diagenesis which took place during burial and subsequent erosion (Figure 2.11).

Faulting, subsidence, and other nondiagenetic processes occurred infrequently in post-McMurray times. The Bitumount Basin (Carrigy, 1959) shows signs of some post-McMurray rejuvenation of the underlying evaporite bed solution. Other high angle faults within the McMurray Formation are largely a result of differential compaction of channel and back-swamp deposits. Tectonic faulting has been reported (Sproule, 1938), but is not significant. Gentle southwestward tilting of about 1.4 m/km has occurred since the post-Devonian hiatus.

Erosion began in Late Cretaceous time and continued for over 70 million years, until the onset of continental glaciation in North America. An undetermined quantity of McMurray sands and younger formations has been removed by glacial scour. Outside of river valleys, glacial deposits are ubiquitous (e.g. Bayrock, 1971), and the present valley morphology is largely a result of regional rearrangement of drainage by glacial disruption. Over 2500 m of ice overlay the area during the maximum extent of glaciation, but the geotechnical implications of this geologically recent load have not been assessed fully. Today,

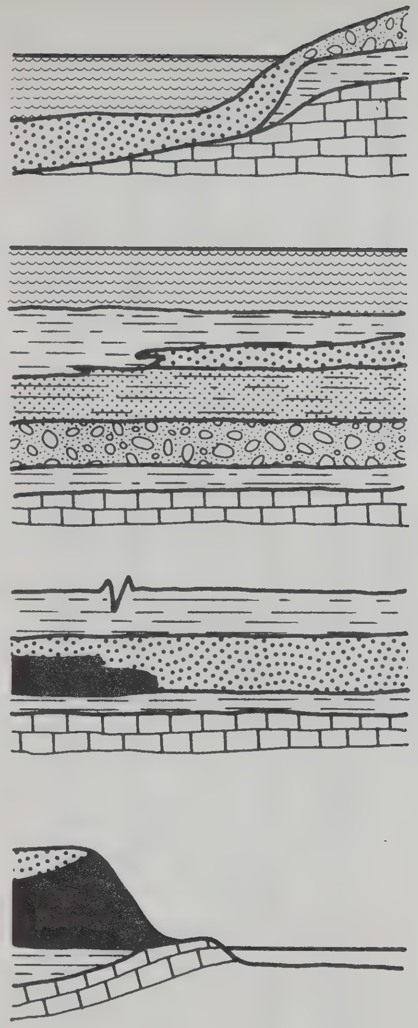

Stage	Materials	Processes
Transport and Deposition (105 my BP)	Coarse-grained sand Fine-grained sand Clayey silts Clays Wood fragments	—Grain rounding —Grain sorting (energy dependency) —Physico-chemical attrition
Shallow burial (to 10 m) to medium burial (to 200 m) (104 my BP)	Sands Mudstones Lignified wood	—Overgrowths —Consolidation (clays) —Compaction (sands) —Minor grain rearrangement
Deep burial (to 1200 m) (80-90 my BP)	Friable sands Clay shales Coaly wood Concretions	—Oil invasion (?) —Chemical diagenesis (ion migration) —Solution and recrystallization of quartz —Joint systems —Continued consolidation
Excavation	Friable oil-saturated sands Basal clays and clay shales Coaly wood Siderite and pyrite concretions	—Rejuvenation of underlying salt solution —Stress-relief joints —Slickensides in clay shales

Figure 2.11 Deposition and Diagenesis in the McMurray Formation

erosive forces continue to act upon all valleys within the oil sands area.

2.5 Athabasca Oil Sands Lithology

2.5.1 Introduction

The lithology of the Athabasca Oil Sands is of great economic importance because lithology directly controls oil occurrence, recovery methods, recovery ratios, and eventually terrain reclamation. The discussion here concentrates on the arenaceous, oil-bearing portion of the McMurray Formation.

2.5.2 Lithological Generalizations: McMurray Formation

The McMurray Formation is heterogeneous with respect to grain size and bedding features but homogeneous with respect to mineralogy. Carrigy's publications (e.g. 1959, 1963a, 1966, 1973) are a relatively complete discussion of McMurray Formation lithology. The following attributes characterize the entire formation:

1. The formation as a whole averages over 94% quartz; hence the term orthoquartzitic is appropriate. There is a tendency for the basal beds to contain some chert, and for the upper beds to contain significant percentages of clay minerals.
2. The clay mineral fraction of any portion is illitic and kaolinitic. Smectite (montmorillonite) appears only in the upper few meters of the formation.
3. The sands are for the most part well sorted.
4. An inverse relationship exists (Figure 2.12) between the

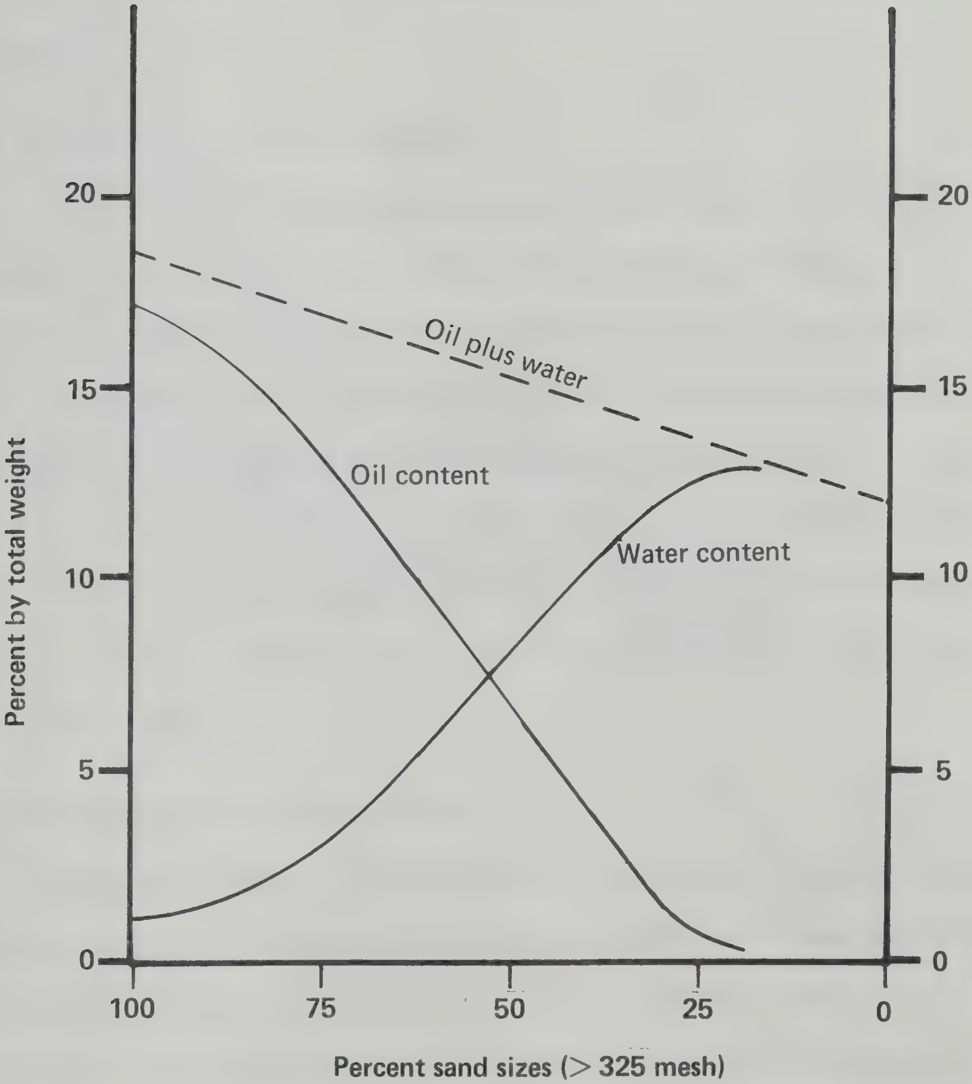

Figure 2.12 Schematic Representation of the Oil Content-Grain Size Relationship

percentage of fine-grained material and the oil content (Carrigy, 1962).

5. Minor but ubiquitous accessory minerals are feldspar and muscovite.

6. The deposit is largely noncemented: calcium carbonate is conspicuously absent.

2.5.3 Lithology of the Lower Member

The majority of grain size curves of the Lower Member sands and pebble conglomerates fall within the boundaries of Group I in Figure 2.13. Chert pebbles and quartzite pebbles are common near the base of the Lower Member, and maximum pebble size observed was 5 x 10 cm. Lithoclastic conglomerates are also common in the Lower Member, and the matrix may vary from a medium-grained sand to a quartz-pebble conglomerate. Sideritic nodules may be associated with these lithoclastic deposits. Pyritic and marcasitic concretions may occur at the base of the Lower Member.

2.5.4 Lithology of the Middle Member

The Middle Member of the McMurray Formation is composed almost entirely of fine- to medium-grained quartzose sands. These sands are in general very well sorted, and fall largely within Group II of Figure 2.13. Other characteristic although less common deposits in the Middle Member include thin coaly seams (one millimeter in thickness), thin lignite bands, thin bands of siderite-cemented sand, and ironstone beds. Lithoclastic conglomerates, consisting of up to 30% rip-off clasts in a matrix of medium-grained sand, are commonly found in the lower portion of the Middle Member, and reverse lithoclastic

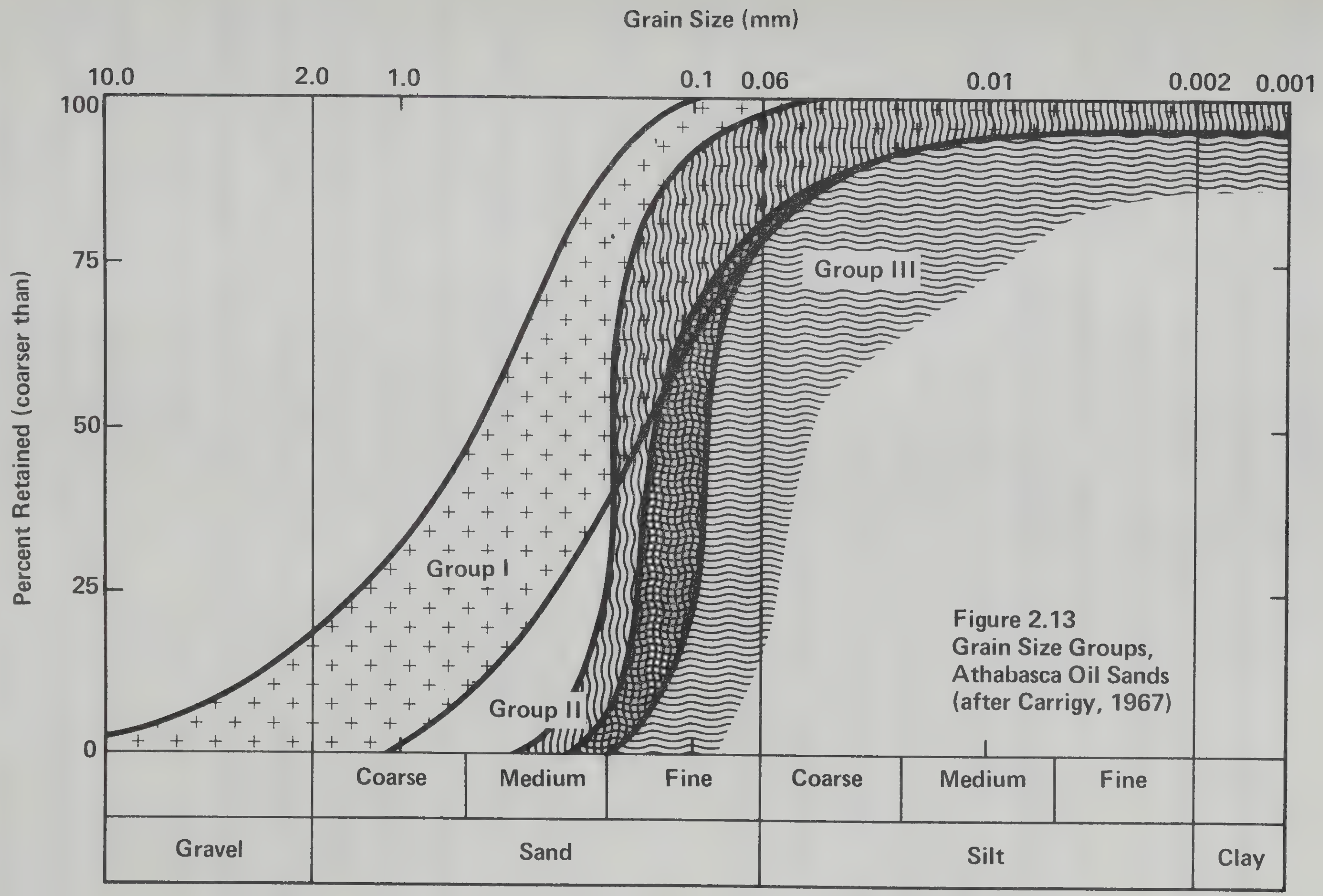

Figure 2.13
Grain Size Groups,
Athabasca Oil Sands
(after Carrigy, 1967)

conglomerates (sand clasts in a clay matrix) have been observed.

2.5.5 Lithology of the Upper Member

Fine-grained quartzose sands to clayey silts are the characteristic deposits of the Upper Member. Grain size curves fall largely within Group III of Figure 2.13. Ironstone bands, usually traceable for several kilometers, are common; intraformational clays up to 0.5 m thick may be observed; and scattered shell beds have been reported (Carrigy, 1959). This is the only portion of the McMurray Formation which can not be classified rigorously as orthoquartzitic, because clay minerals and nonquartz clastics probably form over 10% of the total mineral composition. Muscovite is the most common accessory mineral, and clay minerals form a significant proportion (2% to 6%) of most beds.

2.5.6 Implications of Lithology on Oil Sands Development

The presence of significant quantities of clay minerals and other fine-grained materials has serious implications for the long-term subsidence of tailings ponds (Devenny, 1975). The presence of steeply dipping silt and clay seams has been identified as critical to the stability of high pit walls with respect to block failure (Brooker, 1975). The present study indicates that noncemented lithoclastic conglomerates may form preferential failure zones as a result of the concentration of clay-shale clasts. Finally, the quartzose nature of the deposit is the single most important piece of lithological data; it will be seen in this work that the strength properties of the Athabasca Oil Sands are a direct consequence of the lithology and geological history of the McMurray Formation.

CHAPTER III

NATURAL SLOPES IN THE ATHABASCA OIL SANDS

3.1 Introduction

A study of natural slopes in the oil sands area was undertaken during the summers of 1974 and 1975. The objectives were:

1. To become familiar with the lithology, stratigraphy, and depositional features of the McMurray Formation as they influence engineering behaviour.
2. To examine the morphology of natural slopes to evaluate field slope stability.
3. To observe and describe natural phenomena which could contribute to an understanding of the stability and strength characteristics of oil sand.
4. To compile a photographic record of the slopes and of features of geological and geotechnical interest.

Data collected in this study include a series of sketched and annotated slope profiles (Appendix A), a collection of black and white photographic prints, and the naturalistic observations which are reported in this chapter.

3.2 Occurrence of Slopes in the Athabasca Oil Sands

Exposures of oil sands can occur only in those regions where the oil-bearing portions of the McMurray Formation are at the ground surface, or sufficiently close to the surface to have been exposed

through stream down-cutting. The sites of exposed oil sand slopes coincide therefore with river courses and with the surfaces traces of the McMurray Formation shown on the bedrock geology map (Figure 2.1). The western limit of oil sand outcrops is in the valley of the Athabasca River about 50 km west of Fort McMurray, where oil sands crop out close to river level beneath 190 m of younger sediments. To the southeast, the outcrop limit occurs along the Christina River about 25 km from its mouth, where oil sands dip below river level under about 100 m of sediments. On the Clearwater River, the outcrop on Cottonwood Creek in Range 5W4 represents the easternmost exposure of oil sands, although oil-free McMurray Formation is exposed to the east on into Saskatchewan. To the northwest, outcrops along the MacKay and Ells Rivers about 15 km west of the Athabasca River valley mark the limit of oil sand slopes. The northern and northeastern limits are not well defined because of irregular removal of sediments by glacial processes. Outcrops about 50 km north of Fort MacKay delineate the approximate northern limit of major oil sand slopes. More than 800 km of river banks therefore contain oil sand deposits, and perhaps 100 km consist of excellent exposures with little or no colluvial cover.

All significant oil sand slopes are found within 115 km of the town of Fort McMurray, and most of them may be reached via the streams along which they occur. A large number of slopes have been visited; profiles of many of these slopes, along with structural data, sample locations, general stratigraphy, and other observations, may be found in Appendix A. Aerial photograph interpretation and measurements provided information on the morphology of covered oil sand slopes and the effect of exposure azimuth on steepness.

3.3 Variables Controlling the Gross Morphology of Slopes in the Athabasca Oil Sands

3.3.1 Morphological Agents

The origins, agents, and products in geomorphological processes have been topics of debate for decades (Penck, 1929; Scheidegger, 1970; Carson and Kirby, 1972; Crickmay, 1974; and others). The relationship between slopes and stream erosion discussed in Crickmay (1974) is particularly useful in understanding slope development in the oil sands. The basic reason for the existence of slopes in oil sands is the down-cutting action of young, vigorous streams, but many other factors control individual slope morphology. For the oil sands, the pertinent variables are: (1) the local lithology, stratigraphy, and thickness of the McMurray Formation; (2) the amount and type of material overlying the oil sand slopes; (3) the presence of debris removal agents and the efficiency with which they operate; (4) the thickness and lithology of the materials constituting the slope base; (5) stream size and fit to the occupied valley; (6) slope exposure azimuth; and (7) structural discontinuities. Less important variables, the geomorphological effects of which are minor (or not fully understood or appreciated), include: glacial drag and disturbance, the effects of groundwater upon the McMurray Formation, underlying evaporite solution, differential compaction, and relief and steepness of the Paleozoic erosion surface.

Four distinct end members can be identified among the array of slopes in oil sands: exposed (active) slopes (Plate 3.1), where debris removal keeps a majority of the slope free of colluvium and prevents

PLATE 3.1 Steepbank River Outcrops. 90m high slopes, details may be found in Appendix A, Slope 51. Horizontal vegetation bands correspond to oil-poor zones.

PLATE 3.2 High Hill River. Oil-free coarse- to medium-grained sand lying at slope angles of 70°-80°. Note the 5cm clay band and the excellent exfoliation fractures.

significant basal scree deposition; colluvial (semiactive) slopes without vegetation or with very sparse vegetation; barren scree (semiactive) slopes, where the depth of debris is great, but vegetation is absent or sparse; and covered (inactive) slopes, which consist of significant quantities of scree or colluvium with admixed clay and silt from overlying deposits, organic matter, and generally lush vegetation. All slopes are considered to be in balance with the forces acting upon them over a short time scale; that is, they are in a state of relative equilibrium. Glacial influence operated a short time ago (in the geological sense); therefore all slopes can be considered immature or very young. Slope flattening and recession processes, as a result of active river down-cutting, are occurring to some degree in almost all river reaches.

Inactive slopes not deeply covered with upslope debris show angles of repose close to, but somewhat less than, the angle of repose of loose sand, and much less than the steep angles observed in coarse-grained granular material by some authors (e.g. 41.3°: Rahu, 1969). The most common angle of repose of covered granular slopes is about 29° (Chandler, 1973). This angle is close to the upper limit observed for slopes not actively eroded in the recent past. Most slopes are less steep because of vegetative disturbance, freeze-thaw phenomena, colluvial cover development, and deposition of upslope (generally clay-rich) debris.

3.3.2 Morphological Effects of Stream Erosion

The entire array of slopes in the Athabasca Oil Sands can be attributed directly to the erosive forces of the streams along which

they occur. Steep active slopes occur only where debris removal forces are maximized: on the outside of river meander loops (Figure 3.1) or on the valley walls of vigorously down-cutting streams. Active slope angles are invariably steeper than 40°, vegetative and colluvial cover is sparse, and scree aprons are small or totally absent. Abandonment of a slope by direct river forces conversely results in reduction of slope angle, scree accumulation, and vegetation. In the absence of other forces, the slope angle of these inactive slopes can be expected to stabilize at or somewhat below the maximum angle of shearing resistance of granular material at low stresses.

Stream size in recently excavated valleys seems to have no significant effect on the sectional morphology of active slopes. The planar morphology of slopes along a small, meandering river is distinctly curvilinear. The meander amplitude and spacing, which are functions of stream flow and gradient, result in a sequence of slopes which reflect, in a subdued fashion, the incised stream path. With the exception of the Clearwater River valley, all streams in the study area are actively eroding their valley walls and floors because of meander migration and steep gradients in their lower reaches.

The Clearwater River (Figures 3.2 and 3.3) occupies a large glacial meltwater channel, which at one time carried volumes of water sufficient to excavate a channel averaging 4000 m in crest-to-crest width with a maximum depth of 200 m (60 km east of Fort McMurray). The basal plain of the valley is often more than 1500 m in width, whereas the river itself is usually less than 200 m in width. The Clearwater River is definitely underfit, but nevertheless it possesses considerable hydraulic energy: as it crosses Alberta it drops 35 m,

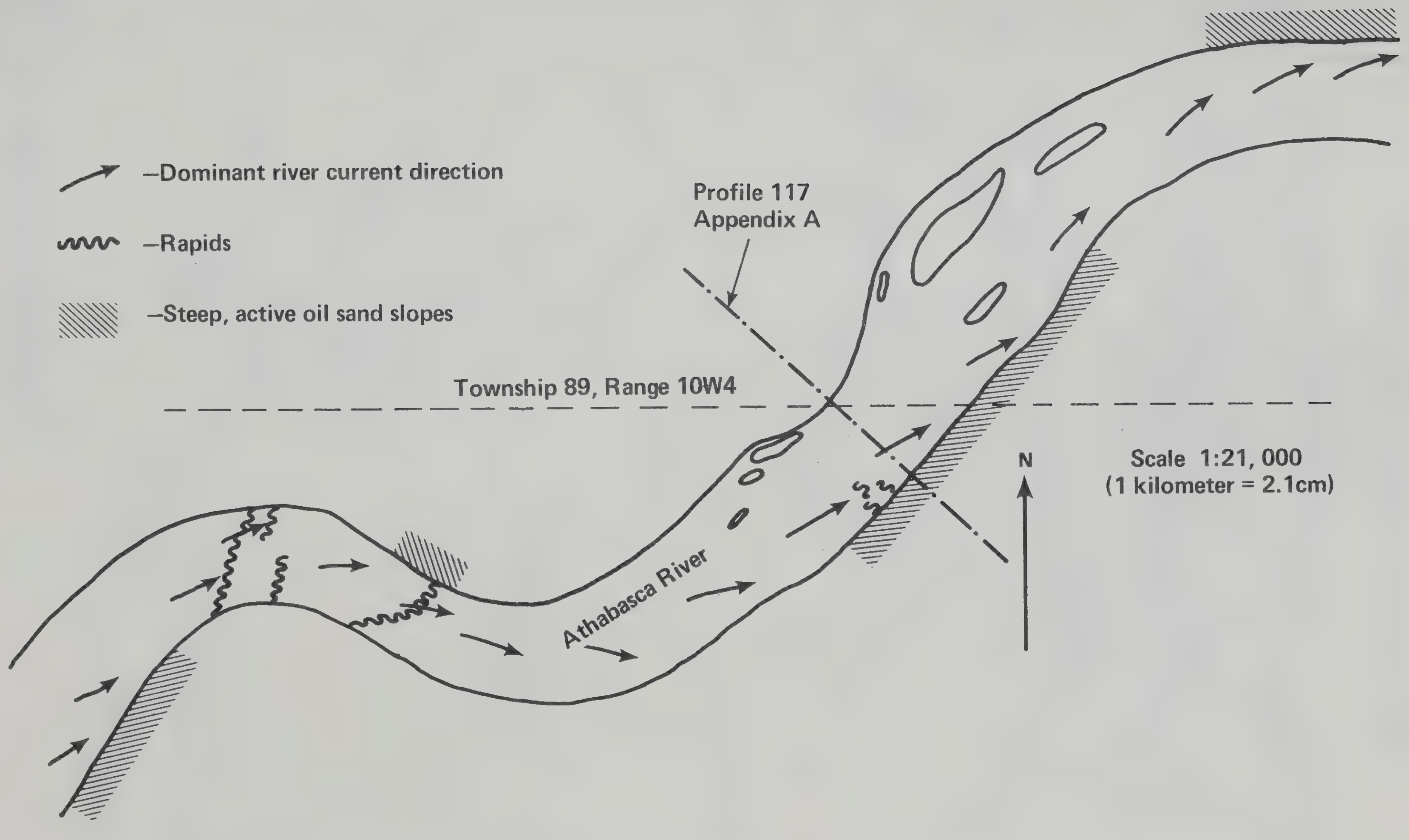

Figure 3.1 Effects of River Current Location on the Occurrence of Steep, Active Oil Sand Slopes

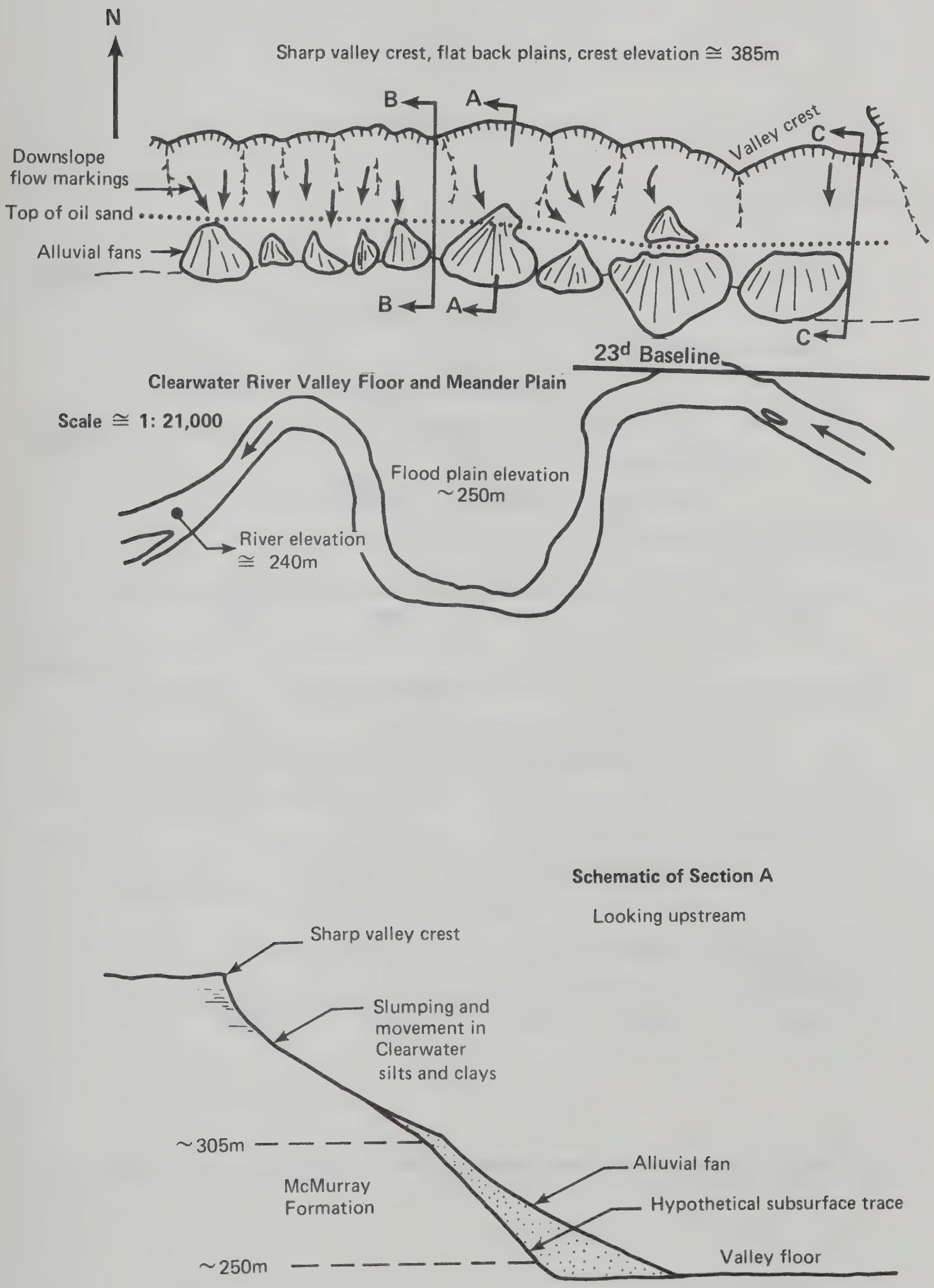

Figure 3.2
Alluvial Fans Coalescing into an Alluvial Apron, Clearwater River Valley, Townships 88, 89; Range 8W4

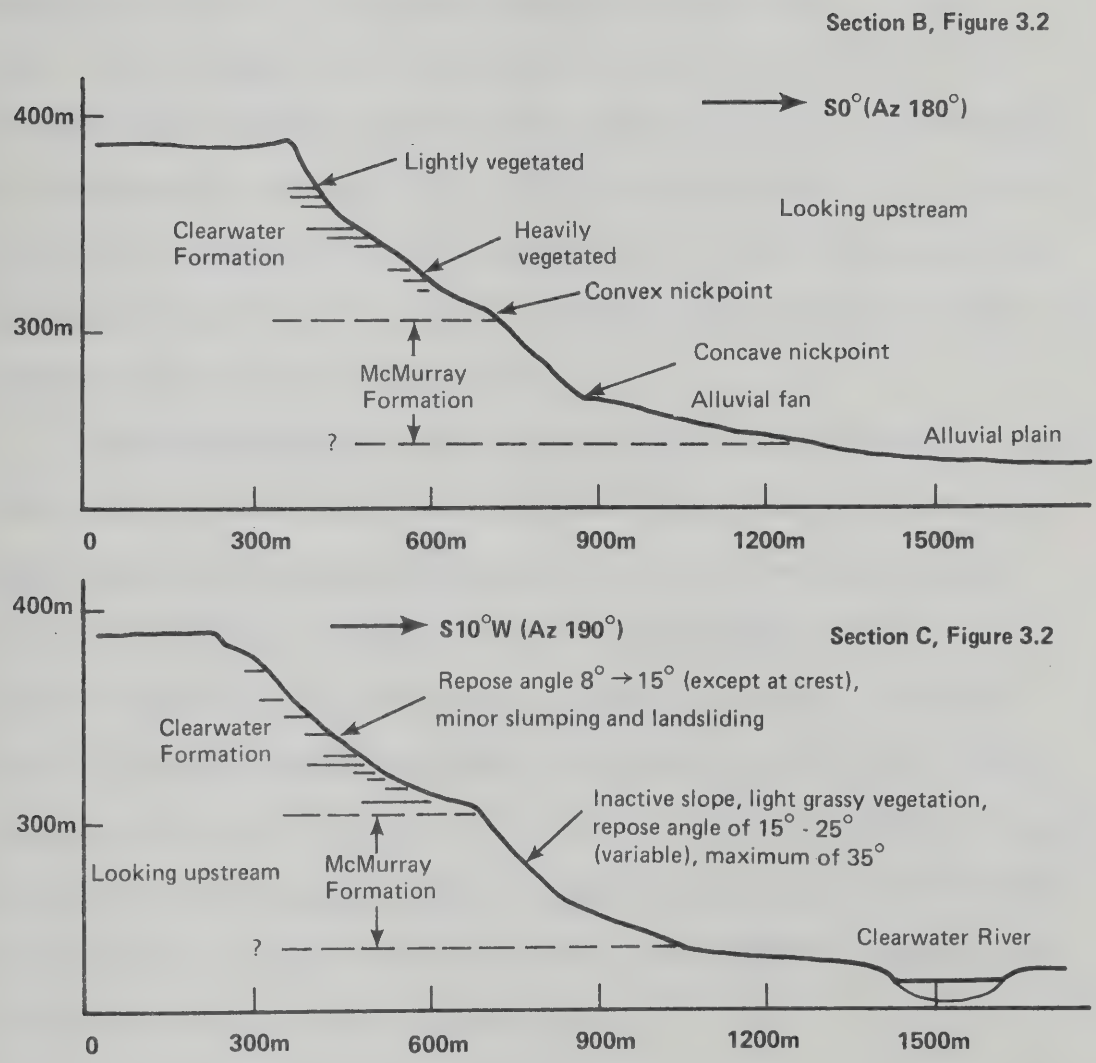

Figure 3.3 North Bank of the Clearwater River, 10 km East of Fort McMurray

a considerable descent for such a large stream. Most of this descent, however, is accommodated in a series of rapids and waterfalls east of the High Hill River (R3W4), resulting in reduced vertical and lateral erosive capability in the lower (western) reaches where oil sands occur. As a consequence of the reduced valley wall erosion, slopes are gentle and densely vegetated, and do not correspond geometrically to the meandering stream course. Significant exposures of oil sands do not occur along the Clearwater River, but the oil-free portion of the McMurray Formation outcrops in numerous locations east of Range 3W4, where the higher stream gradients occur.

Notwithstanding the lack of basal erosion, the covered oil sand slopes west of Range 3W4 in the Clearwater valley can be identified readily on the valley walls where they have not been deeply covered by slump deposition. The top of the oil sand strata is marked by a convex nickpoint and the bottom by a concave nickpoint. Oil sands usually form the steepest portions of the valley walls, and in many cases they stand out distinctly in vertical aerial photography. Along much of the valley, slump debris or basal alluvial fans obscure these features, but the trace of the top of the Fort McMurray Formation can be followed for many miles (Figure 3.2).

3.3.3 Morphological Effects of Bitumen Saturation

The slope angles of fine-grained oil-free to oil-poor portions of exposed slopes approach the angle of repose of loose granular media: 30° to 35° (Appendix A; Slopes 17b, 51). Exceptions occur where sufficient amounts of clay minerals are present to act as a binder for the drier surface layer; or at slope tops, where stresses are low,

and fine-grained oil-free sections may form short, almost vertical slopes. Fine-grained oil-rich slopes, however, tend to be considerably steeper than the oil-poor or barren slopes, with inclinations varying from 35° to 75° over short sections.

Coarse-grained oil-free to oil-poor sections in active oil sand slopes are found only as minor strata close to or at the bases of slopes, or in that portion of the McMurray Formation lying east of Range 5W4. The morphological effects of a thin oil-free coarse-grained sand layer are negligible. Several outcrops of oil-free McMurray Formation were visited, and slope angles were found to be as steep as in the western oil-saturated areas; therefore bitumen saturation has little or no effect on the slope angles of coarse-grained McMurray Formation sands.

The above apparently contradictory observations are related to the role of bitumen as a pore sealant acting to exclude meteoric water. Where bitumen is absent, or present only in small quantities, ingress of water from the surface or from groundwater sources permits the degradation of fine-grained material by freeze-thaw strains (e.g. Plate 2.1) Coarse-grained oil-free material has much lower capillary suction, is therefore relatively free draining, and remains unsaturated for greater distances into the slope face. The unsaturated voids permit freezing without structural disruption.

These interpretations are supported by the behaviour of oil-free slopes along the High Hill River and Cottonwood Creek, and the largely oil-saturated slopes along the Steepbank River. The High Hill River outcrop visited is about 36 m high. The uppermost 16 m consist of very fine-grained oil-free sand (with high capillarity) lying at

a slope angle of about 35°, whereas the lower 20 m consist of medium- to coarse-grained clean oil-free sand (low capillarity, well-drained) lying at a slope angle of 75° (Appendix A; Slope 65, Plate 3.2). Throughout the outcrop, the sand is so friable that surface graines can be brushed off by hand, but incomplete saturation provides some apparent cohesion. The lower sands yielded bulk densities approaching the _in situ_ bulk density of oil sand (2.20 gm/cc), indicating little disturbance.

At Cottonwood Creek (Appendix A; Slope 66), coarse-grained oil-free sands directly underlie coarse-grained oil-saturated sands. No morphological difference is discernible; the angles of repose (70°) are identical. On the Steepbank outcrop, two sections of oil-free fine-grained silty sand about 10 m thick form the only portions of the slope which lie at angles of less than 40° (Appendix A; Slope 51), implying behaviour similar to that of normal sand. Little depositional structure remains; freeze-thaw processes have totally destroyed the fabric. Above and below the oil-free silty sands, oil-rich fine-grained sands lie at angles above 40°.

The bitumen in oil sand is not a cementing agent in the engineering sense. It does not contribute to stress-independent strength; that is, it does not provide true cohesion. As a viscous material, it can not contribute significantly to long-term strength, although it resists rain impact and short-term corrasive forces. However, in the surface meter or so of the outcrops, and in the basal scree and debris piles, weathering phenomena have increased the viscosity of the bitumen, possibly through a combination of evaporation of volatiles, and oxidation-polymerization of other molecules. A sample of bitumen extracted from hard talus yielded an absolute viscosity of 20×10^6 poises at 90°C, whereas typical

unweathered oil at 90°C has a viscosity of much less than 1000 poises.

The viscosity of the talus bitumen could not be measured by the available apparatus at temperatures less than 60°C, even under very high pressure gradients. At room temperature (20° to 25°C), an inverted specimen of the talus bitumen displayed no movement after one year. Natural slopes display a "case-hardened" outer surface; this may be a result of the bitumen acting as a true cementing agent at the low stresses and normal temperatures found in the outer few meters of slope face. The nature of the surface and the scree piles usually belies the true nature of the oil sand within the back slope, where bitumen viscosities are much lower and stresses are higher.

Several conclusions regarding the strength of oil sands may be drawn from the discussion to this point:

1. Bitumen is not the source of strength in oil sands.
2. If freeze-thaw strains destroy the structure, strength is lost.
3. Disturbed oil sands usually behave like normal sands.
4. Intact oil sands display exceptional strengths resulting in high, steep slopes.

3.3.4 Morphological Effects of Cementation and Concretions

Carrigy (1959) has reported the existence of zones of silica-cemented sand within the McMurray Formation. Where they occur, slope angles are steep, and noticeable ledges form. They are, however, rare, and limited in vertical extent.

Cementation by clay minerals has an effect on dry slopes, where the clay can contribute significantly to the dry cohesion of a silt or

fine-grained sand. This is readily observed in outcrops along the MacKay River, where bitumen-poor clayey silts and sand-silt-clays occur at the top of slopes at angles often approaching vertical (Appendix A; Slopes 7a, 59; Plate 3.3). Quantities of clay minerals sufficient to provide cementation do not occur in the medium- or coarse-grained sands.

Siderite (ironstone) concretions result in ledges which tend to steepen underlying beds considerably. Siderite bands are most common in the Upper Member of the Formation, but are found occasionally at the very base of the oil-saturated sands, associated with basal clays or directly overlying the Paleozoic strata.

Local oxide cementation (limonite, geothite) may occur in oil-poor sections, but it is very limited in extent.

Widespread carbonate cementation has not been found by the writer in any portion of the oil sands visited.

The small number of true chemically cemented beds which do exist in the McMurray Formation constitute no more than several percent of any given section. The great majority of the oil sands display few well-developed joint systems. Where cemented strata occur, usually in the upper third of the Formation, they display regular sub-vertical orthogonal joint systems (Babcock, 1975). Furthermore, exfoliation fractures may continue through the cemented strata. The specific effect of these "reinforcing layers" upon slope stability is not considered herein.

3.3.5 Morphological Effects of Grain Size and Bedding Features

Mean grain size in the McMurray Formation generally decreases upwards, although the local variability in absolute grain size may be great. Coarse-grained oil sands usually occur at the base of exposures and, in

PLATE 3.3 Block Falls and Exfoliation Scars on Slope #7 (Appendix A)

active slopes, commonly display steeper angles than overlying, finer-grained beds. This results in convex slopes, with steep portions at the slope bottom (Appendix A; Slopes 51, 61, and 66). On the other hand, slopes displaying more or less uniform grain sizes are linear to slightly concave (Appendix A; Slopes 16a, 17a, 19). It may be concluded that effective field strength increases somewhat with grain size.

Bed thickness and frequency, cross-bedding, and other stratigraphic variables are, in many cases, highly correlated with other morphologically more important variables. Bed frequency, as well as bitumen content, is a function of grain size. Large-scale cross-bedding is the dominant depositional feature of the coarse-grained oil-rich portions of the Middle and Lower Members of the McMurray Formation, but any morphological effect of the cross-bedding is obscured by the physical discontinuities such as exfoliation fractures and diagenetic jointing. Other bedding features (small-scale cross-bedding, slump bedding, clay rip-off clast "breccias", bioturbic features) are rare, minor in extent, and without gross morphological effect.

The specific effects of any of the lithological variables on inactive slopes are not determined easily because of the heavy vegtative cover. The vegetated slopes are less steep, more uniform in slope angle, and in most cases covered by a significant thickness of colluvium. It may be concluded that lithological variables are not of great importance in inactive slope morphology.

In summary, the lithological variables of grain size and bedding do not influence inactive or semiactive slope morphology, but on active slopes, coarse-grained sands lie at somewhat steeper angles.

3.3.6 Morphological Effects of Exposure Angle

Exposure to solar radiation results in drier, steeper, less vegetated slopes. A plot of the relationship between total slope angle and azimuth of slopes of randomly chosen sections illustrates this (Figure 3.4). Field observations and stereoscopic examinations of the Steepbank, MacKay, and portions of the Athabasca River valleys indicate that northward-facing slopes are more densely vegetated, and gentler.

Scarcity of water on the outcrop surface is the major reason for the steeper slopes: vegetative growth is inhibited and freeze-thaw effects are reduced on south-facing slopes. The low albedo of oil sand results in high surface temperatures and consequent moisture deficiency. Vegetative growth follows slope flattening, and is accompanied by increased moisture and clay contents, and consequent soil formation.

3.3.7 Morphological Effects of Basal Stratigraphy

Three common basal stratigraphic configurations exist: the oil sand slope may be founded on carbonate rock, on oil sand, or on lime-free clays. Several minor basal stratigraphies have been noted: coarse-grained goethite-cemented sandstone (observed on one outcrop only), loamy paleosol, and coarse-grained oil-free sand. The goethite sandstone (found in a six-meter layer: Appendix A; Slope 20) displays a morphology similar to that of competent limestone. Paleosol and coarse-grained oil-free sands (both observed in thicknesses of 1.6 m or less) have little effect on overall slope morphology (Appendix A; Slopes 51 and 53).

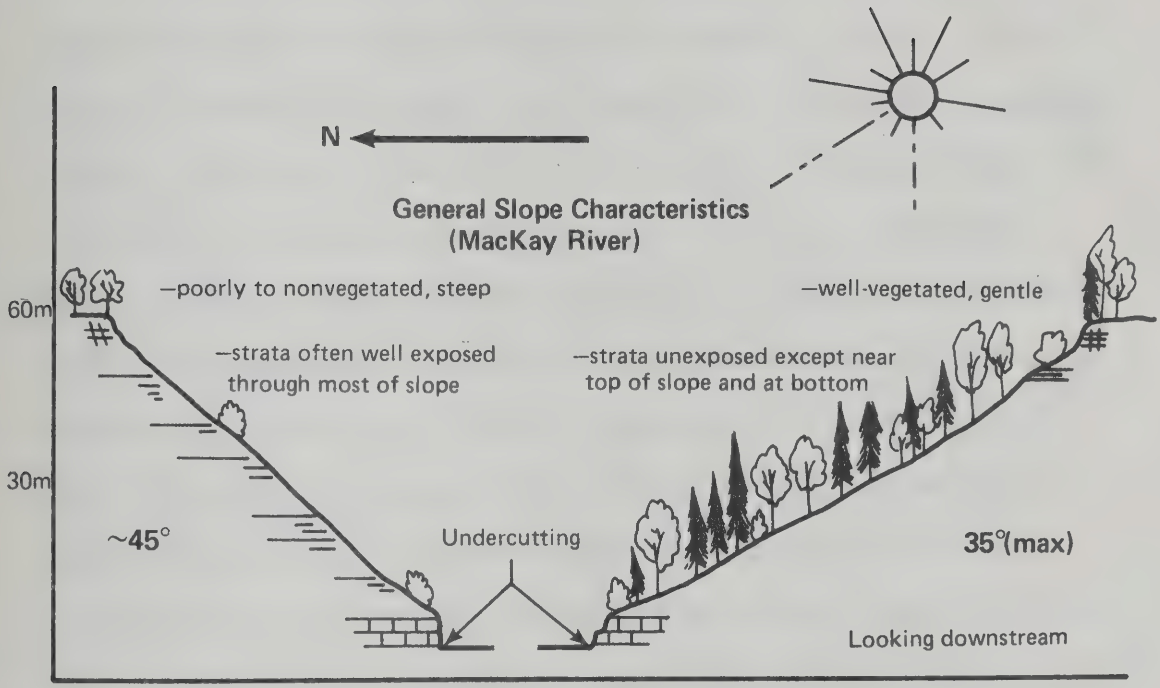

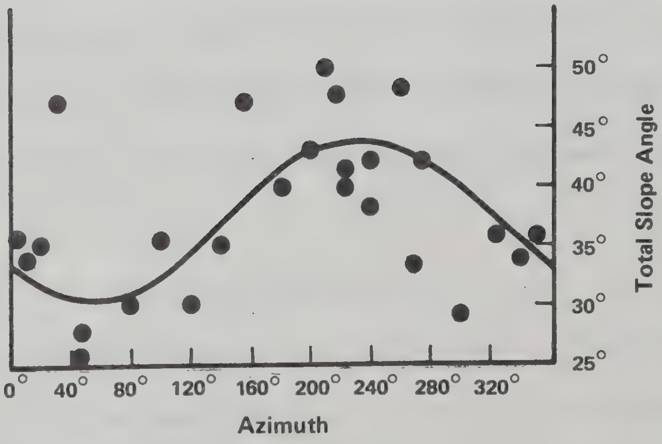

Effect of azimuth on total slope angle, MacKay River, (all slopes undercut, all slopes 45m - 60m in height, and no significant basal clay observable)

Figure 3.4 Effect of Azimuth on Slope Morphology

The carbonate rocks underlying the Athabasca Oil Sands are indurated Paleozoic strata consisting of competent, jointed, fossiliferous limestone and nuggety, less competent, argillaceous limestone (micritic limestone). The presence of competent limestone results in a ledge as a consequence of its resistance to slope undercutting. Weathering and mass-wasting then predominate in the upper slope and reduce the slope angle. The high, steep slopes by the Moberly Rapids (Appendix A; Slope 16) are directly underlain by a thick competent bed of well-jointed limestone, and this bed in turn is underlain by argillaceous limestone, which is eroded during high water stages. The consequence is block failure along joints in the competent limestone: because of this process, a steep slope is maintained in the overlying oil sands. Along the MacKay River, incompetent limestone is underlain by river level competent limestone (Appendix A; Slope 12a). Overlying slopes are less steep and often covered with a veneer of shaley, limey colluvium displaying high angles of repose (i.e. 35° to 44°).

Few differences are observed between active slopes based on oil sands and those based on argillaceous limestone (Figure 3.5), because both materials display similar erosion resistance and repose angles.

Because of the presence of stable basal scree, and because of the lack of debris removal forces, no differences in morphology of covered, inactive slopes based on limestones or on oil sands can be detected.

Significant quantities of lime-free clay at the bases of slopes result in a distinctive planar and sectional slope morphology (Figure 3.6). During the initial study of active oil sand slopes, three slopes

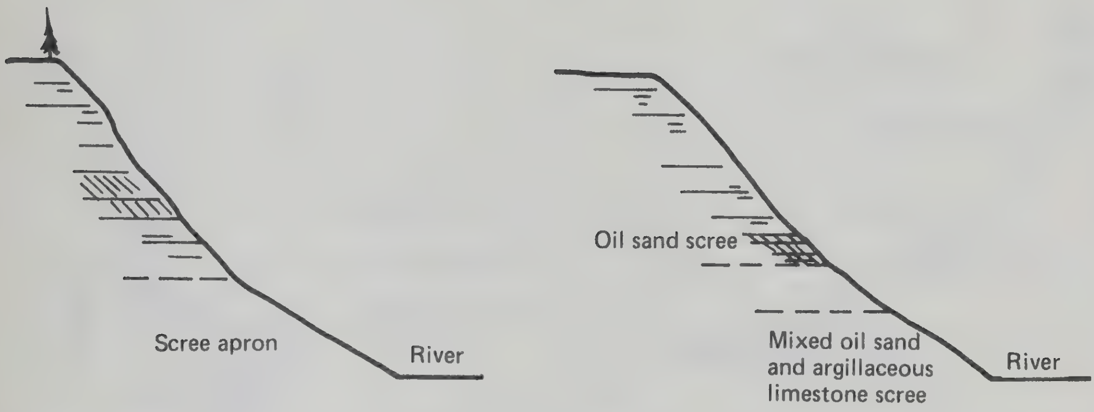

a) Oil Sand Base
(eg: Appendix A, Slopes #21, #22)

b) Argillaceous Limestone Base
(eg: Appendix A, Slope #61)

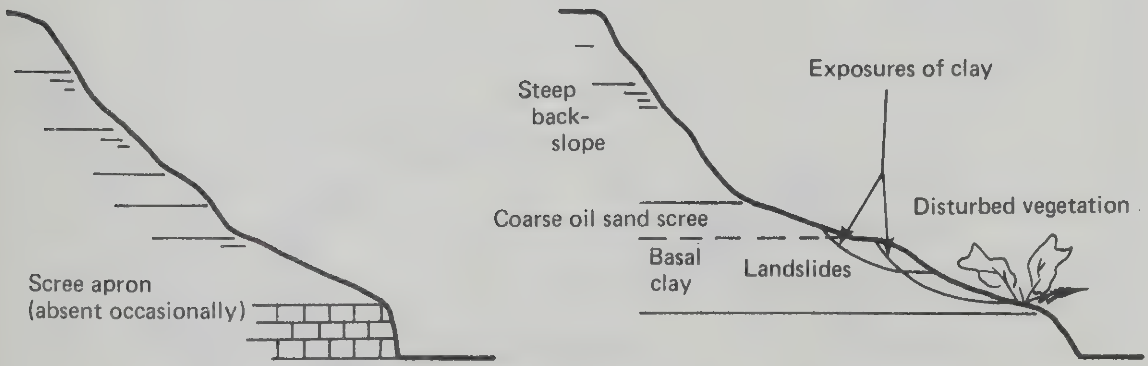

c) Competent Limestone Base
(eg: Appendix A, Slope #9, #10, #16)

d) Basal Clay Base
(eg: Appendix A, Slope #7, #19)

Figure 3.5 Morphological Effect of Basal Stratigraphy on Active Oil Sand Slopes

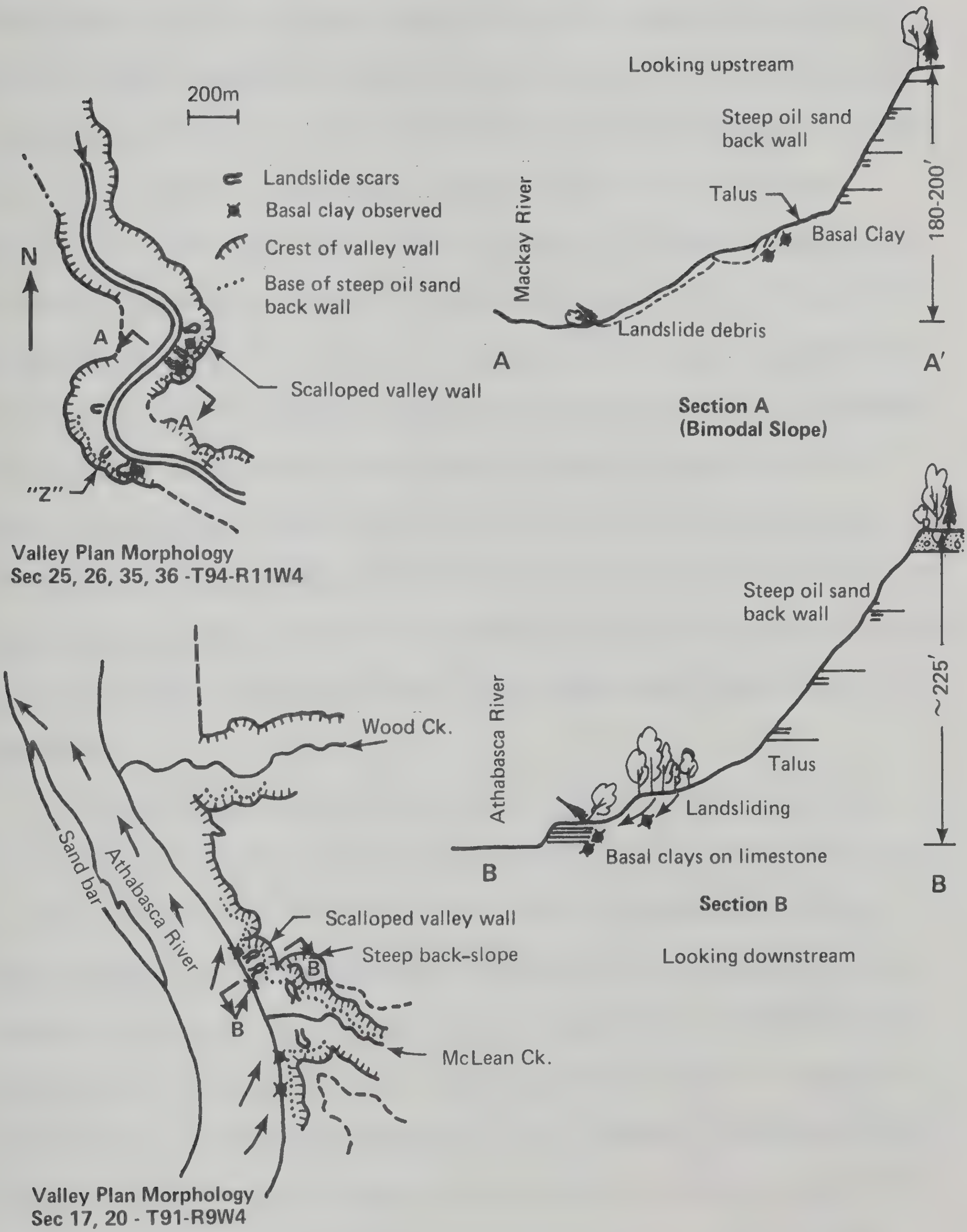

Figure 3.6
Planar and Sectional Morphology
in the Presence of Basal Clay, Little
to No Overlying (Clearwater) Sediments

founded on basal clay were visited and were found to display unique characteristics: high, steep back-slopes of oil sand with a distinctive scalloped appearance; basal portions lying at gentle angles and covered with oil sand debris; and slump and landslide features in the gentle basal portion. To test the general applicability of these observations, five additional sites displaying the above characteristics were chosen on the basis of stereoscopic examination of vertical aerial photographs. The five were visited, and it was discovered that four of them had basal clay strata ranging from 1 to 10 m in thickness, and the fifth had a considerable basal thickness (greater than six meters) of a reddish, clayey material tentatively identified as clay-rich paleosol (Figure 3.6; Site Z). In addition, at numerous other sites along the lower reaches of the MacKay River, where slump features were observed at river level, basal clay strata were found above the limestone.

The scalloped back-slope at basal clay sites may be seen in many locations on aerial photographs (Figure 3.6), but only where the oil sand overburden is thin; that is, north of Township 90. This feature should not be confused with scalloping due to repeated landsliding of overlying argillaceous strata (found south of Township 90). Large deposits of basal clay are much less common south of Township 90, partially because of lower elevation of the Paleozoic surface south of this line. The presence of basal clay on inactive slopes usually can not be verified because of vegetative cover, but the scalloped back-slope is considered diagnostic in those covered slopes lying north of Township 90.

The distinctive morphology of oil sand slopes founded on basal

clay is the consequence of the time-dependent nature of clay strength, and of rebound upon valley excavation. Overconsolidated clays "soften" with time (time-dependent cohesion loss). Exposed clays generally have water contents above 20%, although in borehole cores the water content is 10% to 14% (corresponding to porosities of 15% to 25%). Landsliding and slumping in basal clays result in quasi-equilibrium at inclinations of 10^o to 20^o. Rebound and horizontal movements towards the valley upon excavation result in significant strain differences between the basal clays and the stiffer materials overlying and underlying them. If the difference in elastic moduli is large, failed (slickensided) and softened zones develop within the clay, and result in rapid back-slope exfoliation and recession. Large scree and debris fields at the bases of slopes containing basal clay (Appendix A; Slope 7a) indicate that extensive raveling has occurred in the past, perhaps because the large difference in elastic moduli results in tension in the lower portion of the oil sand slope.

A concise summary of the effects of basal stratigraphy is appropriate. The presence of significant quantities of basal clays results in bimodal slopes, scalloped back-slopes, and basal landslide features. The rates of undercutting of argillaceous limestone and of oil sands are similar and result in steep active slopes. Competent basal limestone effectively reduces erosion rates, and overlying slopes therefore are somewhat less steep and covered with colluvium.

3.3.8 Morphological Effects of Overlying Strata

Oil sand slopes are topped by glacial deposits, by younger Cretaceous strata (Clearwater Formation), or by thin deposits of

aeolian sand, ironstone, or soil. South of McLean Creek (Township 91, R9W4), all oil sand slopes are directly overlain by Cretaceous silts and clays. The thickness of Cretaceous deposits increases southwards to a maximum of approximately 170 m (west of Crooked Rapids in Township 87, R13W4). North of McLean Creek along the Athabasca River, progressively greater amounts of oil sands have been stripped from slope tops by Tertiary erosive processes or Pleistocene glaciation, but eastwards and westwards from the major valley, Cretaceous formations again outcrop above oil sands in increasing thicknesses.

Till is the most common glacial deposit directly overlying oil sands. It usually forms vertical or very steep cliffs displaying vertical jointing (Appendix A; Slope 52). The portion of oil sands directly underneath is characteristically steep, but the slope generally becomes less steep several meters below the till (Figure 3.7).

Thick sequences of overlying formations are the rule south of Township 90, but no significant effect can be observed on the steepness and morphology of the oil sand portions of the slopes. The overall slope morphology, however, is grossly different: the clay-rich Clearwater shales are subject to landslides; the slope of the materials above the McMurray Formation is gentle (10^{o} to 20^{o}); and vegetation is lush, even above active slopes (Figure 3.7). The top of the oil sands is distinctly steeper than the overlying material, and the boundary between the two is marked by an abrupt disappearance of vegetation on active slopes. In many areas, such as the Clearwater valley, the Athabasca valley west of Fort McMurray, and the upper reaches of the MacKay and Steepbank valleys, extensive slumping has obscured the McMurray Formation altogether. Thick sediment layers above active

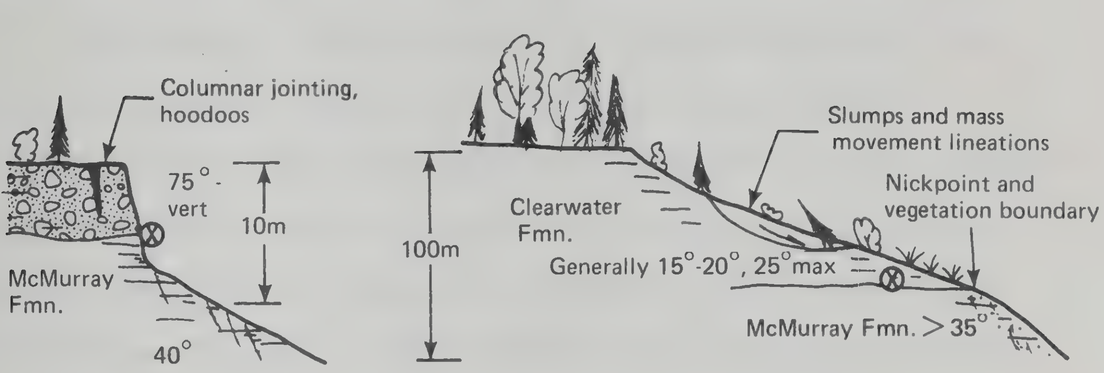

a) **Glacial till, active slopes (eg: Appendix A, Slope 51)**

b) **Thick sequence of Clearwater Formation above an active oil sand slope. (eg: Appendix A, Slopes 58, 59)**

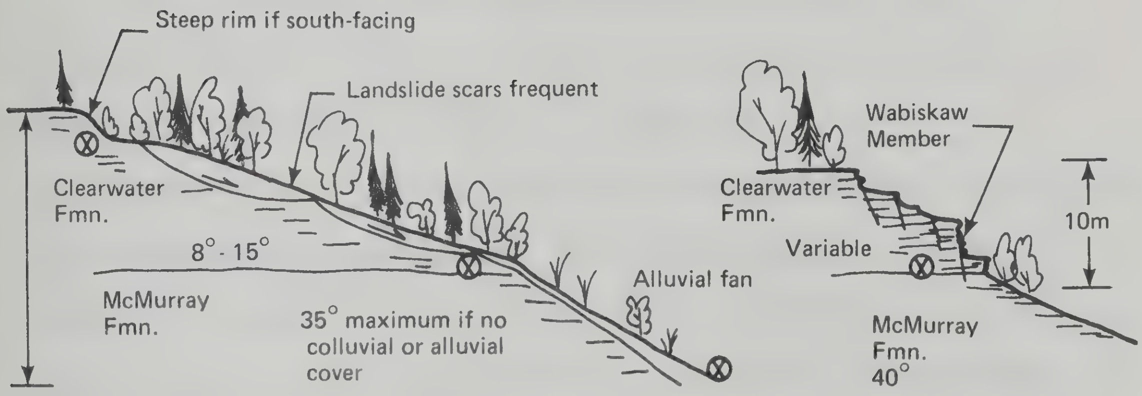

c) **Thick sequence of Clearwater Formation above an inactive oil sand slope. (eg: Figure 3.3)**

d) **Thin sequence of Clearwater Formation (eg: Appendix A, Slope 53)**

⊗ **Possible spring point**

Figure 3.7 Morphological Effects of Overlying Strata

slopes are somewhat steeper than those above inactive slopes.

Thin veneers (1 to 10 m thick) of Clearwater silts and clay-shales overlying oil sands are commonly very steep (Appendix A; Slopes 9 and 59). Excellent drainage, controlled by stress-relief and diagenetic joints, keeps the shales in a semidry state, permitting slopes of 80° to 90° to occur. Where extensive wet terrain behind the slope crest occurs, or where stratigraphic variations are important, a thin veneer of Clearwater silts and shales may lie at inclinations of less than 25°.

3.3.9 Minor Factors Affecting Slope Morphology

The present-day river system along which slopes occur is a function of the disruption of drainage networks by glacial processes, resulting in postglacial excavation of valleys.

Pleistocene continental glaciation has left distinctive landforms on the surrounding highlands, and has removed unknown quantities of oil sands. Erratics of oil sands are common in the Edmonton area and have been reported specifically in the Egg Lake district (Township 56 R25W4). Evidence of glacial disturbance of oil sands was mentioned by Sproule (1951) and Carrigy (1959) in reference to sequences of beds along the Firebag River (Figure 2.1). No evidence of glacial disturbance in oil sands as a result of basal drag has been observed by the writer in the more southern regions around Fort MacKay. This area, however, has been significantly eroded by postglacial meltwater flow (evidence of which is clearly visible on the plains behind the valley walls), and removal of glacially disturbed material is likely.

The Athabasca Oil Sands are not a well-jointed sediment, but

indurated bands within the oil sands commonly display vertical to sub-vertical diagenetic joints. The joints occur in cemented strata, or in medium- to coarse-grained (usually cross-bedded) uncemented sequences in the Middle and Lower Members of the McMurray Formation. Locally, these joints contribute to the formation of ledges and other prominent structures on the slope faces, but their effect is usually obscured by the system of stress-relief joints which lies sub-parallel to the slope face, is more closely spaced, and occurs on all oil sand slopes.

3.3.10 Summary of Morphological Agents and their Effects

Table 3.1 summarizes the main agents controlling slope morphology and describes their effects. The slope profiles presented in Appendix A permit more complete understanding of the effect of morphological agents on natural oil sand slopes. Slope profiles are presented of active slopes only; however, inactive slopes constitute the majority of the river valley walls. Slope profiles have been restricted to those of active slopes because effects of azimuth, lithology, structural discontinuities, bitumen saturation, and overlying and underlying strata are either greatly or completely subdued in inactive slopes, but strongly affect active slope morphology.

Figure 3.8 shows the relationship between maximum observed height and slope angles for all active slopes visited. Extremely steep slope angles over short distances are largely a function of minor cementation or rapid undercutting of a short slope. All other natural slopes in oil sands lie beneath the envelope of Figure 3.8; but it should be emphasized that active slopes are invariably steeper than inactive slopes. The lower slope angle limit for exposed,

TABLE 3.1

SLOPE MORPHOLOGY VARIABLES

PERTINENT VARIABLE	EFFECTS ON OIL SANDS SLOPE MORPHOLOGY
STREAM EROSION	-ACTIVE: SLOPES GREATER THAN 35°, BARE -ABSENT: SLOPES LESS THAN 35°, COVERED
LITHOLOGY	(EFFECTS PERTAINING TO ACTIVE SLOPES)
a) Bitumen Saturation	-high: uniform, steep active slopes, bare -low: variable morphology, more vegetation
b) Grain Size	-coarse to medium-grained: steep slopes -fine-grained: steep with bitumen, but gentle with low bitumen contents
c) Cementation and Concretions	-minor slope steepening
EXPOSURE ANGLE	-south-facing slopes are steeper, dryer, less vegetated than north-facing slopes
BASAL STRATIGRAPHY	
a) Basal clay	-scalloped back-slopes, bimodal slope faces, landsliding in the clays
b) Limestone	-very steep slope base in the limestone, but often somewhat gentler upper slopes due to reduced recession rates
OVERLYING DEPOSITS	-little effect on oil sand slope morphology -slope tops are steep if only a thin veneer is present, but landsliding and slumping are common in thick occurrences

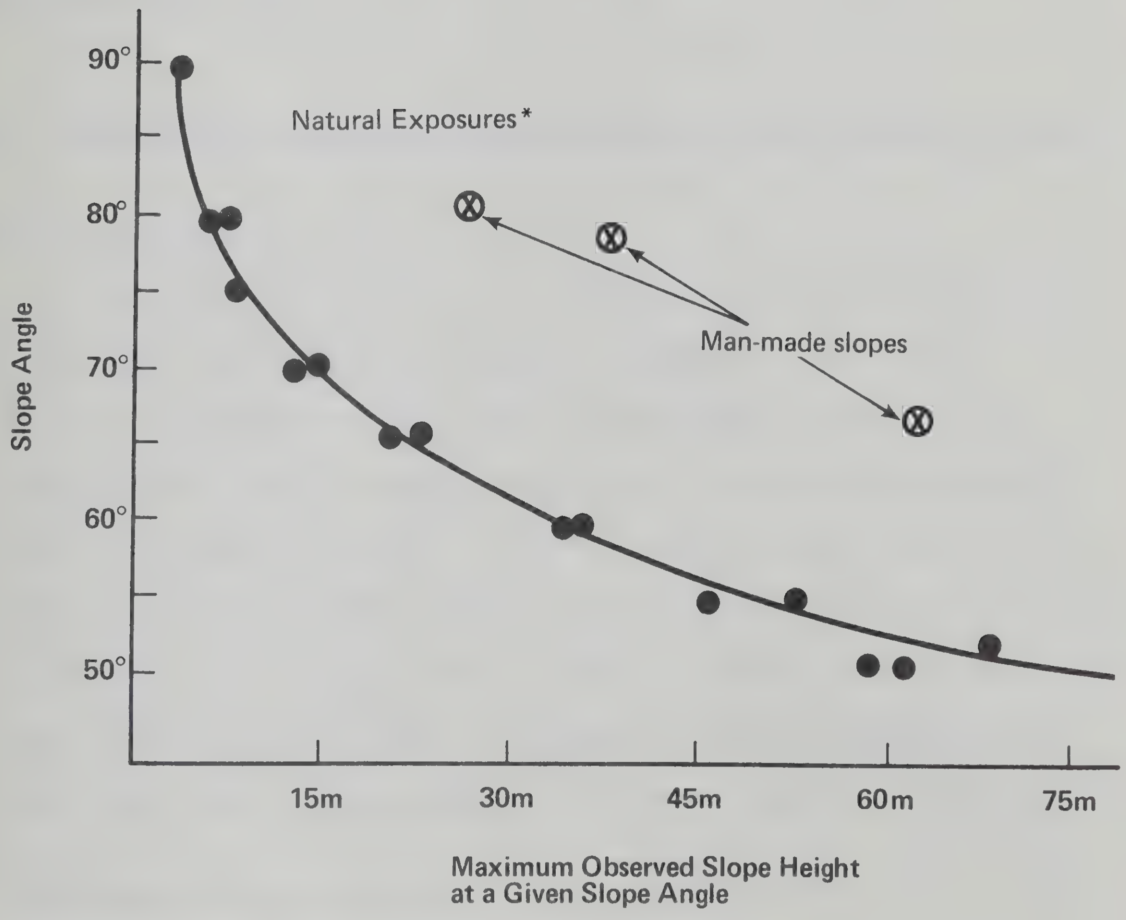

* Most of these data may be found in Appendix A

Figure 3.8 Natural Slope Heights and Maximum Inclinations

undercut oil sand strata is 35° to 45° (depending on locality), whereas the upper limit for inactive slopes is about 35° (the angle approaching the maximum angle of shearing resistance of oil sand scree). Most overgrown inactive slopes are less steep than this upper limit because of creep, surface wash, or a covering of upslope colluvium and scree.

3.4 Mass-Wasting Phenomena on Active Slopes in the Athabasca Oil Sands

3.4.1 Introduction

Active slope development and recession involve a reduction of undisturbed slope material into smaller fragments, which are susceptible to downslope movement under gravitational, corrasive, or erosive forces, and to eventual removal from the slope base by gravitational or aqueous transport. Inactive slopes display the normal phenomena of downslope mass movement of cohesionless materials: extensive creep, some corrasion, and a minimum of surface wash. Active slopes, however, display slope development processes sufficiently different from those of common materials to justify special discussion.

3.4.2 Slope Denudation Processes

Debris removal from a slope face is dominated by a process referred to herein as exfoliation. This mechanism consists of the detachment and eventual fall from the slope face of a planar slab of material from 30 cm to several meters in both length and width, and from 5 to 25 cm in thickness (Plate 3.3). This phenomenon is by far the major slope recession process in oil sands and is entirely the result of the formation of a pervasive sub-parallel joint system

that has been observed on all active oil sand slope faces.

The steep, relatively short fractures (Plate 3.4) lie subparallel to the slope face and are analagous to the onion skin exfoliation observed in poorly foliated igneous rock. Stress-relief through valley excavation in an elastic material with high remnant horizontal stresses (high value of K_o) results in a rotation of the stress field near the slope face so that the major principal compressive stress lies parallel to the slope face and is much higher than the minor principal compressive stress (Figure 3.9). If the effective stress ratio is sufficiently high, or if the slope face experiences tensile stresses (e.g. by gas release pressures), failure takes place, and a redistribution and reduction of stress occurs through formation of planes of minute movement (fracture systems) approximately sub-parallel to, but usually slightly steeper than, the dominant slope face.

The stress-relief joints are enlarged by freezing and thawing of water in the joints and by thermal expansion and contraction, both of which are important processes in the outer meter of slope face. The thermal characteristics of the black oil sands result in expansion of gas-filled voids in the slope, also contributing to the development of the joint system. The extremely low permeabilities result in impeded evolution of gases, and the high bitumen viscosities retard diffusion; therefore a significant pressure increase may occur upon heating. On a favourably oriented exposure, a decrease in fracture frequency with increasing depth was observed, but no quantitative data expressing the relationship of spacing to depth have been obtained.

Insufficient data have been collected on the stress-relief joint systems to identify the major principal stress direction before

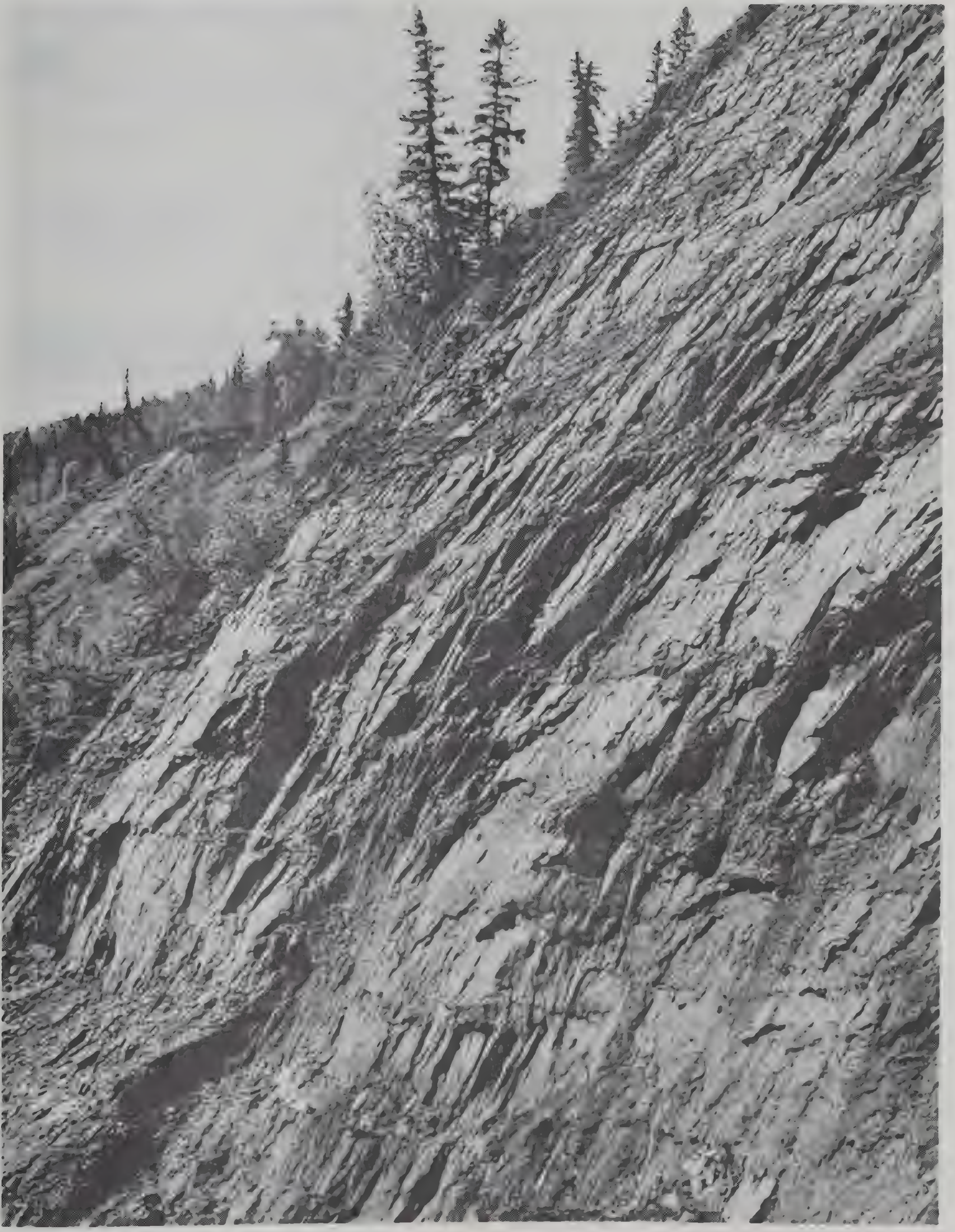

PLATE 3.4 Well-developed Exfoliation Fractures. Slope #16a. Slope angle is about 65° over a 20m height.

a) Conditions before excavation

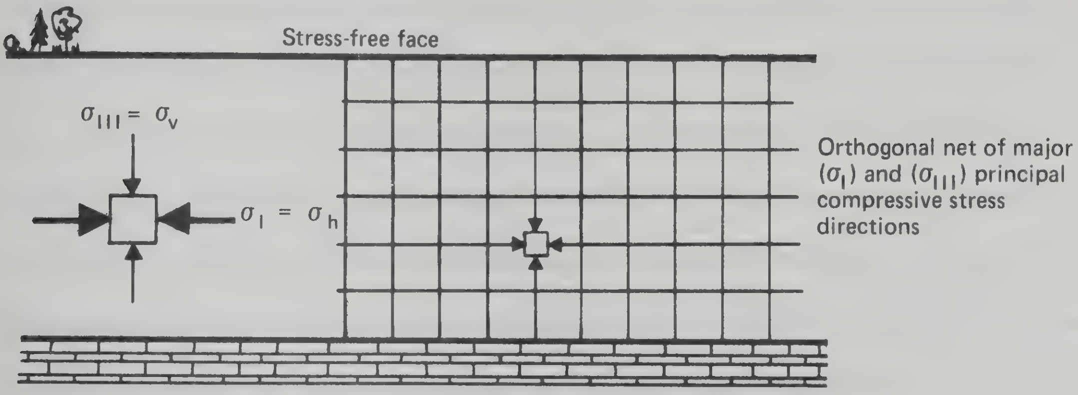

b) Conditions after excavation

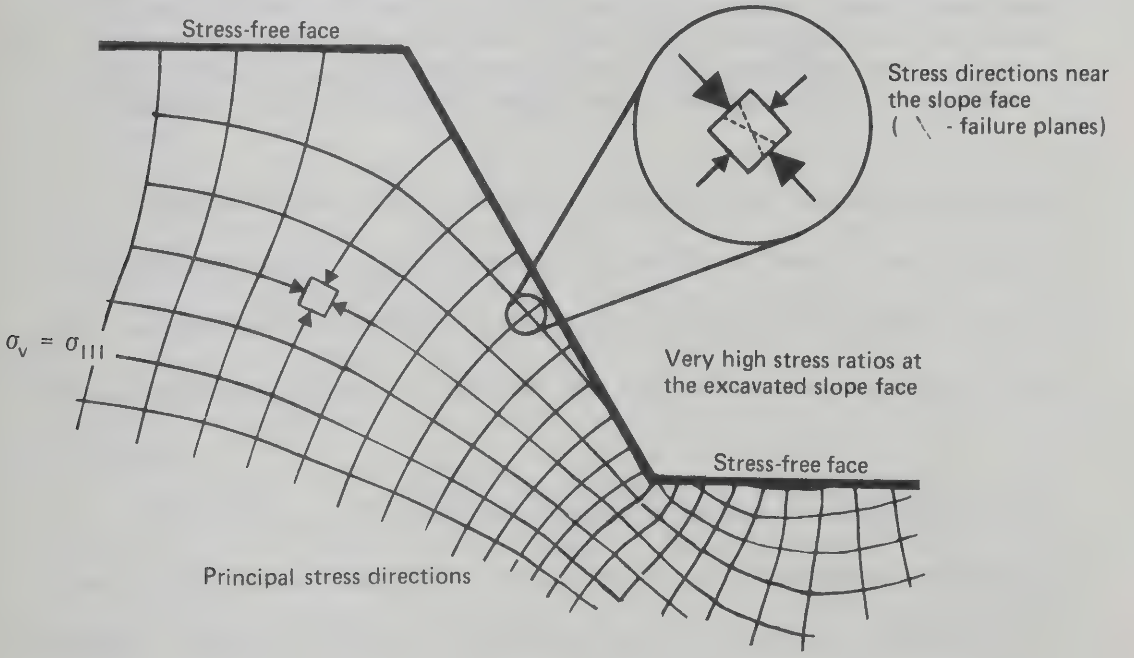

Figure 3.9 Stress Field Rotation Upon Excavation

excavation, but evidence strongly suggests that it is horizontal. Joint data favour a northeast to southwest orientation for the major principal compressive stress at surface (Babcock, 1975), which is consistent with the crustal compression model for the Interior Plains.

The final stage in the process of exfoliation, the detachment and fall, is extremely temperature dependent: the frequency of mateial falls is usually directly related to the heat generated by solar radiation, which causes the softening and straining required for failure. A former resident of Fort McMurray described this phenomenon:

> On hot summer days when we went fishing on the Horse River, we could hear tar sand falling into the river almost continually. The top of a mat of tar sand would curl over and roll up into a shape like a rug and the whole lot would tumble down the slope, breaking up into smaller chunks and finally falling into the river.

Rainfall serves as a further agent in the final detachment of an exfoliation slab. Accumulation of water in the joints results in a net outward force acting on the back of the slabs, and may precipitate immediate failure, or render the slab more susceptible to thermal effects.

The process of exfoliation and sloughing is accompanied by irreversible volume expansion resulting in consistently decreasing material densities as the denudation sequence reaches completion. Consequently, recent scree at slope bases is often extremely soft, particularly during warm weather; whereas in the back-slope, less disturbed oil sands display significantly higher strength, and have a higher density.

No deep-seated rotational or slump failure of a significant portion of the oil sands deposit has occurred recently, nor can

conclusive evidence be found for large-scale failures in the past. This observation, based on detailed study of aerial photographs and numerous on-site examinations, is crucial to the understanding of strength and stability in the oil sands, considering that many slopes in excess of 60 m lie at angles of 50° or greater, and yet the interstitial bitumen does not act as a true cementing agent.

Block falls, like exfoliation, may contribute to the denudation processes on an active oil sand slope (Plate 3.3). The distinction between block falls and exfoliation is one of proportion: block falls consist of the physical detachment and fall of a large, intact, roughly equidimensional unit of material from the slope face, whereas the minor dimension of exfoliation slabs is about an order of magnitude less than the other two dimensions. Block falls result from the development of several planes of weakness (joints, fractures, bedding) in orientations that render downslope movement kinematically possible. Block falls occur only on steep slopes where portions of the slopes have been "oversteepened" by rapid sloughing or undercutting, allowing exfoliation fractures to reach the surface of the slope face. Large, intact blocks in scree piles are rare, because the gross disturbance attending the downslope movement causes rapid disintegration of blocks.

Other slope reduction processes in the oil sands are minor in effect. Direct surface erosion by rain is a significant factor only in those portions of the McMurray Formation which are fine grained (fine-grained silty sand) and which lack bitumen.

Corrasion accounts for very little slope reduction. Flows and slides of overlying material have little or only local effect on the surface of undisturbed oil sands.

Organic slope reduction processes are limited to root disturbance in bitumen-poor zones in the active slopes. Bitumen is generally hostile to plant life, although admixed clay and oil-free silts and sands on a slope face or a debris pile permit the fixing of vegetation, which is prolific on most inactive slopes.

3.4.3 Debris Removal Agents

Lack of significant debris removal results in vegetated slopes lying at angles close to 30°. Where debris removal from the slope base by stream action or landsliding in basal clay is rapid, a dynamic balance is achieved and the activity of mass-wasting becomes a function of the rate of stream undercutting.

Scree or talus slopes may occur anywhere on the face of an oil sand slope. They vary in height from one meter to over 30 m. The angle of repose of colluvial veneer in shaley material has been measured as high as 44°. Gentler slopes in the range of 25° to 38° are most common. Slopes of scree lying at angles of less than 25° are usually the result of failure in underlying basal clay, or of viscous flow of the basal scree pile. The maximum observed angle of 44° in shaley colluvial slopes represents the maximum angle of shearing resistance of scree at low stresses. Colluvial slope angles may be high under conditions of low normal stress and significant shaleyness (Chandler, 1973). As the thickness of debris increases, the slope angle decreases because of lower friction angles associated with higher normal stress. Gradation of basal scree piles is similar to other observed screes, with larger blocks towards the base.

Scree accumulation is the result of shaley sloughing and

exfoliation. Shaley sloughing occurs in fine-grained, oil-poor silts and silty sands where bedding plane fissility and desiccation strains result in small platey debris. Further downslope movement of scree occurs mainly through creep, but minor slumping may occur, particularly in oil-poor material in basal scree slopes. Landsliding and major slumps in basal scree piles have been observed only in conjunction with basal clay.

Viscous flow (Plate 3.5) may result from complete disruption of structure by sloughing, from supersaturation with bitumen by slope surface bitumen seeps, or from increased mobility of warm bitumen. Ells (1926) postulated that the origin of this material was particularly oil-rich beds forced out of the slope by normal stresses. Close examination of the heads of several flowing masses showed discrete lumps, which became less discrete farther down the flow body. In addition, similar viscous flow phenomena have been observed at the bases of slopes varying from 10 to 35 m in height. Carrigy (1967) observed a general northwards decrease in in situ bitumen viscosity, and significant viscous flow of basal scree has been observed only north of Fort MacKay. Slope surface bitumen seeps are also somewhat more common in regions north of Fort MacKay. No supportive evidence for Ells's hypothesis of "squeezing out" of bitumen has been observed on any slope; all phenomena are readily explained by viscous flow of talus.

Interesting similarities exist between viscous flow morphology and classical glacier morphology. Viscous flows exhibit forms analogous to ice falls, bergschrunds, glacier snouts, and tension crevasses.

Bitumen seeps, or "tar springs", are frequently mentioned in the

PLATE 3.5a Viscous Flow in Remoulded Oil Sand. The remoulded talus in the centre of the photograph has formed a viscously flowing 15° toe. Close examination shows other flows in the background.

PLATE 3.5b Viscous Flow in Remoulded Talus. Orthogonal crevassing in a viscously flowing mass, looking upwards along the flow axis.

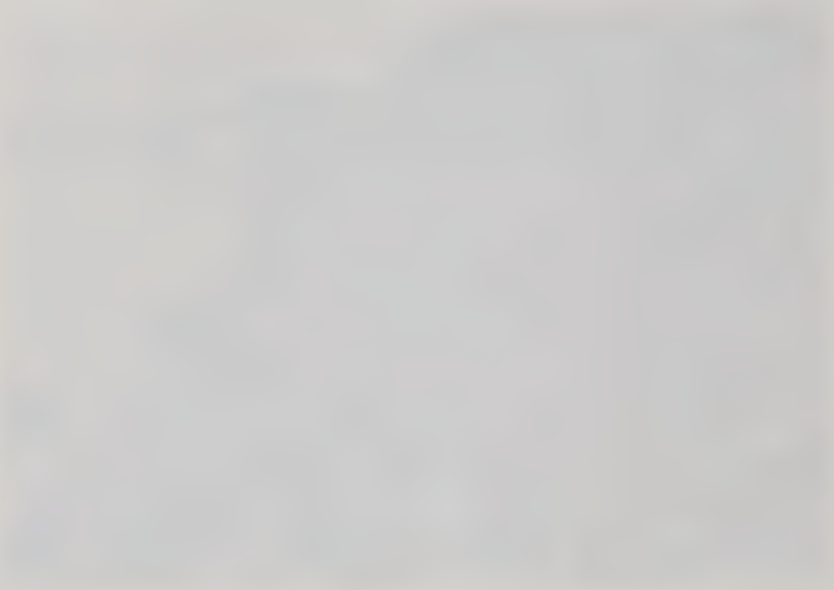

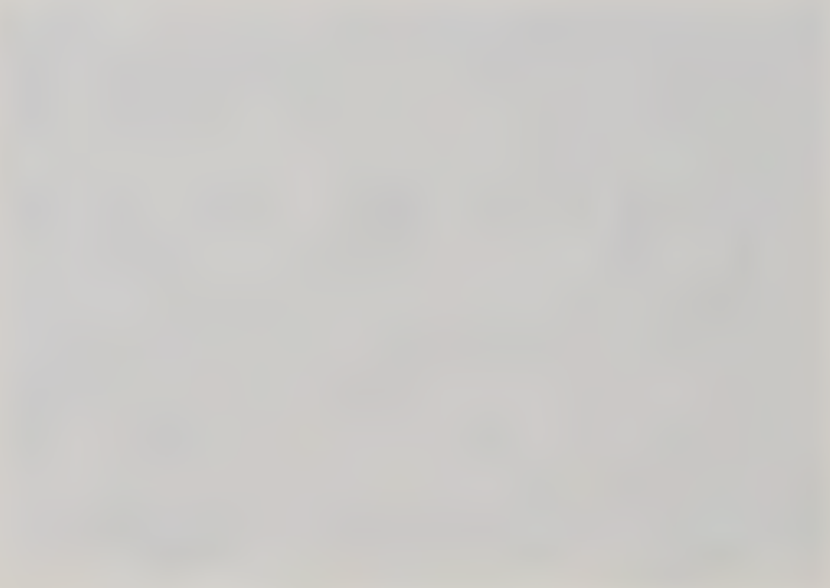

literature on the oil sands (e.g. Ells, 1926; Sproule, 1951; Falconer, 1951). No evidence has been reported in the literature, nor has any evidence been observed on outcrops, that these bitumen seeps are anything but a surface phenomenon limited to the 5 to 15 m of slope face affected by solar heating. Migration of oil from depth is not known to occur at present, nor has it occurred in the recent geological past (Carrigy, 1966). However, migration along joints and fissures remains a possibility.

Minor downslope flows of mixtures of sand, oil, and water (resulting from soaking of debris by rain water) have been observed by the writer, but these were rare, small in magnitude, and unimportant as debris removal agents.

3.4.4 Summary of Mass-Wasting Processes in Oil Sands

Slope reduction and debris removal processes are summarized in Figure 3.10. Table 3.2 evaluates the relative importance of several natural variables in these processes.

The most important factor in mass-wasting of oil sands is the presence of the stress-relief joints. These joints provide the major discontinuities in all oil-rich back-slopes. The susceptibility of the black or dark grey oil sand to solar heating and its consequences is perhaps unique among natural arenaceous materials.

3.5 Slope Recession Rates

The net result of mass-wasting is a gradual recession of exposed slope faces. The recession rate is difficult to measure because the process is a long-term phenomenon, and also because it is a function of

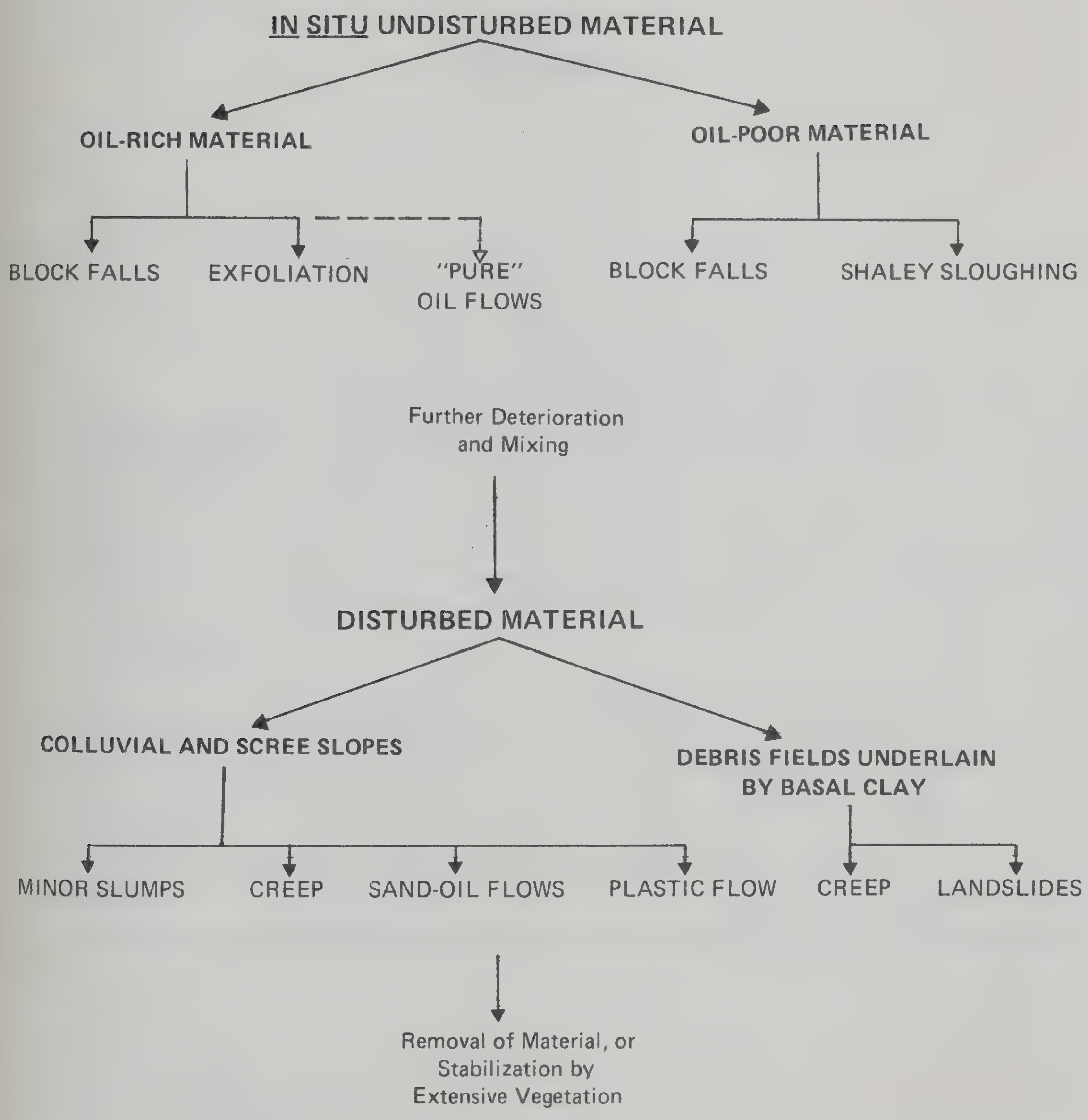

Figure 3.10 Mass-Wasting Processes in Oil Sand Slopes

TABLE 3.2

CAUSALITY MATRIX

UNDISTURBED MATERIAL	STRESS RELIEF	BEDDING-PLANE DISCONTINUITIES	SLOPE STEEPNESS	"OIL-RICHNESS" OF THE MATERIAL	FREEZE-THAW STRAINS	TEMPERATURE SUSCEPTIBILITY	HYDROSTATIC (FLUID) FORCES	DESSICATION STRAINS	ACTIVE TOE EROSION	RAINFALL	OTHER
SHALEY SLOUGHING	M.	V.I.	I.	N.A.	M.	M.	-	I.	-	I.	gas-release strains
BLOCK FALLS	V.I.	M.	V.I.	-	M.	M.	M.?	-	M.	?	
EXFOLIATION	V.I.	-	M.	I.	I.	I.	I.	M.?	-	V.I.	
OIL FLOWS	-	-	-	V.I.	-	V.I.	I.	-	-	-	
DISTURBED MATERIAL											
CREEP	N.A.	N.A.	I.	M.	V.I.	M.	-	M.	-	?	
PLASTIC FLOW	N.A.	N.A.	M.	V.I.	-	V.I.	I. (oil)	-	M.	?	
SAND-OIL (FLUID) FLOW	N.A.	N.A.	M.	I.	-	I.	I(oil & H_2O)	-	-	V.I.	
MINOR SLUMPS	N.A.	N.A.	I.	-	-	-	I. (H_2O)	-	I.	I.	
LANDSLIDES	N.A.	N.A.	I.	-	-	-	V.I. (H_2O)	-	V.I.	V.I.	

LEGEND

V.I. -: Very important relationship of causality
I. -: Relatively important causal relationship
M. -: Minor factor
\- -: Of little or no importance
N.A. -: Not applicable to the particular phenomena
? -: Relationship unclear

many variables. Nevertheless, some examples can be given of slope reduction rates.

Syncrude Canada Limited (formerly Canadian Cities Service, Athabasca, Limited) excavated a 30 m test pit in the side of a valley wall at angles of 55° to 60° during the period 1959 to 1961; in 1974, the talus had accumulated to within six meters of the top. Assuming past and present conditions as in Figure 3.11, the closed form of the rectilinear slope reduction equation (Scheidegger, 1970) yields a slope volume loss of about 115 m^3/m of slope length, and a consequent scree accumulation of 150 m^3/m (assuming a bulking factor of 1.3). By the same analysis, the slope crest has receded by about nine meters in the last 13 years. No active undercutting or debris removal has occurred.

Approximately 60 years ago, a road was constructed directly west of Fort McMurray at the base of an active oil sand slope (Appendix A; Slope 15). All traces of the road on the active slope have disappeared because of river undercutting and consequent slope recession. If the road width was originally about five meters, the river is undercutting that slope at a minimum rate of eight centimeters per year. The volume of material removed is irrelevant, since the road was at the base of the slope.

Rates of recession in inactive oil sand slopes are unknown, and because the entire array of river slopes in this area is geomorphologically immature (8000 to 11,000 years old), few conclusions may be drawn with respect to long-term slope flattening.

Removal of material from an undisturbed slope face with active basal debris removal seems to occur rectilinearly: slope profiles are not generally a function of slope heights within a given slope.

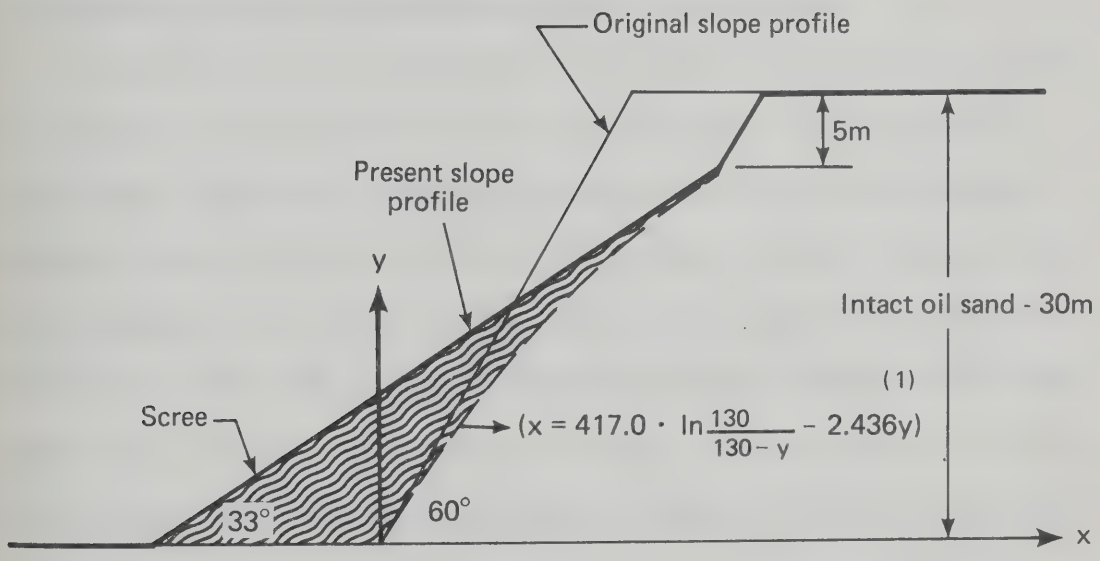

Bulking factor = 1.3
Stable scree = 33°
Original angle = 60°

(1) from Scheidegger, 1970

Figure 3.11 Scree Accumulation, Cities Service Test Pit, 1975

Few materials with significant long-term cohesion display rectilinear slopes. Recession rates, and hence slope reduction rates, are directly related to slope steepness, because steepness results in acceleration of the process of exfoliation in order to maintain equilibrium.

3.6 Hydrogeological Observations on the Natural Slopes

Ground water table elevations near exposed slopes of oil sands are unknown. Minor surface seeps on active slopes are common but their greatly increased rate of occurrence after rainfall suggests that they are solely of surface or near-surface origin. The presence of exfoliation fractures (stress-relief joints) permits the percolation of rain water and surface meltwater into the surface of the backslopes, and this water is released gradually along oil-free or oil-poor seams, resulting in the surface dampness observed. Soluble salt deposition is minor: only a thin white film is observed at the surface, and usually this is confined to a limited area. The consistent association of seeps with zones of low oil content indicates that rich oil sand, because of its very low permeability, forms a barrier to water flow, at least at and near the outcrop surfaces.

The oil sand certainly forms a local barrier and may form a regional barrier to water flow. Spring lines at the tops and bottoms of oil sand outcrops support this contention (Appendix A, Slope 59). In the oil-free sands along the Clearwater River, springs occur in the coarse-grained sands at the base of the McMurray Formation. The finer-grained sands above the coarse-grained sands are moist, but contain no springs. No spring lines are seen at the top of the McMurray Formation where it is oil-free (i.e. along the Clearwater River valley).

It might be hypothesized, therefore, that regional seepage rates are low and evaporation rates exceed flow rates. The presence of springs in the Clearwater and Athabasca River valleys, both above and below the oil-rich McMurray Formation, refutes this hypothesis. Water table levels are generally close to the surface as indicated by extensive areas of muskeg directly behind slope crests.

Thus, the presence of oil sands results in a perched water table on the upper surface. The base of the oil sands is free draining because of the presence of jointed limestone, coarse-grained oil-free sands, and pebble conglomerates (Figure 3.12). These conclusions are still conjectural, as adequate borehole pore pressure data and water table information concerning the oil sands area are unavailable.

3.7 Engineering Implications of the Study of Natural Slopes

Two findings from the natural slope study are crucial to this research:

1. Slopes are high and steep.
2. There are no significant massive rotational earth movements.

The first observation suggests high natural strengths; the second low cohesion or the absence of transient landslide agencies (pore pressures or earthquake forces). Efficient dragline mining requires pit walls over 60 m high at inclinations of at least 55°. Confidence in pit wall stability is necessary, and these initial natural slope observations are reassuring. Nevertheless, the implications of the different time scales between a mining operation and natural slope development must be examined.

The natural slopes in oil sands have probably existed since

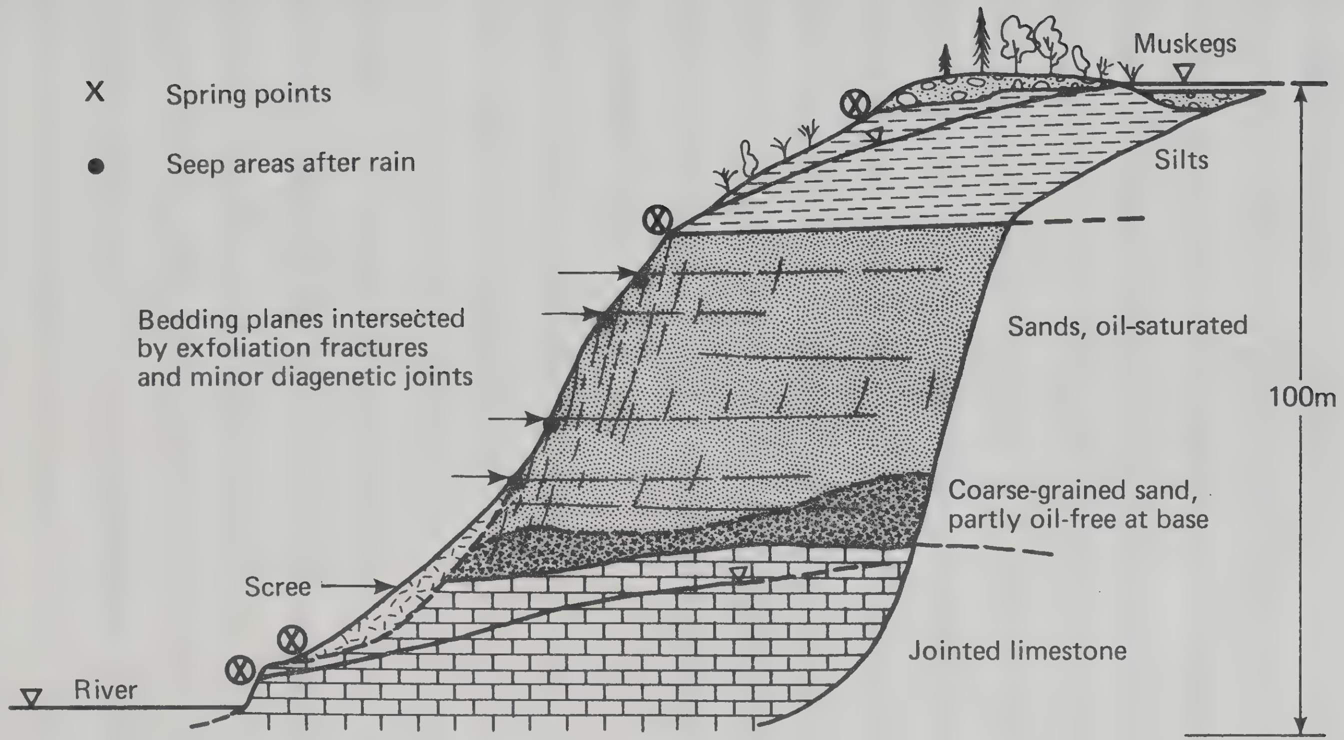

Figure 3.12 Probable Hydrogeological Conditions in a Typical Oil Sand Slope

drainage of the last proglacial lakes to the north of the slopes, and subsequent valley formation, a period of at least 8000 years. This does not suggest that inactive slopes are in a condition of long-term equilibrium: these slopes are in momentary balance with the existing forces of undercutting and debris removal. Even assuming rapid lateral erosion rates, it becomes apparent that slope angles of 55° to 60° over slope heights of 50 to 60 m indicate long-term engineering stability. It would be expected, therefore, that high, steep slopes in oil sands mining operations are feasible. Because weathering processes reduce strength, and because mining operations are of relatively short duration, slopes somewhat steeper than those common in nature are feasible in oil sands mining operations. Trial pits excavated by Syncrude Canada Limited and by Shell Canada Limited to depths beyond 60 m confirm the preceding observations.

The presence of basal clay apparently does not affect back-slope angle. The basal clays invariably contain slickensided strata, and the mineralogy and grain size distribution of the clay suggest a low residual ϕ (Appendix H). The morphology of natural slopes with basal clay suggests that rapid raveling may be a problem in open pit mines founded on basal clay. Smectite is conspicuously absent in these clays (Appendix H); therefore they have little tendency to swell. However, the factor of strain incompatibility as a consequence of differing elastic moduli has yet to be assessed in the case of rapid, steep excavations. Minimum safety factors with respect to pit wall landsliding occur at the end of excavation because the slickensided strata are already close to a residual strength state. The overlying oil sands seem sufficiently

competent to accommodate the upwards stress transfer required to adjust to the strains in the basal deposits.

Paleosol, because of its loamy nature, is likely to act as a granular material in an excavation. Significant quantities of carbonate cement may be present, adding a cohesive component to the inherent frictional resistance. The paleosols examined on natural slopes show a great deal of variability; materials ranged from a competent paleocaliche 10 cm thick to a clayey, calcareous residual soil at least six meters thick. Generalizations are therefore difficult to make.

Extensive diagenetic joints are uncommon and are obscured by the presence of the stress-relief (exfoliation) joints. If the diagenetic joints are steep (greater than 75° is usual), and free of clayey materials, their effects on pit wall stability are expected to be insignificant. Stress-relief joints result from any excavation and may produce large masses of loose debris at the pit floor, which must be salvaged for processing.

3.8 Conclusions

The following conclusions can be drawn from the natural slope study:

1. Bitumen *per se* is not a source of strength in oil sands, although it retards disruptive freeze-thaw phenomena.
2. Oil-free coarse-grained oil sands may form very steep slopes up to 70 m in height.
3. All oil sand slopes show few well-developed diagenetic joints but numerous well-developed exfoliation (stress-relief) joints.
4. Exfoliation raveling is the major slope denudation process;

solar heating and percolation of rain water accelerate raveling.

5. Basal clays, which are common, result in distinct slope morphologies, and must be considered in open pit mine development.

6. Landslides do not occur on natural oil sand slopes; minor blockfalls do occur.

7. The absence of active debris removal agencies results in vegetated slopes at or below the expected angle of repose of granular material.

CHAPTER IV

SAMPLING DIFFICULTIES IN THE ATHABASCA OIL SANDS

4.1 Introduction

The geology and lithology of the McMurray Formation supply a useful interpretative framework for many natural features but provide no specific engineering strength data. The study of natural slopes indicated high strengths, but the source of the additional component of strength beyond that of a normal dense sand was not identified. The absence of significant carbonate cement was noted, but the task of identifying the origin of the high strengths remains.

This chapter discusses sampling problems, the known physical properties of oil sand, and the interpretation of these properties. Various existing hypotheses accounting for the observed strengths are discussed; all are shown to be untenable.

4.2 Sampling Oil Sands

Physical properties measured under conditions differing from those *in situ* are subject to error because of the changes brought about by sampling. This error is especially evident in the reported physical properties of the Athabasca Oil Sands. Samples which are undisturbed or only slightly disturbed are extremely difficult to obtain from the oil-rich, medium- to coarse-grained sections of the McMurray Formation.

Sample disturbance arises from expansion of the oil sands and

the consequent disruption of the dense fabric. The three major reasons for the expansion are:

1. High densities: The high _in situ_ unit weights of the oil-rich sands (2.15 to 2.25 gm/cc as recorded in geophysical logs) prevent the successful use of standard tube-type sampling devices because of high penetration resistance and dilative behaviour during shear.

2. Dissolved gases: Reduction of confining stress on oil sand samples causes an immediate expansion of the material because of exsolution of gas.

3. Temperature sensitivity: The viscosity of the bitumen is highly sensitive to temperature change. Although the bitumen is not a true cement, it does provide temporary cohesion at low stresses; therefore, further yielding of the structure may occur because of bitumen fluidization. The rate of exsolution of gas is also temperature dependent.

Early reference to sampling difficulties was made by Blair (1951). Hardy and Hemstock (1963) graphically described the effects of gas exsolution from cores. A sampling program (reported in Appendix F), undertaken by the writer in 1974, utilized the best available coring methods; nevertheless, all cores displayed expansion. Two illustrations are given:

1. The bit gauge (8.89 cm) was smaller than the plastic core liner (9.453 cm I.D.) to prevent core jamming, yet oil-rich oil sands usually completely filled the liner. This represents a minimum volume expansion of 11.6%.

2. After the core lengths of 6.10 m (30 ft) were cut into four

sections for transportation and storage, rich oil sands quickly extruded from the core liner ends. This extrusion from a 150 cm core length often amounted to three centimeters. Extrusion was accompanied by bubbling of escaping gases. The greater the expansion and extrusion, the greater the intensity of bubbling. The oil-rich, coarse-grained sections of oil sands displayed the most intense gas bubbling.

In the sampling program undertaken by the writer, the core obtained from the oil sands borehole was stored at low temperatures. During the course of the laboratory program, many measurements of the bulk densities of core specimens were made, usually followed by bitumen content measurements and grain size analyses. All bulk densities of core specimens were obtained by measuring the dimensions of right circular cylinders, followed by weighing on an accurate balance.

The geophysical logging data from the sample borehole were available, and the mean _in situ_ bulk densities were determined for the stratigraphic horizons corresponding to those assessed in the laboratory program. Comparisons of the two bulk densities are shown in Table 4.1; these and other density data are plotted in Figure 4.1. Approximate boundaries between the visually determined grain sizes are drawn to emphasize the relationship between grain size and _in situ_ bulk density. The differences between the density data obtained in the laboratory and those values reported in geophysical logs are not unexpected: they are common in the sampling of oil sands (Brooker, 1975). Dry densities of hand specimens collected from oil-free outcrops were determined by drying, weighing, careful sealing with liquid wax, and lastly, volume measurement by mercury displacement in a lucite

TABLE 4.1

SELECTED COMPARISON OF LABORATORY AND GEOPHYSICAL BULK DENSITIES

DEPTH (FEET)	LABORATORY DENSITY	GEOPHYSICAL DENSITY	LITHOLOGICAL DESCRIPTION	OIL CONTENT
91	2.28	2.30	clay-shale	0
93	2.06	2.25	silt & fn.-gr. sand	5-9%
97	2.04	2.21	fn.-gr. sand	9%
101	2.06	2.27	fn.-gr. slty. sand	7%
109	2.03	2.18	fn.-gr. sand	6%
118	2.05	2.26	fn.-gr. sand	6.5%
119	2.32	2.38	clay shale	0
121	2.03	2.20	fn.gr. sand	12%
122	2.06	2.20	fn.gr. sand	11%
124	1.99	2.18	fn.gr. sand	11%
131-132	2.15	2.34	silty sand	0
133	2.238	2.35	silty sand	<1%
135	2.31	2.34	silt	0
136	2.00	2.32	fine sand	10%
151	2.04	2.17	silt	6%
152	2.12	2.25	clayey silt	1%
173	1.92	2.12	med.-gr. sand	13%
190	1.85	2.10	coarse-gr. sand	14.9%
190.2	1.91	2.09	coarse-gr. sand	14.6%
209	1.86	2.10	coarse-gr. sand	14%
218	2.33	2.42	basal clay-shale	0

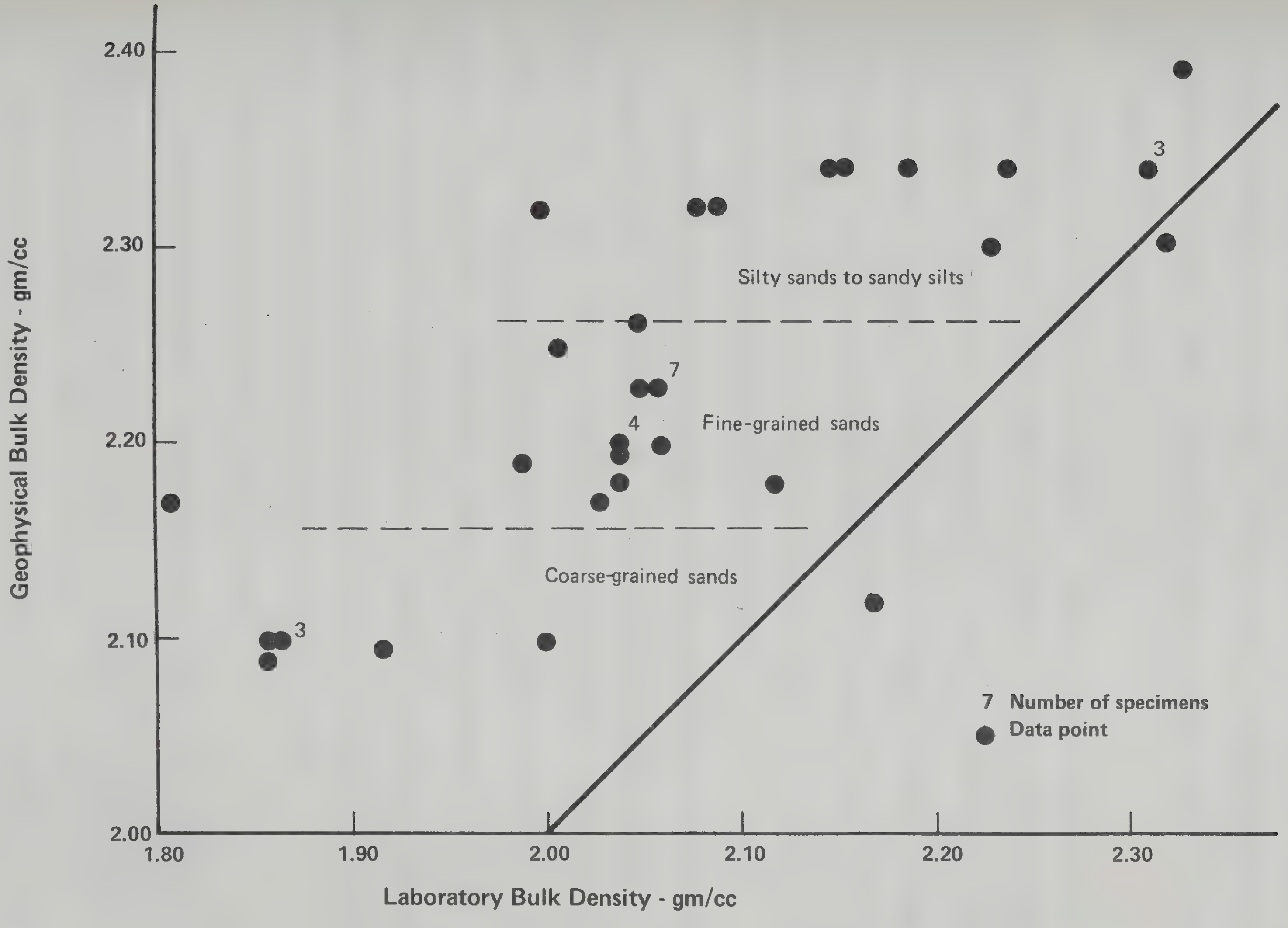

Figure 4.1 Mean Bulk Density from Geophysical Logs Plotted versus Laboratory Determinations

displacement cell. The dry bulk density obtained by this method was converted to saturated bulk density to permit a more direct comparison with data obtained from oil-rich core materials. Several determinations on materials from the same locations show consistent results. The data are reported in Table 4.2.

The conclusions to be drawn from these data are clear: all oil-rich sands expand considerably upon sampling, and coarse-grained oil-rich sands expand more than medium- or fine-grained oil-rich sands. Oil-free borehole samples from the High Hill River, Cottonwood Creek, and Christina River outcrops yield bulk densities much closer to the values obtained from geophysical data, despite the total stress release resulting from outcrop excavation and weathering.

Because of the discrepancy between geophysical and laboratory bulk density data, the methods of calibrating and interpreting geophysical logs have been seriously questioned. Brooker (1975) concluded that the _in situ_ bulk densities of oil sands as reported in geophysical logs were essentially correct, and presented a density profile obtained by geophysical means. Appendix G contains a presentation of typical borehole geophysical data and a discussion of geophysical methods of borehole assessment in the oil sands.

Carrigy (1967) concluded that his data:

> . . . show qualitatively that tar sands maintain the characteristics of a sand regardless of depth, temperature, and bitumen content provided the confining load is removed at a sufficiently slow rate to allow dissipation of pore pressure without disruption of the granular fabric of the sand. (pp.578-579)

On natural slopes and in slowly excavated pit walls, the pore gases probably dissipate slowly, without totally rupturing the fabric. In any sampling method employed to date, the rate of stress relief has

TABLE 4.2

BULK DENSITIES OF OIL-FREE McMURRAY FORMATION SANDS

SAMPLE (1) NUMBER	LOCATION (2)	STRATIGRAPHIC POSITION (2)	SATURATED BULK DENSITY gm/cc	COMMENTS
MD-75-1-1A	High Hill River	Upper Member	2.078	Fine sand, coaly fragments
MD-75-1-1B	High Hill River	Upper Member	2.083	Fine sand, worm casts
MD-75-1-2	High Hill River	Middle Member	2.076	Medium-grained X-bedded sand
MD-75-1-4	High Hill River	Lower Member	2.168	Coarse-grained sand
MD-75-1-5A MD-75-1-5B	High Hill River	Top of Upper Member	2.112 2.123	Very fine sand
MD-75-2-4	Cottonwood Creek	Upper Member	2.183	Medium-grained, trace of oil
MD-75-2-6	Cottonwood Creek	Lower Member	2.151	Coarse-grained sand
MD-75-61-4	Christina River	Basal Sand, Lower Member	2.213±.01	Four analyses, coarse-grained

(1) Grain size analyses may be found in Appendix D.

(2) Refer to Appendix A.

been rapid, causing extensive bulk density reduction. Disturbance of samples therefore has resulted in laboratory data not directly applicable to design problems in undisturbed, in situ oil sands.

4.3 Properties of Oil Sands

4.3.1 Bulk Density

Bulk density figures from several sources are reported in Table 4.3; further geophysical data may be found in Appendix G. Pore fluid (i.e. bitumen) density has a negligible effect on bulk density, since bitumen density is close to that of water (i.e. 1.015 gm/ml). Misinterpretation of geophysical data is a direct result of the anomalies shown in Tables 4.1 and 4.3.

In situ bulk densities from geophysical data for the various lithologies may be summarized as:[1]

1. 2.11 (±0.06) gm/cc for very well-sorted, fine-grained, clean sands, and for medium- to coarse-grained sands (i.e. the major portion of the Middle and Lower Members of the McMurray Formation).
2. 2.21 (±0.06) gm/cc for fine-grained sands (typical of the Middle Member).
3. 2.32 (±0.06) gm/cc for sandy and clayey silts and intraformational clays (found predominantly in the Upper Member).

Figure 4.2 is a plot of the relationship between oil contents and bulk densities from a number of cores analyzed in commercial laboratories. Although the variability of grain size is not quantified,

---

[1] These figures are approximate values only; actual values vary according to location, overburden thickness, and drilling method.

TABLE 4.3

SELECTED BULK DENSITY DATA: ATHABASCA OIL SANDS

BULK DENSITY	SOURCE	COMMENTS
1.96	Blair, 1950	Porosity = 39.2% Saturation = 89% oil and water
2.03-2.08	Blair, 1950	Porosity = 33.0 - 35.5%
1.75-2.09	Clark, 1957	Porosity = 34% to 46%
----	Hardy and Hemstock, 1963	Void ratios from 0.55 to 0.80
----	Doscher et al, 1963	Porosity = 38% - 42%
1.86-2.36	Carrigy, 1967	Geophysical density log Porosity = 17.6% to 43.3%
1.98-2.08	Carrigy, 1967	Geophysical density log Mean porosity = 40% 60 m below surface
2.10-2.19	Carrigy, 1967	Geophysical density log Mean porosity = 34% 300 m below surface
----	Camp,	Mean porosity = 35%
----	Carrigy and Kramers, 1974	Maximum porosity = 35%
2.1 - 2.3	Brooker, 1975	Geophysical density log
2.04-2.40	This volume, 1976	Laboratory data and Geophysical density log Porosity = 16% for clayey silt to 35% for coarse sand

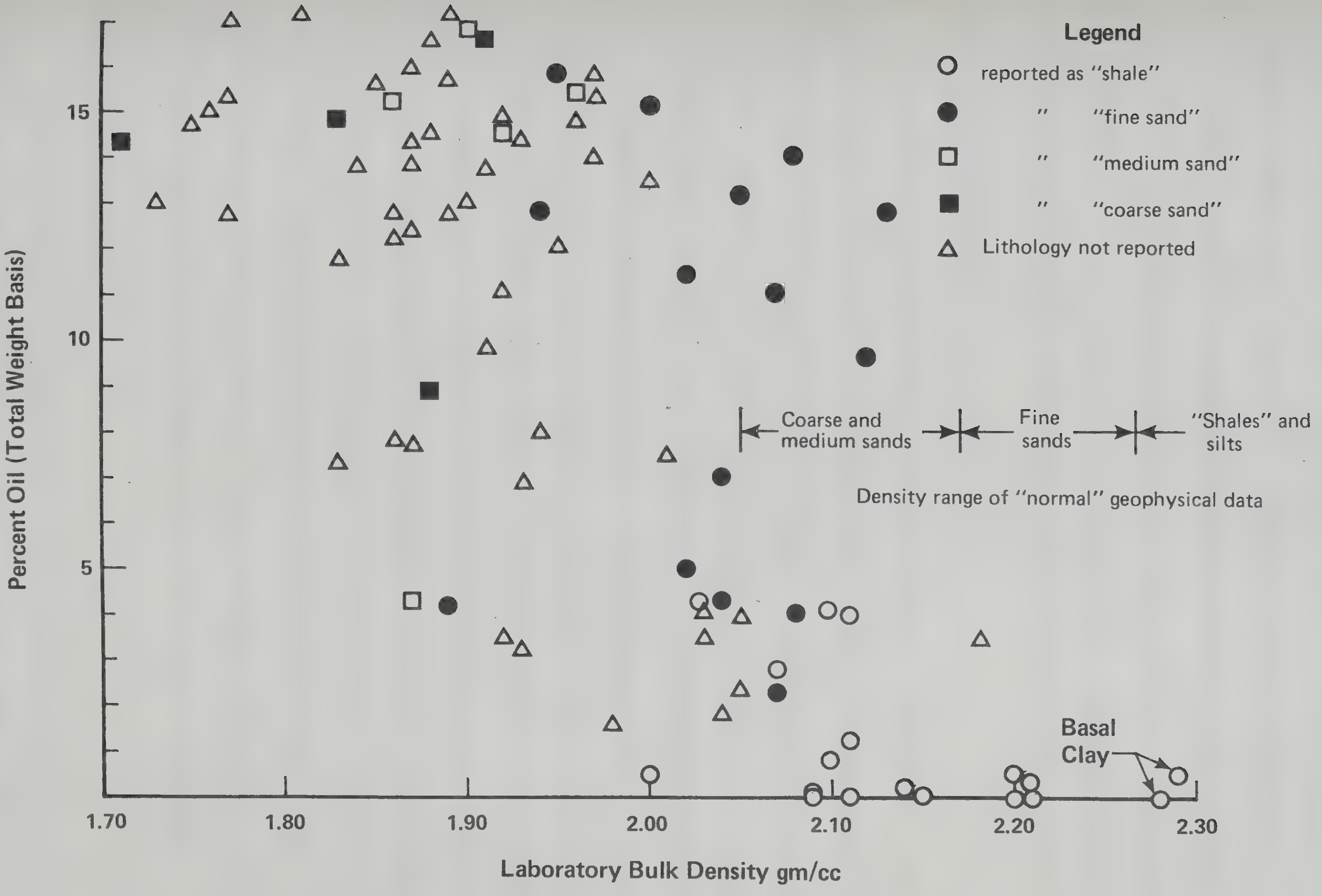

Figure 4.2 Bitumen Content Versus Laboratory Bulk Density

there is a significant reduction in apparent bulk density with increasing oil content. Few values approach reasonable in situ bulk density values; and, in general, coarse-grained oil-rich sands display much greater sample disturbance than fine-grained oil-poor sands. In conclusion, all published bulk density data obtained in laboratories were determined from highly disturbed samples: geophysical methods of in situ bulk density determination are much more reliable.

4.3.2 Porosity and Saturation

Virtually all laboratory analyses report liquid (oil and water) saturations of less than 90% (e.g. Clark, 1957). In general, the sums of the weight percentages of oil and water from analyses performed on medium- to coarse-grained oil-rich sands are relatively constant at 15.5% to 18.0%. These figures correspond to porosities of 29.0% to 32.3%, assuming complete saturation, a mean mineral specific gravity of 2.65, and a pore fluid density of 1.00 gm/ml. Geophysical data indicate that below a burial depth of 20 to 30 m, liquid saturation of oil sands is almost complete, and therefore back-calculated porosity is more representative of the in situ conditions. For example, Clark (1957) reported fluid saturation values of 61% to 100% with a mean of 83%. These saturation and porosity values are a result of sample alteration before testing. Any saturation value of less than 95% must be considered unrepresentative of in situ conditions.

4.3.3 Permeability

Permeabilities determined from oil-rich laboratory specimens are probably much higher than those in situ. For example, values up to 5000 md (millidarcies) were reported by Carrigy and Kramers (1974).

Clark (1959) reported a mean air permeability of 50 md, with a range of 10 to 650 md. Hardy and Hemstock (1963) concluded that these values were markedly affected by gross sample disturbance. In any case, air permeability values may not be directly applicable to fluid flow because of the interfacial tensions which must be overcome. Unfortunately, no data on in situ permeability determinations have been published; therefore it is impossible to estimate the magnitude of the permeability change.

4.3.4 Strength Properties

Few adequate data from strength tests on oil sands have been reported, because strength properties are extremely sensitive to sample disturbance. The difficulties of adequate and representative sampling and testing of oil sands are so great as to render all reported results not directly characteristic of in situ conditions.

Carrigy (1967) reported results from triaxial tests as a plot of the relationship between shear stress and normal stress. The cohesion intercept was zero and the angle of internal friction was 46.6°. The maximum confining stress was 7.03 kg/cm^2 (100 psi); however, test conditions were not described in detail.

Brooker (1975) presented the first detailed assessment of the strength of oil sands. The minimum void ratio of samples tested was about 0.60 (a porosity of 37.5%), equivalent to a saturated bulk density of about 2.03 gm/cc. This value is much lower than mean in situ bulk densities. Brooker's data indicate increasing shear resistance as sample void ratio decreased. Dilative behaviour correlated highly with the strength data: volume decrease at high void ratios (i.e. large

disturbance) and strong dilation at lower void ratios (lesser disturbance). By extension to field data, higher strengths at lower void ratios were postulated. The reported angle of shearing resistance (Mohr-Coulomb envelope) was slightly below 45°, with a cohesion intercept of about 1.0 kg/cm (10 to 15 psi).

Several plate bearing tests (performed on a 0.25 square foot area) demonstrated initially linear load-displacement behaviour (Carrigy, 1967). The lower the depth of the test, the more gentle the slope of the linear portion, reflecting an increased structural disturbance because of gas release.

A series of tests on samples of varying quality was performed by Hardy and Hemstock (1963) in an attempt to rationalize strength data for open pit wall design. Several findings from their research are pertinent to this discussion:

1. Remoulded "saturated" oil sands invariably displayed low shear strengths, regardless of the laboratory bulk densities achieved.

2. The behaviour of slightly disturbed samples was essentially that of a "normal dense sandstone". (The meaning of the term "normal dense sandstone" was not clear.)

3. The exsolution of gases resulted in serious sample disturbance, despite the extraordinary precautions taken.

4. Strength loss increased with burial depth of samples; however, natural slopes displayed much higher strengths than those measured in the laboratory testing program.

Standard penetration tests have yielded values of 60 to 500 blows per foot of oil sands. Vane shear tests (which are impossible to

interpret in this material) showed remoulded strengths approximately one-fifth of peak strength (Carrigy, 1967).

Strength data on the oil sands are limited in quantity, test descriptions are often incomplete, and estimates of sample disturbance are sometimes absent. Therefore, the interpretations of available test results are open to question. Brooker (1975) provided some useful and interesting data from a consulting research study. Unfortunately, gross sample disturbance hampers the extension of Brooker's data to *in situ* material characteristics.

4.4 Source of Strength of Oil Sands

Many sources of strength have been postulated for the observed behaviour of natural oil sand slopes. Artificial slopes over 60 m high at angles over 65° have been standing for long periods; therefore it is obvious that previously published strength hypotheses and informally held theories must be re-examined. This section presents these strength hypotheses and shows why they are not applicable to *in situ* oil sands behaviour.

4.4.1 Bitumen Viscosity

Hardy and Hemstock (1963) reported an oil sands bitumen viscosity of 1.3×10^5 poises at 6°C. Bowman (1967) stated that the bitumen in oil sands is a viscous Newtonian fluid. Because a Newtonian fluid provides no shear resistance at a zero rate of shear, the bitumen can not provide a true cohesive (stress-independent) component of strength. At a rapid strain rate, the viscous component increases the apparent strength. For example, if bitumen viscosity is

5×10^6 poises and the strain rate is 0.10/sec (very rapid), the viscous resistance component amounts to somewhat less than one kg/cm^2, assuming the viscous action takes place over the entire failure surface. At lower strain rates, viscous resistance becomes negligible.

Unless in situ bitumen is grossly different from the laboratory-extracted bitumen, it can provide no significant long-term strength. The term "oil-cemented" (Carrigy, 1959, 1973) can not be used in the engineering sense of "cemented".

4.4.2 Bitumen-Water-Quartz Interfacial Tensions

The surface tensions of bituminous materials are in the range of 40 dynes/cm^2 at 25°C (Mack, 1964), and pure water has a surface tension of about 100 dynes/cm^2 at a similar temperature. Interfacial tensions, however, are negligible in coarse-grained materials because of low interphase surface areas, and therefore can not be a significant source of strength in the Athabasca Oil Sands.

4.4.3 Clay Mineral Cementation

In the absence of interplatelet diagenetic bonds, "clay" cementation becomes true cohesion only when the clay is in a dry state: in a moist state its frictional resistance is much less than that of quartz. For this reason, interstitial clay or clay bands can act as cementing agents only within dessicated outcrop faces. Moreover, only very small quantities of clay are present in the medium- and coarse-grained McMurray Formation sands which constitute the majority of the Athabasca Oil Sands deposit. It is apparent, therefore, that clay can not be a source of long-term pit wall or valley wall strength. The term "clay-cemented sandstone" has often been applied to sandstones

with a clay matrix (e.g. Carrigy and Mellon, 1964). Unless the clay mineral exhibits diagenetic bonding, the term "clay-cemented" is not justified in an engineering sense.

4.4.4 Carbonate or Silica Cementation

Carrigy (1959) reported considerable cementation in the McMurray Formation; however, the writer has not observed any extensive carbonate- or silica-cemented sands. Cementation occurs locally, but in such small amounts as to be inconsequential as a source of strength. Furthermore, zones of oil sands of an indurated nature also exhibit well-developed diagenetic joint systems which completely traverse the cemented strata. The great majority of the oil sands do not display well-developed diagenetic joint arrays and are not cemented.

4.4.5 Siderite, Pyrite, and Iron Oxide Cementation

McMurray Formation sands occasionally occur as local bands (up to 0.6 m) of siderite-, pyrite-, or iron oxide-cemented strata. These strata often are discontinuous, usually are dissected by an orthogonal set of diagenetic joints, and comprise less than 2% to 3% of the McMurray Formation. Because they are discontinuous, jointed, and limited in extent, cemented beds probably do not contribute significantly to pit wall or outcrop strength.

4.4.6 Pore Pressures

Data are not generally available concerning pore pressure redistribution behind pit walls upon excavation. Natural slopes have existed for thousands of years: pore pressures therefore are likely to have equalized and steady state conditions apply. Hence, negative

(or highly reduced) pore pressures are not considered a possible source of strength in natural slopes.

4.4.7 Strength of Granular Materials

Extensive review of the literature has indicated that artificially assembled sands of similar mineralogy and grain shape characteristics have angles of shearing resistance of no more than 46^{o} at very low stresses and high densities (e.g. Nash, 1953; Rowe, 1969). This does not account for the observed long-term stability of natural and man-made oil sand slopes.

4.5 Summary

All published data based on laboratory investigations of oil sands are open to question because of the effects of sample disturbance during sampling and testing. This disturbance is a consequence of the high densities and uncemented character of oil sands, combined with the effects of gas exsolution and the temperature-dependent viscosity of bitumen. The disturbance results in low bulk densities, low total saturation values, low strength parameters, and high porosities, as measured in laboratory investigations.

The commonly held strength hypotheses are untenable, and geotechnical literature has yielded no adequate explanation for the high strength of oil sands.

CHAPTER V

SHEAR STRENGTH OF ATHABASCA OIL SANDS

5.1 Introduction

A program of laboratory testing was designed to determine the source of strength of the Athabasca Oil Sands. Strength tests were performed on artificially densified Ottawa Sand, on densified oil-free sand from the Athabasca Oil Sands, on recompacted oil-rich sand, and, lastly, on specimens of high quality oil sand core obtained from the mining area of the Athabasca deposit (Figure 1.2). The various series of tests and the reasons for undertaking each series are discussed in this introductory section.

5.1.1 Gelatin-Sand Triaxial Tests

Triaxial undrained tests on densified Ottawa Sand were performed using a "solidified" gelatin-water mixture as a pore fluid. The purpose of this test series was to assess the effects of a non-Newtonian pore fluid on the strength of a dense sand mass. The effect of stress history also was explored by employing different stresses for gelatin-setting and for testing.

5.1.2 Dense Ottawa Sand Triaxial Tests

Triaxial undrained tests with pore pressure measurement were performed on densified specimens of Ottawa Sand using de-aired water as a pore fluid. Various stress levels and back pressures were employed to assess the tendency of a dense competent sand to reduce

pore pressures through dilatancy, and to assess the overall strength characteristics of artificially densified sand.

5.1.3 Triaxial Tests on Densified Tailings Sand

Triaxial undrained tests with pore pressure measurements and volume change measurements were performed on oil-free densified tailings sand from the Athabasca Oil Sands. A direct comparison of strength data to those obtained from Ottawa Sand was possible, permitting assessment of the effects of the grain parameters (i.e. roundness, surface rugosity, size, and sorting) on the shear strength of oil sands material.

5.1.4 Triaxial Tests on Recompacted Oil Sand

Triaxial undrained tests were performed on oil-rich (13.5% of total weight) recompacted oil sand. Samples were refrigerated during testing. This test series was designed to explore the role of bitumen in the shear strength characteristics of oil sand. The use of temperatures similar to those _in situ_ provided a direct measure of the effects of bitumen viscosity.

5.1.5 Triaxial Tests on Oil Sand

Several triaxial tests on oil sand specimens were performed to assess the strength of the material; to assess the effects of sample expansion, oil content, and grain size upon the strength; and to assess the consolidation, compressibility, and permeability characteristics of the oil sands.

5.1.6 Shearbox Tests on Densified Ottawa Sand

The major testing apparatus for undisturbed oil sands was a circular shearbox. Several shearbox tests on two grades of densified Ottawa Sand (medium- and coarse-grained) were performed to provide comparative data for the oil sands shearbox tests. The effects of sample density and grain size on strength were explored; the stress-displacement characteristics and the peak and residual strengths were assessed over a stress range from 1 to 10 kg/cm^2; and dilation data were carefully collected for comparison to subsequent shearbox tests.

5.1.7 Shearbox Tests on Athabasca Oil Sands

The major testing program on oil sands consisted of several series of shearbox tests on circular oil sand specimens. Mohr-Coulomb failure envelopes were generated for various materials: oil-poor fine-grained oil sand, oil-rich fine-grained oil sand, oil-rich coarse-grained oil sand, and intraformational oil-free clay. Dilative behaviour was assessed carefully; the effects of varying displacement rates were explored; and the variability of the oil sands materials tested permitted evaluation of the effects of bitumen content, density, and grain parameters upon the strength characteristics and the stress-displacement behaviour. Residual stress ratios were determined for all tests.

5.2 General Comments on the Laboratory Program

5.2.1 Test Equipment

The test equipment consisted of standard triaxial cells with minor modifications and standard circular shearboxes. More detailed

descriptions of each apparatus may be found in Appendix C.

5.2.2 Data Acquisition

Electronic data-gathering methods were used in all tests, with the exception of volume change measurement during triaxial testing (where burette measurement techniques were used). The remote-controlled data acquisition system employed was a multichannel Hewlett-Packard apparatus with variable sampling times and a printed output. Displacements were measured by linear voltage displacement transformers, loads were measured by load cells with a Wheatstone Bridge strain gauge configuration, and pore pressures were monitored with very low compliance metal diaphragm transducers. All electronic measuring devices were recalibrated periodically to eliminate error due to zero point drift or to sensitivity alteration. Sufficient data were collected to permit precise evaluation of peak strength.

Upon completion of a given test, data were selected from the printed tape, transcribed to computer forms, punched on cards, and processed by computer programs to yield both printed and graphical output.

5.3 Gelatin-Sand Triaxial Tests

5.3.1 Sample Preparation

The sand was sedimented under water in a membrane-lined, three-piece brass mould designed to fit a 10.16 cm triaxial cell base. The triaxial cell base was attached securely to a vibrating table equipped with a variable vibration amplitude control: vibration was continuous throughout the sedimentation process. The density of samples was

increased further by shock loading with a wooden mallet on the side of the mould, and by gentle rodding during vibration. After the porous stone, the top cap, and the membrane O-rings were in place, varying surface normal loads (up to 1.0 kg/cm^2), large amplitude vibrations, and suctions of -0.1 kg/cm^2 were applied simultaneously to achieve the maximum possible density. The mould was removed with the negative pore stress shut in; the specimen height was calculated as the mean of three separate measurements; the mean specimen diameter was determined from nine separate diametric measurements; corrections were applied for membrane thickness; and specimen volume was calculated. Bulk densities were calculated when the total dry weight was determined after testing, and saturated bulk densities of 2.13 gm/cc were achieved.

Standard latex membranes of relatively uniform thickness (0.032 cm) were used; Teflon porous end plates (0.32 cm thick) provided end drainage; and all specimens were constructed to a pretest length/diameter ratio of about 2.0.

After densification and volume determinations were completed, the triaxial cells were assembled, and a small cell pressure was applied. Cell pressure and pore fluid pressure were increased simultaneously until sample saturation was considered complete (2.0 kg/cm^2 pore pressure); then a consolidation cell pressure was applied while the volume of efflux water was measured. Void ratio decrease was negligible, since the majority of the volume efflux accompanying a positive effective stress change could be attributed to membrane penetration, porous end plate readjustment, and system compliance.

A chilled mixture of gelatin and water was used as a pore fluid

in an attempt to "lock in" stresses during a pretest unloading phase in order to evaluate the hypothesis that strongly non-Newtonian (Bingham) fluid behaviour could result in high strengths. The gelatin was premixed with hot water and displaced into the sample under a small back pressure differential. Sample fluid volume was about 525 ml, and 1500 ml of gelatin mixture were flushed through to assure complete pore fluid replacement. The sample was chilled to 1°C to allow the gelatin to set.

5.3.2 Sample Description

Ottawa Sand (C-109) was used as the granular mineral material in the gelatin-sand tests. The pore fluid consisted of gelatin-water mixtures of various concentrations with a maximum water-to-gelatin ratio of 15 ml/gm adopted for the final six tests. The specimen saturated densities, with two exceptions, fell within the range 2.12 to 2.14 gm/cc, which corresponds to a porosity range of 30.7% to 32.3%.

5.3.3 Testing Procedure

When the gelatin was set, all pore fluid lines were closed, the cell pressure was reduced to the desired test cell pressure, and a slow, undrained test at a constant strain rate was performed. Strain rates used were 8.7×10^{-6}/sec or 22×10^{-6}/sec, with the exception of Test 2, which was failed at a rate of strain of 40×10^{-6}/sec. The pore fluid pressure and volume change could not be monitored because gelatin was used as a pore fluid.

5.3.4 Results of Testing

Table 5.1a contains the pertinent test data for the series of

TABLE 5.1 a

GELATIN-SAND TESTS

TEST NO.	n_b*	n_a*	γ_s*	T*	σ'_c*	σ_3*	u_i*	$\dot{e}$*	G*	$\left(\frac{\sigma_1-\sigma_3}{2}\right)_f^*$	$\left(\frac{\sigma_1+\sigma_3}{2}\right)_f^*$	$\left(\frac{\sigma'_1+\sigma'_3}{2}\right)_f^{*(1)}$	ϕ'_f *(1)
2	31.7	30.8	2.14	20	7.17	14.13	6.96	40	30	17.3	31.4	32.4	32.3
3	32.0	--	2.14	22	2.81	3.52	0	8.7	30	4.1	7.6	8.6	28.5
4	32.1	31.3	2.13	2	2.81	3.52	0	8.7	30	6.6	10.1	11.1	36.5
5	31.7	--	2.14	1	3.52	3.52	0	8.7	25	5.4	8.9	9.9	33.0
6	31.9	--	2.14	2	3.52	3.52	0	8.7	25	5.8	9.3	10.3	34.3
7	31.9	--	2.14	4	3.52	3.52	0	8.7	25	5.5	9.0	10.0	33.4
8	36.8	34.9	2.07	2	6.82	8.09	6.68	22	25	8.4	16.4	17.4	28.9
9	32.7	31.6	2.13	1	7.11	8.44	6.96	22	25	11.7	20.1	21.1	33.7
10	34.9	33.2	2.10	1	7.17	8.58	7.17	22	25	10.5	19.1	20.1	31.5
11	32.6	31.8	2.12	1	6.82	8.16	6.75	22	30	12.2	20.4	21.4	34.8

* Refer to Table 5.1 b

(1) Assuming pore fluid cavitation at $u = -1.0$ kg/cm^2

TABLE 5.1a(continued)

TEST NO.	n_b*	n_a*	γ_s*	T*	σ_c'*	σ_3*	u_i*	$\dot{e}$*	G*	$\left(\frac{\sigma_1-\sigma_3}{2}\right)_f^*$	$\left(\frac{\sigma_1+\sigma_3}{2}\right)_f^*$	$\left(\frac{\sigma_1'+\sigma_3'}{2}\right)_f^{*(1)}$	$\phi_f'^{*(1)}$
12	31.9	31.4	2.13	1°	7.2	14.1	6.96	22	30	17.2	28.5	29.5	35.7
14	32.3	31.7	2.13	1°	7.2	8.3	6.9	22	25	10.5	18.8	19.8	32.0
15	32.1	31.5	2.13	3°	7.03	8.4	7.03	22	25	12.8	21.2	22.2	35.2
16	32.3	31.8	2.12	2°	7.03	8.4	7.03	22	25	8.23	16.7	17.7	27.7
17	31.9	--	2.12	-	6.96	8.4	6.96	22	No Gel	15.1	23.5	24.5	38.0
19	33.0	32.3	2.12	4°	7.03								
20	32.0	31.2	2.14	4°	7.03	4.9	3.52	22	15	7.6	12.5	13.5	34.2
21	31.3	30.7	2.14	2°	7.03	4.9	3.52	22	15	8.6	13.6	14.6	36.1
22	31.9	31.2	2.14	3°	7.03	4.8	3.44	22	15	9.6	14.5	15.5	38.3
23	31.4	30.8	2.14	3°	7.03	4.9	3.52	22	15	7.5	12.4	13.4	34.0
24	32.5	31.9	2.12	3°	3.5	2.8	1.76	22	15	6.9	9.7	10.7	40.2
25	32.1	31.6	2.13	3°	3.5	2.8	1.76	22	15	5.8	8.58	9.58	37.3

TABLE 5.1b

SYMBOLS USED IN TRIAXIAL DATA TABLES

SYMBOL	UNITS	DEFINITION
n	percent	Porosity (from dry weight and dimensions)
n_b	percent	Porosity before consolidation stress
n_a	percent	Porosity after consolidation stress
γ_s	gm/cc	Saturated unit weight
T	degrees C	Test temperature
σ'_c	kg/cm^2	Maximum effective consolidation stress
σ_3	kg/cm^2	Cell pressure during test
u_i	kg/cm^2	Initial shut-in back pressure
$\dot{e}$	10^{-6}/sec	Strain rate during test
G	$\frac{ml\ H_2O}{gm\ Gel.}$	Gelatin concentration in ml H_2O /gm of gelatin powder
$\left(\frac{\sigma_1-\sigma_3}{2}\right)_f$	kg/cm^2	Maximum total deviatoric stress (failure)
$\left(\frac{\sigma_1+\sigma_3}{2}\right)_f$	kg/cm^2	Mean total stress at failure
$\left(\frac{\sigma'_1+\sigma'_3}{2}\right)_f$	kg/cm^2	Mean effective stress at failure
ϕ'_f	degrees	Secant angle of friction at failure (at maximum deviatoric stress)
$\frac{\sigma'_1}{\sigma'_3}\ _f$	---	Maximum effective stress ratio
e_f	percent	Axial strain at failure
k	cm/sec	Axial permeability
BD	gm/cc	Bulk density (oil sand) (pre-test)
Oil	percent	Oil content (post-test)
σ'_{3f}	kg/cm^2	Effective confining stress at failures
ΔV_f	percent	Volume change at failure
A	---	Pore pressure parameter "A"

gelatin-sand triaxial tests. The porosities in the second column were calculated directly from the volume-weight data, whereas the porosities in the third column were calculated with the assumption that fluid efflux during consolidation was due only to specimen compression. The true test porosity must lie within these two values. The saturated bulk density was calculated directly from the porosity data; a quartz specific gravity of 2.65 was assumed. The temperature reported is the mean internal cell temperature during testing.

The failure data should be commented on, since data in the final two columns were calculated under an assumption of pore fluid cavitation at -1.0 kg/cm^2. A hot mixture of gelatin and water was used to displace the pore water, and the air pressure system used to provide the motive pressure probably resulted in considerable dissolving of air. Cavitation likely occurred at pore fluid pressures above -1.0 kg/cm^2; therefore the reported value of $\frac{\sigma_1 + \sigma_3}{2}$ is too high, and the value of $\frac{\sigma_1}{\sigma_3}$ is too low. The assumption of cavitation at -1.0 kg/cm^2 provides a measure of the minimum effective stress ratios which could have occurred during testing, and is employed only to permit comparison to Tests 20 to 25, in which careful de-airing was enforced. For Tests 20 to 25 inclusive, pore water was preboiled to remove dissolved air, and the pressures employed during flushing with the gelatin solution were much lower than those of the previous tests (1.0 kg/cm^2 maximum). A Mohr-Coulomb failure stress plot of these final six tests is presented in Figure 5.1. The effective stress circles presented assume cavitation occurred at -1.0 kg/cm^2.

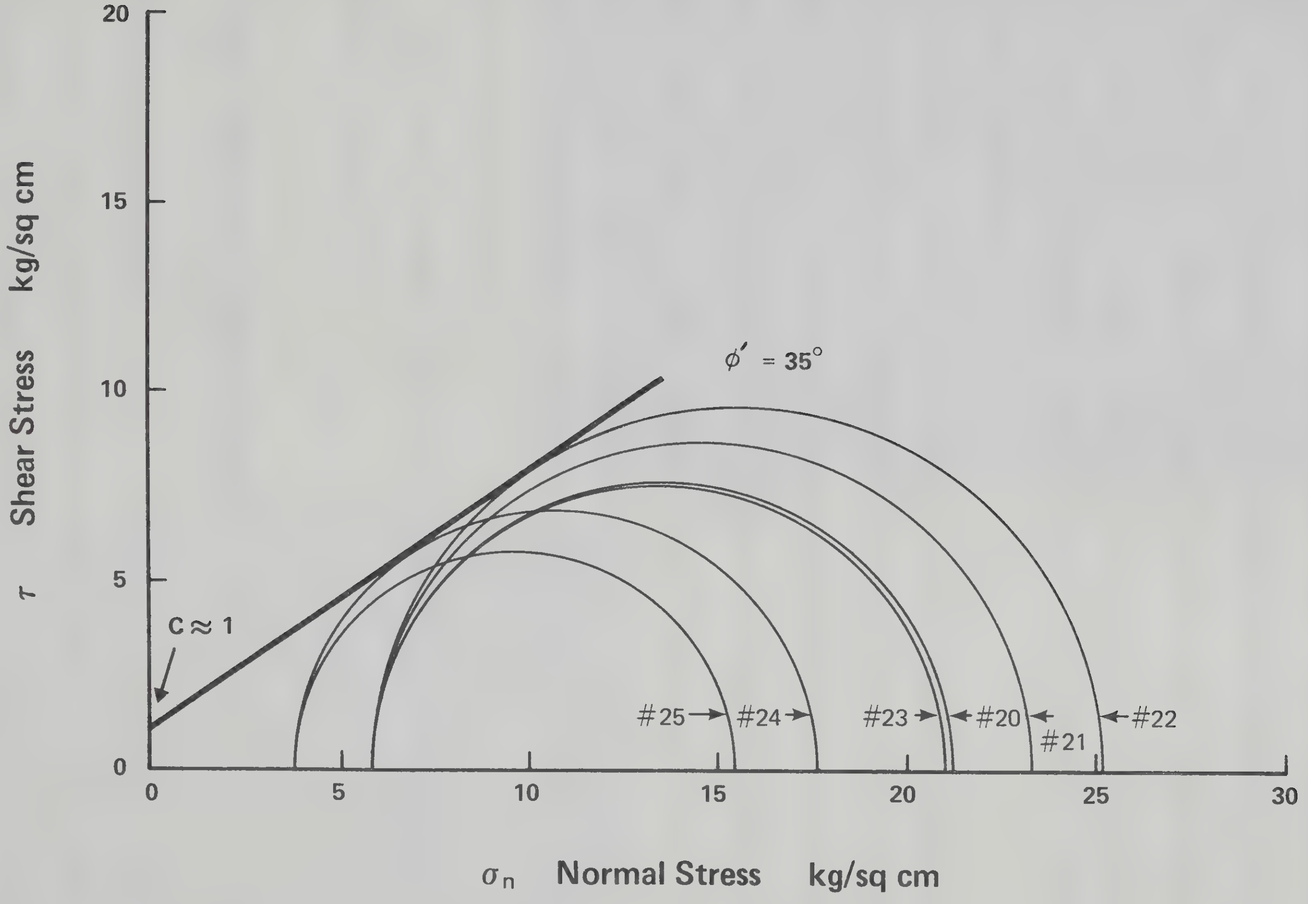

Figure 5.1. Mohr-Coulomb Plot for Gel-Sand Tests # 20 to # 25 (Assuming $\mu_f = -1.0$ kg/sq cm)

5.3.5 Conclusions

Strength envelopes are no steeper, nor are apparent cohesions any greater than those of normal, dense sands. Assuming a linear failure envelope, a cohesion intercept of 1.0 kg/cm^2 and a ϕ of 35° are obtained. Increasing the gelatin concentration and varying the stress history after gelatin setting have no effect on strength; therefore the cohesion intercept is not a result of "locked in" stresses or of true cohesion.

The use of gelatin as a pore fluid provided some unexpected and unusual information. Prefailure cavitation resulted in the inclusion of lines of minute air bubbles coinciding with the lines of maximum dilative behaviour. These lines are clearly visible in Plates 5.1 and 5.2. They indicate that general dilative behaviour occurs before a single plane becomes the preferential failure plane. This reflects the homogeneous and isotropic nature of a dense, artificially compacted quartzose sand.

This test series provided the basis for the remainder of the laboratory program.

5.4 Dense Ottawa Sand Triaxial Tests

5.4.1 Sample Preparation

Samples were prepared as described in Section 5.3.1 with the exception that specimen pore water was not displaced by gelatin. De-aired water was used to prevent cavitation of pore fluid except at very low pressures.

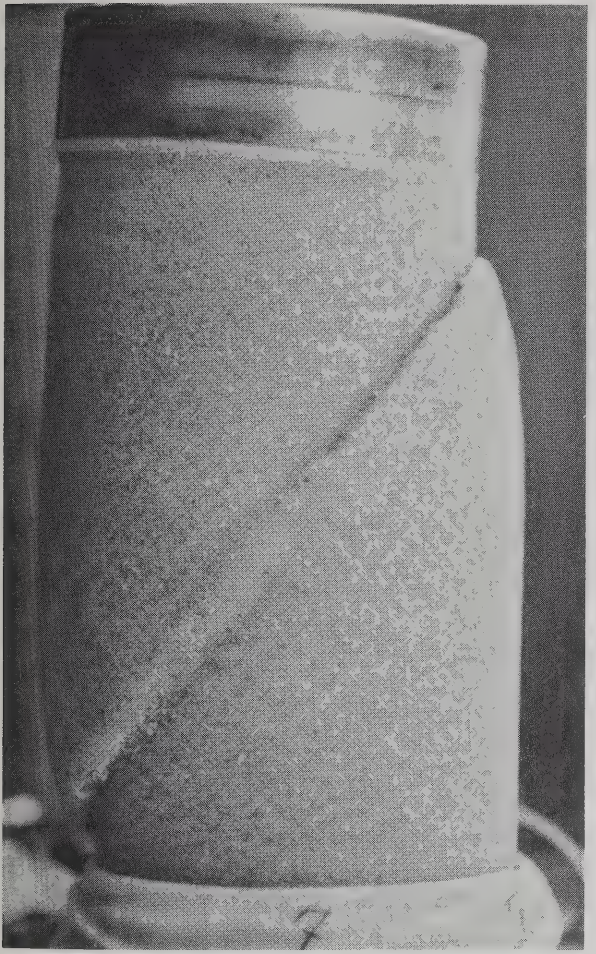

PLATE 5.1 Gelatin Sand Test #7. Development of a net of potential failure surfaces.

PLATE 5.2 Gelatin Sand Test #24. Gross movement has occurred along three elliptic planes, one of which is the major failure plane.

[illegible]

[illegible]

5.4.2 Sample Description

Six tests were performed on specimens with calculated saturated bulk densities varying from 2.09 to 2.14 gm/cc. With careful preparation, densities greater than 2.12 gm/cc could be achieved. All specimens had diameters of 10.05 cm and heights of 20.2 to 20.7 cm. The sand used was Ottawa Sand C-109, a well-rounded, well-sorted, competent quartz sand.

5.4.3 Testing Procedure

After specimens were mounted in the triaxial cells, they were subjected to an effective consolidation stress. The pore water pressure and the cell pressure were adjusted to the desired test values; the pore water pressure was shut in; and the specimens were failed in an undrained state at a constant strain rate with continual monitoring of pore water pressure. To assess the tendency of a dense sand to reduce pore water pressure, the test cell and shut-in back pressures varied from 16.2/12.6 kg/cm^2 to 2.8/1.8 kg/cm^2.

5.4.4 Results of Testing

All stresses and failure data are reported in terms of effective stress, as the test technique permitted assessment of pore fluid pressure. Values of secant ϕ at failure and effective stress ratios at failure are reported in Table 5.2, and the effective stress conditions at failure are plotted as semicircles on a stress diagram to provide a Mohr-Coulomb failure envelope (Figure 5.2). The maximum effective stress ratios decrease and the strains to failure generally increase as confining stress (σ_3) increases.

Appendix E.2.1 reports in detail the relationships between

TABLE 5.2

UNDRAINED TRIAXIAL TESTS: DENSE OTTAWA SAND

TEST NO.	n*	γ_s*	σ_c'*	u_i*	$\left(\frac{\sigma_1-\sigma_3}{2}\right)_f$*	$\left(\frac{\sigma_1'+\sigma_3'}{2}\right)_f$*	ϕ_f'*	$\frac{\sigma_1'}{\sigma_3'}{}_f$*	e_f*
26	31.4	2.13	7.03	7.03	15.2	24.3	38.8	4.35	5.98
27	31.5	2.13	7.03	3.52	9.98	15.5	39.9	4.58	3.24
28	31.2	2.14	3.52	1.76	6.39	9.68	41.3	4.88	3.56
29	32.8	2.11	7.03	12.6	24.1	41.0	36.0	3.86	4.90
30	32.2	2.12	7.03	10.5	22.1	36.9	36.9	4.00	5.22
31	34.1	2.09	14.1	12.7	20.8	36.6	34.6	3.63	6.87

* Refer to Table 5.1b

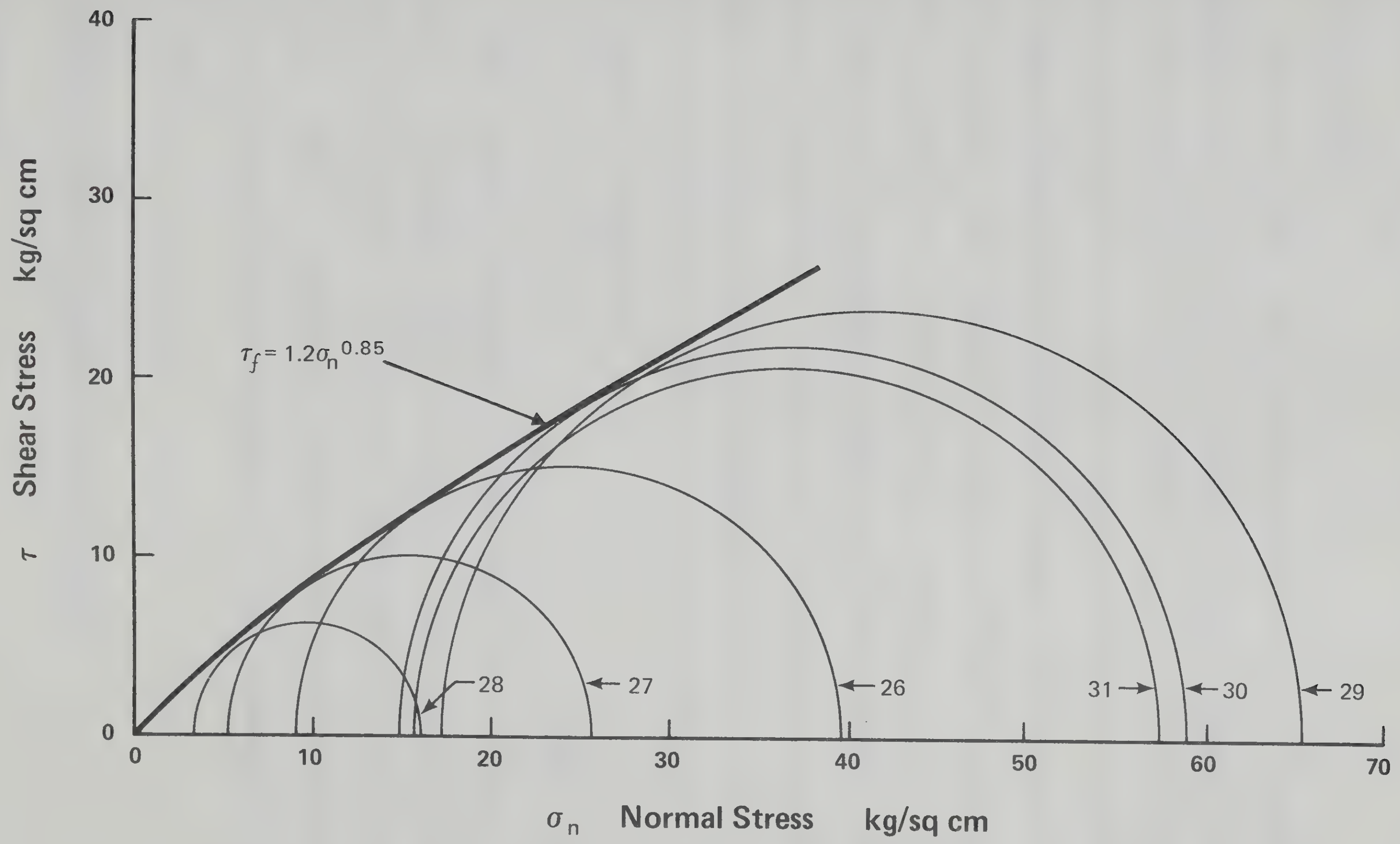

Figure 5.2. Undrained Triaxial Tests: Dense Ottawa Sand

axial strain and measured values of deviatoric stress, pore pressure, effective stress ratio, and the "A" parameter.

5.4.5 Conclusions

Given the minor, unavoidable scatter of data as a result of specimen density variation, the behaviour of this material is precisely that expected of a dense quartzose sand. Cell pressures as high as 16.2 kg/cm^2 with a shut-in back pressure of 12.6 kg/cm^2 did not prevent a reduction of pore water pressure to the point of cavitation initiation. This behaviour is a result of the individual grain competence and the high initial densities (Seed and Lee, 1967).

The failure envelope in Figure 5.2 is deliberately drawn as a curvilinear relationship. The extension of the envelope to the origin is fully justified as the saturated sand exhibits no strength at zero normal stress. The failure envelope corresponds closely to a power law curve with the formula:

$$\tau_f = 1.12 \cdot \sigma_n^{0.85} \qquad \text{Equation 5.1}$$

This equation represents a drawn tangent to the Mohr's circles. It should be emphasized that this equation, and all other equations of this type generated in this work, are phenomenological equations; they do not imply a fundamental relationship. Envelope curvature is directly related to the suppression of dilative behaviour as stress level rises.

5.5 Triaxial Tests on Densified Tailings Sand

5.5.1 Sampling

Tailings sand was obtained from a small tailings pond at the

Syncrude Canada Limited oil sands extraction pilot plant located in Edmonton. The process sand was shipped to Edmonton from an open pit mine 50 km north of Fort McMurray; most of the oil was removed during processing; and coarse-grained tailings were sludged into a pond for settling. Portions from several zones of the tailings pond were mixed to provide a representative sample for specimen preparation.

5.5.2 Sample Preparation

The tailings sand contained 5% to 10% water and approximately 0.5% residual bitumen. The bulk sample was dried, the remaining bitumen was removed by reflux extraction with trichloroethylene, and the sample was oven dried at 100°C to remove all traces of the solvent.

Triaxial specimens were prepared by the methods used in the previous two test series. The sand was premoistened by thorough mixing with boiling water before sedimentation and densification.

5.5.3 Sample Description

The tailings sand tested was obtained from the "oil-saturated" portion of the McMurray Formation, and therefore it displays the grain characteristics of that deposit. A representative grain size curve is presented in Appendix E.2.2; it is characteristic of a well-sorted, fine-grained sand. The individual grains displayed a wide range of grain roundness varying from rounded to very angular. The sand was 98% to 99% quartz, and the dominant accessory mineral was muscovite.

All triaxial specimens were 10.05 cm in diameter with length-to-diameter ratios slightly greater than 2.0. Saturated bulk densities varied from 2.03 to 2.05 gm/cc. These densities are less than those achieved in the Ottawa Sand triaxial tests; the density difference is

due primarily to the angularity of the oil sand grains.

5.5.4 Testing Procedure

The densified tailings sand specimens were saturated by applying an appropriate back pressure, an effective consolidation stress was applied, and the cell and pore water pressures were adjusted to the levels desired for testing. The pore water pressure was shut in, undrained tests were performed at a constant strain rate, and cell fluid volume change was measured.

5.5.5 Results of Testing

Table 5.3 summarizes test data, with the failure data presented in terms of effective stresses. Failure shear plane angles were about 63°, and the values of the maximum effective stress ratio and the secant ϕ decreased as the confining stresses increased. Failure strain was greater than that from tests on densified Ottawa Sand, and the failure strain increased as the confining stress increased. Figure 5.3, a plot of the effective stress conditions at failure, shows that a linear envelope is not justifiable. The curvilinear envelope may be approximated by a power law relationship:

$$\tau_f = 1.12 \cdot \sigma_n^{0.89} \qquad \text{Equation 5.2}$$

This phenomenological relationship is justifiable only in the range of confining pressures used for testing, and only because the tested material is completely cohesionless. The relationships between stress and strain, and other individual test data, are reported in Appendix E.2.2.

5.5.6 Conclusions

The behaviour of densified tailings sand is that of a dense

TABLE 5.3

UNDRAINED TRIAXIAL TESTS: DENSIFIED TAILINGS SAND

TEST NO.	n*	γ_s*	σ_c'*	σ_3*	u_i*	$\left(\frac{\sigma_1'-\sigma_3'}{2}\right)_f^*$	$\left(\frac{\sigma_1'+\sigma_3'}{2}\right)_f^*$	ϕ_f'*	$\left(\frac{\sigma_1'}{\sigma_3'}\right)_f^*$	e_f*	COMMENTS
T-1	37.6	2.03	8.45	10.68	5.27	16.4	27.2	37.1	4.03	8.48	β=63°
T-2	37.9	2.02	7.60	---	--	---	---	----	---	----	Membrane rupture
T-3	36.1	2.05	7.60	14.64	7.04	26.0	41.5	38.8	4.35	7.94	β=59° to 67°
T-4	36.2	2.05	3.53	7.07	5.27	15.3	23.1	41.5	4.91	5.56	
T-5	37.3	2.03	3.50	5.10	3.40	11.8	17.6	42.1	5.04	5.13	Density data inaccurate β = 64.5°
T-6	37.2	2.04	7.04	13.7	12.4	22.4	36.7	37.6	4.13	7.48	Bulge failure

* Refer to Table 5.1b

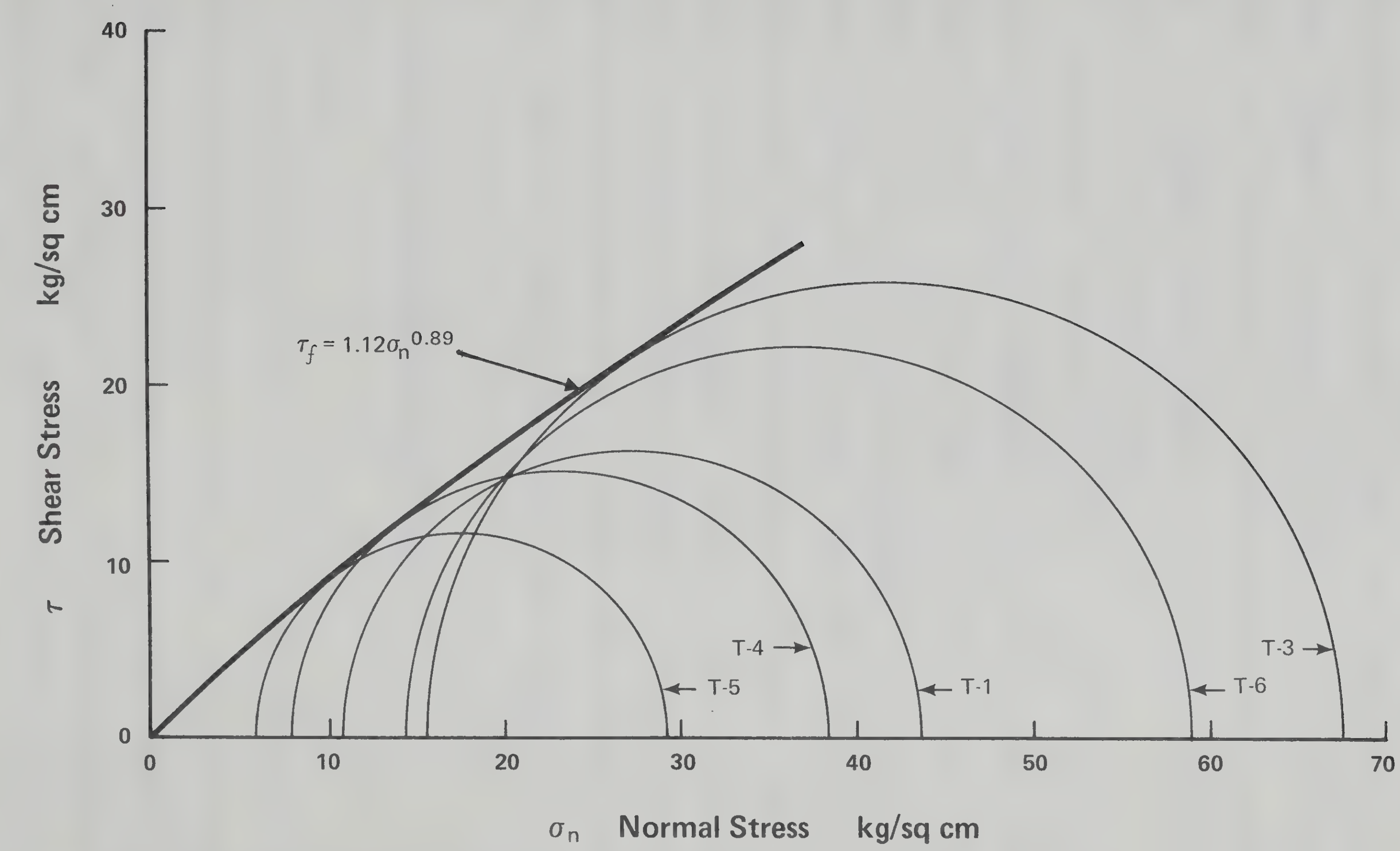

Figure 5.3. Undrained Triaxial Tests on Densified Tailings Sand

quartzose sand. Regardless of the initial shut-in back pressure, pore water pressure in the tailings sand was reduced to the point of cavitation, generally at a pressure of about -0.7 kg/cm^2. The maximum angle of shear resistance is precisely that expected for a fine-grained, subangular, dense quartzose sand: a maximum of about 41° (e.g. Bishop, 1966). The envelope curvature again is due to a suppression of dilative behaviour as confining stress increases.

No additional component of strength resulting from angularity or rugosity of grains has been observed in the data on oil-free sands. The densities obtained with the compactive effort employed are considerably less than those which exist _in situ_. The minimum specimen porosity obtained was 36.1%, although geophysical logs report _in situ_ mean porosities of 29%, calculated from density log data for a similar material (assuming a quartz specific gravity of 2.65, saturated conditions, and a bitumen density of 1.0 gm/ml). It is impossible, without considerable grain crushing, to repack the grains from oil sand to a density as great as that which exists _in situ_.

5.6 Triaxial Tests on Recompacted Oil Sand

5.6.1 Sampling

The oil-rich fine-grained sand used in this test series was obtained from the Syncrude Canada Limited pilot plant, which also provided the fine-grained tailings sand used in the previously described tests. The sample was obtained in a completely disaggregated and blended state and was stored in a sealed container to prevent further moisture loss.

5.6.2 Test Specimen Preparation

Any apparent lumps or pieces of concretions, clay clasts, or limestone were removed from the oil-rich sand by hand, and the raw sand was compacted in a kneading compactor using a one-piece 10.16 x 20.3 cm cylindrical stainless steel mould.

Ten to twelve lifts were used during the sample compaction: a four centimeter initial lift, then a series of 1.5 cm lifts to the full height. Ram pressures used were low (10 kg/cm^2 maximum) because the oil-rich, fine-grained, well-sorted sand tended to extrude from under the ram foot at higher pressures. The compaction of each layer required low initial pressure (two kg/cm^2) gradually increasing to the maximum pressure. A heated ram foot (80° to 90°C) was used throughout the procedure to minimize sticking of the oil sand during compaction. The final lift, after compaction at 10 kg/cm^2, was levelled by continuing the compaction process using gradually diminishing pressures until a flat surface was obtained. A static stress of 30 kg/cm^2 was applied over the entire sample area for one minute using a close-fitting metal disc to prevent side extrusion. The mould, with the top and bottom discs in place, was stored in a cold room at -2°C for 24 hours under a static stress of 0.87 kg/cm^2. This chilling was necessary to permit sample extrusion from the compacting mould without specimen damage.

Once extruded, the specimens were measured, weighed, and enclosed in a latex rubber membrane coated internally with a thin layer of silicon high-vacuum grease to ensure an excellent side seal. Sliced latex membranes were inserted between the specimen ends and the Teflon porous end plates to minimize clogging of the plate by bitumen, while

providing adequate end drainage.

5.6.3 Sample Disturbance

The process described in the previous section resulted in uniform specimens 10.16 cm in diameter and 20.0 cm in length; that is, with a length/diameter ratio of 1.97. As sampled, the material contained (on a total weight basis) 84.4% solid mineral matter, 13.7% bitumen, and 1.9% water. The amount of desiccation which had occurred to that point is not known. The grain size curve obtained from several analyses of this material is presented in Appendix E.2.3.

The density values were calculated by determination of volume before testing and of total weight after testing, since pretest saturation had been accomplished by back pressure. Densities ranged from 2.06 to 2.11 gm/cc, although the latter figure is anomalous and may be somewhat in error. Densities of 2.06 to 2.08 gm/cc were achieved readily by the compactive process.

5.6.4 Testing Procedure

The specimens were mounted in a triaxial cell, subjected to a confining pressure (σ_3), cooled to a temperature of about 4°C, and subjected to a high back pressure until saturation was considered complete. Constant head axial permeability tests at high internal gradients ("i" of 50 cm/cm) were performed on the specimens.

A pore fluid back pressure was shut in, the test temperature was held constant at about 4°C, and an undrained test was performed with continual pore pressure monitoring. Appropriate strain rates were used to ensure at least 95% pore pressure equalization as estimated from the permeability data. Volume change measurements

were not made: the volume change characteristics after cavitation of pore fluid were considered to be similar to those of the redensified tailings sand, as the grain size distribution and the degree of compaction achieved were similar.

Post-failure moisture contents and oil contents were determined. It was assumed that saturation had been achieved before testing; therefore these moisture and oil contents were used to calculate a specimen pretest porosity. No change in moisture content could have occurred during testing since the tests were performed with no drainage.

5.6.5 Results of Testing

Table 5.4 presents the most pertinent test data; Figure 5.4 is a plot of the effective stress circles at maximum deviatoric stress. Test results are similar to those of the triaxial series on redensified tailings sand. The best-fit power law relationship to the Mohr-Coulomb failure envelope is expressed by the equation:

$$\tau_f = 1.13 \cdot \sigma_n^{0.88} \qquad \text{Equation 5.3}$$

This indicates no significant difference from the relationship derived from the oil-free tailings sand tests.

The major difference in the two test series was the failure mode: bulging failure occurred five of six times in this test series, but only once in the previous series on redensified tailings sand.

Permeabilities of the recompacted oil-rich sand ranged from 35.7×10^{-7} to 1.4×10^{-7} cm/sec. A value of 10×10^{-7} cm/sec is considered an appropriate estimate of permeability in a recompacted state. The low permeabilities made it impossible to remove all pore fluid containing dissolved gas by repeated specimen flushing; therefore

TABLE 5.4

UNDRAINED TRIAXIAL TESTS: RECOMPACTED PIT RUN OIL SAND

TEST NO.	* n	* BD	* T	OIL	H_2O	* σ'_c	* σ_3	* u_i	* $\left(\frac{\sigma_1-\sigma_3}{2}\right)_f$	* $\left(\frac{\sigma'_1+\sigma'_3}{2}\right)_f$	* ϕ'_f	* $\frac{\sigma'_1}{\sigma'_3}\ f$	* e_f $\left(\frac{\sigma_1-\sigma_3}{2}\right)_m$	$\left(\frac{\sigma'_1}{\sigma'_3}\right)_m$	* k X10-7	COMMENTS
T-50	32.7	2.11	3°	13.5	2.5	7.12	14.06	7.04	19.15	32.76	35.8	3.81	8.17		5.6	Shear failure 65°
T-51	35.8	2.06	3°	13.3	3.3	10.5	10.70	5.50	13.95	23.9	35.7	3.80	6.19		1.4	Bulge failure
T-52	36.1	2.05	3°	13.5	3.3	---	ELECTRONICS BREAK DOWN				---	----	----		---	Bulge failure
T-53	35.9	2.06	4°	13.4	3.9	5.3	7.05	3.52	9.68	16.4	36.2	3.99	7.7	4.4	35.7	Bulge failure
T-54	35.9	2.06	4°	13.4	3.7	3.50	3.50	1.73	6.46	9.98	40.3	4.74	7.0	4.8	13.5	Bulge failure
T-55	34.7	2.08	7°	13.4	3.4	5.3	7.03	3.46	12.16	19.14	39.4	4.51	7.0	4.9	7.6	Bulge and Shea failure

* Refer to Table 5.1b

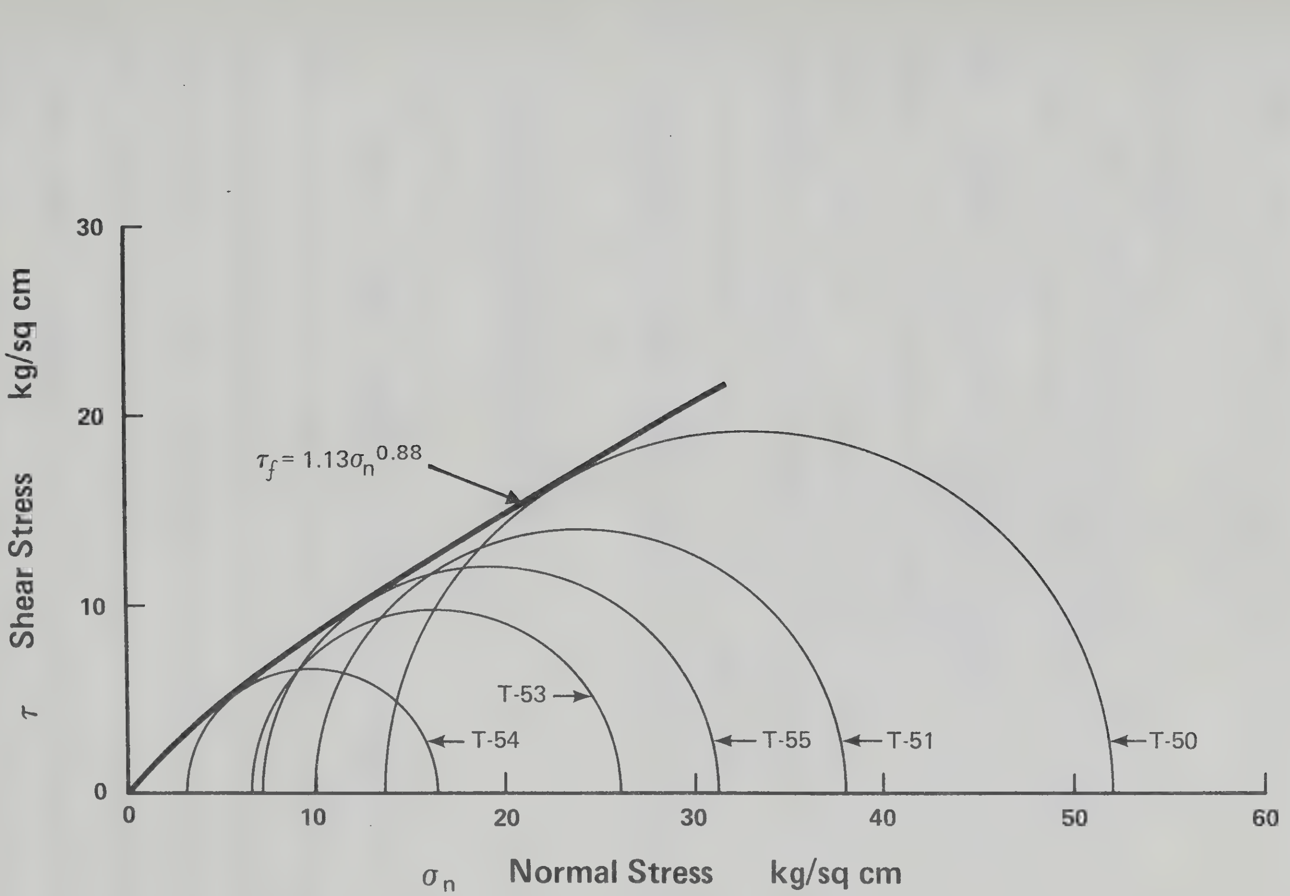

Figure 5.4. Undrained Triaxial Tests on Recompacted Oil-Rich Sand

the specimens tended to cavitate at pore fluid stresses somewhat higher than atmospheric pressure (0.5 kg/cm^2).

Appendix E.2.3 reports individual stress-strain curves as well as other pertinent data not found in Table 5.4.

5.6.6 Conclusions

The bitumen-rich recompacted oil sand acted as a dense quartzose sand; the interstitial bitumen did not contribute in any way to shear strength, even though bitumen temperatures during testing were lowered to 4°C. The porosities obtained in this test series were slightly lower than in the previous test series, probably because of the different compactive method used, and because of the assumption of a bitumen density of 1.0 gm/ml for calculations. The actual density of the bitumen may have been slightly different from this value.

5.7 Triaxial Tests on Oil Sand

5.7.1 Sampling

All oil sand specimens tested during the course of the laboratory investigations of shear strength were obtained from a continuously cored borehole located 50 km north of Fort McMurray. Seven cores, each 6.1 m long, were obtained beginning at a depth of about 30 m. Borehole refrigeration techniques were employed in an effort to reduce sample expansion, and the core was transported carefully and stored in a chilled state before specimen selection and preparation. Further details of the sampling program may be found in Appendix F.

5.7.2 Sample Preparation

The core, in lengths of about 150 cm, was stored in the specimen preparation room at temperatures between -14°C and -18°C. It had been determined that, despite the precautions taken, coarse-grained oil-rich core had expanded a minimum of 12%; and therefore strength testing for the most part was confined to those portions which had undergone the least expansion, i.e., fine-grained oil-poor to oil-rich sand. The selection was based on a rough interpretation of the geophysical borehole logs available for the cored interval (Appendix G); most specimens were from the Upper Member of the Formation.

Use of fine-grained oil sands resulted in some difficulties; the inherent variability of the Upper Member of the McMurray Formation made it impossible to obtain four or five uniform 18 cm long specimens for triaxial testing. Upon opening a 150 cm section of core liner, zones of differential expansion usually were discovered; oil-rich fine-grained sand had expanded considerably, whereas adjacent oil-poor fine-grained silty sands had expanded very little, resulting in corrugated core lengths. Separation of the core along bedding planes had also taken place, with each 150 cm core section containing perhaps two or three such separations. A uniform specimen about 28 cm long was required to obtain a high-quality 18 cm specimen; therefore much of the fine-grained core could not provide adequate specimens. The triaxial testing program had to be limited to performing a series of comparative triaxial tests which assessed general behaviour rather than attempting to obtain failure data over a wide stress range.

Specimens were trimmed on a lathe at low temperatures. Descriptions of equipment and procedure are lengthy, but important, and are

summarized in Appendix B. The procedure yielded uniform right cylinders with square parallel ends, a diameter of 7.6 cm, and a length/diameter ratio of 2.1 to 2.6. Three measurements of length, nine measurements of diameter, and total weight values were obtained for each specimen.

5.7.3 Testing Procedure

The chilled specimens (-15°C) were mounted in the normal manner without side drains on a triaxial cell base modified to accomodate 7.62 cm diameter specimens. To prevent possible sample expansion during the filling of the triaxial cells with warm water (17°C), the specimens were assembled completely in a cold room (-15°C), and 3.0 kg/cm^2 air pressure was introduced into the cell. The cell assembly was brought to the testing laboratory, and cell water was introduced against the 3.0 kg/cm^2 air pressure until the cell was filled. The cell was mounted in the loading frame and a pore fluid pressure was applied in an attempt to saturate the specimens. The difference between the confining stress and the pore fluid stress was generally about 1.0 kg/cm^2; a pore fluid stress of 2.0 to 3.0 kg/cm^2 was employed to achieve saturation.

Specimens were permitted to reach equilibrium with respect to both temperature and pore fluid ingress; for some of the fine-grained specimens, equilibrating pore fluid flow required up to three days. After specimen pressures were stable, some specimens were subjected to an excess effective stress to assess the consolidation characteristics. After consolidation testing, permeability tests were performed on several of the specimens to provide a check on the consolidation data. The pore fluid stress and the cell pressure were adjusted to

the desired test levels, the specimens were allowed to reach equilibrium, and testing followed in either a drained mode with constant back pressure or an undrained mode with measurement of pore fluid stress. Several specimens were tested in a refrigerated triaxial cell (1^{o} to 5^{o}C) to assess temperature effects.

For a specimen of low permeability (e.g. Test 129, Table 5.5a), the procedure from mounting, to assessment of consolidation properties and permeability, to triaxial testing, required 21 days. Notwithstanding the relatively low values of compressibility coefficients, test strain rates employed were deliberately very low. This ensured pore fluid equalization with respect to flow (drained tests) or to stress (undrained tests).

5.7.4 Test Results

Table 5.5a presents the most important test and failure data; Figure 5.5 delineates the relationship between maximum effective stress ratio and normal stress; Table 5.5b reports permeability values, coefficients of consolidation and coefficients of compressibility for three selected tests; and Appendix E.2.4 contains stress-strain curves, grain size data, failure plane sketches, and other pertinent test data.

Although there is a large scatter of stress circles on the Mohr-Coulomb plot, a probable upper bound envelope has been sketched. This envelope corresponds very closely to a power law equation:

$$\tau_f = 2.80 \cdot \sigma_n^{0.84} \qquad \text{Equation 5.4}$$

Secant ϕ values and effective stress ratios increase as confining stress decreases. The failure strains show a general increase as effective confining stress increases, but the total strain to failure

TABLE 5.5

TRIAXIAL TESTS ON ATHABASCA OIL SANDS

SAMPLE NUMBER (DEPTH)	BD *	OIL *	TEST TYPE *	σ_3 *	u_i *	$\dot{e}$ *	$\left(\frac{\sigma_1'-\sigma_3'}{2}\right)_f$ *	$\left(\frac{\sigma_1'+\sigma_3'}{2}\right)_f$ *	σ_3' f *	e_f *	ϕ_f *	$\frac{\sigma_1'}{\sigma_3'}_f$ *	ΔV_f *	"A" *	COMMENTS
109	2.03	6	Undr.	7.03	3.37	1.16	21.02	26.7	5.7	3.1	51.9	8.4	10.3	-.05	Mostly fine sand
117	2.053	12.4	Drained 24°C	8.03	4.00	28.8	30.1	34.2	4.03	1.9	61.9	15.9	10.5	---	Fine-gr. oil-rich silty sand
124	1.990	11.1	Drained 3°C	7.04	0.0	---	13.7	20.7	7.04	6.2	41.4	4.9		---	Fine-gr. sand
129	2.068	10.0	Drained 4°C	2.90	2.00	0.87	11.17	12.07	0.90	1.5	67.7	25.7	+1.43	---	Fine-gr. silty sand, variable saturation
130	2.190	2.7	Drained 2°C	3.01	2.00	0.87	6.39	7.40	1.01	1.7	59.8	13.7	0.1	---	Lean fn.-gr. silty sand, X-bedded
133	2.238	<1.0	Undr. 3°C	8.33	3.46	1.6	15.23	17.10	1.87	1.5	64.4	19.3	---	0.13	42.3° cross-bedded fine-gr. sand
173	1.92	15% in Sand	Drained 5°C	14.8	1.06	~100	16.3	30.0	13.7	8.4	33.0	3.4	---	---	1/3 clay clast breccia -failed in clay
209	1.86	14.6	Drained 25°C	4.0	3.0	5.2	2.57	3.54	1.0	4.3	45.9	6.1	+0.1	---	Coarse-Gr., rich, uniform sand (Bulge)

* Refer to Table 5.1b

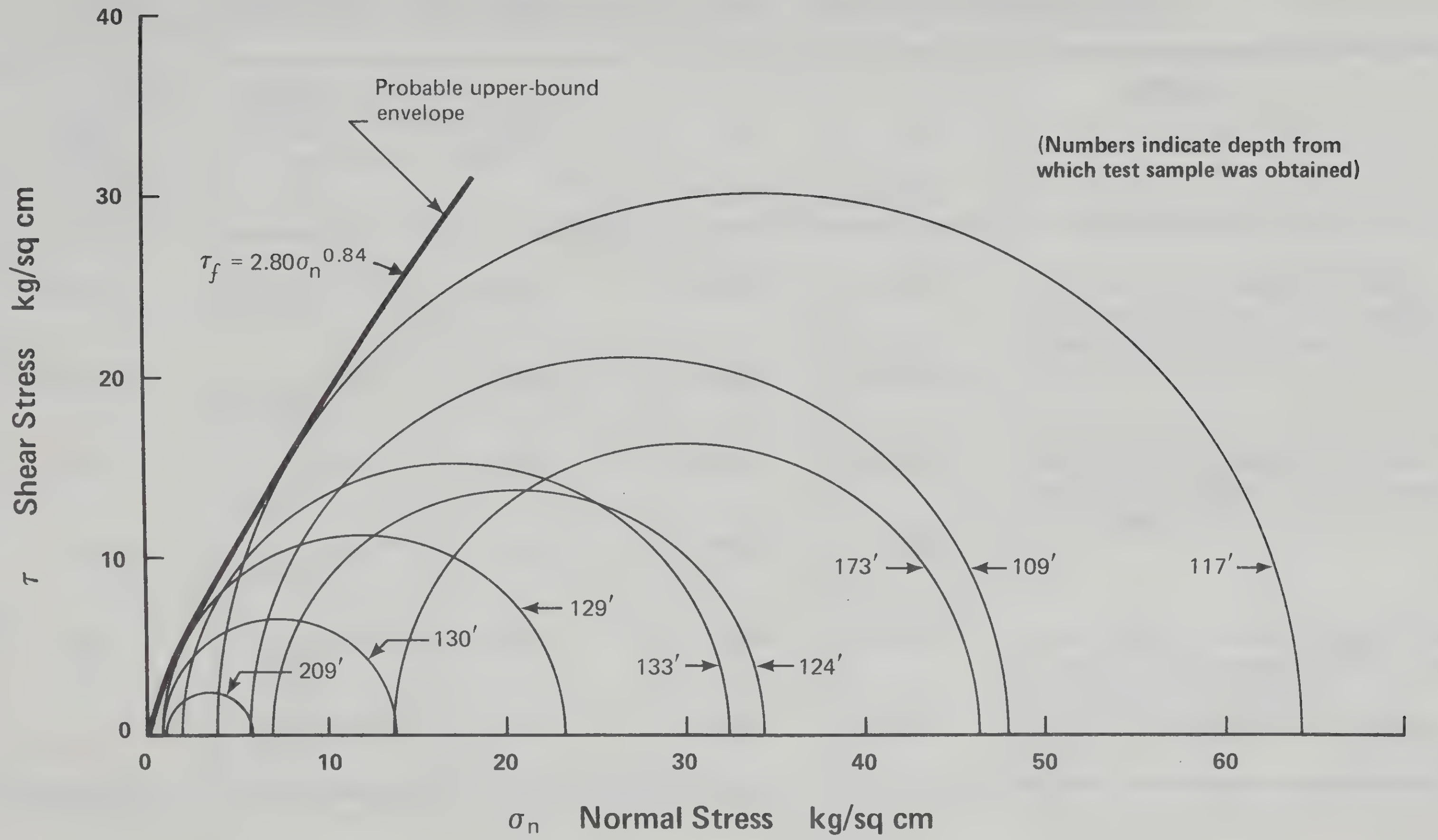

Figure 5.5. Triaxial Tests on Athabasca Oil Sand

TABLE 5.5b

TYPICAL PERMEABILITY AND COMPRESSIBILITY DATA: OIL SAND TRIAXIAL TESTS

SAMPLE	EFFECTIVE STRESS CHANGE (kg/cm^2)	PERMEABILITY cm/sec. (Δp-kg/cm^2)	C_v $cm^2/sec.$ (from t_{100})	(1) m_v cm^2/kg	(2) m_v cm^2/kg	COMMENTS
Triaxial Test 117'	1--5	7.0×10^{-8} (0.5)	0.125	0.00056	0.00063	-High quality sample, fine-grained, little oil, swell upon sampling approximately 6%
	5--9	7.0×10^{-8} (0.5)	0.098	0.00071	0.00055	
Triaxial Test 129'	4--6	3.15×10^{-8} (1.0)	0.044	0.0072	0.00078	-High quality sample, fine-grained, little oil, 6% swell upon sampling
	6--10	3.05×10^{-8} (1.0)	0.038	0.00083	0.00068	
Triaxial Test 209'	1--3	5.25×10^{-6} (0.5)	0.24	0.0194	0.0018	-Low quality sample, swell at least 12% (probably 20%) coarse-grained, oil-rich (Note differences in values of m_v)
		5.25×10^{-6} (0.5)	0.36	0.0145	0.0013	

(1) m_v calculated from $m_v = \frac{k}{\gamma \cdot C_v}$

(2) m_v calculated from $m_v = \frac{\Delta e}{(1+e_o) \cdot \Delta\sigma}$

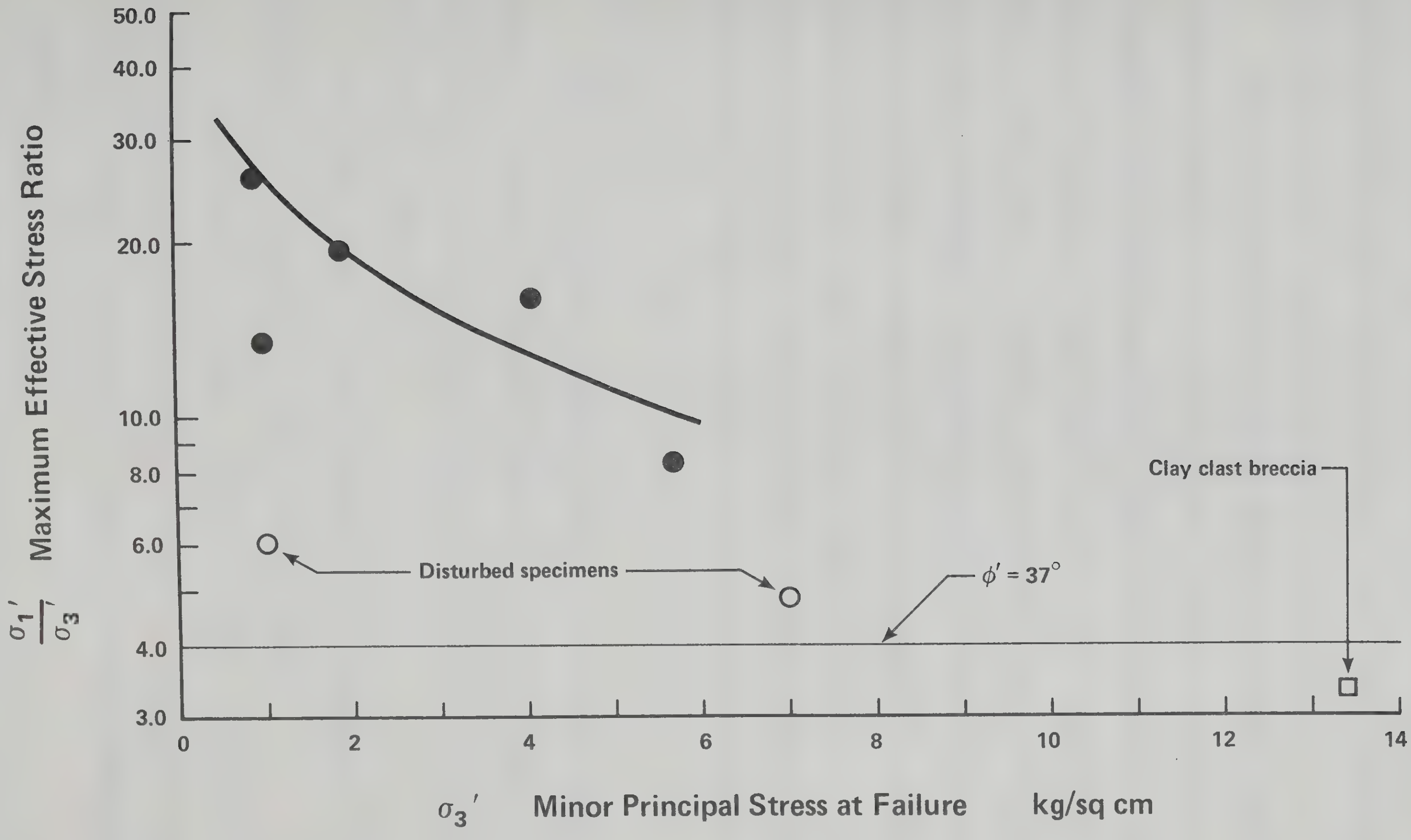

Figure 5.6. Confining Stress versus Maximum Effective Stress Ratio - Oilsand Triaxial Specimens

is approximately one-third that of the redensified oil sand, the densified tailings sand, or the Ottawa Sand. Drained tests on high quality specimens indicate that the volumetric strain before failure was small: about one-tenth that of a normal dense uniform sand.

No relationships are apparent between grain size and strength, or between bitumen content and strength. Tests 124 and 209, performed on materials which had experienced considerable expansion, displayed lower peak strengths, higher failure strains, and higher porosities than the other tests. Test 173, performed on a specimen consisting of one-third lithoclastic conglomerate and two-thirds oil-rich medium-grained sand, failed almost entirely in the clay-rich portion: no strain in the sand could be detected except for small portions of the numerous failure planes adjacent to the clay clast zone. No additional strength due to testing in a chilled state (1^{o} to 5^{o}C) could be detected.

5.7.5 Conclusions

The large degree of scatter evident in test data led to one important conclusion: shearbox testing on small specimens would prove more valuable than triaxial testing, as sample uniformity could be more closely controlled.

The extension of the Mohr-Coulomb failure envelope to the origin of the axes is justified for the following reasons:

1. Specimens of oil-free sandy silts from a borehole depth of 42 m were immersed in water for 24 hours: they disaggregated almost totally, indicating the absence of stress-independent cohesion.
2. Outcrop samples from the oil-free portions of the McMurray

Formation (60 km east of Fort McMurray) displayed no significant cohesion in a saturated state.

3. The insight afforded by the extensive series of shearbox tests (Section 5.9) justified an assumption of no cohesion.

Dilative behaviour in these specimens was not as pronounced as in the densified tailings sand tests; it must be concluded that dilation occurred largely within a narrow plane, obscuring the effects of dilation when compared with the relatively large specimen volume (800 cc). Nevertheless, the extreme steepness and the curvature of the failure envelope can be explained only in terms of high dilatancy due to granular interlock, and a progressive suppression of this dilatancy as effective confining stress increased. Stress-strain curves (Appendix E.2.4) show that at low stresses, post-failure stress reduction may be abrupt; residual strength is reached after a total strain about twice the value of the failure strain. This extreme decrease in strength can be explained only through a disruption of structure.

Tests 124 and 209 demonstrate clearly the effect of structure change through excessive expansion: very low strengths compared to the other triaxial tests at similar confining stresses. Because all specimens have been altered somewhat by the sampling procedure and are therefore less than perfect, the strength envelope presented may be considered as a lower limit: _in situ_ strength must be equal to or higher than the values reported herein.

5.8 Shearbox Tests on Densified Ottawa Sand

To provide comparable strength and dilatancy data for shearbox tests on oil sands, 13 direct shear tests were performed on Ottawa

Sand: 12 in a very dense state, and one in a loose state.

5.8.1 Test Specimen Preparation

The 12 dense specimens were prepared in specially constructed circular shearboxes equipped with screw-fastened porous bronze bases and top caps loosely sealed against the shearbox sides by O-rings (Appendix C; Figure C.2). The dry sand was densified on a vibrating table, with concomitant shock loading using a wooden mallet, and by application of a varying normal load (also during vibration) of up to 1.5 kg/cm^2. Porosity data were calculated from shearbox volumes and total dry weight of sand, assuming a specific gravity of 2.65 for quartz grains.

The single loose specimen was constructed by pouring dry sand into a shearbox, affixing the top cap, and flooding with water.

5.8.2 Specimen Description

Two grades of Ottawa Sand were used: 20 to 30 mesh (referred to as coarse Ottawa Sand), and C-109 grade (referred to as fine Ottawa Sand), with a median grain diameter (D50) of approximately 0.4 mm (actually a medium-grained sand). Six tests were performed on each material. The mean pretest porosities achieved were 33.88% for the coarse Ottawa Sand, and 32.75% for the C-109 grade sand. All specimens were approximately 3.16 cm in height.

The single loose specimen had a pretest porosity of 37.5%; C-109 grade Ottawa Sand was employed.

5.8.3 Testing Procedure

The assembled densified specimens were mounted in a standard

direct shear device, the normal load was applied, the specimens were flooded with water, the shearbox retaining screws were removed, and a standard shearbox separation of 0.4 mm was enforced. Testing proceeded at a constant displacement rate; rapid rates were employed because of excellent specimen drainage. Time to failure was approximately 20 min; all tests were continued beyond failure to residual strength conditions.

5.8.4 Results

Table 5.6 contains pertinent test data; Figure 5.7 shows the relationship between normal stress and shear stress at failure and at a residual state; and Appendix E.1.1 reports the relationships between displacement, stress ratio, and volume change.

Given the slight variability in the pretest densities, the test results are consistent. The secant ϕ values and the dilative rate at failure were somewhat higher for low normal stresses (1 to 3 kg/cm^2), but remained relatively constant for higher normal stress (3 to 10 kg/cm^2). The results for the six tests on C-109 sand (OS-FINE-1 to OS-FINE-10) demonstrated a uniform increase in displacement to failure as the stress level increased. The maximum total dilatancy (in the first displacement cycle) was slightly greater for the coarse Ottawa Sand. The residual secant ϕ values (ϕ_r^s) were greater in the finer-grained sand.

As shown on Figure 5.7, a curvilinear failure envelope is justified from the origin to three kg/cm^2 normal stress, but above that stress, a linear envelope may be used. A linear approximation, as shown on the figure, would display a ϕ of about 40^o, and an apparent cohesion of 0.4 kg/cm^2.

TABLE 5.6 OTTAWA SAND SHEARBOX TESTS

*- see Table 5.7(b) for a complete legend	n *	B.D. *	σ_n *	τ_f *	$\frac{\tau_f}{\sigma_n}$ *	ϕ^s_f *	d_f *	ΔV_t *	$\Delta \dot{V}_f$ *	ϕ^s_r *
Sample Number	Medium-Grained Ottawa Sand Test Series									
OS-FINE-1	31.3	2.13	1.0	1.07	1.07	47.1	0.089	1.43	9.5	32.7
OS-FINE-2	32.8	2.11	2.0	2.03	1.02	45.5	0.084	1.38	9.3	31.8
OS-FINE-3	34.0	2.09	3.0	2.65	0.88	41.4	0.087	2.06	7.1	31.5
OS-FINE-4	32.8	2.11	4.0	3.80	0.95	43.5	0.102	1.42	8.3	31.8
OS-FINE-6	33.1	2.10	6.0	5.06	0.84	40.2	0.130	1.45	6.6	30.6
OS-FINE-10	32.5	2.11	10.0	9.16	0.92	42.5	0.181	1.29	7.1	29.7
OS-LOOSE-4.0	38.9	2.01	4.0	2.56	0.64	32.6	0.249	-1.49	1.2	31.7
Sample Number	Coarse-Grained Ottawa Sand Test Series									
OS-COARSE-1	35.5	2.06	1.0	0.99	0.99	44.7	0.150	1.51	7.4	30.9
OS-COARSE-2	34.4	2.08	2.0	1.77	0.88	41.5	0.128	1.78	8.0	29.9
OS-COARSE-3	33.2	2.10	3.0	2.81	0.94	43.2	0.131	2.02	8.6	30.1
OS-COARSE-4	32.9	2.11	4.0	4.07	1.02	45.5	0.140	2.06	9.3	29.0
OS-COARSE-6	33.5	2.10	6.0	5.48	0.91	42.4	0.120	1.89	7.8	29.2
OS-COARSE-10	33.8	2.09	10.0	8.44	0.84	40.2	0.150	1.55	7.2	29.3

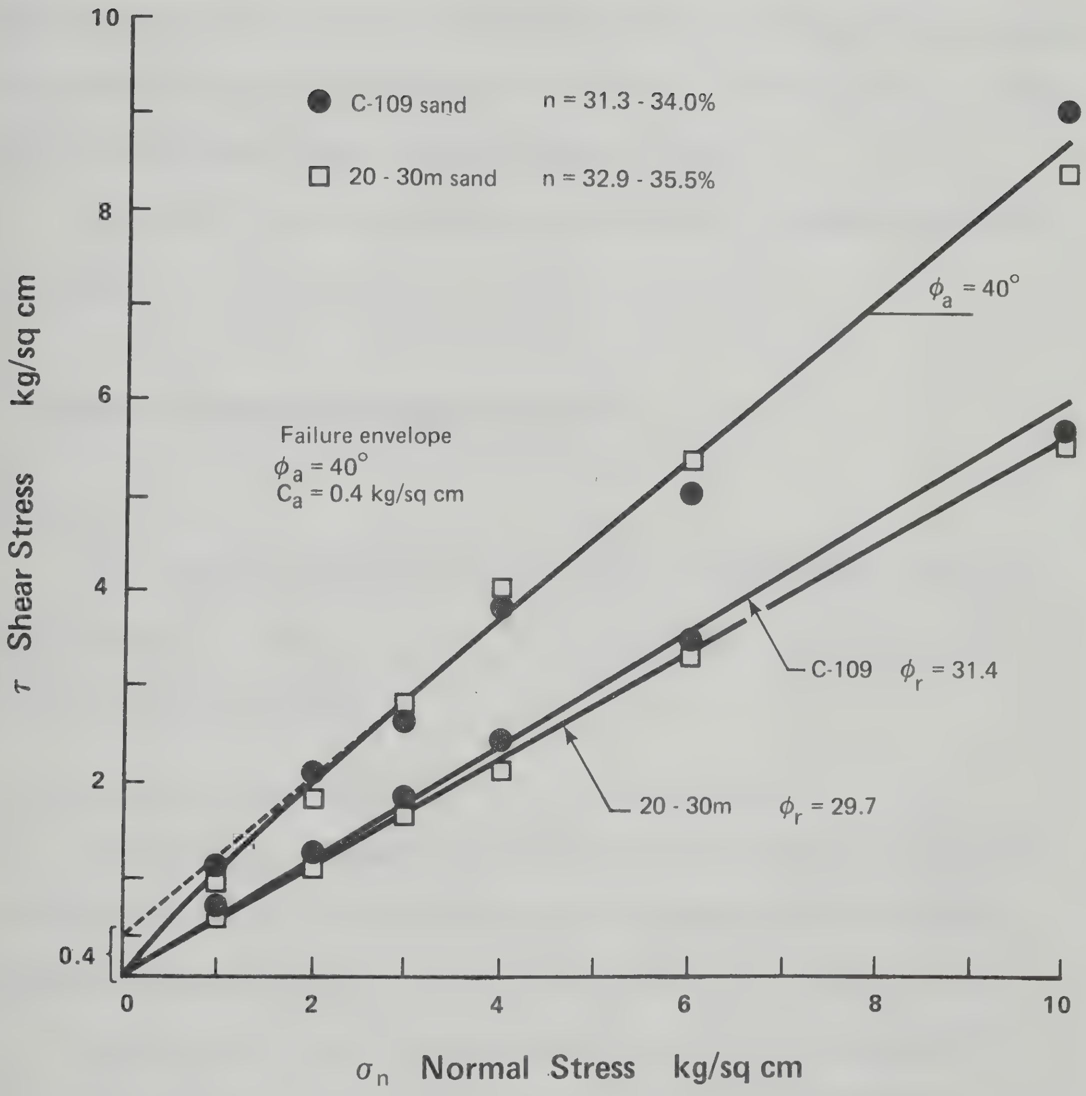

Figure 5.7. Ottawa Sand Shearbox Test Series

5.8.5 Conclusions

The 12 tests performed displayed the typical characteristics of a dense quartzose sand undergoing shear. The linearity of the envelope above stresses of 3.0 kg/cm^2 is evidence of the competent quartzose grain nature: no gross suppression of dilation has occurred. This observation is confirmed by the dilative rates at failure, which show little change within the test stress range.

The low ϕ_r^s values are a function of grain roundness and grain smoothness.

5.9 Shearbox Tests on Athabasca Oil Sand

5.9.1 Sampling

The samples came from the same suite of core which provided the triaxial specimens: Section 5.7.1 describes the sampling and storage of these specimens.

5.9.2 Specimen Preparation

All shearbox specimens for Test Series A to E were prepared on a lathe in a cold room. Further details of sample preparation are reported in Appendix B.1.

Specimens G-1 to G-5 were prepared by direct trimming of refrigerated but unfrozen sections of core using a circular brass trimming ring and scalpel. The technique used was similar to the method outlined in Appendix B.2.1.

5.9.3 Specimen Description

Several different materials were tested during the course of the

shearbox tests on Athabasca Oil Sand. Complete descriptions, sketches, and grain size curves for each undisturbed specimen may be found in Appendices E.1.2 to E.1.7 for the six groups of tests. A general description of each test series follows:[1]

1. Oil Sand Shearbox Series A: Twelve specimens were tested. Specimen heights varied from 3.05 to 3.30 cm. This series of tests was performed on more disturbed specimens than those of the subsequent four test series: all specimens displayed some disturbance due to expansion. Series A specimens were chosen to represent a wide range of bitumen contents. Specimens A-1 to A-3 contained an average of 4% bitumen (by total weight); bulk densities of these specimens varied from 2.01 to 2.08 gm/cc. Specimens A-4 to A-8 contained no bitumen; their pretest bulk densities had a mean of 2.15 gm/cc. The four remaining specimens, A-9 to A-12, were oil-rich (5% to 13% bitumen), and their bulk densities were low (with a mean of 2.00 gm/cc).

2. Oil Sand Shearbox Series B: Three tests were conducted on a laminated, silty, oil-poor material of unusually high laboratory densities: 2.25 to 2.36 gm/cc. All specimens displayed cross-bedding at dip angles of 25° to 30° from the horizontal. Specimen thickness for these and all remaining tests ranged from 2.30 to 2.65 cm.

3. Oil Sand Shearbox Series C: Seven shearbox tests were performed on a section of oil-rich core (with a mean bitumen content

---

[1] All bulk densities are from pretest volume and weight measurements; all bitumen contents are expressed as percentages of total pretest weights.

of 11%), which displayed less disturbance than any other oil-rich section. Mean pretest bulk density was 2.062 gm/cc with little variation (standard deviation of .0065). All specimens displayed bedding dips of 20^{o} to 30^{o} from the horizontal.

4. Oil Sand Shearbox Series D: This series consisted of four tests on a material displaying horizontal bedding. The mean bitumen content for these samples was 6.5%; bulk densities varied from 2.04 to 2.06 gm/cc.

5. Oil Sand Shearbox Series E: An intraformational clay from the Upper Member of the McMurray Formation was selected. Four specimens were tested, none of which contained any detectable bitumen. The mean bulk density of specimens in this test series was 2.32 gm/cc.

6. Oil Sand Shearbox Series G: This series consisted of a number of comparative tests on various samples. Five specimens of intraformational clays, all visibly disturbed, were tested to assess residual strength properties. These specimens displayed horizontal bedding, and contained little or no bitumen. For these five specimens, bulk densities in a highly disturbed pretest state varied from 2.06 to 2.21 gm/cc. One specimen of remoulded material from Test A-5 was tested at a saturated remoulded density of 2.06 gm/cc. Two specimens of highly disturbed coarse-grained oil-rich sand (with a bitumen content of 14.8%) were tested at bulk densities of 1.85 and 1.91 gm/cc.

5.9.4 Testing Procedure

All specimens were trimmed by lathe in a cold room, mounted in

a cold state, and allowed to warm to room temperature only when the total normal load had been applied. The shearbox was flooded with water, and left to stand for one hour to allow specimens to equilibrate. All tests were conducted in the same shearbox (Appendix C; Figure C.1) and testing frame, with identical shearbox separations of 0.4 mm; all tests but one were carried to a state of residual strength. Series A tests were conducted at varying displacement rates to assess the effect (if any) of negative pore stresses developed during testing. Other tests were conducted at displacement rates considered conservative for the particular material being tested. For example, Series E tests were displaced at a rate of 8.67×10^{-7} cm/sec, resulting in times to failure of 12.5 hr at low normal stress, to 37 hr at a normal stress of 3.5 kg/cm^2. Since the materials had very low compressibilities, the coefficient of consolidation was probably low, and even the minimum time to failure of 12.5 hr may be considered conservative. The oil-bearing sands and silty sands were tested at very slow (about 10^{-5} cm/sec) rates of displacement to preclude misinterpretation of results.

To illustrate this, consider the lowest value of the coefficient of consolidation obtained in the triaxial tests: 0.038 cm^2/sec. Assuming a shearbox specimen thickness of 3.5 cm, and drainage only from the ends (in fact, radial drainage also occurs), solution of the time to failure formula given by Bishop and Henkel (1962) yields a value of 537 sec, or somewhat less than 9 min. The minimum test time to failure was 108 min, and most tests had times to failure of more than 360 min.

After failure had occurred, the displacement rate was increased in order to reach conditions of constant void ratio in a reasonable time, and a final cycle of displacement at displacement rates of

approximately 5 x 10^{-4} cm/sec was performed to assess residual strength. For argillaceous materials, the rate of displacement for this final cycle was somewhat slower: 1.2 x 10^{-5} cm/sec to 5 x 10^{-6} cm/sec, again to guarantee against any nonequilibrated pore pressures. Arenaceous materials displayed residual strength characteristics within 1.5 full cycles (three reversals). It was discovered that even at the maximum displacement rate possible (about one centimeter in three minutes) the sandy oil-rich specimens showed no detectable shear strength component as a result of either bitumen viscosity or pore fluid stresses. Nevertheless, a conservative approach was favoured, and much slower displacement rates were employed consistently.

5.9.5 Test Results

1. Oil Sand Shearbox Series A: Table 5.7 contains pertinent test and failure data; Figure 5.8 presents a Mohr-Coulomb plot of failure and residual stress conditions; and Appendix E.1.2 reports other test data, including the relationships between horizontal displacement and stress ratio, and individual sample descriptions.

2. Oil Sand Shearbox Series B and D: The results for these two test series are combined. Table 5.8 reports the most important test and failure data; Figure 5.9 shows the resultant Mohr-Coulomb plot; and Appendices E.1.3 and E.1.5 contain test plots, grain size curves, and sample descriptions.

3. Oil Sand Shearbox Series C: Table 5.9 lists important test and failure data; Figure 5.10 is a plot of stress conditions at failure and at the residual state; and Appendix E.1.4 contains further test and sample data.

TABLE 5.7 a OILSAND SHEARBOX SERIES A

Test Property / Sample Number	n *	B.D.*	σ_n *	τ_f *	$\frac{\tau_f}{\sigma_n}$ *	ϕ_f^s *	d_f *	ΔV_t *	$\Delta \dot{V}_f$ *	ϕ_r^s*	T_f*	% Oil *	Depth in Feet	Test Property / Comments
OILSAND A-1	31.7	2.01	0.635	1.00	1.57	57.5	0.32	1.14	7.7	-	-	-	146'	Dessicated
OILSAND A-2	31.6	2.08	1.01	1.55	1.54	57.0	0.23	1.21	10.3	33.8	-	3.9	132.2	X-Beds at 30-35°
OILSAND A-3	33.7	2.06	1.71	3.17	1.85	61.7	0.18	2.53	26.7	33.3	-	4.3	132.3	X-Beds at 30-35°
OILSAND A-4	27.2	2.14	5.53	6.04	1.09	47.5	0.16	1.13	7.5	34.3	1.8	3.8	131.8	Worm Casts 8-10° X-Beds
OILSAND A-5	28.5	2.15	8.45	8.14	0.96	43.9	0.21	1.00	11.0	33.0	2.8	0	132.9	34° X-Beds
OILSAND A-6	27.4	2.17	11.4	9.55	0.84	39.9	0.18	0.68	4.9	31.5	2.7	0	132.8	40° X-Beds
OILSAND A-7	28.0	2.13	4.94	5.05	1.02	45.6	0.30	0.78	3.5	32.7	2.3	0	132.5	30-35° X-Beds
OILSAND A-8	26.5	2.16	1.94	2.36	1.22	50.6	0.20	1.51	9.5	34.6	2.4	0	132.6	25-30° X-Beds
OILSAND A-9	38.8	1.98	0.543	0.92	1.69	59.4	0.11	3.86	19.4	34.3	6.7	13.2	136.2	25° X-Beds
OILSAND A-10	33.4	2.06	1.08	1.84	1.71	59.6	0.12	2.49	19.0	36.0	11.0	8.8	136.8	25° X-Beds
OILSAND A-11	38.8	1.97	2.37	2.40	1.01	45.4	0.14	1.36	10.4	33.2	12.0	12.5	136.6	25° X-Beds
OILSAND A-12	34.0	1.99	5.50	5.59	1.02	45.5	0.12	1.06	10.5	33.0	11.3	4.8	136.4	25° X-Beds

* See Table 5.7 b for a full explanation of symbols and units used.

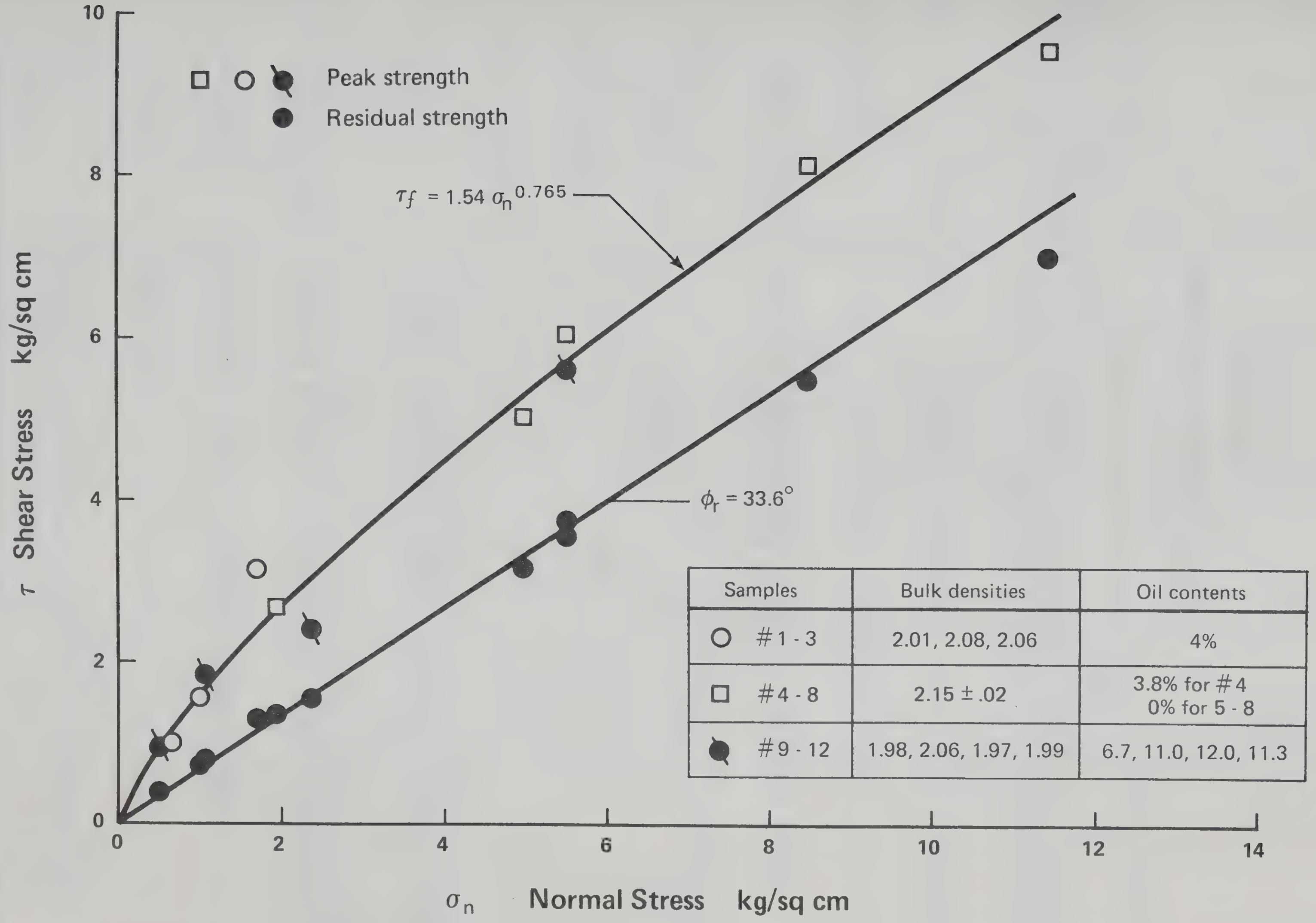

Samples	Bulk densities	Oil contents
○ #1 - 3	2.01, 2.08, 2.06	4%
□ #4 - 8	2.15 ± .02	3.8% for #4 0% for 5 - 8
● #9 - 12	1.98, 2.06, 1.97, 1.99	6.7, 11.0, 12.0, 11.3

Figure 5.8. Oilsand Shearbox Series A

TABLE 5.7 b

SYMBOLS USED IN DATA TABLES

SYMBOL AND NAME		UNITS	COMMENTS
n	Porosity	Percent (%)	Calculated from volume, dry mineral weight, oil content, and moisture content
B.D.	Bulk Density	gm/cc	Direct volume/weight determination before testing
σ_n	Normal Stress	kg/cm^2	Held constant throughout test
τ_f	Shear Stress at Failure	kg/cm^2	Maximum shear stress is defined as the shear stress at failure
$\frac{\tau_f}{\sigma_n}$	Maximum Stress Ratio	-	Maximum shear stress divided by the normal stress
ϕ_f^s	Secant ϕ at Failure	Degrees	$= \text{ARC TAN } (\tau_f/\sigma_n)$
d_f	Displacement to Failure	cm	
ΔV_τ	Total Volume Change	Percent (%)	Maximum volumetric expansion in the first cycle of the shear test (at peak if negative)
$\Delta\dot{V}_f$	Rate of Volume Change at Failure	%/cm	Rate of volume change at and just preceding failure; averaged over several data points
ϕ_r^s	Residual Secant ϕ	Degrees	$= \text{ARC TAN } (\frac{\text{Residual Shear Stress}}{\sigma_n})$
T_f	Time to Failure	Hours	
% Oil	Oil Content	Percent (%)	Expressed as a percent of original total weight of specimen

TABLE 5.8 OILSAND SHEARBOX SERIES B AND D

	n *	B.D.*	σ_n*	τ_f*	$\frac{\tau_f}{\sigma_n}$ *	σ_f^s*	d_f*	ΔV_t*	$\Delta \dot{V}_f$*	ϕ_r^s*	T_f*	% Oil	Depth	Comments
OILSAND SHEARBOX SERIES B														
OILSAND-B-1	18.4	2.355	1.00	2.29	2.29	66.4	0.088	5.41	55.0	36.4	8.0	0.8	135'	30° X-Beds Silt and Clay
OILSAND-B-2	23.3	2.248	2.00	2.86	1.43	55.0	0.116	2.15	25.0	33.8	11.0	1.1	135'	35° X-Beds Silt and Fine Sand
OILSAND-B-4	19.2	2.320	4.00	7.08	1.77	60.5	0.144	4.62	46.0	35.0	14.0	1.4	135'	30° X-Beds Silt and Fine Sand
OILSAND SHEARBOX SERIES D														
OILSAND-D-1	33.4	2.061	0.885	1.93	2.19	65.4	0.060	1.56	22.0	36.7	7.5	5.4	118.15'	Horizontal Bdg.
OILSAND-D-2	34.2	2.035	2.00	2.88	1.44	55.2	0.088	1.18	13.0	36.3	8.3	6.9	118.25'	Horizontal Bdg.
OILSAND-D-4	33.9	2.057	4.00	4.63	1.16	49.2	0.106	0.546	10.0	32.9	11.2	6.0	118.35'	Horizontal Bdg.
OILSAND-D-8	33.9	2.042	8.00	10.51	1.31	52.7	0.138	0.647	20.0	34.3	14.6	7.8	118.45'	Horizontal Bdg.

* See Table 5.7 b
For a Complete
Legend

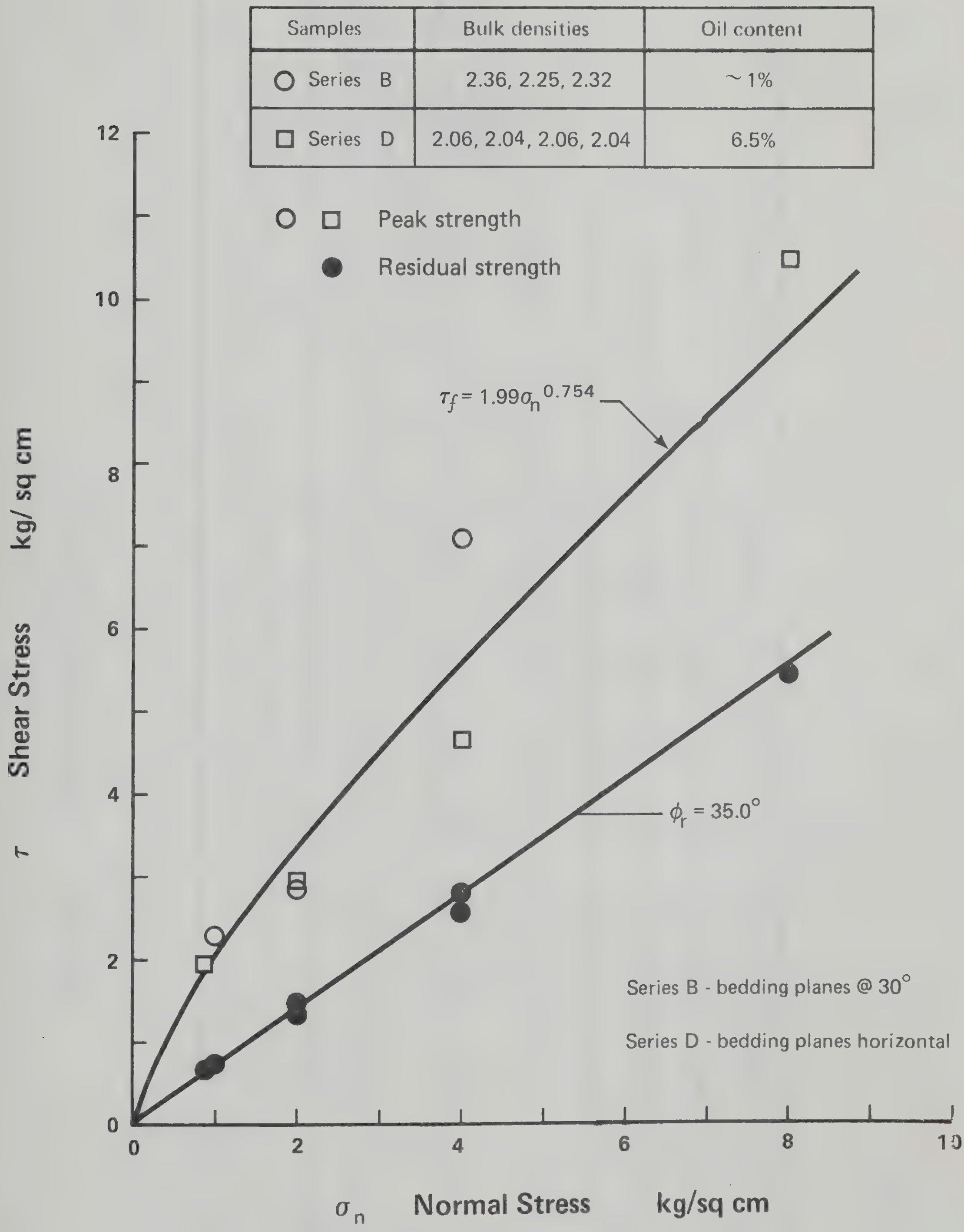

Figure 5.9. Oilsand Shearbox Series B and D

TABLE 5.9 OILSAND SHEARBOX SERIES C

	n *	B.D.*	σ_n*	τ_f*	$\frac{\tau_f}{\sigma_n}$*	ϕ_f^s*	d_f*	ΔV_t*	$\Delta\dot{V}_f$*	ϕ_r^s*	T_f*	Oil %	Footage	Comments
OILSAND-C-0.5	32.8	2.065	0.50	1.40	2.79	70.3	0.085	2.62	46.0	34.9	4.5	9.5	122.1′	All samples BDG. DIP @ 22-35°
OILSAND-C-1.0	33.6	2.072	1.00	2.50	2.50	68.2	0.080	2.63	33.0	38.0	4.3	11.7	122.25′	High ϕ_r^s value (ignored in mean
OILSAND-C-2.0	31.9	2.054	2.001	4.05	2.02	63.7	0.136	0.82	21.0	37.0	24.0	5.7	122.4′	
OILSAND-C-4.0	35.7	2.054	4.026	5.85	1.45	55.5	0.130	0.74	17.0	33.2	47.0	12.1	122.55′	
OILSAND-C-6.0	34.6	2.064	6.019	8.92	1.48	56.0	0.148	1.30	23.0	33.0	15.6	12.8	122.7′	
OILSAND-C-8.0	34.4	2.063	7.985	12.08	1.51	56.6	0.158	1.23	18.0	34.2	16.7	12.7	122.85′	
OILSAND-C-10.0	34.4	2.066	10.00	14.20	1.42	54.8	0.185	1.12	15.0	-	19.5	12.6	122.9′	

* See Table 5.7 b
For a Complete
Legend

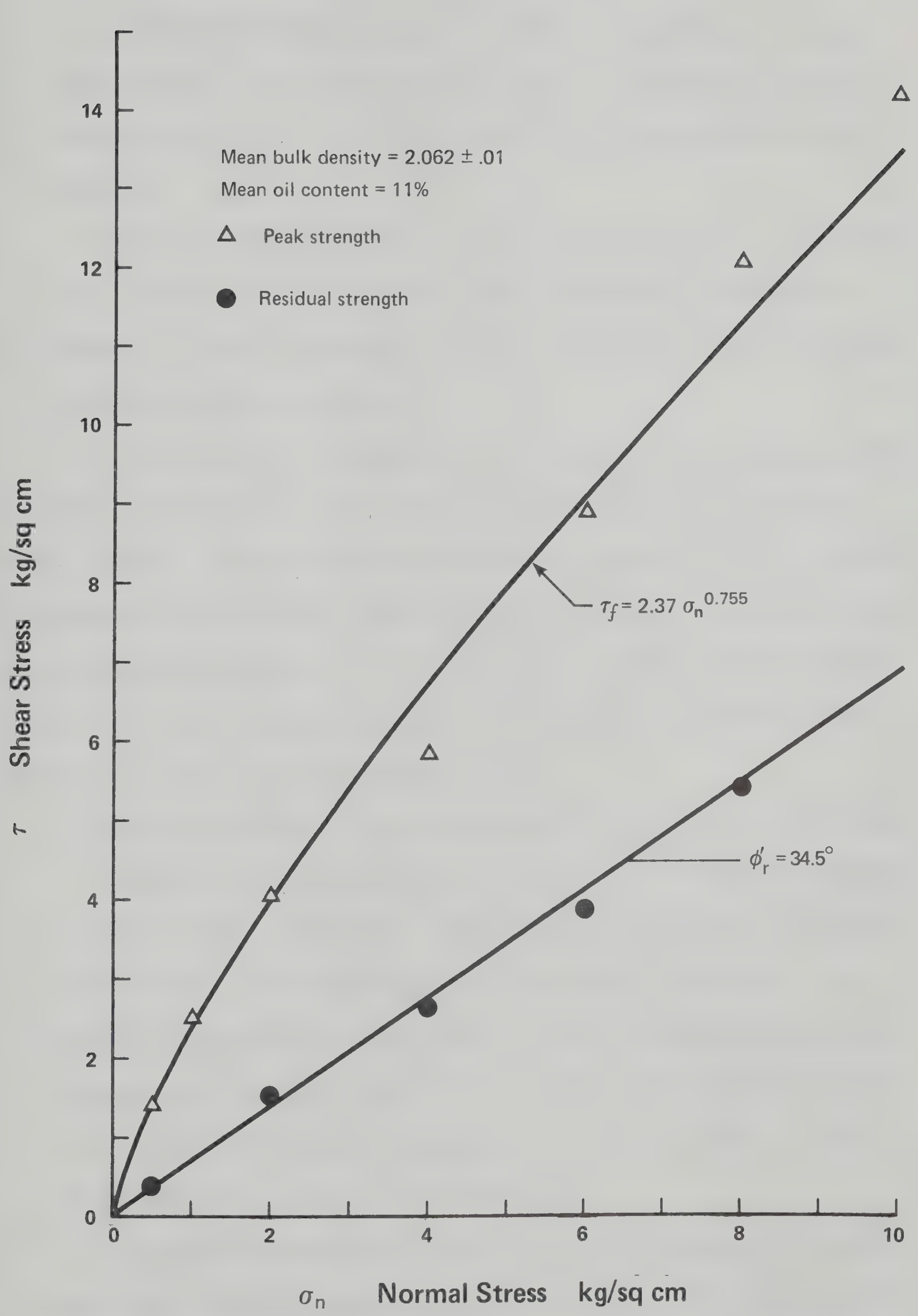

Figure 5.10. Oilsand Shearbox Series C

4. Oil Sand Shearbox Series E: Table 5.10 contains the most important test and failure data; Figure 5.11 shows the resultant Mohr-Coulomb stress plot; and Appendix E.1.6 presents additional test data.

5. Oil Sand Shearbox Series G: Table 5.11 is a list of pertinent test and failure data; Figure 5.12 shows stress conditions at residual strength for Series G tests; and Appendix E.1.7 contains further individual test data.

The dilative rate at failure is the ratio of the volume increase (vertical displacement) to the horizontal displacement immediately before failure. It corresponds therefore to the slope of the relationship between volume change and displacement immediately before failure. The relationships between the dilative rate at failure and the normal stress for the 12 dense Ottawa Sand tests and for Oil Sand Shearbox Series A to E are plotted in Figure 5.13.

The major results of the test series are summarized as follows:

1. Maximum ϕ_r^s for arenaceous oil sands is 36°, which corresponds to a stress ratio of 0.726. (Notwithstanding a small but persistent tendency to curvilinearity of the residual envelope, the residual data have been presented as linear envelopes with angles of shearing resistance equal to the means of all determinations.)

2. Minimum ϕ_r^s for argillaceous beds in the oil sands is 18°, corresponding to a stress ratio of 0.325.

3. Regression analyses to yield the best fit power law envelope have large positive correlation coefficients. Table 5.12 presents the failure envelopes and correlation coefficients for the various

TABLE 5.10 OILSAND SHEARBOX SERIES E

	n *	B.D.*	σ_n*	τ_f*	$\frac{\tau_f}{\sigma_n}$*	ϕ^s_f*	d_f*	ΔV_t*	$\Delta\dot{V}_f$*	ϕ^s_r*	T_f*	Oil* %	Depth From Surface (ft.)	Comments
OILSAND-E-1	19.6	2.35	1.00	1.52	1.52	56.7	0.039	2.75	35.0	21.7°	12.5	0	119.35	Horizontal Bedding
OILSAND-E-2	20.1	2.35	2.00	1.88	0.94	43.3	0.062	1.10	13.0	17.9°	20.0	Trace	119.45	Silty Seams
OILSAND-E-3.5	23.2	2.29	3.50	3.78	1.08	47.2	0.099	1.03	8.9	18.1°	37.0	0	119.15	Horizontal Bedding
OILSAND-E-5	22.8	2.29	5.00	4.61	0.92	42.6	0.083	0.51	2.3	17.3	33.0	0	119.25	Horizontal Bedding

*See Table 5.7 b
For a Complete
Legend

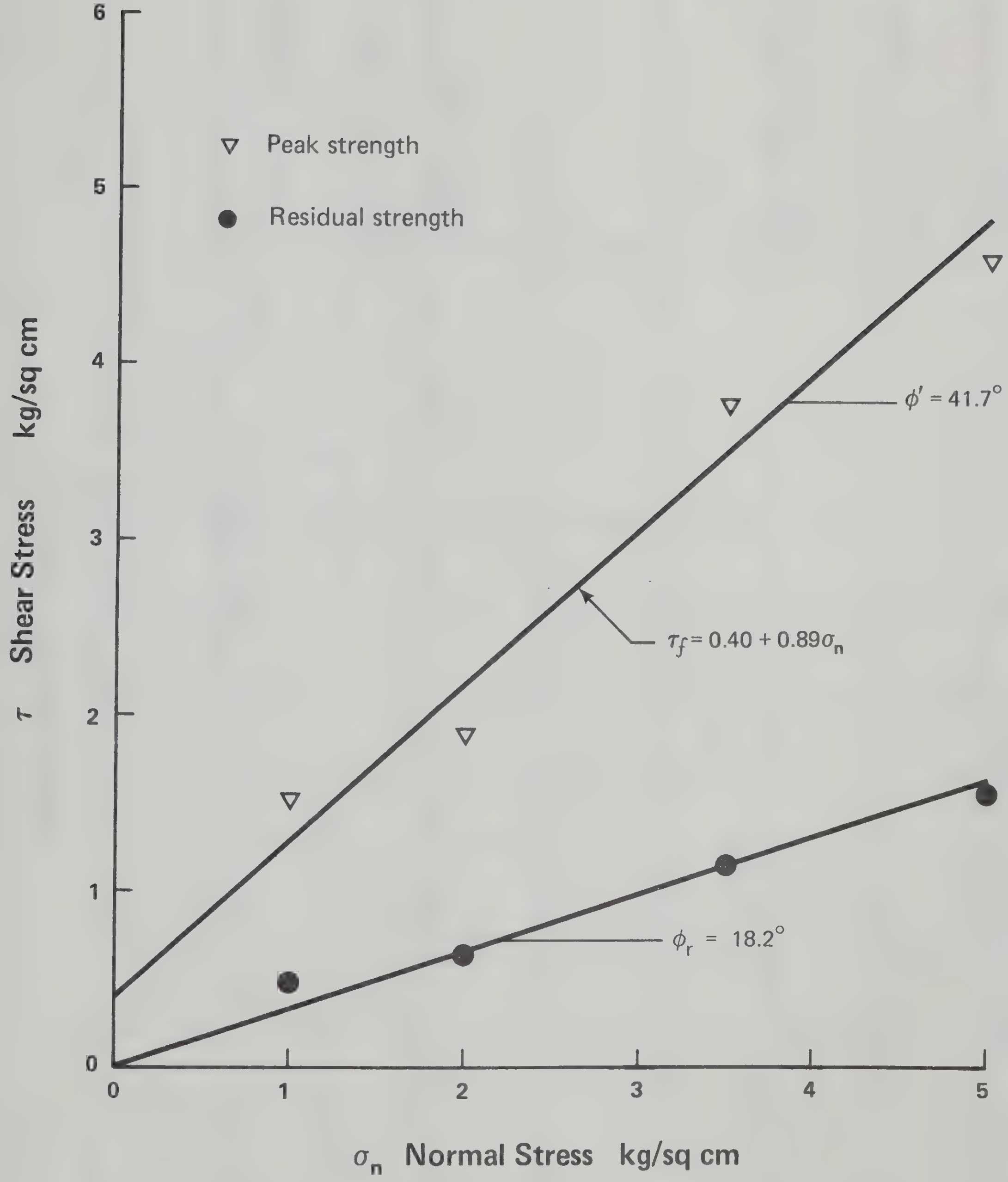

Figure 5.11. Oilsand Shearbox Series E

TABLE 5.11

OILSAND SHEARBOX SERIES G

SAMPLE * see Table 5.7b	B.D.	σ_n*	τ_n*	$(\frac{\tau_f}{\sigma_n})_f$*	ϕ^s_f*	d_f*	ΔV_t*	$\Delta \hat{V}_t$*	ϕ^s_r*	T_f*	Oil* %	Footage	Comments
G-1 AOS-CLAY 158.75-158.90	2.21	5.00	3.57	0.71	35.5°	0.18	0.06	1.0	29.5°	13.6	0	158.8'	Friable clayey silt, somewhat dessicated
G-2 AOS-CLAY 158.65-158.75	2.16	0.50	0.48	0.97	44.1°	0.16	--	---	32.2°	12.0	0	158.7'	Same as above - no test data given
G-3 OILSAND 174.7' Clay Rich	2.08	1.00	0.71	0.70	35.0°	0.27	0.21	1.5	18.8°	--	Trace	174.7'	Crazed and dessicated T_{100}≃50 min
G-4 OILSAND 174.8' Clay Rich	2.13	2.00	1.09	0.55	28.6°	0.20	0.23	2.0	18.3°	--	---	174.8'	T_{100}≃65 min
G-5 OILSAND 174.9' Clay Rich	2.06	4.00	2.43	0.61	31.3°	0.31	-.08	+0.10	27.5°	--	1.2%	174.9'	Sandy seam in failure plane
G-6 REMOULDED Shear "A" #5	2.06	3.00	2.09	0.70	35.0°	1.17	-3.1	-0.5	34.5°	3.2	0	--	Remoulded, consolidated from oilsand A-5
G-7 OILSAND -G-0.314	1.85	0.314	0.270	0.861	40.7°	0.37	0.98	+2.3	37.0°	6.3	14.9	190.0'	Coarse to medium oilsand
G-8 OILSAND -G-6.002	1.91	6.002	3.83	0.636	32.4°	2.49	-2.1	+0.90	31.6°	14.	14.6	190.2'	Coarse to medium oilsand

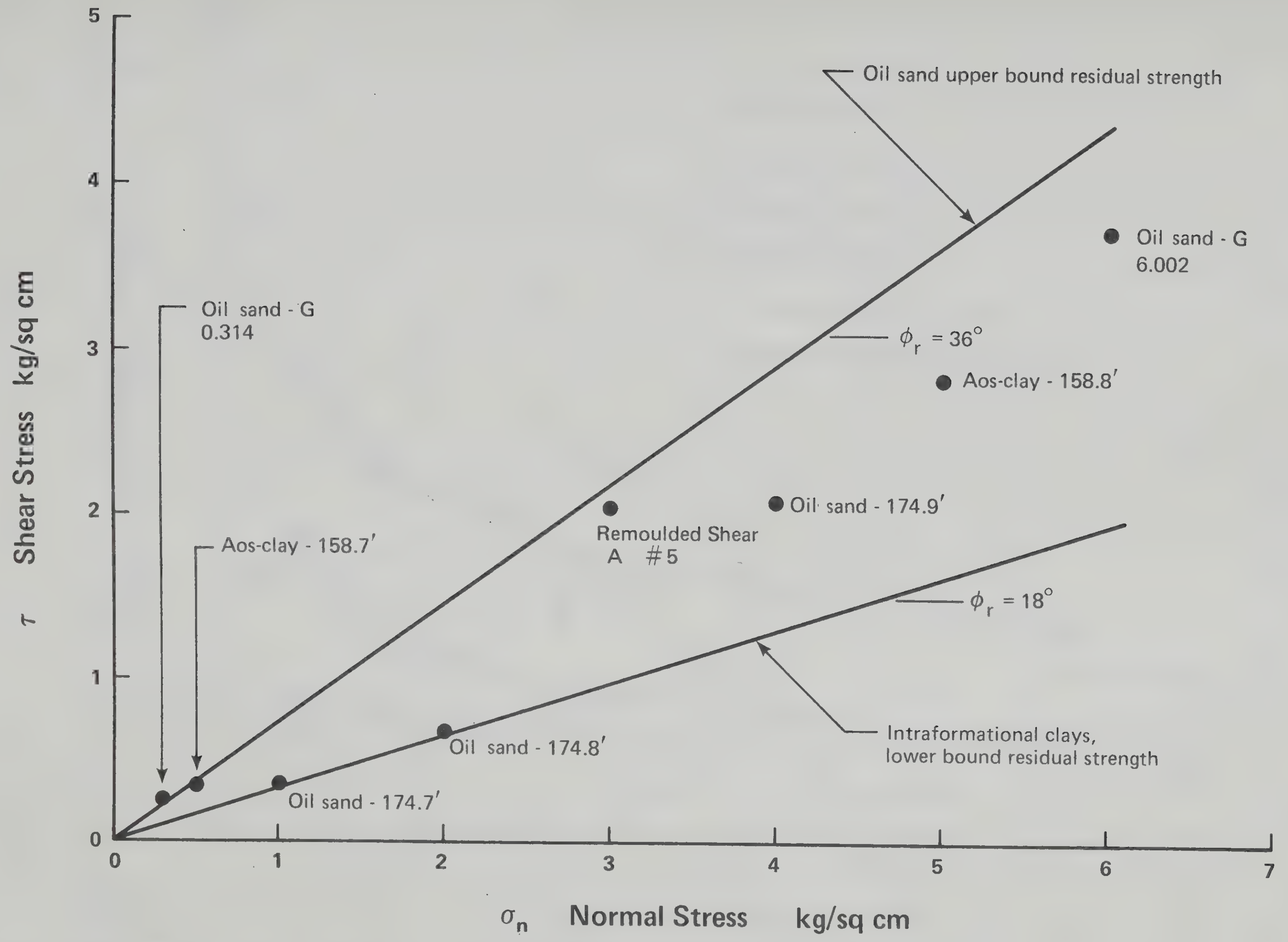

Figure 5.12. Residual Strength Data –Oilsand Series G

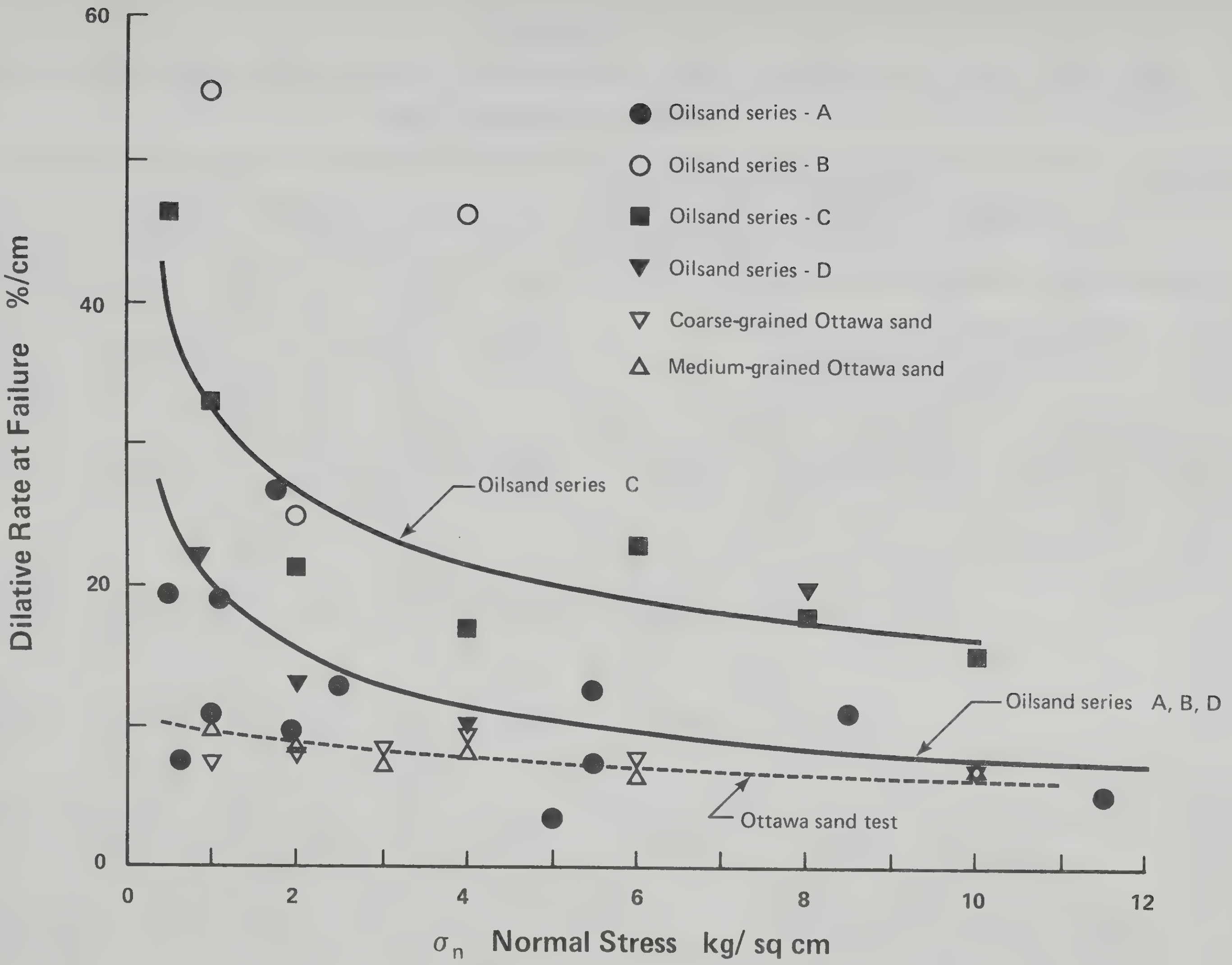

Figure 5.13. Dependence of Dilative Rate at Failure Upon Normal Stress

TABLE 5.12

FAILURE ENVELOPE COEFFICIENTS AND RESIDUAL STRENGTH DATA FOR ALL SHEARBOX TESTS ON OTTAWA SAND AND ATHABASCA OIL SAND

TEST SERIES	FAILURE CURVE	COEFFICIENT "a"	COEFFICIENT "b"	CORRELATION COEFFICIENT (REGRESSION)	RESIDUAL STRENGTH (TAN ϕ_r')	COMMENTS
Ottawa Sand Shearbox	$\tau_f=a+b\cdot\sigma_n$	0.40	0.84	--	0.610 0.570	Upper Figure For Finer Sand
Oilsand Series A	$\tau_f=a\cdot\sigma_n^b$	1.54	0.765	0.987	0.664	
Oilsand Series B and D	$\tau_f=a\cdot\sigma_n^b$	1.99	0.754	0.962	0.700	
Oilsand Series C	$\tau_f=a\cdot\sigma_n^b$	2.37	0.755	0.996	0.687	
Oilsand Series E	$\tau_f=a+b\cdot\sigma_n$	0.40	0.899	Insufficient Data	0.325	Hand Drawn Failure Envelope
Oilsand Series G	--	--	--	--	0.726 0.325	Residual Data For Sand and Clay

oil sand shearbox test series.

4. Within a given test series, displacement to failure increases with increasing normal stress, whereas the total volume change, the dilative rate at failure, and the minimum stress ratio decrease with increasing normal stress level.

5.9.6 Conclusions

Examination of the strength values obtained and of the variations in displacement rates employed in Series A and C shows conclusively that bitumen does not contribute to long-term shear strength, either by viscous resistance or by generation of negative pore fluid stresses. All data indicate that pore pressures were equilibrated at failure, and therefore drained conditions existed throughout the test series.

Specimen density per se can not be correlated directly with strength. The very dense specimens from Series A and B displayed lower strengths than those from Series C; therefore mineralogy must be an important factor (since Series C was more quartzose and coarser grained than Series A or B). Density in oil sands is largely a function of sorting: silty sands have larger grain size ranges (poor sorting) and can produce a more compact structure without forming the texture responsible for the high strengths.

Series D data indicate that strength parallel to bedding may be lower than strength across bedding. The relationship between normal stress and dilative rate at failure (Figure 5.13) shows that high dilative rates are correlated with high strengths. The mean grain size of the Ottawa Sand used for the comparative tests is much higher than the mean grain size of Series C specimens (or that of any other series); yet the

dilative rates at failure are much lower than those of the oil sand specimens. The total dilatancy in the first one-half cycle (failure cycle) of displacement is approximately the same for the Ottawa Sand as for the great majority of the oil sand specimens, since the grain size of Ottawa Sand is comparatively large. Diminution of the dilative behaviour as normal stress rises is more noticeable in the oil sand specimens than in the Ottawa Sand. This is a function of individual grain competence and of mineralogy: Ottawa Sand is an extremely competent, rounded, well-sorted sand; the quartz in oil sands is less rounded, and oil sands always contain minor feldspar and muscovite fragments, which cleave and crush at lower stresses than those necessary for quartz. Furthermore, the competence of the individual quartz grains in oil sands is probably less than that of Ottawa Sand grains. As dilative behaviour is suppressed, cleavage of mineral grains must occur for movement along the shear plane to be kinematically possible; therefore a tangent to the failure envelope at intermediate or at high normal stresses yields a cohesion intercept, which is a measure of the amount of cleavage and grain shear taking place.

The Mohr-Coulomb failure envelopes have been drawn as curvilinear relationships. The assumption of curvilinearity is reasonable: the dilation suppression phenomenon in these materials is gradual, because of random distribution of grain contact angles; and a gradual process must give rise to a gradual curvature. Bilinearity occurs only on idealized failure surfaces with constant inclination of contacts (Patton, 1966). Statistically, the power law fit provides a large positive coefficient of correlation. This does not constitute proof of the curvature, but it does provide support of the

concept. Nevertheless, the use of a power law is not intended to suggest a fundamental physical relationship: it is a phenomenological curve-fitting process applicable only to the stress range explored in the study.

Further support of the concept of failure criteria curvilinearity and of the hypothesis of no cohesion is provided by two simple but important qualitative tests: slaking tests (24 hr) on fine-grained borehole specimens, and saturation tests on medium-grained oil-free outcrop specimens. Both tests indicate little or no cohesive component of strength at zero stress.

5.10 General Comments and Conclusions

5.10.1 Rejection of Previous Strength Hypotheses

The testing program described in this chapter has led to the rejection of numerous hypotheses concerning the source of strength in the Athabasca Oil Sands:

1. Stress-independent physical cohesion does not exist in the great majority of the oil sands materials tested: although carbonate, silica, dry clay, or oxide cementation may be a local and minor feature, the majority of oil sands generate cohesionless Mohr-Coulomb strength envelopes.
2. Viscous strength or yield strength resulting from the interstitial bitumen has not been detected: in the long term, bitumen acts as a liquid, and pore water is in sufficient continuity to preclude the generation of long-term negative pore stresses.
3. Interfacial tensions are negligible as a strength source in

the oil sands: the general coarseness of the material precludes large interphase surfaces, and bitumen-water and bitumen-air systems have lower surface tensions than water-air systems.

4. The strength of oil sands is not a direct function of material density: residual strengths are within the normal range, and recompacted sand specimens display no anomalous behavioural characteristics. Strength parallel to bedding may be lower than in other directions.

5.10.2 Source of Strength in the Oil Sands

Many facts concerning the strength of oil sands have become apparent during the course of the testing program:

1. In general, oil sand specimens display no stress-independent cohesion.

2. Oil sands are marked by an extremely high dilative rate at failure; this rate decreases as stress level increases and results in a curvilinear failure stress relationship.

3. The value of the apparent cohesion intercept increases as stress level increases and as dilative behaviour decreases.

4. The component of additional strength is greater in more quartzose, coarser-grained materials.

5. The source of strength is lost with the gross textural disturbance caused by expansion upon sampling.

These facts lead to one conclusion: the fabric of the quartz grains is responsible for the unusually high shear strengths of oil sands.

CHAPTER VI

COMPARATIVE STRENGTH STUDIES OF ORTHOQUARTZITES

6.1 Introduction

According to the geological principle of uniformitarianism, the fabric of the McMurray Formation responsible for the unusual strength behaviour can not be unique: other geologically similar materials must display similar stress-strain-strength behaviour. The three characteristics considered critical with respect to the unusual stress behaviour of the McMurray Formation sands are the quartzose nature, the lack of cohesion at zero stress, and the age of the material. On the basis of these criteria, three materials were selected for comparative testing:

1. St. Peter Sandstone: a well-rounded quartzose sand of Ordovician age.
2. Swan River Sandstone: a well-sorted, angular quartzose sand of Lower Cretaceous age, stratigraphically very similar to the McMurray Formation.
3. Swan River Preglacial Sand: a poorly-sorted, angular quartzose sand, likely of Lower Pleistocene age.

All of these materials were tested in direct shear, and a limited number of drained triaxial tests were performed on the St. Peter Sandstone samples.

6.2 St. Peter Sandstone

6.2.1 Sampling

St. Peter Sandstone samples were obtained from a storm drainage tunnel under construction during 1975 beneath the city of Minneapolis in Minnesota, U.S.A. A low-pressure water-jet was used for mining, a slush pump removed the slurry of water and sand, a time-setting mixture of a silicate compound was used to reduce the permeability of the unsaturated sand, and shotcrete was applied for the initial tunnel support. The tunnel was excavated at the rate of 6 to 7 ft (two meters) per mining sequence, with a two-foot (0.6 m) wide central column left for roof support before the silicate compound was sprayed on. Block samples were obtained from the central pillar before it was removed.

The bed chosen consisted entirely of cohesionless sand. The sand was unsaturated, and displayed some apparent cohesion because of pore water capillarity. To test for true cohesion, a small elongated block was cut from the selected stratum and placed on end. Water was dripped on the specimen; if it collapsed, then lack of true cohesion was assumed.

Four large blocks, each roughly 50 x 30 x 30 cm, were cut by hand saw, and carefully brought to the surface. The blocks were trimmed by spatula to fit into a 20 l bucket, and a rapidly setting mixture of silicate was applied by hand to the exterior of the specimen to provide some strength. It had been determined previously that a concentrated mixture of the silicate and its setting agent would penetrate only 1 or 2 cm of the specimens before setting, leaving the interior sand uncemented and unsaturated. The cylindrical samples were packed with

loose sand to ensure adequate shock protection during transport. All samples arrived intact at the testing laboratories.

6.2.2 Sample Preparation

Great difficulty was experienced in trimming specimens for testing. The St. Peter Sandstone samples were extremely brittle and lacked true cohesion. Shaping specimens by lathe or tube methods was not feasible; therefore, a time-consuming, but successful, method of hand-trimming was used.

Shearbox specimens were cut with hack saw blades, scalpels, and a brass ring. Very gentle pressing of the ring into the specimen and simultaneous removal of excess grains by scalpel or hack saw blades eventually resulted in a full brass ring. The ends were trimmed carefully to provide planar surfaces for uniform load distribution. Great care was taken at all stages to prevent chipping of edges, gouging of the specimen, or cleavage of the untrimmed block. Full details of specimen preparation techniques are reported in Appendix B.2.1.

It proved considerably more difficult to obtain specimens sufficiently cylindrical in shape with flat parallel ends for triaxial testing. The four successful tests reported in this chapter are the result of 12 attempts: six specimens were ruined during either trimming or mounting, and two other specimens failed by end crushing, as a result of nonuniformity of stresses at the specimen ends. The apparatus employed for trimming was the common vertical frame used for soft clay specimens. A wire trimming saw was not effective in the medium-grained sand; therefore sharpened hack saw blades were used to achieve the necessary cylindrical sample. A U-shaped end trimmer with a flat,

sharp hack saw blade was used to trim planar ends. Further details are reported in Appendix B.2.2.

6.2.3 Geology and Sample Description

St. Peter Sandstone was chosen as a comparative test material because it met the three basic requirements for comparison with the Athabasca Oil Sands: it is geologically old, it is quartzose, and those portions sampled displayed no cohesion at zero stress.

St. Peter Sandstone is an orthoquartzite of Lower Paleozoic (Ordovician) age; it is characteristically a transgressive beach deposit, and it unconformably overlies a series of largely carbonate rocks, which display progressively greater ages toward the northeast (Dapples, 1955). The deposit has a mean thickness of 23 m, and is found over a very large area of the central United States (580,000 km^2). Roundness, good sorting, and the monomineralic nature of the grains indicate extensive winnowing and multi-cycle reworking in high energy, persistent depositional regimes (i.e. stable coastlines with beaches and barrier bars). In the vicinity of Minneapolis, Minnesota, the St. Peter Sandsone is well sorted and has a mean diameter of 0.13 to 0.26 mm. The mineralogy is simple: more than 99% of the grains are quartz.

The specimens obtained for testing had porosities varying from 25.8% to 28.5% for undisturbed specimens (much of the variation may be a result of sample trimming and errors in dimension determinations.). To ensure that the specimens tested were essentially cohesionless, small intact pieces left from the trimming procedure were saturated, and they usually collapsed under their own weight. If any strength in a saturated state was apparent, the specimen from which the piece

was obtained was rejected.

6.2.4 Test Procedure

Shearbox specimens were mounted in the same shearbox and testing frame employed for all the Athabasca Oil Sands shear tests. Specimens were subjected to the normal load desired for testing, and then flooded with tap water. The shearbox retaining screws were removed, a shearbox separation of 0.4 mm was enforced, and testing followed. Rapid displacement rates were possible because of the high permeabilities (1.9×10^{-3} to 4.5×10^{-3} cm/sec) and the negligible compressibilities. The time to failure for all tests was one-half to one hour; displacement rates were quadrupled after failure to reach residual strength conditions rapidly.

Triaxial specimens were trimmed to diameters of 3.81 cm with length-to-diameter ratios of 2.0 to 2.5, mounted on a standard 3.81 cm triaxial cell with porous stainless steel end plates, and subjected to an effective confining stress. Permeability determinations were made on two specimens before testing. From the results of previous tests on dense sands it could be assumed that the pore pressures would drop to the point of cavitation before failure; therefore only drained tests with volume change measurements were performed. Tests were continued to the point where the stress-strain relationship showed a residual strength state. This proved possible in the triaxial apparatus only because of the complete loss of fabric after failure.

6.2.5 Test Results

Table 6.1 contains pertinent test and failure data for the shearbox tests on St. Peter Sandstone; the Mohr-Coulomb envelopes at

TABLE 6.1 ST. PETER SANDSTONE SHEARBOX TESTS

	n *	B.D.*	σ_n *	τ_f *	$\frac{\tau_f}{\sigma_n}$ *	ϕ_f^s *	$\dot{\Delta V}_f$ *	ΔV_t *	d_f *	ϕ_r^s *	Comments
STP-A-0.5	26.7	2.21	0.50	0.675	1.35	53	12	1.0	0.073	36.0	Disturbed During Loading
STP-B-0.5	27.5	2.20	0.50	1.59	3.18	72	47	1.4	0.048	31.7	Semi-Brittle Rupture
STP-C-0.5	26.6	2.21	0.50	1.96	3.93	76	88	1.7	0.061	33.7	Brittle Rupture
STP-2.0	27.0	2.20	2.00	4.96	2.48	68	25	1.0	0.088	31.0	Brittle Rupture
STP-A-3.0	-	-	3.00	4.72	1.57	58	14	1.1	0.085	33.4	Edge Broken During Trimming
STP-B-3.0	27.4	2.20	3.00	5.82	1.94	63	22	1.0	0.098	32.2	Brittle Rupture
STP-4.0	26.5	2.21	4.00	10.1	2.52	68	34	1.6	0.127	32.6	Brittle Rupture
STP-5.0	25.8	2.22	5.00	13.4	2.68	70	26	1.5	0.146	35.4	Brittle Rupture
STP-6.0	28.5	2.18	6.00	10.9	1.82	61	17	1.5	0.123	32.7	Sudden Expansion at Failure
STP-8.0	26.6	2.21	8.00	16.4	2.04	64	25	1.0	0.146	31.9	Brittle Rupture

* See Table 5.7 b for a complete legend

the point of failure and at a residual strength state are presented in Figure 6.1; and Appendix E.1.8 contains further stress-displacement data.

The results of 10 tests are reported in the table; two of the specimens were damaged before testing, and those test results reflect the damage. Much of the remaining data scatter in Figure 6.1 is likely a result of irregularities in the sample preparation technique. (Compare, for example, the two tests at 5.0 and 6.0 kg/cm^2 normal stress.) Rejecting the results from the two obviously disturbed specimens, the remaining eight data points fit a power law curvilinear relationship with a high correlation coefficient. The curve equations and correlation coefficients, along with those from other test series discussed in this chapter, are reported in Table 6.5.

The main characteristics of the shearbox test results are: high dilation rates at failure, total (first cycle) dilatancies considerably smaller than those displayed by Ottawa Sand, a mean residual angle of shear resistance of 32.4^o (rejecting the outlying data), and a gentle envelope curvature.

Triaxial specimen data show more variability as a result of the difficulties in obtaining parallel-ended, right circular cylinders with no edge chipping. The data from the four successful tests are reported in Table 6.2; the corresponding effective stress circles are presented in Figure 6.2; and further test data may be found in Appendix E.2.5. A hand-sketched envelope is drawn in Figure 6.2, since four data points are considered insufficient for statistical correlation. The power law relationship was obtained by plotting the envelope on double logarithmic graph paper to determine the appropriate coefficients. The residual

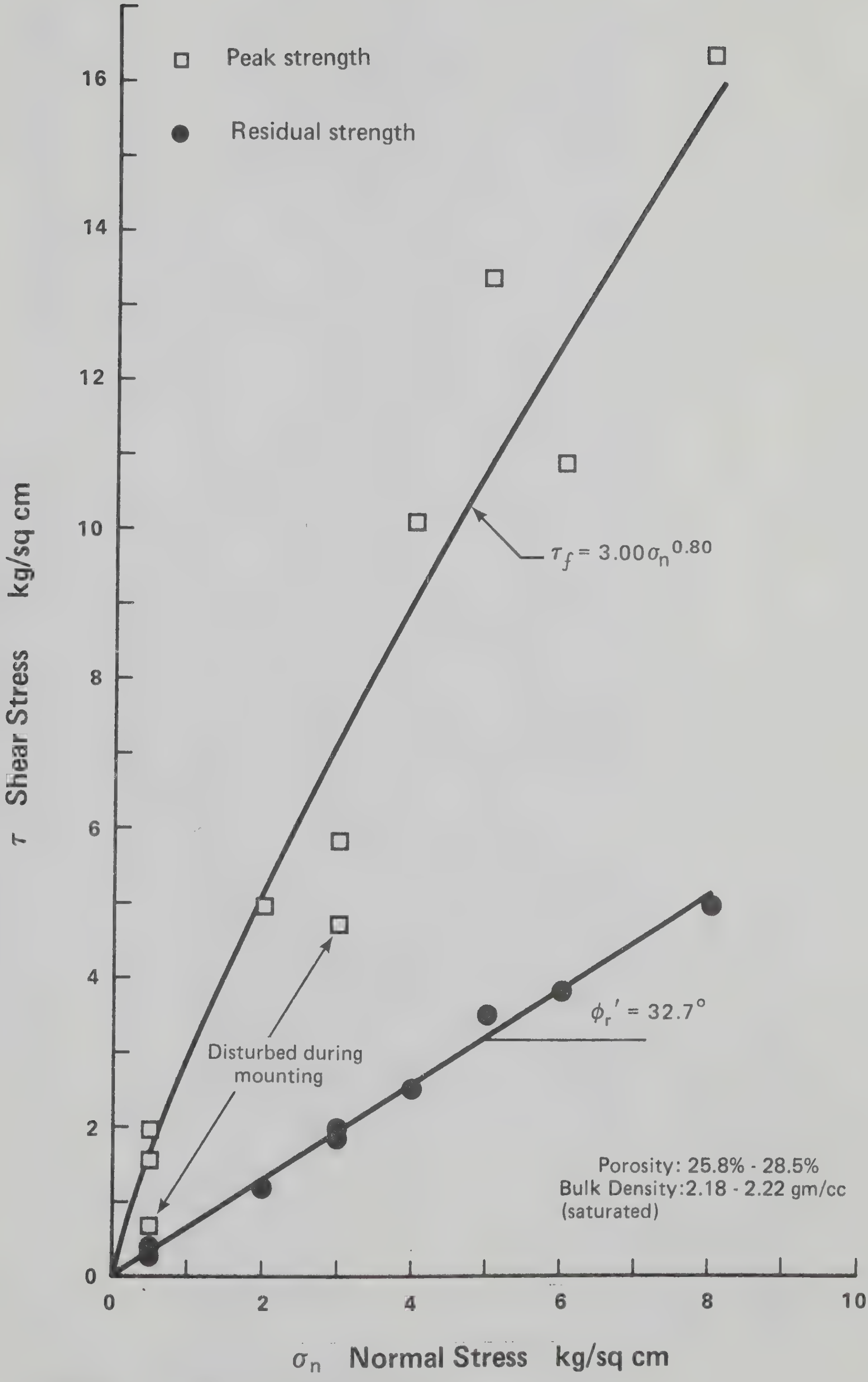

Figure 6.1 St. Peter Sandstone Shearbox Series

TABLE 6.2

DRAINED TRIAXIAL TESTS ON ST. PETER SANDSTONE

	n^*	B.D.*	$\sigma_3'^*$	$\left(\frac{\sigma_1-\sigma_3}{2}\right)_f^*$	$\left(\frac{\sigma_1'+\sigma_3'}{2}\right)_f^*$	ε_f^*	$\left(\frac{\sigma_1'}{\sigma_3'}\right)_r^*$	ϕ_r^{s*}	$\left(\frac{\sigma_1'}{\sigma_3'}\right)_m^*$	ϕ_{max}^{s*}	Comments
STPT-0.526	27.3	2.20	0.526	4.83	5.36	0.64	4.69^{**}	$40.4°^{**}$	19.4	64.3°	ΔV=0.277% at failure = 2.0% at ε=4.8%
STPT-1.0	26.1	2.22	1.00	5.73	6.73	0.50	3.67	34.9°	12.47	58.4°	ΔV=0.15% at failure 69° failure plane
STPT-3.0	26.9	2.21	3.00	14.18	17.18	0.73	3.50	33.7°	10.45	55.6°	No ΔV data, failure plane = 68°
STPT-5.0	28.7	2.18	5.00	16.65	21.65	1.07	3.42	33.2°	7.66	50.3°	ΔV=0.13% at failure, 62° failure plane

* See Table 5.1 b for a complete legend

** Residual Probably Not Reached

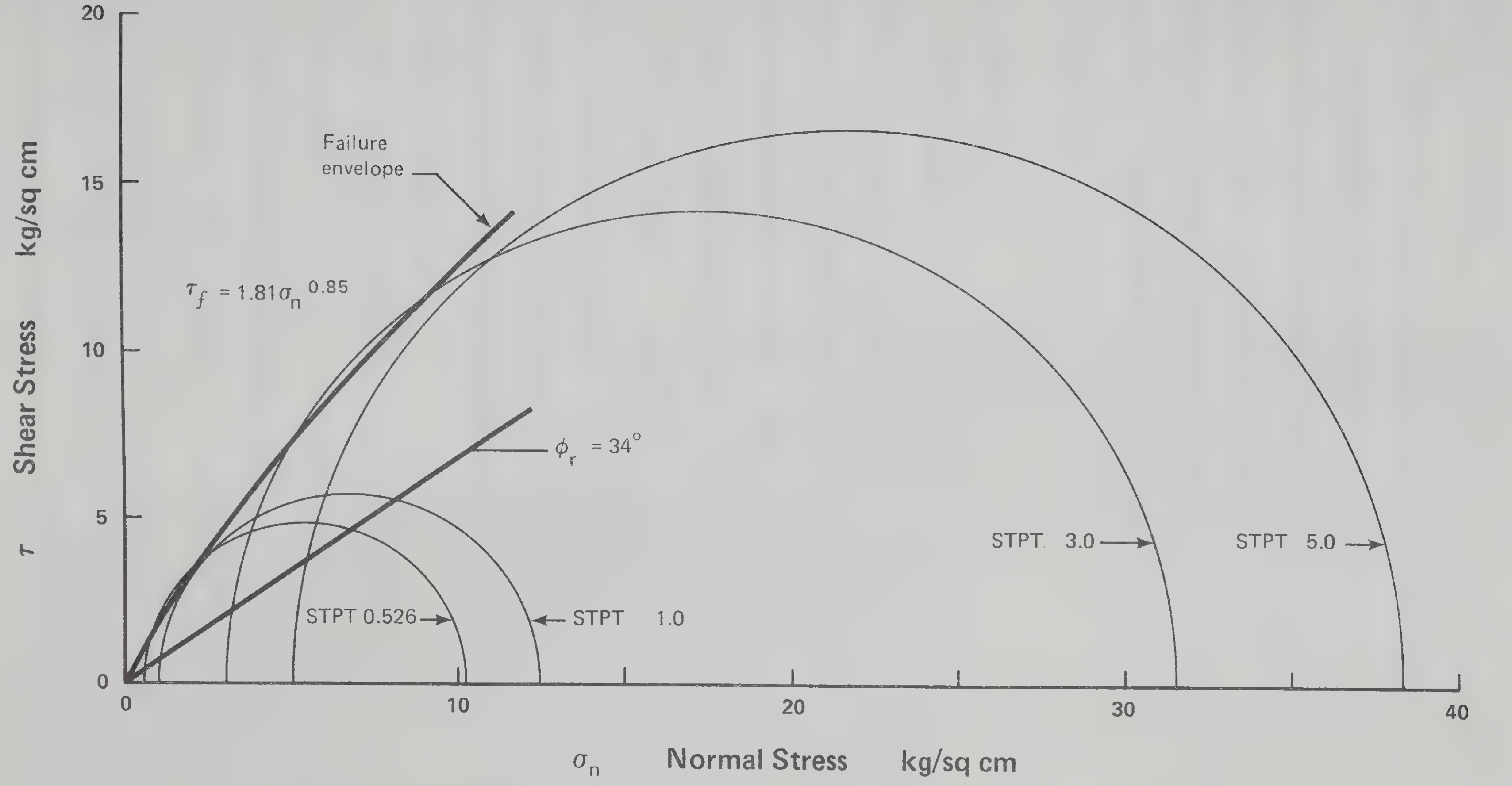

Figure 6.2 Drained Triaxial Tests on St. Peter Sandstone

envelope at an inclination of 34° is drawn on the assumption that a residual state had not been reached in Test STPT-0.526.

The strength results are not surprising in the light of the data reported in the previous chapter, but the very small volumetric expansion before failure is remarkable. Although largely a function of strain energy storage in the testing apparatus, the sudden nature of the failure, at both low and high stresses, attests to the brittleness of the material.

6.2.6 Conclusions

The behaviour of St. Peter Sandstone, in both direct shear and triaxial test configurations, is similar to that of Athabasca Oil Sand (particularly the Series C tests). It may be argued that the envelopes presented are minimum envelopes; that is, strength <u>in situ</u> must be at least equal to (and probably higher than) that obtained in the laboratory. Sampling, specimen preparation, and test procedures can not in any way add to the strength: they can only decrease it; therefore the uppermost data points are probably the most reliable. Nevertheless, a statistical curve-fitting technique has been employed where applicable to eliminate personal bias.

The component of strength above that of a normal dense sand is quite remarkable for the St. Peter Sandstone. Its grains display a much greater degree of roundness than the sand grains from the McMurray Formation, and in general the grains are more equant; yet the degree of textural interlock is sufficient to yield shear strengths at least twice as high as those of a dense sand (within the test stress range) and considerably higher than the strengths from Series C of the

oil sand shearbox tests. The envelope curvature is somewhat less than that of the other materials tested, as the individual grains of the St. Peter Sandstone are more competent because of the multi-cyclic nature of the deposit: incompetent, cleavable, and stressed grains have been eliminated. The tendency for dilative behaviour to be suppressed in favour of grain shear is therefore less than in other test materials.

6.3 Swan River Sandstone

6.3.1 Sampling

Block samples of Swan River Sandstone were obtained from the banks of the Swan River, eight kilometers downstream (east) of the town of Swan River in Manitoba (Figure 6.3). A single block large enough to provide 20 shearbox specimens was trimmed by hand from the back-slope, placed inside a plastic bag to prevent desiccation, and carefully set on a layer of loose sand in a cardboard box. Only partial success in obtaining samples was achieved: upon arrival at the testing laboratories, the block specimen had already lost close to 50% of its volume through attrition of grains and cleavage along pre-existing planes of weakness.

6.3.2 Specimen Preparation

Specimens of Swan River Sandstone were prepared for shearbox testing by the same methods used in the preparation of St. Peter Sandstone specimens (Section 6.2.2).

The block sample of Swan River Sandstone provided only four intact specimens. During the trimming of the fifth specimen, the remainder of the block (about 4×10^4 cc in volume) disintegrated

Legend

- ▲ Swan River, Manitoba
- ○ Sample locations, Swan River Sandstone and preglacial sand
- ● Sample locations for basal clay study

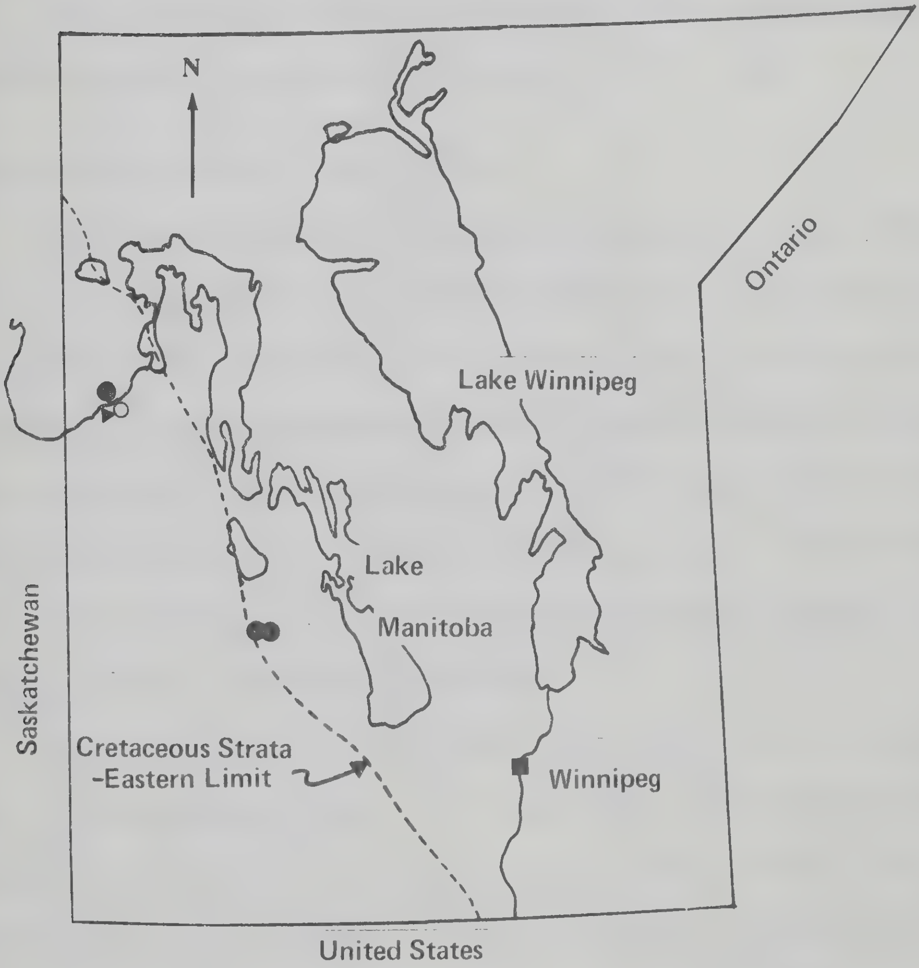

Figure 6.3 Manitoba Sample Locations

into chunks, none of which were large enough to serve as shearbox or triaxial specimens.

The porosities and bulk densities of the specimens were calculated from pretest dimensions within the brass trimming ring, and from post-test dry weight. The calculated saturated bulk densities varied from 2.04 to 2.10 gm/cc, corresponding to porosities of 37.0% to 33.7% respectively.

Irregularities of the specimens within the brass trimming ring probably account for most of the variation in the data.

6.3.3 Geology and Sample Description

The Swan River Formation, which crops out in west central Manitoba (Figure 6.3), consists largely of quartzose, arenaceous sediments approximately 60 m in depth, and is of a general transgressive nature. It is the lithologic equivalent of the McMurray Formation, although it may be somewhat younger stratigraphically. The Swan River Formation lies unconformably upon a Paleozoic erosion surface, but the limestones underlying it may be somewhat older than the limestones underlying the McMurray Formation in Alberta.

The primary source of the Swan River Sandstones was the igneous rocks of the Canadian Shield to the northeast. Repeated reworking in the final depositional environment is not evident from the grain characteristics. This indicates that the unit likely represents a single major transgression over a geologically short time period.

At the base of the Swan River Formation is a sequence of fine-grained materials which consist of clays and clayey silts with occasional lignite bands and minor pyritic concretions. Although they are separated

by somewhat over 800 km, the similarities between the Swan River Formation and the McMurray Formation are striking. Even the sub-parallel stress-relief joints evident in the McMurray Formation outcrops are found in the outcrops of Swan River Sandstone.

The sandstone displays grain characteristics similar to those of the McMurray Formation sands; for example, the mineral content is almost entirely quartzose, the grain shape varies from rounded to angular, the grain surfaces display less rugosity than that observed in the oil sands, and a good degree of sorting is evident.

6.3.4 Testing Procedure

Five intact specimens were tested by direct shear, but only four generated adequate failure data. (The sample tested at 8.0 kg/cm^2 had been disturbed before testing.) The sixth specimen was disaggregated and redensified in a shearbox by the methods described in Chapter V (Section 5.8.1). The same shearbox and testing frame used in previous shearbox tests was employed for these specimens, and the shearbox separation was again 0.4 mm. Test displacement rates employed were relatively rapid (5.4 x 10^{-5} cm/sec) because permeabilities were high. All tests were continued to a residual strength state.

6.3.5 Test Results

Table 6.3 reports test data for the shearbox tests on the Swan River Sandstone; Figure 6.4 is a graph of the relationship between normal stress and shear stress at failure; and individual plots of the relationships between displacement and volume change, and between displacement and stress ratio, may be found in Appendix E.1.9.

The failure envelope in Figure 6.4 is drawn as a power law

TABLE 6.3 SWAN RIVER SANDSTONE SHEARBOX TESTS

	n^*	B.D.*	σ_n^*	τ_f^*	$\frac{\tau_f}{\sigma_n}^*$	d_f^*	ϕ_f^{s*}	ΔV_t^*	$\Delta\dot{V}_f^*$	ϕ_r^{s*}	Comments
Swan River Shearbox Series A 0.5 kg.	33.7	2.10	0.50	1.03	2.07	.069	64.2	1.97	28	33.8	Bedding Planes Within 10° of Shearbox Failure Plane
" " 1.0 kg.	34.0	2.09	1.00	2.93	2.93	.093	71.1	2.46	35	35	" "
" " 2.0 kg.	36.4	2.05	2.00	3.81	1.91	.137	62.3	2.02	18.8	-	" "
" " 4.0 kg.	37.0	2.04	4.00	7.94	1.98	.129	63.3	1.01	18.2	33.5	" "
" " 8.0 kg.	37.0	2.04	8.00	7.52	0.94	.194	43.2	0.49	5.3	31.5	" " (Disturbed during trimming)
Disagg. Redensified Swan River Sandst. 4.0	37.2	2.04	4.00	3.23	0.81	.180	38.9	1.19	6.8	31.5	

* See Table 5.7 b for a complete legend

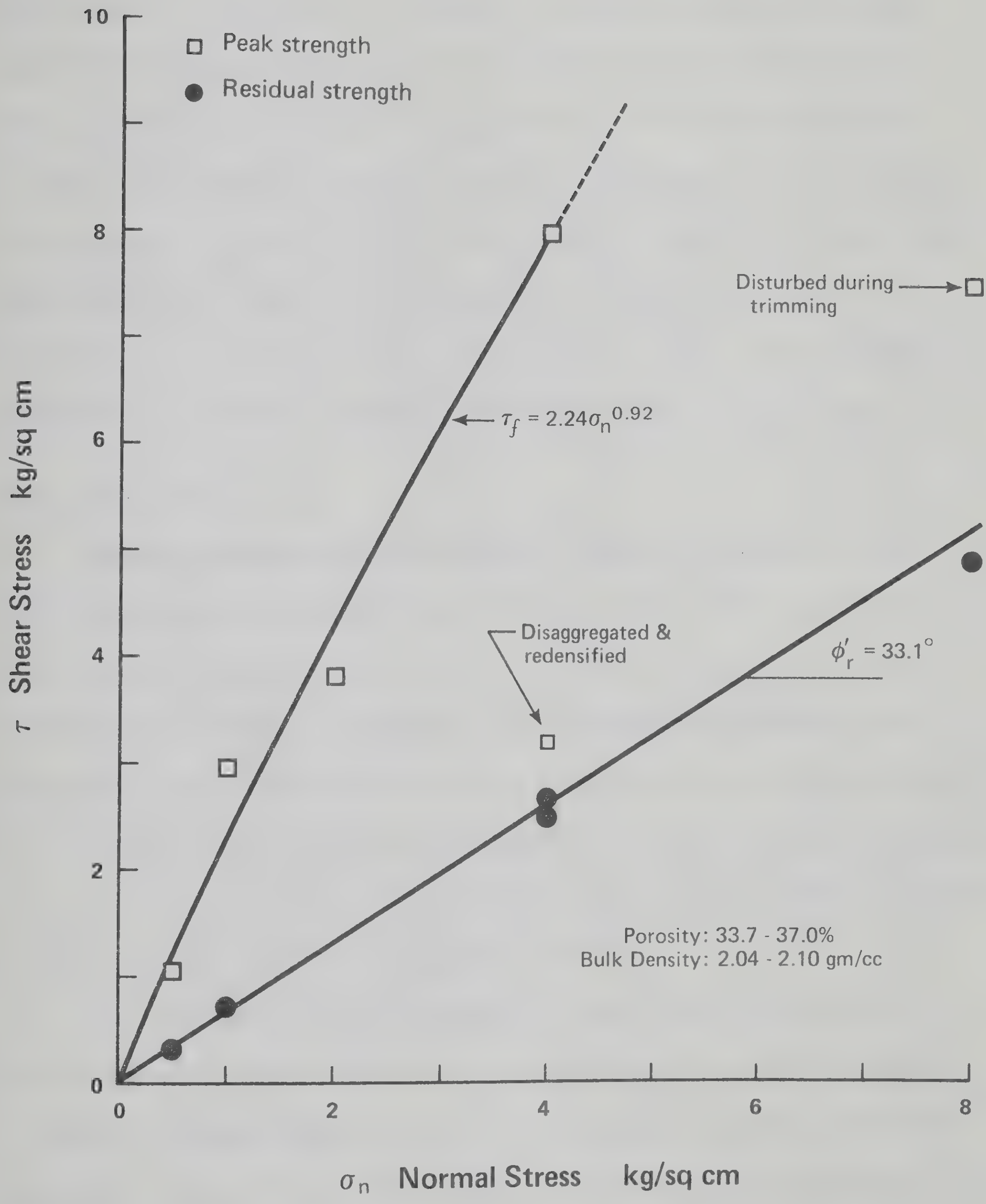

Figure 6.4 Swan River Sandstone Shearbox Series

curvilinear relationship (the results of the test performed at 8.0 kg/cm^2 were not included.). Actually, the data points may be connected by a straight line, but the previous shearbox data indicate that a curvilinear envelope is more probable. The coefficients of the power law regression equation and the coefficients of correlation are presented in Table 6.5. The stress-displacement and strength characteristics are similar to those generated in previous test series: displacement to failure increases with normal stress, and progressive suppression of dilative behaviour occurs at higher stress levels.

6.3.6 Conclusions

Notwithstanding the high porosity (35.3%) compared to the St. Peter Sandstone, the strength results are similar. Only four tests over a limited stress range could be performed, but sufficient data were generated to permit comparison. The porosity achieved in the redensified test (37.2%) is close to the porosity of undisturbed samples, but it is obvious that the fabric responsible for the unusual strengths can not be duplicated by artificial densification. The fabric is therefore not a direct function of specimen density.

The dilation rates at failure are lower than those of the St. Peter Sandstone; nevertheless the total dilatancy in the first cycle is higher. Increased angularity of the specimens may aid in vertical propagation of the failed (dilating) zone, making it larger than in the well-rounded St. Peter Sandstone. Therefore an overall greater total dilatancy may be obtained even though dilation rates at failure are lower. The much lower porosities (27%) of the St. Peter Sandstone support this hypothesis, since, if other conditions were constant,

greater dilatancy would be observed in denser specimens.

6.4 Swan River Preglacial Sand

6.4.1 Sampling

A bed of sand (presumably interglacial or preglacial, since it is overlain by till) was observed during the field trip to obtain specimens of Swan River Sandstone. Although this sand is geologically young, it was sampled for comparative study since the overall lithology is quartzose and no cohesion is displayed. Block specimens were obtained by shaping a circular pedestal on the outcrop, then slowly trimming down a circular tin to provide a flush fit to the sample block. Loose sand was poured in the sides as required to provide lateral support. The specimens arrived at the testing laboratories intact.

6.4.2 Sample Preparation

The method used to prepare specimens for shearbox testing was identical to that used in the preparation of specimens of St. Peter and Swan River Sandstones (Section 6.2.2).

6.4.3 Geology and Sample Description

Swan River preglacial sand occurs in a layer at least four meters thick in a river outcrop 12 km east of the town of Swan River in Manitoba (Figure 6.3). It is a horizontally bedded, slightly ferruginous sand displaying no wet cohesion, but some dry cohesion due to desiccated interstitial clay. Current bedding is characteristic of the medium-grained sands, whereas horizontal laminae are the

dominant feature of the fine-grained sands. No till underlying the sand was observed, although outcrops were not extensive enough to preclude this possibility. The sand is thought to be preglacial or interglacial, perhaps deposited in a preglacial lacustrine delta regime.

The medium-grained sands are incompetent and proved impossible to sample, but a number of fine-grained specimens were obtained. The horizon sampled and tested was classified as a quartzose sandy silt, with a ferruginous reddish hue. Thin section examination revealed a few lithic fragments and accessory clay minerals and feldspars. Pretest porosities of 35.0% to 36.2% were measured. Mineralogic assessment of a fine-grained sand fraction revealed significant quantities of montmorillonite, confirming a Quaternary origin for these sands.

6.4.4 Test Procedure

The procedures used were identical to those used in the Swan River Sandstone series of shearbox tests. Specimens were trimmed with the bedding planes within five degrees of the shear plane. Only four specimens were tested; further testing was considered unnecessary.

6.4.5 Test Results

Table 6.4 lists important test and failure data; Figure 6.5 shows the relationship between normal and shear stresses at failure and at a residual state; and Appendix E.1.10 contains computer plots of the relationships between displacement and stress ratio and between displacement and volume change.

Dilative rates at failure, secant ϕ values, and stress ratios at failure are much lower than those of the test series reported previously in this chapter, but residual envelope data are very similar.

TABLE 6.4

SWAN RIVER PREGLACIAL SAND SHEARBOX TESTS

	n^*	B.D.*	σ_n^*	τ_n^*	$\frac{\tau_f}{\sigma_n}^*$	d_f^*	ϕ_f^{s*}	ΔV_t^*	$\dot{\Delta V}_f^*$	ϕ_r^s	Comments
Swan River Shearbox Series B 1.0 kg.	35.2	2.07	1.00	0.93	0.93	.114	42.9	1.00	8.5	35	Bedding Planes within 5° of shearbox failure plane
" " 2.0 kg.	35.0	2.08	2.00	1.702	0.85	.148	40.4	0.83	8.5	34	" "
" " 3.5 kg.	36.1	2.05	3.50	2.82	0.81	.212	38.8	7.08	6.0	33	" "
" " 5.0 kg.	36.2	2.05	5.00	3.98	0.80	.229	38.5	0.91	5.8	34	" "

* See Table 5.7 b for a complete legend

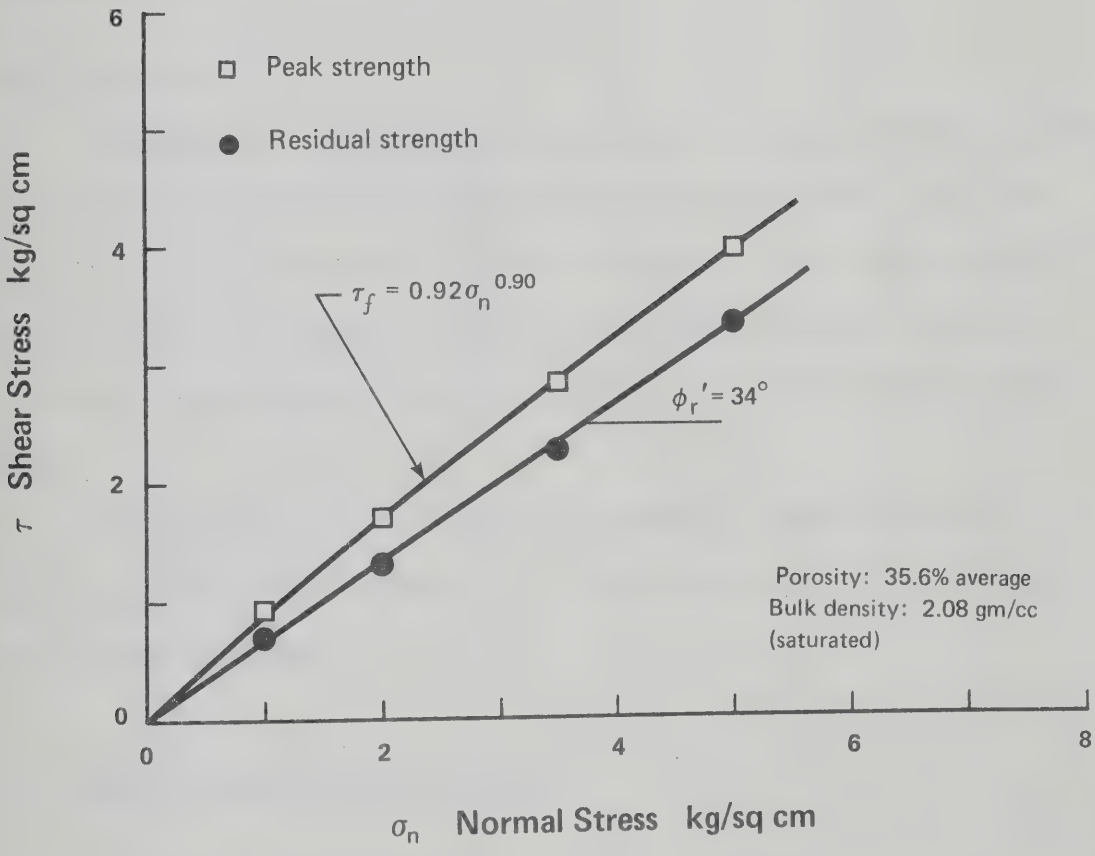

Figure 6.5 Swan River Preglacial Sand Shearbox Series

Envelope curvilinearity is again demonstrated, but is less pronounced than in the other test series. Failure envelope coefficients and statistical coefficients of correlation may be found in Table 6.5. Displacement to failure is considerably greater, and the total dilatancy in the first cycle is less than that of the intact materials previously tested.

6.4.6 Conclusions

Porosities of the Swan River preglacial sand are similar to those of the Swan River Sandstone, but strengths are much lower. The component of strength at failure is very similar to that obtained in the series of tests on compacted Ottawa Sand, and the dilative rates at failure are also similar, notwithstanding a gross difference in grain size.

The component of extra strength related to great geological age is missing in this material: it is a young sand, and it behaves as a normal dense sand.

6.5 General Comments and Conclusions

6.5.1 Dilative Behaviour and Displacement

Figure 6.6 presents the dilation characteristics of the three materials reported in this chapter; curves generated from the Ottawa Sand tests and from Oil Sand Shearbox Series C tests are included for comparison. The conclusions to be drawn are incontrovertible. The high strength is a result of high dilative rates before and during failure; the source of the high dilative rates is the intergranular fabric; and the intergranular fabric is a result of the geological,

TABLE 6.5 POWER LAW FAILURE ENVELOPE CORRELATIONS

Test Series	Curve Equation	Value of Coefficient a	Value of Coefficient b	Correlation Coefficient r	Residual Stress Ratio (tan ϕ_r)	Comments
St. Peter Triaxial	$\tau_f = a \cdot \sigma_n^{\,b}$	1.81	0.85	Insufficient Data	0.674	No Statistical Test Performed: Hand Sketched
St. Peter Shearbox	$\tau_f = a \cdot \sigma_n^{\,b}$	3.00	0.800	0.986	0.642	Eight Valid Data Points
Swan River Sandstone	$\tau_f = a \cdot \sigma_n^{\,b}$	2.24	0.922	0.976*	0.652	Four Valid Data Points
Swan River Pre-Glacial Sand	$\tau_f = a \cdot \sigma_n^{\,b}$	0.922	0.901	1.000	0.674	Four Valid Data Points

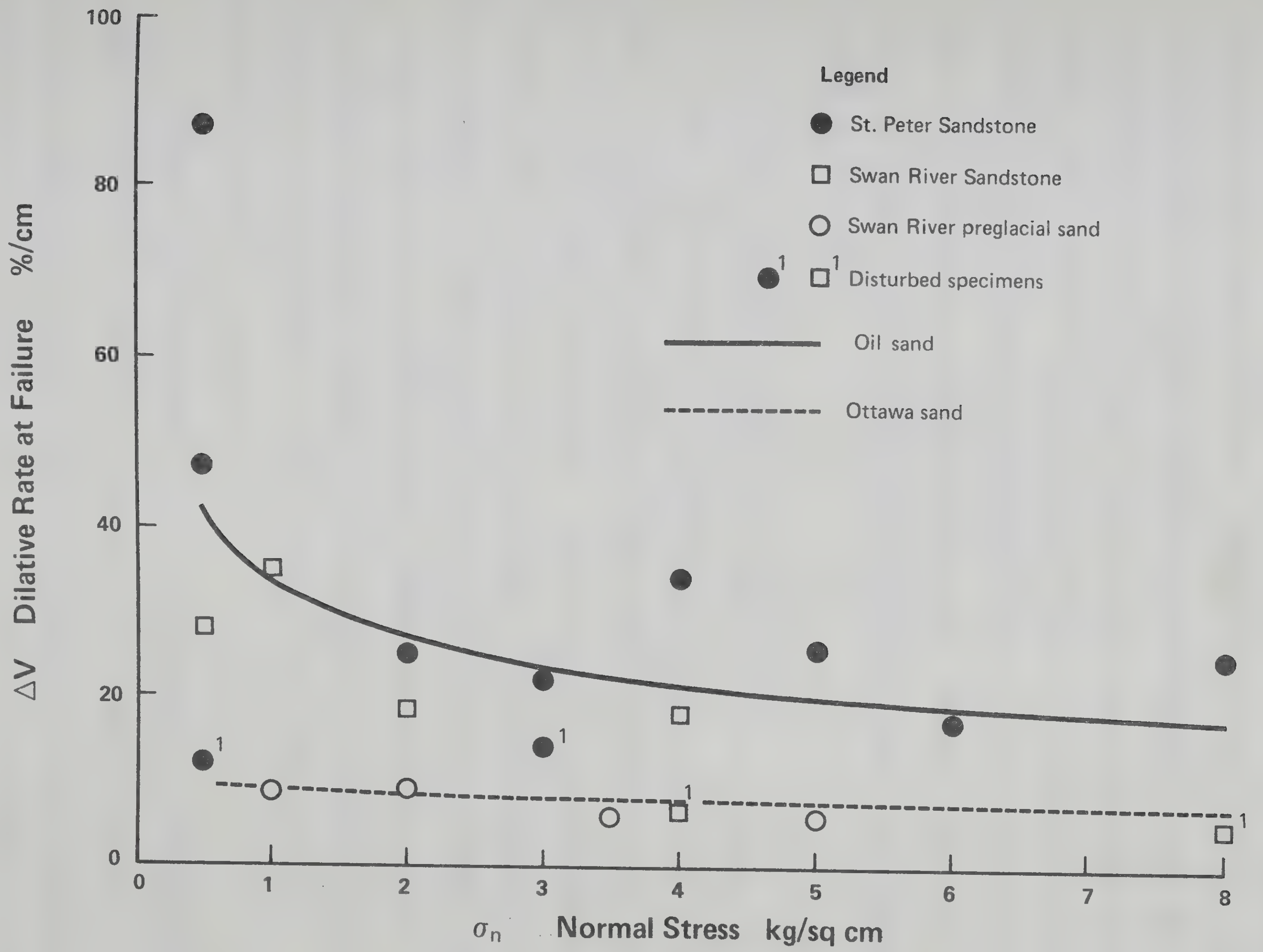

Figure 6.6 Dilative Behavior at Failure as a Function of Normal Stress

postdepositional history of the sands.

Figure 6.7 demonstrates the increase in total displacement to failure in specimens displaying lower strengths. The St. Peter Sandstone shows the least displacement, although it was the coarsest-grained natural material tested; the Swan River preglacial sand, which was the finest-grained material tested, displays the largest displacement to failure. The relationships presented in Figure 6.7 are sketched as straight lines: it should be emphasized that this was done to accentuate the differences between the data groups. In fact, there is reason to believe that a curvilinear relationship exists, as indicated by the data points.

6.5.2 Envelope Curvature, Coefficients, and Correlation Methods

Table 6.5 presents the coefficients of the statistically fitted power law curves for the three materials tested. In most cases, the power law correlation coefficient is greater than the correlation coefficient derived from a linear assumption. The single exception to this statement is the Swan River Sandstone group of tests, which have a coefficient of correlation of 0.987, assuming a linear envelope. Insufficient data were generated to fully assess the strength of this material, but further data at higher stress levels would probably emphasize envelope curvilinearity.

The power law relationships are not applicable to significantly higher stress levels than those employed in the testing program. A power law equation of the form used in this work has an ever-decreasing tangent value as stress level increases. This is unrealistic, and it may be assumed that at higher stress levels the failure envelope will

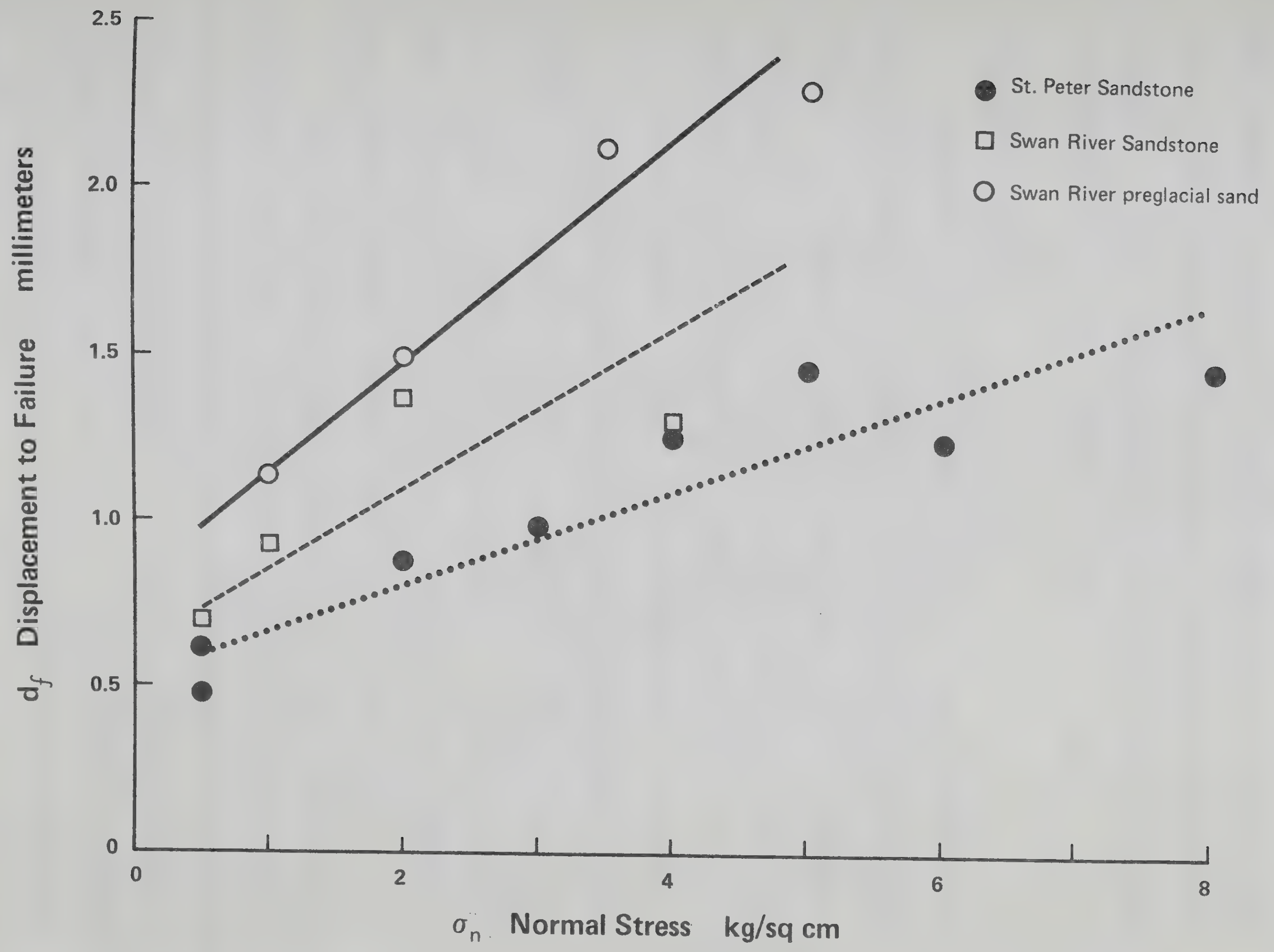

Figure 6.7 Displacement to Failure as a Function of Normal Stress

parallel the residual stress envelope. Parallelism would be expected to occur at that stress where the dilative rate at failure is zero. Higher normal stresses may, however, cause fracture of grains and destruction of the intergranular texture responsible for the high strengths: failure envelopes would then be lower than anticipated by an assumption of fabric disruption only by shearing.

6.5.3 Conclusions

Synthesis of the data reported in this chapter with the data reported in Chapter V indicates that geological, postdepositional texture (i.e. diagenetic fabric) is responsible for the strength of these materials. The intergranular texture responsible appears to be characteristic of geologically old quartzose sands which do not contain true cementing agents to provide a stress-independent cohesion.

Although all three "old sands" tested are underlain directly by carbonate rocks, none contain any significant interstitial carbonate cement. Nevertheless, if the materials contained sufficient cement to result in a significant true cohesion, failure envelope curvilinearity and high strengths would still be expected.

Diagenetic processes have acted for millions of years on these geologically old sands: tectonic and metamorphic processes have not noticeably altered the deposits; therefore a diagenetic strength source is the only possible explanation. The only significant diagenetic processes operating on quartzose sands at shallow depths of burial are those of quartz solution and deposition; Chapter VII discusses these processes.

CHAPTER VII

THE FABRIC AND SINGLE GRAIN CHARACTERISTICS OF LOCKED SANDS

7.1 Introduction

The term "locked sands" was chosen as an appropriately descriptive name for old, quartzose sands displaying little or no cohesion at zero stress, and having a particularly large dilative strength component during shear. When the dilative component is suppressed by high normal loads, particle shear and a markedly curved failure envelope result. The postulate of the existence of a distinct class of engineering materials with unique stress-strain-strength characteristics requires supporting data. This chapter identifies the specific textural and fabric features responsible for the engineering behaviour of locked sands.

Microscopic techniques were used to determine the microtextural and microfabric characteristics responsible for the high dilatancy rates during shear, and to define the geological framework in which these characteristics could be placed. Four natural materials discussed in the preceding two chapters were examined: McMurray Formation sands, St. Peter Sandstone, Swan River Sandstone, and Swan River preglacial sands. Optical and electron microscopes were used.

7.2 Sandstone Nomenclature

The term "sandstone" implies a material with a stress-independent cohesion sufficient to provide a definite competence to saturated, hand-held specimens. "Sand" implies no cohesion. Sandstones may vary from low-porosity quartzites which display unconfined compressive strengths in the order of 700 kg/cm^2 (10,000 psi) to friable strata from which it is impossible to obtain a specimen for compressive strength testing. The frequent occurrence of the term "friable sandstone" in geological literature, particularly in reference to sandstones from nonmetamorphic, nontectonic areas, suggests the existence of a separate class of engineering materials, viz., locked sands. The following definitions are suggested for arenaceous materials:

1. Sand: an aggregate of dominantly sand-sized particles displaying little or no cohesion (less than 0.3 kg/cm^2) in a saturated state, with an approximately linear peak strength envelope that is less than 10° to 12° steeper than the residual envelope.

2. Locked sand: an aggregate of dominantly sand-sized particles displaying little or no cohesion in a fully saturated, stress-free state, characterized by a curved peak strength envelope that is more than 10° to 12° steeper than the residual envelope.

   Geological age and quartzose mineralogy seem to be prerequisites for locked sands. Porosities somewhat lower than those of a dense sand are characteristic. The material displays a large dilative strength component during shear which is progressively suppressed by higher normal loads.

3. Sandstone: an aggregate of sand-sized particles having

either interparticle physical cementation, or a degree of interlock sufficient to impart an appreciable stress-independent cohesion in a saturated state. In the absence of true mineral cement, porosities are low, probably less than 20% in a well-sorted material.

Although the definition of locked sand is based on a limited number of materials, it is likely that locked sands are common in the Cretaceous and Tertiary strata of western Canada. Among Cretaceous sands which probably display some locked sand characteristics are the Milk River Sandstone; the Cadomin Formation, the Cutbank Sandstone, the Ellerslie Formation, and other quartzose, sandy equivalents of the Lower Manville; as well as other quartzose sands which are not cemented by calcium carbonate or iron oxide. Tertiary sands which may display similar behaviour include the Ravenscrag and Paskapoo Formations (where not cemented), although the necessary diagenetic alteration is diminished because of lower burial depths and lesser age.

7.3 Optical Microscope Studies

7.3.1 Equipment

The optical microscope used was a Carl-Zeiss Mono-Binocular Petrographic Microscope, with a built-in 35 mm camera. In addition to the usual petrographic microscope accessories, an automatic exposure device was used to obtain correct exposure at all light levels. Magnification ranges used in this study ranged from 10 to 250 times, as measured on the 35 mm colour slides or the black and white negatives. Further tenfold magnification during photographic printing was achieved without significant loss of grain density.

7.3.2 Thin Section Preparation

Representative samples of the locked sands (Athabasca Oil Sands, St. Peter Sandstone, Swan River Sandstone) were set aside for the manufacture of optical microscope thin sections of standard thickness (30 μ). The friability of the material, the presence of bitumen in the oil sands, and the lack of cohesion when wet necessitated the use of unusual preparatory techniques.

Oil-free medium- or coarse-grained sandstones (St. Peter Sandstone, Swan River Sandstone, and oil-free McMurray specimens) were relatively simple to prepare. Careful handling was required to avoid disintegration during impregnation with plastic resin, but no complex or unusual procedures were necessary.

Equant specimens (20 to 100 cc) were cut from hand specimens and block samples through careful use of a coarse-toothed hack saw blade. The specimens were allowed to air dry, heated in an oven to 80° to 90°C, then placed carefully in a shallow dish containing premixed and heated (100°C) epoxy resin. Capillary tension caused the epoxy to flow into the specimens (at these temperatures the viscosity of the epoxy appeared to be similar to that of water at 25°C); the epoxy was permitted to harden; and standard thin section preparatory techniques were then followed.

High quality thin sections could be obtained consistently through this method: grain plucking was minimal, uniform thickness was achieved readily, and the microfabric was preserved. Nevertheless, the high incidence of cracked grains suggests that great care must be taken during the cutting and grinding of thin sections. For future work the use of a strong dye mixed with the impregnating resin is suggested. Clear

resin and quartz are difficult to differentiate microscopically in plain light, and the addition of a strong dye would permit the use of nonpolarized light during microscopic examination.

Thin section preparation of fine-grained oil-poor sands and silty sands was more complex than the preparation of coarse-grained oil-free locked sands.

Oil Sand Shearbox Series A consisted mainly of fine-grained sands and silts, with the first eight specimens having relatively low bitumen contents or no bitumen whatsoever. Drying the samples in a cold storage room (at -20°C) or in a heated room (at 20°C) resulted in extensive crazing; therefore the samples were freeze-dried. Specimens at -20°C were placed in a vacuum flask, and the flask was surrounded by dry ice while vacuum was developed. Twenty-four hours were required at a vacuum of 250 μ of mercury pressure (3.3×10^{-4} atmospheres) to assure drying.

When dry, the samples were encased in polyester casting resin and allowed to set. This method has not proved entirely satisfactory: reaction occurred between the small quantity of bitumen and the resin, resulting in bubbling and separation of the resin from the specimen. This method, however, was satisfactory for oil-free specimens. Some penetration of the high molecular weight resin into the oil-free specimens was achieved through repeated evacuation while specimens were totally immersed in the casting resin.

The encased specimens were cut in the desired orientation, but grinding soon revealed inadequate penetration of resin into the fine-grained layers. To achieve high-quality, uniform surfaces, further impregnation was required. After a relatively flat surface was

obtained (on 360 mesh silicon carbide paper), the specimens were heated slowly to approximately 80°C, and several drops of premixed, rapid-setting epoxy were applied. The specimen heat resulted in rapid flow and absorption of some of the epoxy, and the impregnation process was furthered by pressing a flat, heated spatula blade on the specimen surface. After it had hardened, the excess epoxy was ground off. When necessary, the process was repeated several times to ensure that the epoxy penetrated at least 30 μ into the specimen surface. The flat surface was then attached to a glass slide, and normal thin section techniques were followed.

All attempts to make high-quality thin sections of medium- and coarse-grained oil-rich sands from borehole specimens failed. No resin was found to meet the following three requirements: low temperature applicability, nonreactive with bitumen, and sufficiently penetrative to permit adequate grain cementation.

Comparison of bulk density data from laboratory specimens and from borehole geophysical devices indicates that coarse-grained oil-rich sands undergo 10% to 20% volumetric expansion (Chapter IV), and therefore microfabric must be somewhat disturbed. Examination of thin sections prepared by a coking-impregnation technique developed at the Alberta Research Council revealed a "sand-grain-floating-in-matrix" structure. This method, although adequate for mineralogy, was inadequate for the purposes of this research.

The only coarse-grained oil-rich specimens prepared were several hand specimens obtained from outcrops. The bitumen had hardened sufficiently to permit encasement, but the results of thin sectioning were

not consistently satisfactory because of excessive grain fracture.

Over 500 black and white negatives and colour transparancies were obtained from the optical microscope study. The study material consisted of 53 thin sections, approximately 25 of which were of low quality because of grain plucking, excessive grain fracture, improper thickness, or fabric disruption. The experimental nature of thin sectioning techniques in these materials, and the difficulty of dealing with specimens containing bitumen, were responsible for most of the poor-quality thin sections.

7.4 Scanning Electron Microscope Studies

7.4.1 Equipment

The scanning electron microscope used was a Cambridge Stereoscan (Model S-4). The secondary electron emission at excitation levels of 10 to 30 kV from a coated specimen in a vacuum chamber (10^{-5} torr) was viewed directly on a cathode ray screen, and also occasionally photographed on a 57 mm square negative. All specimens were coated with carbon, then gold (each layer approximately 50 to 75 Å thick) in a hot-wire vacuum evaporator (Edwards High Vacuum Company). Nonconductivity and otherwise nonideal behaviour of quartz sand specimens resulted in a maximum resolution level of about 500 Å. This value is, however, well below the minimum resolution range used in this study (2000 Å), and was therefore not detrimental to the interpretation of the photographic data. The specimen mounting frame used during observation had rotational, translational, and tipping controls, which provided almost complete access to the specimen surface at any desired

orientation, and also permitted stereoscopic pair photography.

7.4.2 Specimen Preparation Techniques

Surface textures and shapes of individual grains were studied by scanning electron microscope methods. For oil-rich sands, all bitumen was removed by extraction with toluene. For all natural sands, the grains were disaggregated in water, cleaned ultrasonically or by gentle shaking for several minutes, thoroughly dried, and then sieved. The small metallic stubs used in the scanning electron microscope were cleaned, coated with a thin layer of low-resistance contact cement, and immediately dusted with a few dry grains to provide a low grain density, resulting in the best possible photographic conditions.

Undisturbed specimens of several arenaceous materials were mounted for electron microscopy. Freeze-dried oil-poor oil sand specimens, and dried intact specimens of other locked sands were trimmed carefully to form small cylinders or polygonal prisms about 0.8 cm in diameter and 0.8 to 1.5 cm in length. The base of the cylinder was attached to the metallic scanning electron microscope stub with low-resistance contact cement, and some of the cement was painted on the sides of the specimen with a soaked cotton swab. This was found necessary to insure a continuous conductive layer which would permit electron travel between the specimen surface and the stub. Before viewing, a fresh fracture face was created and the specimen was coated in vacuo with a layer of carbon and two layers of gold, each about 50 to 75 Å thick. A double gold coating was used because of the excessive "charging" observed in the first specimens which were single coated. The charging was due to incomplete conductive communication with the

base, and resulted in intensely bright areas on the viewing screen.

It has not proved feasible to date to study undisturbed coarse-grained oil-rich specimens by scanning electron microscope methods: bitumen tends to bubble or move when subjected to high vacuum; coating does not adhere well to the bitumen, resulting in charging; and coarse-grained specimens have little coherence and tend to fly apart during the rotational coating process. Only individual grain mounts of coarse-grained material with the bitumen removed were viewed.

Table 7.1 is a list of the individual specimens examined by scanning electron microscope methods. Because the scanning electron microscope produces a photograph of a surface in three dimensions, it is particularly useful to study grain shapes and textures. Therefore, over 90% of the specimens listed in Table 7.1 were individual grain mounts. Over 400 photographs were taken; selected photographs are presented here.

To avoid experimental bias, a random selection method for grain shape and surface texture examination was employed. The scanning electron microscope operator (a technician with no geological background) was instructed to mount specimens, to randomly turn the translation controls, and to choose the nearest grain to the center of the viewing screen. Two photographs were taken: one showing the entire grain, and one showing the surface texture of the center portion of the grain. This procedure eliminated personal bias in the selection of surface texture specimens.

7.5 Grain Shapes

All materials tested were highly quartzose; quartz generally

TABLE 7.1

SUMMARY OF SCANNING ELECTRON MICROSCOPE MATERIALS

Specimen Identification	Description and Comments	Usable Negatives
A. Undisturbed Specimens	-Diagenetic fabric study	43
(1) B1 to B7	-Oil sand specimens, fine-grained, 16-17 meters (1)	29
(2) STP-1A	-St. Peter Sandstone, Minneapolis	7
(3) SR-A-1	-Swan River Sandstone, Manitoba	7
B. Grain Mounts	-Study of size, shape and surface texture	327
(1) ATS 134'-135'	-Fine oil sand grains, borehole specimen, 17 m (-100+200,-200+300)(2)	7
(2) ATS 156.8'	-Oil sand, borehold specimen 23 m (-100+200, -200+325)	16
(3) ATS 189.75'	-Oil sand, borehole specimens, 33.4 m (-10+20, -20+40, -40+60, -60+100, -100+200)	40
(4) ATS 190.5'	-Oil sand, borehole specimens, 33.6 m (-100+200, -200+325)	16
(5) ATS 210'	-Coarse-grained oil sand, borehole specimens, 40 m (-20+40, -40+60, -60+100, -100+200)	32
(6) MD-75-1-2	-High Hill River, crossbedded sand, Middle Member (-60+100, -100+200)	16
(7) MD-75-1-4	-High Hill River, Coarse sand just above basal conglomerate (-100+200)	8
(8) MD-75-2-1	-Cottonwood Creek, coarse sand 3 m below oil (-20+40, -60+100)	16

(1) depth below top of McM. Fmn.
(2) sieve ranges studied

TABLE 7.1 (continued)

Specimen Identification	Description and Comments	Usable Negatives
(9) MD-75-3-1	-Mouth of Christina River, Middle Member McM. Fmn. (-60+100)	8
(10) MD-61-4	-Zebra-striped sand, Christina River outcrop, base of McM. Fmn. (-20+40, -40+60, -60+100)	24
(11) MD-75-6-2	-Coarse sand, 5 meters above basal clay, Mackay River (-60+100, -100+200)	16
(12) STP-1A	-St. Peter Sandstone, Minneapolis (-60+80, -80+100, -100+140, -140+200)	52
(13) SR-A-1	-Swan River Sandstone, Manitoba (-60+100, -100+200, -200+325)	32
(15) River Sand	-North Saskatchewan River sand, Edmonton (.2mm - .4mm fraction)	8
(16) Ottawa Sand	-Coarse Ottawa Sand, as received (-20+30)	3
(17) Crushed Ottawa Sand	-Crushed and sieved (-100+200)	5

displays no strong cleavage and only occasional rough partings (Berry and Mason, 1959). The quartz grains of the McMurray and Swan River Sandstones came largely from igneous terrain; therefore the initial detrital grains were roughly equant. In addition, transport has sharply decreased the incidence of acicular or tabular grains. St. Peter Sandstone grains likely have been derived from older arenaceous materials, and the lengthy time period in high energy environments has resulted in a high degree of sphericity and roundness (Dapples, 1955). Diagenetic alterations, however, reduce the expected equant grain nature. In addition, since larger, heavier particles are more susceptible to transport attrition, the incidence of nonequant grains increases with decreasing grain size, as does the individual grain angularity.

7.5.1 Grain Shapes of McMurray Formation Sand

Within the limited sampling interval, grain shapes varied from equant to subequant, and a distinct relationship was observed between grain size and shape. Because the sand is quartzose, equant grains predominate (Plate 7.1a), especially in the coarse-grained fraction. In the finer-grained fractions, however, the incidence of equant grains is lower, and the incidence of acicular, prismatic, and tabular grains is greater (Plate 7.1b). Nonequant grains observed in the oil sands (i.e. acicular, prismatic, or tabular) generally reflected the mineralogy of the grains (feldspar and muscovite); for example, the deformed mica visible in Plate 7.1b.

Mellon (1956) indicated a plutonic source for the detrital McMurray sands, but the proximity of significant bodies of Paleozoic sandstones (the Athabasca Formation in northwest Saskatchewan) suggests

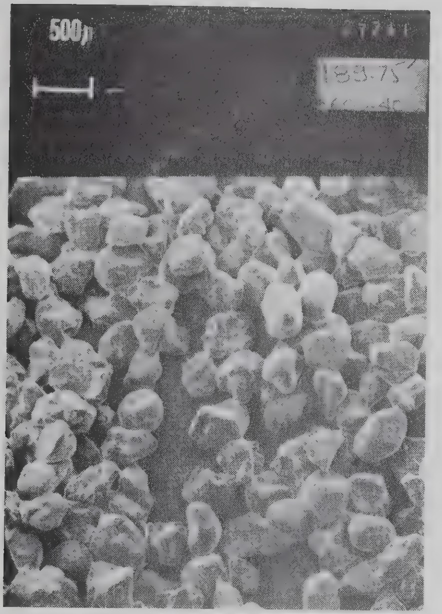

7.1a McMurray Formation
Middle Member, medium-grained fraction.
(-40mesh +60mesh)

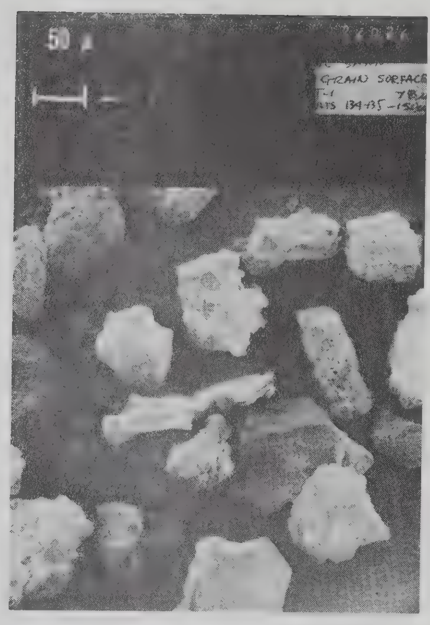

7.1b McMurray Formation
Upper Member, very fine-grained sand fraction.
(-200mesh, +325mesh)

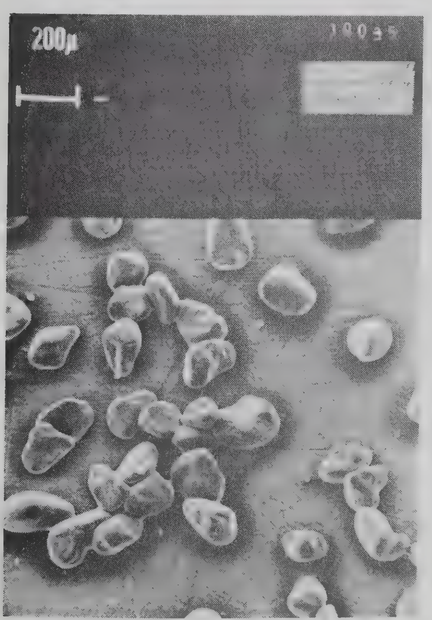

7.1c St. Peter Sandstone
Fine-grained sand fraction.
(-100mesh, +140mesh)

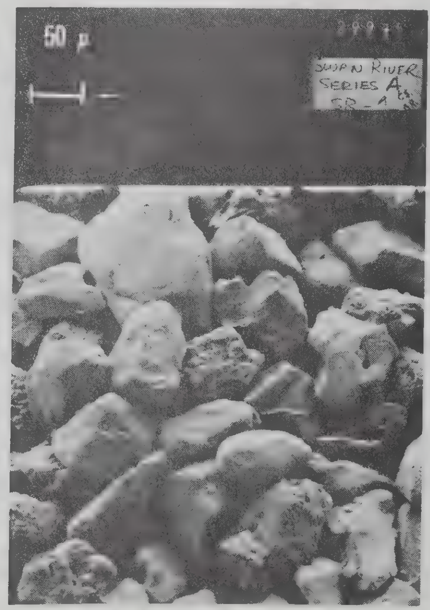

7.1d Swan River Sandstone
Fractured face of an undisturbed specimen.

PLATE 7.1 Grain Shapes

multiple sources contributing quartzose detrital materials to the sediment paleo-transport system.

7.5.2 St. Peter Sandstone

The individual grains of this very quartzose sand are generally equant, but numerous kidney-shaped and ellipsoidal grains are present (Plate 7.1c). Acicular, prismatic, and tabular grains are absent. The source of the St. Peter Sandstone materials was probably pre-existing sands and sandstones which had experienced significant rounding as a result of several erosional-depositional cycles, and which were deposited in their present form in a high-energy beach environment. The absence of nonequant grains is the direct consequence of this extensive predepositional reworking.

7.5.3 Swan River Sandstone

The influence of the quartzose mineralogy upon grain shape is also evident in micrographs of Swan River Sandstone (Plate 7.1d). Most grains are roughly equant, but a few acicular grains may be observed. Swan River Sandstone has a slightly greater incidence of nonequant grains than McMurray Formation sands of similar size. This may be due to a more plutonic source area (Paleozoic sandstones were locally absent), and to less time in the transport-deposition regimes before sedimentation.

7.6 Individual Grain Characteristics

Grain roundness is a grain parameter distinct from grain shape (Pettijohn, 1975), although the two are often confused. It may be assumed that, in these materials, grain roundness was at a maximum

at or shortly after the time of deposition. Minor overgrowths, deposited soon after burial (Dapples, 1959), decrease surface rugosity slightly, but the long-term effect of diagenetic processes (as observed in these materials) is to increase rugosity and hence to decrease roundness. Diagenetic roundness reduction is accompanied by an increase in surface rugosity because of pressure solution re-entrants, crystal faces, and pyramidal crystal truncations. In general, an equant, rounded quartz sand can be expected to lose some of its depositional characteristics as a result of diagenesis.

Three scanning electron microscope photographs are presented for comparison: a classic example of crystal overgrowth (Plate 7.2a), showing crystal faces and pyramidal truncations on a grain of Ottawa Sand; a sample of crushed quartz (Plate 7.2b), demonstrating the high degree of fracture smoothness, the lack of cleavage, and the edge sharpness of fresh quartz; and an example of a contact point pressure solution concavity (Plate 7.2c) on a grain of St. Peter Sandstone. Not all solution features result from contact point pressure solution: pitting of interstitial quartz surfaces was observed frequently.

7.6.1 Grain Roundness

Grains from St. Peter Sandstone are very well-rounded (Plate 7.1c), whereas the McMurray sands and the Swan River sands display grain roundness ranging from very angular to very well-rounded (Plates 7.1a, 7.1d). The absence of crystal faces and of pyramidal crystal truncations in St. Peter Sandstone indicates that solution phenomena were dominant, and indeed, to this date, little evidence for significant first cycle crystal overgrowth in the material sampled has been

7.2a Ottawa Sand
Crystal overgrowths on a very well-rounded quartz grain.

7.2b Ottawa Sand
Crushed quartz sand: edge sharpness and fracture mode are clearly visible.

7.2c St. Peter Sandstone
Pressure solution has resulted in numerous grain surface re-entrants.

7.2d McMurray Formation
Crystal overgrowth faces and perhaps some minor pitting.

PLATE 7.2

Grain Surface Textures

[illegible]

[illegible]

[illegible]

[illegible]

[illegible]

found. This implies that (at least locally) an open system diagenetic process existed: quartz has probably been removed from the system.

The mixed nature of the McMurray Formation grains can be attributed either to multi-source deposition or to significant amounts of solution and overgrowth processes. Photographic evidence (Plates 7.2d, 7.3a, 7.3b, 7.3c, 7.3d) favours diagenetic alteration: individual grains showing both solution and overgrowth features were occasionally observed (Plates 7.1d, 7.4a). Since the diagenetic processes of overgrowth and solution may be concurrent, closed system conditions may have existed, or several sequences of solution and overgrowth may have occurred in an open system. In general, the McMurray and Swan River sediments show more overgrowth than solution features.

7.6.2 Grain Surface Texture

No rigorous system of classification for diagenetic textures of quartz grains has yet been reported in the literature reviewed. Although researchers have studied thousands of specimens, their emphasis has been on qualitative texture assessments as a diagnostic tool to identify depositional environments (e.g. Krinsley and Donahue, 1968; Krinsley and Margolis, 1969). Pittmann (1972) presented excellent examples of overgrowths but few examples of pressure solution. The most useful comparative study is the <u>Atlas of Quartz Sand Surface Textures</u> by Krinsley and Doornkamp (1973).

Probably the most consistent feature of the oil sand grains is the surface rugosity. Both crystal overgrowth truncations and solution pits contribute to rugosity. Evidence for superimposition of several stages of overgrowth and pitting was observed. Two excellent examples,

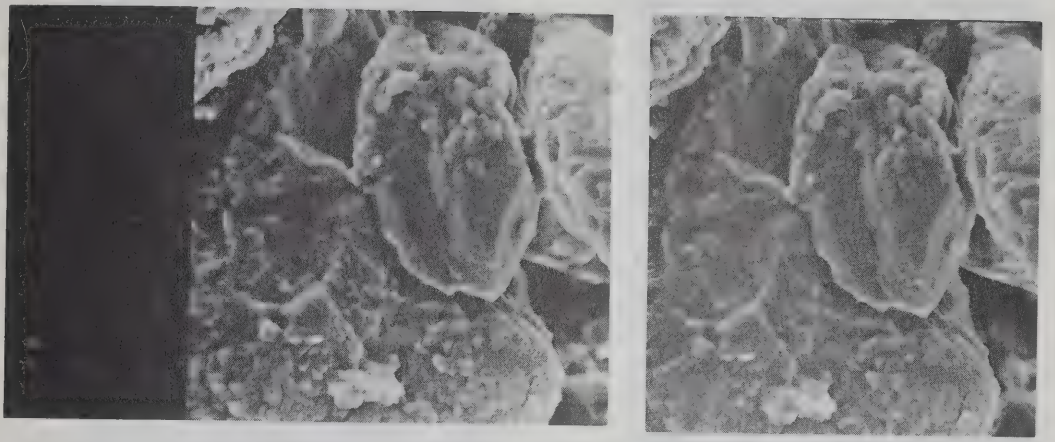

7.3a Stereoscopic pair of an intact specimen showing mainly crystal overgrowth features. Flat particles are clay minerals. Pendular bitumen is visible in upper right corner.

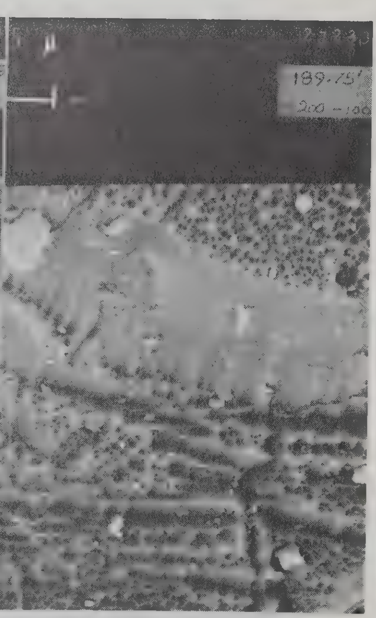

7.3b Overgrowths and minor solution pits.

7.3c Interpenetrative contacts as a result of overgrowths and minor solution.

7.3d Oriented pits on a quartz grain as a result of solution.

PLATE 7.3

Fabric and Surface Textures

McMurray Formation

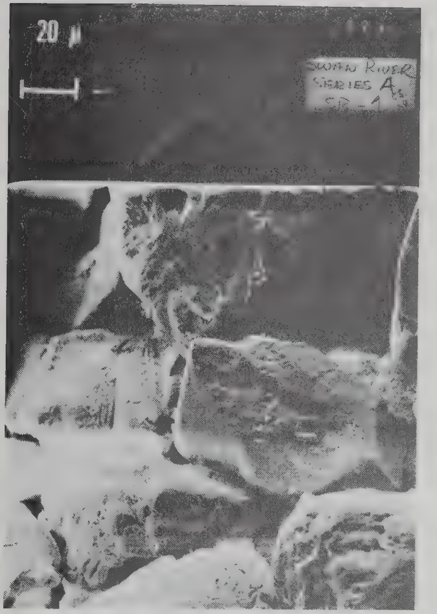

7.4a <u>Swan River Sandstone</u>
Pyramidal crystal truncations as a result of overgrowths.

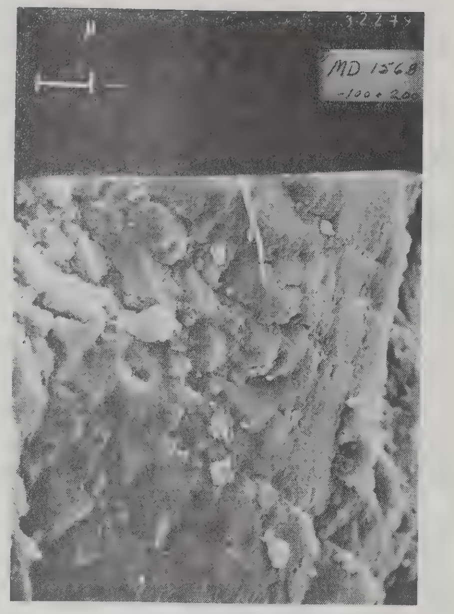

7.4b <u>McMurray Formation</u>
A small field of aligned overgrowths 1 µ in diameter. Note merging faces on adjacent pyramids.

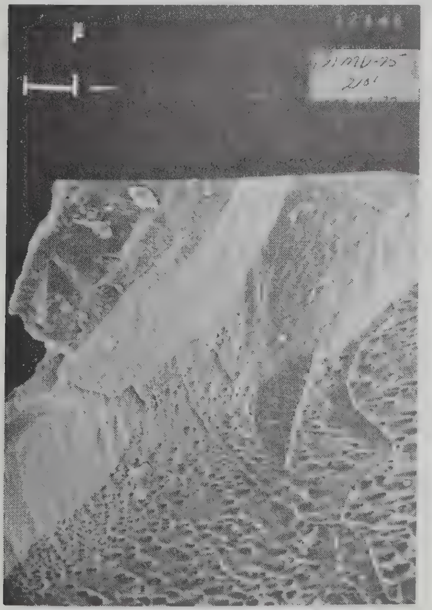

7.4c <u>McMurray Formation</u>
Oriented solution pits, several preferential directions may be detected.

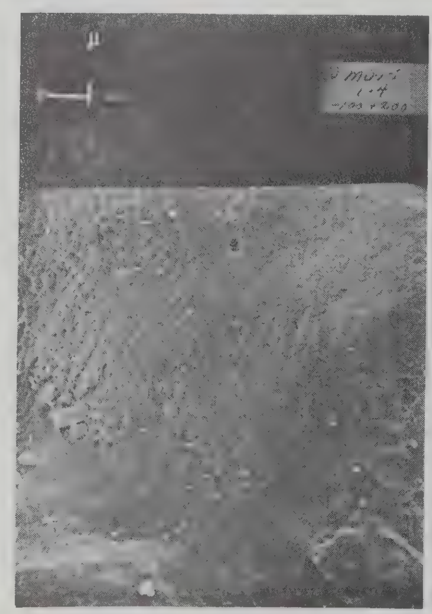

7.4d <u>McMurray Formation</u>
Solution pitting on a quartz grain from the oil-free High Hill River outcrop.

<u>PLATE 7.4</u>

<u>Grain Surface Textures</u>

[illegible]

one of overgrowth and one of pitting, are shown in Plates 7.4b and 7.4c. Oil-free specimens of the McMurray Formation sands from the High Hill River area display the same features but in a subdued fashion (Plate 7.4d). These photographic data suggest that the McMurray Formation had a gas cap above the oil sand deposits, as the presence of a gas cap would tend to inhibit diagenesis.

In St. Peter Sandstone, solution indentations are commonly visible on grain surfaces and likely represent points of grain contact pressure solution (Plate 7.2c, 7.5a). The effects of diagenesis are much more uniform and therefore appear less intense in this sand than in the McMurray Formation sands. Because the great majority of the St. Peter Sandstone is likely of multi-cycle origin, previous high-energy depositional regimes have eliminated those grains most susceptible to chemical attack and to physical attrition, leaving only high-quality, pure, unstressed quartz. The surfaces often display depositional textural features (such as conchoidal fractures), somewhat subdued by solution pits and crystal overgrowths. Chemical etching is often visible adjacent to incipient or poorly developed overgrowths (Plate 7.5b). In this material, solution was considered to be the dominant porosity reduction mechanism (measured porosity was 26%). In general, however, visual diagenetic alteration is not as striking in the St. Peter Sandstones as in the McMurray Formation sands.

In Swan River Sandstone, solution pits are relatively common (Plate 7.5c); areas of overgrowth with or without crystalline texture are more common (Plates 7.1d, 7.4a, 7.5c). The most commonly observed and most strongly developed surface feature of the fine-grained fraction ($74\ \mu$ to $150\ \mu$) is a saw-tooth or apicular texture showing strong

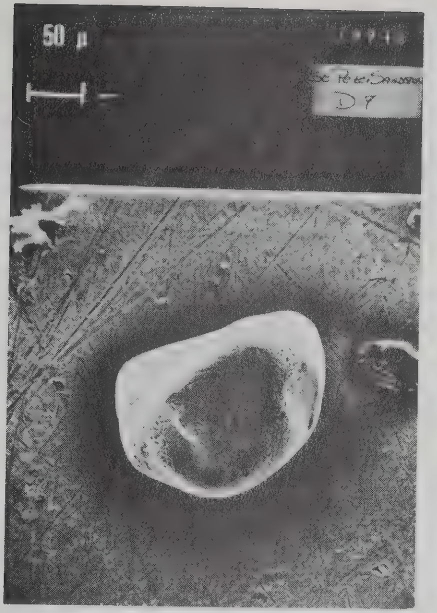

7.5a <u>St. Peter Sandstone</u>
Surface re-entrants on a typical well-rounded and ellipsoidal quartz grain.

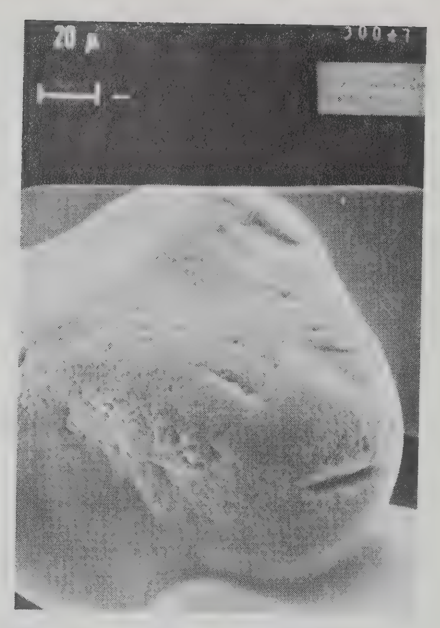

7.5b <u>St. Peter Sandstone</u>
Crystal overgrowths and solution pits on a well-rounded quartz grain.

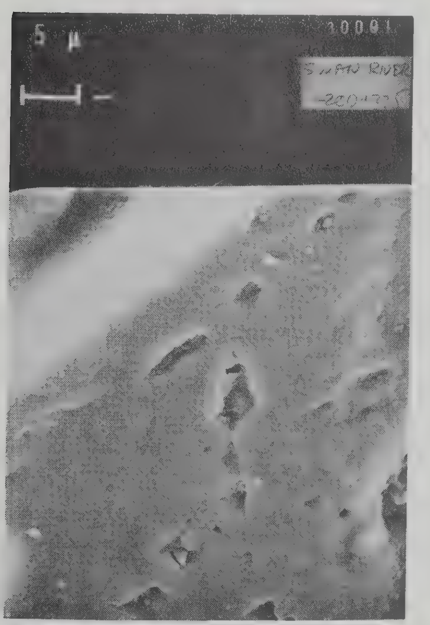

7.5c <u>Swan River Sandstone</u>
Solution Pitting. Note lower left to upper right features which control the shape of the pits.

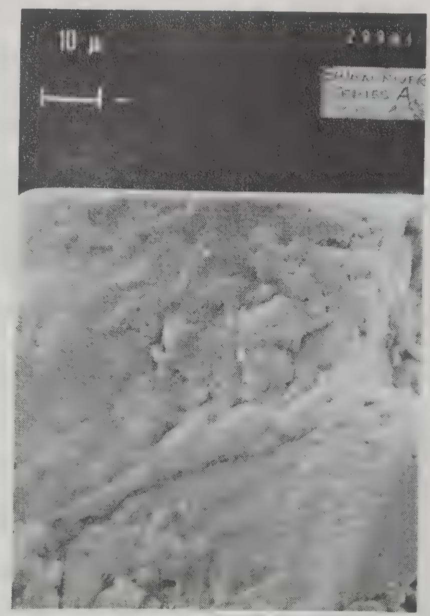

7.5d <u>Swan River Sandstone</u>
"Plastered" overgrowth displaying a poor crystal face development.

<u>PLATE 7.5</u>

<u>Grain Surface Textures</u>

evidence of underlying order resulting from cleavage plates (Plate 7.6a). Literature on this topic refers to these structures as etching features. The myriad pits probably represent selective solution at points of grain defects on cleavage plates. (Similar, although less-developed, features were found in most of the materials studied; for example, Plate 7.6b.)

Swan River Sandstone shows less diagenetic alteration than either McMurray Formation sands or St. Peter Sandstone. The characteristic surface textures, however, closely resemble those shown by the McMurray Formation sands, suggesting that recrystallization and overgrowth have been the dominant diagenetic agents in the Swan River Sandstone.

7.7 Intergranular Relationships in Locked Sands

An artificial or recently deposited assemblage of rigid, equant particles displays only tangential intergranular contacts. Artificial densification, by any means other than grain rupture, does not significantly alter the characteristic tangential fabric. At the other end of the geological spectrum, orthoquartzites of low porosity show a great intimacy of intergranular contact (Plate 7.7a). In geological and geotechnical literature, quartzose arenaceous materials between these two end members have been categorized by qualifying adjectives: friable, weak, crumbly, competent, and other descriptive terms. These modifiers are used without direct relation to fabric, and usually no intergranular fabric assessments are performed. Nevertheless, the nature of the grain-to-grain contacts observed in locked sands is associated qualitatively with the shear strengths, and fabric assessment

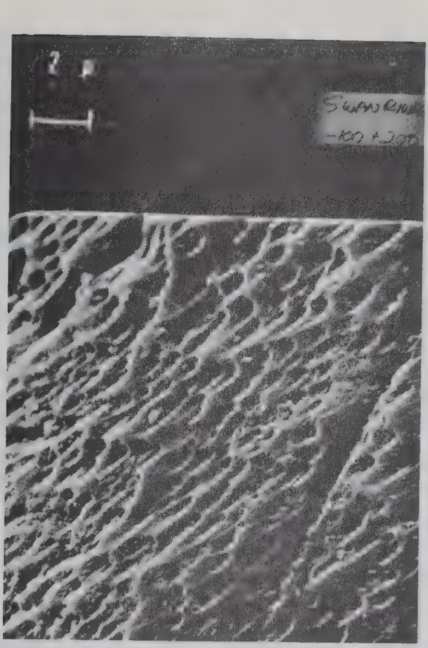

7.6a Swan River Sandstone
Solution pits in an oriented field creating an apicular (saw tooth) effect.

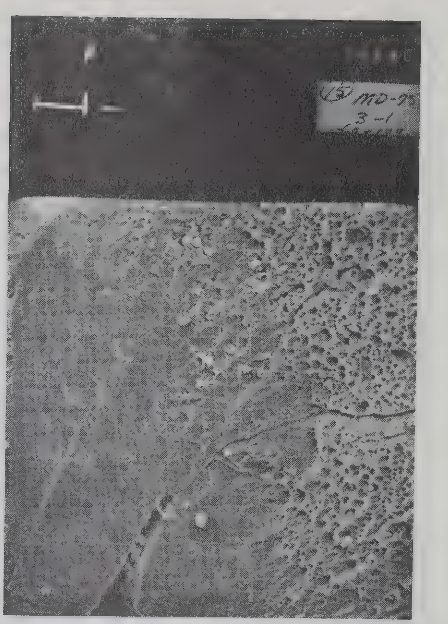

7.6b McMurray Formation
Surface etching on a grain of quartz. No signs of overgrowth are visible.

7.6c McMurray Formation
Deep pit. The concavities on the top and the right are contact points typical of interpenetrative sands.

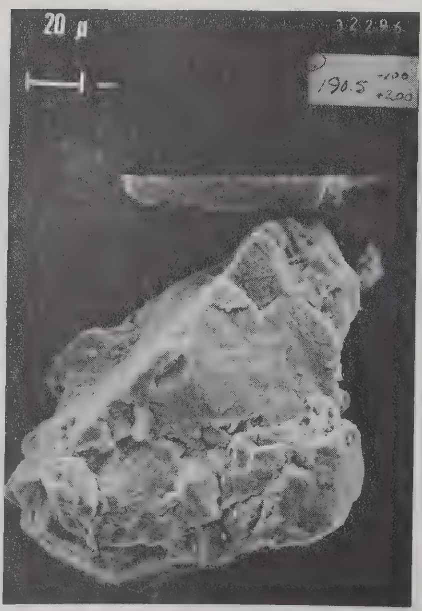

7.6d McMurray Formation
Numerous crystal facets. A grain from the Middle Member, an oil-rich zone.

PLATE 7.6

Grain Surface Textures

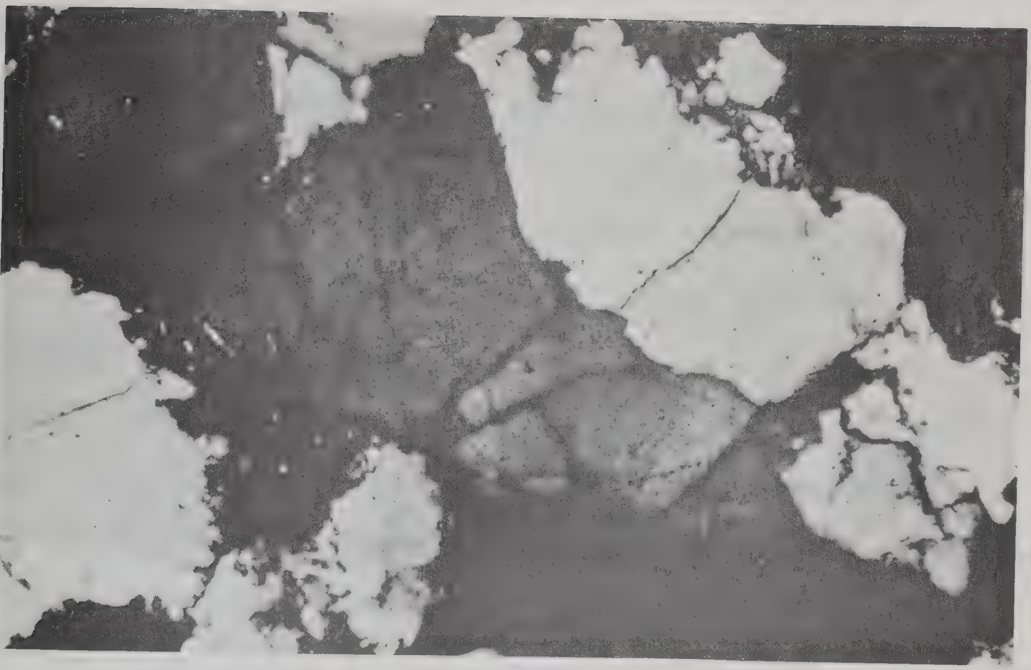

PLATE 7.7a Orthoquartzite from the Rocky Mountains showing extensive suturing at all grain contacts. Porosity is less than 5%. X130.

PLATE 7.7b A cemented orthoquartzite. The grains show little diagenetic alteration, but are cemented together. X130.

PLATE 7.7. Optical Micrographs of Diagenetic Textures

would be valuable.

Four types of intergranular contacts have been identified (e.g. Siever, 1959; Dapples, 1959): (1) tangential, (2) straight, (3) concavo-convex (or interpenetrative), (4) sutured (or micro-stylolitic). These four categories are shown in Figure 7.1. These grain contact fabric categories are used only as convenient divisions into which data may be placed: materials exist at all diagenetic stages between a tangential sand and a dense, sutured quartzite.

Tangential grain contacts in a quartz arenite preclude cohesion in a saturated state, provided there is no matrix or pendular cement. The porosity may be high in near-surface, poorly graded deposits (40%), or low in well-graded sands which have been vibrated, shock-loaded, or gravitationally compacted (18% to 25%). Capillary tension, the presence of a clay matrix, or the deposition of minor amounts of dissolved salts at grain contacts (in a dry or semidry state) may result in a qualitative assessment of significant cohesive strength where in fact little exists.

Weak diagenesis may result in straight (or linear) contacts, likely as a result of quartz overgrowths at early burial stages (Siever, 1959), but perhaps also as the result of minor amounts of pressure solution. Densification may have taken place along with minor porosity reduction.

Deeper burial provides greater effective stresses, and grain contact points become favourable locations for solution. Usually the dissolved quartz is deposited on the stress-free quartz faces in adjacent interstices, but it may be taken out of the local area by groundwater. Concurrent solution and overgrowth produce an interpenetrative

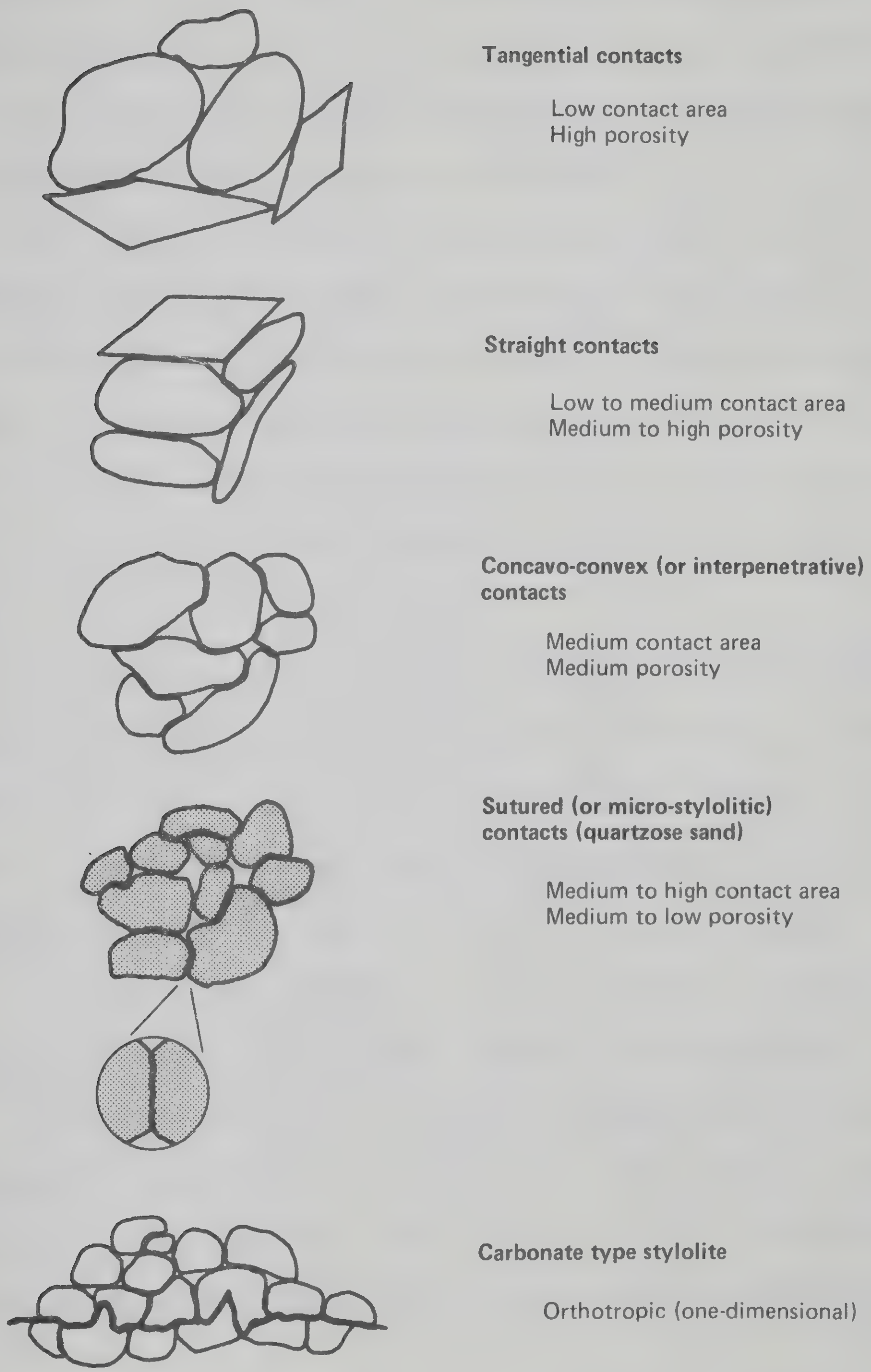

Tangential contacts

Low contact area
High porosity

Straight contacts

Low to medium contact area
Medium to high porosity

Concavo-convex (or interpenetrative) contacts

Medium contact area
Medium porosity

Sutured (or micro-stylolitic) contacts (quartzose sand)

Medium to high contact area
Medium to low porosity

Carbonate type stylolite

Orthotropic (one-dimensional)

Figure 7.1. Intergranular Fabric Classification

structure, and the development of the interpenetrative fabric is an approximate measure of the extent of diagenesis. The material may at this stage begin to display some true cohesion as the three-dimensional interlocked structure becomes better developed.

Continuation of solution-deposition processes without true metamorphic alterations results in welded quartz arenites or quartzites displaying high cohesion because of the intimate grain fabric. Contacts are interpenetrative and usually sutured (Plate 7.7a). The majority of the surface area of each grain is in direct physical contact, although not in crystallographic union, with other surrounding grains.

The processes of solution and overgrowth are often assumed to be contact point and interstitial phenomena respectively. Evidence was found for etching and pitting of quartz grains at points of non-contact, and overgrowths may form directly at points of contact, occasionally pushing the original grains apart (Pettijohn et al., 1972). Quartz overgrowths are invariably in crystallographic continuity with the parent grain but do not always display a crystalline outer surface; plaques and layers may be uniformly deposited without any diagnostic crystal truncations (Plate 7.5d). The degree of perfection of crystal form of deposited quartz has been interpreted as being a function of the rate of quartz precipitation (Krinsley and Doornkamp, 1973).

The topic of processes and agents in quartzose sand diagenesis has been discussed in considerable detail by Milligan (1976), and therefore only a list of variables affecting diagenesis will be included here. Some of these variables are: orientation of grain crystallographic

axes, amounts of minerals other than quartz in the sand, pore water chemistry, depth and time of burial, tectonic stress fields, quartz availability, and quartz crystal purity (Park and Schat, 1968).

McMurray Formation sands, St. Peter Sandstone, and Swan River Sandstone all fall into the same intergranular fabric category. The incidence of tangential contacts is high, but straight and interpenetrative contacts are relatively common and are probably best developed in the St. Peter Sandstone. Definite evidence of subtle diagenetic grain fabric is visible in all samples of these materials.

7.7.1 McMurray Formation Sands

Both crystal overgrowth and solution features can be observed in the McMurray Formation sands (Plates 7.2d and 7.3d). The absence of dust lines and the fine-grained nature of portions of the sands obscure the amount of crystal overgrowth in optical microscope study (Plate 7.10), but the overgrowths are readily visible in scanning electron micrographs of individual grains (Plate 7.4b). Interpenetrative fabric, however, may result from either solution or recrystallization; optical microscope methods are probably superior in identifying solution fabric. Dense grain assemblages with evidence of both solution and overgrowth are common, but in general overgrowth seems to be the dominant mechanism (Plates 7.3a, 7.3c). The intimacy of contacts occasionally can be seen in scanning electron micrographs (Plates 7.3c and 7.8a).

Specimens from oil-free outcrops show similar evidence of solution and overgrowth, but overall material transfer is significantly less (Plates 7.4d, 7.9c, 7.9d). Areas of rapid postdepositional

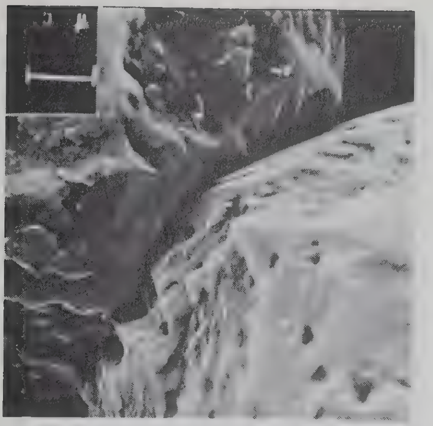

7.8a Interpenetrative grain contact.

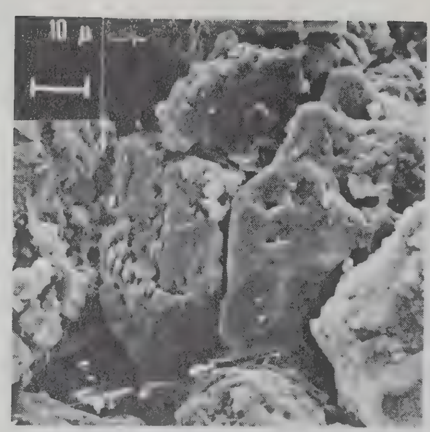

7.8b Linear grain contacts.

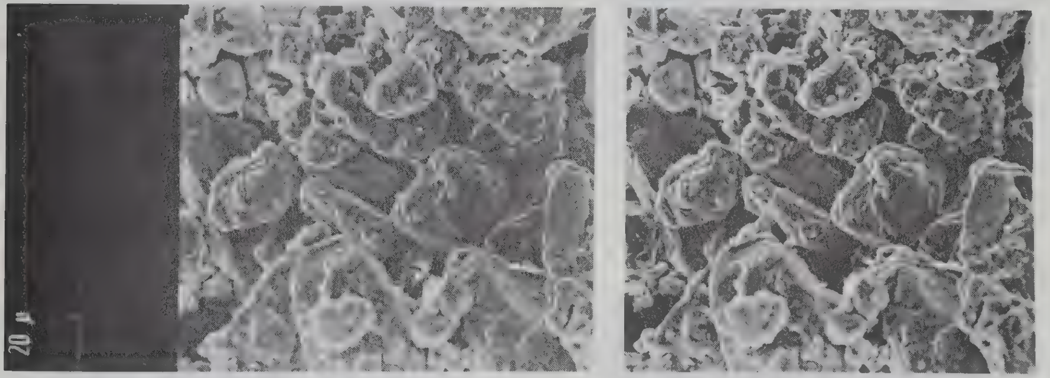

7.8c Stereoscopic pair of the fabric of the McMurray Formation, Upper Member, fine-grained sand.

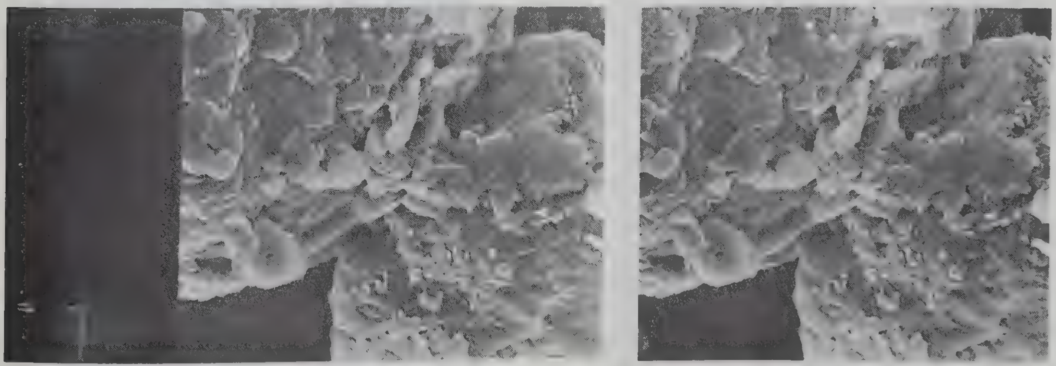

7.8d Stereoscopic pair of an interpenetrative contact. Note the clay platelets on the quartz grain surface.

PLATE 7.8

McMurray Formation Fabric

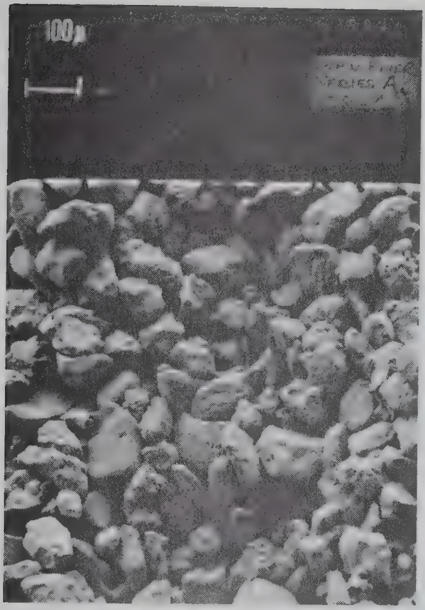

7.9a Swan River Sandstone
Fabric of an undisturbed specimen.

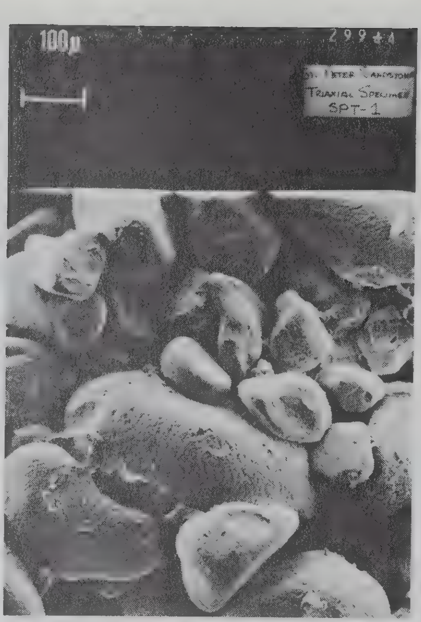

7.9b St. Peter Sandstone
The deposits at grain contact points are soluble salts which provide no true cohesion when saturated.

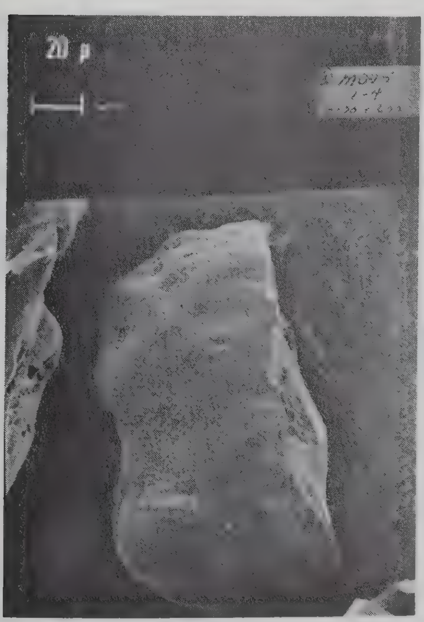

7.9c McMurray Formation
Grain from an oil-free outcrop showing the lack of a well-developed diagenetic texture.

7.9d McMurray Formation
From an oil-free sand at the base of the oil-rich Christina River outcrops.

PLATE 7.9

Fabric and Textures

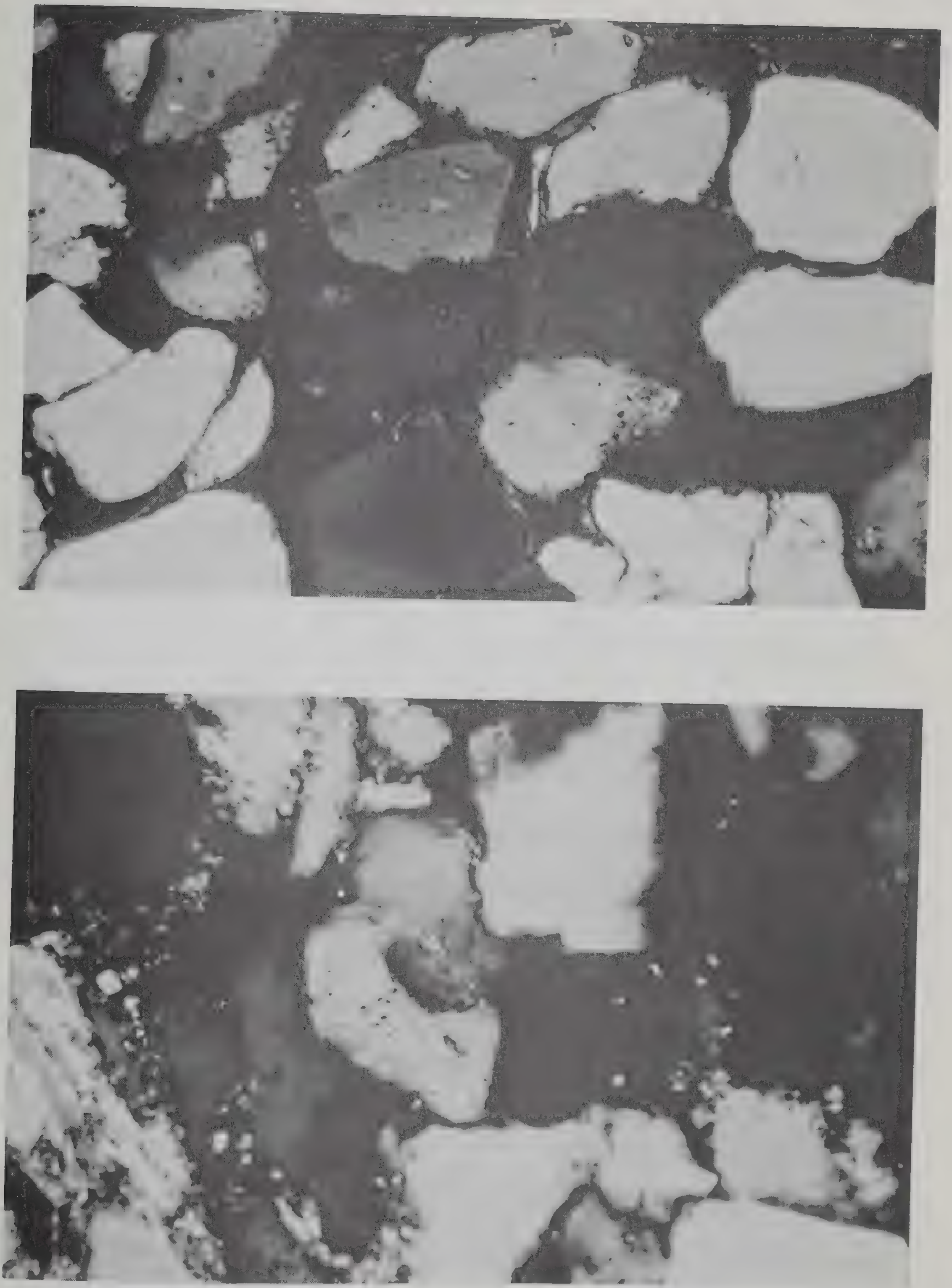

PLATE 7.10 McMurray Formation Fabric; Optical Micrograph.
Top: oil-free outcrop, X130.
Bottom: fine-grained sand, X520.

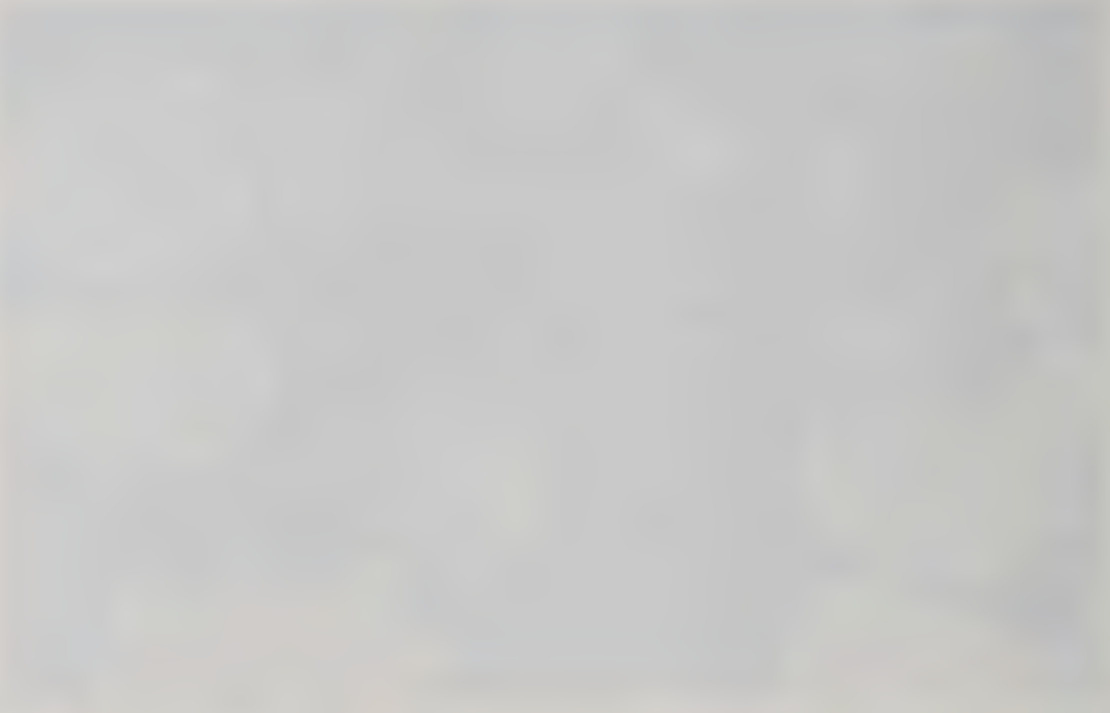

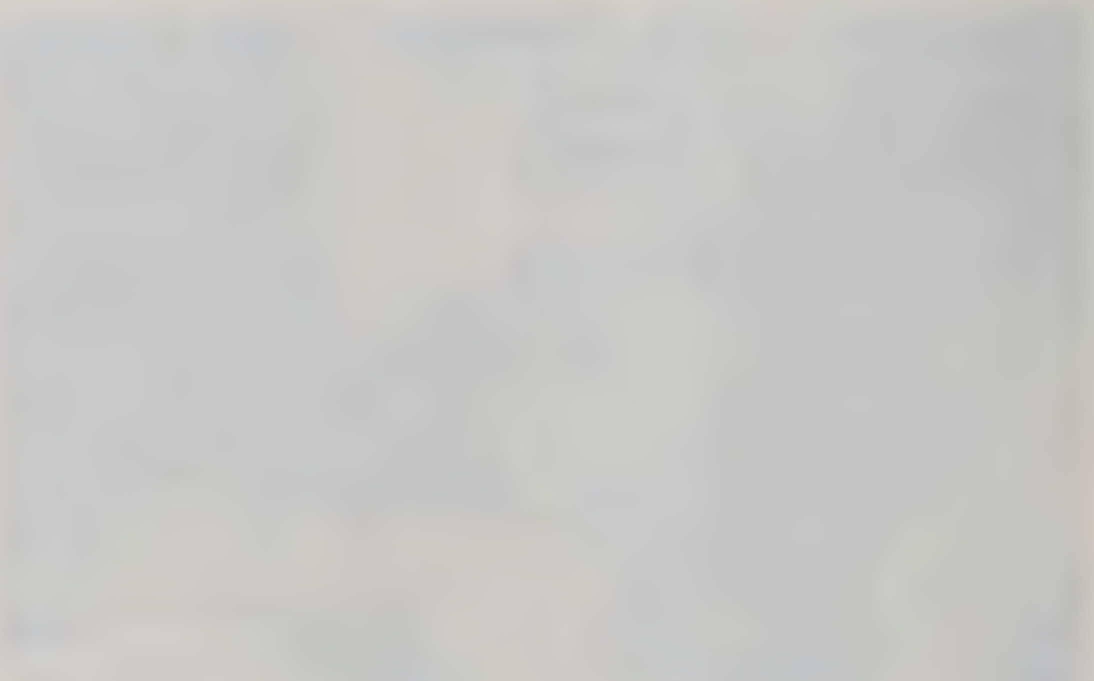

[illegible]

precipitation (resulting in smooth surfaces with few crystal truncations) are more common than in the oil-bearing sands.

7.7.2 Swan River Sandstone Fabric

Optical micrographs (Plate 7.11) reveal a fabric similar to that of the McMurray Formation sands. Scanning electron micrographs (Plate 7.9a) show a similar intimate grain assemblage, although with somewhat less interpenetrative fabric. The Swan River Sandstone displays less surface rugosity, and the _in situ_ porosity (34% to 35%) indicates that diagenetic fabric is less well-developed than that of the McMurray Formation sands of similar grain size and sorting. Nevertheless, the research reported in Chapter VI indicates that high strengths exist in the Swan River Sandstone, although the diagenetic fabric is less intense.

7.7.3 St. Peter Sandstone Fabric

Crystal overgrowth features have been identified in St. Peter Sandstone, but pressure solution features are much more common. The distinct indentations (Plate 7.9b), the large areas of grain surface contact, and the absence of visible crystal overgrowth revealed in the optical microscope studies (Plate 7.12) all indicate the predominance of solution over recrystallization as a densification agent in these portions of St. Peter Sandstone. The intraformational transfer of silica is shown by examination of other portions of the St. Peter Sandstone which could be classified as competent, lithic orthoquartzites, although in general the formation is incompetent (Pettijohn _et_ _al_., 1972).

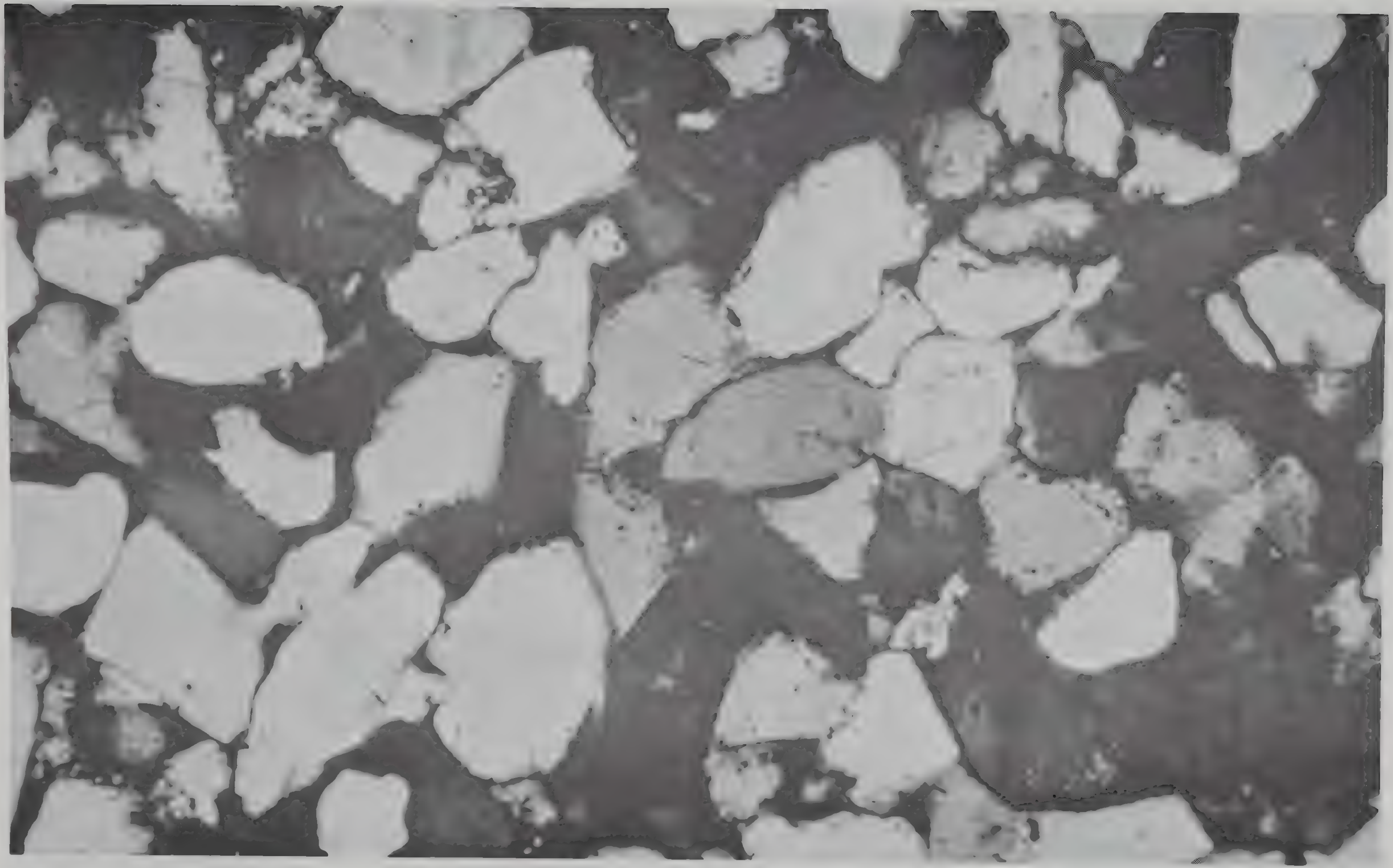

PLATE 7.11 Swan River Sandstone Fabric; Optical Micrograph. X180.

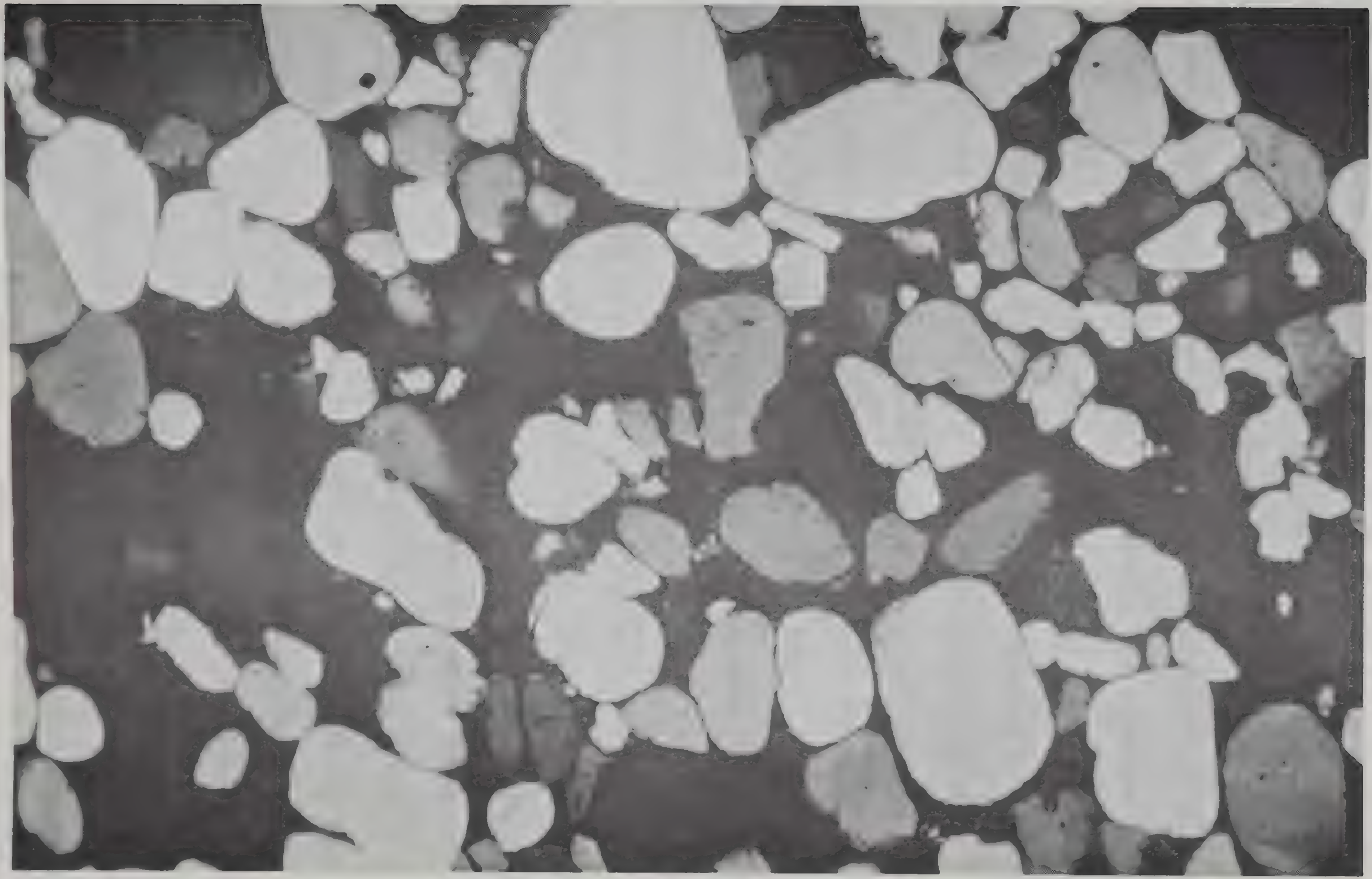

PLATE 7.12 St. Peter Sandstone Fabric; Optical Micrograph. X72.

7.8 The Diagenetic Model in Locked Sands

The processes and consequences of diagenesis are not understood clearly (Pettijohn et al., 1972). It has been established in this thesis that a minor amount of diagenesis is sufficient to radically alter engineering strength and stress-strain characteristics. Quantification of diagenetic alteration is desirable, but assessment of diagenetic fabric at the present time must remain qualitative. Nevertheless, diagenesis in orthoquartzites may be discussed in a semiquantitative manner to place the topic in an engineering framework.

The minimum porosity of well-sorted sands subjected to normal laboratory densification procedures is about 30% to 35% (e.g. Lambe and Whitman, 1969). The density achieved is a function of the compactive effort, the compactive method, the grain shape, and the grain surface rugosity. During this experimental program, a minimum porosity of 31.5% was achieved using medium-grained Ottawa Sand (C-109), by employing the maximum vibratory and compacting effort possible without crushing of grains. It is unlikely that relatively well-sorted sands such as the fine- to medium-grained McMurray Formation sands, the St. Peter Sandstone, and the Swan River Sandstone were deposited in a state more dense than 35% porosity. Moreover, further postburial compaction could not account for more than 2% to 3% decrease in the porosity, because of the competence of the quartz grains and the low compressibility of sands (Athy, 1939). The relatively low borehole log porosities for medium-grained McMurray Formation sands (n = 27%) and from oil-free outcrops (n = 28% to 32%) indicate diagenetic porosity reductions. St. Peter Sandstone porosities (n = 26% to 28%) also indicate diagenetic postdepositional porosity reduction similar to, or greater in magnitude

than, that of the medium- to coarse-grained sands of the McMurray Formation.

Overgrowth and contact point solution both tend to reduce porosity. A porosity reduction of four percent (from 32% to 28%), achieved solely by quartz overgrowths in interstitial voids requires the importation of vast quantities of quartz (5.88% weight increase). This is, however, considered possible (Pettijohn _et_ _al_., 1972), and the overgrowth structure alone can account for the unusual strength properties by providing an interpenetrative structure (Figure 7.2a). On the other hand, pressure (contact point) solution is a much more effective process in porosity reduction than is quartz precipitation (Figure 7.2b). To reduce the porosity by four percent (from 32% to 28%) in an assemblage of ideal spheres with body-centered packing requires a percentage mineral loss at the contact points of only 0.23%.

The effectiveness of pressure solution can be demonstrated by analyzing three packing arrangements of ideal spheres: (1) cubic open packing, (2) cubic body-centered packing, and (3) cubic face-centered packing. It is assumed that:

1. Equal amounts of material are removed from each grain during solution at the contact points.
2. Unit-cell volume changes are homogeneous and isotropic, as are the solution phenomena themselves.

If the initial radius of spheres is taken as unity, the following expression for volume reduction is obtained (Figure 7.3) for one-half of a contact point:

$$\wedge V = \frac{\pi \bar{a}^2 (3r - \bar{a})}{3} \quad .$$

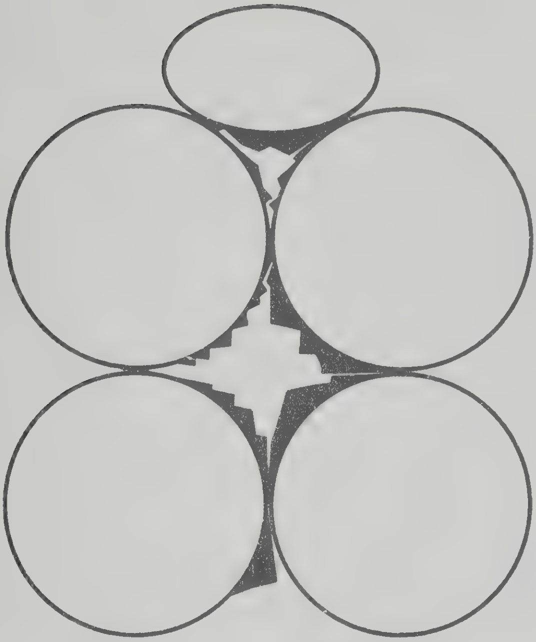

7.2a Crystal Overgrowths

—Recrystallization of quartz

—Material added to the strata

—No volume change (overall)

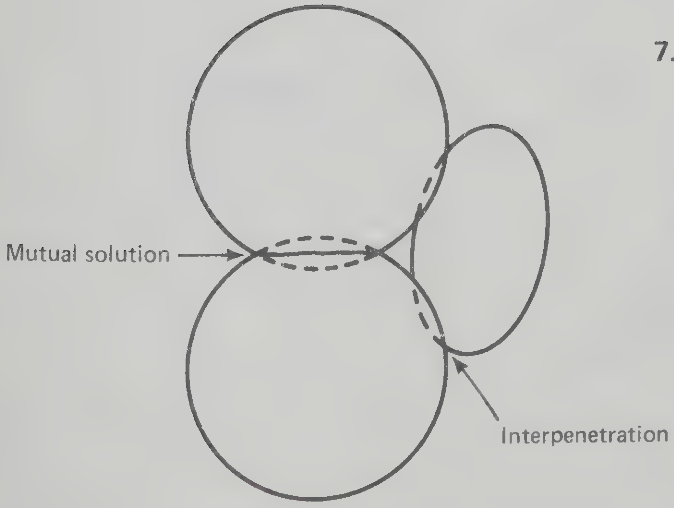

7.2b Contact Point Solution

—Contact point solution only

—Material removed from the strata

—Volume diminution

Figure 7.2 Porosity Reduction Mechanisms

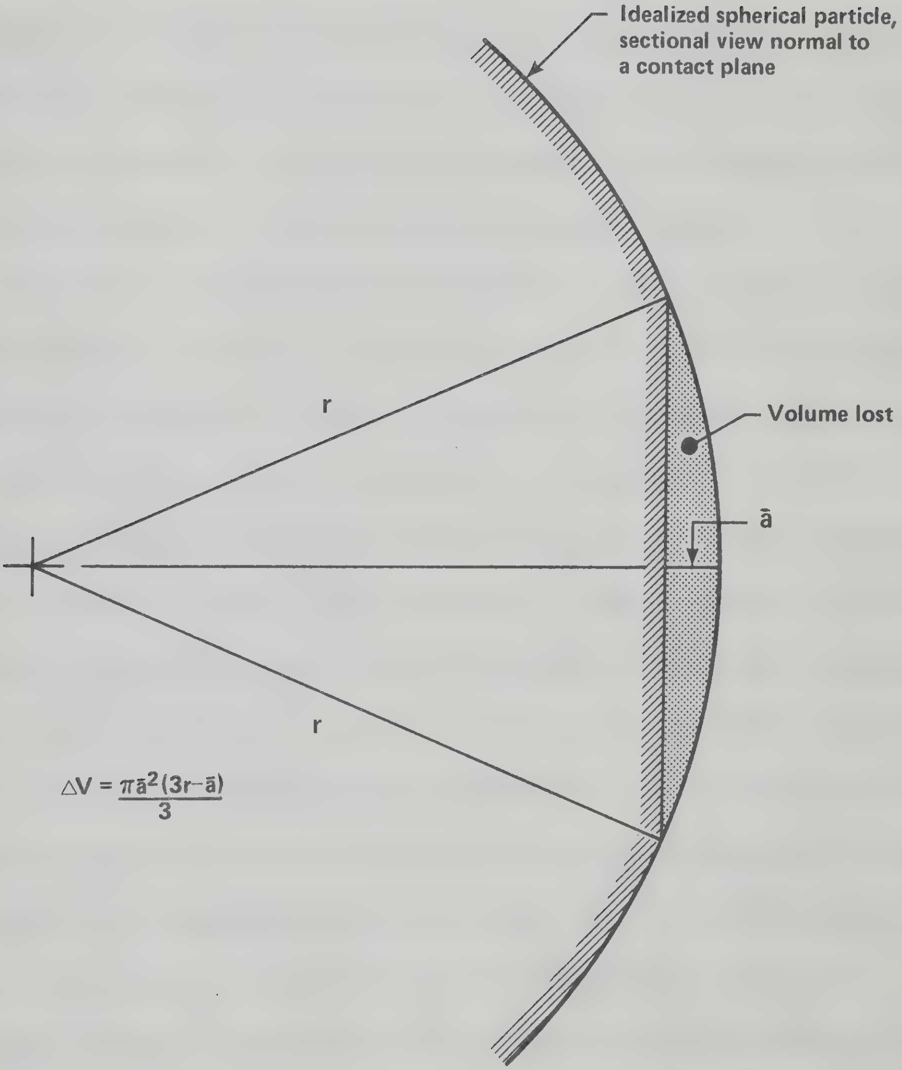

Figure 7.3 Volume Loss at One-Half of a Contact Point

Application of this formula to unit-cell algebra results in the equations presented in Table 7.2. Volume change formulae for one-dimensional solution of contact points in a cubic open packing are also presented.

These formulae are valid only for small radial solution (Figure 7.4) and become invalid when contact point overlap occurs. The porosity reduction for isotropic solution and one-dimensional solution on a cubic open structure is presented in Figure 7.5 for comparison with the porosity reduction through crystal overgrowth alone.

Packing of natural grains is distinctly different from packing of ideal spheres. Preferred solution directions exist in crystals, and solution phenomena are never isotropic and probably never homogeneous. Nevertheless, the great reduction of porosity for a small material loss through solution alone indicates that it is a powerful mechanism in bulk density increases. For example, to reduce porosity by five percent by recrystallization alone, the amount of material necessarily introduced would be close to 10%. Solution porosity reduction of five percent, however, would require the removal of only 1.45% of the mineral weight in an ideal isotropic solution of a cubic open lattice. Closed-system solution-overgrowth, where dissolved quartz is redeposited locally, is an even more powerful porosity reduction mechanism.

This analysis demonstrates that subtle pressure solution phenomena have a much greater effect on porosity than overgrowth phenomena; nevertheless, in microscopic examination, it is probably much easier to identify subtle crystal overgrowth than to identify subtle solution features. Quantitative measurement of these phenomena is difficult but is being developed to some extent (e.g. Cathodoluminescence: Sippel, 1968).

TABLE 7.2

GRAIN CONTACT PRESSURE SOLUTION POROSITY REDUCTION

Packing Type	Number of Spheres in a Unit Cell	Original Length of Side of Unit Cell (Radius=Unity)	Original Porosity (Percent)	Total Number of Solution Grain Contact Points Per Unit Cell	Amount of Material Lost Through Ideal Contact Point Solution (Percent)	Porosity After Contact Point Solution (Percent)
Cubic Open Packing	1	2	47.64	6	$\left[\frac{3}{2}\,\bar{a}^2\cdot(3-\bar{a})\right]\cdot 100$	$\left[1-\frac{\pi}{12}\left(\frac{2-3\bar{a}^2\cdot(3-\bar{a})}{(1-\bar{a})^3}\right)\right]\cdot 100$
Cubic Body-Centered Packing	2	$\frac{4}{\sqrt{3}}$	31.98	16	$\left[2\bar{a}^2\cdot(3-\bar{a})\right]\cdot 100$	$\left[1-\frac{\pi\sqrt{3}}{8}\left(\frac{1-2\bar{a}^2\cdot(3-\bar{a})}{(1-\bar{a})^3}\right)\right]\cdot 100$
Cubic Face-Centered Packing	4	$\frac{4}{\sqrt{2}}$	25.95	48	$\left[3\bar{a}^2\cdot(3-\bar{a})\right]\cdot 100$	$\left[1-\frac{\pi\sqrt{2}}{6}\left(\frac{1-3\bar{a}^2\cdot(3-\bar{a})}{(1-\bar{a})^3}\right)\right]\cdot 100$
One-Dimensional Solution, Cubic Open Packing	1	2	47.64	2	$\left[\frac{\bar{a}^2}{2}\cdot(3-\bar{a})\right]\cdot 100$	$\left[1-\frac{\pi}{12}\left(\frac{2-\bar{a}^2\cdot(3-\bar{a})}{(1-\bar{a})}\right)\right]\cdot 100$

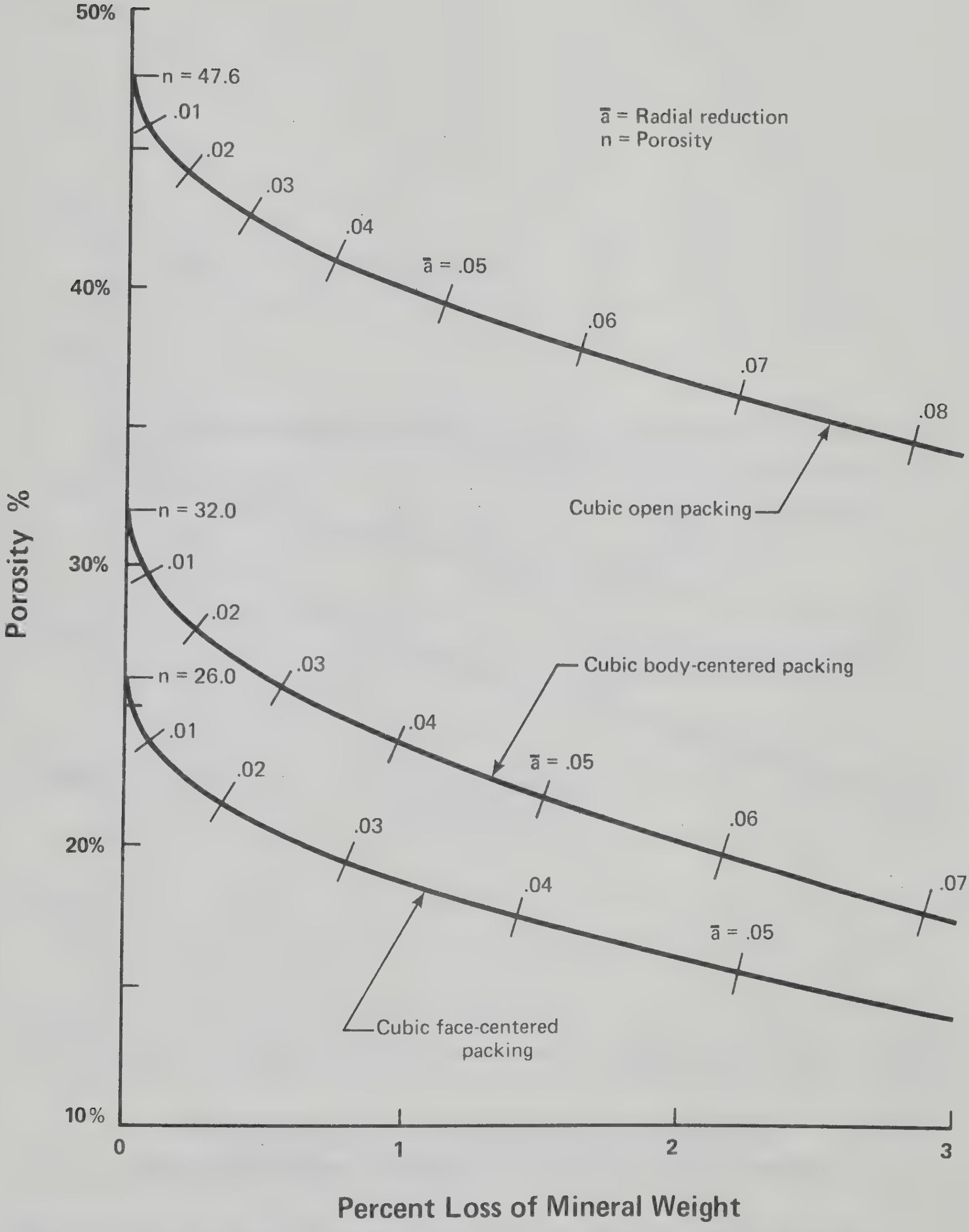

Figure 7.4 Porosity Reduction Through Idealized Contact Point Solution on Perfect Spheres

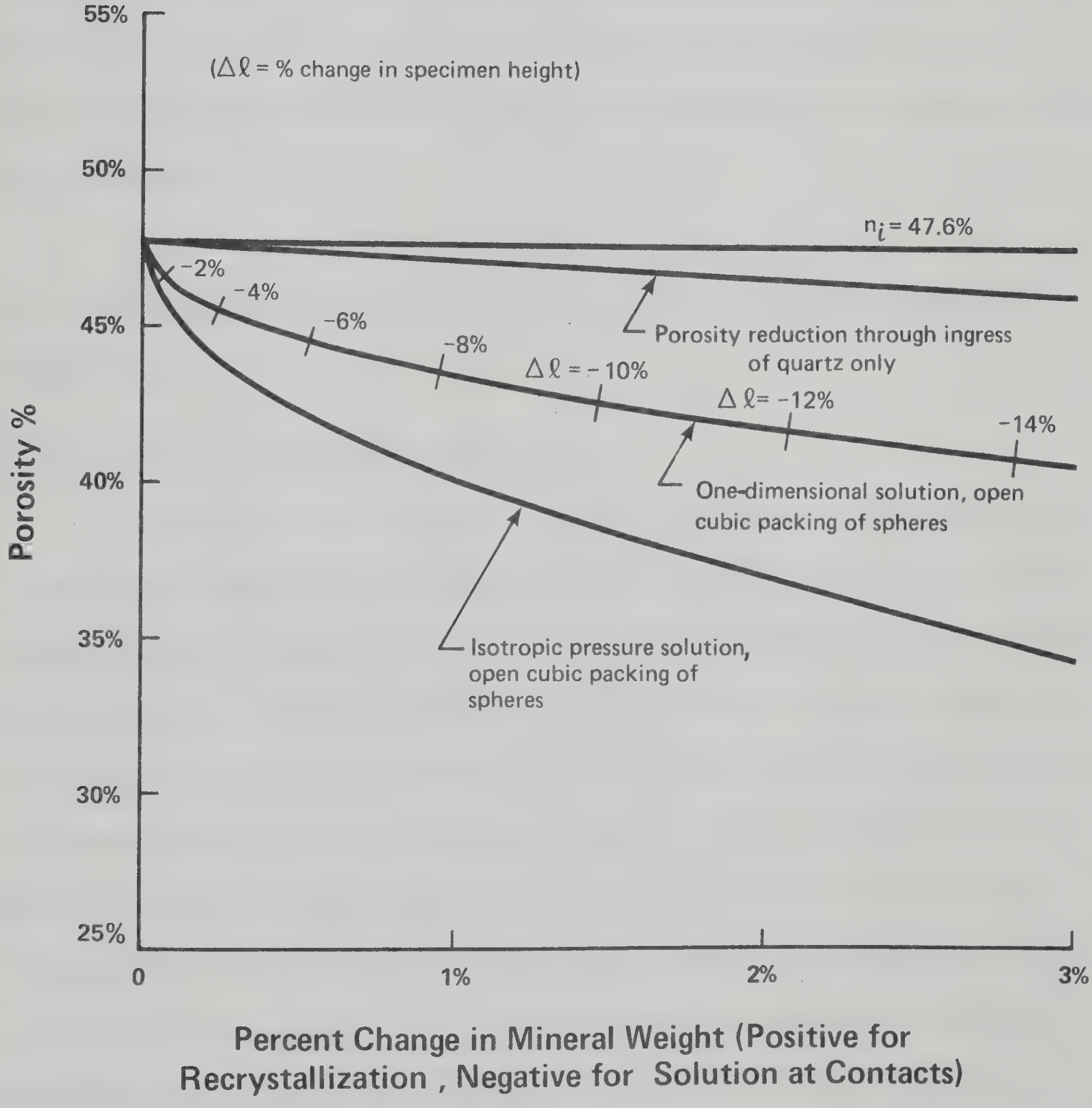

Figure 7.5 Comparison of Porosity Reduction Through Pure Isotropic Solution, Pure Orthotropic Solution, and Pure Recrystallization; Idealized Cubic Open-Packed Spheres

The data generated in the optical and scanning electron microscope studies constitute direct observational proof of the diagenetic model for "locked sands". Which particular process has been dominant is not important to engineering behaviour, since both phenomena, or either phenomenon, can give rise to the cohesionless, highly dilative behaviour exhibited by these sands. The fabric acquisition is a one-way, irreversible process, and its continuation must enhance strengths at low stresses.

7.9 The Effect of Fabric and Texture on the Strength Properties of Locked Sands

7.9.1 Residual Strength of Locked Sand

Both Swan River Sandstones and McMurray Formation sands approach a residual strength state before one-half cycle (five millimeters) of displacement is completed. The equant particles (as compared to micaceous and clay minerals) and the competent nature of quartz result in a residual state being reached soon after the fabric has been disrupted. St. Peter Sandstone approaches the residual state even more rapidly. Failure may be so abrupt that no further displacement after failure is necessary to create the residual voids ratio in the failure plane, even in a triaxial test. The extreme particle roundness is likely responsible for this rapid approach to residual friction angles. Although the triaxial apparatus is not considered suitable to assess residual stress states, the brittle nature of locked sands usually results in a quasi-residual state after little strain (less than three percent).

The values of the residual ϕ reflect the added component of intergranular friction resulting from surface rugosity and grain angularity. Densified Ottawa Sand friction angles are 31° at the residual state; St. Peter Sandstone residual friction angles are 32.7°; Swan River Sandstones, McMurray Formation sands, and Swan River preglacial sands have a mean of about 34.5° for residual friction angles. The grain angularity and the grain surface rugosity of the test materials indicate consistent trends. Smooth glass balls (ballotini) have a residual angle of friction of 24° (Rowe, 1962); crushed, extremely angular glass has a residual friction angle of approximately 43° (Parikh, 1967).

7.9.2 Peak Strength of Locked Sands

The characteristic high peak strengths of locked sands are a direct consequence of (1) the interpenetrative grain fabric, and (2) the quartzose nature of the sands. The interpenetrative fabric results in a high degree of particle interlock, and the quartzose grain mineralogy of the locked sands reduces grain shear; therefore dilation is fully developed at low stresses. As normal stress increases, an increasing number of the diagenetic quartz grain contacts shear rather than dilate, resulting in curvature of the failure envelope. The interpenetrative fabric results in high dilatancy at low stresses, and the quartzose nature reduces the tendency to grain shear at higher stresses, permitting dilatancy to develop. The presence of significant quantities of other (typically arenaceous) minerals such as feldspars, micas, and cherts results in grain cleavage and deformation at low stresses; and this in turn would result in a rapid suppression of

dilative behaviour and, consequently, envelopes showing less curvature and lower slopes. This peak-strength behaviour is therefore likely to be typical of quartz arenites; and arkoses or graywackes having similar diagenetic fabric should generally be less competent at a given stress level.

7.10 Conclusions

The source of the unusually high strength of quartz arenites which have undergone mild diagenesis has been identified. The high strengths of locked sands are associated with exceptionally large dilative rates at failure, and these rates are a result of a characteristic diagenetic fabric identifiable by microscope methods. Either solution or overgrowth may be responsible for the strength behaviour, and evidence for both processes exists. Pressure solution at points of grain contact is an extremely efficient porosity reduction mechanism. Overgrowth and solution increase the surface rugosity of quartz sands, resulting in somewhat higher residual angles of friction than in recent, subrounded to subangular sands.

The engineering characteristics of a new class of engineering materials, locked sands, have been placed in a geological-textural framework. Microscope studies have proved invaluable in arriving at a rational explanation of the stress-strain-strength behaviour of locked sands.

CHAPTER VIII

SLOPE STABILITY OF THE ATHABASCA OIL SANDS

8.1 Introduction

The rationale for a curvilinear, power law failure criterion for oil sands has been established, and it has been shown that the strength source is constant through time: it is not related to transient phenomena such as excavation pore pressures or viscosity. These findings may now be applied to the design of high steep pit slopes.

This chapter analyzes the stability of high steep pit walls by a wedge method, and presents a method of estimating the factor of safety. A finite element analysis of stress conditions within slopes is used to assess the potential for progressive failure, for tension zone development, and for pit-face raveling. The analyses and results are applicable to natural slopes.

8.2 Planar Wedge Failure: Analytic Design and Rationale

The stability of high steep slopes with tension cracks in the back-slope may be analyzed, without gross error, by assuming a planar failure surface. The assumption of curvilinear (circular or log-spiral) failure surfaces results in solutions closer to true lower-bound solutions (Chen, 1975), but using the planar failure surface will generally result in less than five percent error, given the assumptions employed in this section.

Tension cracks have been observed in steep oil sand slopes

(Morgenstern, 1976). They may be formed as the result of small negative pore pressures and minor cementation of beds. The existence of deep tension cracks is analytically conservative, and is therefore a useful analytic parameter. Excavation of steep slopes in materials with high horizontal stresses results in zones of potential tension failure in the back-slope. The distance from the slope crest of a tension crack of a given depth is not a required parameter; continual mining will eventually result in the tension crack reaching a critical location. Hence this analysis accepts the depth of the tension crack as a fixed parameter, and solves for a failure plane maximizing the total shear stress for a given geometry.

The tension cracks which may exist in the back-slope may be partially filled with water. The hydrostatic forces become significant if steep failure angles are specified, and therefore depth of water in the tension crack is considered to be another design parameter.

The natural slope study reported in Chapter III indicated that natural oil sand slopes are well drained and that water table levels are drawn down significantly near valley walls. When a pit is excavated, stress redistribution in the pit walls causes both elastic strains and dilatant fabric expansion. The consequence is a gradual reduction in pore pressures within the slope. This lowering of pore pressure is furthered if the underlying Devonian strata or water-bearing sands are depressured by pumping before mining. The arenaceous nature of the oil sands also precludes the existence of large negative pore pressures, which increase the stability of an excavated pit face. These considerations lead to the analytic assumption that pore pressures are not a grossly significant variable, and that a total stress analysis, based on saturated unit weights, would be valid.

8.3 Wedge Failure Solution

8.3.1 Derivation of Solution Nomographs

Figure 8.1 presents the geometric configuration for the analysis; Figure 8.2 identifies the forces acting on the wedge; Table 8.1 explains the notation used in the following analysis.

1. For the unit shear stress along the failure surface:

$$\frac{\overline{S}}{L} = C = \frac{\overline{P}.\cos\alpha + \overline{W}.\sin\alpha}{L} \qquad \text{Equation 8.1}$$

2. For the unit normal stress along the failure surface:

$$\frac{\overline{N}}{L} = \sigma_n = \frac{\overline{W}.\cos\alpha - \overline{P}.\sin\alpha}{L} \qquad \text{Equation 8.2}$$

3. From geometric considerations:

$$L = \frac{H - D}{\sin\alpha} \qquad \text{Equation 8.3}$$

$$B = H\,(\cot\alpha - \cot\beta) - D\cot\alpha \qquad \text{Equation 8.4}$$

$$\overline{P} = \frac{g.\gamma_w\,.\,h^2}{2} \qquad \text{Equation 8.5}$$

$$\overline{W} = \frac{g.\gamma_m\,.\,H^2}{2}\left[\cot\alpha\left\{1 - \left(\frac{D}{H}\right)^2\right\} - \cot\beta\right] \qquad \text{Equation 8.6}$$

Substitution of Equations 8.3 to 8.6 in Equations 8.1 and 8.2 yields:

$$\frac{2C}{g.\gamma_m.H} = C_1.C_2.\ \sin\alpha.\cos\alpha - C_1.C_3.\sin^2\alpha \qquad \text{Equation 8.7}$$

$$\frac{2\sigma_n}{g.\gamma_m.H} = C_1.C_4.\cos^2\alpha - C_1.C_3.\sin\alpha\cos\alpha - C_1.C_5.\sin^2\alpha \qquad \text{Equation 8.8}$$

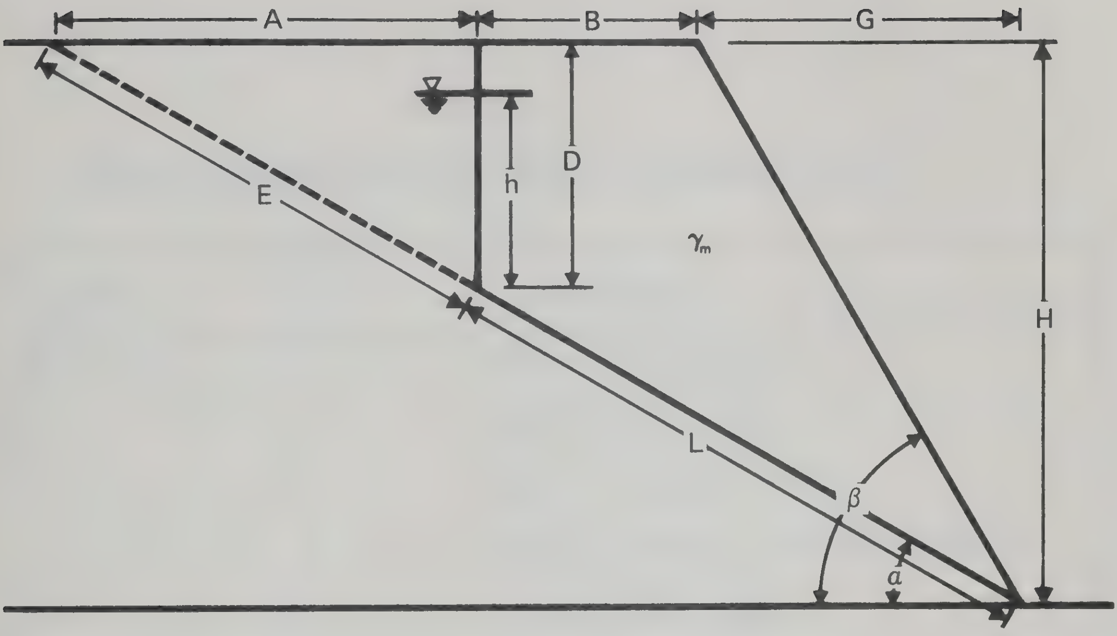

Figure 8.1 Wedge Analysis Geometry

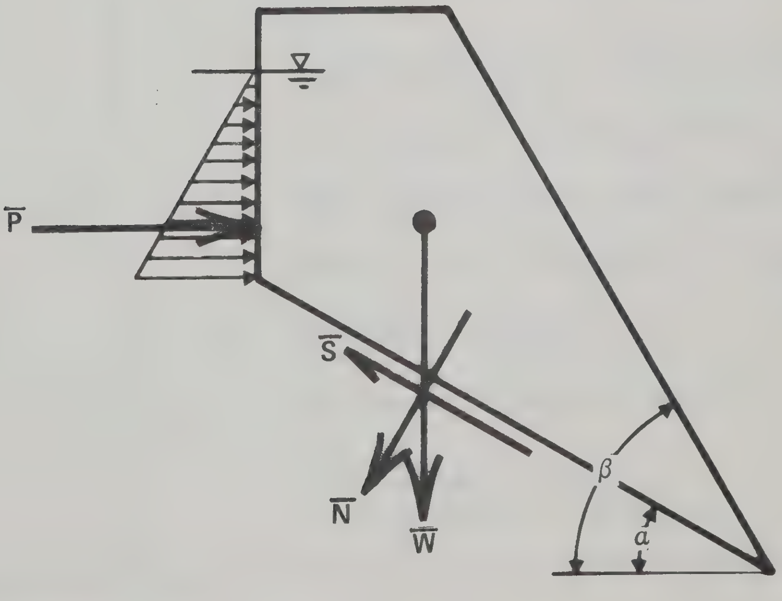

Figure 8.2 Forces Acting on a Wedge

TABLE 8.1

NOTATION EMPLOYED IN WEDGE ANALYSIS (FIGURES 8.1,8.2)

SYMBOL	DEFINITION
A,B,E,G,L	Geometric distances
H	Total slope height
D	Depth of tension crack
h	Height of water in tension crack
α	Failure plane angle
β	Slope angle
C	Mean shear stress
σ_n	Mean normal stress
τ_f	Maximum allowable mean shear stress
$\overline{P}$	Hydrostatic force at back of wedge
$\overline{S}$	Total shear force along failure plane
$\overline{N}$	Total normal force across failure plane
$\overline{W}$	Mass of a unit thickness of the wedge
γ_w	Unit mass of water
γ_m	Unit mass of slope material
g	Gravitational constant (= 9.81 m/sec^2 - SI units)

The constants C_1 to C_5 are given by the following equations:

$$C_1 = \frac{1}{1 - \frac{D}{H}}$$ Equation 8.9a

$$C_2 = 1 - \left(\frac{D}{H}\right)^2 + \frac{\gamma_w}{\gamma_m} \cdot \left(\frac{h}{H}\right)^2 = C_4 + C_5$$ Equation 8.9b

$$C_3 = \cot \beta$$ Equation 8.9c

$$C_4 = 1 - \left(\frac{D}{H}\right)^2$$ Equation 8.9d

$$C_5 = \frac{\gamma_w}{\gamma_m} \cdot \left(\frac{h}{H}\right)^2$$ Equation 8.9e

If all physical parameters in Equations 8.9a to 8.9e are predefined, the unit shear stress and normal stress are functions only of the failure angle (α). It is not necessary to specify the location of the tension crack, since the shear force has a maximum value within the specified domain. Therefore:

$$C = f\ (\alpha)$$ Equation 8.10

$$\frac{d}{d\alpha} \cdot f\ (\alpha) = 0$$ Equation 8.11

These equations define that geometry which yields the maximum planar shear stress; that is, the most critical failure plane. Performing the designated operation yields:

$$\tan 2\ \alpha = \frac{C_2}{C_3}$$ Equation 8.12

This equation, in combination with Equation 8.7, allows for nomographic solution for that plane exhibiting the maximum shear stress (Figures 8.3 to 8.6). The nomographic solutions are based on the

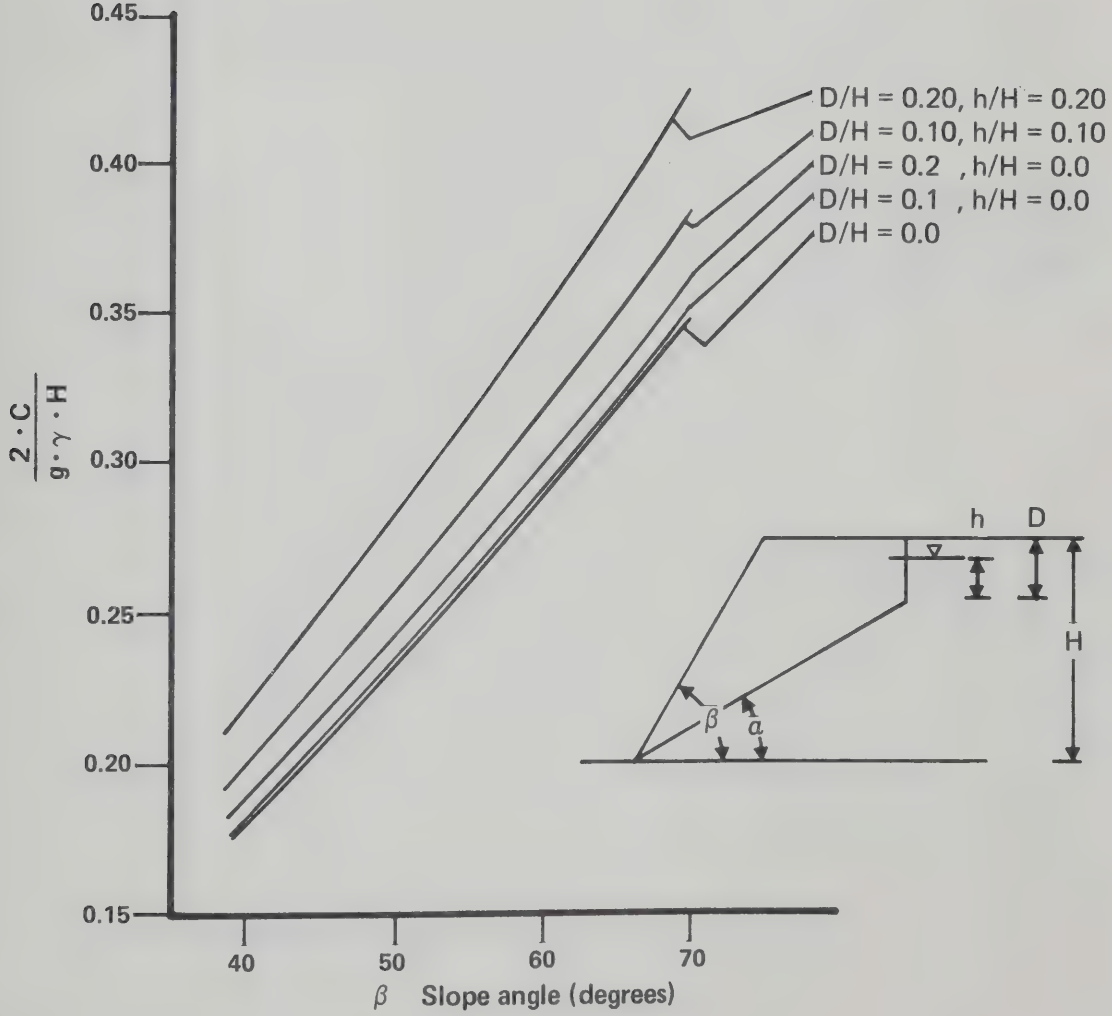

Figure 8.3 Nomographic Solution, D/H = 0.10 and 0.20

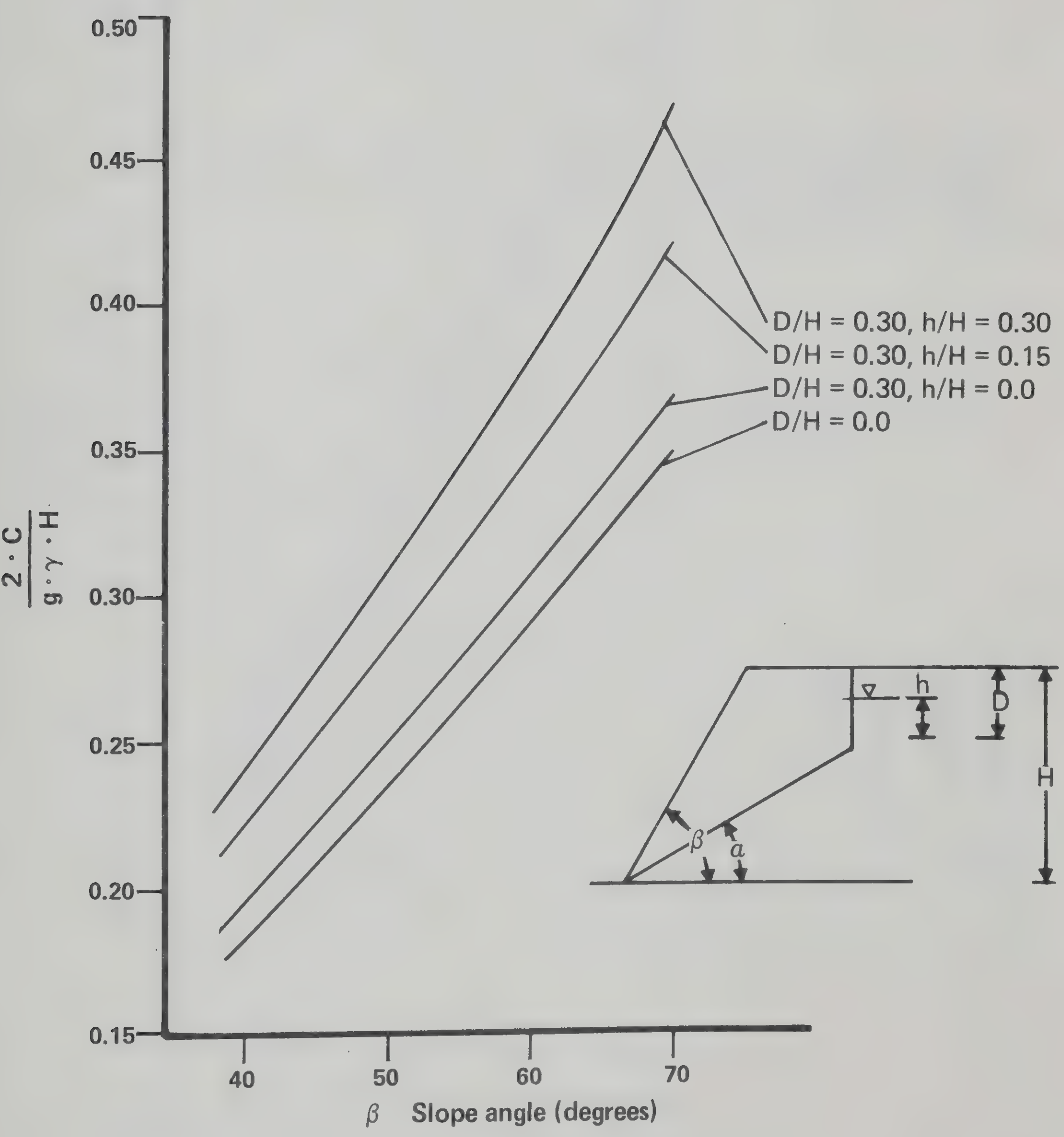

Figure 8.4 Nomographic Solution, D/H = 0.30

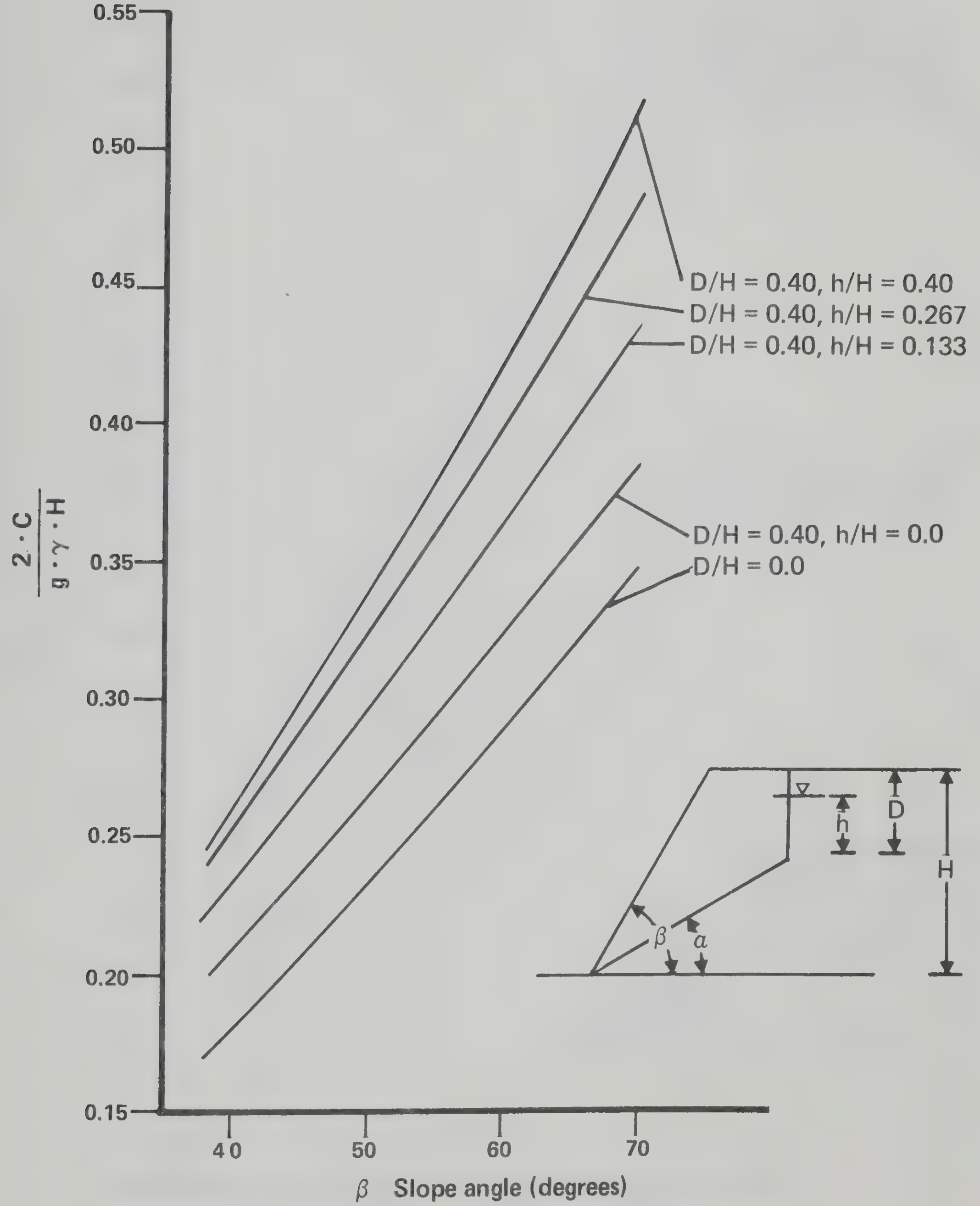

Figure 8.5 Nomographic Solution, D/H = 0.40

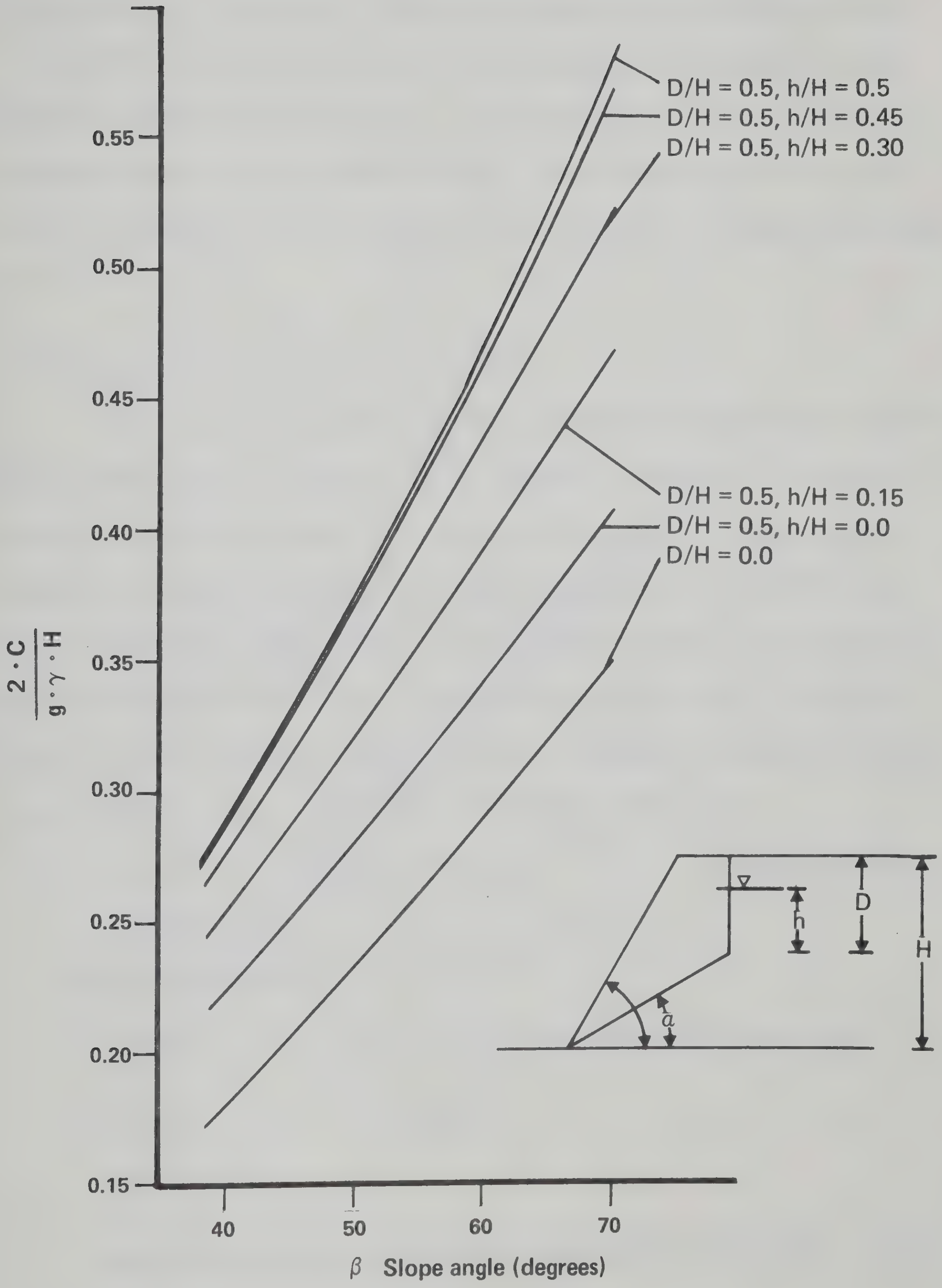

Figure 8.6 Nomographic Solution, D/H = 0.50

assumption that the ratio of the unit weights (e.g. Equation 8.9e) is 0.5. This assumption facilitates nomographic presentation, and error is less than five percent. In addition, the failure plane inclination may be solved (Figure 8.7). The distance from the slope crest to the most critical tension crack location is given by Equation 8.4.

8.3.2 Application of a Failure Criterion

The power law failure criterion delineated in previous chapters may at this point be applied to the analysis. Equation 8.8 provides a measure of the mean normal unit stress on the failure plane. That stress may be used directly in a power law criterion to derive the maximum allowable shear stress. The allowable shear stress may then be divided by the actual shear stress from Equation 8.7 to provide a measure of the factor of safety. Several examples are given to demonstrate the procedure. The failure criterion assumed is:

$$\tau_f = 2.0\,\sigma_n^{0.8} \qquad \text{(in kg/cm}^2\text{ only)} \qquad \text{Equation 8.13}$$

1. Example 1

Analysis Parameters:

$\beta = 65^\circ$ $\quad$ $h = 30$ m (crack filled with water)

$H = 60$ m $\quad$ $\gamma_m = 2.1$

$D = 30$ m

Conversion to consistent units (kilograms, centimeters) yields:

$\frac{D}{H} = 0.5$ $\quad$ $\frac{h}{H} = 0.5$ $\quad$ $\beta = 65^\circ$

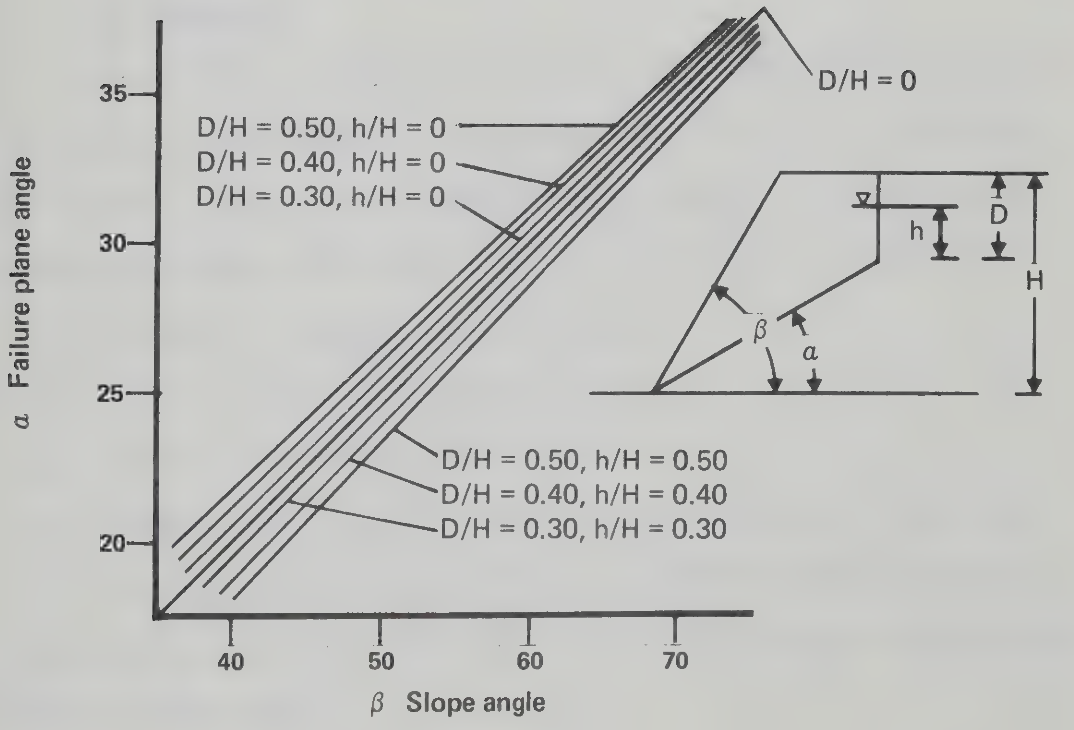

Figure 8.7 Failure Plane Angle Nomograph

$\frac{2\cdot C}{g\cdot\gamma_m\cdot H} = 0.525$ therefore $C = 3.4$ kg/cm^2

and $\alpha = 31^{\circ}$ from Equation 8.12 (or Figure 8.7).

Solving Equation 8.8:

$\frac{2\cdot\sigma_n}{g\cdot\gamma_m\cdot H} = 0.6396$ therefore, $\sigma_n = 4.1$ kg/cm^2

Therefore, from Equation 8.13:

$$\tau_f = 6.2$$

The safety factor, τ_f divided by C, is calculated as 1.8.

2. Example 2

Selection of a specific distance of a tension crack from the slope crest for analysis requires the direct solution of Equations 8.7 and 8.8. If the above example is considered, with the failure angle specified as 40°, the following results can be calculated:

$B = 7.78$ m (from Equation 8.4)

$C = 2.964$ kg/cm^2 (from Equation 8.7)

$\sigma_n = 2.033$ kg/cm^2 (from Equation 8.8)

$\tau_f = 3.528$ kg/cm^2 (from Equation 8.13) therefore, FS = 1.19

If the tension crack were dry, the factor of safety would be 1.96, showing the significant effects of water pressure on thin slabs lying at steep angles.

8.3.3 Extensions to the Wedge Analysis

In a cohesionless material with a linear envelope, the most critical failure surface is that surface where the ratio of shear stress to normal stress is at its maximum. Hence the following equation should be maximized in a given domain to yield a maximum

stress ratio:

$$\frac{C}{\sigma_n} = f(\alpha) \qquad \text{Equation 8.14}$$

Again, a maximum occurs where:

$$\frac{df(\alpha)}{d\alpha} = 0 \qquad \text{Equation 8.11}$$

and the following equation is derived:

$$W \tan^3\alpha + X\tan^2\alpha + Y\tan\alpha + Z = 0 \qquad \text{Equation 8.15}$$

where:

$W = 4C_3C_5$ Equation 8.16a

$X = 3C_3^2 - 3C_2C_5$ Equation 8.16b

$Y = -2C_2C_3 - 2C_3C_4$ Equation 8.16c

$Z = -C_2C_4$ Equation 8.16d

and the constants C_1 to C_5 are defined by Equation 8.9.

This equation may be solved iteratively to find the critical angle and hence the maximum shear stress to normal stress ratio in a given range of values dictated by the geometry. Inspection of a given geometry and set of input parameters will permit the prediction of the logical worst conditions which could occur. Worst conditions will occur where the failure plane is extremely steep, the tension crack coincides with the slope crest, and the tension crack is filled with water. It should be recognized, of course, that the worst possible conditions probably will never be encountered. For example, the closer a tension crack is to the slope crest, the less chance there is that it will retain significant quantities of water.

Furthermore, the adoption of a curvilinear criterion (Equation 8.13) will result in Equation 8.15 not yielding the lowest factor of

safety.

Defining the factor of safety as:

$$FS = \frac{\tau_f}{C} \qquad \text{Equation 8.17}$$

and substituting Equations 8.7, 8.8, and 8.13 yields:

$$FS = \frac{2.0\sigma_n^{0.8}}{C} \qquad \text{Equation 8.18a}$$

$$FS = 4.0 \frac{\left\{g \cdot \gamma_m \cdot \frac{H}{2}\right\}^{0.8} \cdot \left\{C_1C_4\cos^2\alpha - C_1C_3\sin\alpha\cos\alpha - C_1C_5\sin^2\alpha\right\}^{0.8}}{g \cdot \gamma_m \cdot H \cdot \left\{C_1C_2\sin\alpha\cos\alpha - C_1C_3\sin^2\alpha\right\}}$$

Equation 8.18b

This equation could be minimized within a given domain by the same methods used to derive Equations 8.12 and 8.15. Because of the complexity of the equation, this has not been done. Generally, minimizing is not required, since worst conditions can be predicted which yield the minimum factor of safety. Iterative solution using the individual equations is preferred, since the mathematics is simple.

8.3.4 Wedge Analysis: Conclusion and Critique

Repeated solution of the wedge problem for various geometries subject to the criterion expressed by Equation 8.13 show that the factor of safety of oil sand slopes is high. The only cases which approach low factors of safety are those characterized by deep, water-filled tension cracks close to the slope face. Point loads imposed on high steep slopes by heavy equipment can safely be ignored in analysis: they are insignificant compared to the weight of the wedge.

This analysis is subject to the following criticisms: the failure surface is assumed to be planar; progressive failure as a result of unequal

stress distributions on the failure plane is ignored; and structural disturbance at or near the slope face as a result of excavation is ignored. However, research shows high laboratory strengths in oil sands; in situ strengths may be considerably higher still. Thus, the failure criterion defined by Equation 8.13 is conservative, and may be used in analysis.

8.4 Finite Element Stress Distribution Analysis

8.4.1 Introduction to Finite Element Analysis of Oil Sand Slopes

A stress distribution analysis employing finite element methods was performed on two model slopes: a 60° slope (1:1.73), and a 63.4° slope (1:2). A constant value of K_o and a coarse mesh were employed in the 60° slope analysis; a bilinear value of K_o, a finer mesh, and varying basal stratigraphies were employed in the 63.4° slope analysis. Constant strain triangles and linear elastic, isotropic, plane strain analyses were used throughout; single load step analyses were performed and tensile or failed elements were removed in the 63.4° slope analysis. Maximum principal compressive stress, minimum principal compressive stress, and orientation of principal stress axes were contoured for the area of interest; circular toe arcs were drawn through the 63.4° slope; and stress distributions normal and parallel to the arc were determined from the contour diagrams. The solution for maximum allowable shear stresses along the circular arcs was obtained by application of power law failure criteria.

8.4.2 Analytic Rationale

A linear stress-strain relationship was considered justified on the basis of triaxial test results, the stress paths involved, and

the no-failure analysis.

The choice of elastic parameters was based on the knowledge of typical in situ sand properties, and the realization that elastic parameters are grossly affected by even minor sample disturbance. Analysis of geophysical sonic data yields Young's Modulus values of approximately 75,000 kg/cm^2 and Poisson's Ratios of 0.3 to 0.35 for oil sands. This value of Young's Modulus is unrealistic for the high stress changes involved in excavating.

Nonlinear K_o distributions were chosen because calculations based on the curvilinear failure criterion showed that a constant K_o was not logically acceptable, particularly in near-surface strata. Behavioural anisotropy and the effects of gas exsolution or fracturing could not be incorporated into this model.

The finite element analysis was performed as a gross behavioural study to delineate:

1. Regions of stress concentration and potential progressive failure.
2. Regions of potential tensile and shear failure.
3. Deformation patterns under elastic conditions.

Furthermore, delineations of stress distributions along selected circular arcs were derived, and the effects of variations in lithology and stratigraphy were studied.

8.4.3 Analytic Procedure

A plane strain, linear elastic, isotropic analysis does not permit the direct solution of a stress field where K_o is greater than about 0.99 (Desai and Able, 1972); therefore a two-step procedure was

employed (Figure 8.8). The in situ total stresses for the nonexcavated slope were calculated: the total vertical stress was assumed to be equal to the unit density multiplied by the thickness of overburden, and the total horizontal stress was assumed to be equal to the vertical stress multiplied by the value of K_o at that depth. The second step assumed a weightless soil mass with a stress distribution on the excavated face equal but opposite to the in situ stress distribution; the stresses were converted to forces applied at element nodes, and the resultant stress field from finite element analysis was added directly to the stress field from step one.

The displacements derived from step two are correct for the chosen analytic parameters, and are the actual elastic displacements occurring upon excavation.

After the normal and shear stress fields were obtained, the principal stress field was generated, and stress values were contoured for various sets of analytic elastic parameters. The contours of principal stresses and their orientations, and the delineations of a specific circular arc, permitted the calculation of the normal compressive stress and the tangential shear stress along the arc. The shear stress was compared directly with the allowable shear stress generated from substitution of the normal compressive stress along the chosen arc into a power law failure criterion.

Element stresses rather than mean nodal stresses were used to obtain stress contours. Element stresses in constant strain triangles often showed considerable oscillation; but mean nodal stresses tended to overestimate stresses near structure boundaries. Therefore the element stresses were hand contoured to average large oscillations

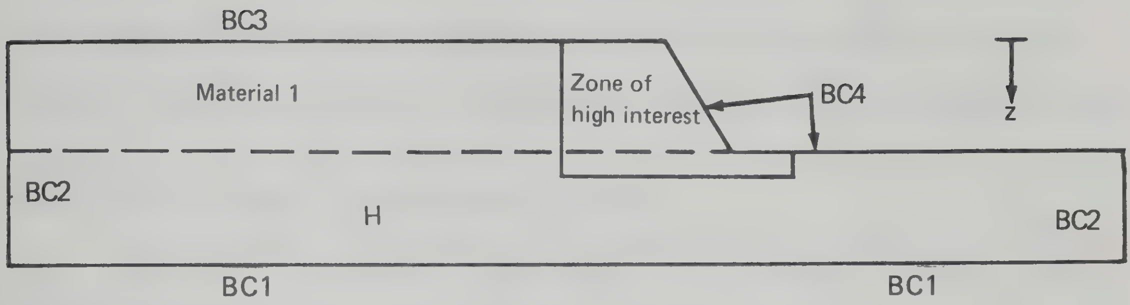

Specification of Boundary Conditions for Step 2 (below)

BC1: $\Delta x = 0$ (Fixed boundary)
$\Delta y = 0$
BC2: $\Delta x = 0$ (Roller boundary)
BC3: $\sigma x = 0$ (Stress-free face)
$\sigma y = 0$
BC4: $\sigma y = \gamma_1 \cdot z$
$\sigma x = \sigma y \cdot K_0 = \gamma_1 \cdot z \cdot K_0$

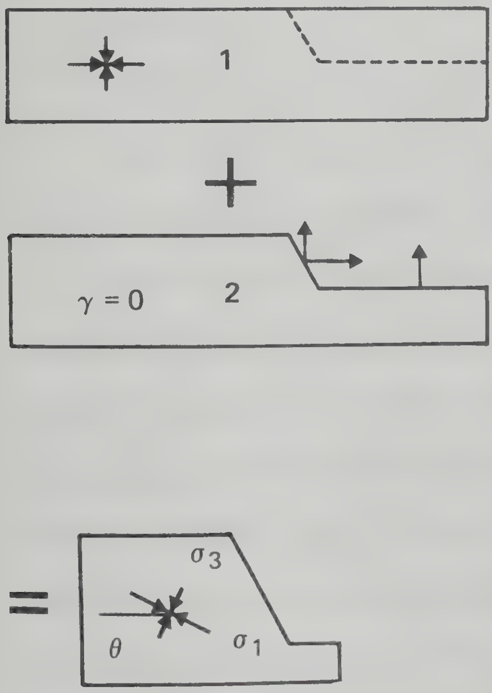

Step 1 (*In situ* conditions)
$(\sigma y)_1 = \gamma \cdot z$
$(\sigma z)_1 = K_0 \cdot \sigma y$ $\tau xy = 0$

Step 2 (Excavation step)
$\left.\begin{array}{l}(\sigma y)_2\\(\sigma x)_2\\(\tau xy)_2\end{array}\right\}$ Solved by finite element analysis

$(\Delta x)_2, (\Delta y)_2$ " "

Step 3 (Complete solution)
$(\sigma y)_3 = (\sigma y)_1 + (\sigma y)_2$
$(\sigma x)_3 = (\sigma x)_1 + (\sigma x)_2$
$(\tau xy)_3 = (\tau xy)_2$
$\Delta x = (\Delta x)_2$
$\Delta y = (\Delta y)_2$

↓

{ Solve for Principal Stresses }

Figure 8.8 Finite Element Analytic Procedure

(e.g. Figure 8.19). The stresses in a limited region only were contoured, since the immediate back-slope is the zone of potential failure.

8.4.4 Finite Element Mesh Characteristics

The following general rules guided mesh design for finite element analysis:

1. Triangle aspect ratios were kept low.
2. Finer mesh divisions were employed in the region of large stress variation (i.e. toe of slope).
3. Mesh height was twice the slope height (although this was not necessary, because of the high Young's Modulus of the basal limestone).
4. Mesh length was greater than ten times the slope height.
5. Side boundaries employed roller-type constraints; basal boundaries employed pin-type constraints (Desai and Able, 1972).

The two meshes employed are shown in Figures 8.9 and 8.10 for the 60° and 63.4° slopes respectively. The second mesh was designed and used because the initial mesh was too coarse to accomodate the large elastic displacements at the slope toe, and because it contained rows of elements which displayed considerable stress oscillation. The second mesh contained approximately double the element density; therefore stress distributions along circular arcs were determined for the second mesh only.

8.4.5 Application of Various K_o Conditions to the Excavated Slope

The 60° slope mesh was subjected to boundary stresses representing values of K_o constant within each analysis, but varying among analyses from a value of 1.0 to 8.0. The resultant horizontal force

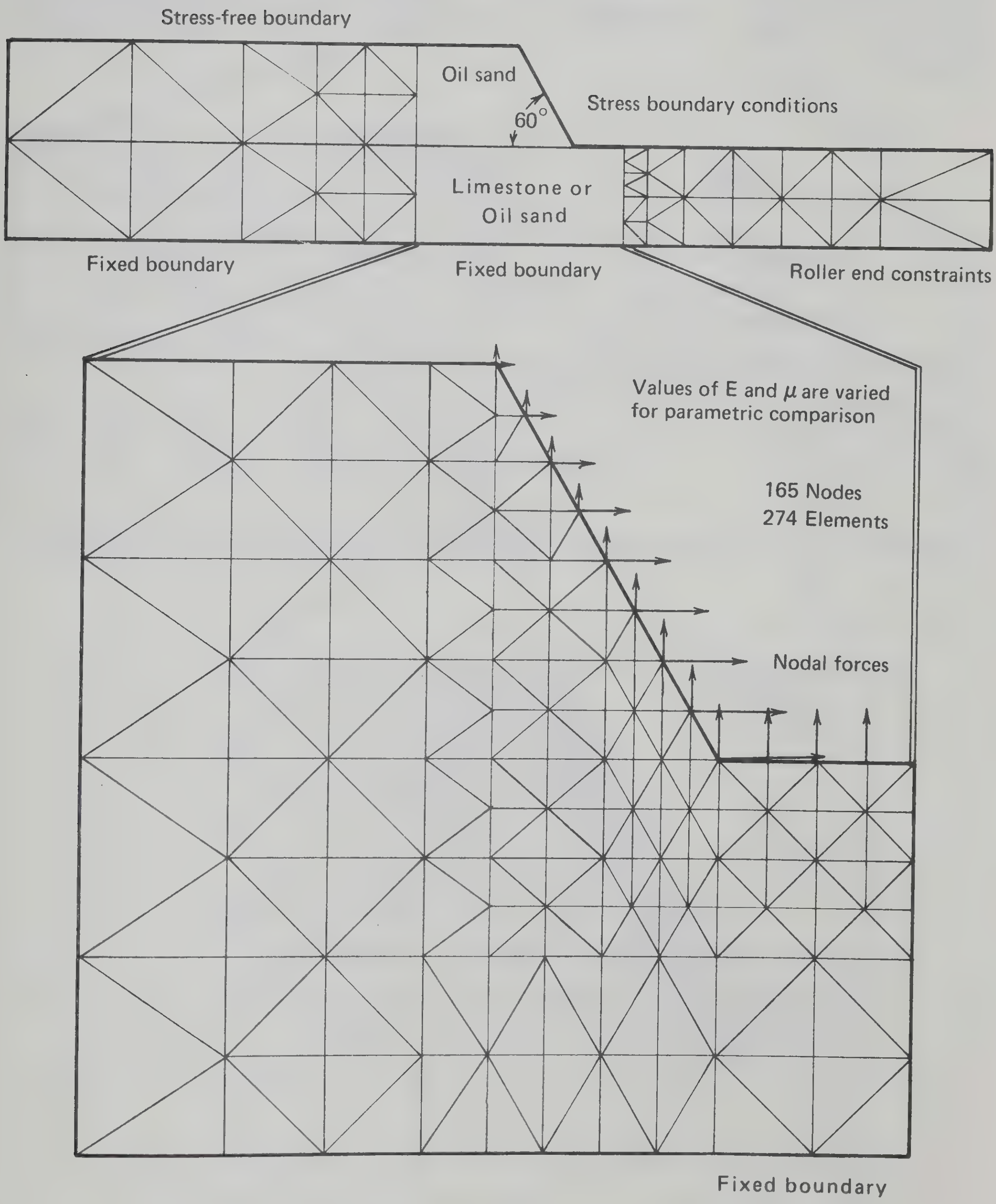

Figure 8.9 Finite Element Mesh, 60° Slope

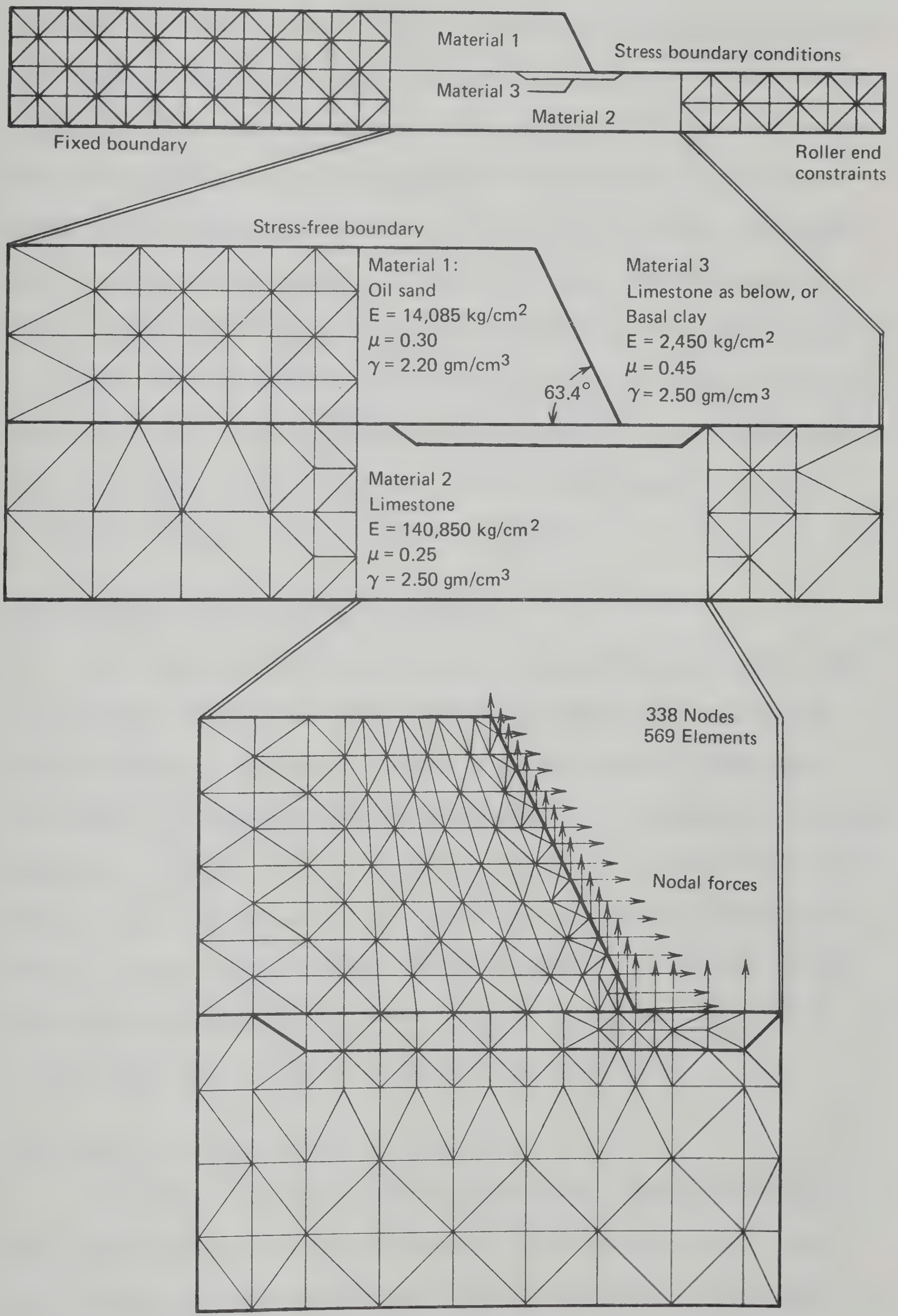

Figure 8.10 Finite Element Mesh, 63.4° Slope

diagrams are linear (Figure 8.11). Recognition that values of K_o may not remain constant with depth resulted in application of a nonlinear horizontal nodal force distribution (Figure 8.11) to the 63.4° slope. The values of the forces were obtained by multiplying a given mean nodal stress by the appropriate value of K_o, by the slope increment, and of course by the tangent of the slope angle. For all analyses on the second mesh, values of K_o were expressed as two numbers (e.g. $K_o = 2,4$). The first number refers to the constant value of K_o which was applied to the entire slope below a depth of H/2; the second number is the value of K_o at surface. Values of K_o between the slope crest and the slope midpoint varied linearly.

8.4.6 Analysis Using the 60° Slope Mesh

The effects of differing moduli ratios between oil sands (Soil 1) and limestone (Soil 2) were examined by keeping K_o constant and varying values of E_1 and E_2; Poisson's ratios remained unchanged. The effects of varying K_o values were assessed by keeping all material properties constant, and by applying slope forces derived for K_o equal to 1.0, 1.5, 2.0, 4.0, and 8.0. Pre-excavation in situ forces were subject to the same K_o values. Moduli ratios (E_1/E_2) of 1:1, 1:20, and 1:50 were employed, while the value of K_o was kept constant at 1.0 and other material properties remained unchanged.

8.4.7 Analysis Using the 63.4° Slope Mesh

The effects of the introduction of a soft layer at the slope base was explored by an initial analysis with two soils only, then by a further analysis introducing a lens of material at the slope base (Figure 8.10) with differing properties. Material properties

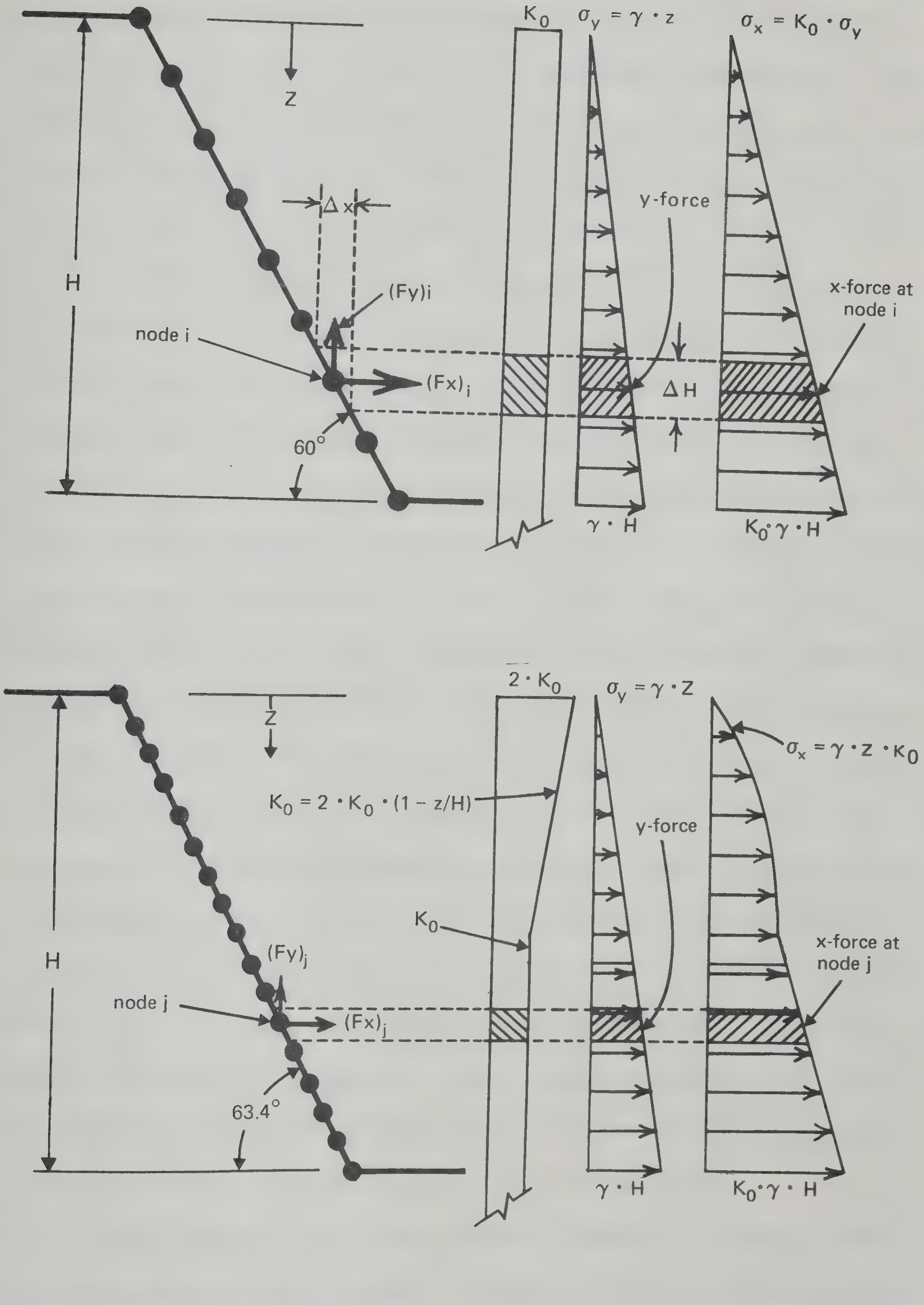

Figure 8.11 Derivation of Nodal Forces

were kept constant for the initial analyses: Young's Moduli ratios for oil sands, limestone, and clay were 1 : 10 : 0.17, and Poisson's Ratio values of 0.30, 0.25, and 0.45 respectively were employed. Non-constant values of K_o were employed, and boundary stresses were derived as shown in Figure 8.11. K_o values of (1,2), (2,4), and (4,8) were used for both of the stratigraphies in Figure 8.8.

A further analytic step was introduced for this slope mesh by a partial removal of tension to examine the effects on slope stress distributions. Any elements in the mesh which yielded tensile stresses (minimum principal stress) in the first analysis were accorded new material properties. Oil sand elements in the upper, tensile zone were given material properties assuming an unchanged bulk modulus (K), and a shear modulus (G) reduced by a factor of 50. Since the program constitutive matrices use Young's Moduli and Poisson's Ratios, conversion to bulk and shear moduli, reduction of shear modulus, and reconversion to standard elastic constants were done by hand calculation. Reduction of shear modulus results in a similar drop in Young's Modulus and a rise in Poisson's Ratios as indicated by well-known elastic relationships (e.g. Jaeger and Cook, 1969). Oil sand elements which had failed, by exceeding the specified (failure criterion) shear stress in the region of the slope toe, were given elastic constants equivalent to a shear modulus reduction by a factor of five. Failed elements in the clay were given a new Young's Modulus lowered by a factor of ten, accompanied by a Poisson's Ratio increase from 0.45 to 0.49.

These steps did not remove tension completely, and new tensile elements were generated; however, incremental loading with progressive tension removal was not considered justifiable. The purpose of the tension

removal increment was only to indicate patterns of stress evolution, and not to generate quantitative data.

8.4.8 Results of 60° Slope Analysis

Slope deflections are presented in Figure 8.12. Values of both K_o and soil properties are varied to show the effects of <u>in situ</u> stress and of varying soil properties on slope surface deflections.

Contours of normalized maximum shear stresses are presented in Figure 8.13 and in Figure 8.14 for selected conditions. The zone of "failure" was derived by applying a simple linear mean total stress failure criterion:

$$\tau_{max} = \left(\frac{\sigma_1 + \sigma_3}{2}\right) \sin 40° = 0.64 \left(\frac{\sigma_1 + \sigma_3}{2}\right) \qquad \text{Equation 8.19}$$

and is intended to show regions of higher probability of failure. The result of application of various total stress ratio failure criteria is shown in Figure 8.14c.

Contours of the change in the first stress invariant are derived:

$$\Delta J_1 = \frac{\Delta \sigma_1 + \Delta \sigma_2 + \Delta \sigma_3}{3} \qquad \text{Equation 8.20}$$

Two selected cases are presented in Figure 8.15. If the change in pore fluid pressure can be expressed as:

$$\Delta u = f(\Delta J_1) \qquad \text{Equation 8.21}$$

then these figures give an idea of the magnitude of the pore pressure change.

8.4.9 Results of 63.4° Slope Analysis

Normalized elastic deflections (tension permitted) are presented in Figure 8.16 for two stratigraphies and for three conditions of K_o.

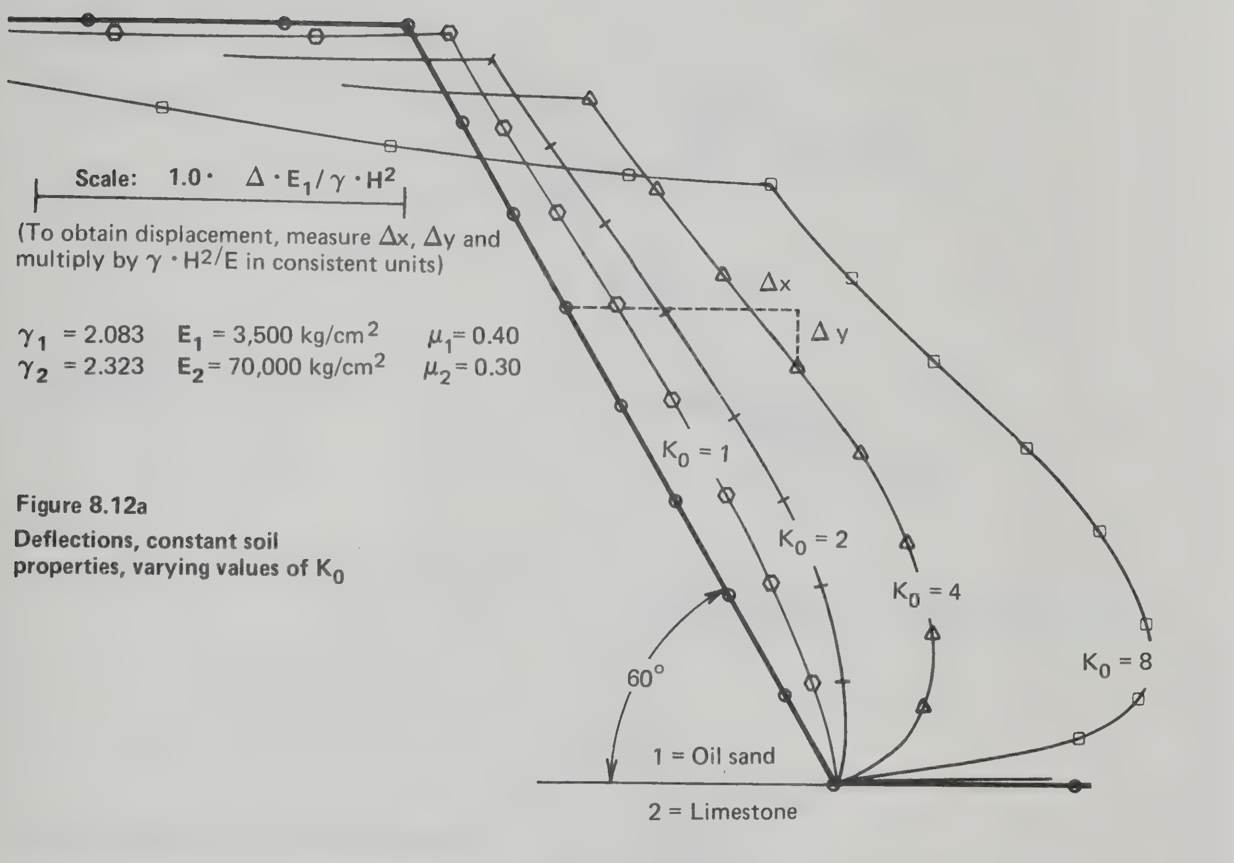

Figure 8.12a
Deflections, constant soil properties, varying values of K_0

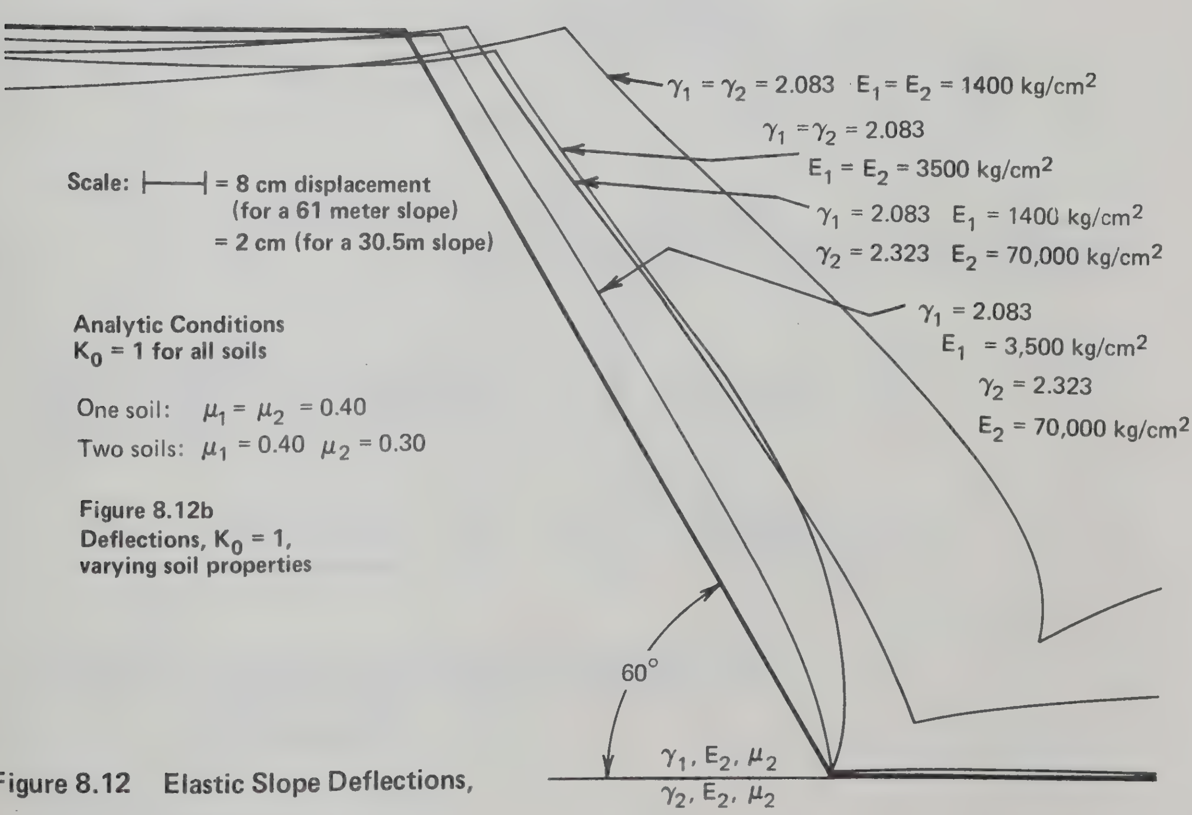

Figure 8.12b
Deflections, K_0 = 1, varying soil properties

Figure 8.12 Elastic Slope Deflections, 60° Slope

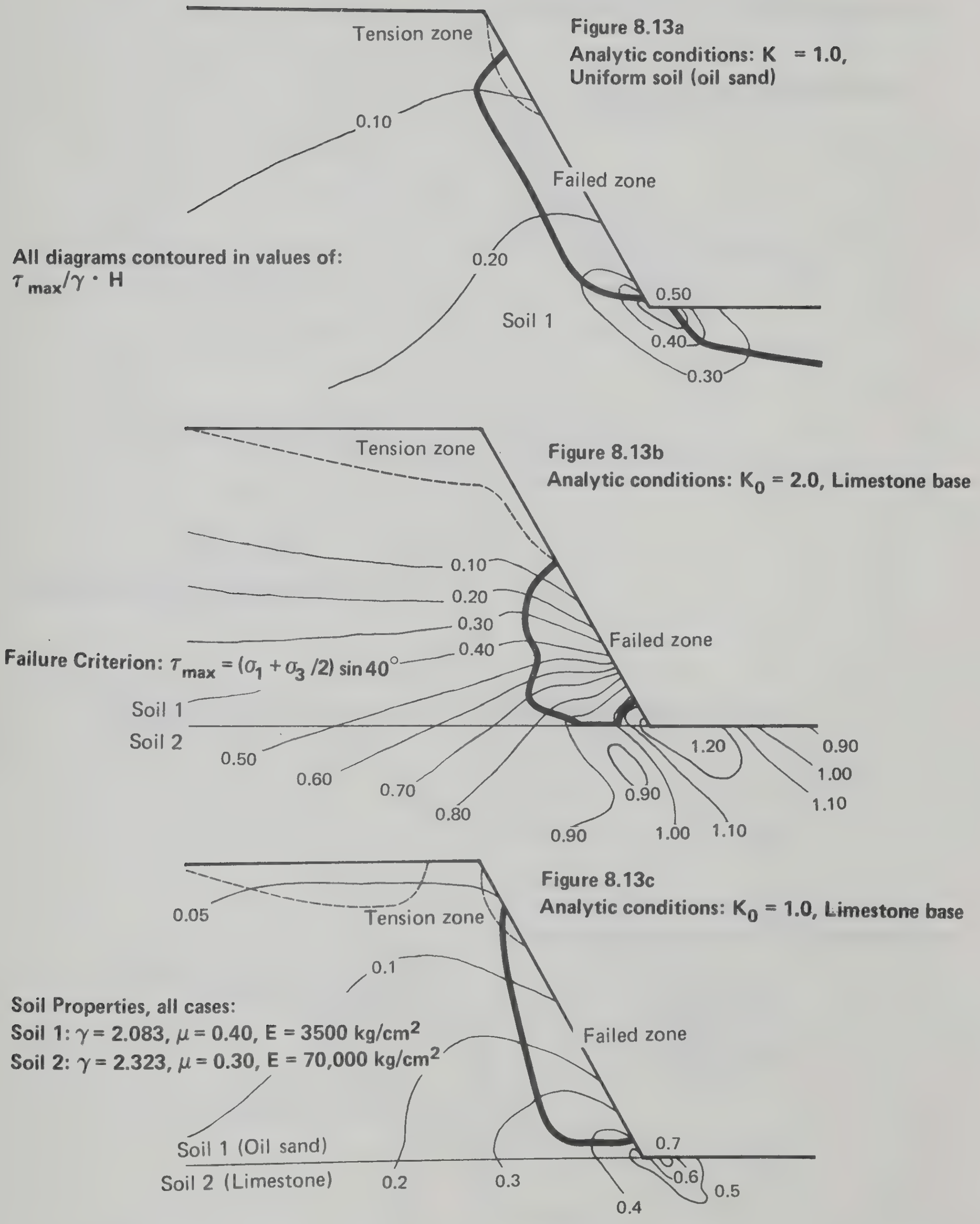

Figure 8.13a
Analytic conditions: K = 1.0,
Uniform soil (oil sand)

All diagrams contoured in values of:
$\tau_{max}/\gamma \cdot H$

Figure 8.13b
Analytic conditions: $K_0 = 2.0$, Limestone base

Failure Criterion: $\tau_{max} = (\sigma_1 + \sigma_3 /2) \sin 40°$

Figure 8.13c
Analytic conditions: $K_0 = 1.0$, Limestone base

Soil Properties, all cases:
Soil 1: $\gamma = 2.083$, $\mu = 0.40$, $E = 3500$ kg/cm^2
Soil 2: $\gamma = 2.323$, $\mu = 0.30$, $E = 70{,}000$ kg/cm^2

Figure 8.13 Contours of Maximum Shear Stress, 60° Slope; Zones of Tension, Zones of Potential Shear Failure Included

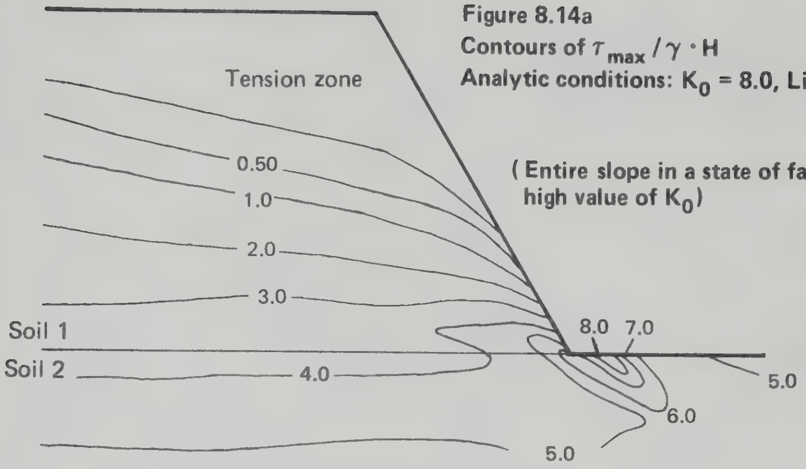

Figure 8.14a
Contours of $\tau_{max}/\gamma \cdot H$
Analytic conditions: K_0 = 8.0, Limestone base

(Entire slope in a state of failure due to high value of K_0)

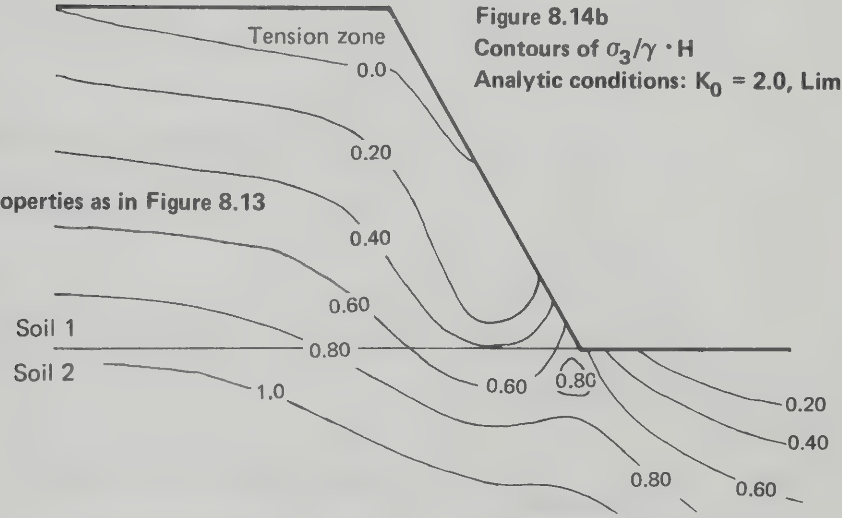

Figure 8.14b
Contours of $\sigma_3/\gamma \cdot H$
Analytic conditions: K_0 = 2.0, Limestone base

All soil properties as in Figure 8.13

Figure 8.14c
Application of a total principal stress ratio failure criterion, K_0 = 2.0, Limestone base

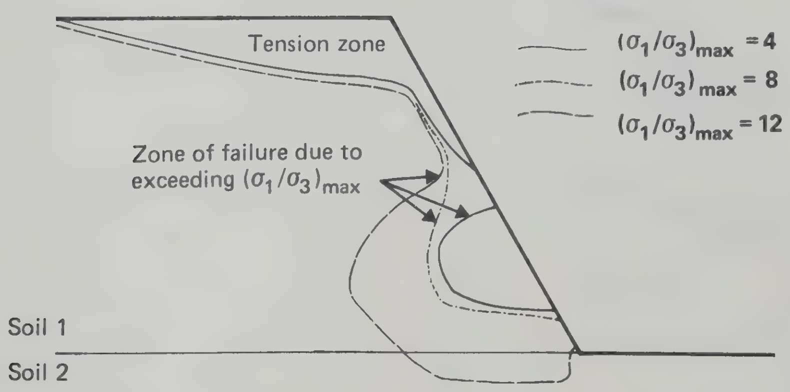

Figure 8.14 Stress Conditions and Failure Zones, 60° Slope; Varying K_0

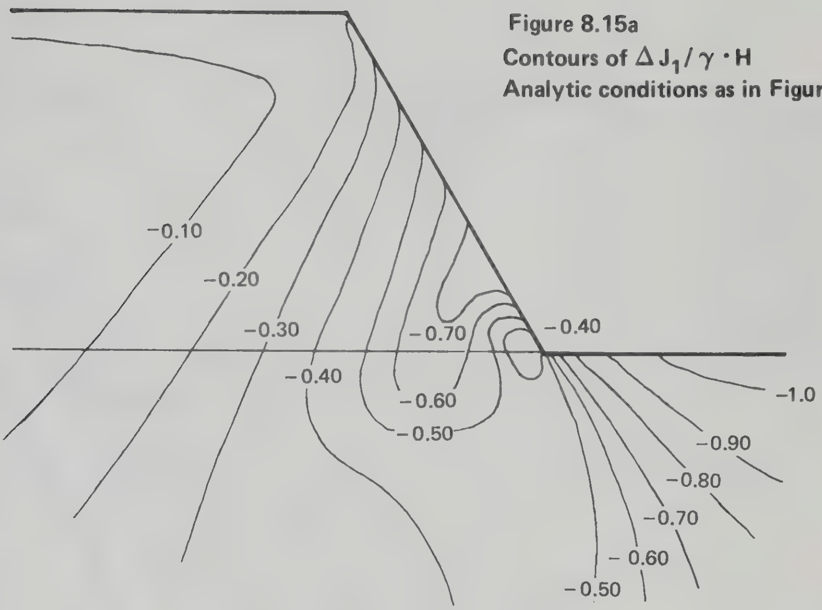

Figure 8.15a
Contours of $\Delta J_1/\gamma \cdot H$
Analytic conditions as in Figure 8.13b

Derivation of ΔJ_1: Plane strain

$$J_1 = \frac{\sigma_1 + \sigma_2 + \sigma_3}{3}$$

therefore:

$$\Delta J_1 = \frac{\Delta\sigma_1 + \Delta\sigma_2 + \Delta\sigma_3}{3}$$

$$\left\{\begin{array}{l} \Delta\sigma_1 = \sigma_{1B} - \sigma_{1A} \\ \Delta\sigma_2 = \sigma_{2B} - \sigma_{2A} \\ \Delta\sigma_3 = \sigma_{3B} - \sigma_{3A} \\ \sigma_2 = \mu(\sigma_1 + \sigma_3) \end{array}\right.$$

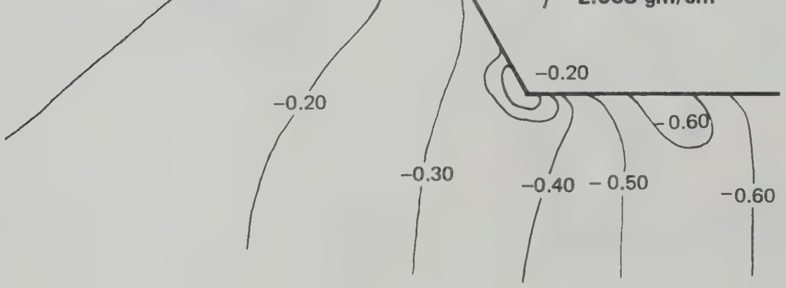

Figure 8.15b
Contours of $\Delta J_1/\gamma \cdot H$
Analytic conditions:
$K_0 = 1.0$
Uniform soil
$\mu = 0.40$
$E = 3{,}520 \text{ kg/cm}^2$
$\gamma = 2.083 \text{ gm/cm}^3$

Figure 8.15 Contours of the Change in Mean Principal Stress, 60° Slope

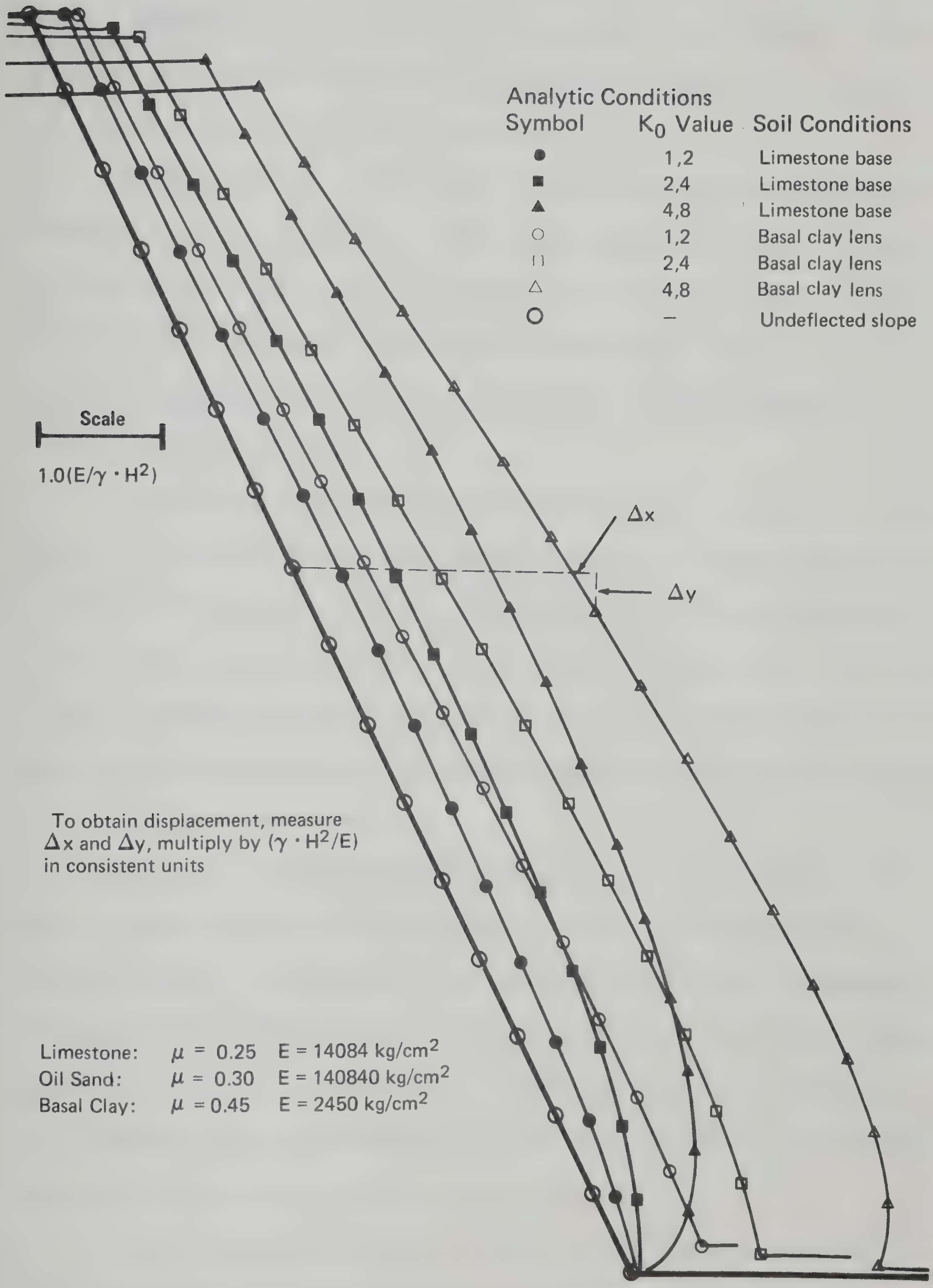

To obtain displacement, measure Δx and Δy, multiply by (γ · H^2/E) in consistent units

Limestone: μ = 0.25 E = 14084 kg/cm^2
Oil Sand: μ = 0.30 E = 140840 kg/cm^2
Basal Clay: μ = 0.45 E = 2450 kg/cm^2

Figure 8.16 Elastic Slope Deflections, 63.4° Slope

Figures 8.17 and 8.18 show the increase in the number of failed elements as tension is removed by increments. Again, two stratigraphies and three conditions of K_o are employed.

Figures 8.19 to 8.23 present principal stress distributions for selected analytic conditions. Each figure contains a contour diagram of maximum principal stress, minimum principal stress, and deviation of the stress axes from the x-y coordinate system: these three contour diagrams completely specify the plane strain stresses computed by finite element analysis.

Figure 8.24 shows an alternate method of stress solution presentation. This method is visually effective, but it is more difficult to employ in stress distribution calculations. No data are included in the tensile failure zone from the initial solution, since the attribution of changed elastic constants results in unrealistic stress distributions in those areas. The actual density of data is much greater than the diagram indicates.

The variation of principal stress along two selected circular arcs is shown in Figure 8.25, indicating how the intersection of a potential failure surface with the principal stresses may be resolved to yield a compressive stress value normal to the arc and shear stresses parallel to the arc, providing the arc and the principal stresses are all quantitatively and geometrically defined. The value of K_o in the slope for the particular analysis is also shown.

Values of normal stress and shear stress under various analytic conditions for three different circular arcs passing through both the slope crest and the toe arc are presented in Figures 8.26 to 8.28. Allowable shear stresses for two different power law failure

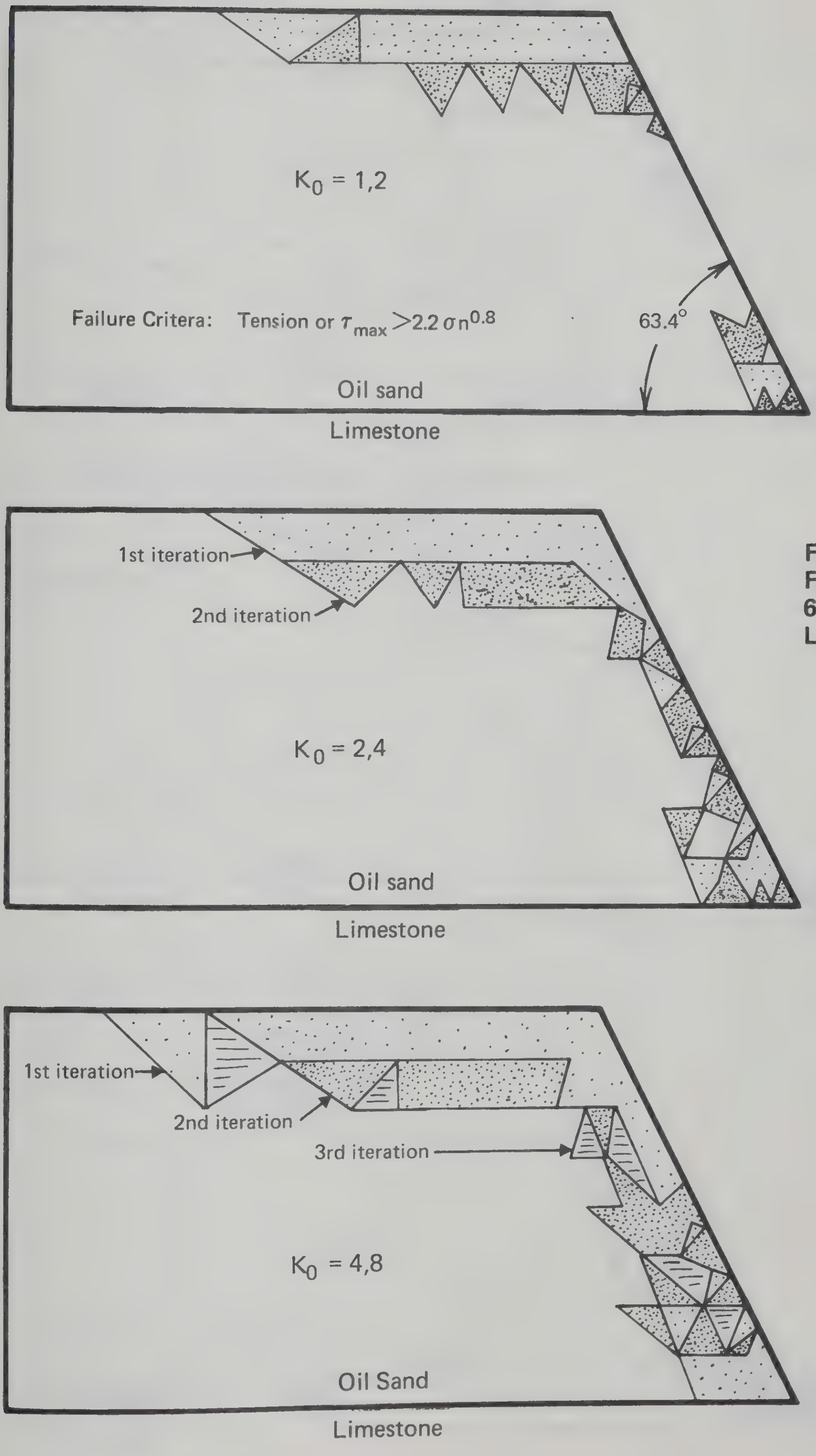

Figure 8.17
Failed Elements,
61 Meter Slope,
Limestone Base

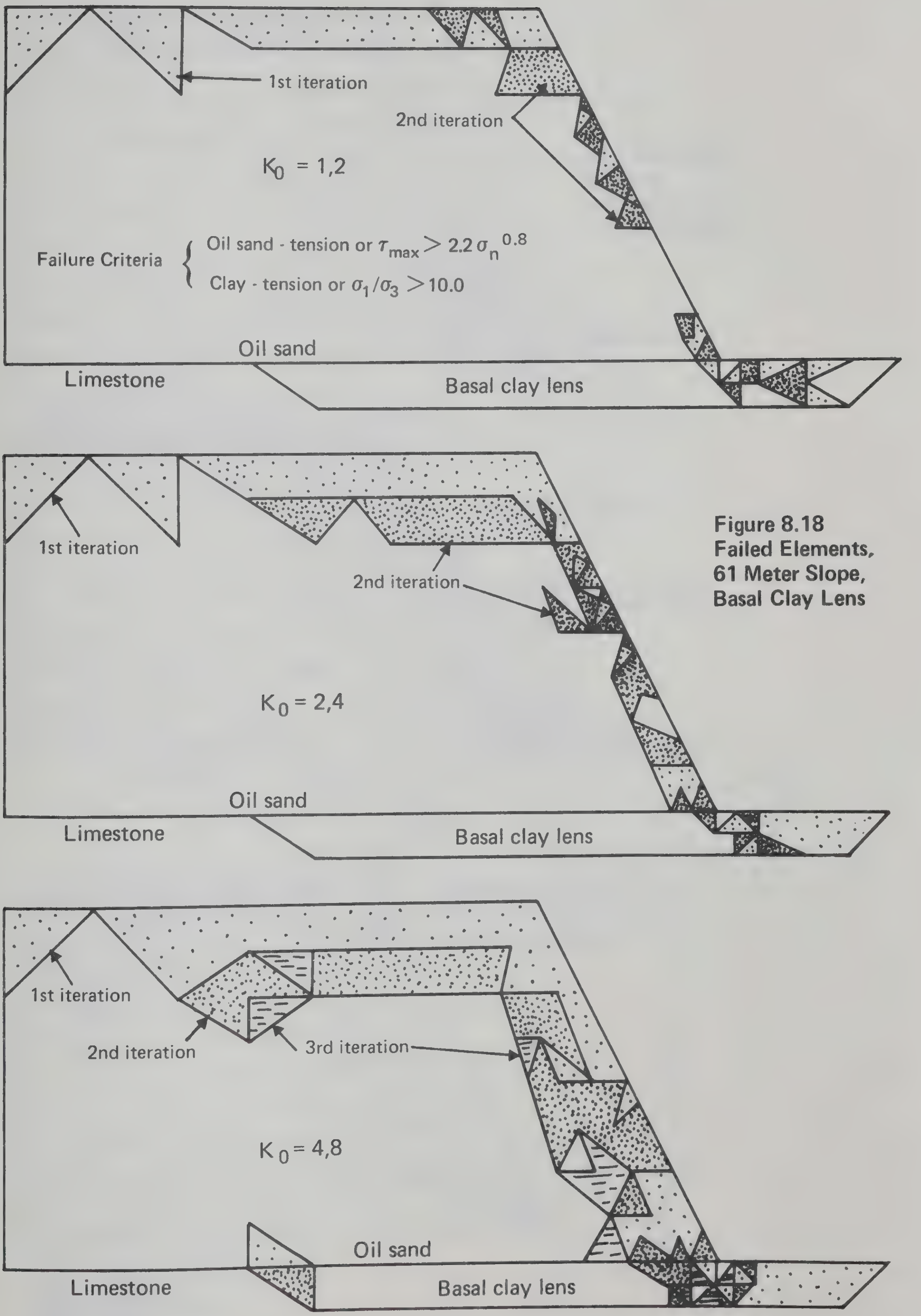

Figure 8.18
Failed Elements,
61 Meter Slope,
Basal Clay Lens

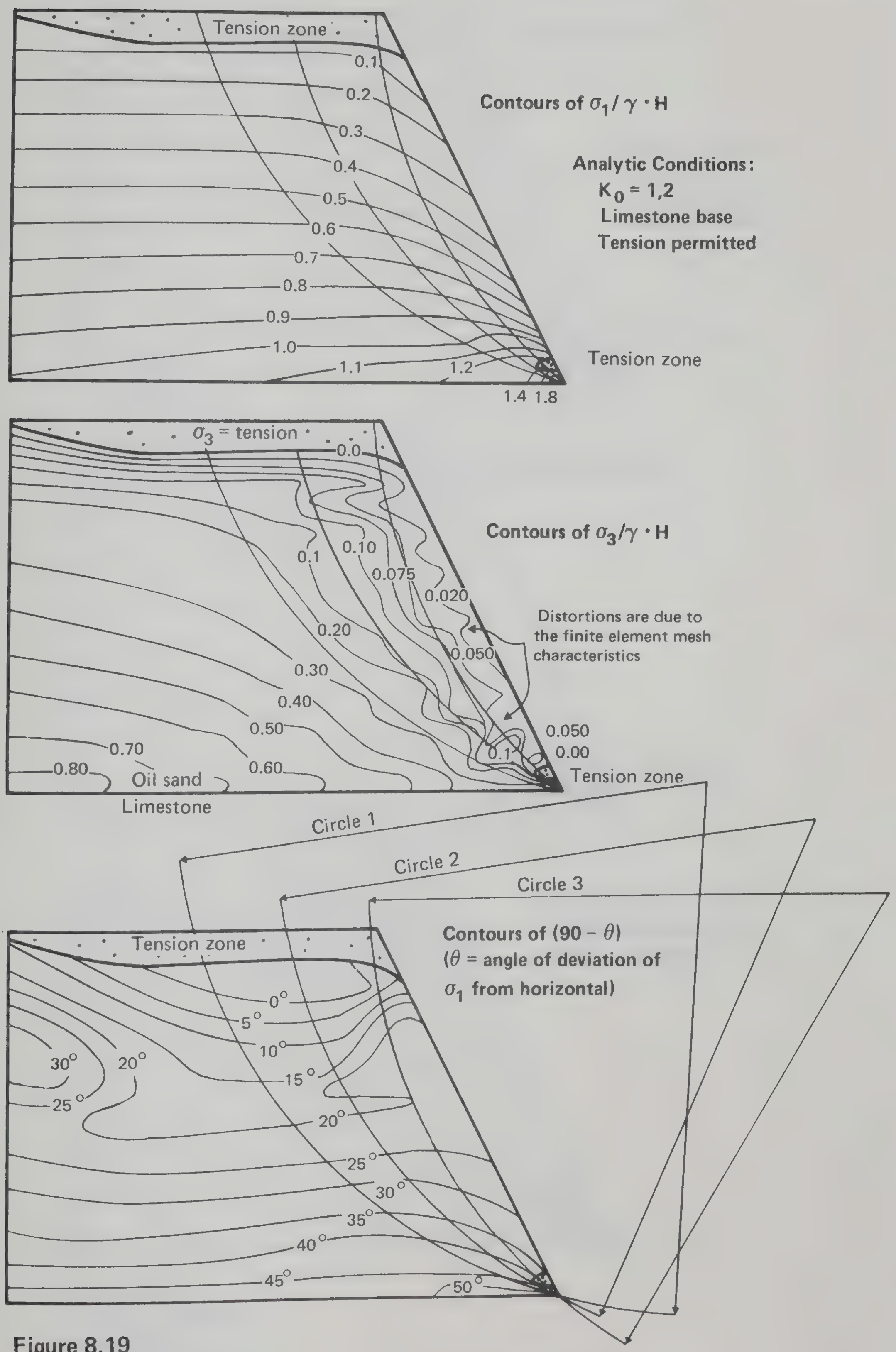

Figure 8.19
Stress Conditions,
63.4° Slope

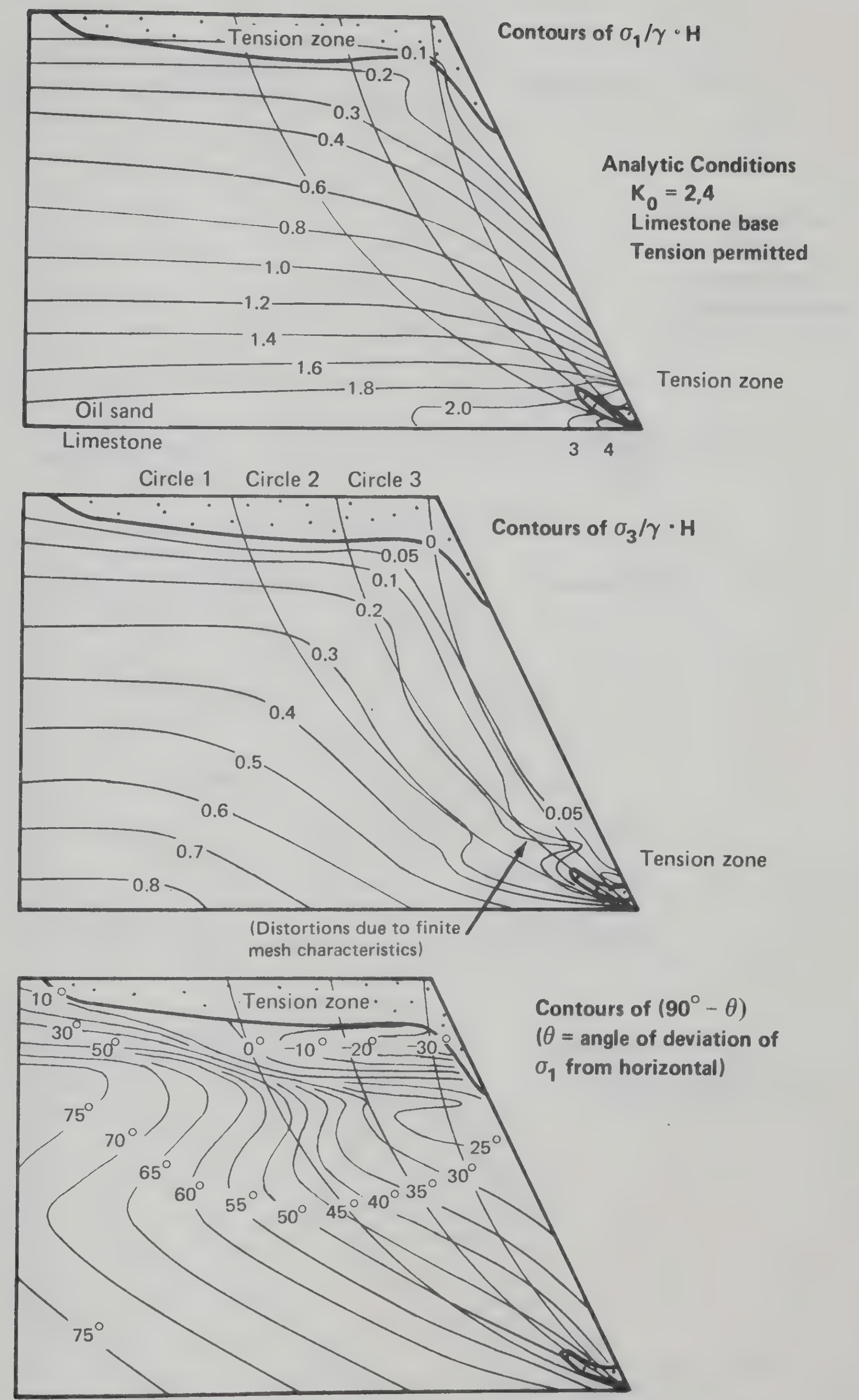

Figure 8.20
Stress Conditions,
63.4° Slope

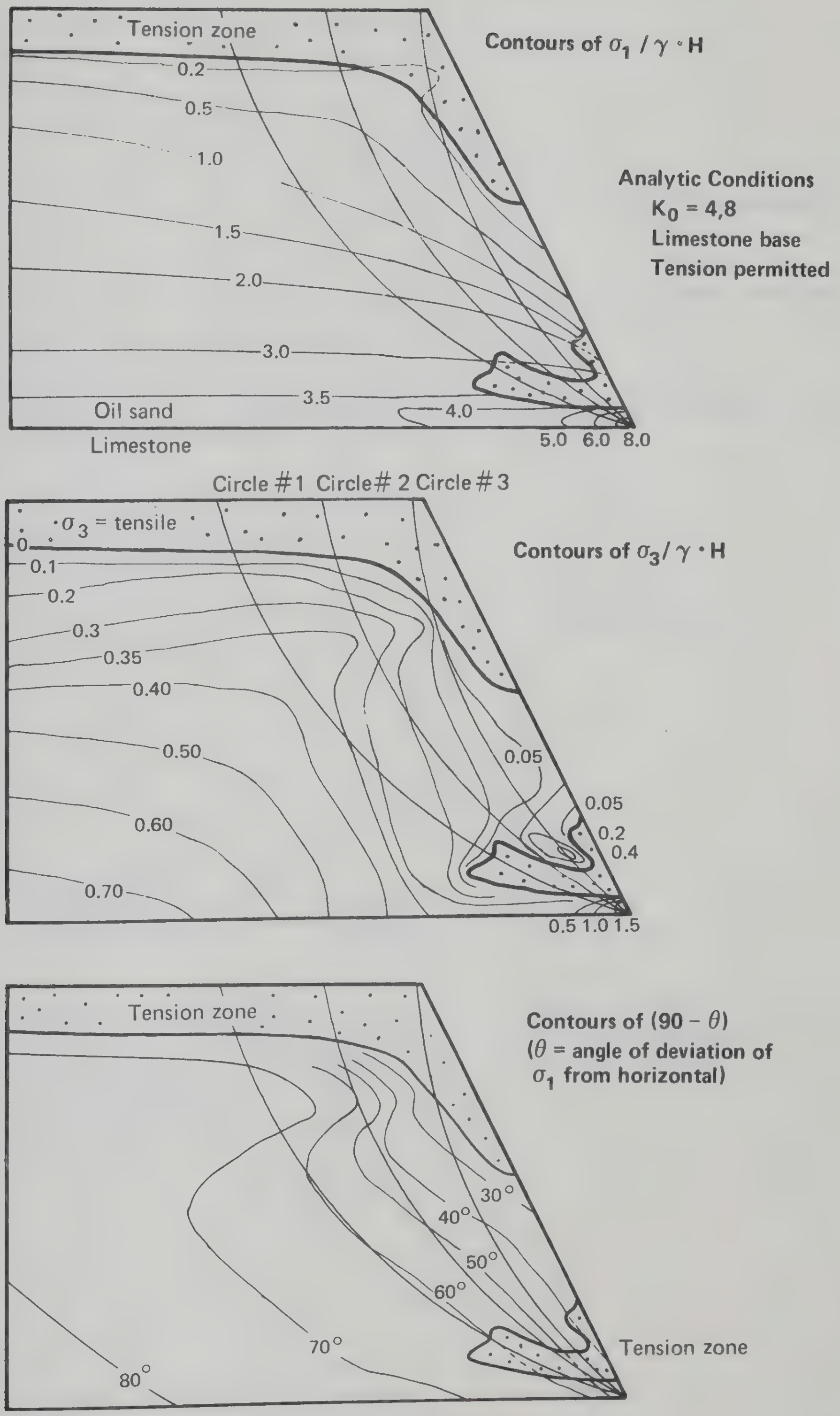

Figure 8.22
Stress Conditions,
63.4° Slope

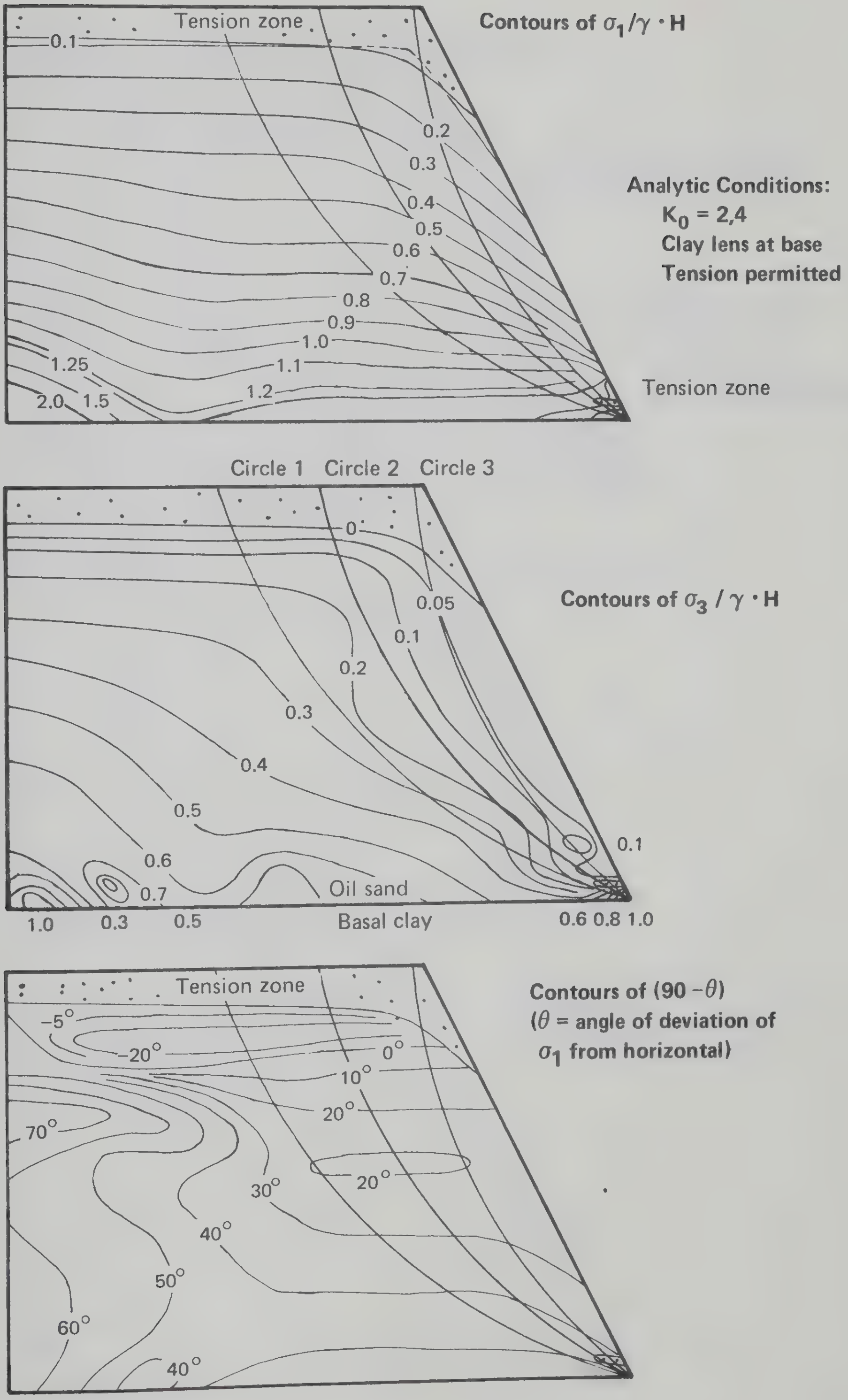

Contours of $\sigma_1/\gamma\cdot H$

Analytic Conditions:
K_0 = 2,4
Clay lens at base
Tension permitted

Contours of $\sigma_3/\gamma\cdot H$

Contours of $(90-\theta)$
(θ = angle of deviation of σ_1 from horizontal)

Figure 8.21
Stress Conditions,
63.4° Slope

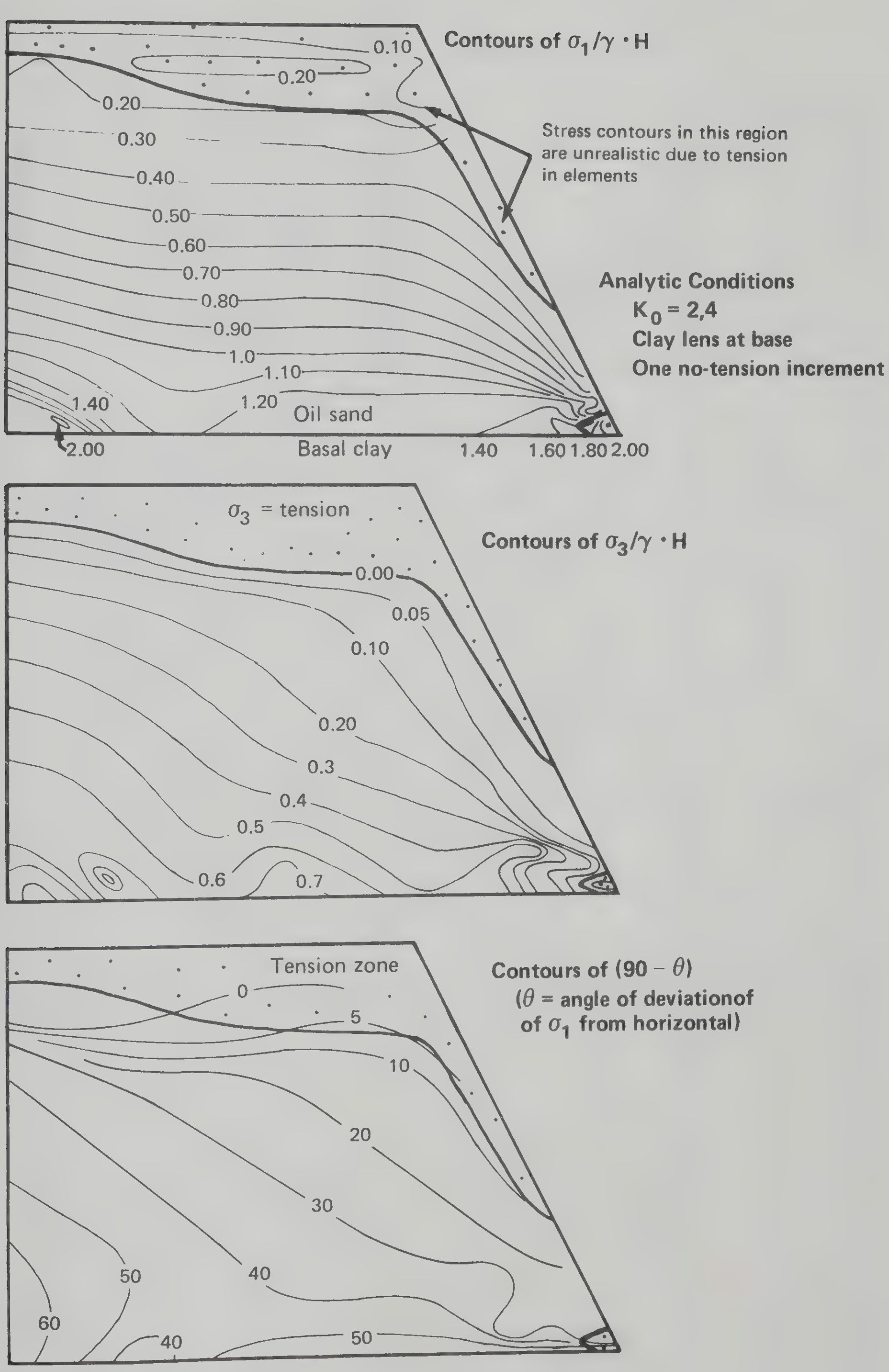

Figure 8.23
Stress Conditions,
63.4° Slope

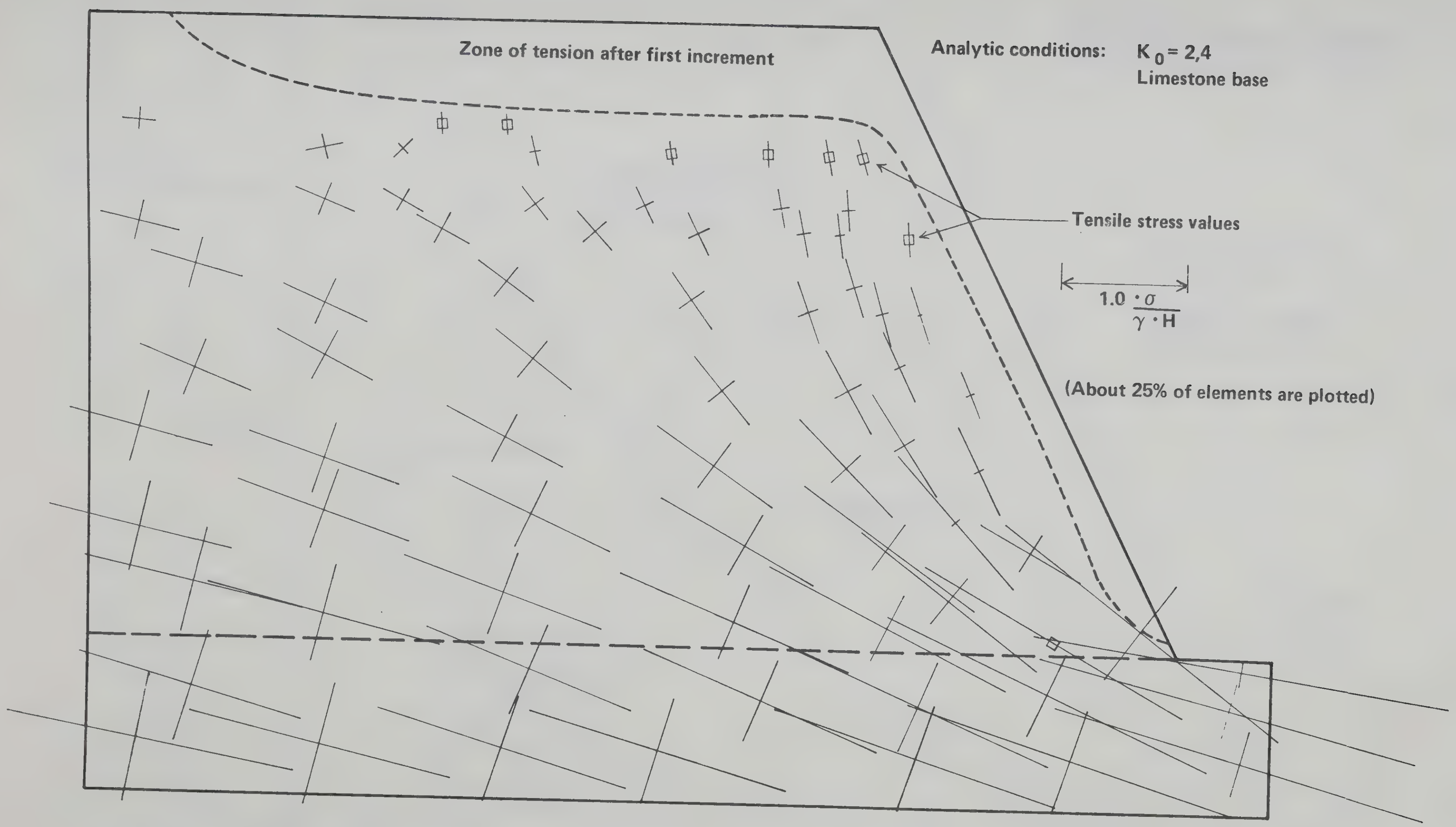

Figure 8.24 Principal Stress Magnitudes and Directions, 63.4° Slope; One No-Tension Increment

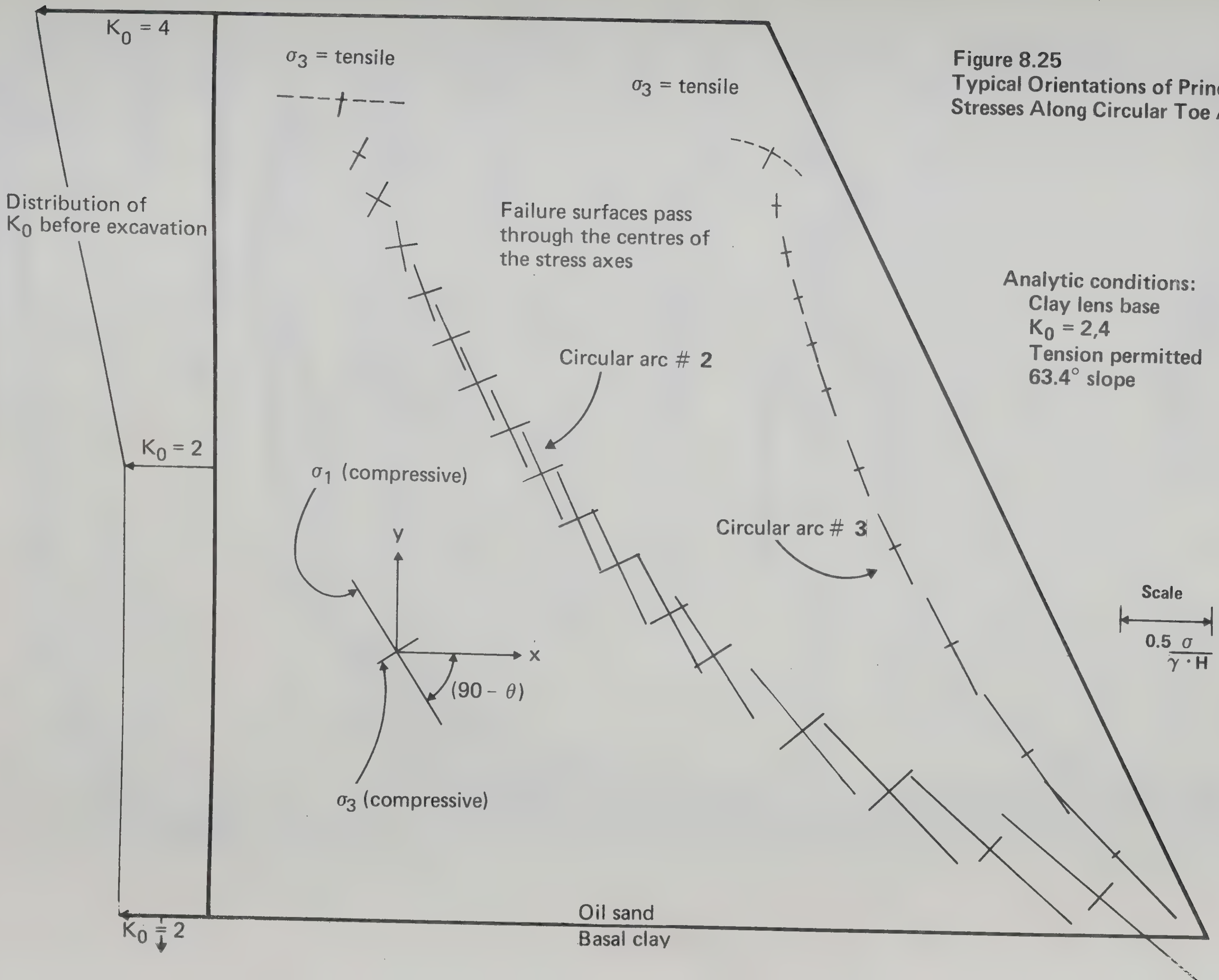

Figure 8.25
Typical Orientations of Principal Stresses Along Circular Toe Arcs

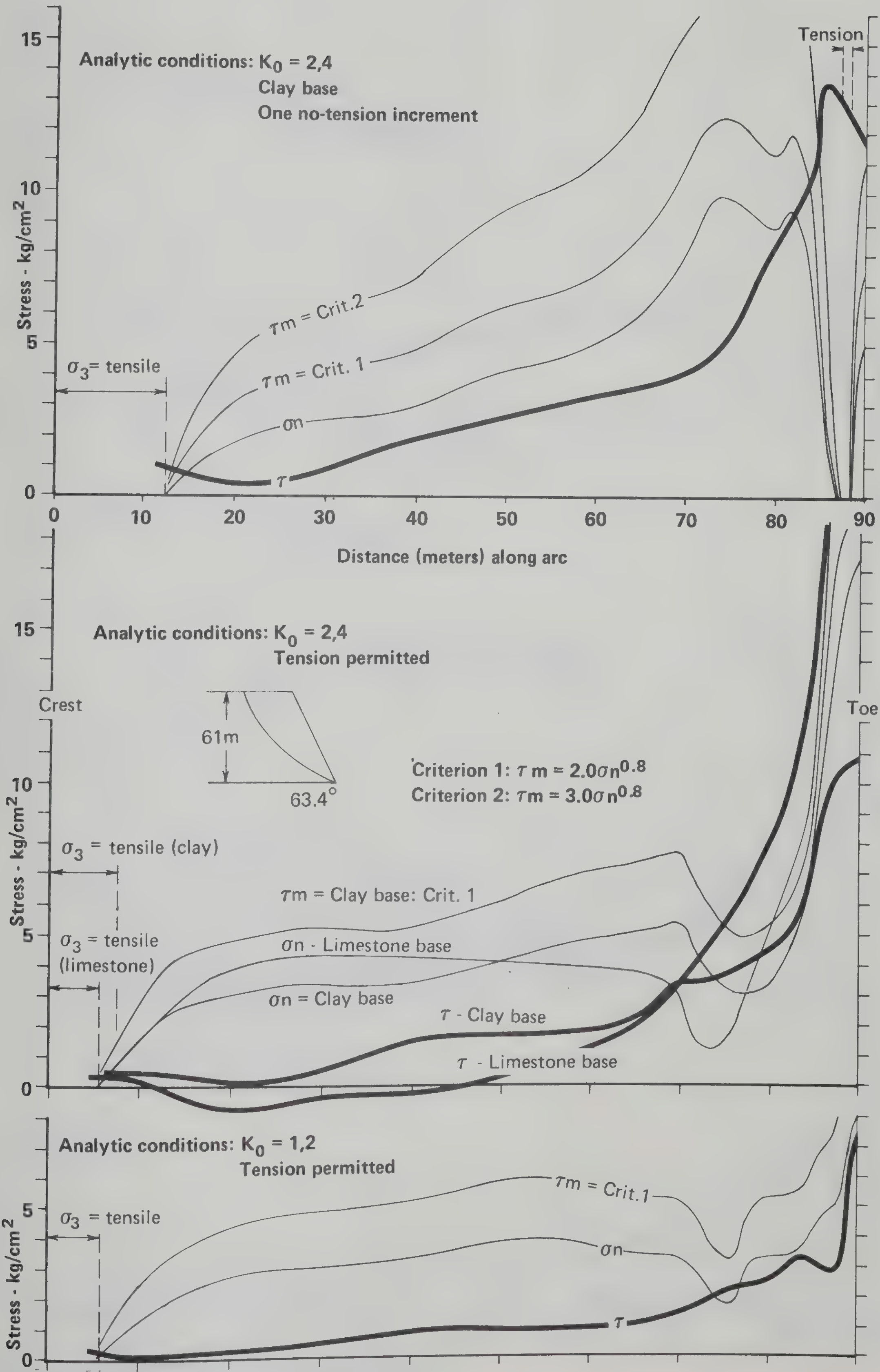

Figure 8.26 Stresses Along Circular Arc #1

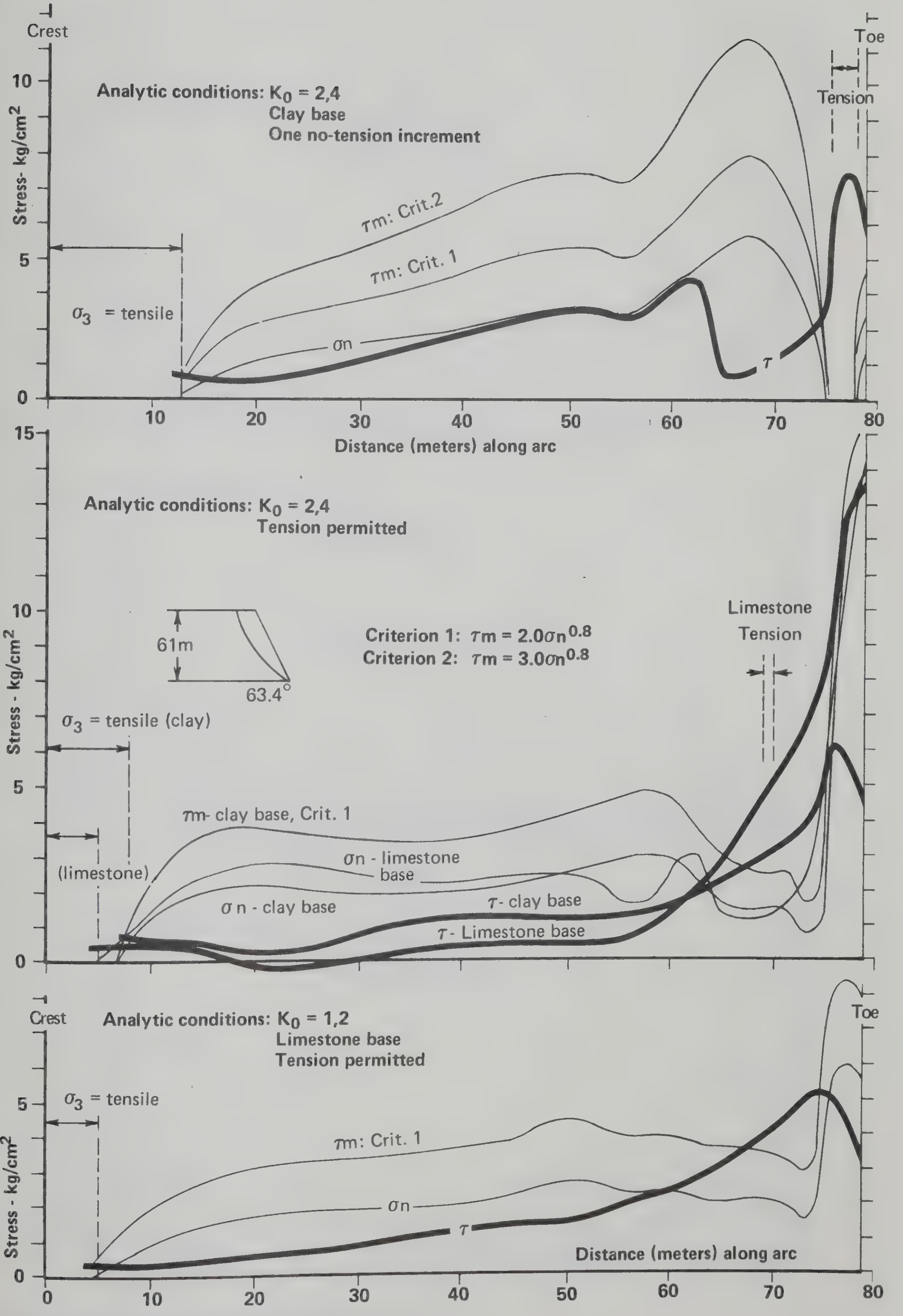

Figure 8.27 Stresses Along Circular Arc #2

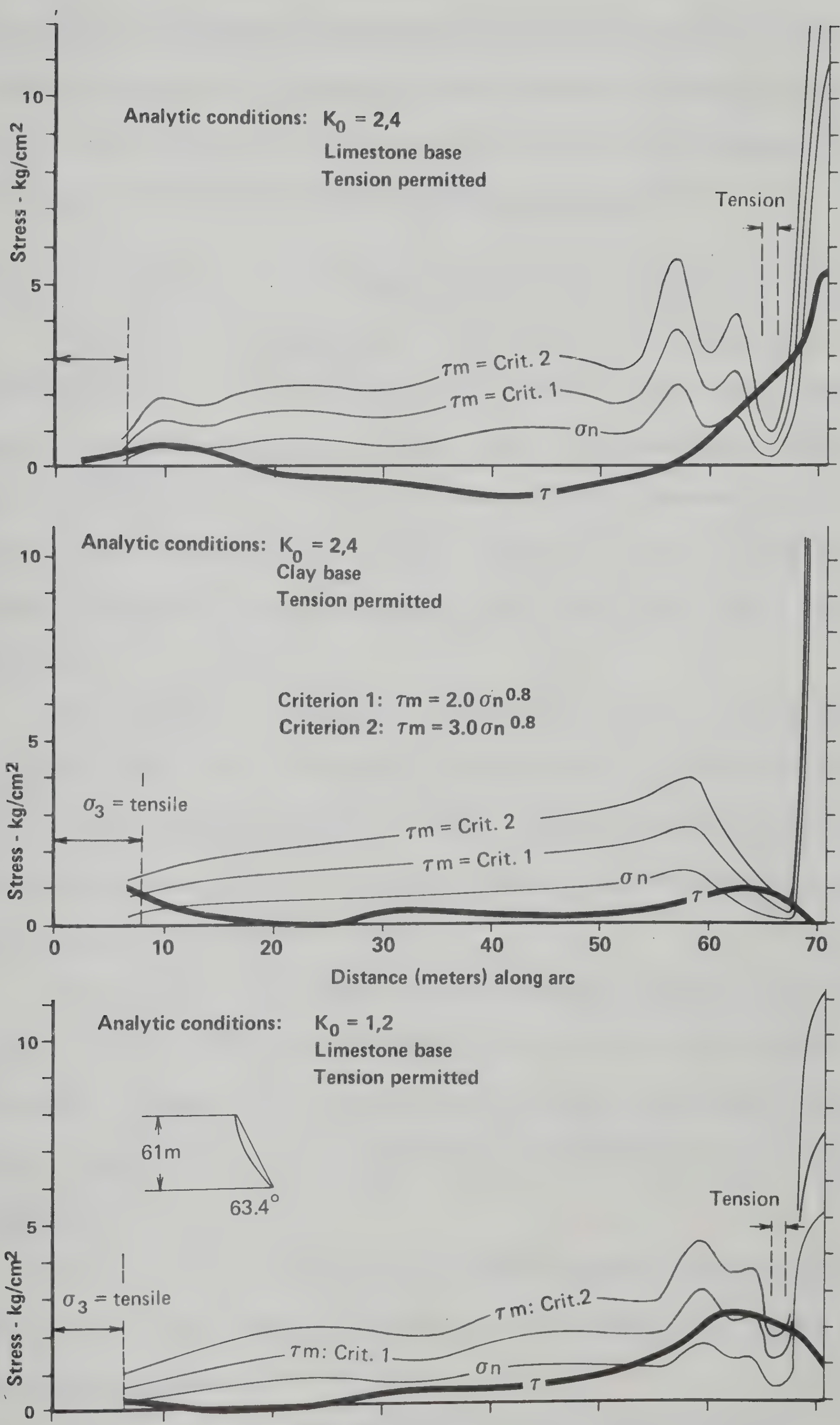

Figure 8.28 Stresses Along Circular Arc # 3

criteria are included for comparative purposes. Zones of tension, in which failure must be assumed, are delineated in each case. In general, the tensile zones are at the slope crest and face, and at the interface between oil sands and underlying materials.

8.4.10 Conclusions of Stress Analysis by Finite Element Methods

Excavation of steep slopes in materials with high *in situ* stresses results in (1) principal stress field rotation such that the maximum principal compressive stress close to the slope face tends to align itself parallel to the slope face; (2) high concentrations of stresses near the slope toe; and (3) creation of zones of tensile minimum principal stress at the slope crest and at the top of the slope face.

An increase in the analytic value of K_o results in an increase in maximum shear stress throughout the slope (but particularly at the toe), a corresponding increase in slope deflection, the generation of an upturned slope crest, and a rapid return to pre-excavation *in situ* stresses away from the slope face.

Introducing a soft clay lens at the slope base has the effect of reducing the shear stress magnitude in the overlying oil sands, increasing outward slope toe movement, increasing the length of the tensile failed zone at the slope crest, and creating a high shear stress concentration in the clay.

The use of a very high modulus ratio between limestone and oil sands has the same effect as eliminating the limestone and using a rough (pinned) base.

Introducing a power law failure criterion with respect to

circular toe arcs demonstrates several important factors: (1) circular arcs closest to the slope face display the greatest stress ratios and are generally less stable than circular arcs farther from the slope face; (2) normal stresses remain relatively constant for a large portion of the circular arc because of stress rotation; and (3) shear strength is exceeded mainly at the slope toe, necessitating upwards redistribution of shear stress.

8.5 Conclusions

The wedge and finite element analyses support the hypothesis of high strengths of oil sands. The analyses show that the strengths of oil sands are sufficient to withstand the high shear stresses caused by excavation of high, steep pit walls. The stress-strain curves generated from oil sand samples indicate that progressive failure phenomena may play an important role in slope stability. Zones of stress concentration predicted from finite element analysis show that the slope toe is the critical zone for progressive failure.

The finite element analysis indicates that tensile zones may exist in the slope crest: the tension cracks assumed in wedge analysis are therefore justified.

The data and analyses lead to the conclusion that major, deep-seated failure of oil sand slopes is unlikely: rapid raveling at the pit face will be the major failure mode.

CHAPTER IX

CONCLUSIONS AND RECOMMENDATIONS

9.1 Restatement of Objectives

The objective of this thesis was described as the investigation of the geotechnical properties of the Athabasca Oil Sands with emphasis on those properties of concern in surface mining operations. The major topics explored in the thesis are the morphology of natural slopes in the Athabasca Oil Sands, stress-strain-strength characteristics, microfabric and microtexture of McMurray Formation sands, stability analysis of oil sand slopes, and computer stress analysis of high steep pit walls. The mineralogy and index properties of the basal clay deposits of the McMurray Formation are discussed in Appendix H.

9.2 Summary of Research

The McMurray Formation, which contains over 95% of the Athabasca Oil Sands, is an orthoquartzitic, transgressive blanket sand with increasing quantities of clay minerals and decreasing grain size towards the top of the formation. It unconformably overlies a Lower Cretaceous paleoerosion surface, and subdues the paleotopographical relief. The grain size of the deposit controlled invasion of oil, resulting in decreasing mean oil contents towards the top of the McMurray Formation.

Natural slopes in the McMurray Formation are generally steep: slopes over 60 m in height at average slope angles of 55° have been observed. Detailed examination of a large number of natural slopes

indicates:

1. Bitumen is not a source of strength except in the outer few meters of slope face.
2. The sands are essentially uncemented.
3. No deep-seated rotational failures in intact oil sands can be found.
4. Hydrogeological boundary conditions in oil sand slopes remain unknown, but water pressures are probably low.

Recession and degradation of oil-rich slopes occur through removal of slabs along exfoliation fractures; the process is accelerated by solar radiation and by water pressure in the fractures. Oil-free slopes are degraded by freeze-thaw structural disruption in capillary-saturated zones of fine-grained sand, and by detachment of exfoliation slabs by gravity and weathering.

Landsliding occurs at the bases of slopes which have significant deposits of basal clays. These landslides are confined to scree and debris piles and underlying clays, and have not been observed to pass through intact oil sands. Slickensided zones in basal clays indicate that residual strength conditions exist in these strata as a result of the differences in strain arising from the low elastic moduli of the clays. Slopes containing significant quantities of basal clay display characteristic morphologies such as bimodal slopes, scalloped backslopes, and basal landsliding.

Natural slopes display high long-term strengths, but previously published laboratory do not provide an explanation for the observed strengths. The reason for this anomaly has been identified as excessive disturbance during and after sampling which has resulted in poor-

quality laboratory data. Several suggested strength sources have been shown to be inapplicable to oil sands behaviour. Cementation by clay minerals, carbonates, or bitumen has been ruled out as a significant source of strength of oil sands; and negative or reduced pore pressures are very unlikely to contribute significantly to the strength of oil sands.

An extensive strength testing program was designed to assess the stress-strain-strength characteristics of Athabasca Oil Sands. Triaxial tests were performed on dense Ottawa Sand, densified oil-free sand from extraction tailings, compacted oil-rich oil sand, and high-quality bore hole oil sand specimens. These tests indicated that:

1. Bitumen does not contribute to shear strength.
2. Sorting, grain angularity, and grain surface rugosity do not contribute significantly to peak strength characteristics.
3. Oil-rich undisturbed Athabasca Oil Sands have low permeabilities and very low compressibilities.
4. Peak stress ratios (or peak deviatoric stresses) are very high, strains to failure are small, post-peak strength loss is sudden and large, and dilative behaviour is characteristic.
5. Small amounts of sample expansion do not destroy the strength characteristics, but large amounts of expansion destroy the structure of the oil sands.

Shearbox testing was undertaken to explore further the shear strength characteristics of the oil sands. Comparative tests were performed on coarse-grained and medium-grained Ottawa Sand, and on a number of specimens of oil sand selected to assess the variability of the Athabasca Oil Sands. The shearbox testing program indicated that:

1. Oil sands display shear strengths much greater than those of dense sands.

2. Typical oil sand Mohr-Coulomb failure envelopes are distinctly curvilinear, display no cohesion intercept, and may be usefully approximated by a power law relationship.

3. The residual strengths of the arenaceous portions of the oil sand deposits are normal with a value of about 35°. Intraformational clayey silts show residual angles of shearing resistance as low as 18°.

4. Secant ϕ angles of oil sand specimens are a function of dilative behaviour; this behaviour is suppressed as normal stress level increases.

Generalization of the strength findings was attempted by testing three quartzose undisturbed natural materials. Two of these materials, St. Peter Sandstone and Swan River Sandstone, are similar to the McMurray Formation sands: they are quartzose, fine- to medium-grained, and geologically old. The third material, a preglacial sand, is quartzose and very fine-grained, but geologically young. Behaviour of these materials showed that the conclusions from the oil sands strength studies are indeed generalizable: the geologically old materials behaved in a very similar manner to the oil sands. Furthermore, the preglacial sand behaved in a manner similar to ordinary dense sand. The results of these studies indicate that diagenetic processes are responsible for the characteristics of the geologically old materials.

The term "locked sands" was chosen to refer to materials showing the following characteristics: high shear strengths, curvilinear strength envelopes, and little or no cohesion at zero normal stress.

An optical and scanning electron microscope study has identified

the specific diagenetic processes responsible for the shear strength of locked sands. Crystal overgrowth and pressure solution have resulted in an interpenetrative grain structure, which creates a degree of interlock without true cohesion. The interlock causes extremely high dilatancy at low normal stress levels. These phenomena are responsible for the curvilinearity of the Mohr-Coulomb envelope. The effectiveness of crystal overgrowth and pressure solution was examined in an idealized analysis which showed that minor amounts of solution result in dramatic decreases in porosity. The porosity reduction is, in turn, associated with the interpenetrative granular fabric responsible for the stress-strain-strength behaviour.

Since oil sand slopes, either natural or man-made, are steep and high, potential failure surfaces may be usefully approximated by planar surfaces. A method of stability analysis based on total stress and planar surfaces has been presented. Back-slope tension cracks containing water are included in the analysis, and curvilinear failure criteria may be employed. Analysis of a number of possible cases has confirmed what has already been demonstrated by nature - that high steep oil sand slopes exist at safety factors much greater than 1.0.

Finite element analyses of two high steep slopes were performed to explore stress redistribution upon excavation. No-tension incremental solution and failure criteria were employed in an attempt to qualitatively assess stability. The computer stress analysis has demonstrated several important points:

1. Tension zones likely exist at the tops of all oil sand slopes.
2. Stress field rotation upon excavation results in very high

stress ratios in the slope face. These high stress ratios are probably responsible for the exfoliation fractures observed on all oil sand slopes.

3. Shear strengths are usually exceeded by the shear stress in the region of the slope toe, indicating that progressive failure must be assumed in these materials.

4. Residual strength conditions probably exist at the bases of slopes founded on basal clay. Thrust faulting in pit floors is a possibility as a result of the high values of in situ horizontal stress and the stress concentrations at the slope toe.

9.3 Limitations of the Research

A number of criticisms can be directed at the research reported in this volume. The most serious of these are associated with Chapter VIII.

The finite element analytic parameters, of necessity, were chosen arbitrarily. No data exists in the public domain on slope deflections, in situ moduli, or pore pressures. Furthermore, a single-step, tension-permitted analysis was performed, mesh divisions in regions of rapid stress change were probably not sufficiently small, and failed element properties were chosen arbitrarily. Plastic behaviour and failure flow laws were not used in the analysis. Nevertheless, it is the writer's evaluation that, until more high-quality data is generated, exotic and expensive computer analysis is not justified in oil sands geotechnique.

The stability analysis in Chapter VIII may be nonconservative because it may err on the unsafe side. Evaluation of the stability analysis indicates that, within the limitations stated, the error is

not gross. The nonconservative error arises from the assumption of planar failure surfaces and from the curvilinearity of the failure criterion (combined with a mean total stress assumption on the failure plane). The assumption of deep tension cracks which do not contribute to shear strength is conservative, and probably offsets the previous nonconservative assumption.

The preceding criticisms are mitigated by the nature of the failure criterion employed in the analysis. The laboratory strength values reported in Chapter V must be less than those which exist <u>in situ</u>, and a further degree of conservatism was introduced by reducing the strength criteria for analyses. More complex stability analyses are not considered justifiable until pore pressure data are available.

9.4 Recommendations for Further Research

The effects of diagenetic processes on engineering characteristics of natural materials are not clearly understood. The present study has, of necessity, confined itself to a few quartzose materials which crop out in accessible locations. The strength of oil sands is important to pit mining programs, but the stress-strain-strength behaviour of this locked sand is important in <u>in situ</u> extraction methods and crucial to the success of any future underground mining project. Shear strength envelopes for oil sands should be extended to higher stress levels approximating those expected in tunnels at some depth (i.e. about 140 kg/cm^2), as underground methods may eventually be employed. Fracture propagation and secondary or tertiary recovery methods are used to enhance productivity of conventional quartzose arenaceous oil resevoirs in Alberta. Knowledge of the behaviour of the reservoir sands is lacking, but it is likely that

many of them behave as locked sands.

In situ stress states in the McMurray Formation sands are not known; nevertheless, knowledge of stress states is vital in fracture propagation and computer modeling of stresses and strains. Pore pressures behind pit walls and natural slopes are unknown; therefore pit wall design at present lacks crucial input parameters which may significantly affect mining economics. Both of these topics are worthy of consideration as minor research projects.

Despite numerous research studies, there is still considerable misinformation concerning the nature and geological history of the oil sands. Much recent research is largely repetition of similar work in the past, although new and useful topics on the Athabasca Oil Sands are numerous. The basal stratigraphy of the oil sands (basal clays, paleosols, oil-free coarse-grained sands) is not understood, and has been largely ignored. These deposits are of great interest in open pit mining and *in situ* extraction techniques. There is still conjecture as to the depositional environment of the McMurray Formation, and studies of areal variation have not been published. One of the less important, but most interesting, topics is the source of the bitumen in the oil sands. Many scientists still do not accept the theory of up-dip migration followed by degradation or loss of volatiles.

9.5 Concluding Statement

Over three billion dollars have now been spent on the development of the Athabasca Oil Sands. It is imperative that useful geological and geotechnical data be generated to properly implement the technology of today and of the immediate future. The end of the era of fossil energy

sources is perhaps at hand, but many decades, possibly even centuries, will pass before petroleum products are no longer employed as energy sources. Development of these resources in the most efficient manner possible is necessary to meet Canada's needs for energy now and for several decades to come.

REFERENCES CITED

Alberta Oil and Gas Conservation Board (1963). A description and reserve estimate of the oil sands of Alberta. Edmonton, Alberta: Govt. of Alberta. 60 pp.

Allen, A.R. and Sanford, E.R. (1973). The Great Canadian Oil Sands operation. Guide to the Athabasca Oil Sands Area (Eds. M.A. Carrigy and J.W. Kramers). Can. Soc. Petroleum Geol. Oil Sands Symp., pp. 103-121.

Ansley, R.W. and Bierlmier, W.G. (1963). Continuity of bedding with McMurray Formation. Res. Coun. Alberta, K.A. Clark Vol. (Ed. M.A. Carrigy), pp. 55.62.

Athy, L.F. (1939). Density, porosity and compaction of sedimentary rocks. Am. Assoc. Petroleum Geol. Bull., Vol. 14, pp. 1-24.

Babcock, E.A. (1975). Fracture phenomena in the Waterways and McMurray Formations, Athabasca Oil Sands region, Northeastern Alberta. Bull. Can. Pet. Geol., Vol. 23, No. 4, pp. 810-826.

Ball, M.W. (1935). Athabaska oil sands: apparent examples of local origin of oil. Bull. Am. Assoc. Petroleum Geol., Vol. 19, No. 2, pp. 153-171.

Bayrock, L.A. (1971). Surficial geology of the Bitumount area. Alberta Mapsheet N.T.S. 74E, 1:250,000 map with notes. Edmonton, Alberta: Research Council.

Bell, R. (1884). Report on part of the basin of the Athabasca River, Northwest Territory. Geol. Surv. Can. Rept. Prog., 1882-83-84, Pt. cc, pp. 5-35.

Bell, R. (1908). The tar sands of the Athabasca River, Canada. Trans. Am. Inst. Min. Eng., Vol. 38, pp. 836-848.

Berry, L.G. and Mason, B. (1959). Mineralogy: Concepts, Descriptions, Determinations. San Francisco: W.H. Freeman and Co. 630 pp.

Bishop, A.W. and Henkel, D.J. (1962). The Measurement of Soil Properties in the Triaxial Test. London: Edward Arnold. 227 pp.

Bishop, A.W. (1966). The strength of soils as engineering materials. Geot., Vol. 16, No. 2, pp. 91-130.

Blair, S.M. (1950). Report on the Alberta Bituminous Sands. Edmonton: Govt. Alberta. 82 pp.

Bowman, C. (1967). Discussion in Proc. Seventh World Petroleum Cong., Mexico City, Vol. 1, Tar Sands Section, pp. 561-650.

Brooker, E.W. (1975). Tarsand Mechanics and Slope Evaluation. Proc. Tenth Can. Rock Mech. Symp., Queen's University, Kingston, Ont., Vol. 1, pp. 409-446.

Carrigy, M.A. (1959). General geology of the McMurray area. Geology of the McMurray Formation, Pt. III, Mem. 1, Edmonton, Alberta: Res. Coun. Alberta. 130 pp.

Carrigy, M.A. (1962). Effect of texture on the distribution of oil in the Athabasca oil sands, Alberta, Canada. Jour. Sed. Petrology, Vol. 32, No. 2, pp. 312-325.

Carrigy, M.A. (1963a). Petrology of coarse-grained sands in the lower part of the McMurray Formation. K.A. Clark Vol., Res. Coun. Alberta, Edmonton, pp. 43-54.

Carrigy, M.A. (1963b). Criteria for differentiating the McMurray and Clearwater Formations in the Athabasca Oil Sands. Res. Coun. Alberta Bull. 14. 32 pp.

Carrigy, M.A. (1965). Athabasca Oil Sands bibliography (1789-1964). Res. Coun. Prelim. Rept. 65-3. 91 pp.

Carrigy, M.A. (1966). Lithology of the Athabasca Oil Sands. Res. Coun. Alberta Bull. 18. 48 pp.

Carrigy, M.A. (1967a). The physical and chemical nature of a typical tar sand: bulk properties and behavior. Proc. 7th World Petroleum Congress, Mexico City, Vol. 3, pp. 573-581.

Carrigy, M.A. (1967b). Some sedimentary features of the Athabasca Oil Sands. Sed. Geol., Vol. 1, pp. 327-352.

Carrigy, M.A. (1973). Mesozoic geology of the Fort McMurray area. Guide to the Athabasca Oil Sands Area (Eds. M.A. Carrigy and J.W. Kramers). Can. Soc. Petroleum Geol. Oil Sands Symp., pp. 77-101.

Carrigy, M.A. and Mellon, G.B. (1964). Authigenic clay mineral cements in Cretaceous and Tertiary sandstones of Alberta. Jour. Sed. Pet., Vol. 34, No. 3, pp. 461-472.

Carrigy, M.A. and Zamora, W.J. (1960). The Athabasca Oil Sands: oil field of Alberta. Alberta Soc. Petroleum Geol., Calgary, Alberta, pp. 38-49.

Carson, M.A. and Kirby, M.J. (1972). Hillslope Form and Process. Cambridge: Cambridge University Press, Cambridge Geographical Studies No. 3. 475 pp.

Chandler, R.J. (1973). The inclination of talus, arctic talus terraces, and other slopes composed of granular materials. Jour. Geol., Vol. 81, pp. 1-14.

Chattopadhyay, P.K. (1972). Residual shear strength of some pure clay minerals. PhD thesis, Dept. of Civil Engineering, University of Alberta, Edmonton.

Chen, Wai-Fah (1975). Limit Analysis and Soil Plasticity: Developments in Geotechnical Engineering (7). New York: Elsevier Scientific Publishing Company. 638 pp.

Clark, K.A. (1957). Bulk densities, porosities and liquid saturations of good grade Athabasca Oil Sands. Edmonton: Res. Coun. Alberta Mimeo. Circ 22. 22 pp.

Clark, K.A. (1959). Permeabilities of the Athabasca Oil Sands. Trans. Can. Inst. Min. Met., Vol. 63, pp. 151-156.

Coates, D.F. (1964). Some cases of residual stress effects in engineering work. State of Stress in the Earth's Crust. New York: American Elsevier, pp. 679-688.

Corbett, C.S. (1955). _In situ_ origin of McMurray oil of northeastern Alberta and its relevance to general problem of origin of oil. Bull. Am. Assoc. Petroleum Geol., Vol. 39, No. 8, pp. 1601-1649.

Crickmay, C.H. (1974). The Work of the River: a Critical Study of the Central Aspects of Geomorphology. London: Macmillan. 271 pp.

Dapples, E.C. (1955). General lithofacies relationship of St. Peter Sandstone and Simpson Group. Am. Assoc. Petroleum Geol. Bull., Vol. 39, pp. 444-469.

Dapples, E.C. (1959). The behavior of silica in diagenesis. Silica in Sediments. Soc. Econ. Paleontologists and Mineralogists Spec. Pub. No. 7, pp. 36-54.

Desai, C.S. and Ahel, J.F. (1972). Introduction to the Finite Element Method, a Numerical Method for Engineering Analysis. New York: Van Nostrand Reinhold Co. 477 pp.

Devenny, D.W. (1975). Subsidence problems associated with reclamation at oil sand mines. Proc. Tenth Can. Rock Mech. Symp., Queen's University, Kingston, Ont., pp. 161-180.

Dickenson, K.A., Berryhill, H.L., and Holmes, C.W. (1972). Criteria for recognizing ancient barrier coastlines. Recognition of Ancient Sedimentary Environments. Soc. Econ. Paleontologists and Mineralogists Spec. Pub. No. 16, pp. 192-214.

Dresser Atlas (1971). Log Review; Log Interpretation.

Ells, S.C. (1914). Preliminary report on the bituminous sands of northern Alberta. Can. Mines Branch Rept. 281. 88 pp.

Ells, S.C. (1915a). Notes on clay deposits near McMurray, Alberta. Can. Mines Branch Bull. 10. 15 pp.

Ells, S.C. (1915b). Bituminous sands of northern Alberta. Can. Mines Branch Summ. Rept. for 1914, Rept. 346, pp. 60-73.

Ells, S.C. (1922). Bituminous sands of Alberta. Can. Mines Branch Summ. Rept. for 1920, Rept. 574, pp. 19-22.

Ells, S.C. (1926). Bituminous sands of northern Alberta: occurrence and economic possibilities; report on investigations to the end of 1924. Can. Mines Branch Rept 632. 239 pp.

Falconer, W.L. (1951). Stratigraphy of McMurray Formation. Oil in Canada, Vol. 3, No. 50, pp. 4440-4443.

Govier, G.W. (1973). Alberta's oil sand in the energy supply picture. Presentation to the 1973 Oil Sands Symp., Can. Soc. Petroleum Geol., Calgary.

Grim, R.E. (1968). Clay Mineralogy. Toronto: McGraw Hill. 596 pp.

Gussow, W.C. (1956). Athabasca bituminous sands. Twentieth Int. Geol. Cong., Mexico, Vol. 3, pp. 63-70.

Halferdahl, L. (1969). Composition and ceramic properties of some clays from northeastern Alberta. Edmonton: Res. Coun. Alberta Rept. 69-3. 24 pp.

Hardy, R.M. and Hemstock, R.A. (1963). Shearing strength characteristics of Athabasca Oil Sands. K.A. Clark Vol., Res. Coun. Alberta, Edmonton, pp. 109-122.

Heckel, P.H. (1972). Ancient shallow marine environments. Recognition of Ancient Sedimentary Environments. Soc. Econ. Paleontologists and Mineralogists Spec. Pub. No. 16, pp. 226-286.

Hitchon, B. (1963). Composition and movement of formation fluids in strata above and below the pre-Cretaceous unconformity in relation to the Athabasca Oil Sands. K.A. Clark Vol., Res. Coun. Alberta, Edmonton, pp. 63-74.

Hubbert, M.K. (1971). The energy resources of the earth. Scientific American, Vol. 225, No. 3, pp. 61-70.

Hume, G.S. (1924). Clay deposits on Athabaska River, Alberta. Geol. Surv. Can. Summ. Rept. for 1923, Pt. B, pp. 16-20.

Hume, G.S. (1947). Results and significance of drilling operations in the Athabasca bituminous sands. Trans. Can. Inst. Min. Met., Vol. 50, pp. 298-333.

Hume, G.S. (1951). Possible Lower Cretaceous origin of bitumen in bituminous sands of Alberta. Proc. Athabasca Oil Sands Conf., Edmonton, pp. 66-75.

Jaeger, J.C. and Cook, N.G.W. (1969). Fundamentals of Rock Mechanics. London: Chapman and Hall Ltd. (Science Paperbacks). 515 pp.

Kenney, T.C. (1967). The influence of mineral composition on the residual strength of natural soils. Proc. of the Geotech. Conf., Oslo, Vol. 1, pp. 123-129.

Kidd, F.A. (1951). Geology of the bituminous sand deposits of the McMurray area of Alberta. Proc. Athabasca Oil Sands Conf., Edmonton, pp. 30-38.

Krinsley, D.H. and Donahue, J. (1968). Environmental interpretation of sand grain surface textures by electron microscopy. Geol. Soc. Am. Bull., Vol. 79, pp. 743-748.

Krinsley, D.H. and Margolis, S. (1969). A study of quartz sand grain surface textures with the scanning electron microscope. Trans. N.Y. Acad. Sci., Vol. 31, pp. 457-477.

Krinsley, D.H. and Doornkamp, J. (1973). Atlas of Quartz Sand Surface Textures. Cambridge: Cambridge University Press. 91 pp.

Krumbein, W.C. and Sloss, L.L. (1963). Stratigraphy and Sedimentation. San Francisco: W.H. Freeman and Company. 660 pp.

Lambe, T.W. and Whitman, R.V. (1969). Soil Mechanics. Toronto: John Wiley and Sons. 553 pp.

Link, T.A. (1951). Source of oil in oil sands of Athabasca River, Alberta, Canada. Proc. Athabasca Oil Sands Conf., Edmonton, pp. 55-65.

Lynch, E.J. (1962). Formation evaluation. New York: Harper and Row. 422 pp.

Mack, C. (1964). Physical chemistry. Bituminous Materials: Asphalts, Tars and Pitches, Vol. 1 (Ed. A.J. Hoiberg). New York: Interscience Publishers, pp. 25-123.

McLearn, F.H. (1932). Problems of the Lower Cretaceous of the Canadian interior. Trans. Roy. Soc. Can., Vol. 26, Sec. 4, pp. 157-175.

McLearn, F.H. (1945). Revision of the Lower Cretaceous of the western interior of Canada. Geol. Surv. Can Paper 44-17. 14 pp.

Martin, R. and Jamin, F.A.S. (1963). Paleogeomorphology of the buried Devonian landscape in northeastern Alberta. K.A. Clark Vol., Res. Coun. Alberta, Edmonton, pp. 31-42.

McConnell, R.C. (1891). Tar sands on Athabasca River. Geol. Surv. Can. Ann. Rept. 5, Pt. 5, pp. 144-147.

Mellon, G.B. (1956). Heavy minerals of the McMurray Formation. Edmonton: Res. Coun. Alberta Rept. 72, Pt. II. 43 pp.

Mellon, G.B. and Wall, J.H. (1956). Geology of the McMurray Formation. Edmonton: Res. Coun. Alberta Rept. 72, Pt I. 43 pp.

Milligan, M.F. (1976). Model studies for a friable sandstone. MSc thesis, Dept. of Civil Eng., University of Alberta, Edmonton.

Mossop, G. (1976). Pers. comm. Alberta Res. Council, Earth Sciences Division, Edmonton, Alberta.

Nash, K.L. (1953). The shearing resistance of a fine closely graded sand. Proc. Third Int. Conf. Soil Mech. and Foundation Eng., Switzerland.

Norris, A.W. (1973). Paleozoic (Devonian) geology of northeastern Alberta and northwestern Saskatchewan. Guide to the Athabasca Oil Sands Area (Eds. M.A. Carrigy and J.W. Kramers). Can. Soc. Petroleum Geol. Oil Sands Symp., pp. 15-76.

Parikh, P.V. (1967). The shearing behaviour of sand under axisymmetric loading. PhD thesis, Manchester University, Great Britain. Referred to in Rowe, 1969, op. cit.

Park, W.C. and Schat, E.H. (1968). Stylolites: their nature and origin. Jour. Sed. Pet., Vol. 38, pp. 175-191.

Patton, F.D. (1966). Multiple modes of shear failure in rock. Proc. First Cong. Int. Soc. Rock Mech., Lisbon, Vol. I, pp. 509-513.

Penck, W. (1929). Die geomorphologische Analyse (Trans. H. Czech and K.C. Boswell). London: Macmillan. 429 pp.

Pettijohn, F.J. (1975). Sedimentary Rocks. New York: Harper and Row. 628 pp.

Pettijohn, P.J., Potter, P.W., and Siever, R. (1972). Sand and Sandstone. New York: Springer-Verlag. 618 pp.

Pittman, E.D. (1972). Diagenesis of quartz in sandstones as revealed by scanning electron microscopy. Jour. Sed. Pet., Vol. 42, pp. 507-519.

Rahu, P.H. (1969). The relationship between natural forested slopes and angles of repose for sand and gravel. Geol. Soc. Am. Bull., Vol. 80, pp. 2123-2128.

Rowe, P.W. (1962). The stress-dilatancy relation for static equilibrium of an assembly of particles in contact. Proc. Roy. Soc. London, Ser. A, Vol. 269, pp. 500-527.

Rowe, P.W. (1969). The relation between the shear strength of sands in triaxial compression, plane strains, and direct shear. Geot., Vol. 19, No. 1, pp. 75-86.

Rudkin, R.A. (1966). Lower Cretaceous; Chapter I. Geological History of Western Canada. Pub. Alberta Soc. Petroleum Geol., Calgary. 232 pp.

Russell, L.S. (1932). Mollusca from the McMurray Formation of northern Alberta. Trans. Roy. Soc. Can., Third Ser., Vol. 26, Sec. 4, pp. 37-43.

Sbar, M.L. and Sykes, L.R. (1973). Contemporary stress and seismicity in eastern North America: an example of intra-plate tectonics. Geol. Soc. Am. Bull., Vol. 84, No. 6, pp.1861-1882.

Scheidegger, A.E. (1970). Theoretical Geomorphology. New York: Springer-Verlag. 435 pp.

Scotland, W.A. and Benthin, H. (1954). Athabasca Oil Sands project. Unpublished report, Calvan Consolidated Oil and Gas Co., Calgary, 3 vols.

Seed, H.B. and Lee, K.L. (1967). Undrained strength characteristics of cohesionless soils. Jour. Soil. Mech. Foundations Div., Am. Soc. Civ. Emg., Vol. 93, No. SM6, pp. 330-360.

Siever, R. (1959). Petrology and geochemistry of silica cementation in some Pennsylvania sandstones. Silica in Sediments. Soc. Econ. Paleontologists and Mineralogists Spec. Pub. No. 7, pp. 55-79.

Sippel, R.F. (1968). Sandstone petrology, evidence from luminescence petrography. Jour. Sed. Pet., Vol. 38, pp. 530-554.

Sproule, J.C. (1938). Origin of McMurray oil sands, Alberta. Bull. Am. Assoc. Petroleum Geol., Vol. 22, No. 9, pp. 1133-1152.

Sproule, J.C. (1951). The McMurray Formation in its relation to oil occurrences. Proc. Athabasca Oil Sands Conf., Edmonton, pp. 6-25.

Sproule J.C. (1955). Discussion to Corbett (1955). Bull. Am. Assoc. Petroleum Geol., Vol. 39, No. 8, pp. 1649-

Starr, C. (1971). Energy and power. Scientific American, Vol. 225, No. 3, pp. 37-49.

Stick, J.C. (1960). Nuclear radiation logging of wells. Lane-Wells Co., Houston, U.S.A.

Vigrass, L.W. (1966). General geology of Lower Cretaceous heavy oil accumulations in western Canada. Can. Min. Met. Bull., Vol. 59, pp. 87-94.

Voight, B. (1967). Interpretation of in situ stress measurements. Proc. First Cong. Int. Soc. Rock Mech., Vol. 3, pp. 332-348.

Ward, S.H. and Clark, K.A. (1950). Determination of the viscosities and specific gravities of the oils in samples of Athabasca bituminous sand. Edmonton: Res. Coun. Alberta Rept. 57. 22 pp.

White, O.L., Karrow, P.F., and Macdonald, J.R. (1974). Residual stress relief phenomenon in southern Ontario. Proc Ninth Can. Rock Mech. Symp., pp. 323-348.

Wickenden, R.T. (1951). Regional correlations of the Lower Cretaceous formations of the McMurray oil sand area. Proc. Athabasca Oil Sands Conf., Edmonton, pp. 39-45.

Youmans, A.H., Hopkinson, E.C., and Wickmann, P.A. (1966). Neutron Lifetime Logging in Theory and Practice. SPWLA Transactions, May, 1966.

APPENDIX A

SLOPES IN THE ATHABASCA OIL SANDS

Introduction

The following pages contain selected slope profiles obtained during field trips to the Fort McMurray area during the years 1973 to 1975. If direct physical access to an entire slope face was possible, measurements were made with a rope and hand inclinometer (e.g. Slope 51); however, extreme steepness occasionally prevented access from the slope base, and in those cases heights reported are visual estimates (e.g. Slope 59). In general, the profiles represent the steepest portions of a given face, and all angular measurements may not have been made directly on a normal vertical plane, but may lie several meters to either side, depending on accessibility. The location (LSD-Section-Township-Range) of each slope has been determined from NTS 1:50,000 topographic maps where available, or NTS 1:250,000 topographic maps. All slopes were studied in stereoscopic aerial photography before and after the field trips.

TABLE A.1

CONTENTS OF APPENDIX A

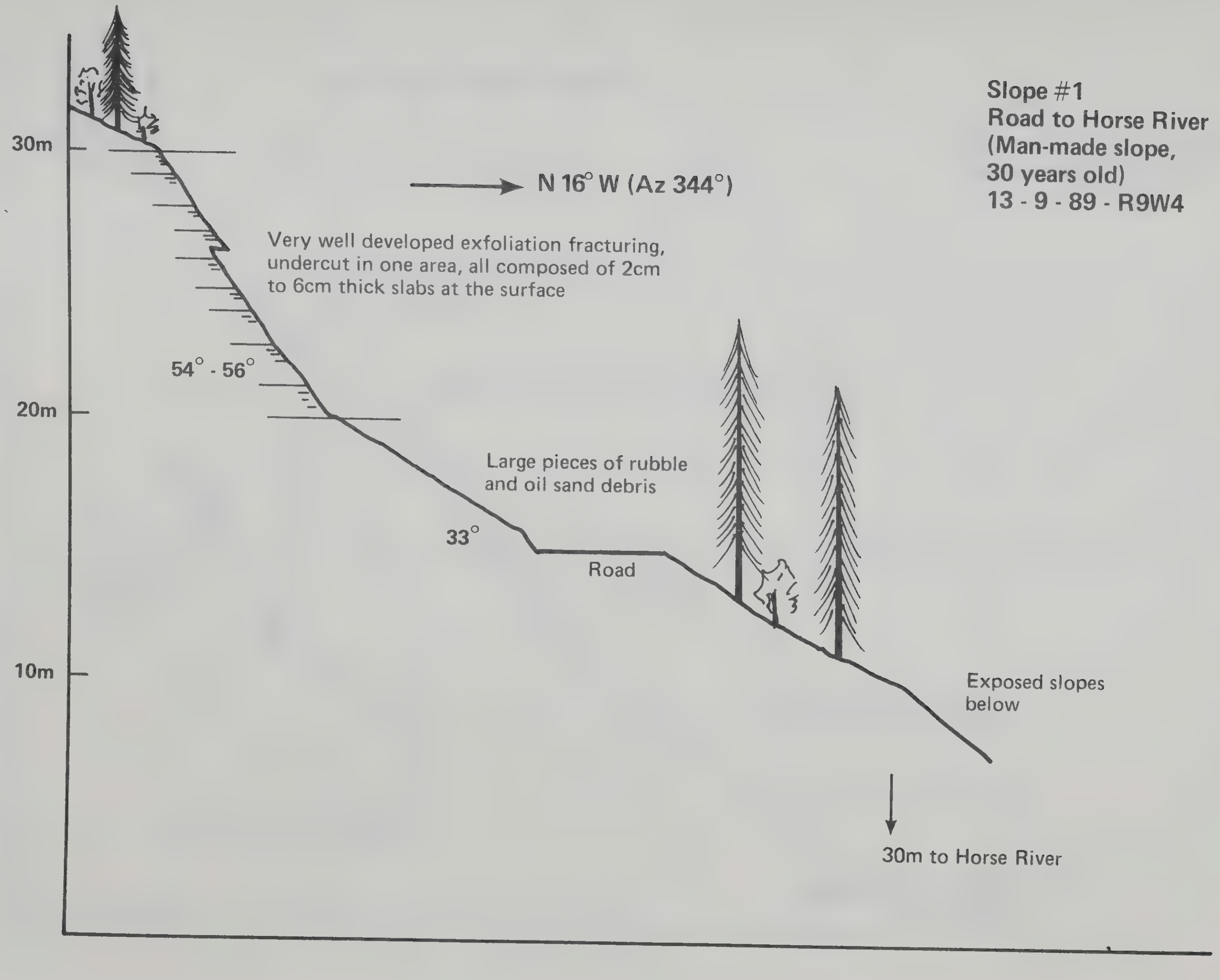
Slope #1
Road to Horse River
(Man-made slope,
30 years old)
13 - 9 - 89 - R9W4
N 16° W (Az 344°)
Very well developed exfoliation fracturing, undercut in one area, all composed of 2cm to 6cm thick slabs at the surface
54° - 56°
Large pieces of rubble and oil sand debris
33°
Road
Exposed slopes below
30m to Horse River
30m
20m
10m

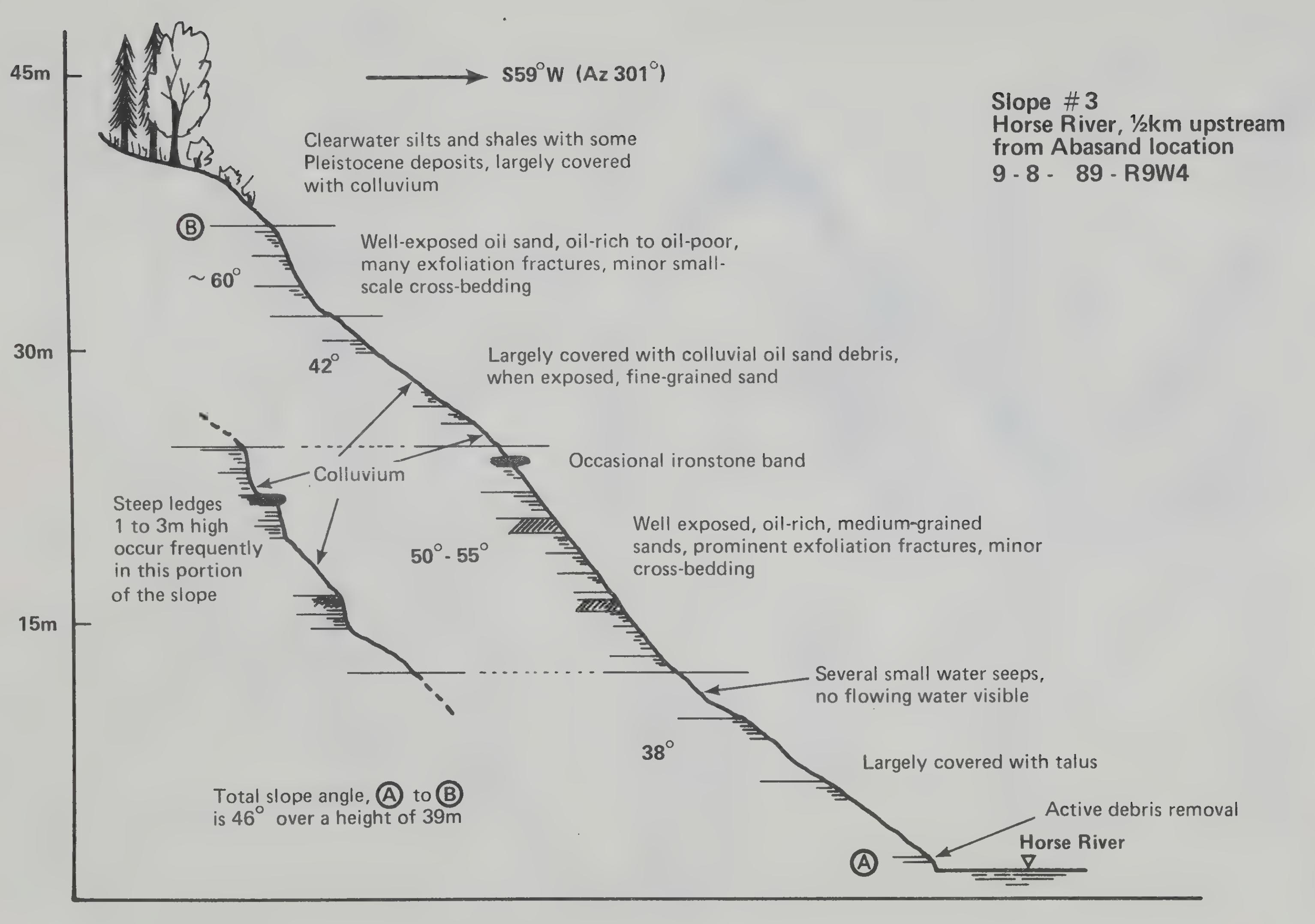
Slope #3
Horse River, ½km upstream from Abasand location
9 - 8 - 89 - R9W4
S59°W (Az 301°)
45m
30m
15m
Clearwater silts and shales with some Pleistocene deposits, largely covered with colluvium
Ⓑ
~60°
Well-exposed oil sand, oil-rich to oil-poor, many exfoliation fractures, minor small-scale cross-bedding
42°
Largely covered with colluvial oil sand debris, when exposed, fine-grained sand
Colluvium
Occasional ironstone band
Steep ledges 1 to 3m high occur frequently in this portion of the slope
50° - 55°
Well exposed, oil-rich, medium-grained sands, prominent exfoliation fractures, minor cross-bedding
Several small water seeps, no flowing water visible
38°
Largely covered with talus
Total slope angle, Ⓐ to Ⓑ is 46° over a height of 39m
Active debris removal
Horse River
Ⓐ

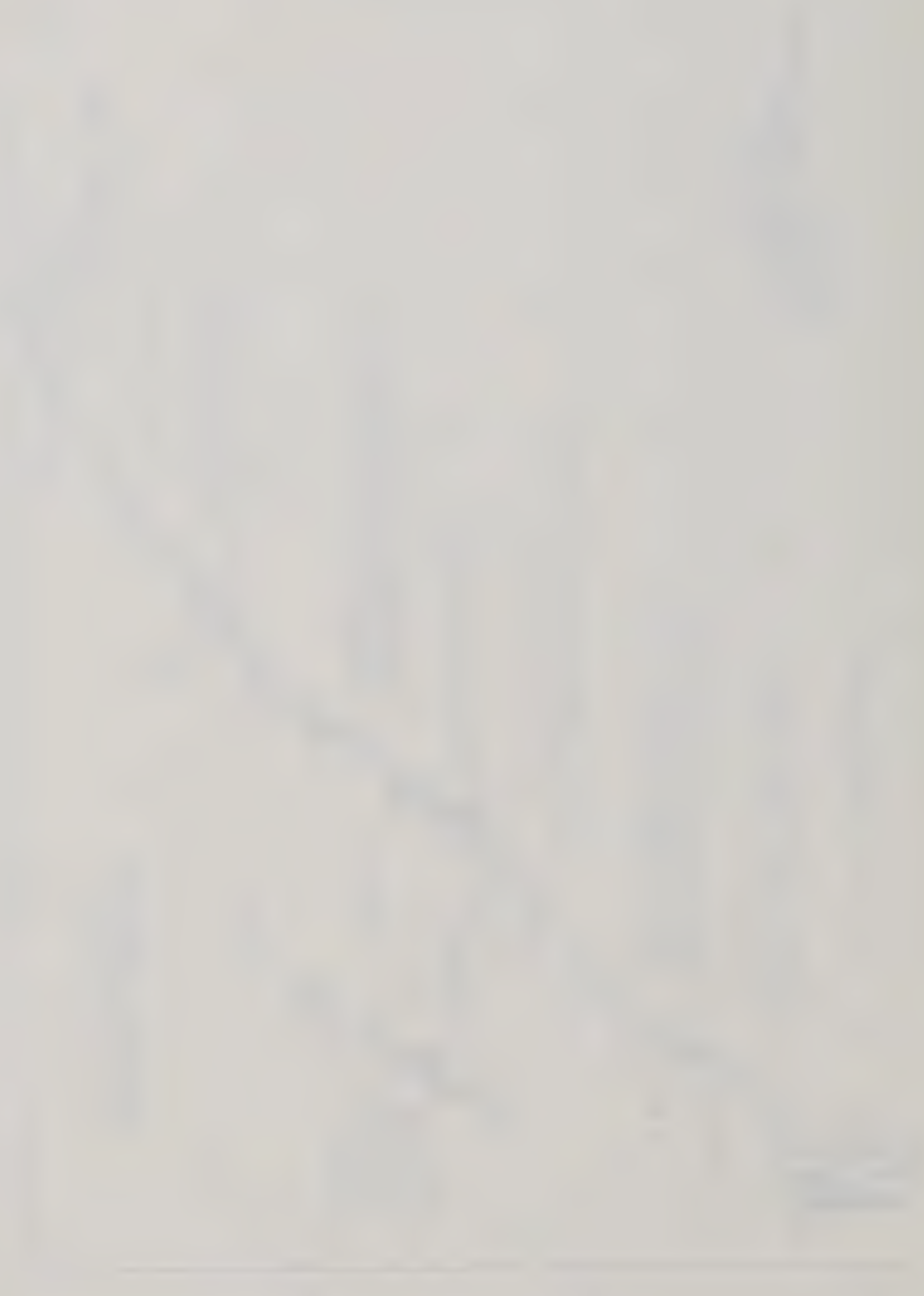

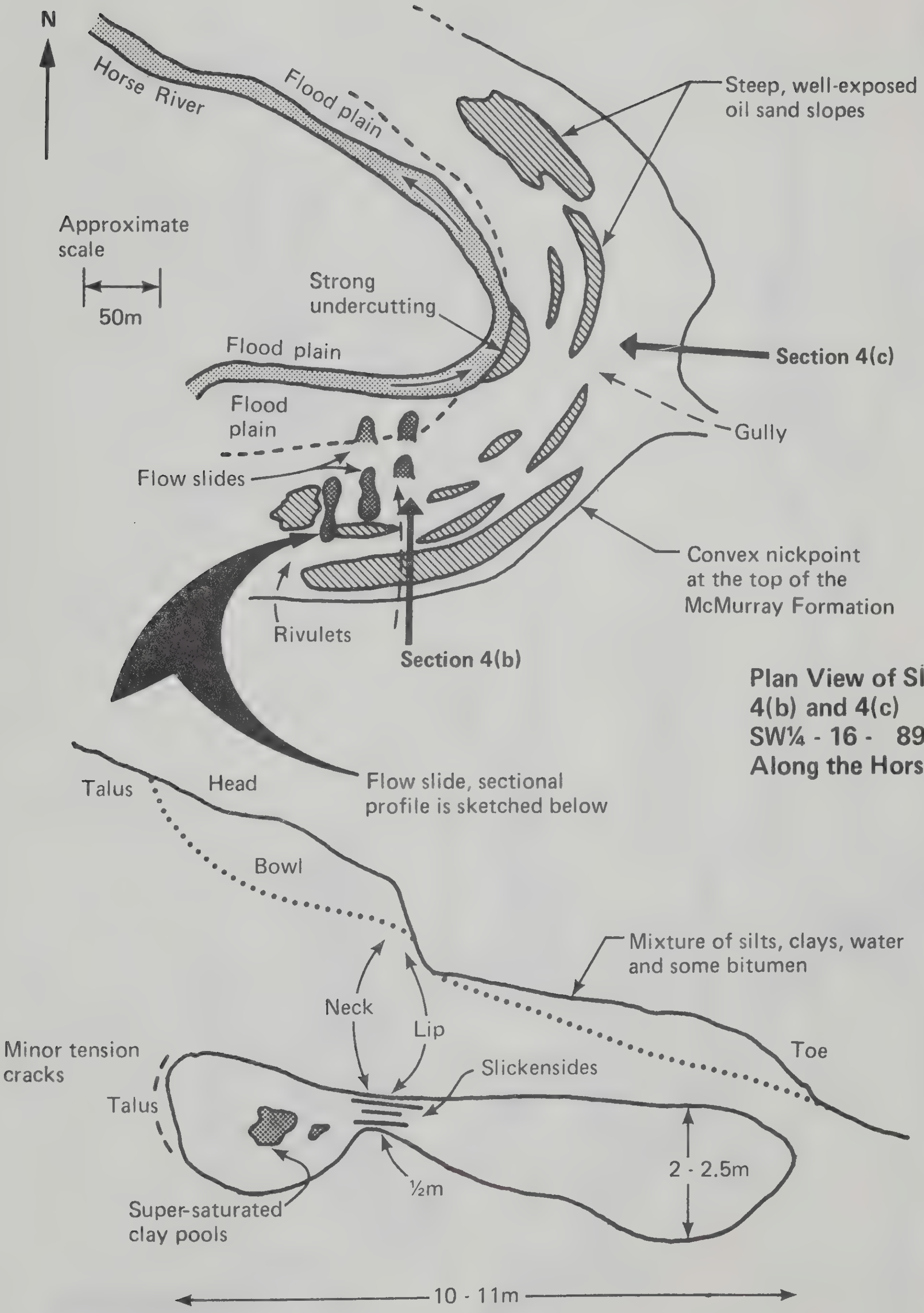

Plan View of Slopes
4(b) and 4(c)
SW¼ - 16 - 89 - R9W4
Along the Horse River

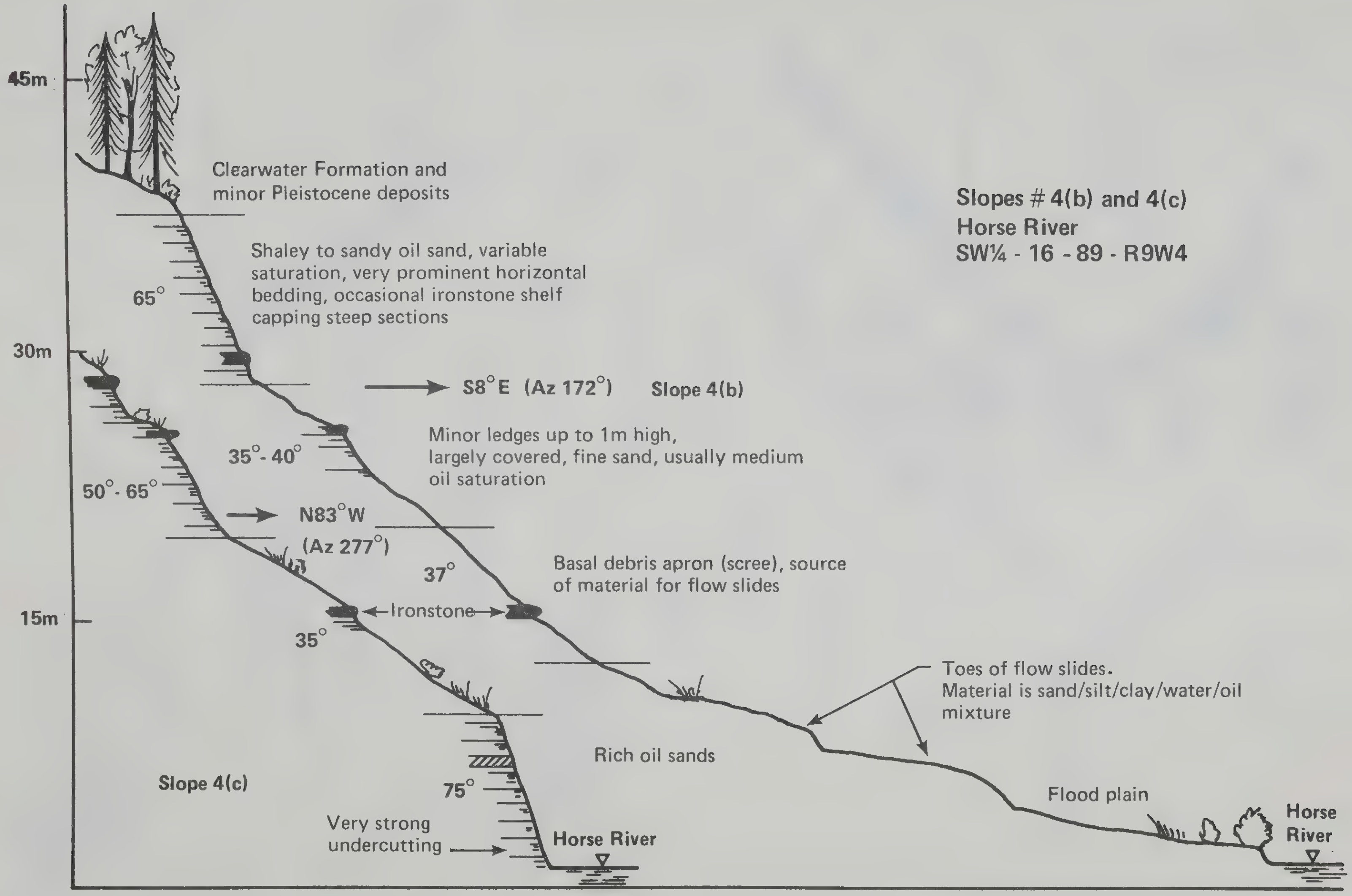

Slopes # 4(b) and 4(c)
Horse River
SW¼ - 16 - 89 - R9W4

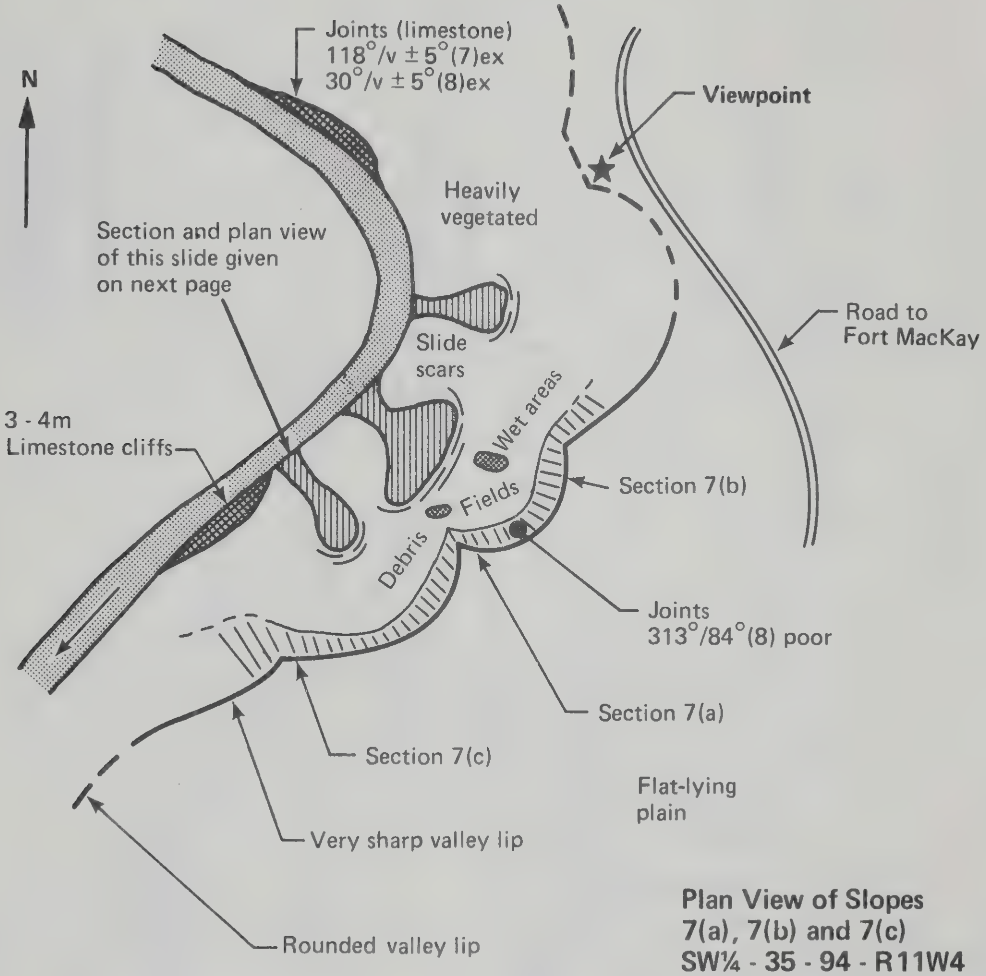

Plan View of Slopes 7(a), 7(b) and 7(c)
SW¼ - 35 - 94 - R11W4

General Profile of Slopes at Site 7

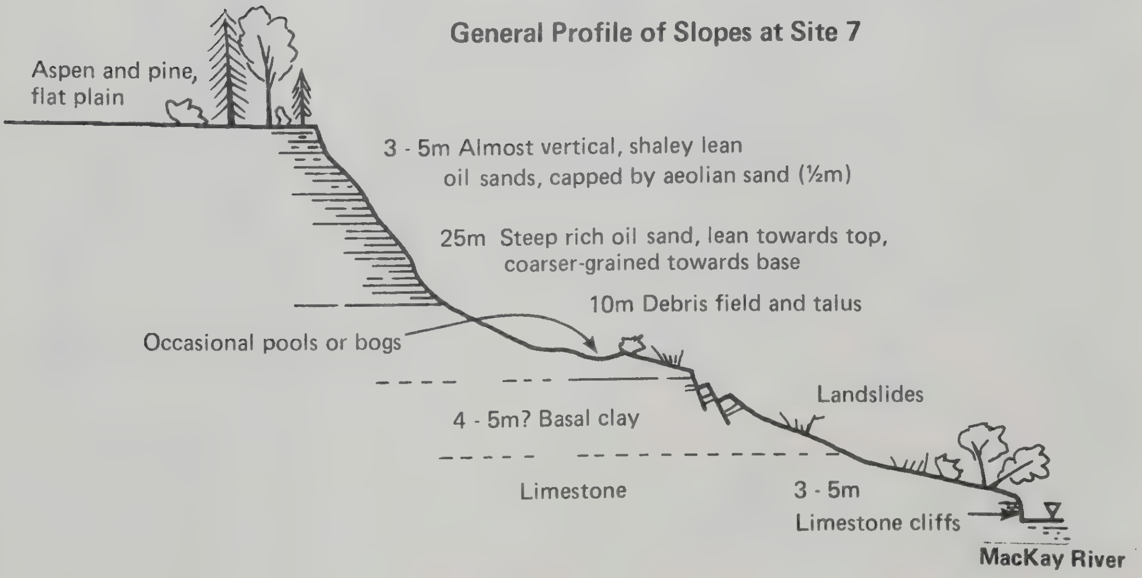

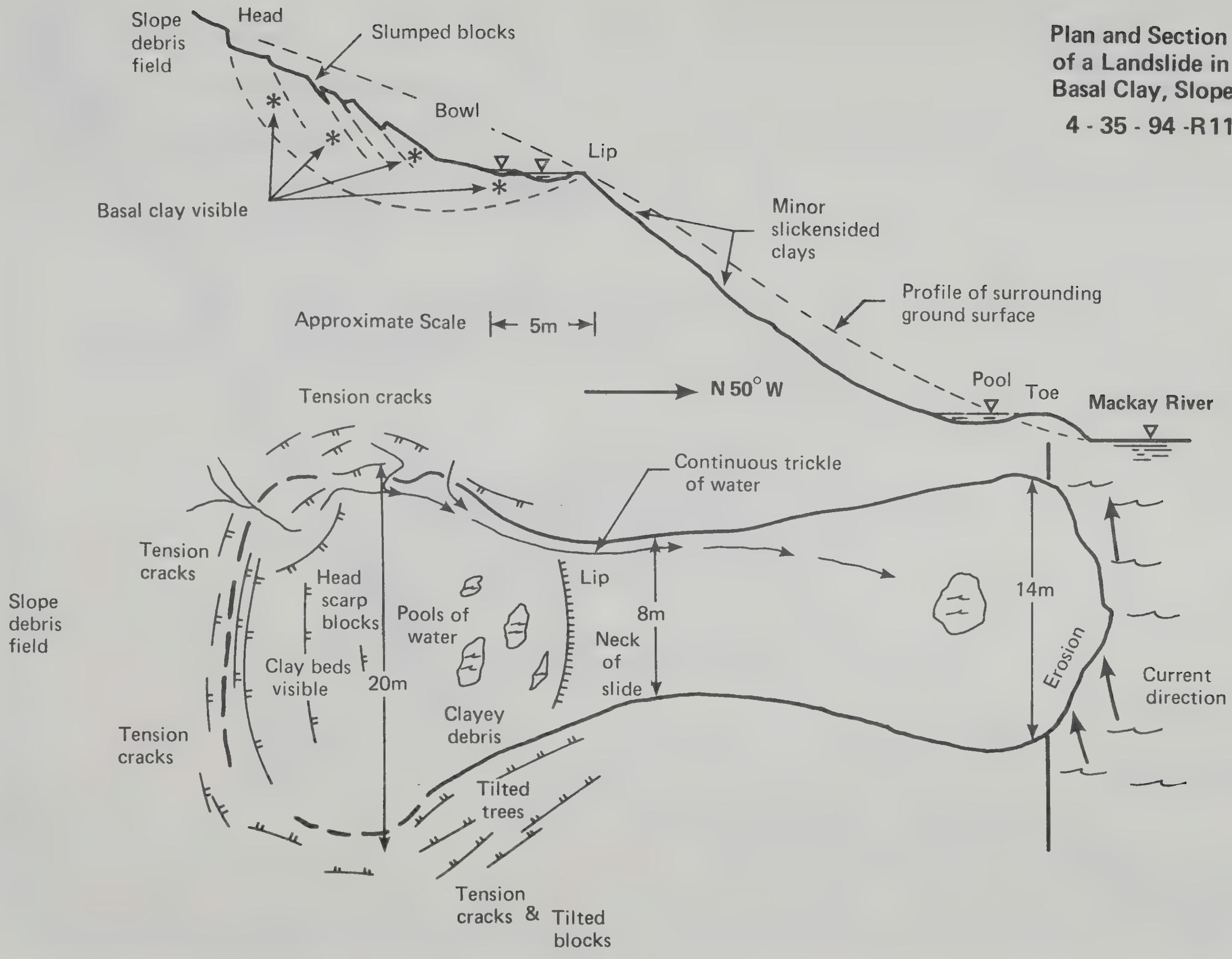

Plan and Section View of a Landslide in Basal Clay, Slope #7

4 - 35 - 94 -R11W4

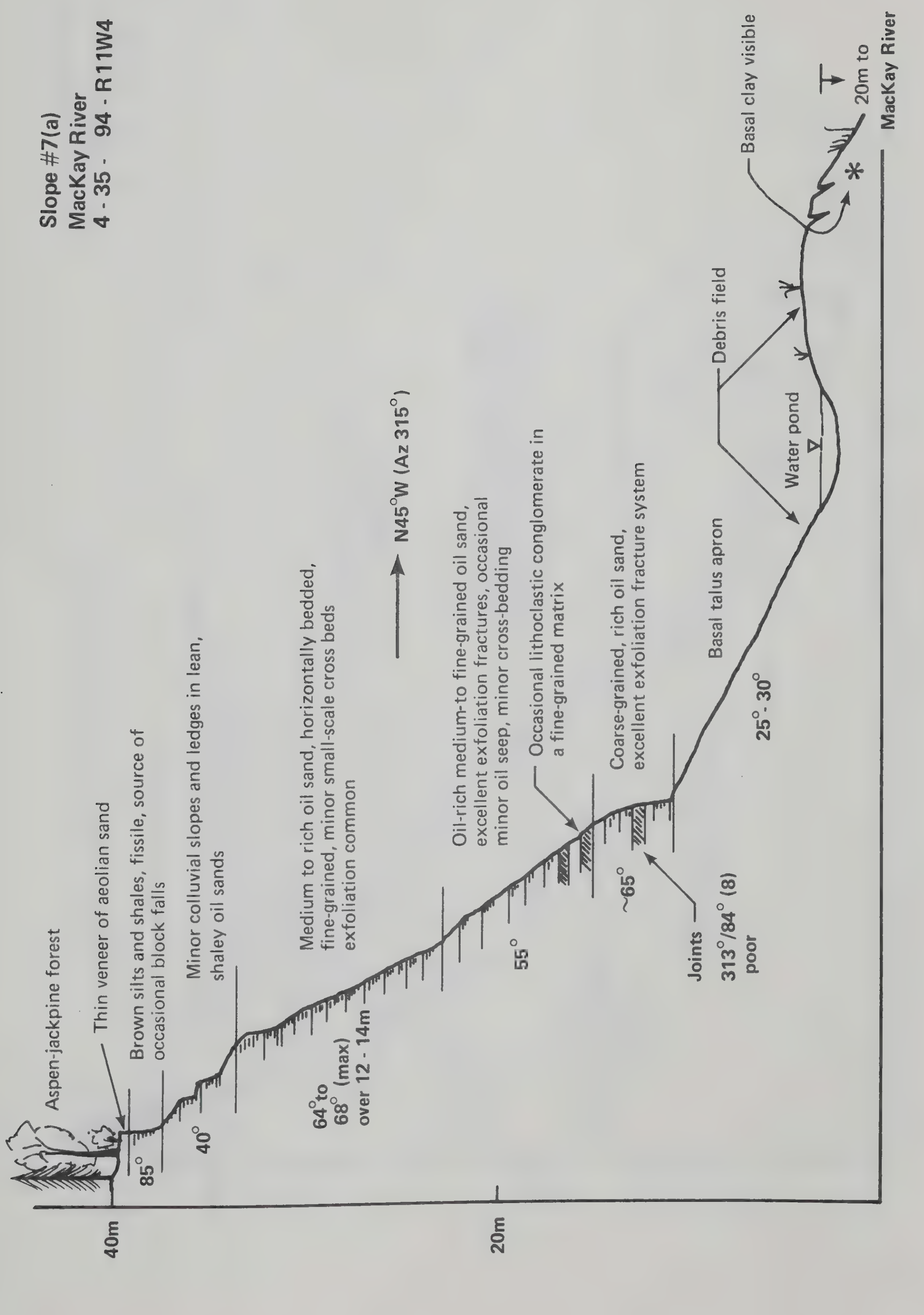
Slope #7(a)
MacKay River
4 - 35 - 94 - R11W4
N45°W (Az 315°)
Aspen-jackpine forest
Thin veneer of aeolian sand
Brown silts and shales, fissile, source of occasional block falls
Minor colluvial slopes and ledges in lean, shaley oil sands
Medium to rich oil sand, horizontally bedded, fine-grained, minor small-scale cross beds exfoliation common
Oil-rich medium-to fine-grained oil sand, excellent exfoliation fractures, occasional minor oil seep, minor cross-bedding
Occasional lithoclastic conglomerate in a fine-grained matrix
Coarse-grained, rich oil sand, excellent exfoliation fracture system
Basal talus apron
Water pond
Debris field
Basal clay visible
20m to
MacKay River
*
85°
40°
64° to
68° (max)
over 12 - 14m
55°
~65°
Joints
313°/84° (8)
poor
25° - 30°
40m
20m

Slopes # 7(b) and 7(c)
MacKay River
4 - 35 - T94 - R11W4

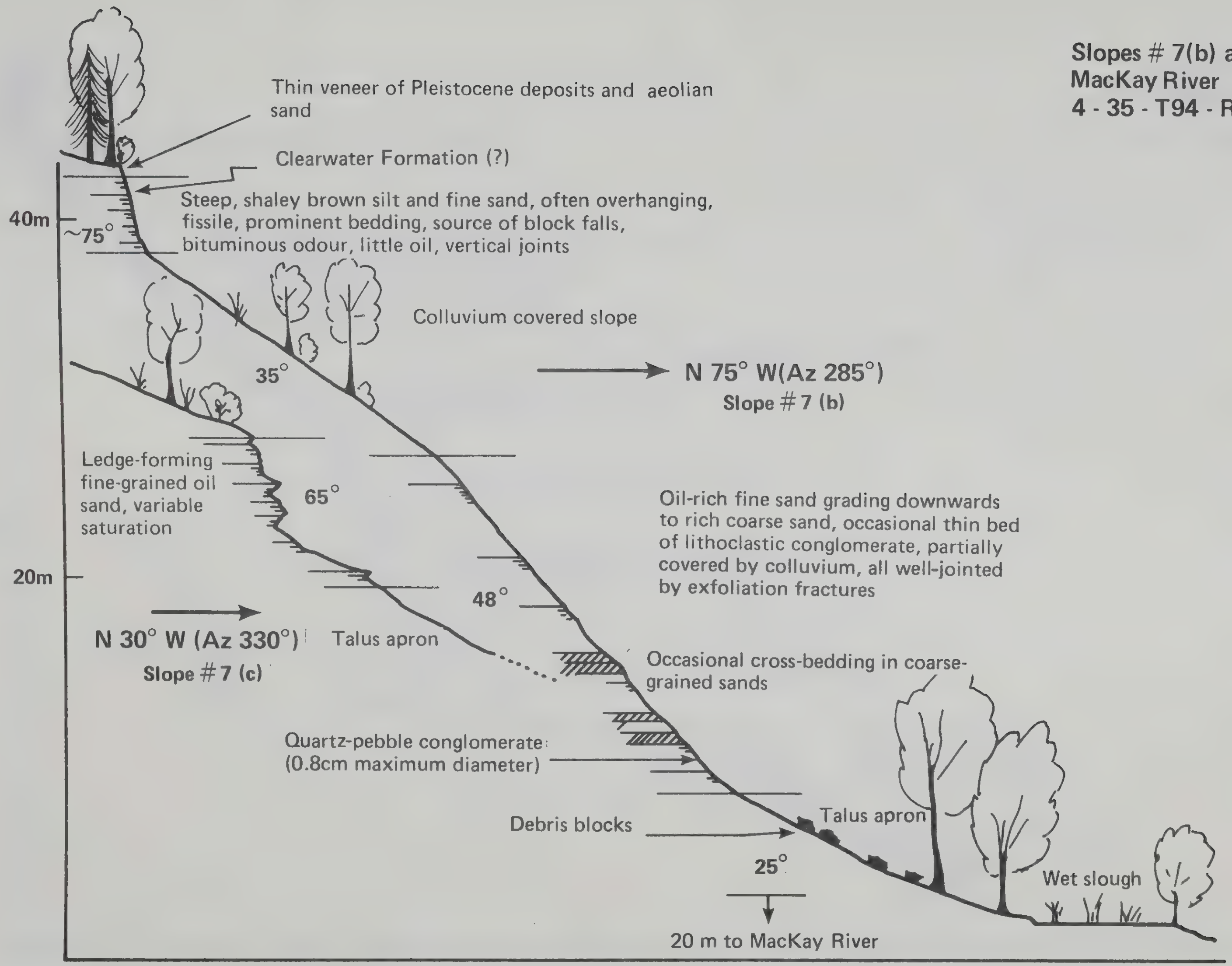

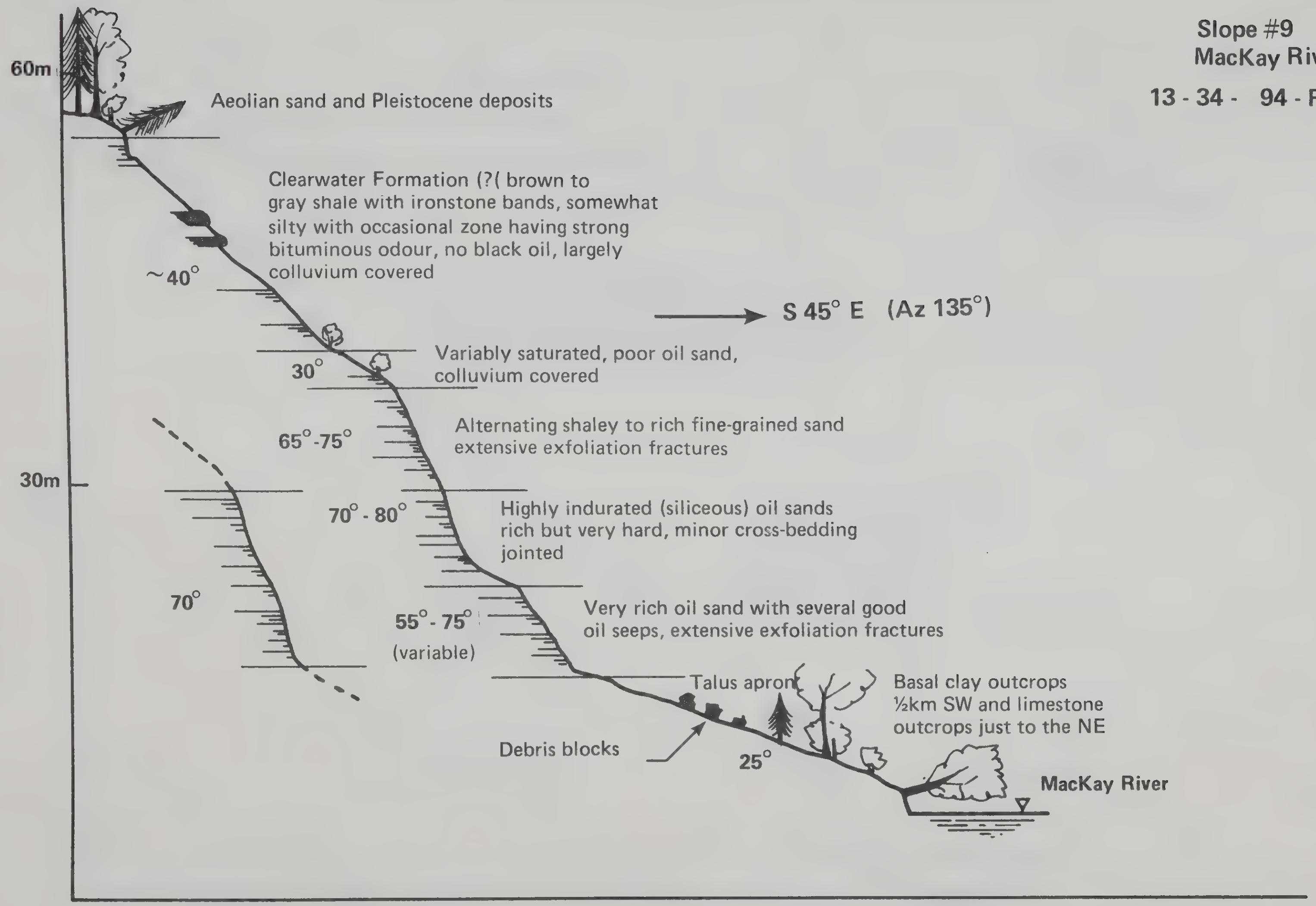

Slope #9
MacKay River

13 - 34 - 94 - R11W4

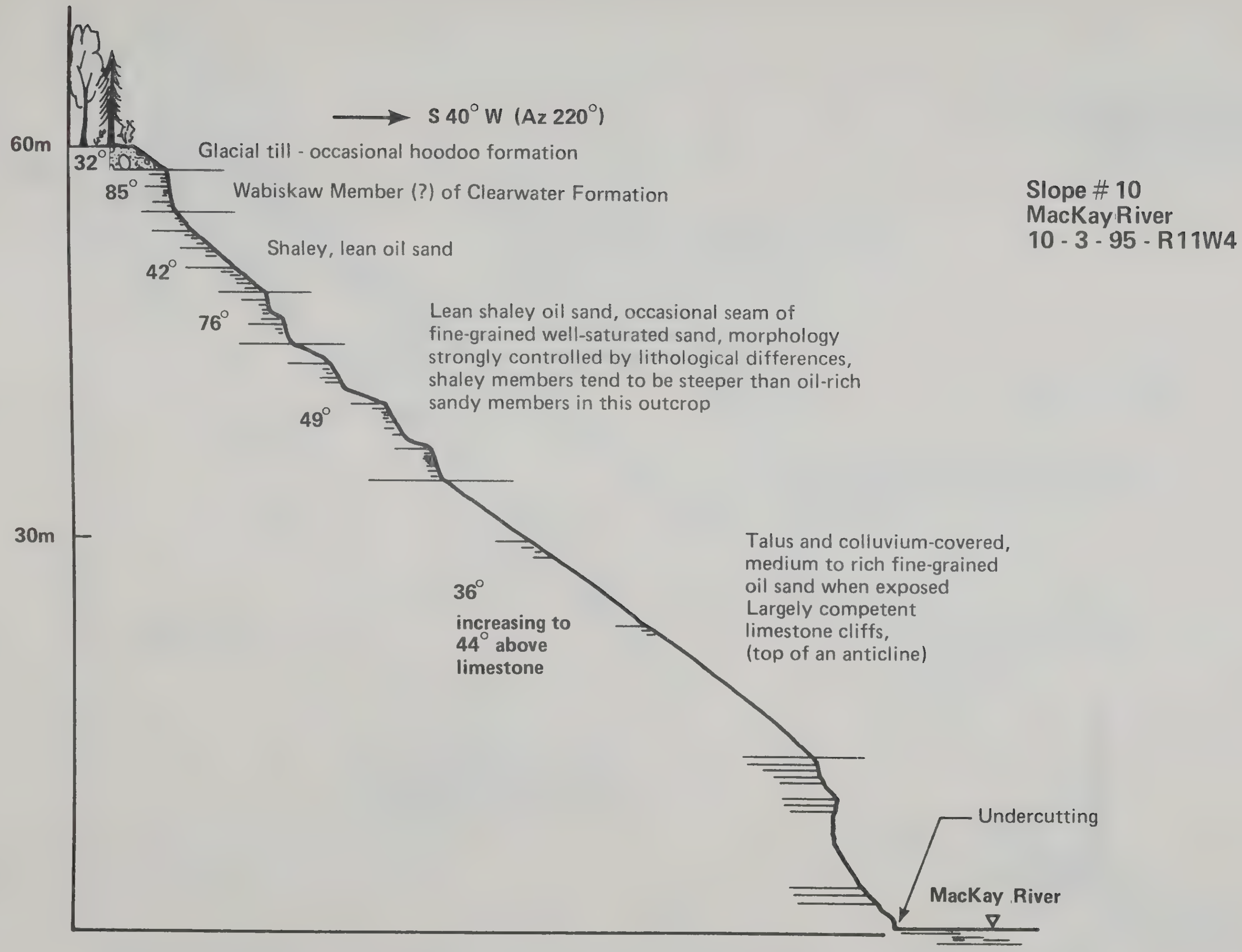

Slope # 10
MacKay River
10 - 3 - 95 - R11W4

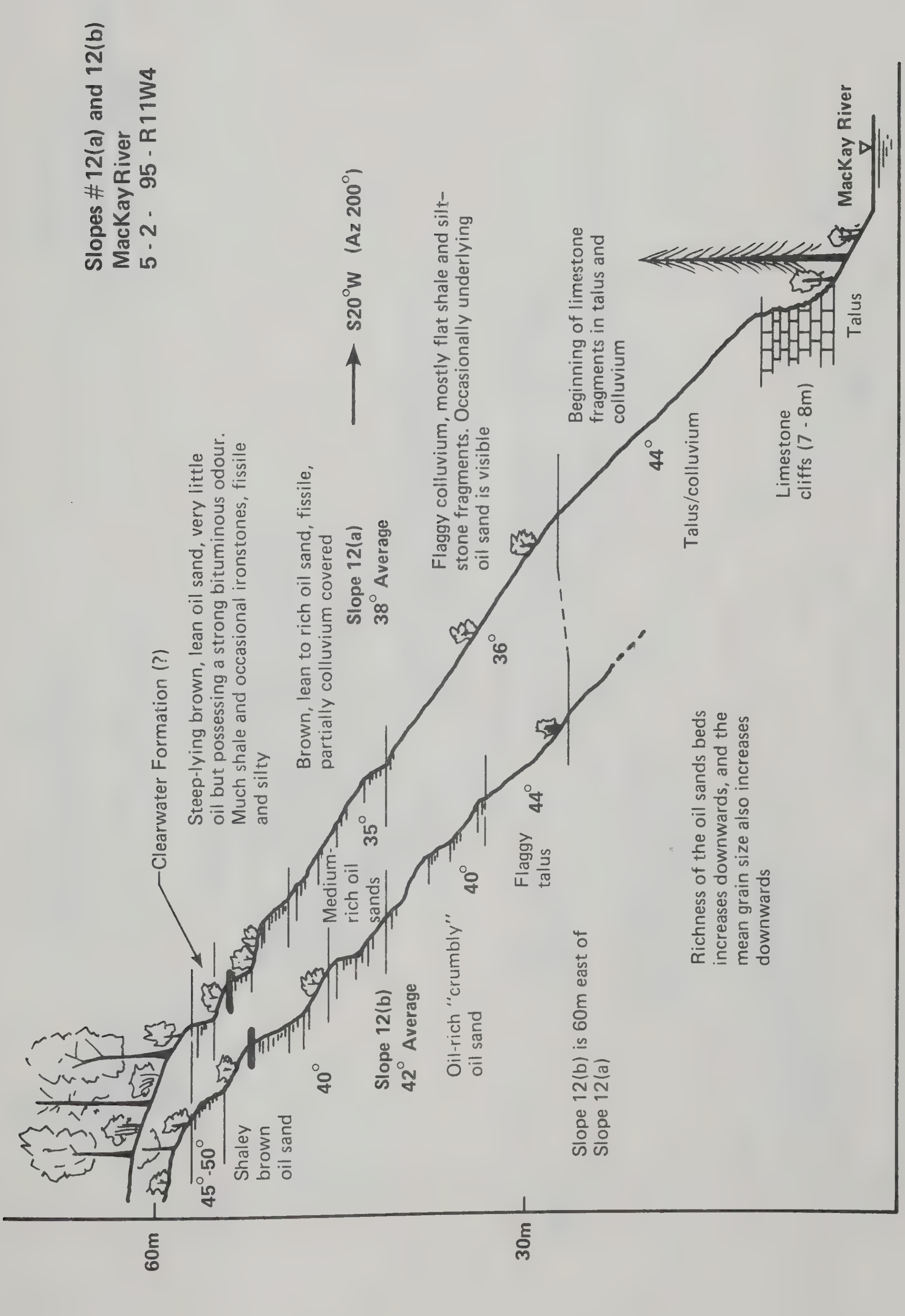
Slopes #12(a) and 12(b)
MacKay River
5 - 2 - 95 - R11W4
S20°W (Az 200°)
60m
30m
45°-50°
Shaley brown oil sand
Clearwater Formation (?)
Steep-lying brown, lean oil sand, very little oil but possessing a strong bituminous odour. Much shale and occasional ironstones, fissile and silty
40°
Medium-rich oil sands
35°
Brown, lean to rich oil sand, fissile, partially colluvium covered
Slope 12(a)
38° Average
Slope 12(b)
42° Average
Oil-rich "crumbly" oil sand
40°
Flaggy talus
44°
36°
Flaggy colluvium, mostly flat shale and silt-stone fragments. Occasionally underlying oil sand is visible
Slope 12(b) is 60m east of Slope 12(a)
Richness of the oil sands beds increases downwards, and the mean grain size also increases downwards
44°
Talus/colluvium
Beginning of limestone fragments in talus and colluvium
Limestone cliffs (7 - 8m)
Talus
MacKay River

Slope # 14
Athabasca River
4km N of Ft. McMurray
8 - 32 - 89 - R9W4

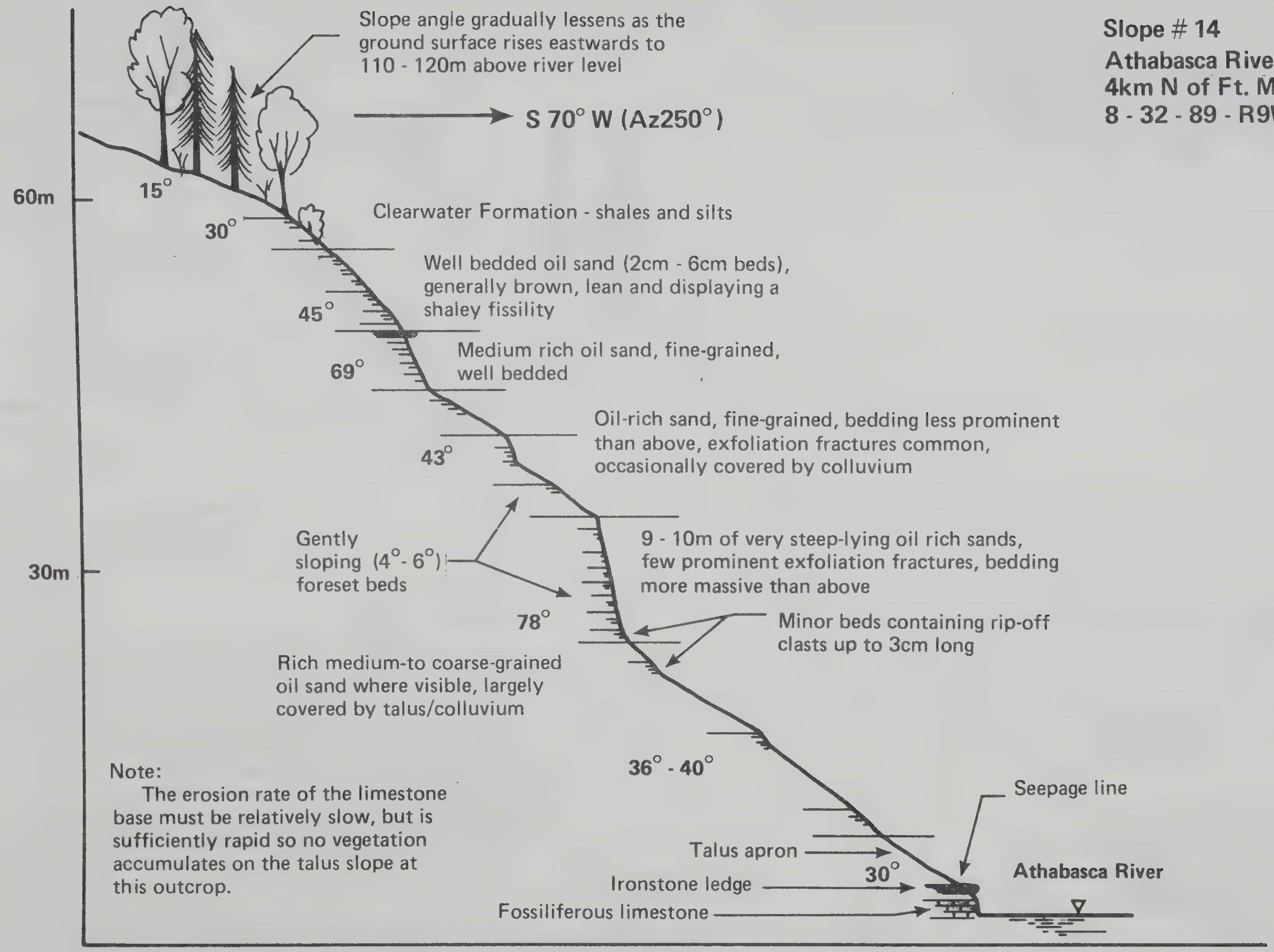

Note:
The erosion rate of the limestone base must be relatively slow, but is sufficiently rapid so no vegetation accumulates on the talus slope at this outcrop.

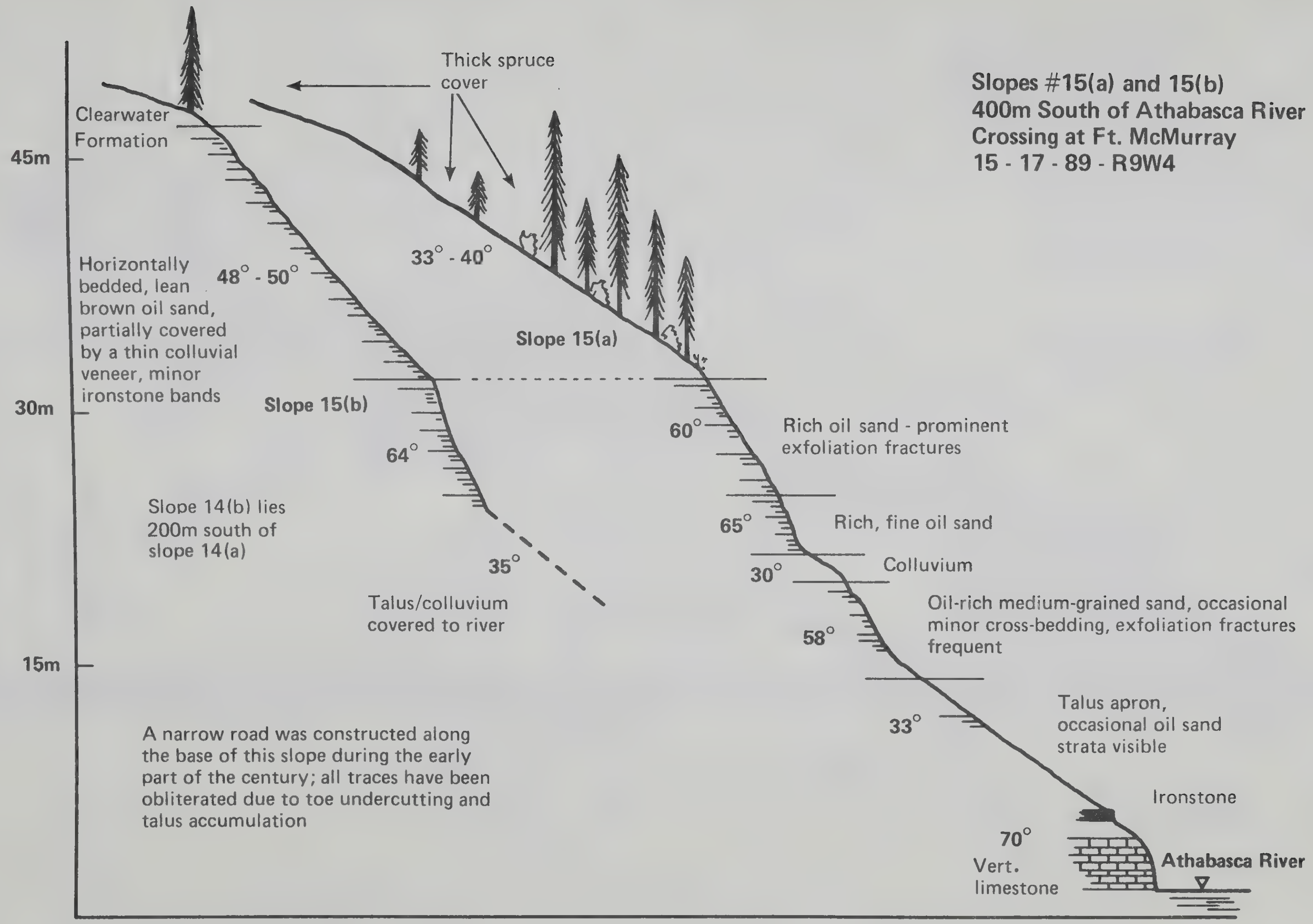

Slopes #15(a) and 15(b)
400m South of Athabasca River
Crossing at Ft. McMurray
15 - 17 - 89 - R9W4

Sketch of Front View of Slopes 16(a) and 16(b) (See Following Page) 10 - 18 - 89 - R9W4

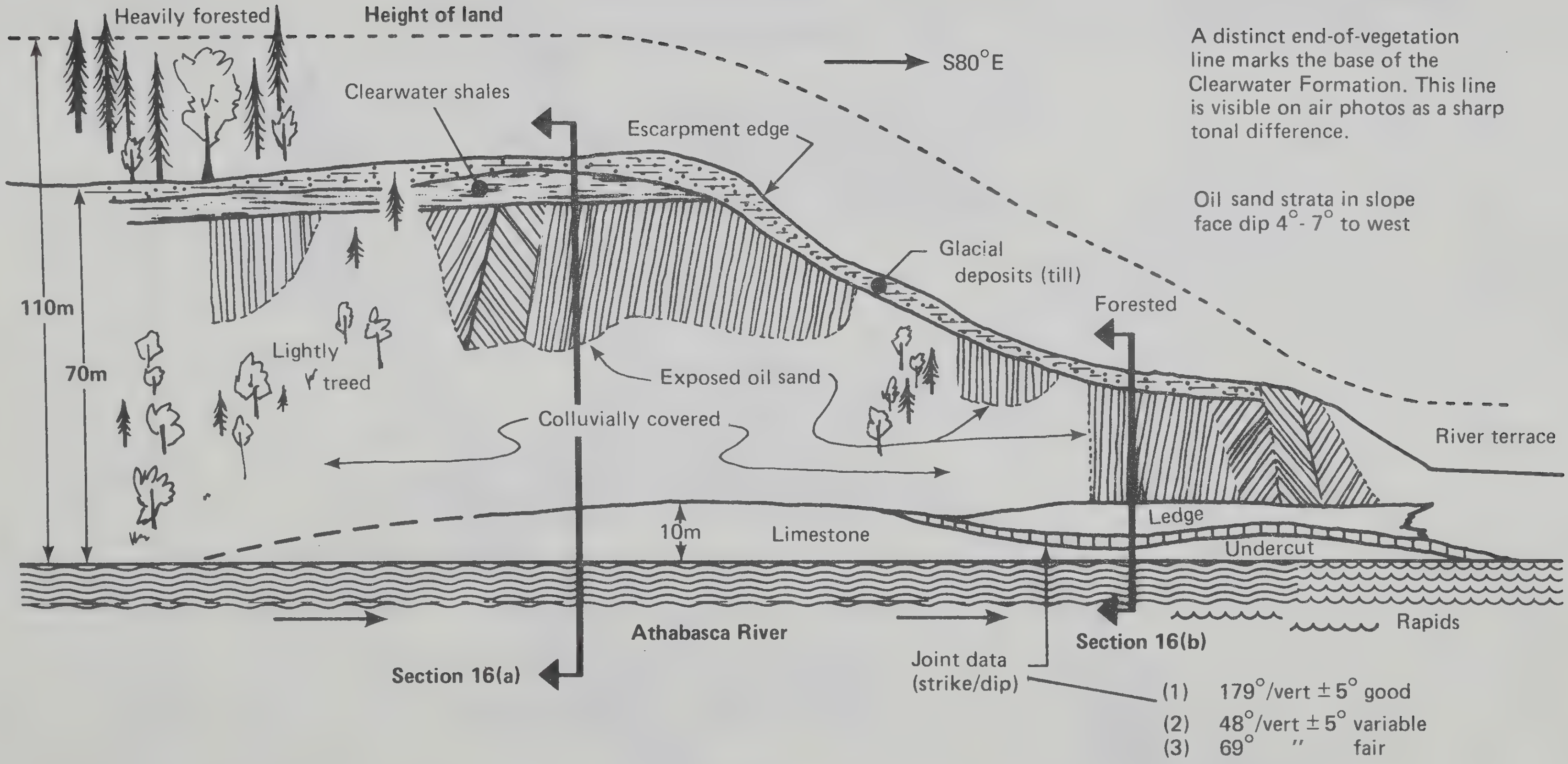

A distinct end-of-vegetation line marks the base of the Clearwater Formation. This line is visible on air photos as a sharp tonal difference.

Oil sand strata in slope face dip 4°- 7° to west

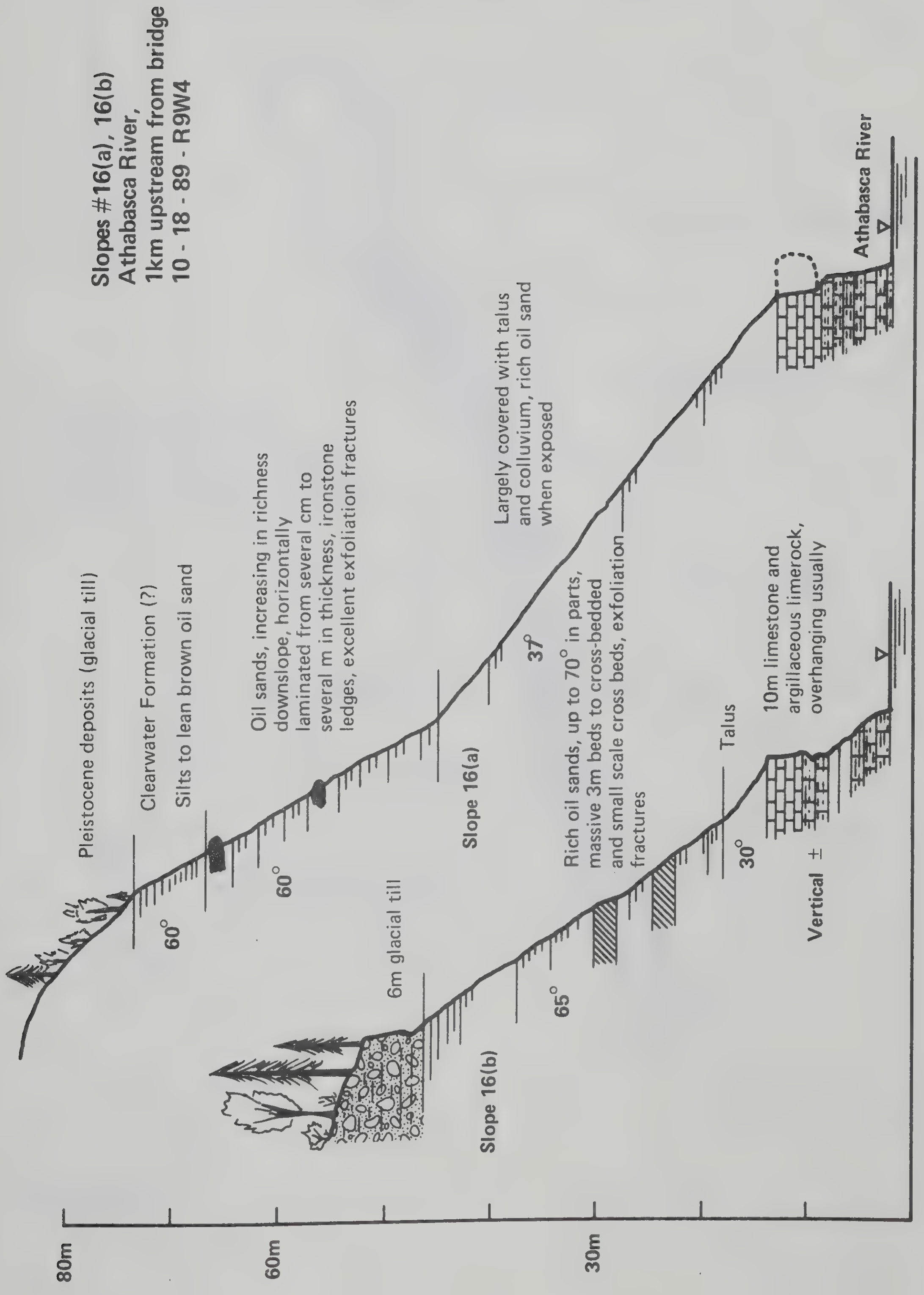
Slopes #16(a), 16(b)
Athabasca River,
1km upstream from bridge
10 - 18 - 89 - R9W4
Pleistocene deposits (glacial till)
Clearwater Formation (?)
Silts to lean brown oil sand
Oil sands, increasing in richness downslope, horizontally laminated from several cm to several m in thickness, ironstone ledges, excellent exfoliation fractures
Largely covered with talus and colluvium, rich oil sand when exposed
60°
60°
37°
Slope 16(a)
6m glacial till
65°
Slope 16(b)
Rich oil sands, up to 70° in parts, massive 3m beds to cross-bedded and small scale cross beds, exfoliation fractures
Talus
30°
Vertical ±
10m limestone and argillaceous limerock, overhanging usually
Athabasca River
80m
60m
30m

Plan of Oil Sand Slopes 3.5km N of Ft. McMurray

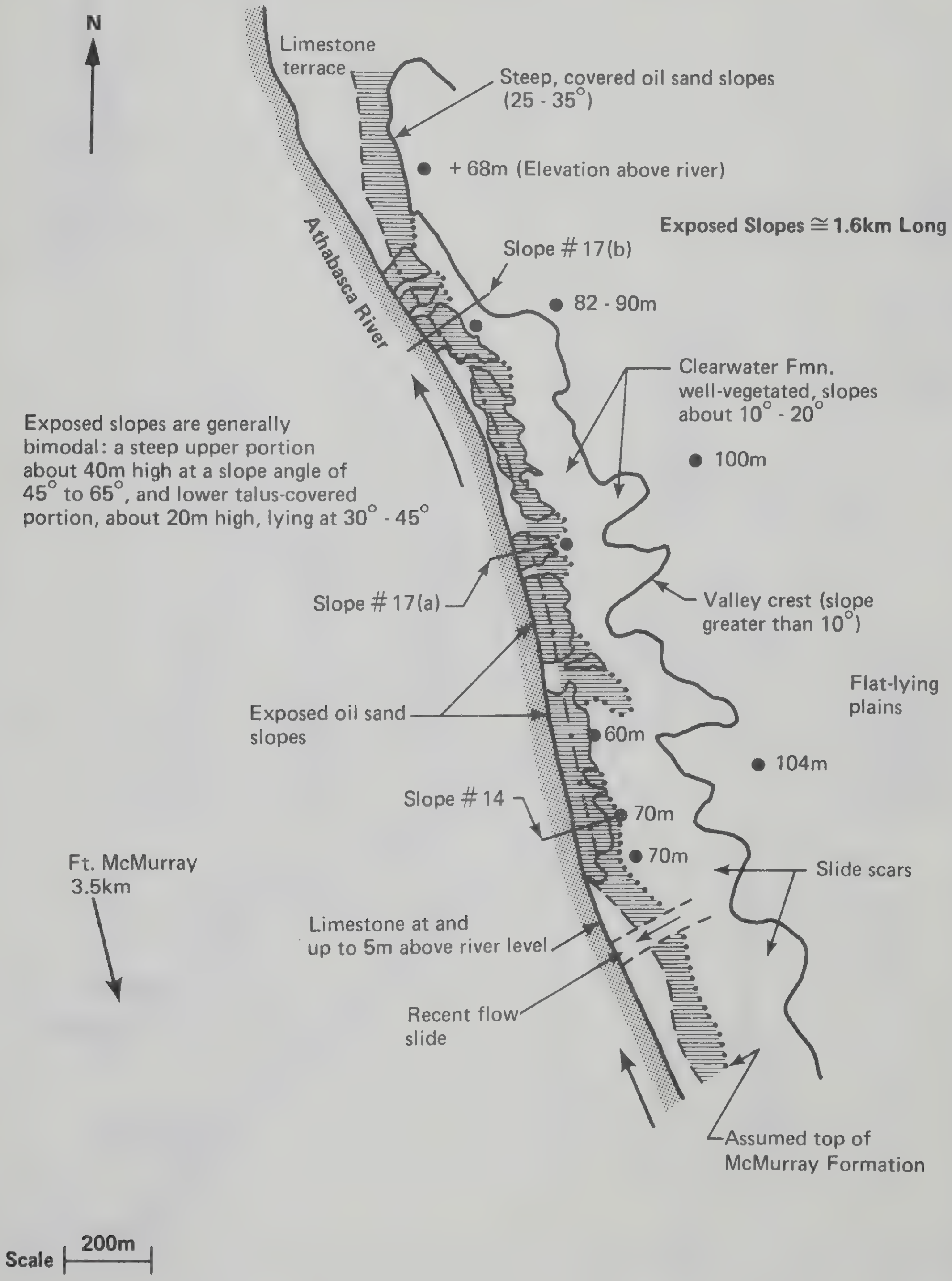

Slope #17(a)
4km north of Ft. McMurray
7 - 5 - 90 - R9W4

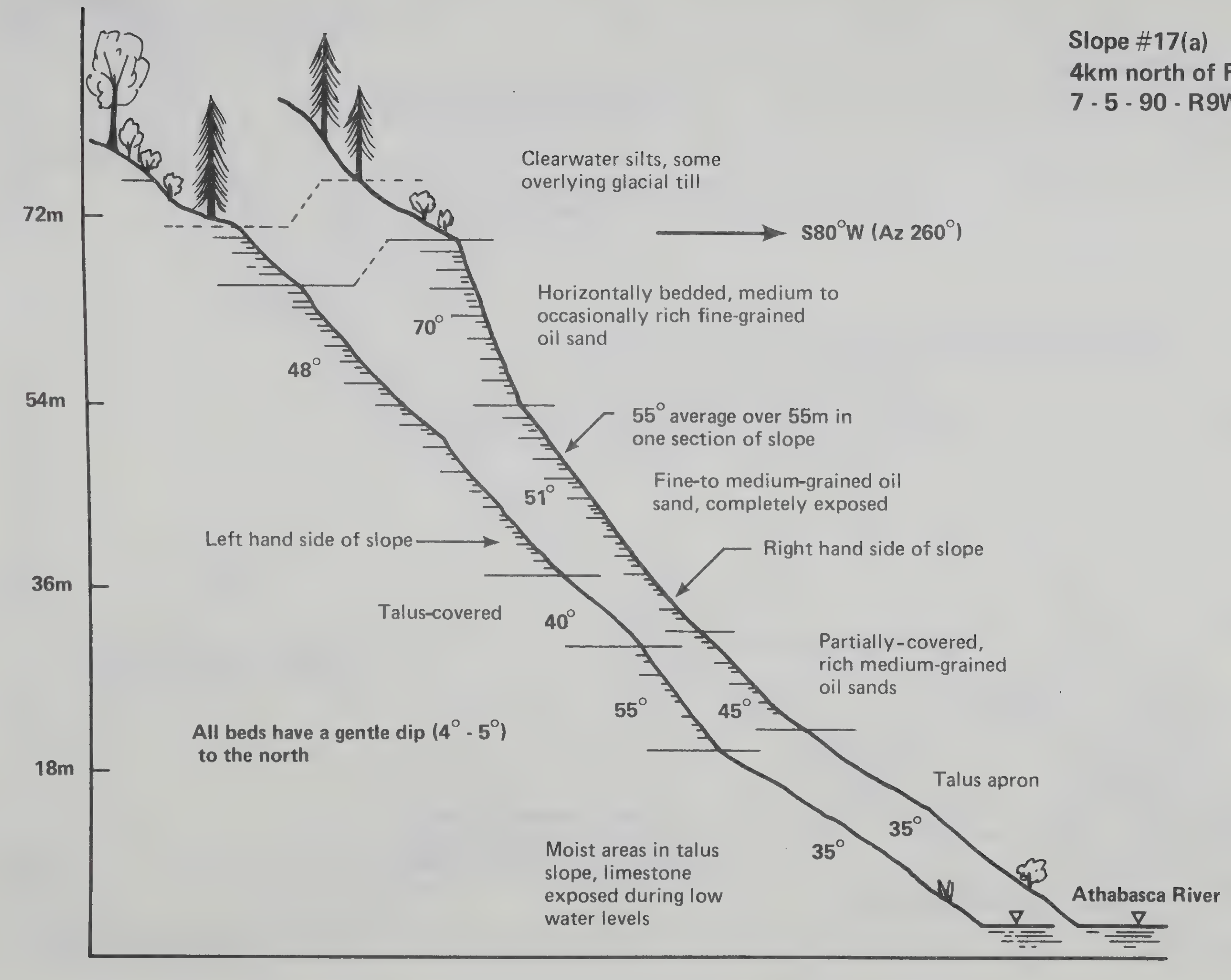

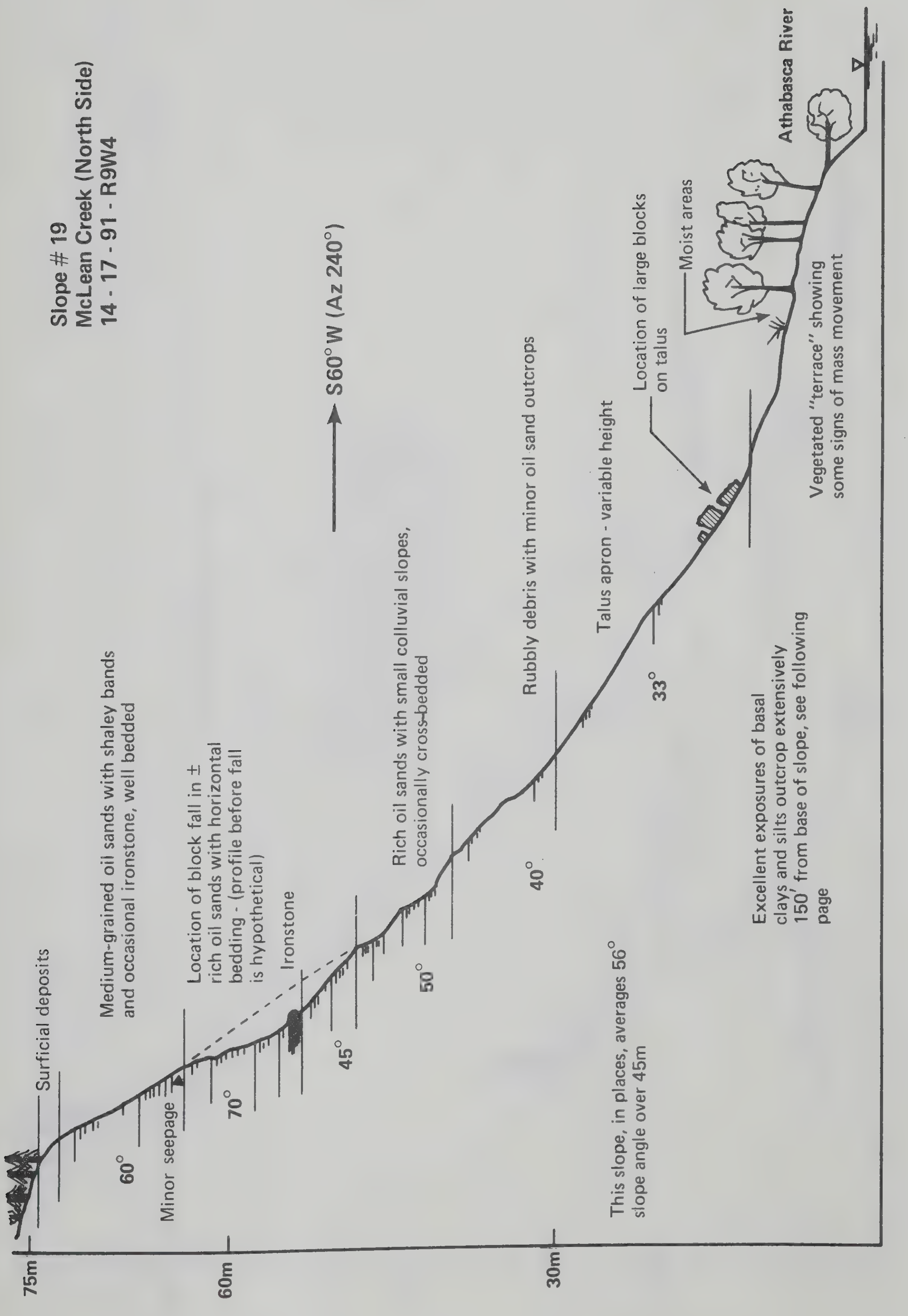
Slope # 19
McLean Creek (North Side)
14 - 17 - 91 - R9W4
S60° W (Az 240°)
75m
60m
30m
Surficial deposits
Medium-grained oil sands with shaley bands and occasional ironstone, well bedded
60°
Minor seepage
70°
Location of block fall in ± rich oil sands with horizontal bedding - (profile before fall is hypothetical)
Ironstone
45°
50°
Rich oil sands with small colluvial slopes, occasionally cross-bedded
40°
Rubbly debris with minor oil sand outcrops
This slope, in places, averages 56° slope angle over 45m
Talus apron - variable height
33°
Location of large blocks on talus
Moist areas
Excellent exposures of basal clays and silts outcrop extensively 150' from base of slope, see following page
Vegetated "terrace" showing some signs of mass movement
Athabasca River

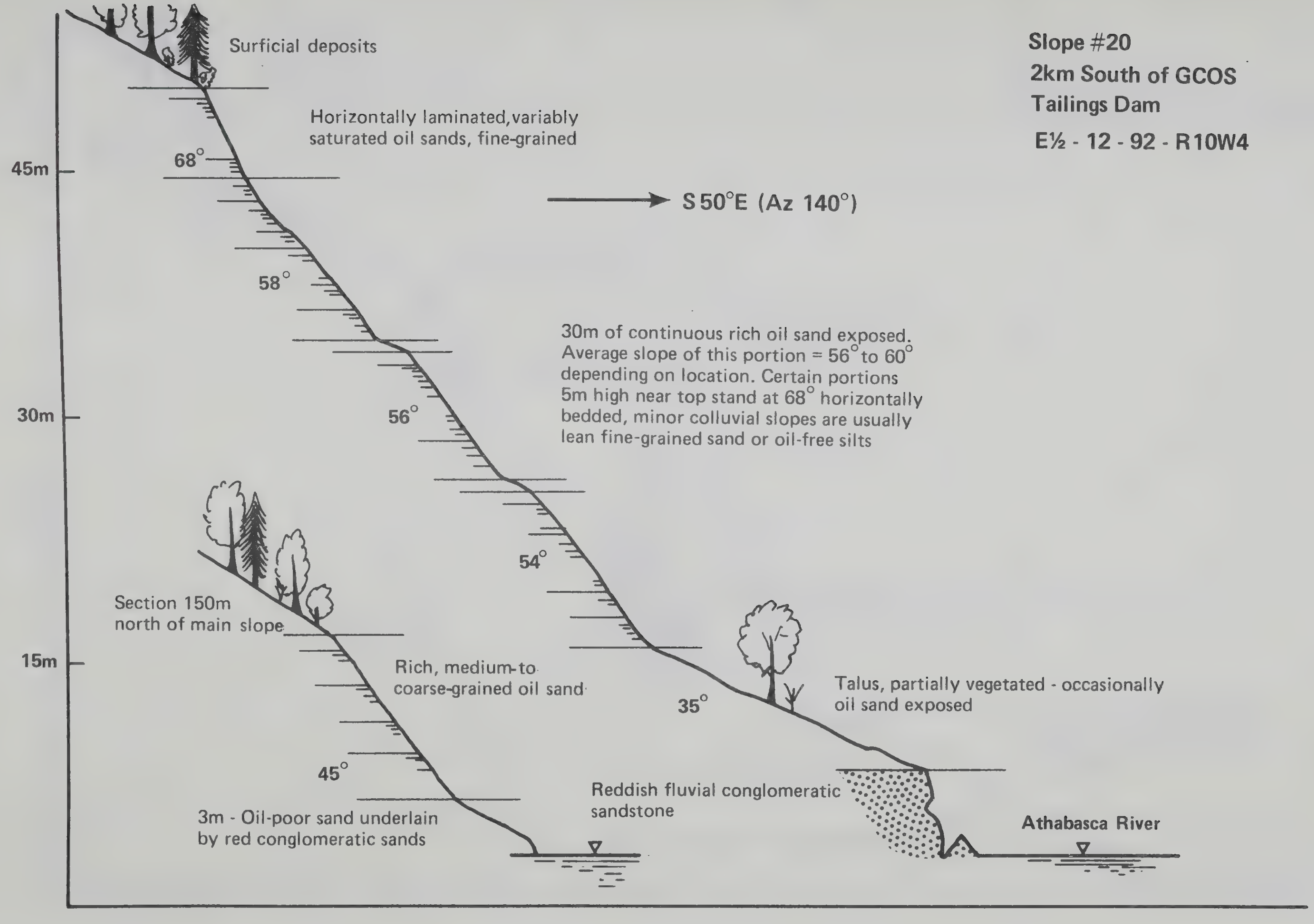
Slope #20
2km South of GCOS
Tailings Dam
E½ - 12 - 92 - R10W4
S 50°E (Az 140°)
Surficial deposits
Horizontally laminated, variably saturated oil sands, fine-grained
68°
58°
56°
54°
35°
45°
30m of continuous rich oil sand exposed. Average slope of this portion = 56° to 60° depending on location. Certain portions 5m high near top stand at 68° horizontally bedded, minor colluvial slopes are usually lean fine-grained sand or oil-free silts
Section 150m north of main slope
Rich, medium-to coarse-grained oil sand
3m - Oil-poor sand underlain by red conglomeratic sands
Talus, partially vegetated - occasionally oil sand exposed
Reddish fluvial conglomeratic sandstone
Athabasca River
45m
30m
15m

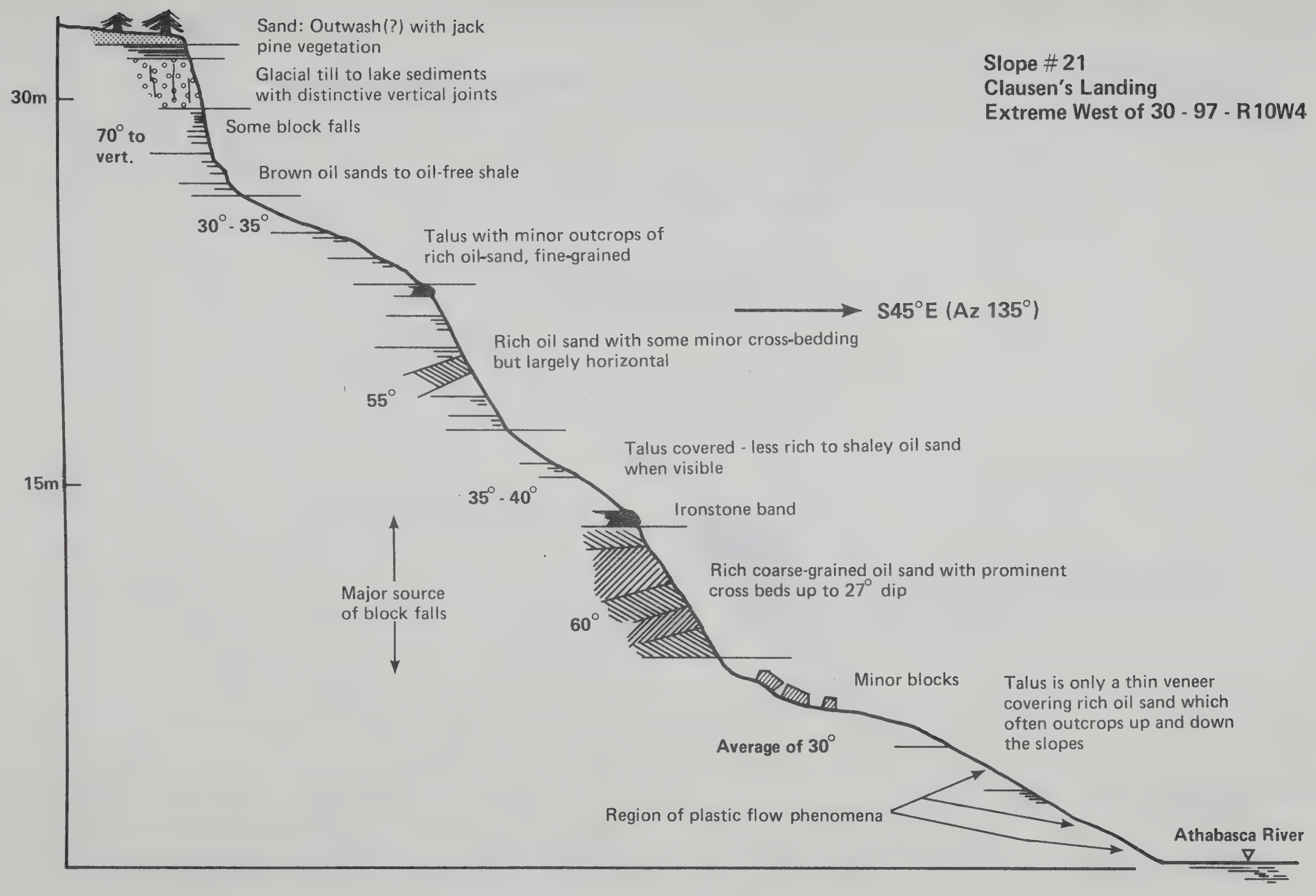

Slope # 21
Clausen's Landing
Extreme West of 30 - 97 - R10W4

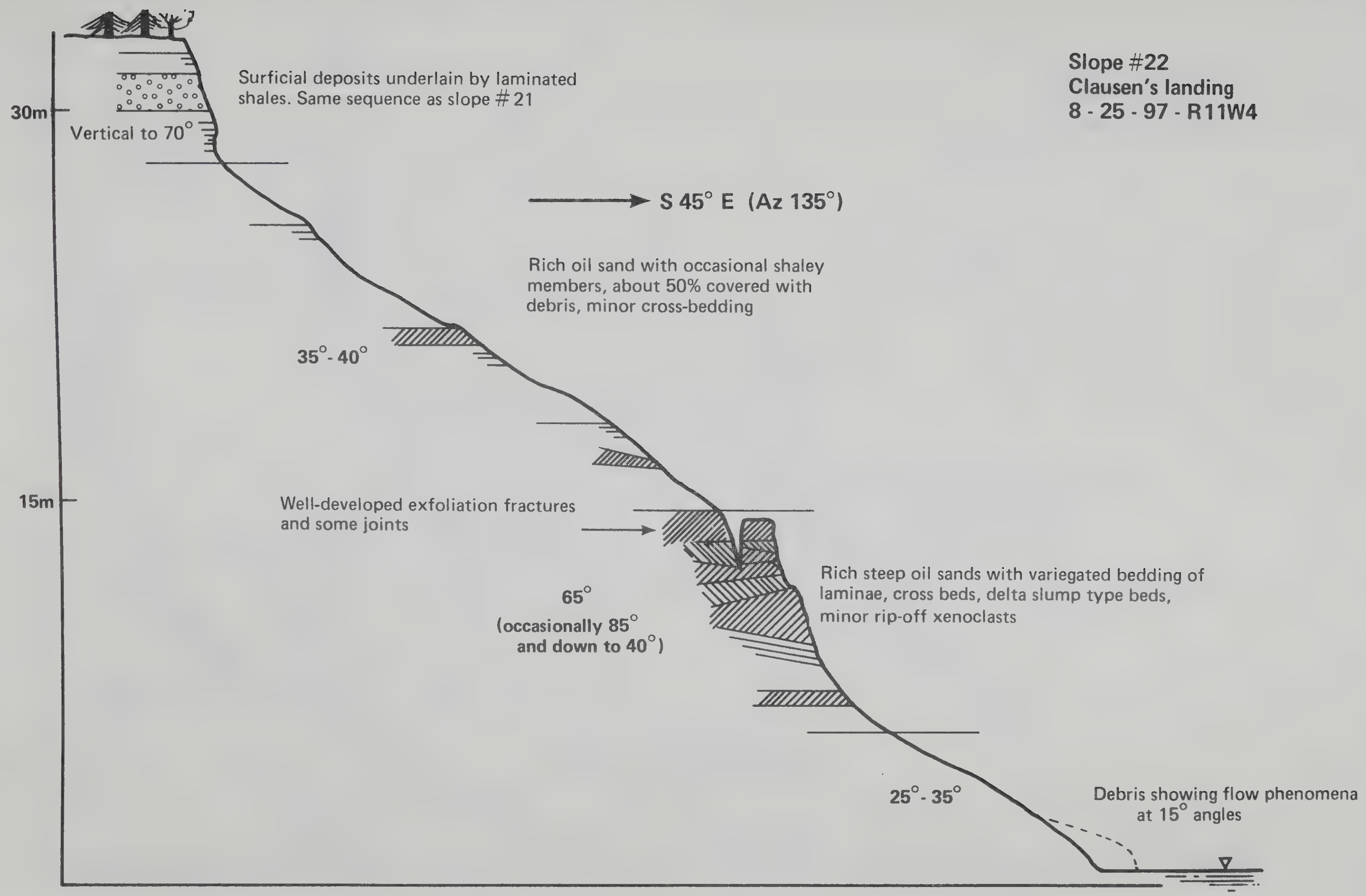
Slope #22
Clausen's landing
8 - 25 - 97 - R11W4
S 45° E (Az 135°)
30m
15m
Surficial deposits underlain by laminated shales. Same sequence as slope # 21
Vertical to 70°
Rich oil sand with occasional shaley members, about 50% covered with debris, minor cross-bedding
35°- 40°
Well-developed exfoliation fractures and some joints
65°
(occasionally 85° and down to 40°)
Rich steep oil sands with variegated bedding of laminae, cross beds, delta slump type beds, minor rip-off xenoclasts
25°- 35°
Debris showing flow phenomena at 15° angles

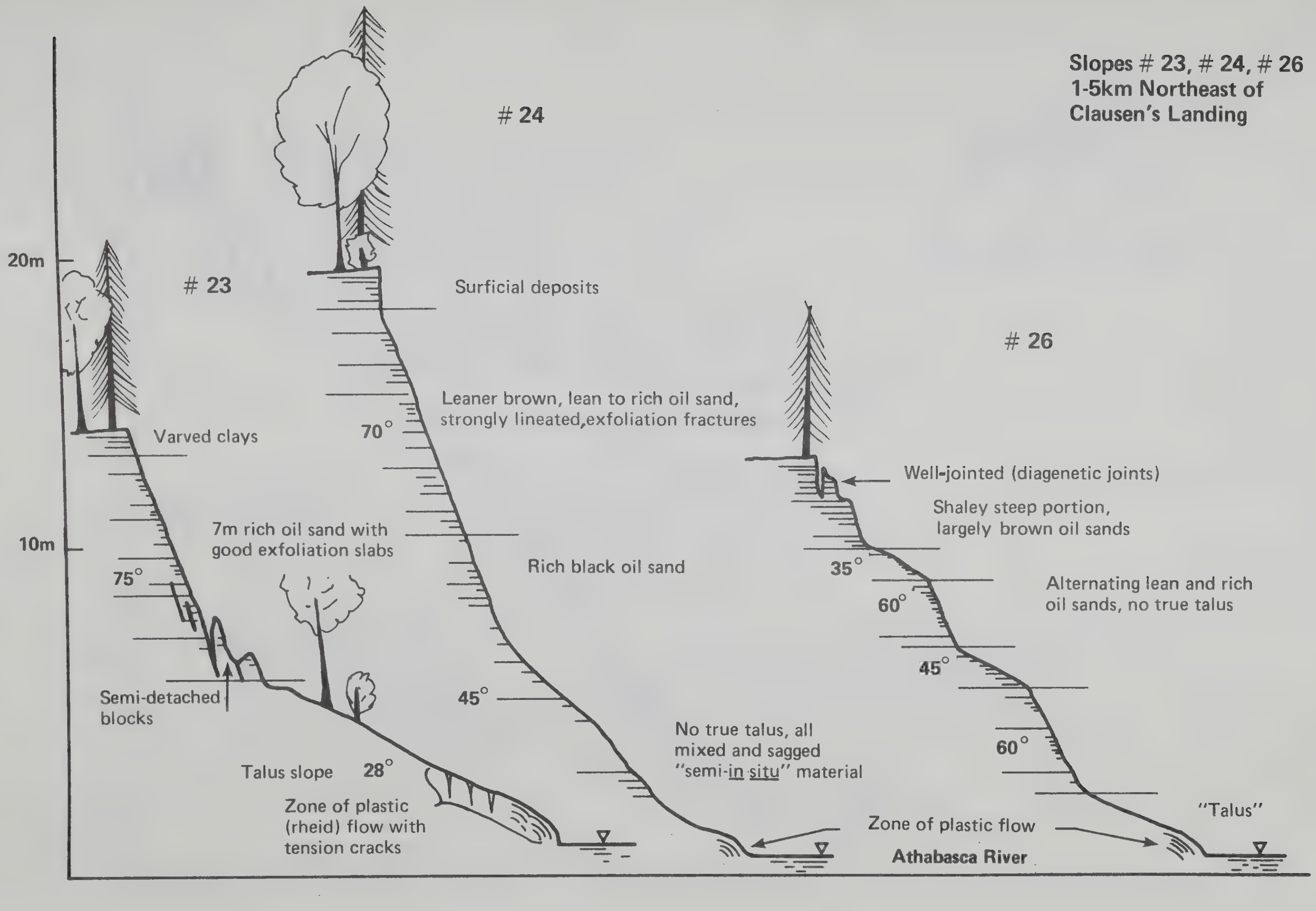

Slopes # 23, # 24, # 26
1-5km Northeast of
Clausen's Landing

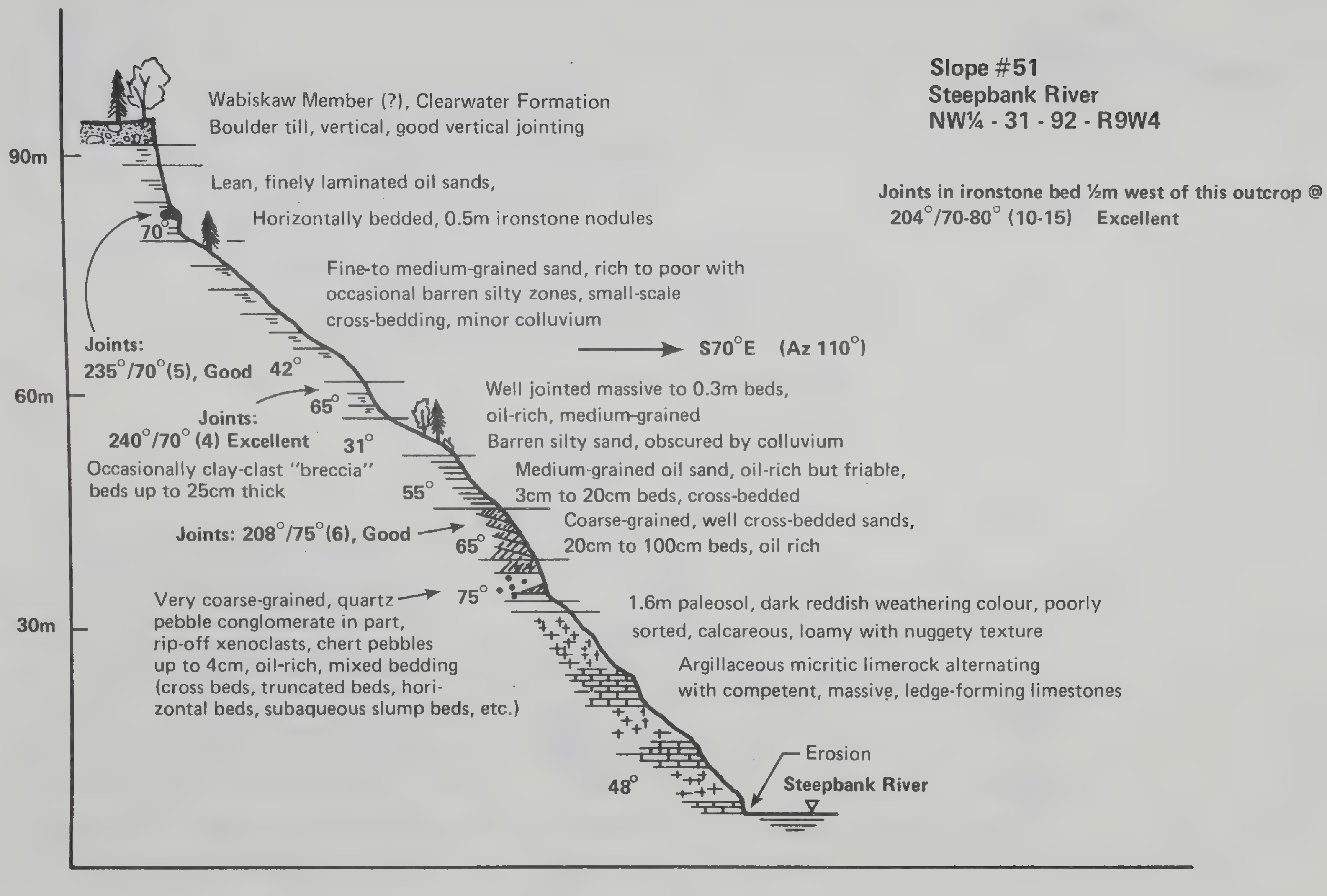

Slope #51
Steepbank River
NW¼ - 31 - 92 - R9W4

Joints in ironstone bed ½m west of this outcrop @ 204°/70-80° (10-15) Excellent

Slope #52
Steepbank River
NW¼ - 31 - 92 - R9W4

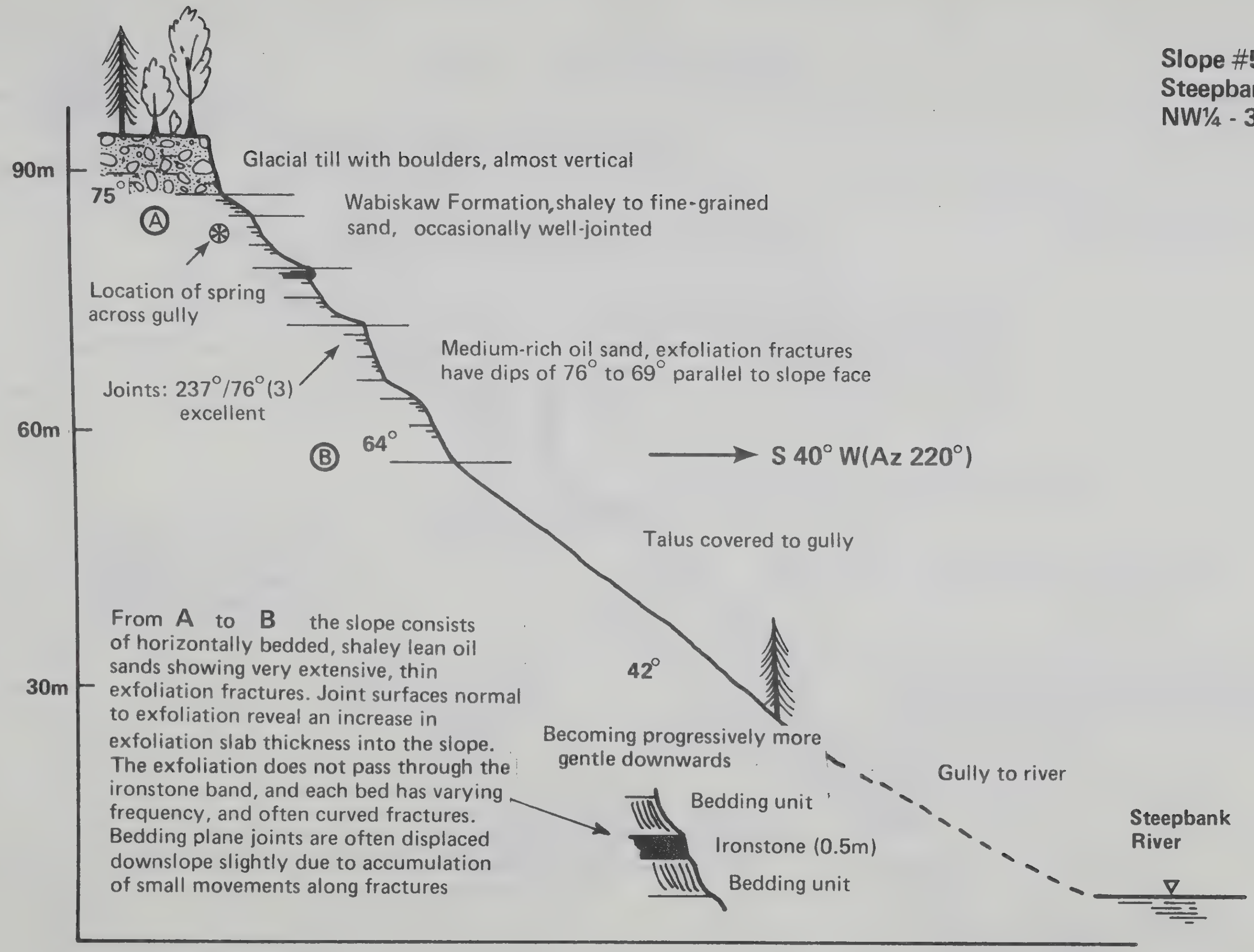

From **A** to **B** the slope consists of horizontally bedded, shaley lean oil sands showing very extensive, thin exfoliation fractures. Joint surfaces normal to exfoliation reveal an increase in exfoliation slab thickness into the slope. The exfoliation does not pass through the ironstone band, and each bed has varying frequency, and often curved fractures. Bedding plane joints are often displaced downslope slightly due to accumulation of small movements along fractures

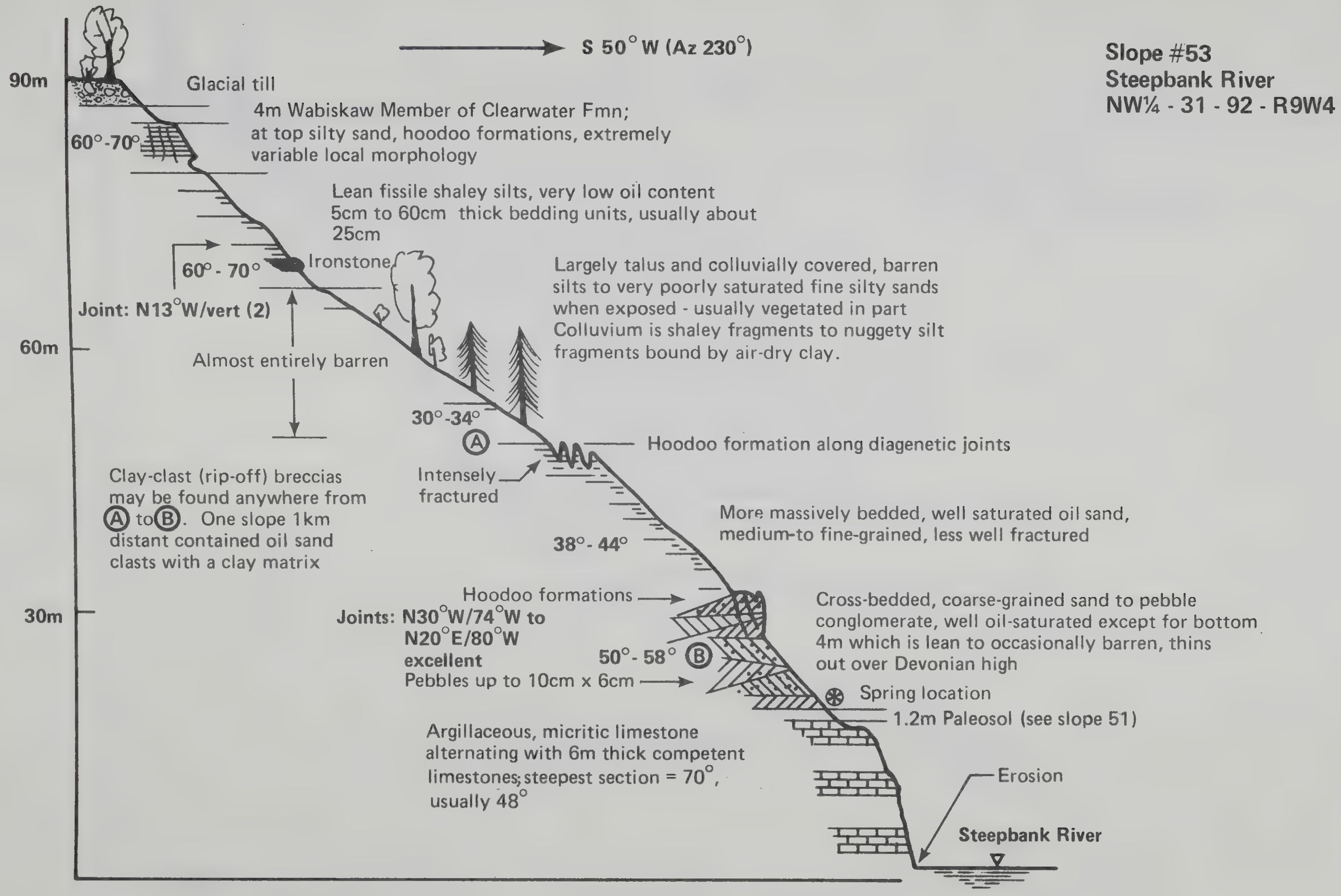
Slope #53
Steepbank River
NW¼ - 31 - 92 - R9W4
S 50° W (Az 230°)
90m
60m
30m
Glacial till
4m Wabiskaw Member of Clearwater Fmn;
at top silty sand, hoodoo formations, extremely variable local morphology
60°-70°
Lean fissile shaley silts, very low oil content
5cm to 60cm thick bedding units, usually about 25cm
60° - 70°
Ironstone
Joint: N13°W/vert (2)
Almost entirely barren
Largely talus and colluvially covered, barren silts to very poorly saturated fine silty sands when exposed - usually vegetated in part
Colluvium is shaley fragments to nuggety silt fragments bound by air-dry clay.
30°-34°
Ⓐ
Hoodoo formation along diagenetic joints
Intensely fractured
Clay-clast (rip-off) breccias may be found anywhere from Ⓐ to Ⓑ. One slope 1km distant contained oil sand clasts with a clay matrix
38° - 44°
More massively bedded, well saturated oil sand, medium-to fine-grained, less well fractured
Hoodoo formations
Joints: N30°W/74°W to N20°E/80°W excellent
Pebbles up to 10cm x 6cm
50° - 58°
Ⓑ
Cross-bedded, coarse-grained sand to pebble conglomerate, well oil-saturated except for bottom 4m which is lean to occasionally barren, thins out over Devonian high
Spring location
1.2m Paleosol (see slope 51)
Argillaceous, micritic limestone alternating with 6m thick competent limestones; steepest section = 70°, usually 48°
Erosion
Steepbank River

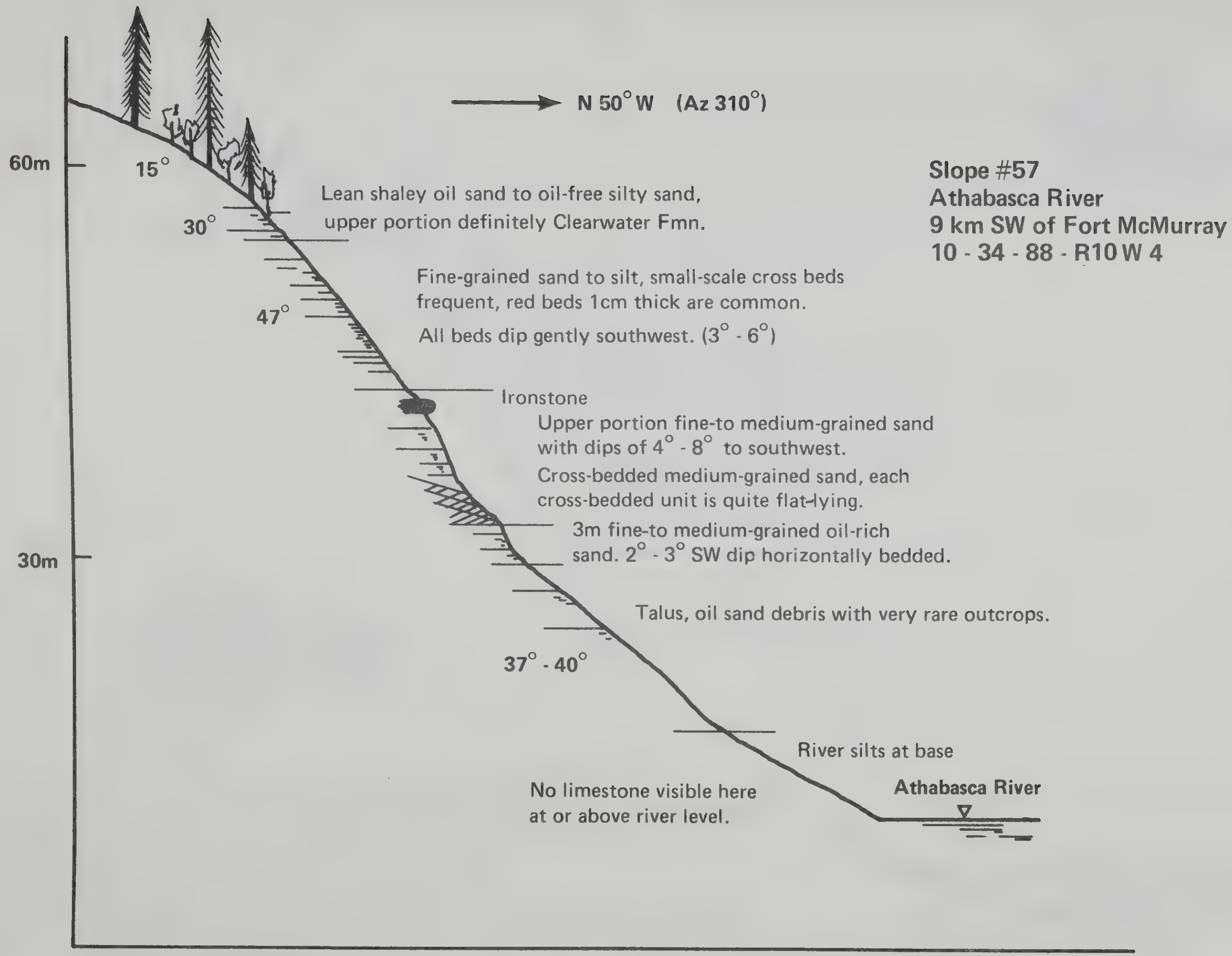

Slope #57
Athabasca River
9 km SW of Fort McMurray
10 - 34 - 88 - R10 W 4

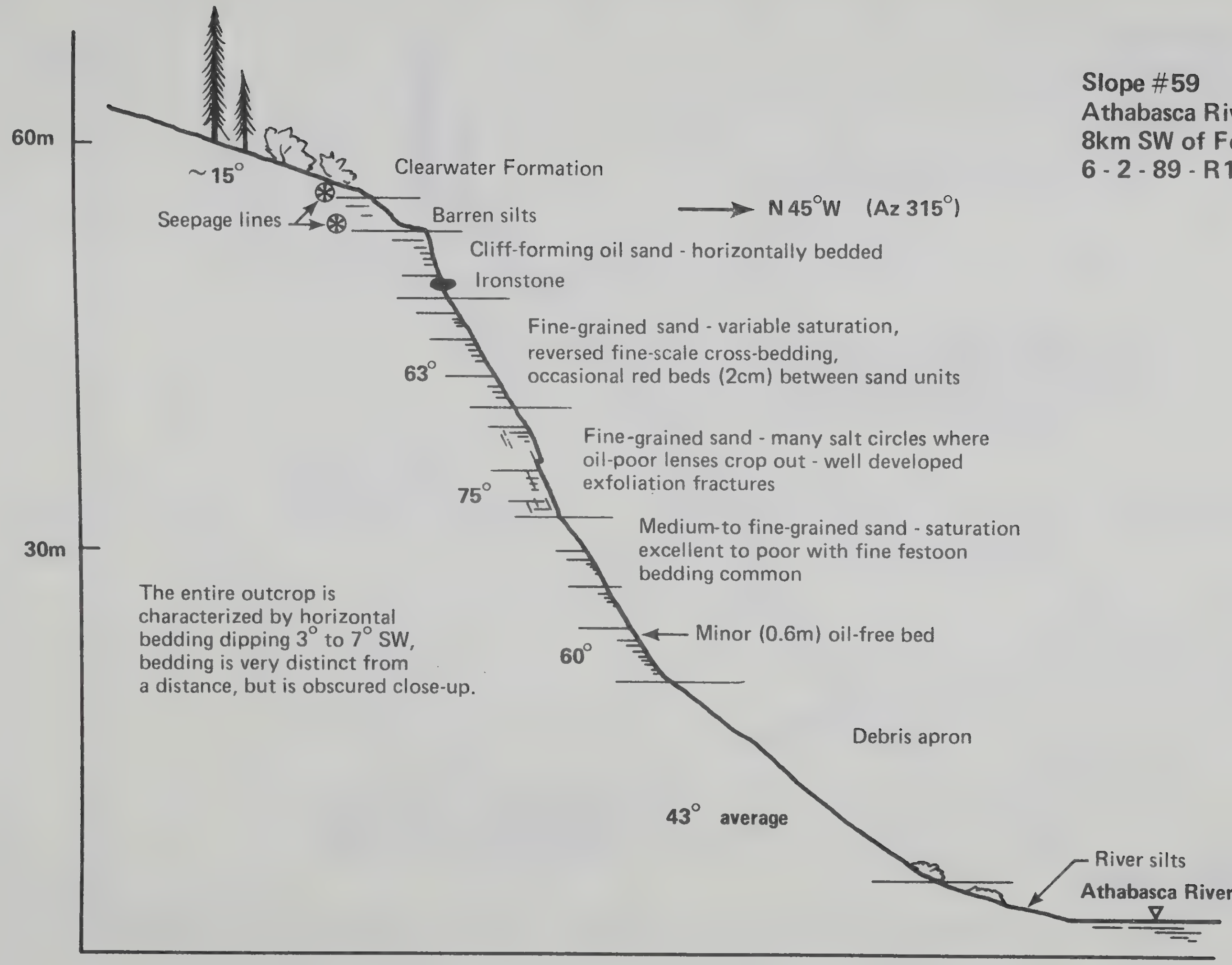

Slope #59
Athabasca River
8km SW of Fort McMurray
6 - 2 - 89 - R10W4

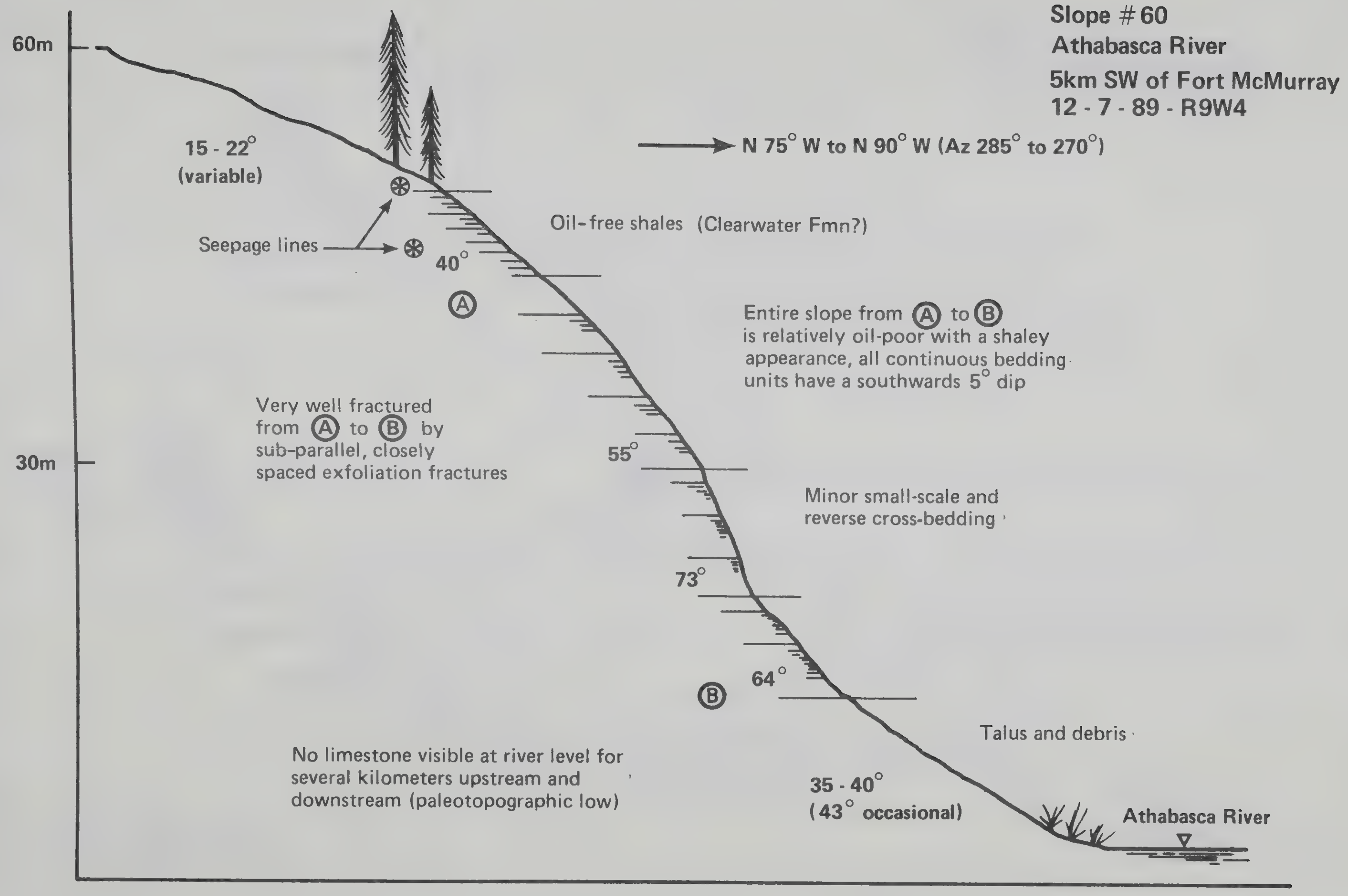
Slope # 60
Athabasca River
5km SW of Fort McMurray
12 - 7 - 89 - R9W4
N 75° W to N 90° W (Az 285° to 270°)
60m
30m
15 - 22°
(variable)
Seepage lines
40°
Ⓐ
Oil-free shales (Clearwater Fmn?)
Entire slope from Ⓐ to Ⓑ is relatively oil-poor with a shaley appearance, all continuous bedding units have a southwards 5° dip
Very well fractured from Ⓐ to Ⓑ by sub-parallel, closely spaced exfoliation fractures
55°
Minor small-scale and reverse cross-bedding
73°
64°
Ⓑ
Talus and debris
No limestone visible at river level for several kilometers upstream and downstream (paleotopographic low)
35 - 40°
(43° occasional)
Athabasca River

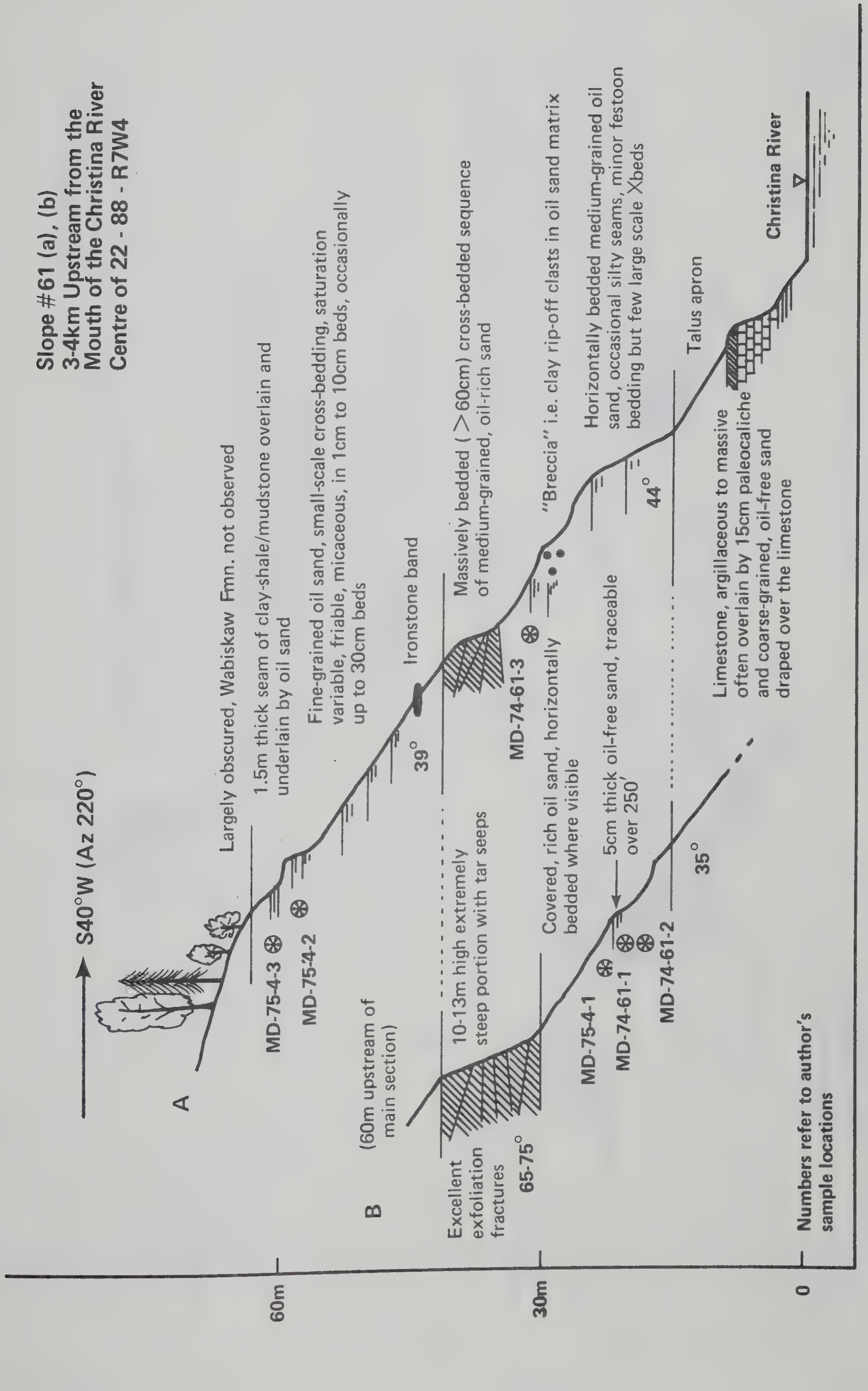
Slope #61 (a), (b)
3-4km Upstream from the
Mouth of the Christina River
Centre of 22 - 88 - R7W4
S40°W (Az 220°)
A
B
(60m upstream of main section)
60m
30m
0
Largely obscured, Wabiskaw Fmn. not observed
1.5m thick seam of clay-shale/mudstone overlain and underlain by oil sand
Fine-grained oil sand, small-scale cross-bedding, saturation variable, friable, micaceous, in 1cm to 10cm beds, occasionally up to 30cm beds
Ironstone band
39°
Massively bedded (>60cm) cross-bedded sequence of medium-grained, oil-rich sand
"Breccia" i.e. clay rip-off clasts in oil sand matrix
Horizontally bedded medium-grained oil sand, occasional silty seams, minor festoon bedding but few large scale Xbeds
44°
Talus apron
Limestone, argillaceous to massive often overlain by 15cm paleocaliche and coarse-grained, oil-free sand draped over the limestone
Christina River
MD-75-4-3
MD-75-4-2
MD-74-61-3
10-13m high extremely steep portion with tar seeps
Excellent exfoliation fractures
65-75°
Covered, rich oil sand, horizontally bedded where visible
5cm thick oil-free sand, traceable over 250'
35°
MD-75-4-1
MD-74-61-1
MD-74-61-2
Numbers refer to author's sample locations

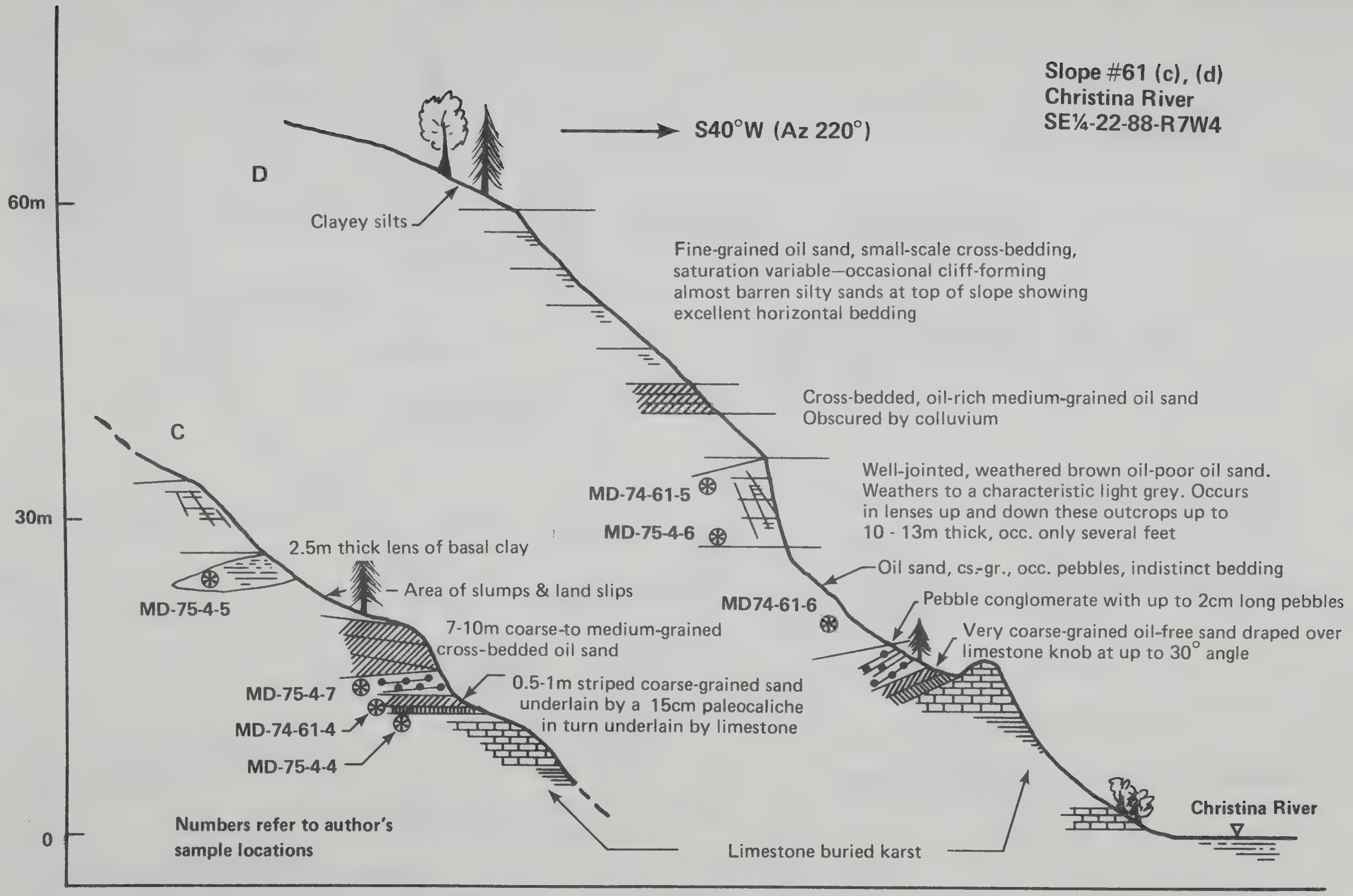
Slope #61 (c), (d)
Christina River
SE¼-22-88-R7W4
S40°W (Az 220°)
60m
30m
0
D
C
Clayey silts
Fine-grained oil sand, small-scale cross-bedding, saturation variable—occasional cliff-forming almost barren silty sands at top of slope showing excellent horizontal bedding
Cross-bedded, oil-rich medium-grained oil sand
Obscured by colluvium
MD-74-61-5
MD-75-4-6
Well-jointed, weathered brown oil-poor oil sand. Weathers to a characteristic light grey. Occurs in lenses up and down these outcrops up to 10 - 13m thick, occ. only several feet
Oil sand, cs.-gr., occ. pebbles, indistinct bedding
MD74-61-6
Pebble conglomerate with up to 2cm long pebbles
Very coarse-grained oil-free sand draped over limestone knob at up to 30° angle
2.5m thick lens of basal clay
Area of slumps & land slips
MD-75-4-5
7-10m coarse-to medium-grained cross-bedded oil sand
0.5-1m striped coarse-grained sand underlain by a 15cm paleocaliche in turn underlain by limestone
MD-75-4-7
MD-74-61-4
MD-75-4-4
Numbers refer to author's sample locations
Limestone buried karst
Christina River

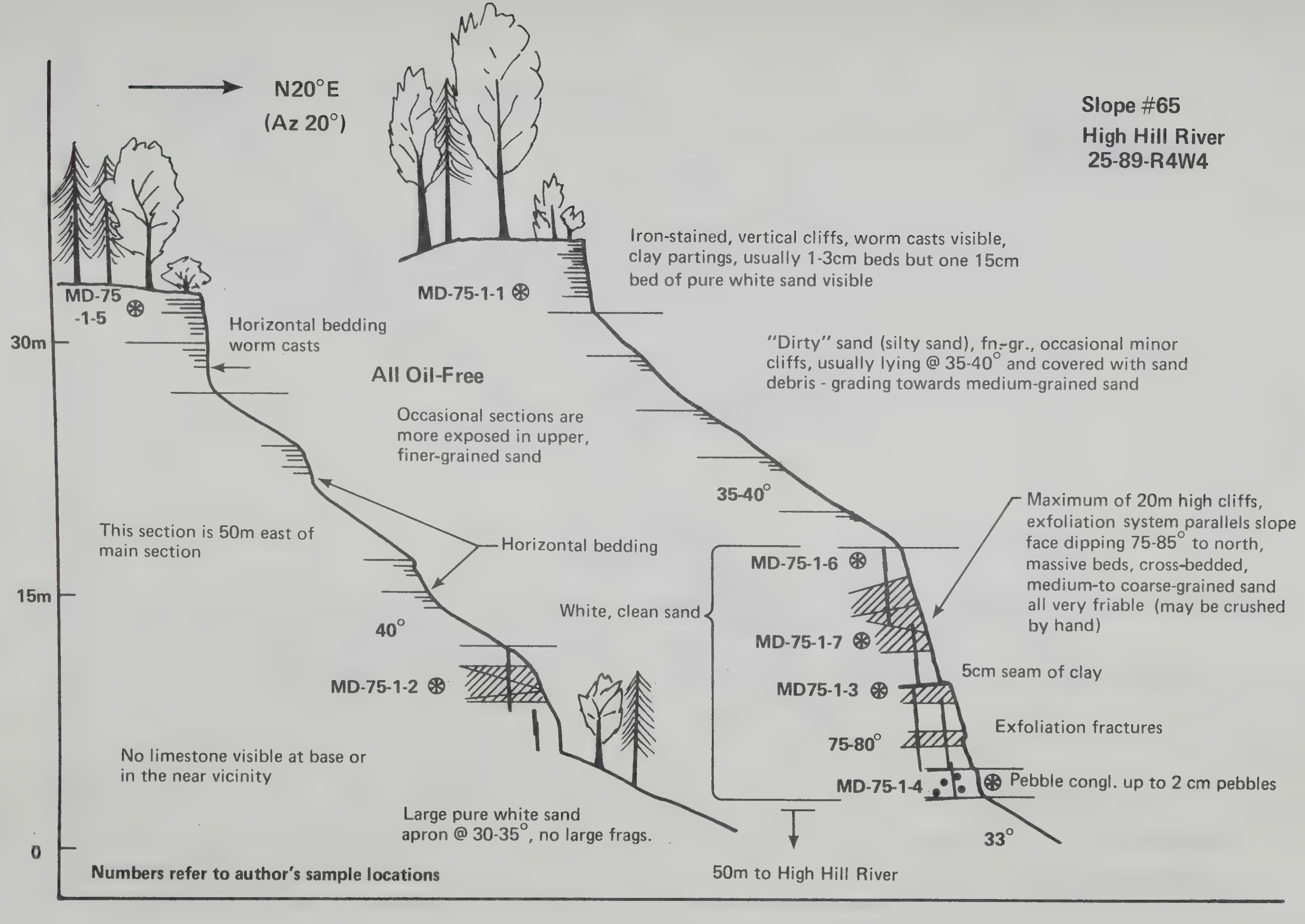
Slope #65
High Hill River
25-89-R4W4
N20°E
(Az 20°)
30m
15m
0
MD-75 -1-5
Horizontal bedding
worm casts
MD-75-1-1
All Oil-Free
Occasional sections are more exposed in upper, finer-grained sand
Iron-stained, vertical cliffs, worm casts visible, clay partings, usually 1-3cm beds but one 15cm bed of pure white sand visible
"Dirty" sand (silty sand), fn.-gr., occasional minor cliffs, usually lying @ 35-40° and covered with sand debris - grading towards medium-grained sand
35-40°
This section is 50m east of main section
Horizontal bedding
40°
MD-75-1-2
White, clean sand
MD-75-1-6
MD-75-1-7
MD75-1-3
75-80°
MD-75-1-4
Maximum of 20m high cliffs, exfoliation system parallels slope face dipping 75-85° to north, massive beds, cross-bedded, medium-to coarse-grained sand all very friable (may be crushed by hand)
5cm seam of clay
Exfoliation fractures
Pebble congl. up to 2 cm pebbles
33°
No limestone visible at base or in the near vicinity
Large pure white sand apron @ 30-35°, no large frags.
50m to High Hill River
Numbers refer to author's sample locations

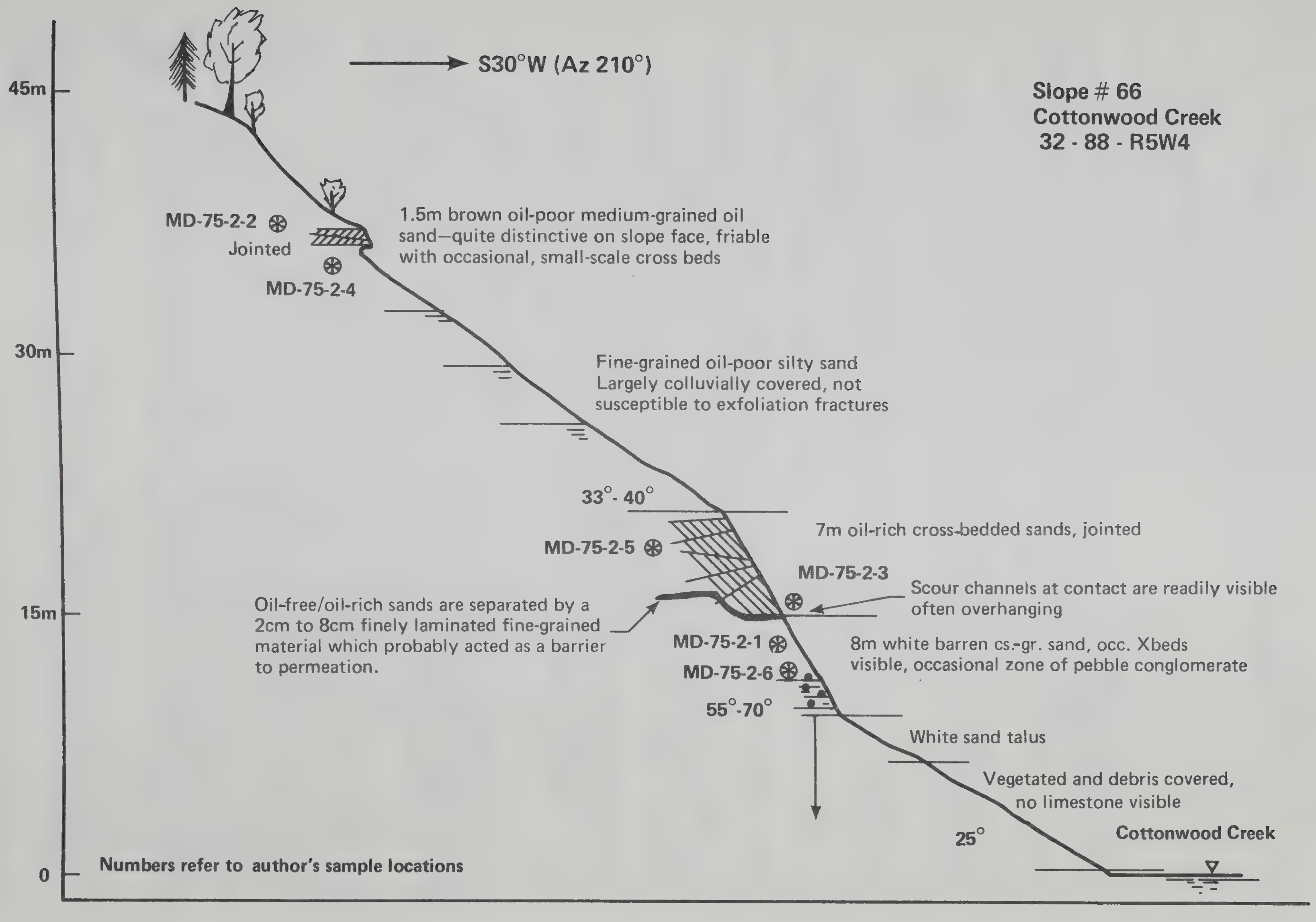
Slope # 66
Cottonwood Creek
32 - 88 - R5W4
S30°W (Az 210°)
45m
30m
15m
0
MD-75-2-2
Jointed
MD-75-2-4
1.5m brown oil-poor medium-grained oil sand—quite distinctive on slope face, friable with occasional, small-scale cross beds
Fine-grained oil-poor silty sand Largely colluvially covered, not susceptible to exfoliation fractures
33°- 40°
MD-75-2-5
7m oil-rich cross-bedded sands, jointed
MD-75-2-3
Scour channels at contact are readily visible often overhanging
Oil-free/oil-rich sands are separated by a 2cm to 8cm finely laminated fine-grained material which probably acted as a barrier to permeation.
MD-75-2-1
MD-75-2-6
8m white barren cs.-gr. sand, occ. Xbeds visible, occasional zone of pebble conglomerate
55°-70°
White sand talus
Vegetated and debris covered, no limestone visible
25°
Cottonwood Creek
Numbers refer to author's sample locations

APPENDIX B

SAMPLE PREPARATION AND MOUNTING FOR SHEARBOX AND TRIAXIAL TESTING

B.1 Oil Sand Specimen Preparation

B.1.1 General Comments

Specimens were prepared in a cold room at a temperature of -15° to -20°C. Initial sampling attempts indicated that special considerations are necessary in preparing oil sand specimens:

1. Warm temperatures must be avoided as they greatly accelerate specimen deterioration.
2. Even at relatively cold temperatures (-15°C), specimen expansion continued slowly when confining stress was relieved (resulting in one case in a further volumetric expansion of 3.6% in two weeks).
3. Normal equipment for specimen preparation (e.g. trimming frames, trimming rings, Shelby tubes) were tested and found to be inadequate.

The following special techniques were used for preparation of all specimens:

1. A four-speed belt-driven lathe with 7.62 cm diameter ends was used as the basic trimming tool.
2. Tungsten carbide-tipped bits proved necessary: oil sand specimens require the use of materials with extremely high resistance to abrasion. Three types of bits were used; their designs and functions are illustrated in Figure B.1.
3. All specimens were stored, opened, trimmed, and mounted in a chilled state; they were allowed to warm to room temperature only after the application of a confining or normal stress.

B.1.2 Shearbox Specimen Preparation

The plastic liner was removed carefully from a length of core, and the ends of the sample were trimmed with a hack saw or with a dry diamond saw to form roughly flat, parallel end surfaces. Samples were centered securely on a lathe, and axial pressure was applied by a screw jack to provide the necessary stability during rotation.

Sample eccentricity was removed by cutting with a general trimming bit at the extremely slow rate of two revolutions per second. The rotation rate was then increased to about four revolutions per second, and the general trimming bit was used to trim the specimen diameter to 64.5 mm (about one millimeter above gauge diameter). Several sharp general trimming bits were required for this process, as the angularity and toughness of the quartz grains caused rapid bit abrasion. Dull bits caused specimen surface corrugations and an increase in specimen temperature; therefore bits were changed as soon as wear became evident.

Initial cuts were made with the general trimming bit; the final gauge cut was made with the gauge bit. Several passes of the gauge bit along the sample were made to assure maximum regularity of the cylinder.

The undercut bit was used to shape flat parallel ends. The bit

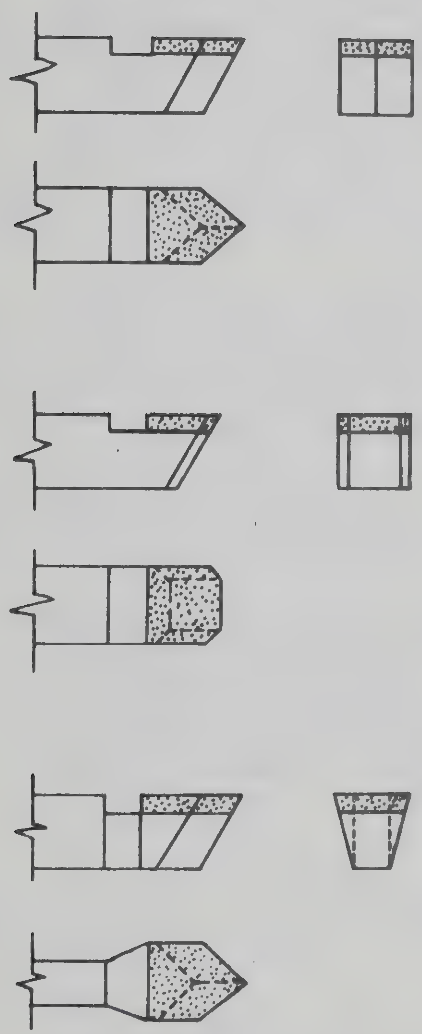

a) General Trimming Bit
  - large scale removal of material

b) Gauge Bit
  - final diametric trimming
  - flat end minimizes gauge wear

c) Undercut Bit
  - cutting slots for ends of specimens
  - undercut edges minimize balling, heat generation, and gouging

Figure B.1 Tungsten-Carbide Tipped Specimen Trimming Bits: Design and Function

was guided directly into the cylinder to create parallel-sided slots with a two-centimeter "neck" remaining between specimens (Figure B.2). Each specimen was about 2.54 cm thick. This procedure assured uniformity of size and shape.

The specimens were removed from the lathe, the connecting necks were broken, and excess material at the neck was trimmed with a scalpel. Hand grinding on coarse (80-C), then fine (280), silicon carbide paper removed end irregularities.

After the final trimming and sanding of specimens, the volumes and total weights were measured. The shearbox was prechilled and assembled in a chilled state. Brass porous end plates and single thicknesses of filter paper were used at both ends of specimens to provide complete drainage during testing.

B.1.3 Triaxial Specimen Preparation

Uniform, right circular cylinders were used for triaxial testing. Because the oil sand core available was 9.4 cm in diameter, standard 10.16 cm diameter triaxial cells were modified to accomodate specimens of 7.62 cm in diameter and 15.5 to 20.0 cm in length.

It was essential that the length of core chosen for trimming be relatively uniform and free of any incipient or actual bedding plane separations. Many core lengths were rejected as unsuitable for testing for various reasons:

1. Differing lithologies in many cases resulted in differential expansion, causing visible discontinuities.
2. Oil-rich specimens displayed excessive expansion, and generally were not suitable for testing.
3. Specimens containing significant sections of clay-rich bands were rejected, as it was desired to test only the arenaceous oil sands which comprise the majority of the deposit.
4. Core lengths of less than 28 cm could not provide the necessary 15.5 to 20.0 cm required for triaxial testing.

The trimming procedure followed after specimens were selected was very similar to that employed in shearbox specimen preparation (Section B.1.2). End pieces were used for bitumen content determinations and grain size analyses.

B.1.4 Triaxial Specimen Mounting

Clean triaxial cells, with silicon grease applied to the base O-ring seal, were chilled in a cold room for several hours prior to mounting. The triaxial specimens were weighed and measured (to determine bulk densities), then sheathed with 7.11 cm diameter latex membranes using a standard membrane stretcher. In the initial tests, porous Teflon end drainage plates were used, but, because the compressive behaviour of the Teflon was unknown, porous stainless steel end plates were used in subsequent tests. The stainless steel end plates were separated from the specimens by finely slotted latex membranes. Side drains were not used because permeability data were of interest. The end caps were coated with a thin layer of silicon grease to ensure an adequate seal. All membranes were sealed to the end caps with double O-rings.

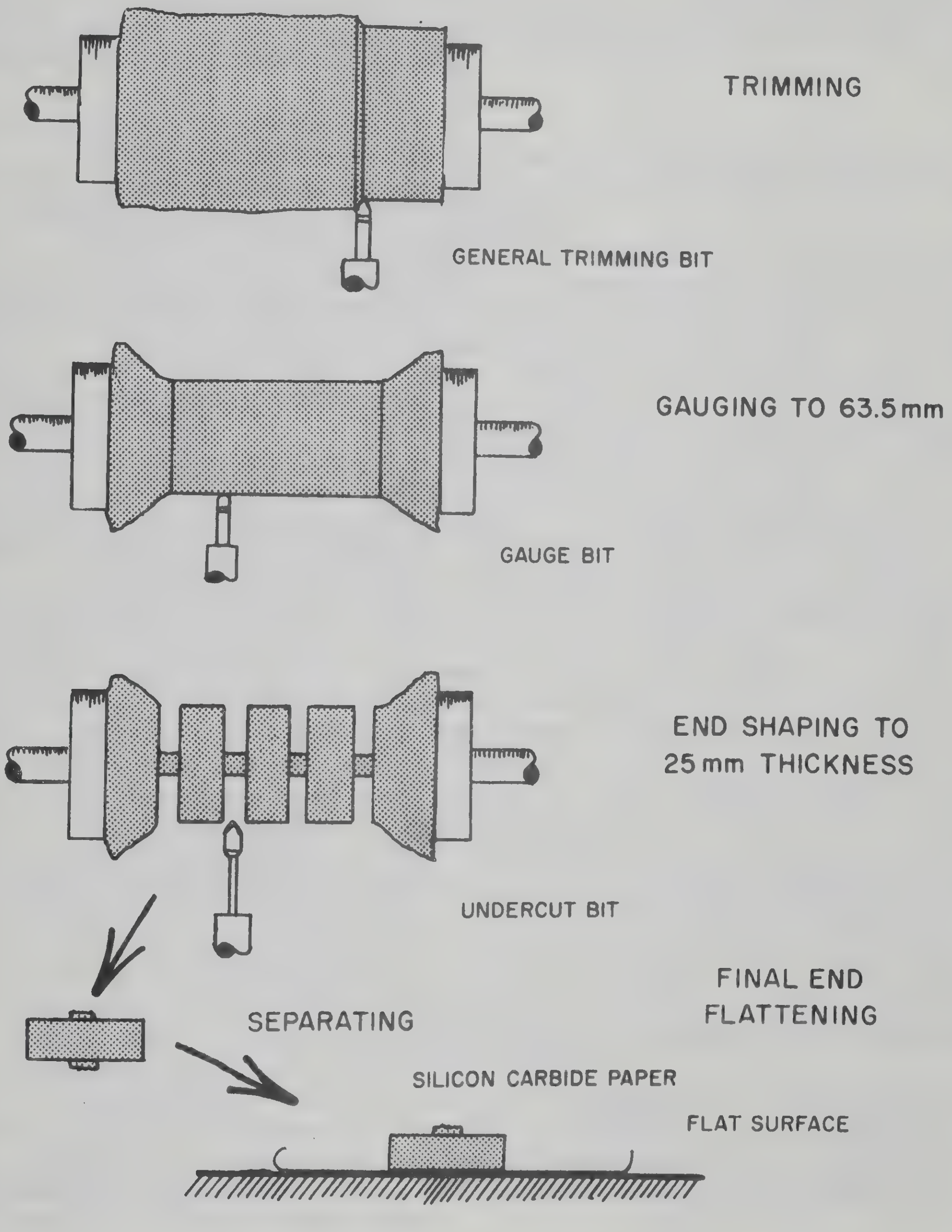

FIGURE B.2

STAGES IN SHEARBOX SPECIMEN TRIMMING

B.2 Specimen Preparation for Oil-Free Orthoquartzites

Different methods were required for the preparation of specimens of oil-free orthoquartzites (i.e. St. Peter Sandstone, Swan River Sandstone, and Swan River preglacial sand) than those employed in the preparation of oil sand specimens.

B.2.1 Shearbox Specimens

Unsaturated medium- and fine-grained uncemented arenaceous materials may, with sufficient care, be sampled in block form by hand to provide adequate laboratory specimens.

Because the materials sampled were generally very brittle and tended to fracture when placed under stress in an unconfined state, the block samples were pretrimmed to yield smaller blocks of suitable size for test specimens. The original St. Peter Sandstone block samples were cylinders about 30 cm in diameter and 50 cm in length. All samples were coated with a silicate solution. The top and bottom five centimeters of each cylinder were cut off with a band saw and discarded. A five centimeter disc was cut from the sample, and divided into seven portions (Figure B.3) by careful cutting with a band saw. The outer skin (three centimeters on all sides) was trimmed and discarded, and individual blocks were wrapped in plastic to prevent dessication.

A 6.35 cm diameter brass ring, 2.54 cm high, with a shaped cutting edge, was designed and built to trim specimens. Sample blocks were set on loose sand on a table in a cool, humid room. The brass ring was placed on top of each sample, and excess sand was removed with a fine- or medium- toothed hack saw blade (or with a small spatula) and a scalpel. The brass ring was pushed through the sample by gentle tapping with the wooden spatula handle. When about five millimeters of the specimen protruded from the top of the ring, the excess sandstone was removed carefully, and the ends were flattened with a sharpened straight edge (Figure B.3). The filled brass ring was weighed, cuttings were preserved for moisture determinations or other analyses, and specimens were inverted onto a porous Teflon end drainage plate which sat on a small pedestal. The close-fitting Teflon end plate served as an extrusion piston to push the specimen into the shearbox, and was left in place during testing as a porous end plate. The shearbox was mounted, a normal load was applied, saturation was accomplished by flooding with water, and testing ensued.

Shearbox specimens of Swan River Sandstone and Swan River preglacial sand were trimmed by the same methods used in trimming St. Peter Sandstone, except that the specimens were trimmed directly from the sample block and were separated by sawing with a hack saw blade at the base of the trimming ring.

B.2.2 Triaxial Specimen Preparation

Of the orthoquartzites discussed in Chapter VI, only St. Peter Sandstone samples were tested in a triaxial apparatus.

The triaxial testing of St. Peter Sandstone required 3.81 cm diameter specimens at least 7.62 cm long. A 12 cm long block with a square 5.6 cm cross section was cut with a band saw from the block sample of sandstone. A small hole was made in each end precisely in the center, two latex squares were placed over each end, and the block was mounted in a wire saw trimming frame normally used in the preparation

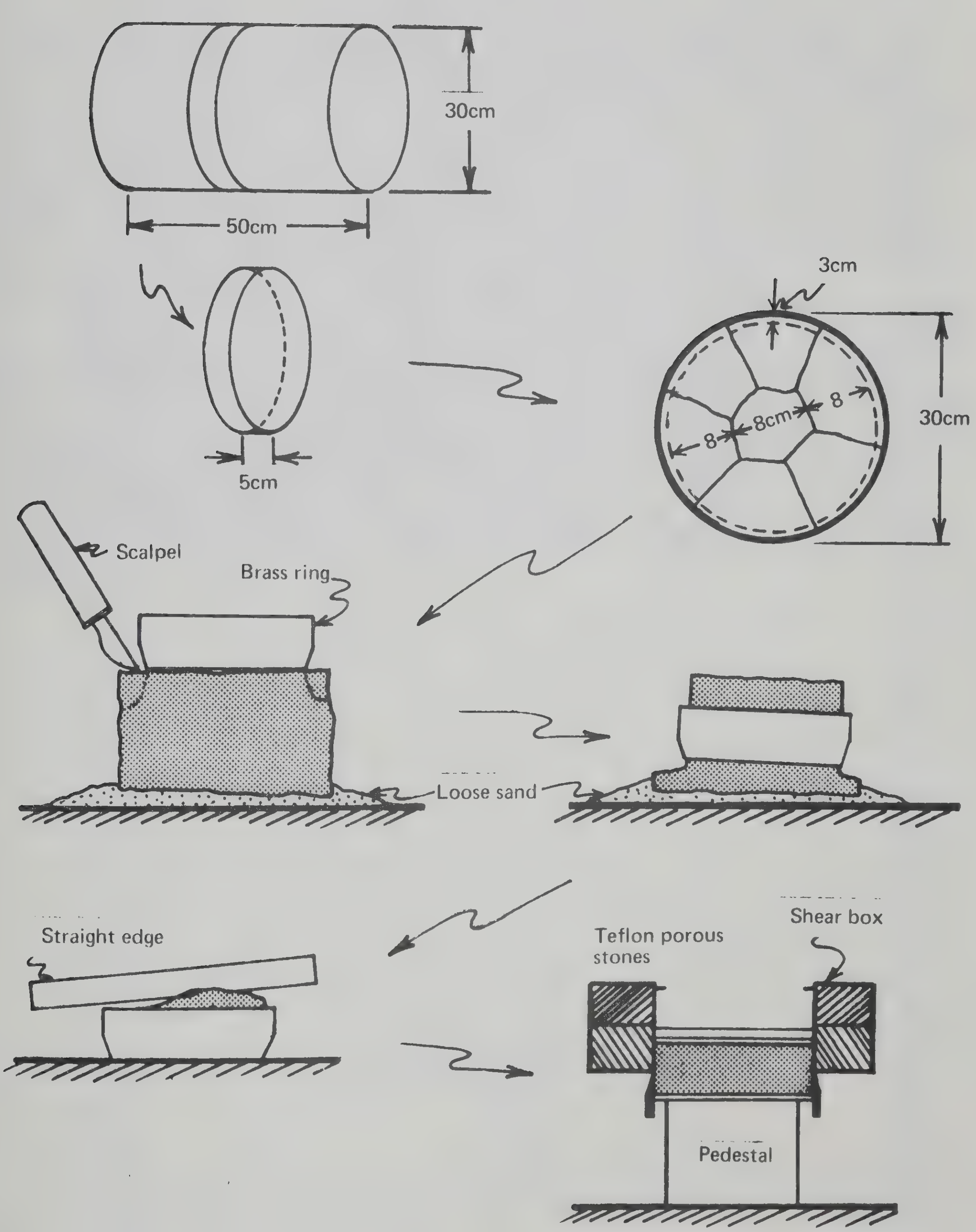

Figure B.3 Preparation of Shear Box Specimen of Locked Sand

of soft clay specimens. The small holes accommodated the metal centering prong on the trimming frame end caps (Figure B.4); without the holes, samples split longitudinally. The latex was necessary both to prevent splitting due to stress concentration at uneven points, and to provide sufficient friction between the end caps and the sample to allow free turning so that a cylindrical specimen could be obtained. A sharpened straight edge was drawn carefully over the specimen surface (normal to the specimen to prevent splitting) until a 3.81 cm diameter cylindrical central portion at least 9.5 cm long was obtained. A U-shaped end trimmer and a coarse-toothed hack saw blade were used to roughly square the ends, and a sharpened straight edge smoothed the end surface for testing. Blowing on the specimens removed loose grains. Specimens were weighed carefully, and measured with calipers.

Extreme care was necessary in all phases of specimen preparation, and, despite the precautions taken, only four successful triaxial tests were completed from 12 original specimen blocks. At no time during mounting, saturation under back pressure, or permeability testing could the pore fluid stress be allowed to approach the cell stress: specimens immediately disaggregated into a mass of loose sand when pore fluid stress equalled the cell fluid stress. Even the exposure of a block to water is catastrophic: capillary tension draws water in, to the point of saturation, and the unstressed block collapses under its own weight.

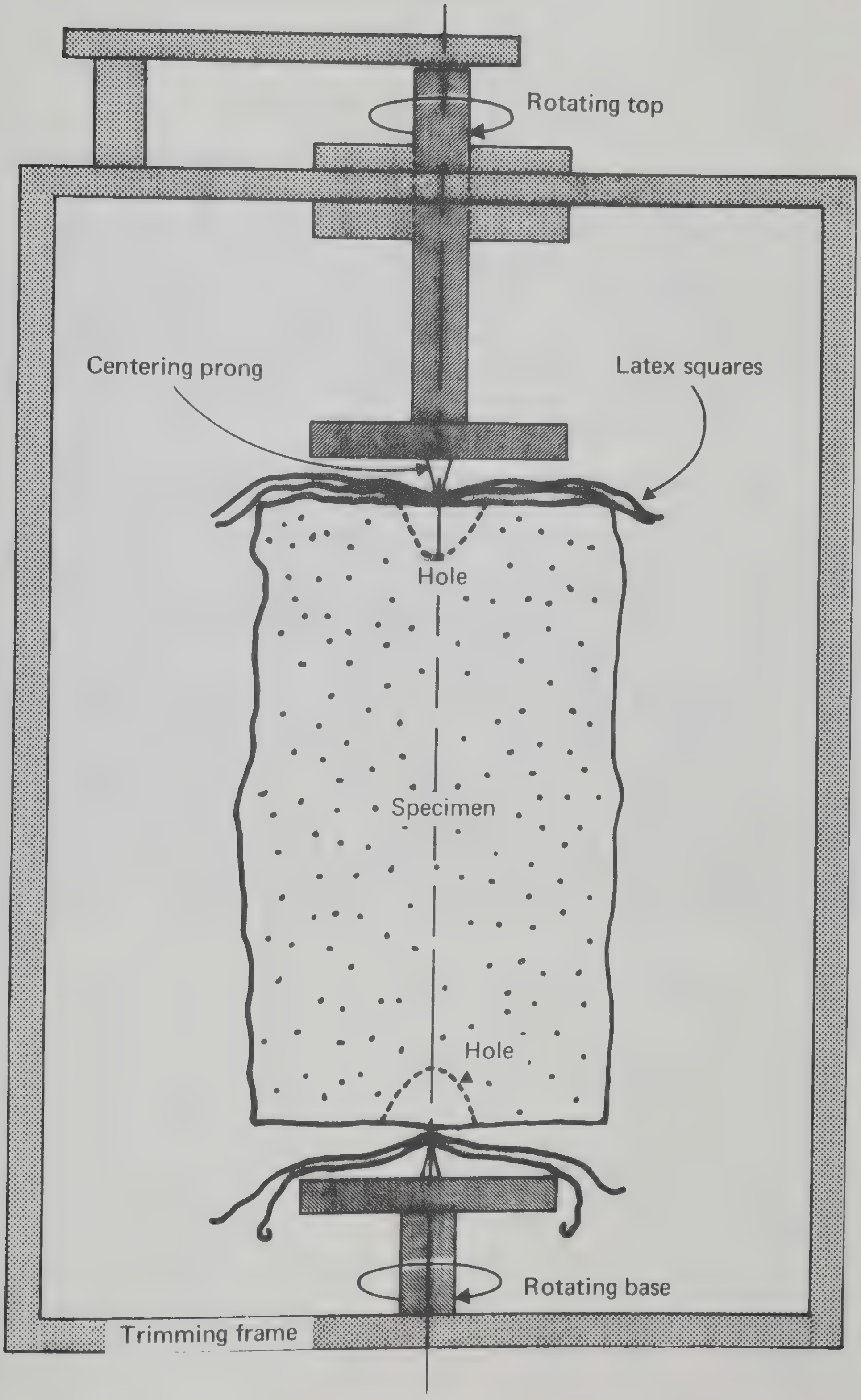

Figure B.4 Trimming Locked Sand Specimens

APPENDIX C

STRENGTH TESTING EQUIPMENT

C.1 Testing Equipment

Because the core obtained in the sampling program was cylindrical in shape and less than 10 cm in diameter, certain limitations were imposed on the strength testing program. A circular shearbox (Figure C.1) was used for all shear tests. This permitted lathe trimming and rapid density determination of circular specimens. Testing of compacted silty sands and fine-grained sands required the design and use of a circular shearbox (Figure C.2) with a sealed end cap which fit sufficiently tightly to prevent the escape of any sand or silt, yet sufficiently loosely to have negligible effect on normal loads.

The designed shearbox met these specifications completely: an upwards force of only one-half kilogram was required to remove the end cap, and friction was reduced further by lubrication of the shearbox sides before testing with silicone spray. Micrometer measurements were used to determine sample height after compaction.

The triaxial testing program employing gelatin as a pore fluid required standard 10.16 cm diameter cells equipped with copper refrigeration coils (Figure C.3). All cells were reinforced with several windings of Fiberglas tape (under tension during wrapping), since cell pressures of up to 16 kg/cm^2 were to be employed. Assembly of the sand specimens took place in a brass, three-part mould sitting on a machined retention ring at the cell base (Figure C.4). Compaction of oil-rich, pit-run oil sands required a one-piece stainless steel mould 10.16 cm in diameter and 20.32 cm in length, with a wall thickness of 1.27 cm. Modifications were made to standard 10.16 cm diameter triaxial cells to accommodate 7.62 cm diameter cylindrical oil sand specimens for testing.

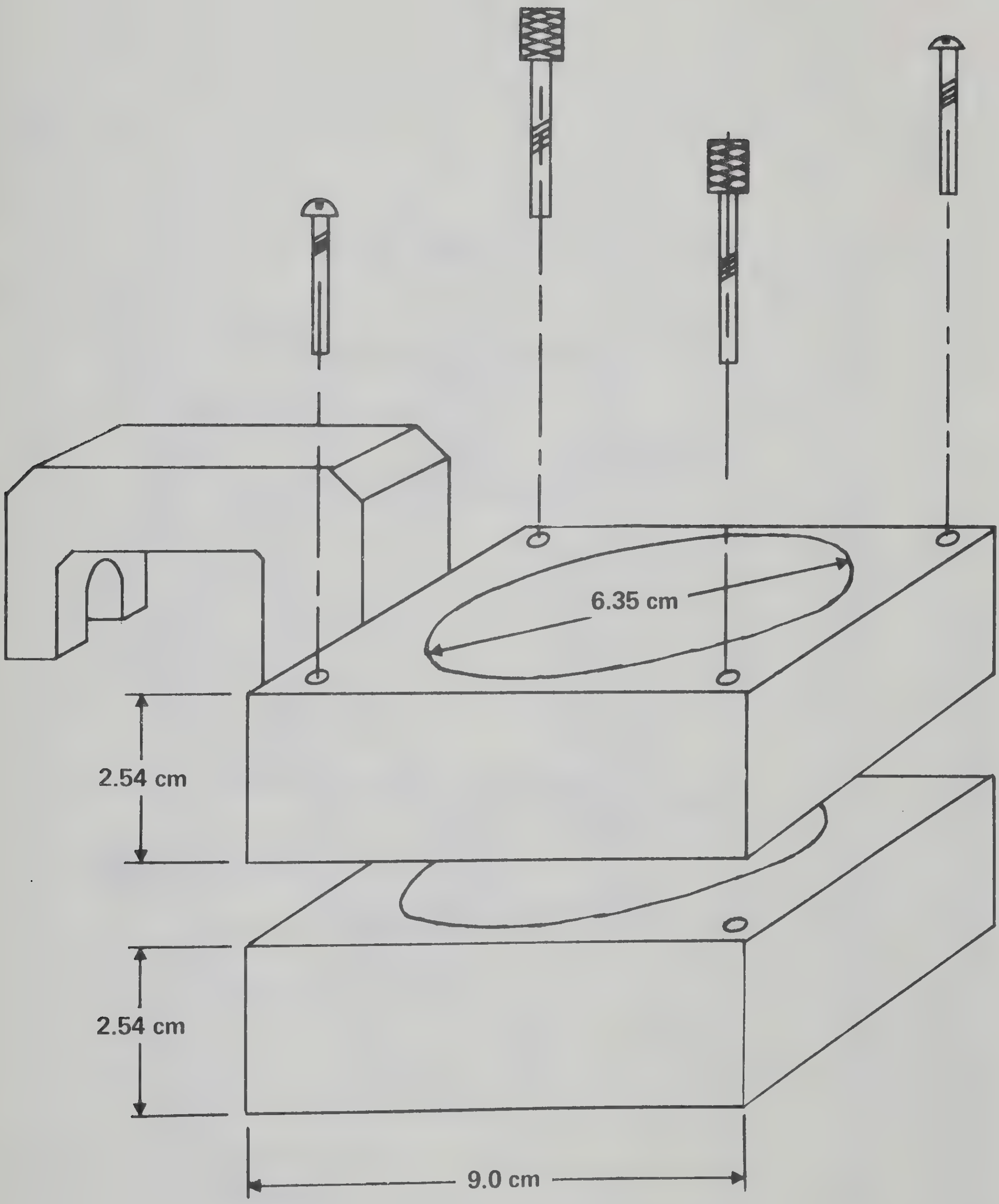

Figure C.1 Circular Shearbox

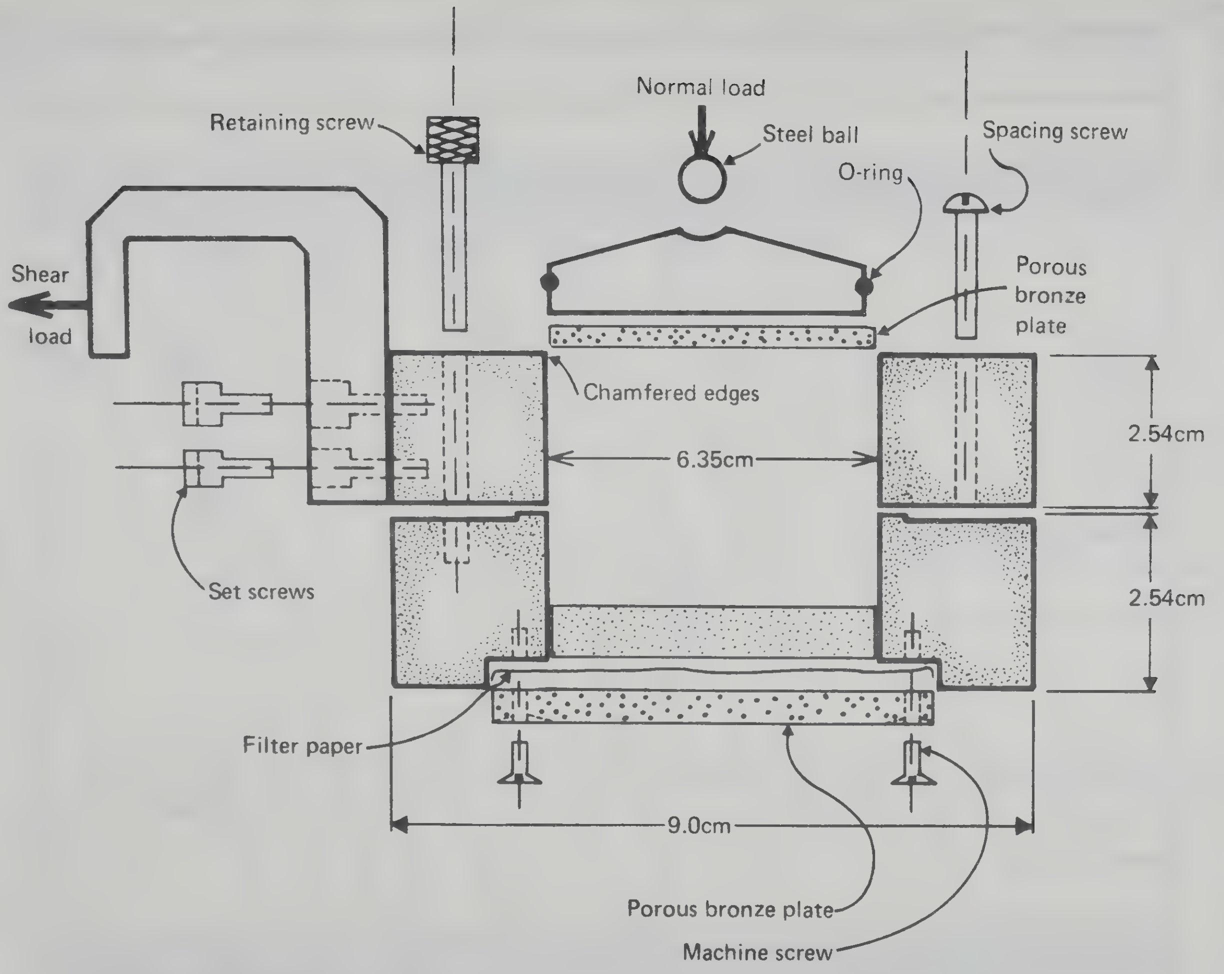

Figure C.2 Circular Shearbox with Modifications for Sand Compaction

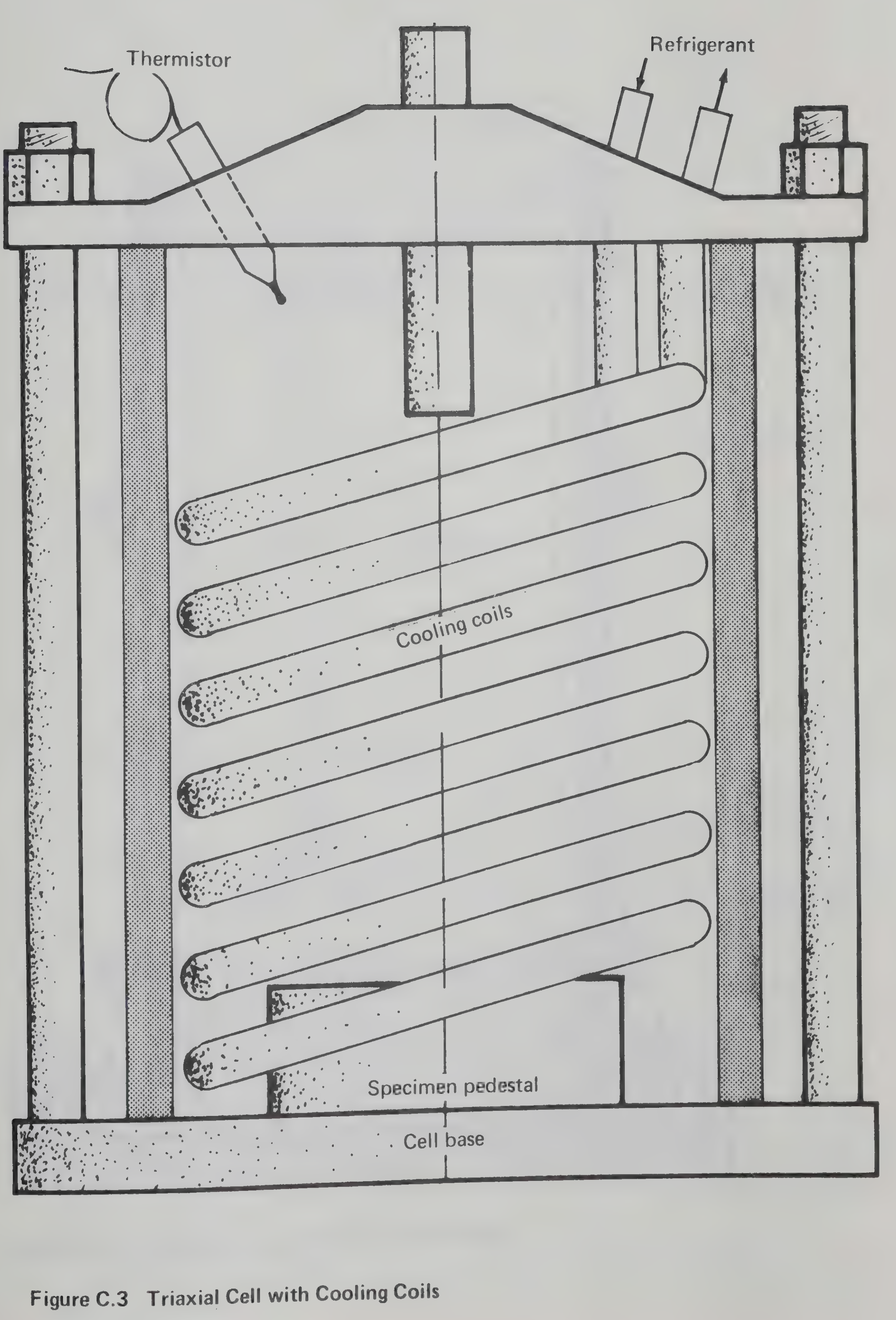

Figure C.3 Triaxial Cell with Cooling Coils

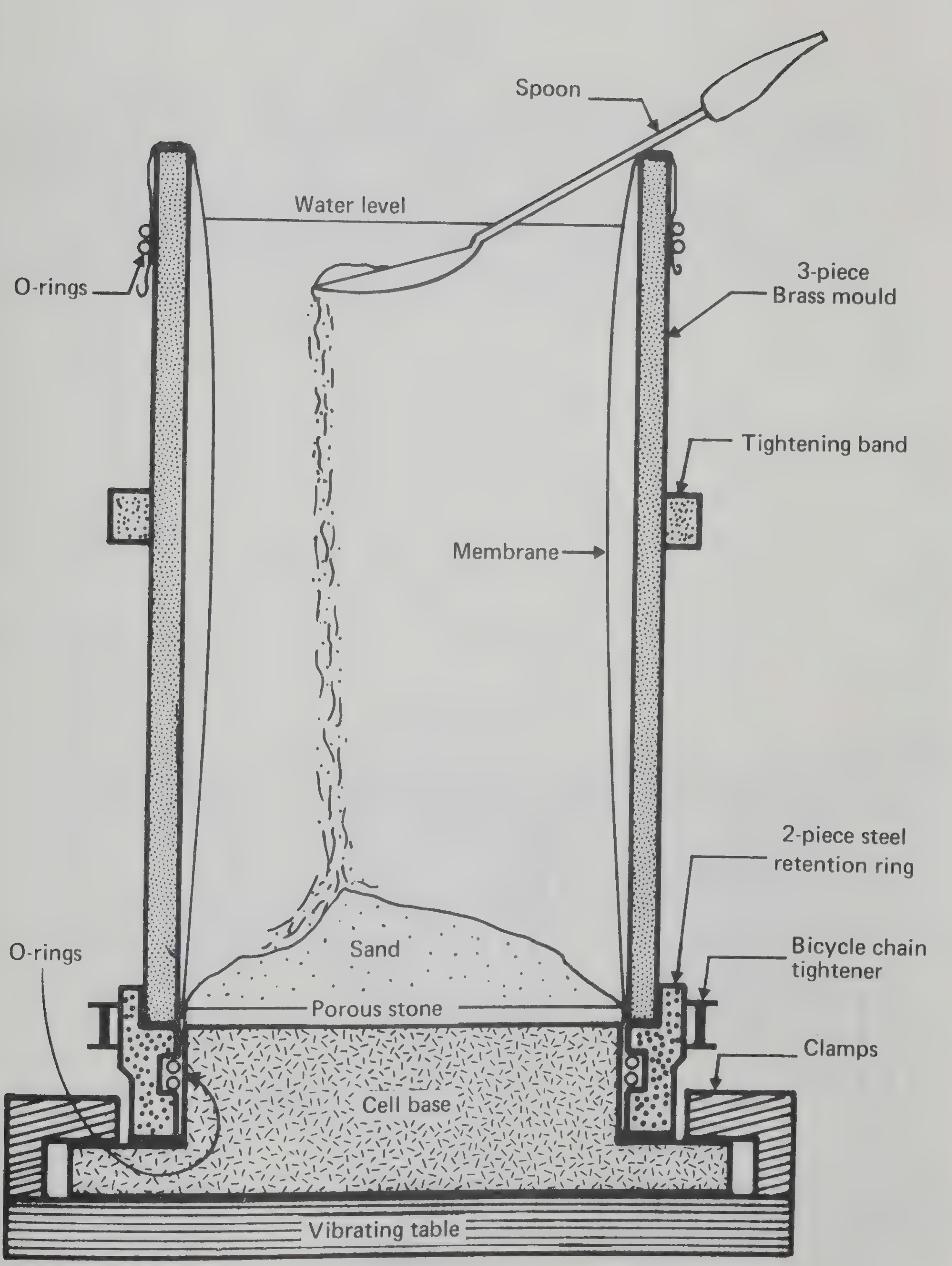

Figure C.4 Moulding Dense Sand Triaxial Specimens

APPENDIX D

The grain size curves below, and in Table D.1 on the following page demonstrate the great lithologic variability of the Athabasca Oil Sands. All specimens in the grain size curves are from the oil-free portion of the Cottonwood Creek outcrop (Appendix A, Slope 66) or from the High Hill River outcrop (Appendix A, Slope 65).

Table D.1 contains data from the borehole which provided the strength testing specimens. The numbers in the column labelled "Specimen" refer to the depths in feet below ground surface.

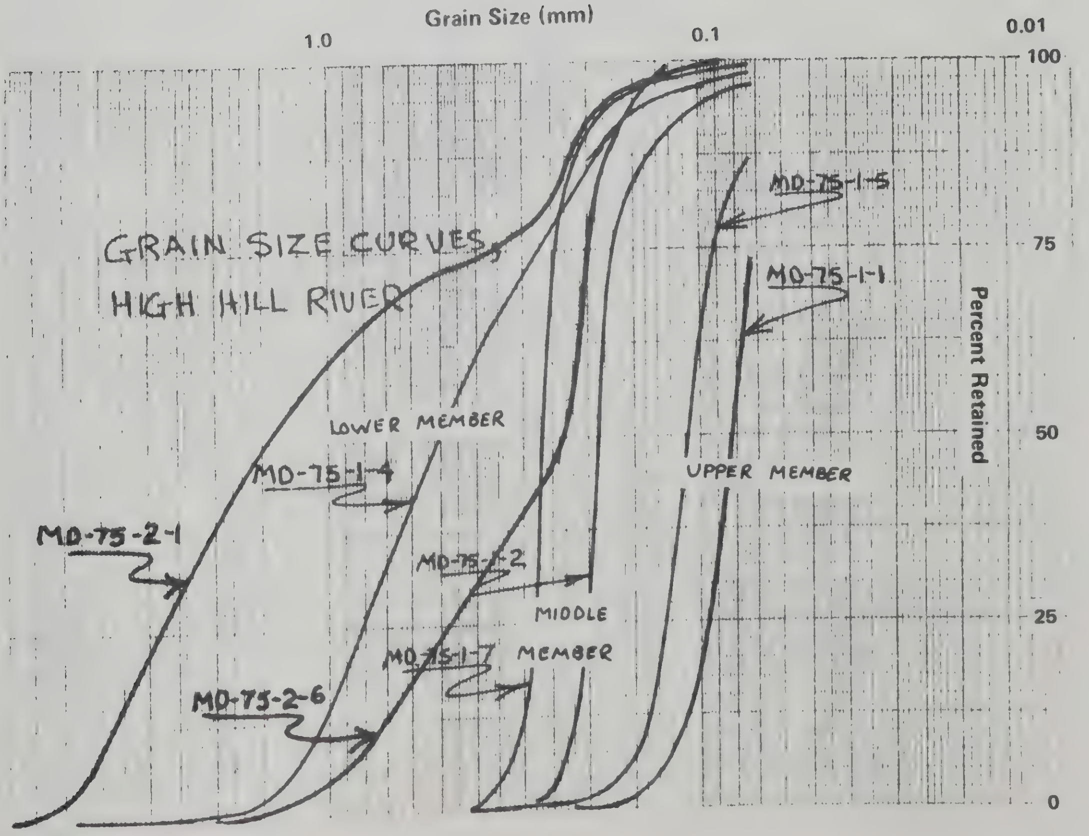

TABLE D.1

SELECTED DATA ON OIL SAND SPECIMENS

(BD = Bulk Density; O = Oil content by total weight; M = percent water; D50 = Median grain diameter in mm)

Specimen	Data and Comments
91.2	BD = 2.23; O = <1%; silt
118.0(A)	O = 11.1%; M = 3.2%
118.0(B)	O = 9.5%; M = 5.7%
119.2	O = 0%; D50 = 0.0050; clay-shale
121.0	BD = 2.19; O = 8.3%; M = 1.3%; concretions
121.5	BD = 2.03; O = 13.8%; M = 2.8%
126.4	BD = 2.04; M = 7.2%; O = 5.0%
126.7	BD = 1.92; M = 7.9%; O = 6.0%
127.0	BD = 1.81; O = 5.8%; M = 9.1%; 2 specimens
127.7	BD = 2.36; M = 1.9%; concretion
127.8	O = 6.3%; D50 = 0.100
127.9	BD = 2.12; O = 6.2%; M = 6.9%
134-135	BD = 2.20; O = 3.3%; M = 7.1%
149	O = 0%; D50 = 0.0150
149.4	O = 2.6%; D50 = 0.108
149.8	O = 2.9%; D50 = 0.105
151.3	O = 3.2%; D50 = 0.109
152.2	O = 5.6%; D50 = 0.115
153	O = 0%; D50 = 0.051; silt
154	O = 0%; D50 = 0.0098; clayey silt
156.7	O = 5.9%; M = 4.3%; dessicated
157.0-157.8	BD = 2.20; O = 0%; M = 11%; 7 samples
158	BD = 2.59; O = 0%; M = 3.4%; concretion
158.6-159.0	O = 0%; M = 11.6%; 5 samples
165	O + M = 15.1% (oil-rich); D50 = 0.160
171.9	BD = 1.86; O = 14.7%; M = 2.0%
174.5	O = 2.0%; M = 13.3%; silty
189.7	O = 12.4%; M = 3.1%; D50 = 0.420
189.8	O = 16.8%; M = 1.4% D50 = 0.415
190.0	O = 14.1%; D50 = 0.440
190.2	O = 14.6%; M = 1.2%; D50 = 0.270
190.3	O = 14.4%; M = 2.5%; D50 = 0.390
190.4	O = 13.5%; M = 4.1%; D50 = 0.390

APPENDIX E

TABLE E.1

TABLE OF CONTENTS

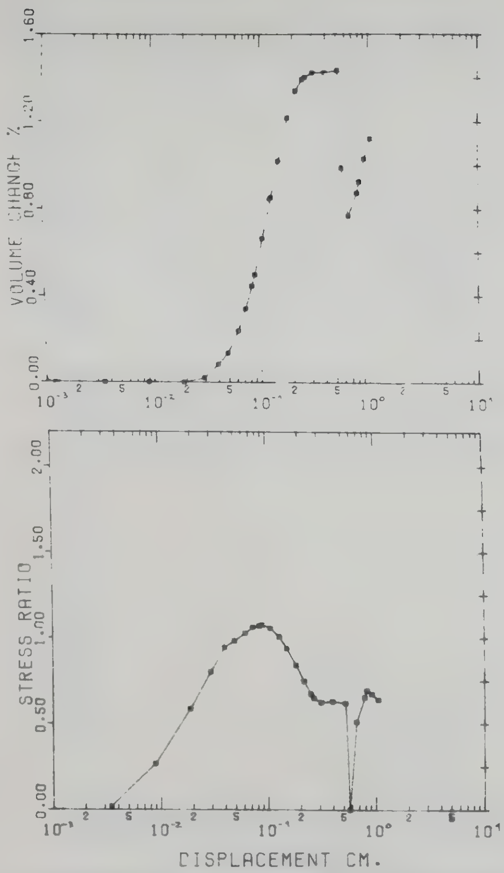

OTTAWA SAND C-109 (FINE) 1.0KG./SQ.CM.

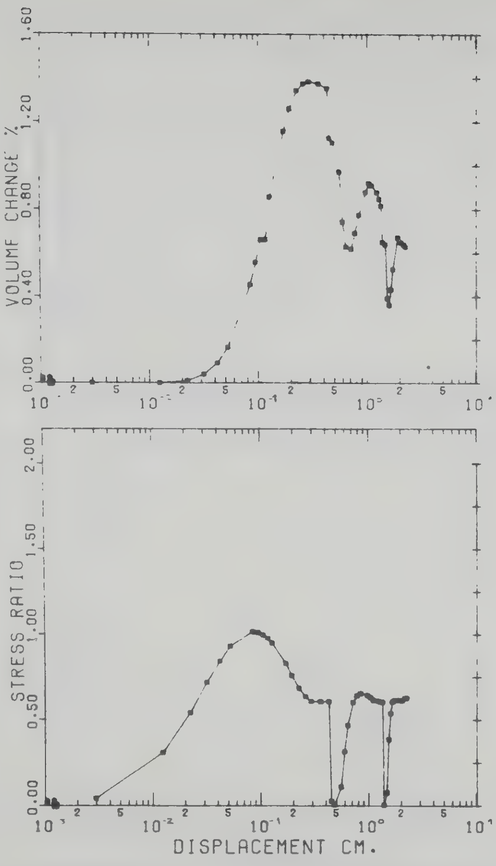

OTTAWA SAND C-109 (FINE) 2.KG./SQ.CM.

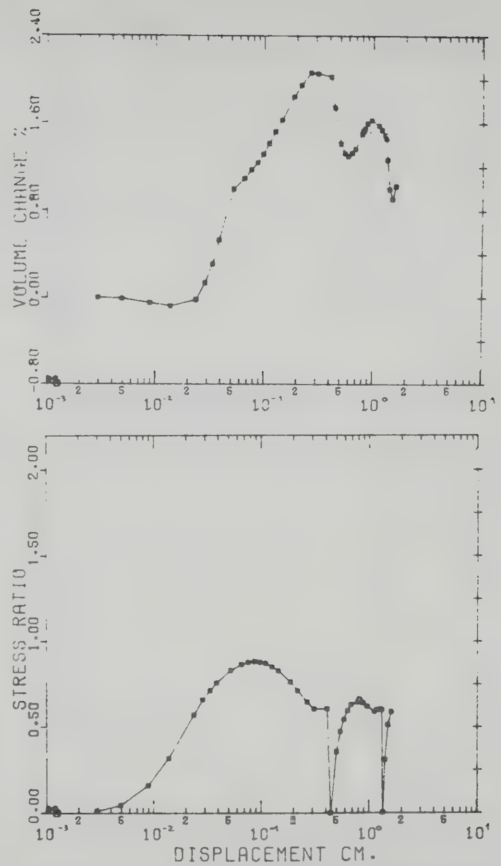

OTTAWA SAND C-109 (FINE) 3.0KG./SQ.CM.

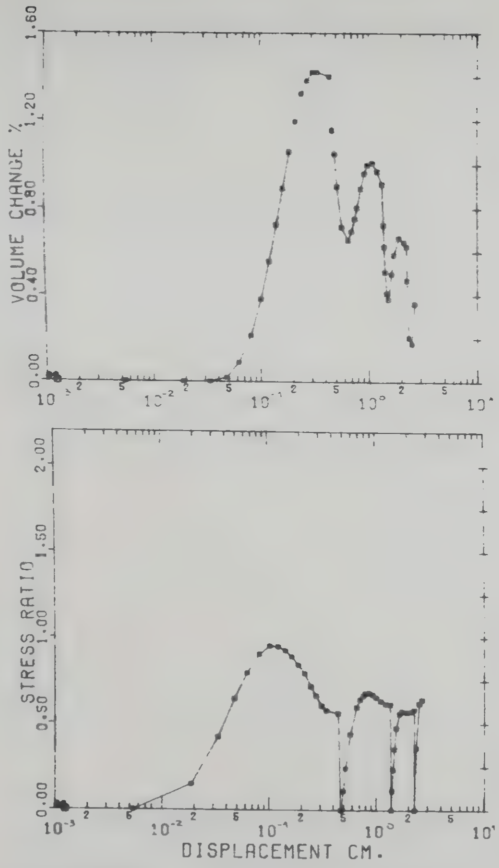

OTTAWA SAND C-109 (FINE) 4.0KG./SQ.CM.

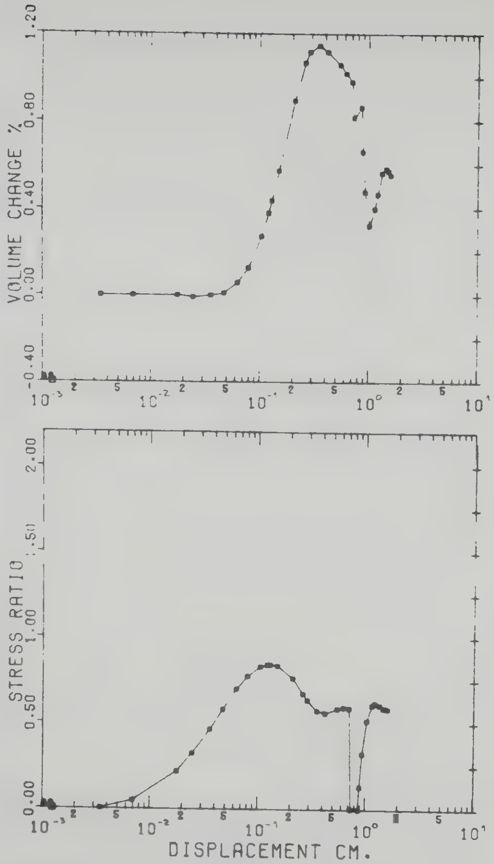

OTTAWA SAND C-109 (FINE) 6.0KG./SQ.CM.

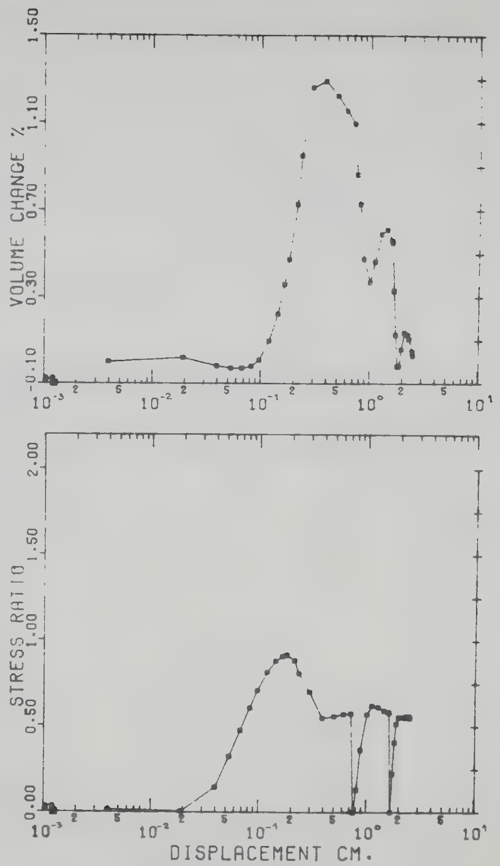

OTTAWA SAND C-109 10 KG/SQ.CM

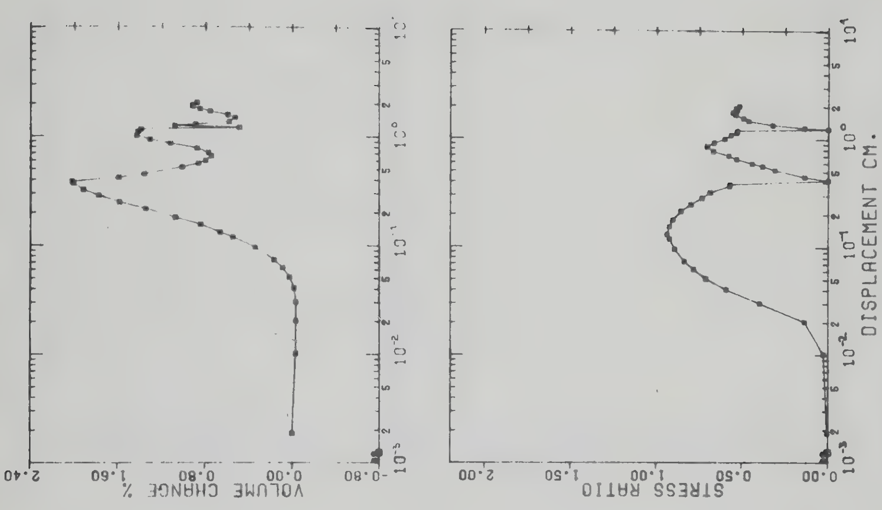

OTTAWA SAND 20-30 MESH 3.0KG./SQ.CM.

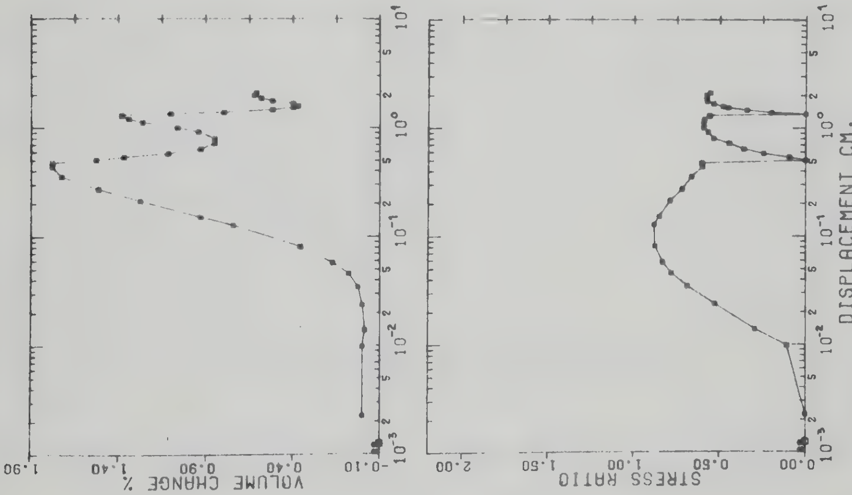

OTTAWA SAND 20-30 MESH 2.0KG/SQ.CM.

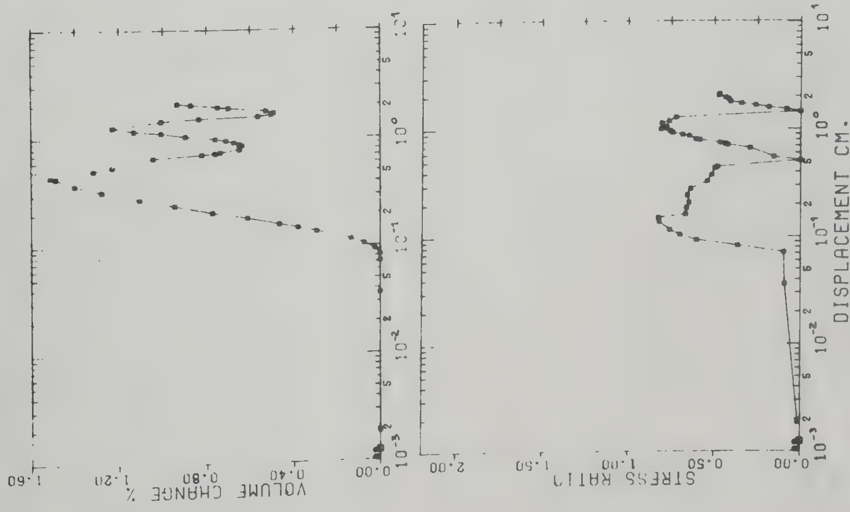

OTTAWA SAND 20-30 MESH 1.0KG/SQ.CM.

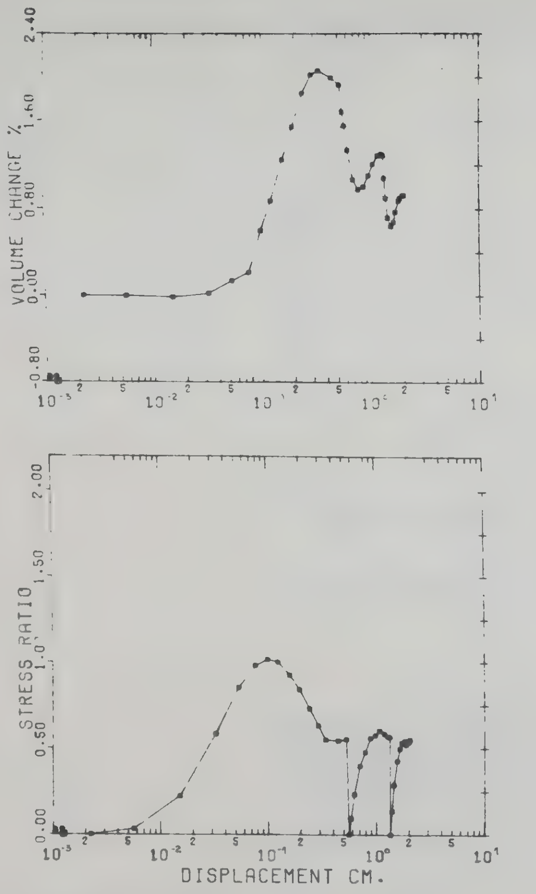

OTTAWA SAND 20-30 MESH 4.0KG./SQ.CM.

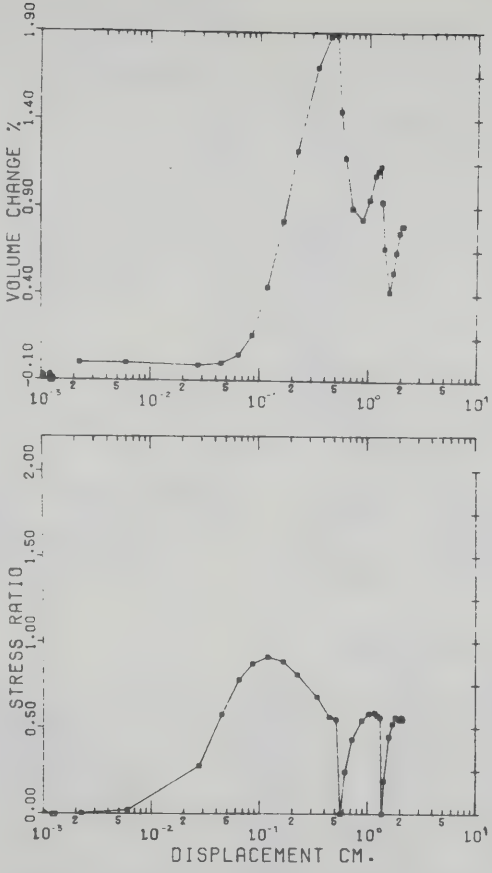

OTTAWA SAND 20-30 MESH 6.0KG/SQ.CM.

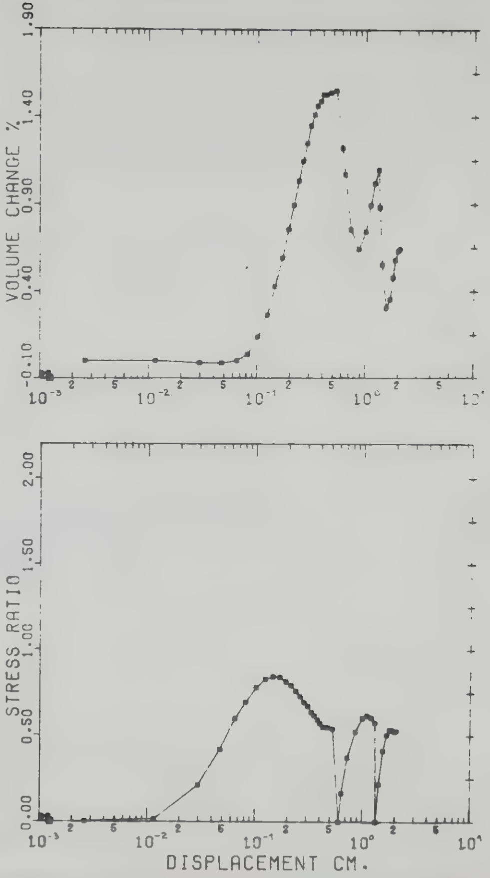

OTTAWA SAND 20-30 MESH 10.0KG./SQ.CM.

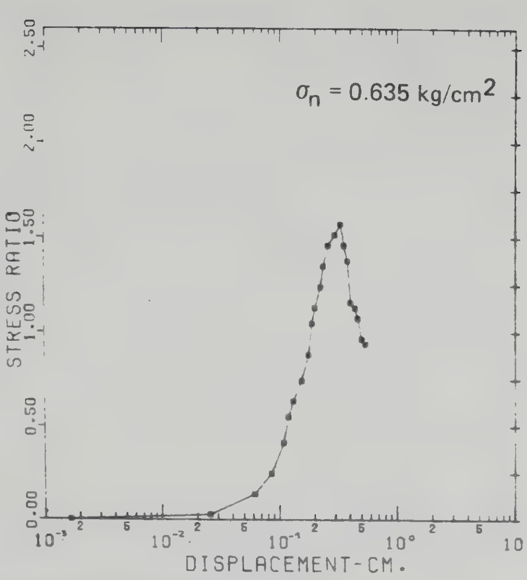

OILSAND SHEARBOX SERIES A TEST 1

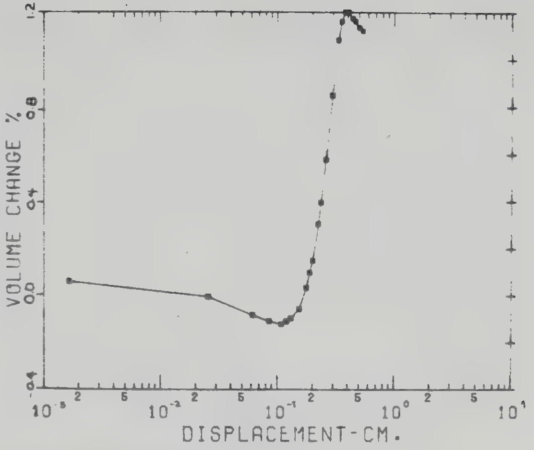

OILSAND SHEARBOX SERIES A TEST 1

Description: Largely oil-free silt, some fine-grained sand; specimen failed in a 6cm square shear box, specimen height = 4.0cm; other specimen bedding features not recorded

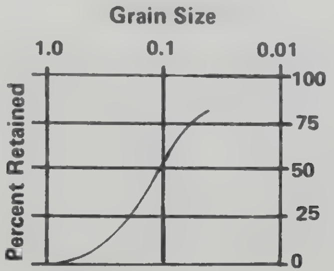

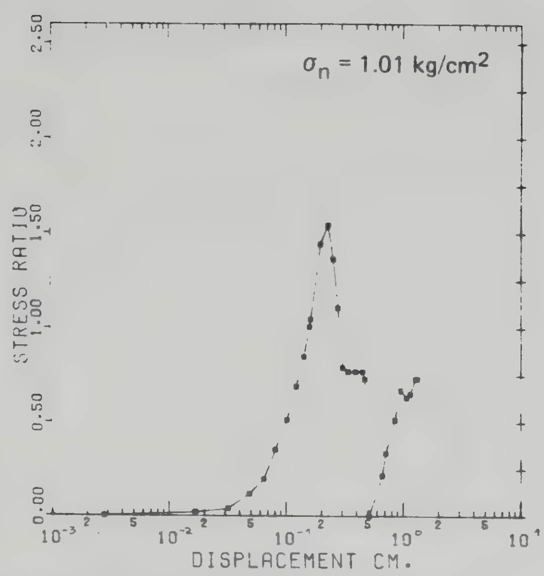

OILSAND SHEARBOX SERIES A TEST 2

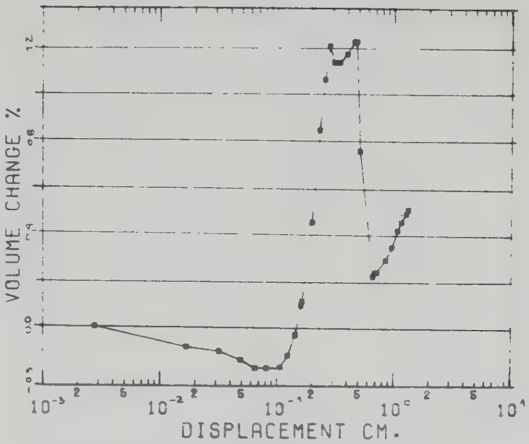

OILSAND SHEARBOX SERIES A TEST 2

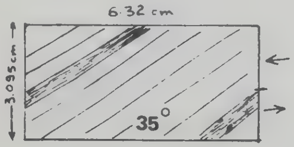

Description: Largely oil-free silt and fine-grained sand, cross-bedded @ 35°

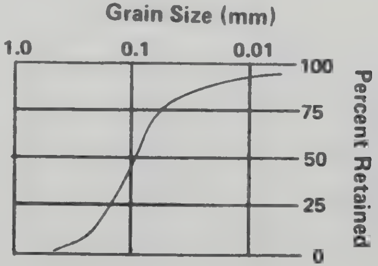

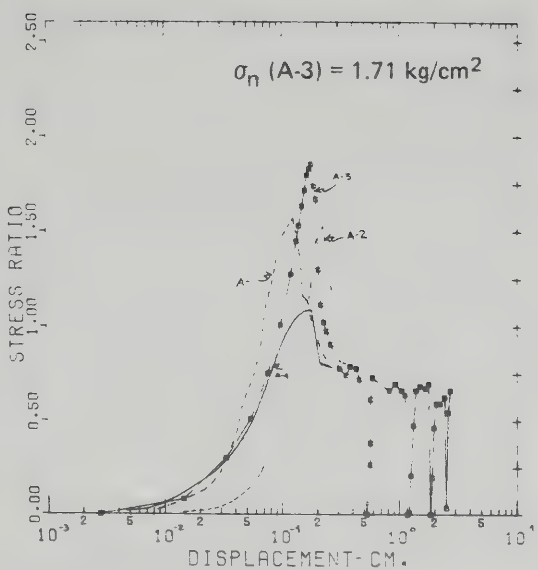

OILSAND SHEARBOX SERIES A TEST 3

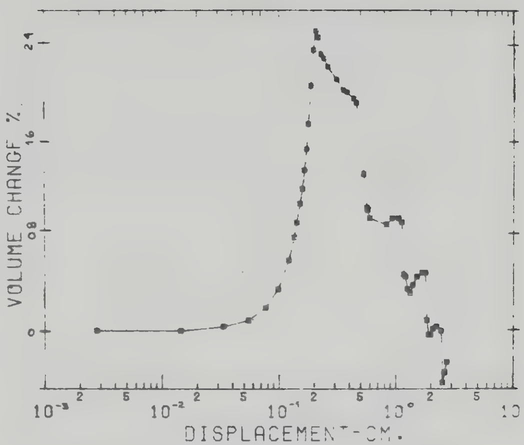

OILSAND SHEARBOX SERIES A TEST 3

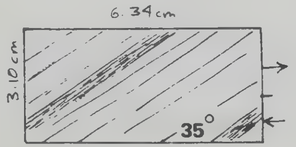

Description: Largely oil-free silt and fine-grained sand, 35° dip to cross beds

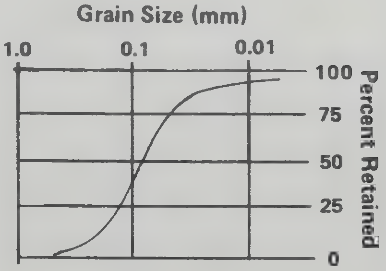

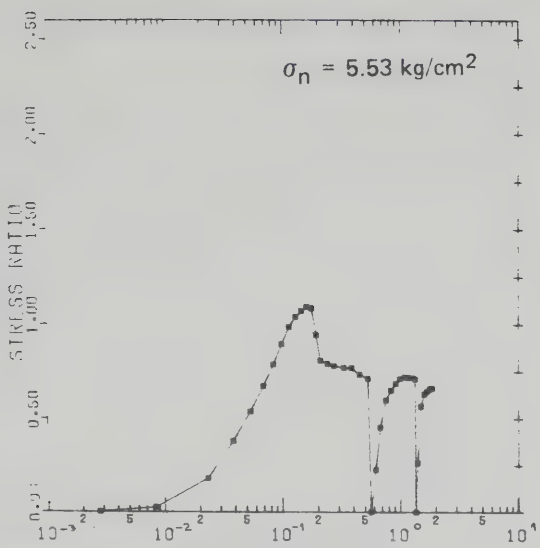

OILSAND SHEARBOX SERIES A TEST 4

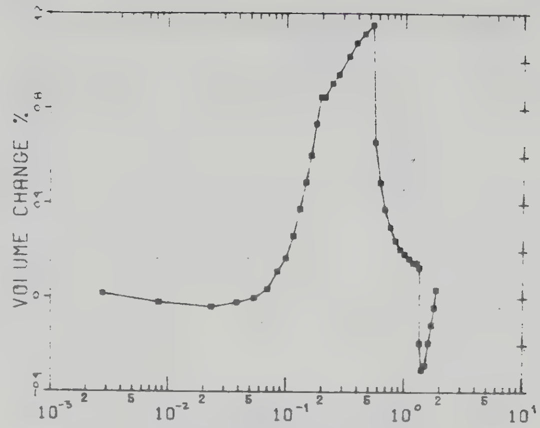

OILSAND SHEARBOX SERIES A TEST 4

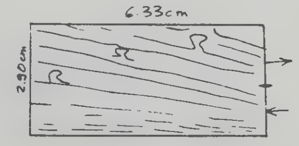

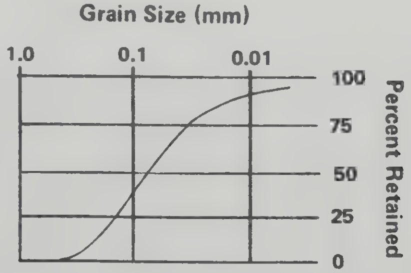

Description: oil-poor fine-grained sand with mottled appearance due to worm casts, clayey band at bottom of specimen. Specimen sheared through sand only.

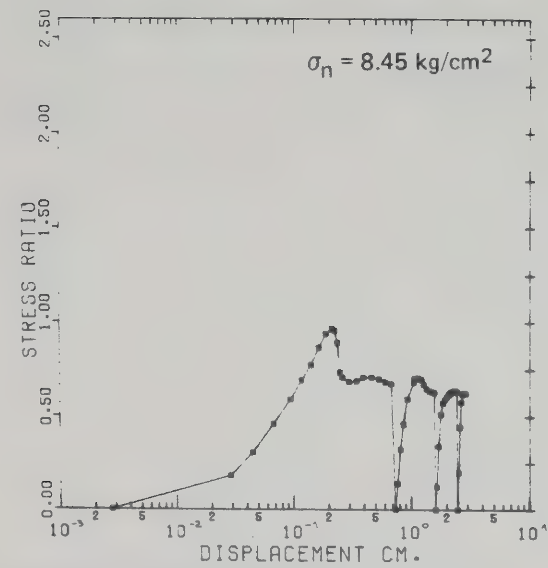

OILSAND SHEARBOX SERIES A TEST 5

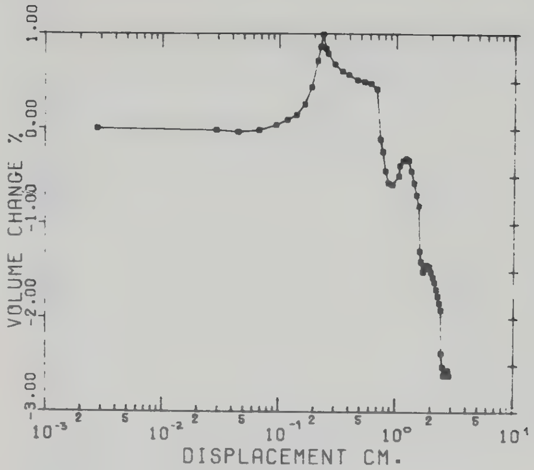

OILSAND SHEARBOX SERIES A TEST 5

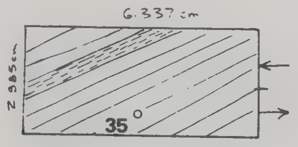

Description: Oil-poor fine-grained sand, bedding dip of 32° - 35°.

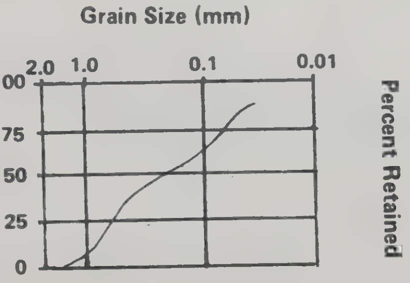

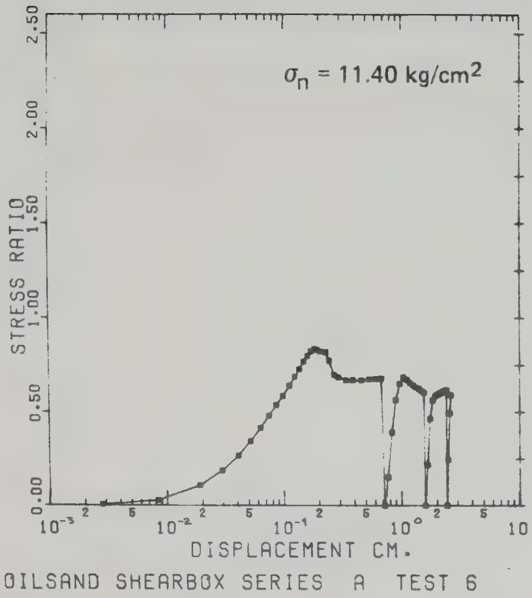

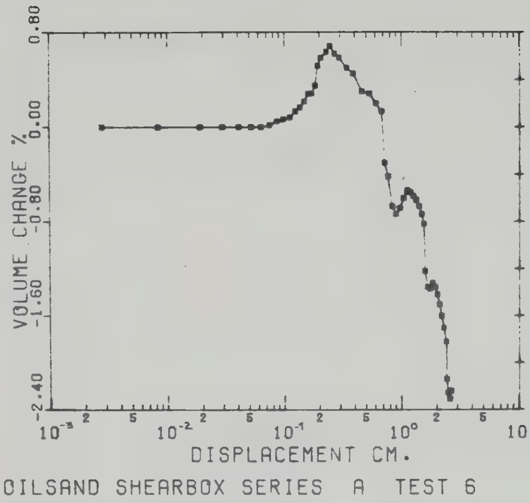

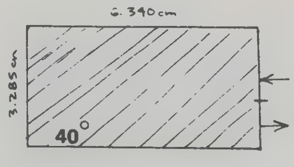

Description: Barren fine-grained sand to silt, cross-bedding averages 40° to plane of specimen

Grain size as for Specimen on previous page

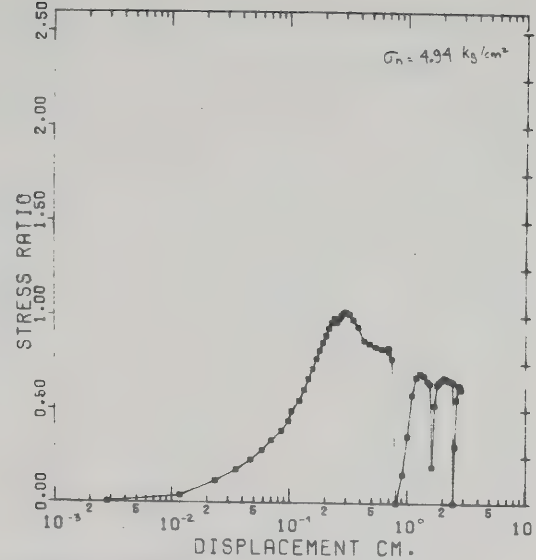

OILSAND SHEARBOX SERIES A TEST 7

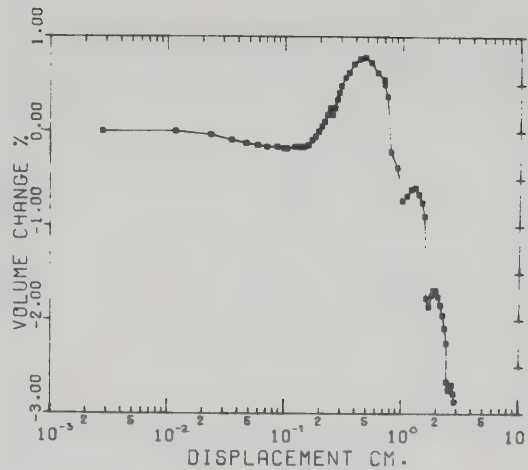

OILSAND SHEARBOX SERIES A TEST 7

OILSAND - A-7

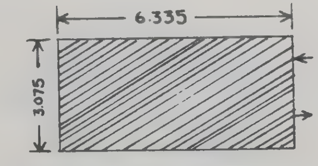

DESCRIPTION : OIL-FREE SILT,
UNIFORMLY CROSS-BEDDED AT 32°,
VARVE THICKNESS ≃ 1 m.m.

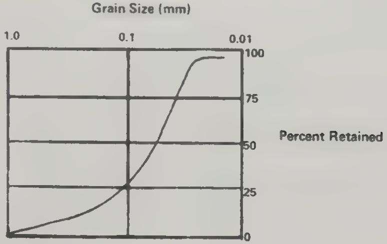

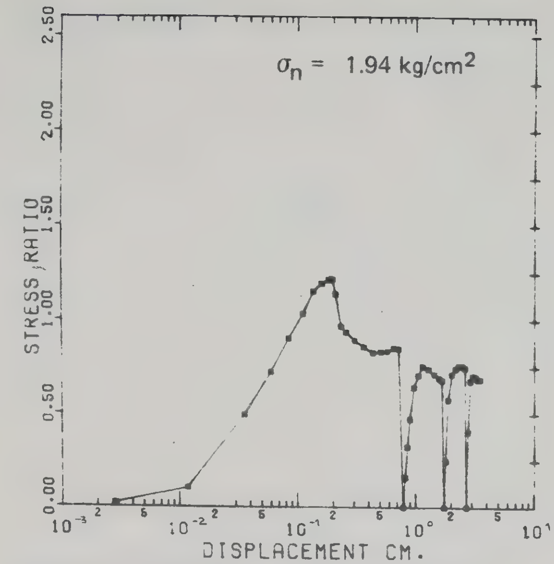

OILSAND SHEARBOX SERIES A TEST 8

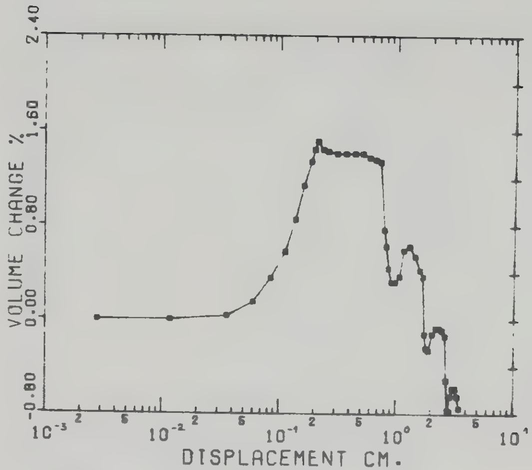

OILSAND SHEARBOX SERIES A TEST 8

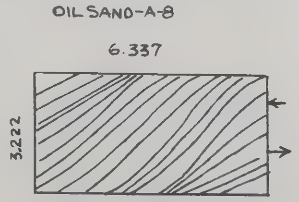

Description: Oil-free silt with distorted bedding at 25° - 35° varve thickness ≅ 1mm.

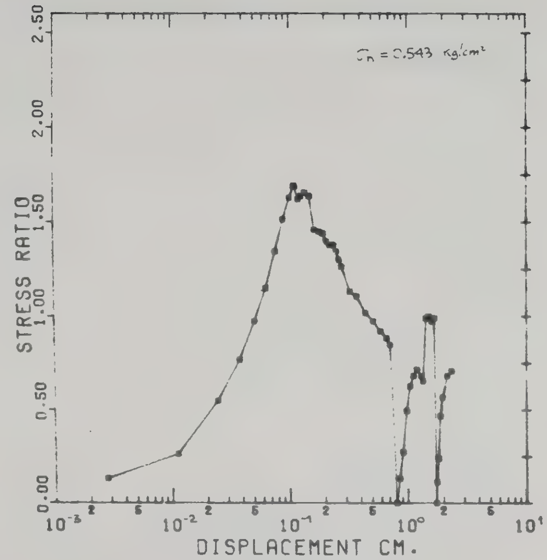

OILSAND SHEARBOX SERIES A TEST 9

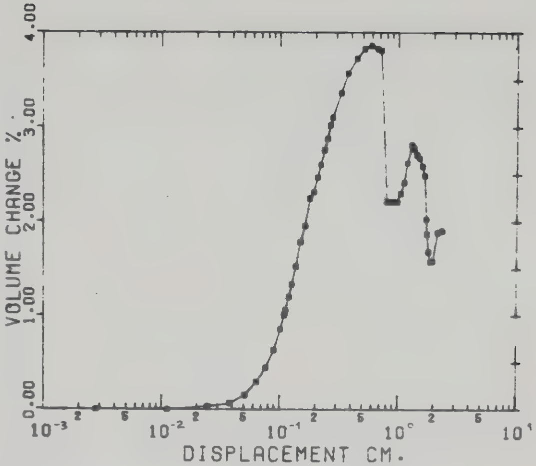

OILSAND SHEARBOX SERIES A TEST 9

OILSAND - A-9

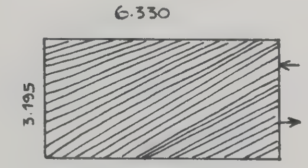

DESCRIPTION: FINE-GRAINED OIL SAND,
~10% OIL, CROSS-BEDDED 15°-25°

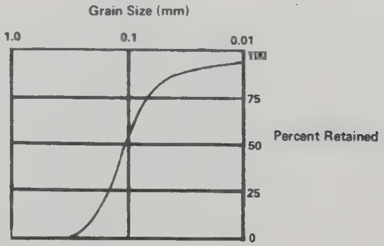

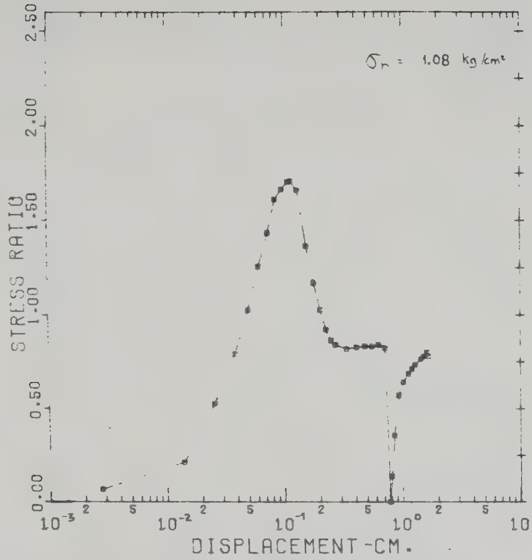

OILSAND SHEARBOX SERIES A TEST 10

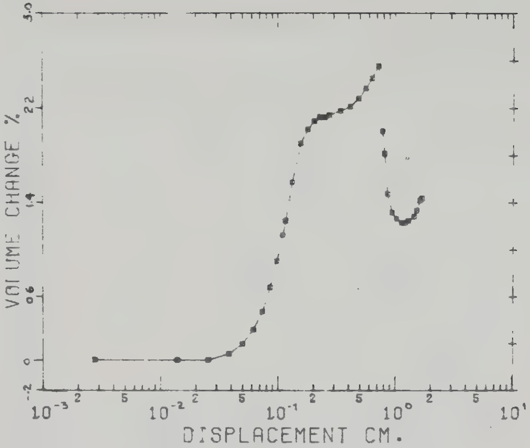

OILSAND SHEARBOX SERIES A TEST 10

OILSAND - A - 10

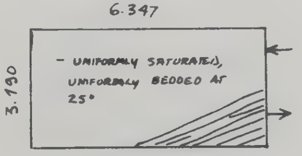

DESCRIPTION: UNIFORM FINE-GRAINED
OILSAND, >10% OIL.

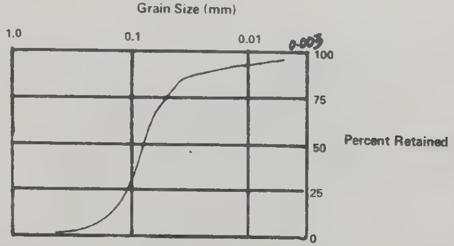

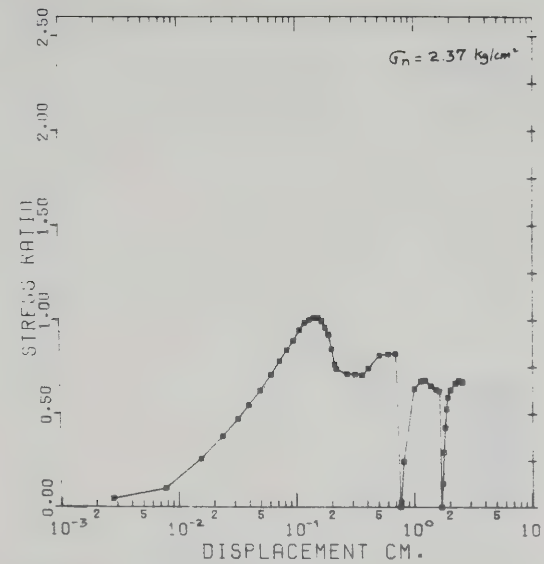

OILSAND SHEARBOX SERIES A TEST 11

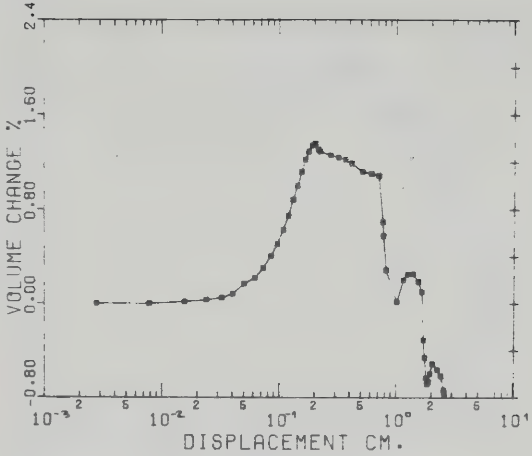

OILSAND SHEARBOX SERIES A TEST 11

OILSAND-A-11

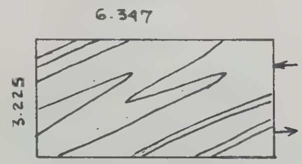

DESCRIPTION: VARIABLY SATURATED FINE-GRAINED SAND. CROSS-BEDDED AT 25°. ~5% OIL.

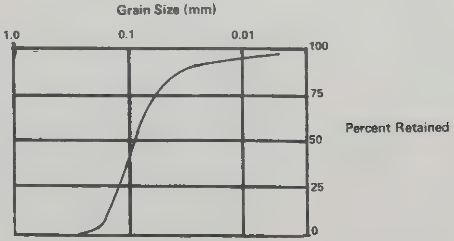

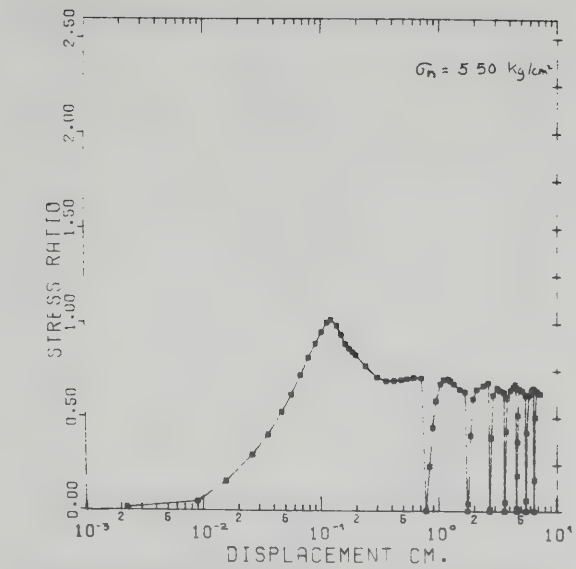

OILSAND SHEARBOX SERIES A TEST 12

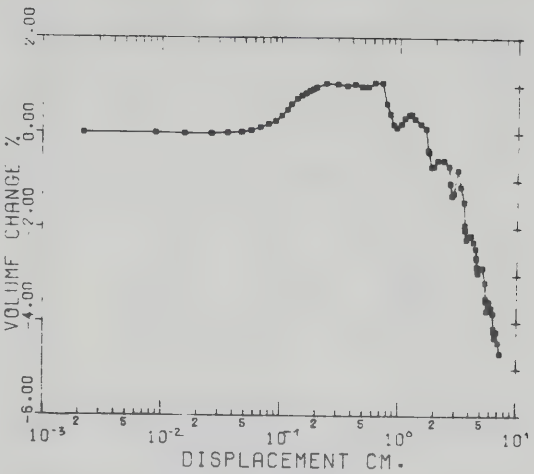

OILSAND SHEARBOX SERIES A TEST 12

OILSAND -A-12

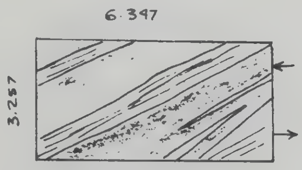

DESCRIPTION: VARIABLY SATURATED FINE-GRAINED OIL SAND, BEDDING DIP 25°-30°, ~10% OIL.

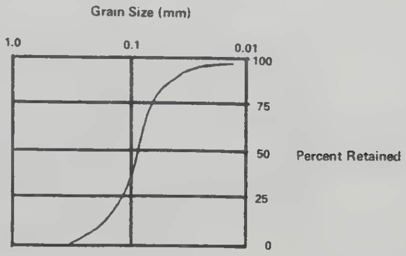

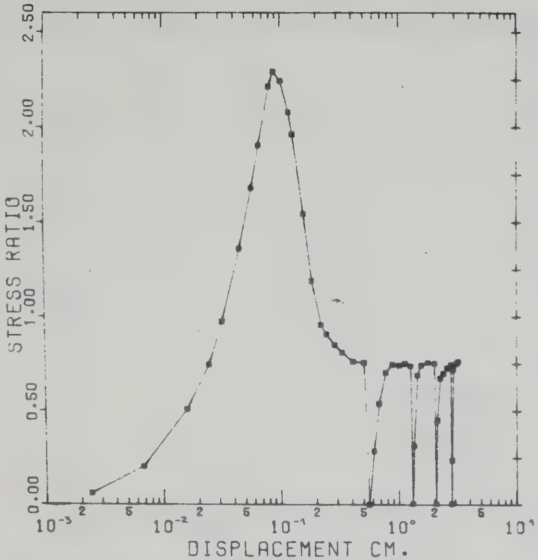

OILSAND SHEARBOX SERIES B 1.0 KG./SQ.CM

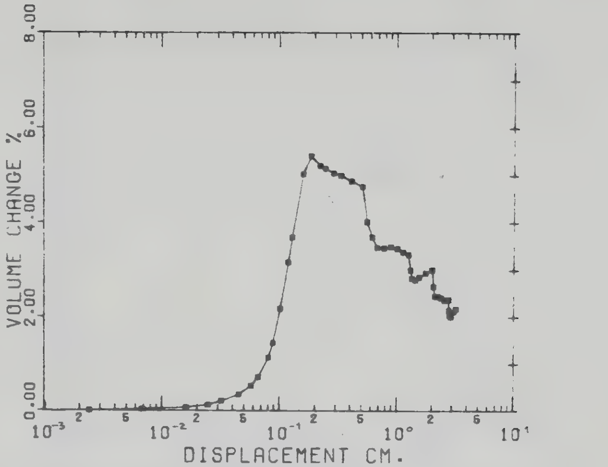

OILSAND SHEARBOX SERIES B 1.0 KG./SQ.CM

OILSAND-B-1

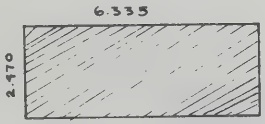

DESCRIPTION: OIL FREE FINE, SANDY SILT, NO CLAY, BEDDED AT 30° TO 25°.

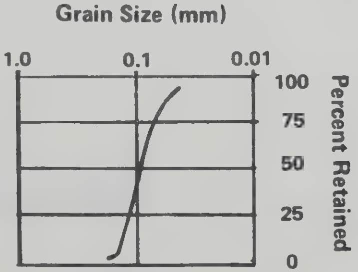

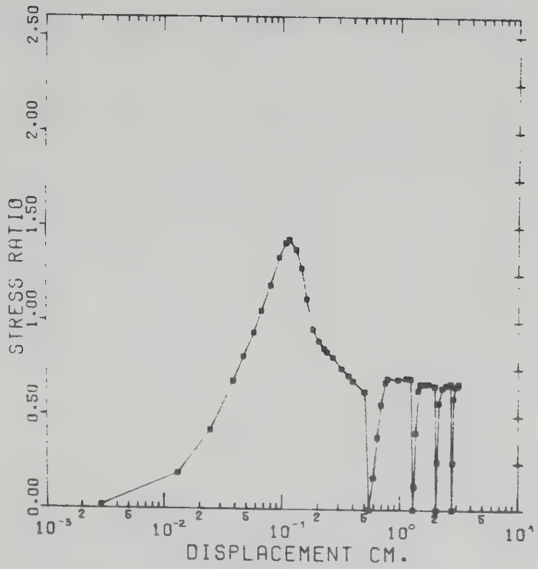

OILSAND SHEARBOX SERIES B 2.0 KG./SQ.CM.

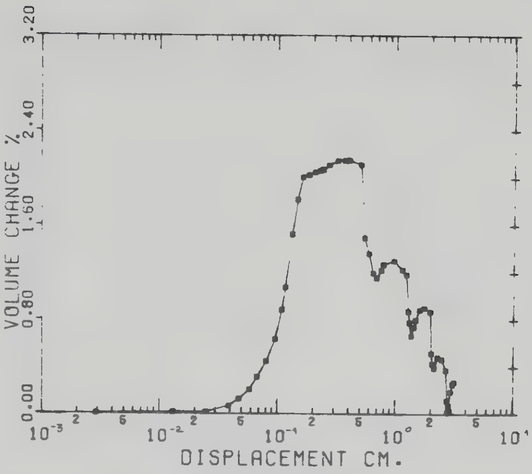

OILSAND SHEARBOX SERIES B 2.0 KG./SQ.CM.

For grain size chart and sample description, see previous page

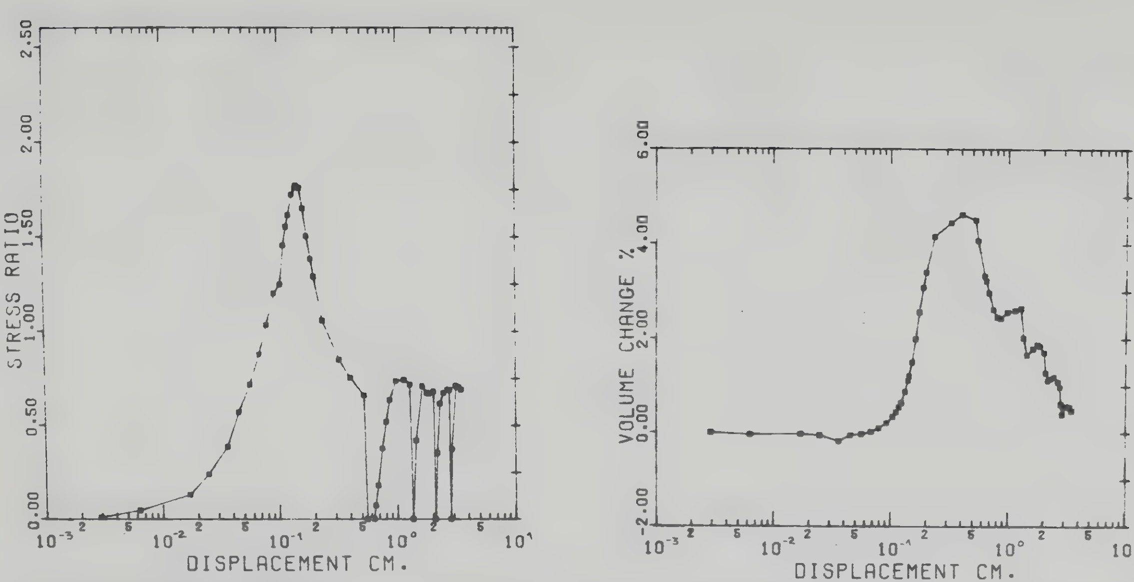

OILSAND SHEARBOX SERIES B 4.0 KG./SQ.CM.

OILSAND SHEARBOX SERIES B 4.0 KG./SQ.CM.

Sample description and grain size curve as for Shearbox Series "B", 1.0 kg/cm^2

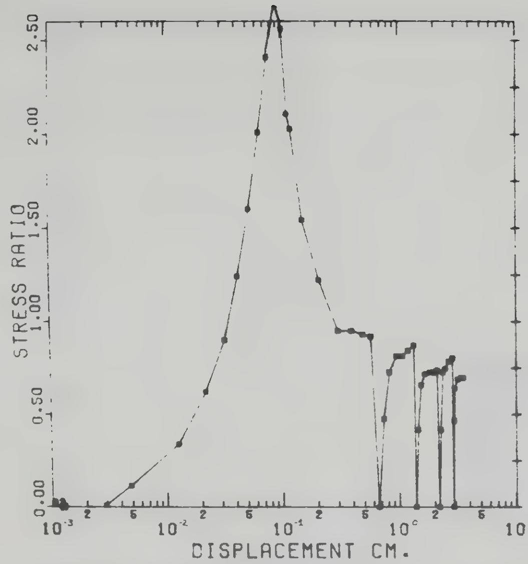

OILSAND SHEARBOX SERIES C 0.5 KG./SQ.CM.

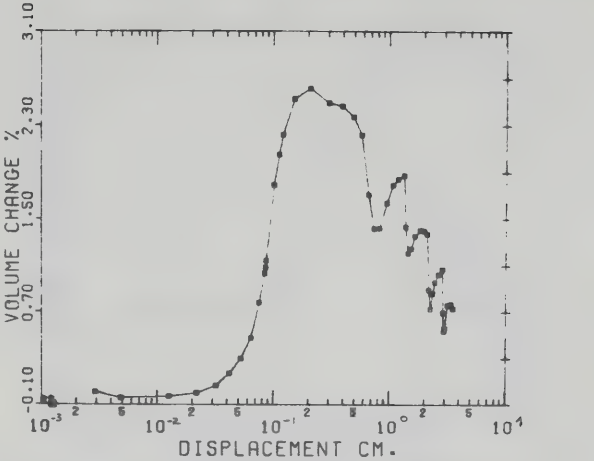

OILSAND SHEARBOX SERIES C 0.5 KG./SQ.CM.

OILSAND – C – 0.5

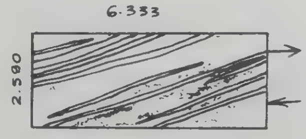

DESCRIPTION: OIL-RICH FINE GRAINED OILSAND WITH NUMEROUS (25%) VERY THIN (<1mm) OIL FREE SILTY STREAKS. 20° BEDDING.

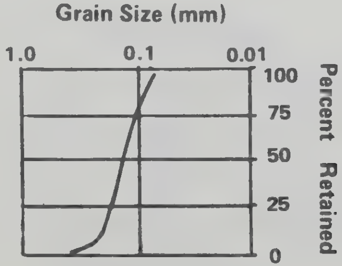

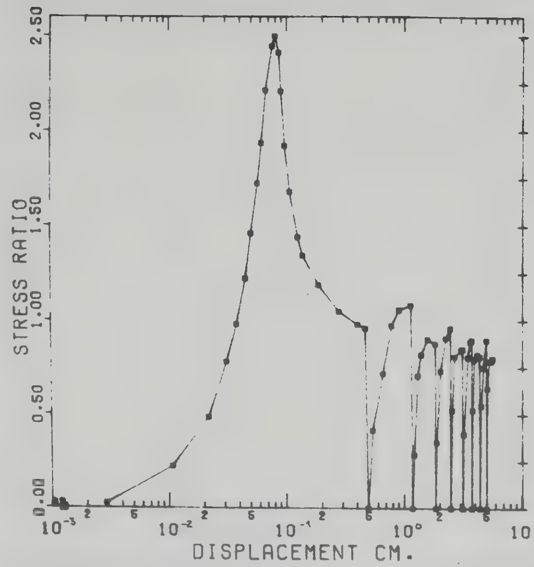

OILSAND SHEARBOX SERIES C 1.0 KG./SQ.CM.

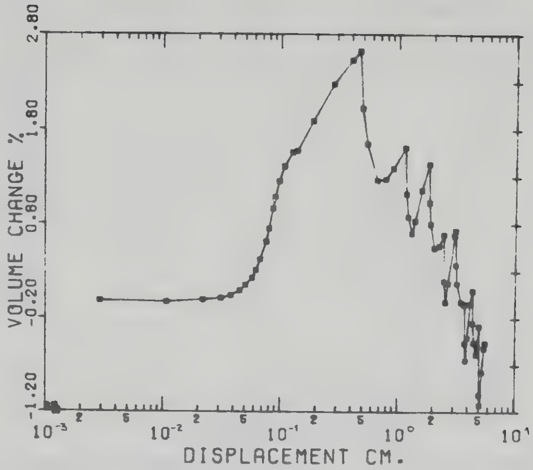

OILSAND SHEARBOX SERIES C 1.0 KG./SQ.CM.

OILSAND -C-1.0

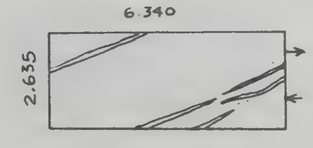

DESCRIPTION: OIL-RICH WITH A FEW WISPS OF OIL FREE SILT DIPPING AT 20°. FINESAND

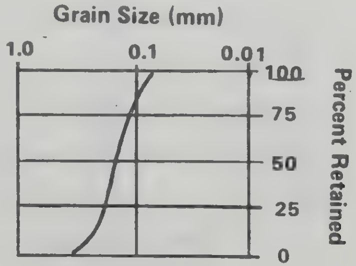

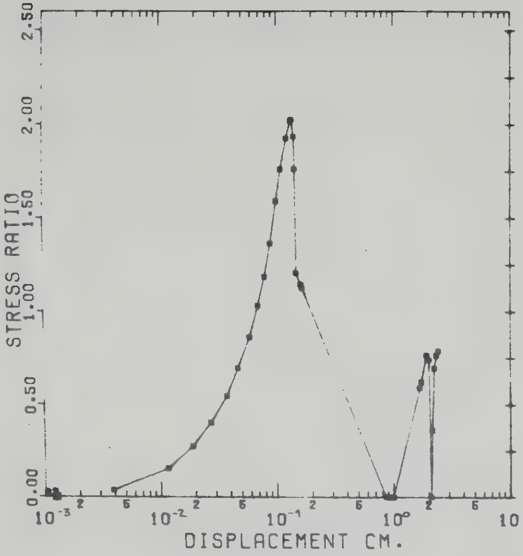

OILSAND SHEARBOX SERIES C 2.0 KG/SQ.CM.

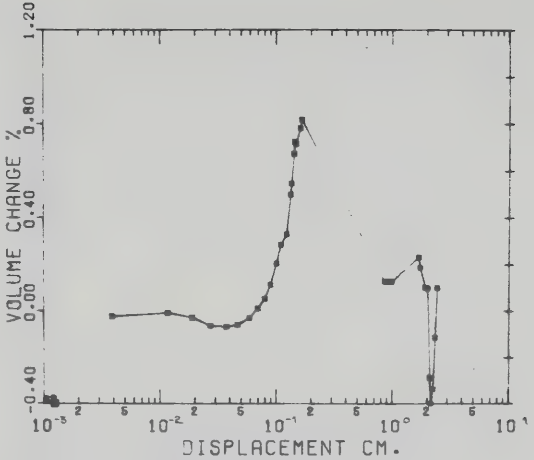

OILSAND SHEARBOX SERIES C 2.0 KG/SQ.CM.

OILSAND - C - 2.0

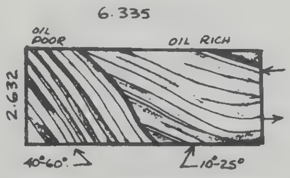

DESCRIPTION: TRUNCATED BEDDING SEQUENCE. OIL-POOR REGION HAS 60% OIL FREE SEAMS, OIL-RICH SECTION <10% OIL-FREE SEAMS.

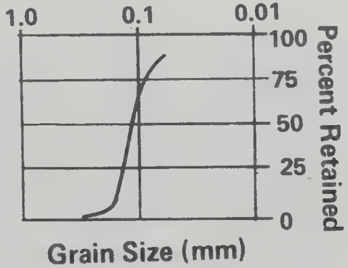

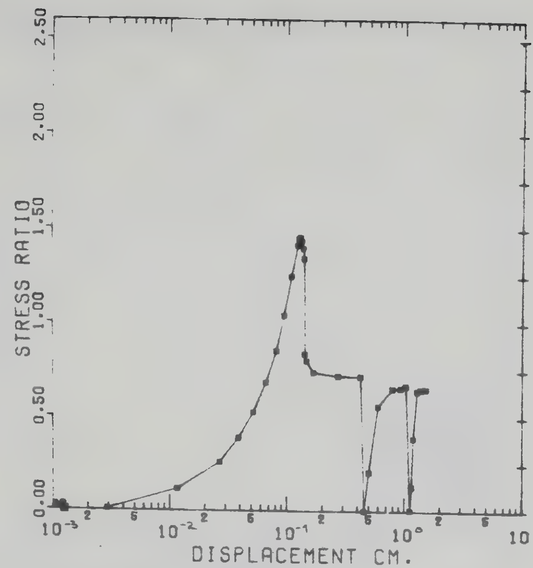

OILSAND SHEARBOX SERIES C 4.0 KG./SQ.CM.

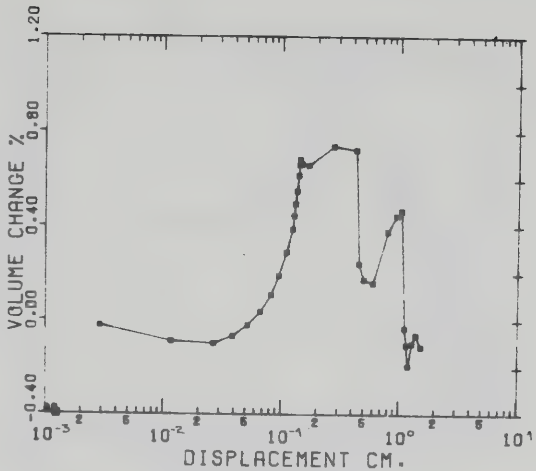

OILSAND SHEARBOX SERIES C 4.0 KG./SQ.CM.

OILSAND -C -4.0

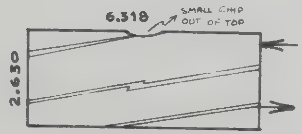

DESCRIPTION: GENTLY BEDDED, OIL-RICH FINE SAND WITH 3% OIL-FREE SEAMS.

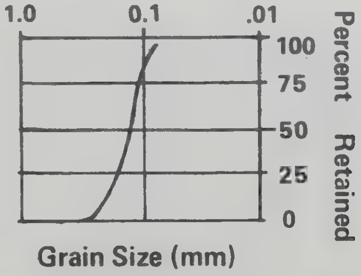

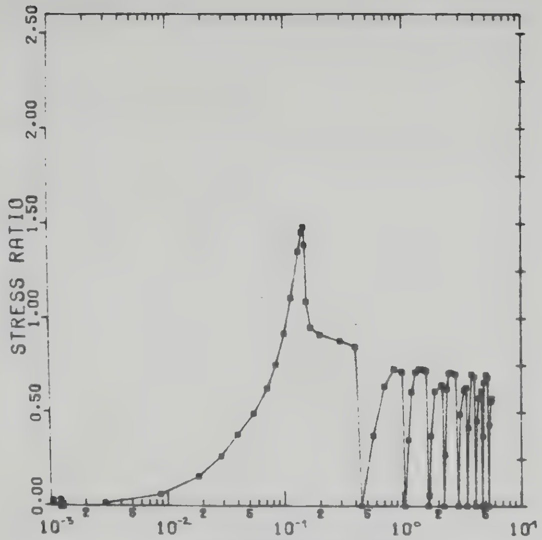

OILSAND SHEARBOX SERIES C 6.0 KG./SQ.CM.

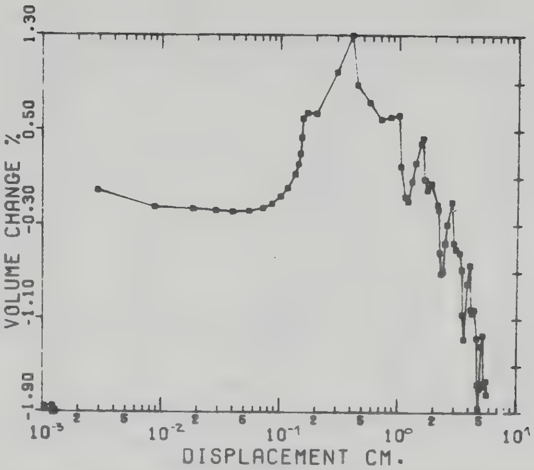

OILSAND SHEARBOX SERIES C 6.0 KG./SQ.CM.

OILSAND-C-6.0

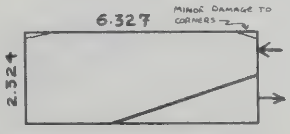

DESCRIPTION: FINE OIL-RICH SAND, ONE ½mm THICK OIL-FREE SEAM DIPPING 15°-20°

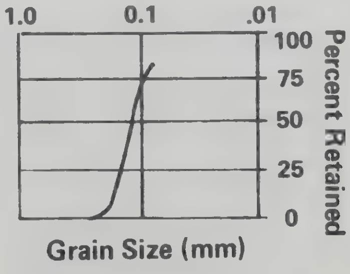

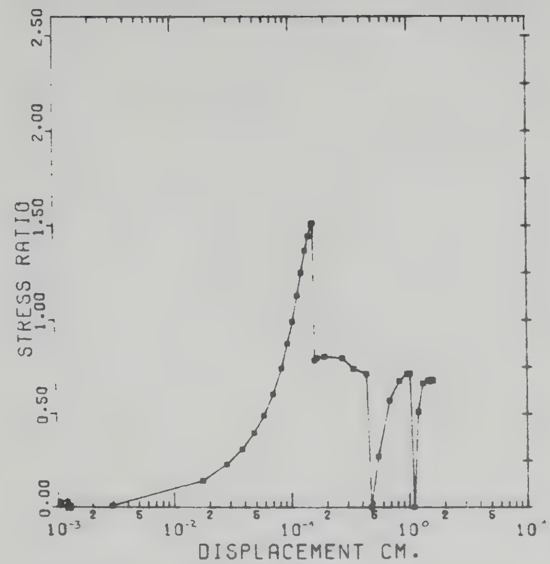

OILSAND SHEARBOX SERIES C 8.0 KG./SQ.CM.

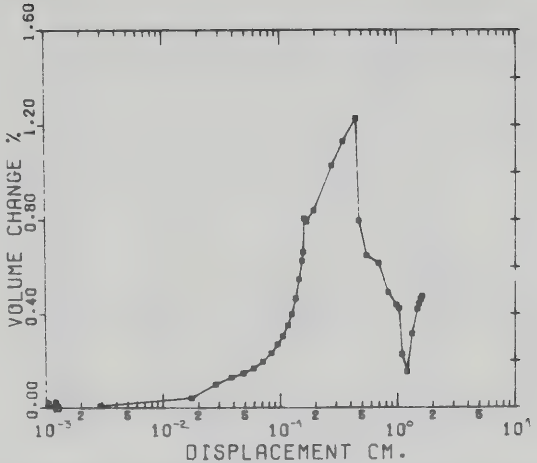

OILSAND SHEARBOX SERIES C 8.0 KG./SQ.CM.

OILSAND-C-B

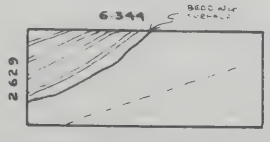

DESCRIPTION: LARGELY UNIFORM, 20° DIPPING FINE OIL-RICH SAND. MINOR BEDDING TROUGH WITH A FEW OIL-FREE SEAMS.

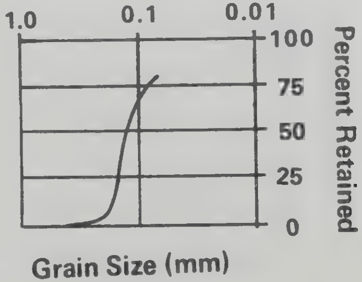

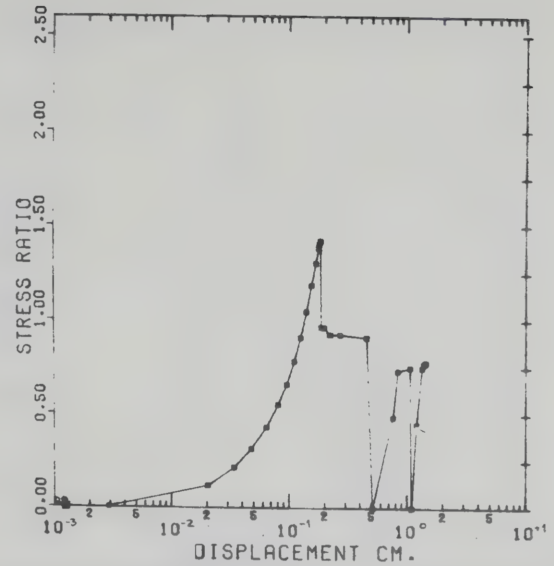

OILSAND SHEARBOX SERIES C 10.0 KG./SQ.CM.

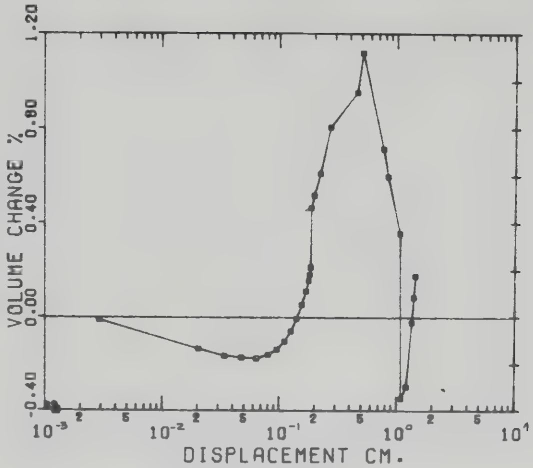

OILSAND SHEARBOX SERIES C 10.0 KG./SQ.CM.

OILSAND -C -10

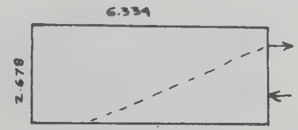

DESCRIPTION: UNIFORM OIL-RICH
FINE SAND: FAINT BEDDING
JUST DISCERNABLE. (20°)

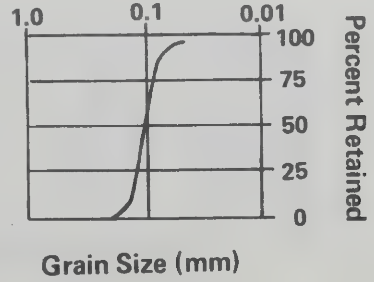

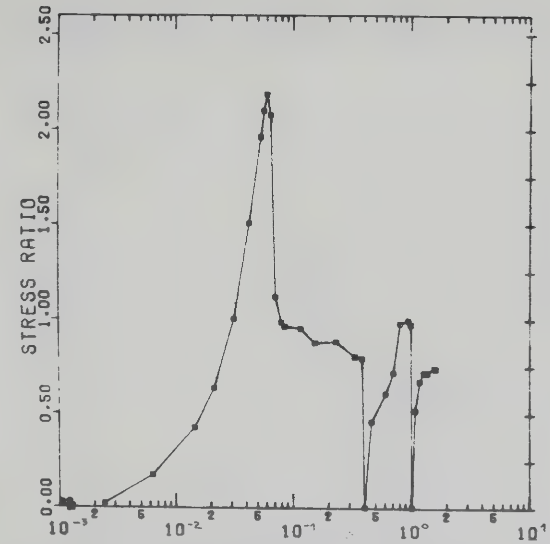

OILSAND SHEARBOX SERIES D 0.885 KG./SQ.CM.

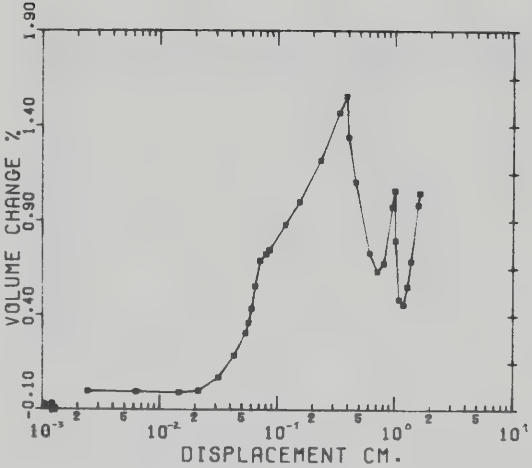

OILSAND SHEARBOX SERIES D 0.885 KG./SQ.CM

OILSAND-D-0.855
(118.10'–118.19')

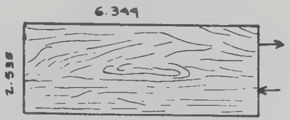

DESCRIPTION: VARIABLY SATURATED FINE SAND AND SILT, HORIZONTAL MEAN BEDDING DIRECTION.

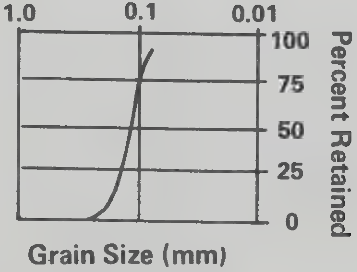

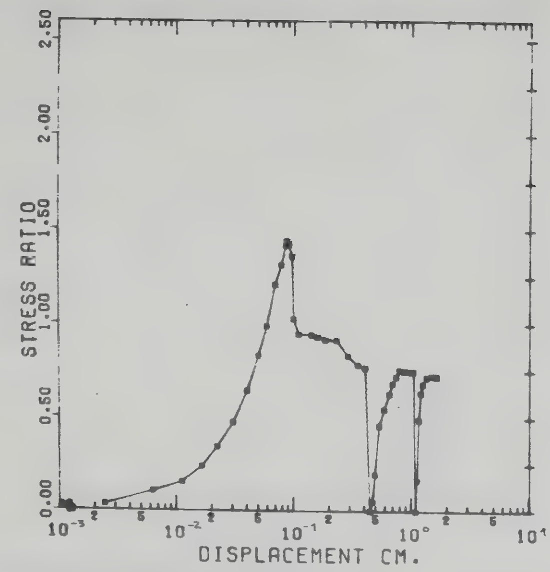

OILSAND SHEARBOX SERIES D 2.0 KG./SQ.CM.

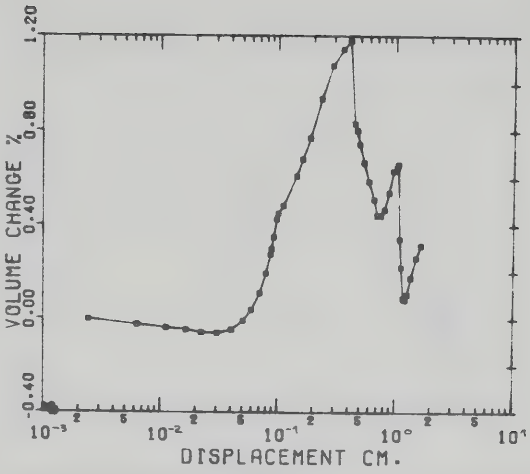

OILSAND SHEARBOX SERIES D 2.0 KG./SQ.CM.

OILSAND-D-2
(118.20'-118.29')

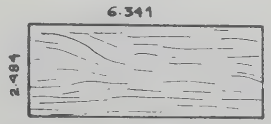

DESCRIPTION: FINE SAND-SILT, BEDDING HORIZONTAL, OIL SAT'N VARIABLE (~6-8% OIL).

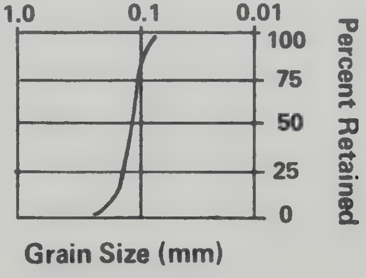

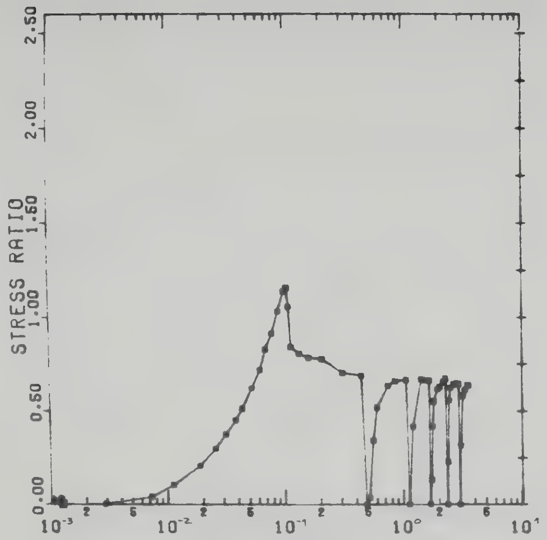

OILSAND SHEARBOX SERIES D 4.0 KG./SQ.CM.

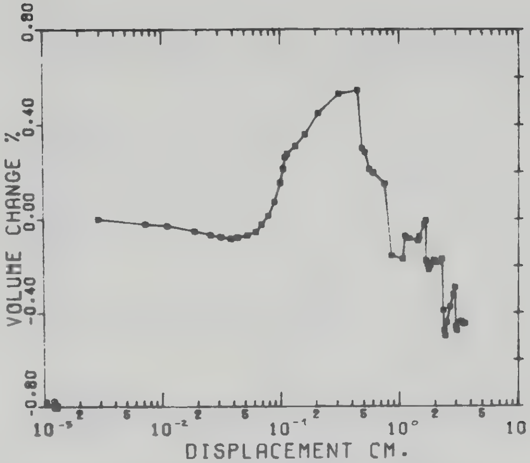

OILSAND SHEARBOX SERIES D 4.0 KG./SQ.CM.

OILSAND-D-4
(118.30'-118.39')

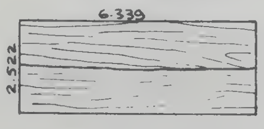

DESCRIPTION: FINE SAND-SILT, BDG. HORIZONTAL, SATURATION VARIABLE. BEDDING TRUNCATION PLANE AT SAMPLE MID-POINT.

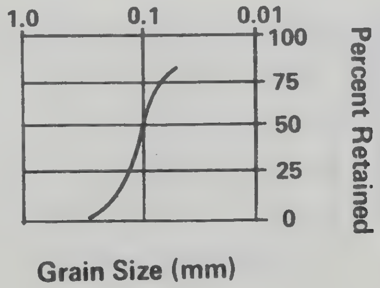

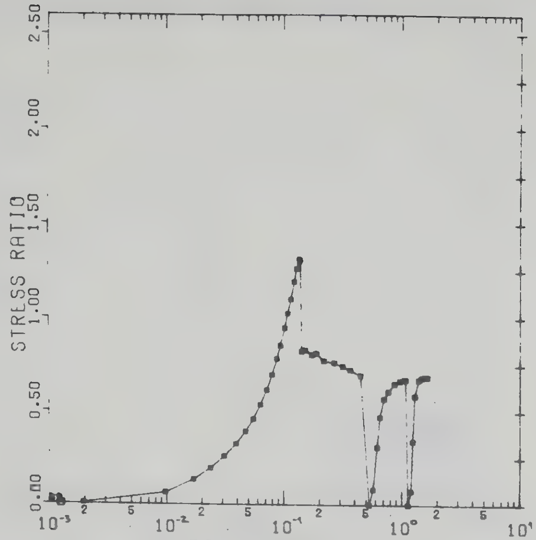

OIL SAND SERIES D 8.0 KG./SQ.CM.

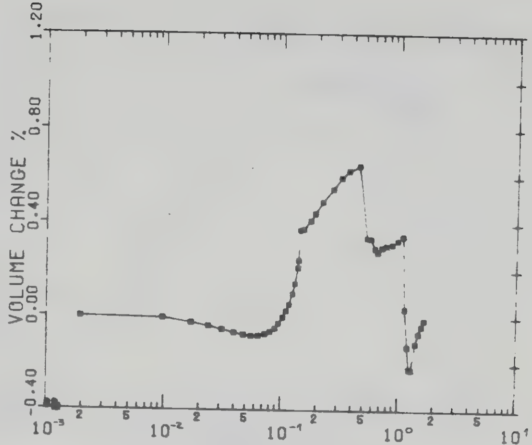

OIL SAND SERIES D 8.0 KG./SQ.CM.

OILSAND - D-8
(118.40' - 118.45')

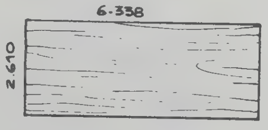

DESCRIPTION: VARIABLY SATURATED, HORIZONTALLY BEDDED, FINE SAND-SILT.

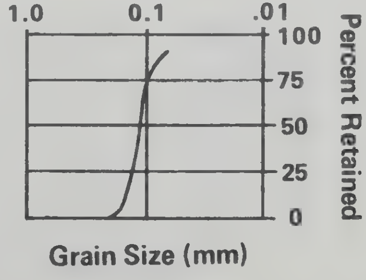

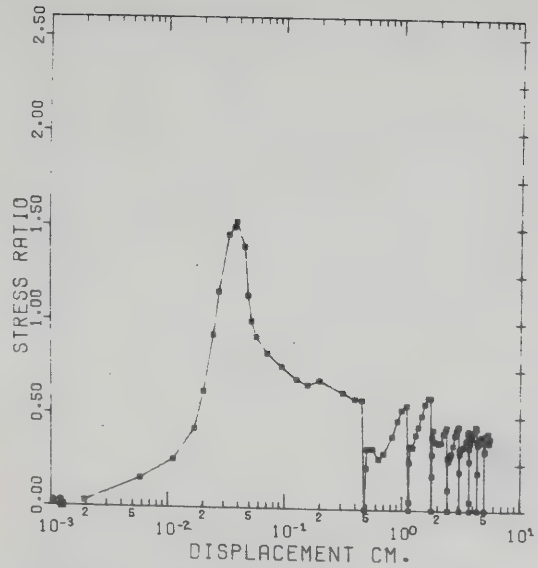

0ILSAND SHEARBOX SERIES E 1.0 KG./SQ.CM.

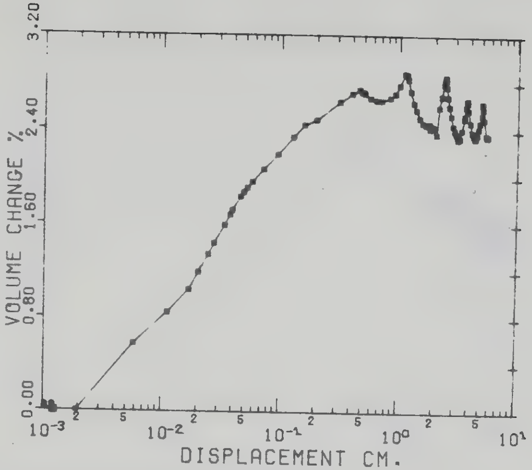

0ILSAND SHEARBOX SERIES E 1.0 KG./SQ.CM.

OILSAND - E - 1
(119.3' - 119.35')

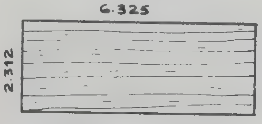

DESCRIPTION: OIL-FREE CLAY,
HORIZONTAL TO 8° BDG.

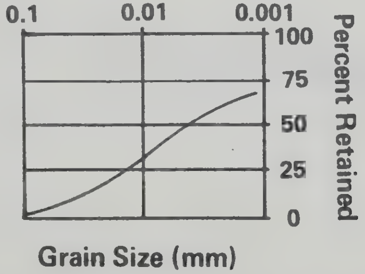

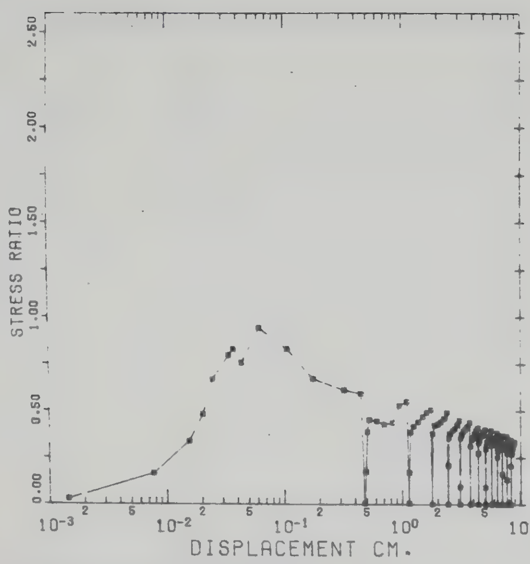

OILSAND SHEARBOX SERIES E 2.0 KG./SQ.CM.

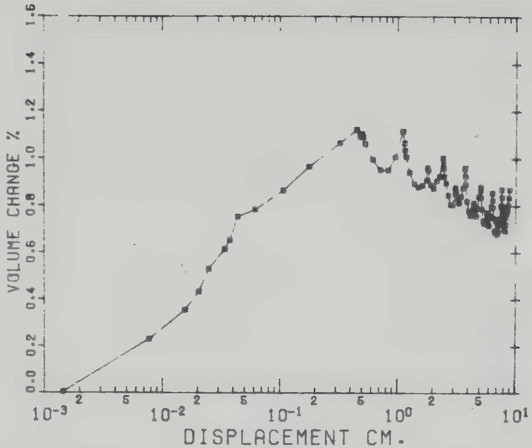

OILSAND SHEARBOX SERIES E 2.0 KG./SQ.CM.

OILSAND-E-2
(119.4'- 119.49')

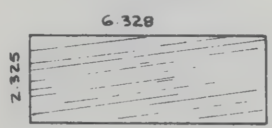

DESCRIPTION: OIL-FREE <u>CLAY</u>,
8° TO 5° BEDDING.

Grain Size as for Oilsand -E-1

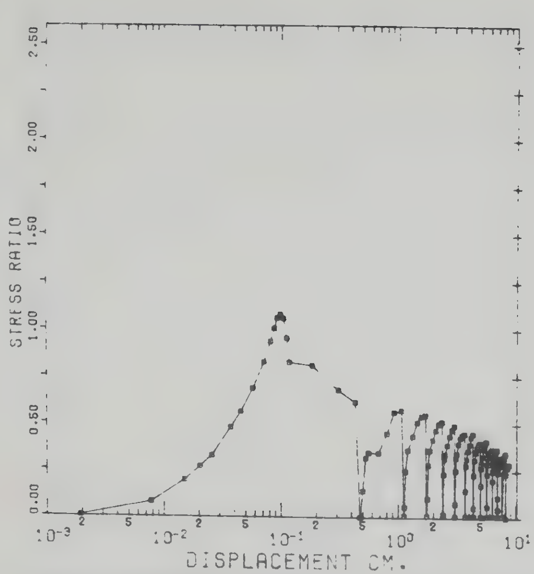

OILSAND SHEARBOX SERIES E 3.5 KG./SQ.CM.

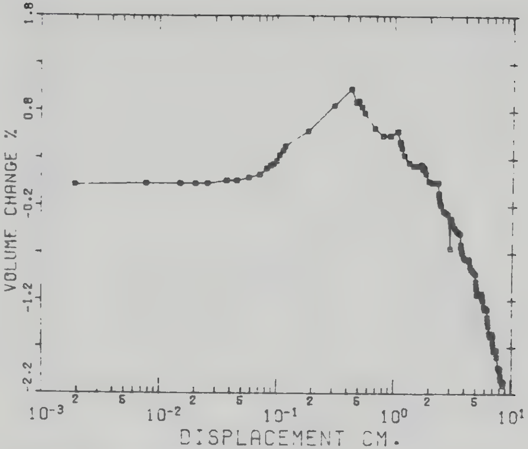

OILSAND SHEARBOX SERIES E 3.5 KG./SQ.CM.

OILSAND-E-3.5
(119.50'-119.59')

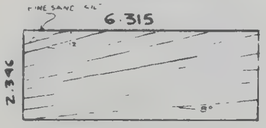

DESCRIPTION: ONE CORNER OF OIL-FREESILT/SAND, REMAINDER 8° TO 12° OIL-FREE CLAY.

Grain Size as for Oilsand-E-1

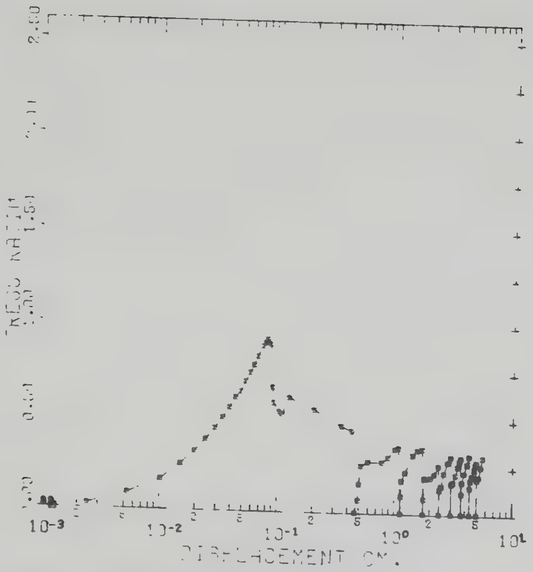

OILSAND SHEARBOX SERIES E 5.0 KG./SQ.CM.

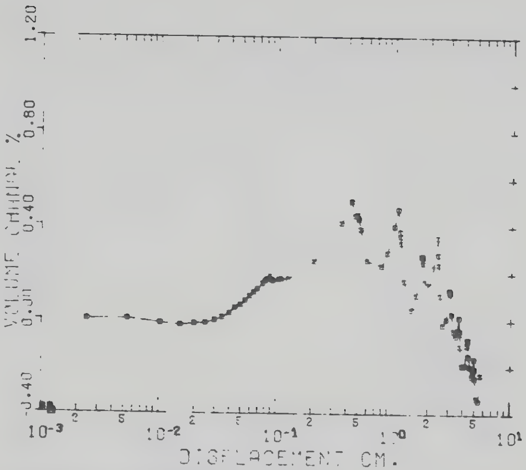

OILSAND SHEARBOX SERIES E 5.0 KG./SQ.CM.

OILSAND - E - 5
(119.2' - 119.29')

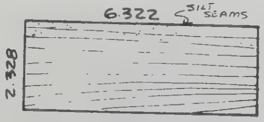

DESCRIPTION: HORIZONTAL TO 6° BEDDING, OIL FREE CLAY. MINOR SILT SEAMS, BUT NOT IN PLANE OF FAILURE.

Grain Size as for Oilsand-E-1

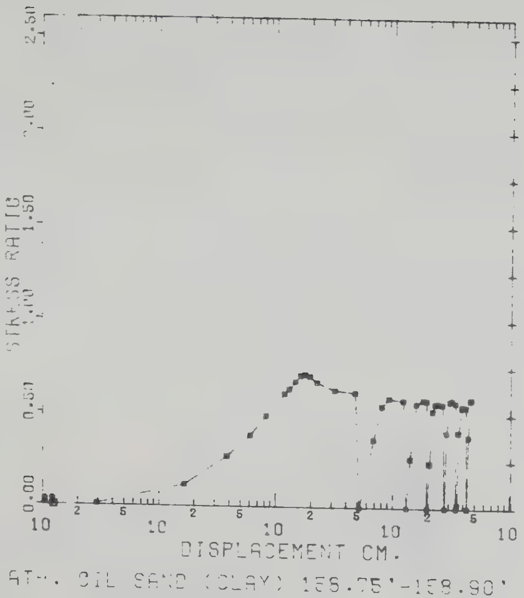

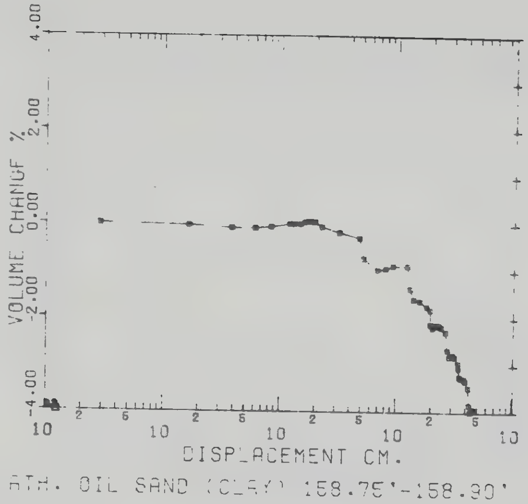

G-1

OILSAND 158.75'-158.90'

SAMPLE DESCRIPTION: FRIABLE CLAYEY SILT, SOMEWHAT DESSICATED Cv VERY HIGH DUE TO FRACTURES, HORIZONTAL BEDDING, SHEARED PARALLEL TO BEDDING

Grain Size as for Oilsand -E-1

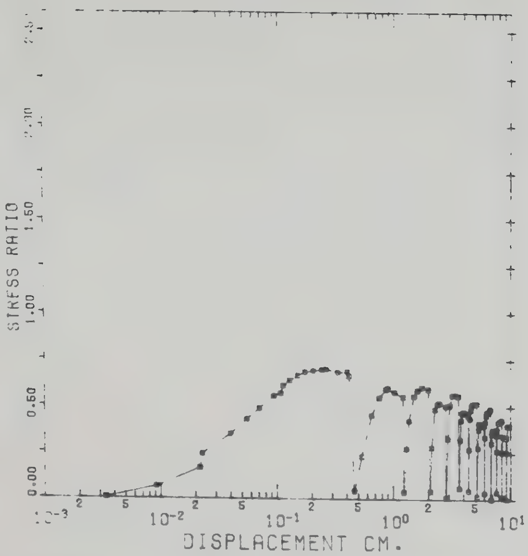

OIL SAND 174.7' 1.0 KG/SQ.CM. (CLAY RICH)

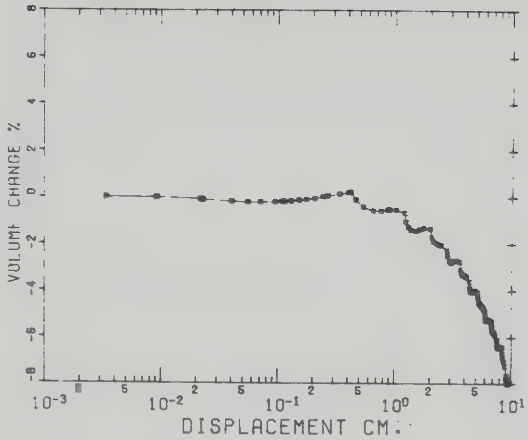

OIL SAND 174.7' 1.0 KG/SQ.CM. (CLAY RICH)

Grain size and limits as for Oilsand 174.8' (next page)

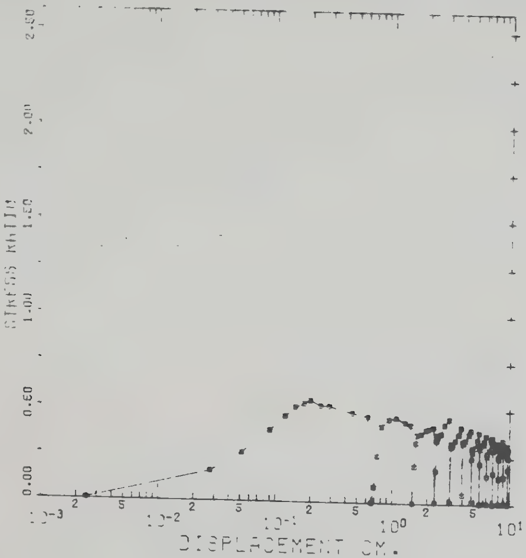

OIL SAND 174.8' 2.0 KG/SQ.CM. (CLAY RICH)

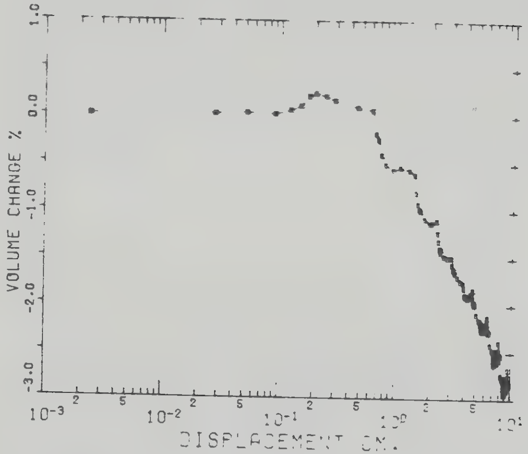

OIL SAND 174.8' 2.0 KG/SQ.CM. (CLAY RICH)

G-4
OILSAND - 174.8'

SAMPLE DESCRIPTION: CLAYEY SILT WITH OCCASIONAL FINE SILTY SEAMS, HORIZONTAL BEDDING TO DIP OF 4°
MEAN MOISTURE CONTENT AFTER SHEAR = 15.5% (TOTAL WEIGHT BASIS)

$W_L = 27.9$
$W_P = 19.6$
$I_P = 8.3$

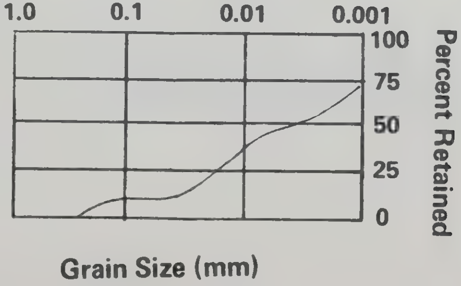

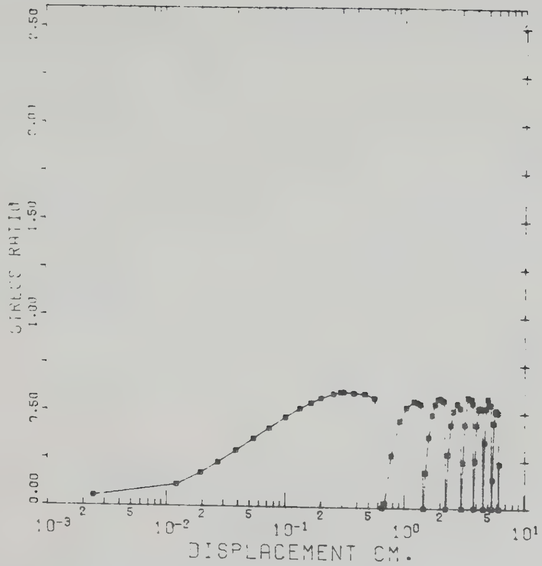

OILSAND SHEARBOX 174.9'(CLAY RICH) 4.0 KG.

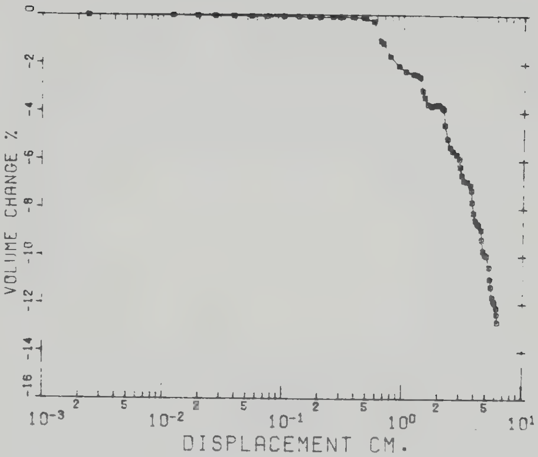

OILSAND SHEARBOX 174.9'(CLAY RICH) 4.0 KG.

G-5
OILSAND - 174.9'

SAMPLE DESCRIPTION FISSLE CLAYEY SILT TO SILTY CLAY, OCCASIONAL 1.0 mm VARVE OF FINE SAND, FINELY LAMINATED THROUGHOUT, HORIZONTAL TO SLIGHTLY DIPPING BEDDING

Grain size and limits as for Oilsand 174.8′ (previous page)

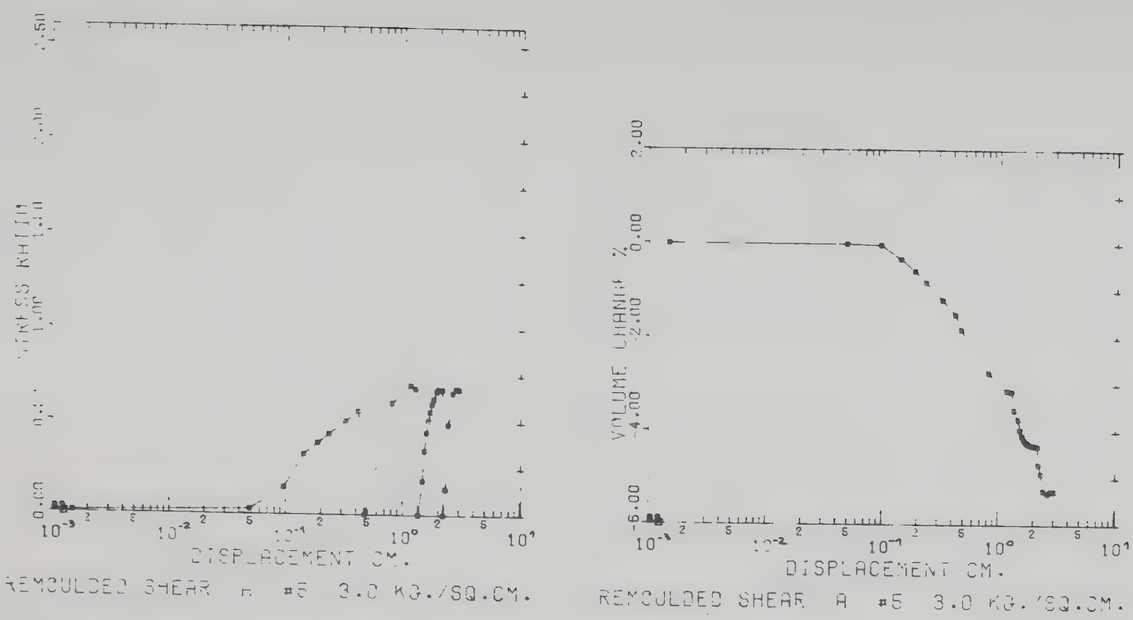

Grain size as for Oilsand A-5

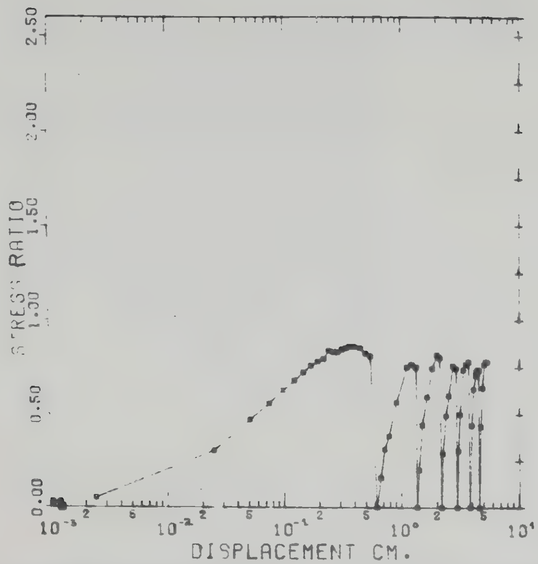

OILSAND SHEAR SERIES G 0.314 KG./SQ.CM.

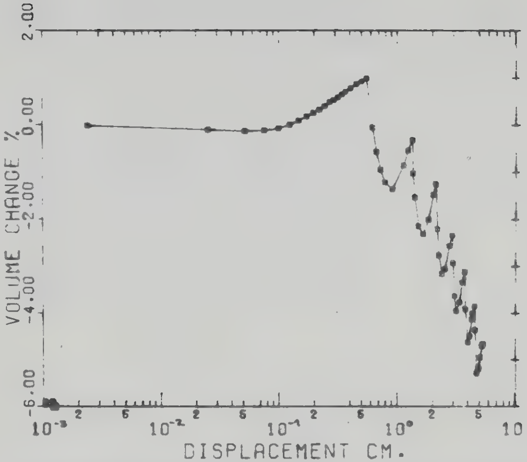

OILSAND SHEAR SERIES G 0.314 KG./SQ.CM.

G-7

OILSAND - 1900'

SAMPLE DESCRIPTION: OIL-RICH
MEDIUM-GRAINED SAND, FAINT
7° CROSS-BEDDING.

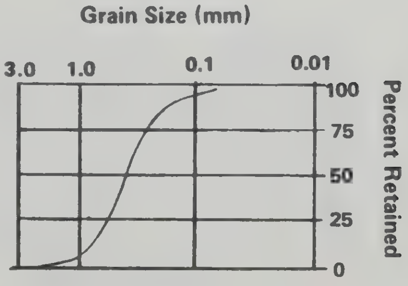

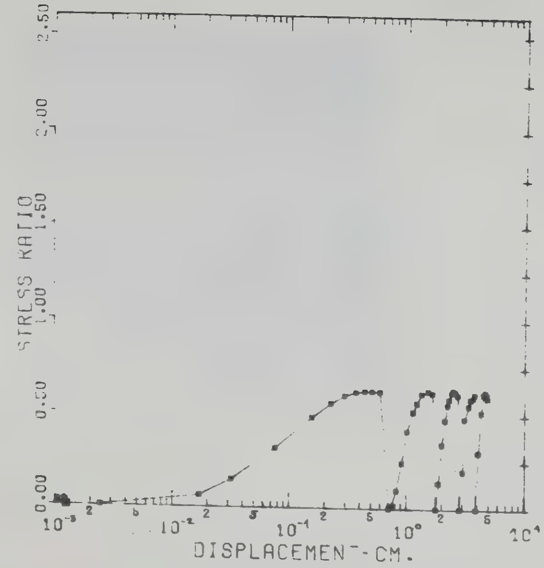

OILSAND SHEAR SERIES G 6.002 KG./SQ.CM.

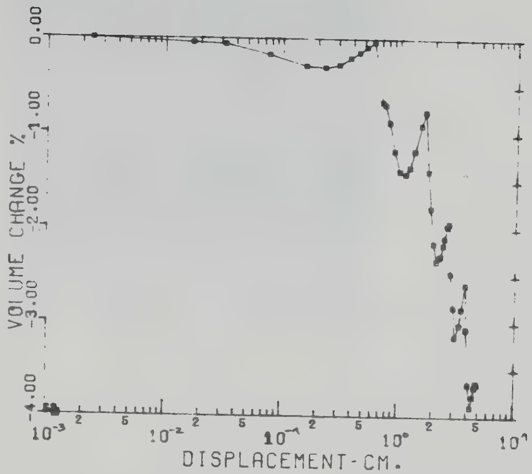

OILSAND SHEAR SERIES G 6.002 KG./SQ.CM.

Oilsand - 190.2

Sample Description: Oilrich medium-grained sand, faint 10° cross bedding

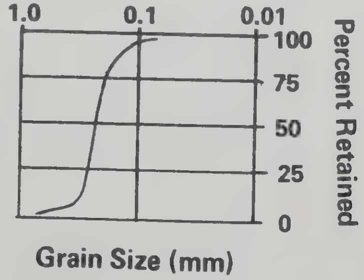

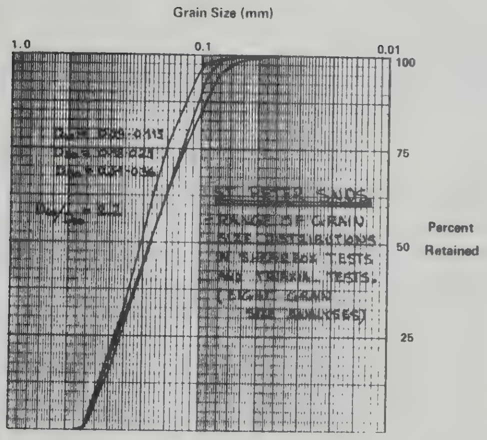

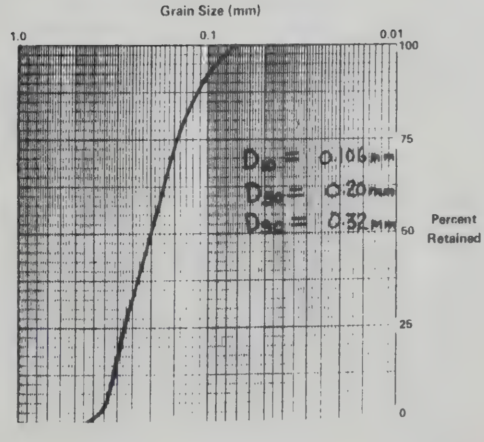

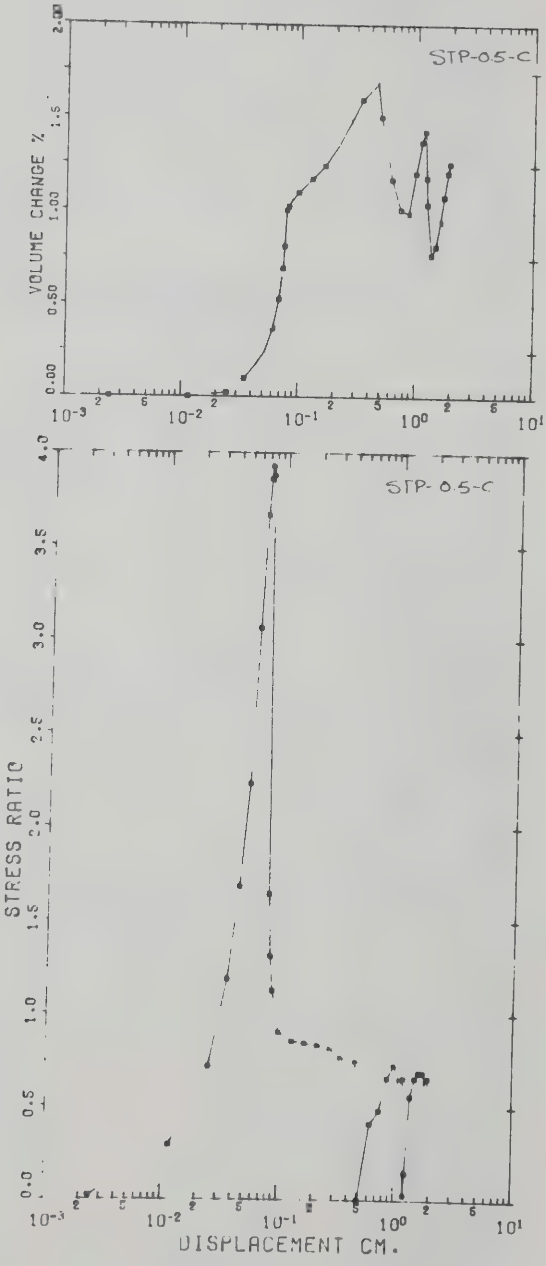

ST. PETER SHEAR 0.5 KG./SQ.CM.(UNDIST.)

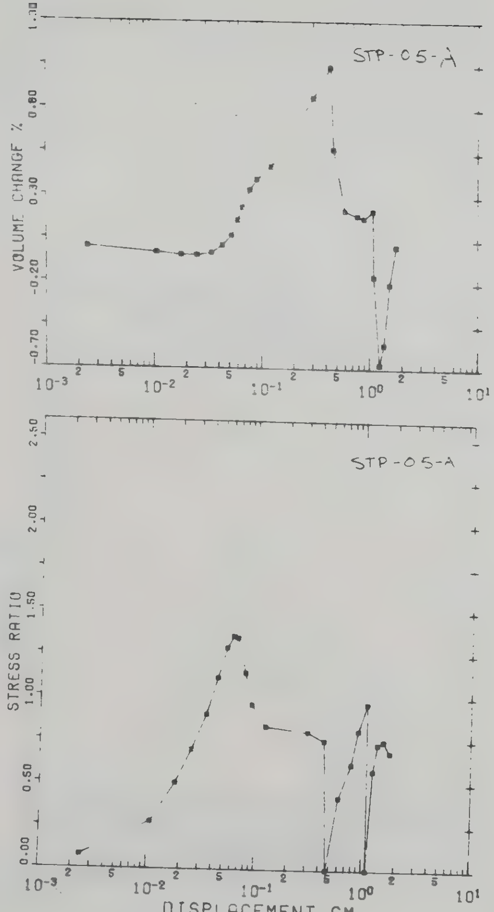

ST.PETER SHEAR 0.5 KG./SQ.CM. (DISTURBED)

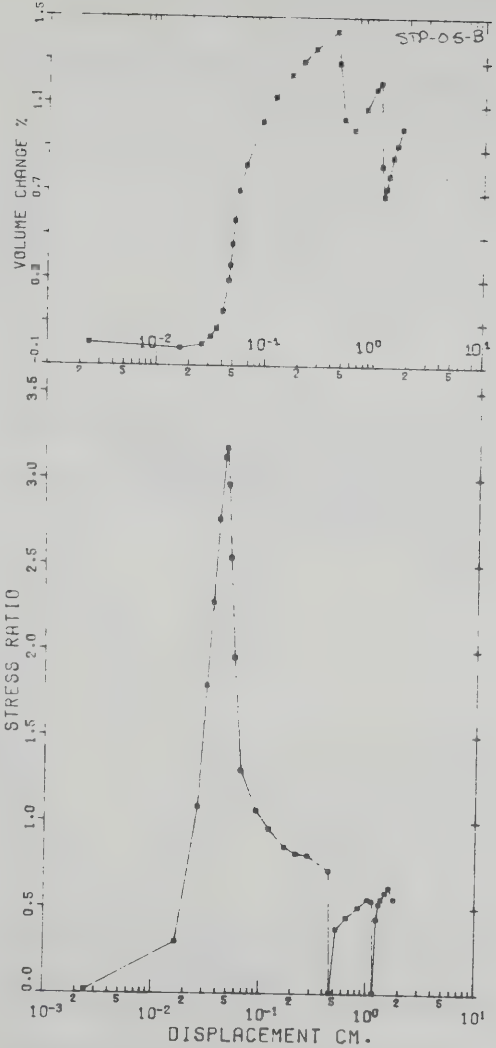

ST. PETER SHEARBOX 0.5 KG./SQ.CM. (UNDIST.)

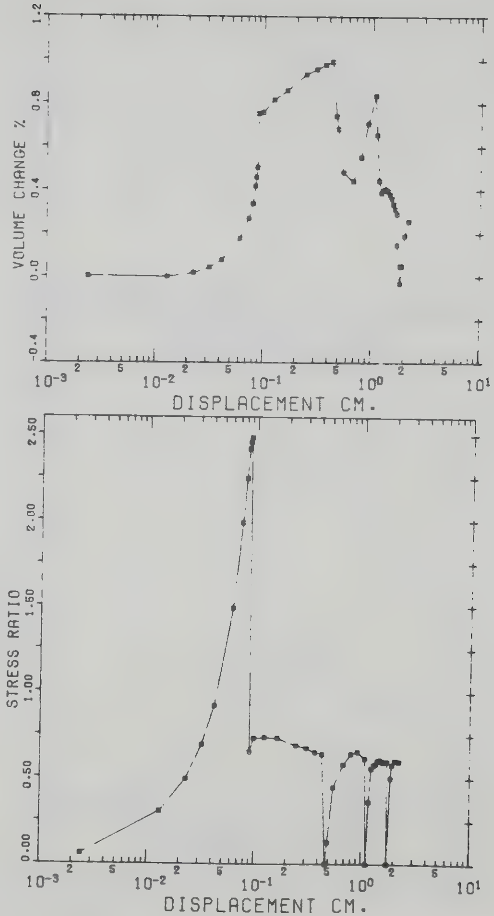

ST. PETER SHEARBOX TEST 2.0 KG./SQ.CM.

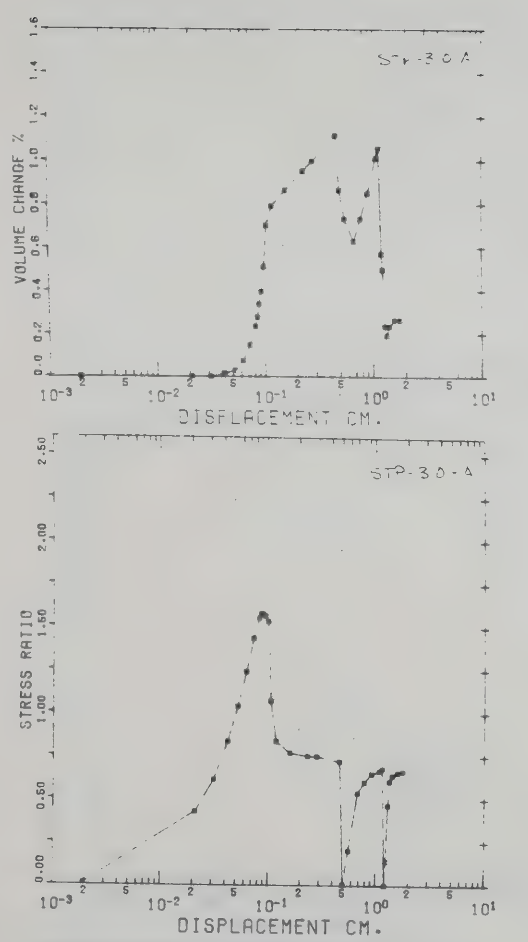

ST PETER SHEAR 3.0 KG./SQ.CM

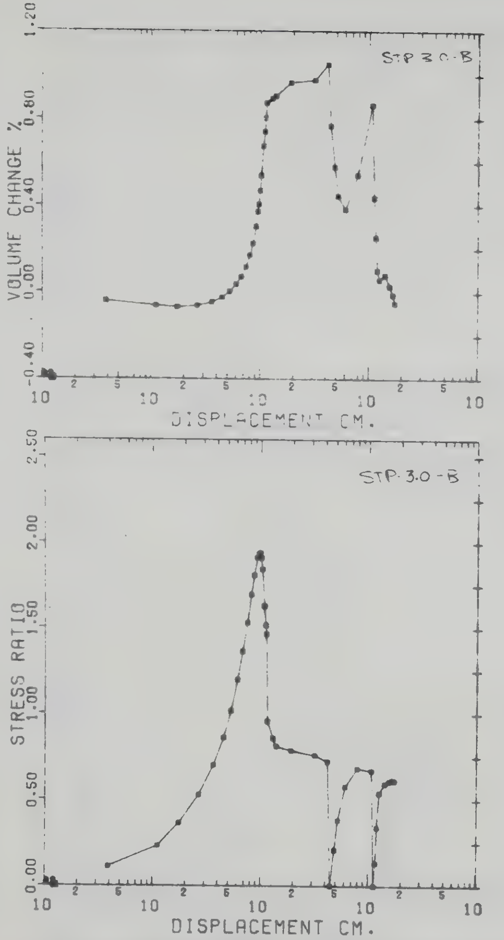

ST. PETER SHEAR TEST -STP 20- 3.0 KG./SQ.CM.

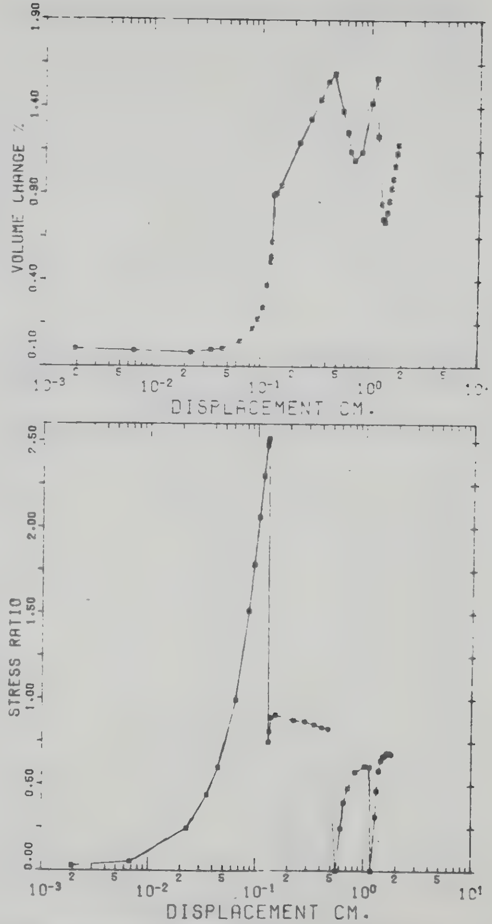

ST. PETER SHEARBOX TEST 4.0 KG./SQ.CM.

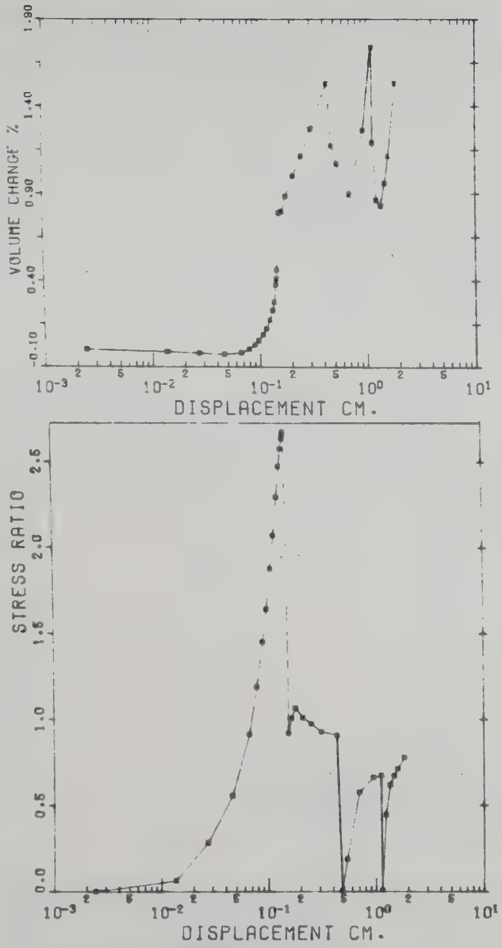

ST. PETER SHEARBOX 5.0 KG./SQ.CM.

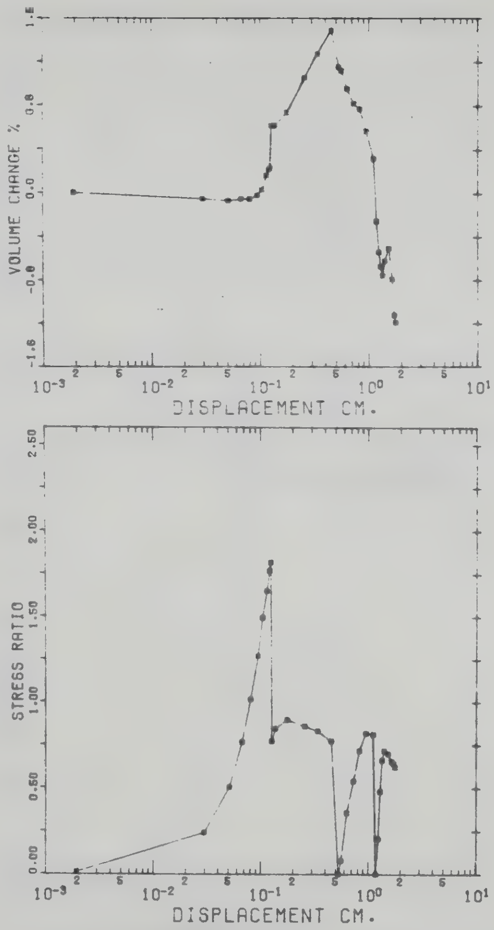

ST. PETER SHEARBOX 6.0 KG./SQ.CM.

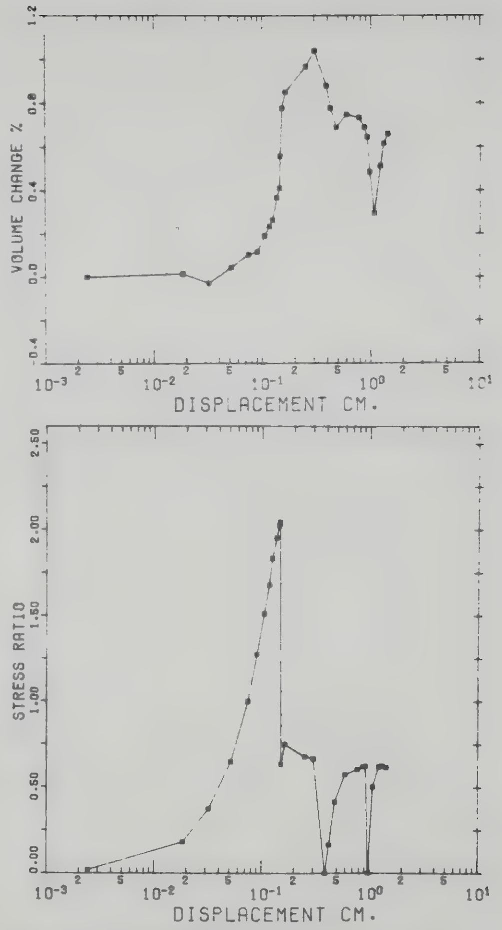

ST. PETER SANDSTONE 8.0 KG./SQ.CM.

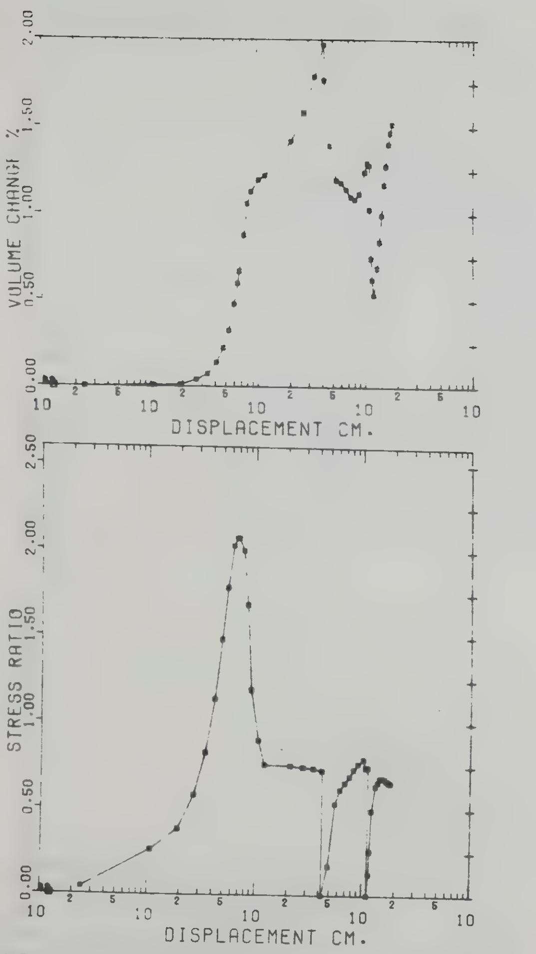

SWAN RIVER SHEAR SERIES A 0.5 KG./SQ.CM.

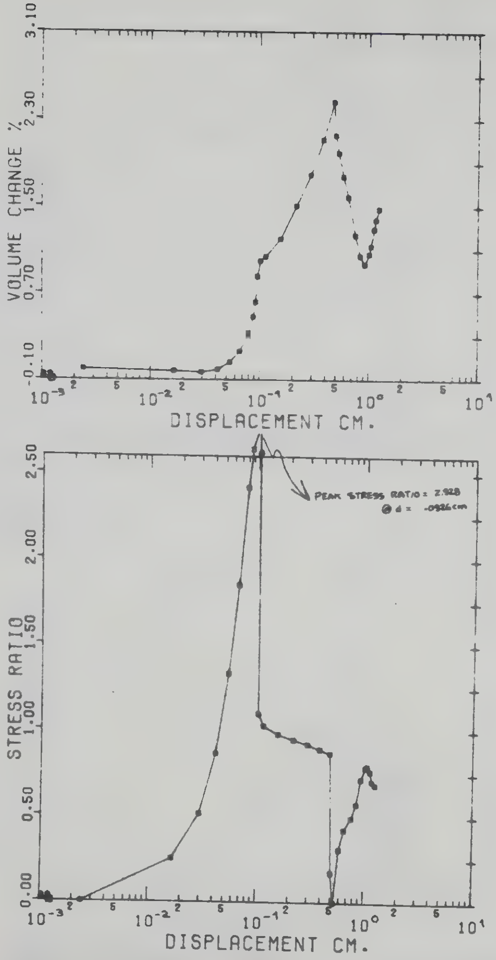

PEAK STRESS RATIO = 2.928 @ d = .0926cm

SWAN RIVER SHEAR SERIES A 1.0 KG./SQ.CM.

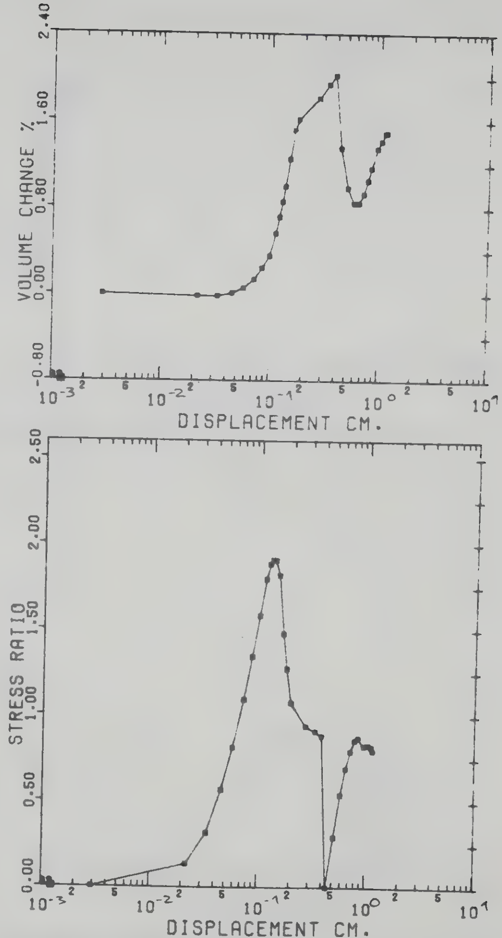

SWAN RIVER SHEAR SERIES A 2.0 KG./SQ.CM.

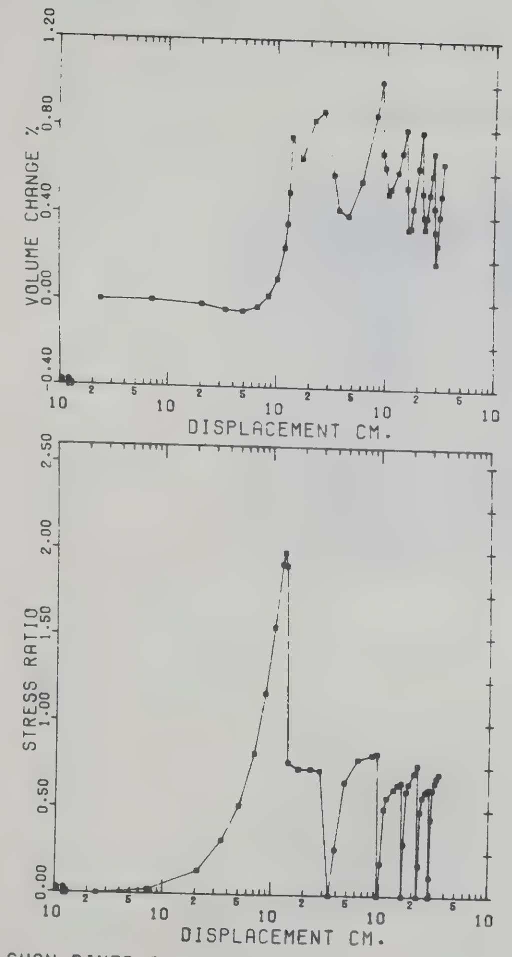

SWAN RIVER SHEAR SERIES A 4.0 KG./SQ.CM.

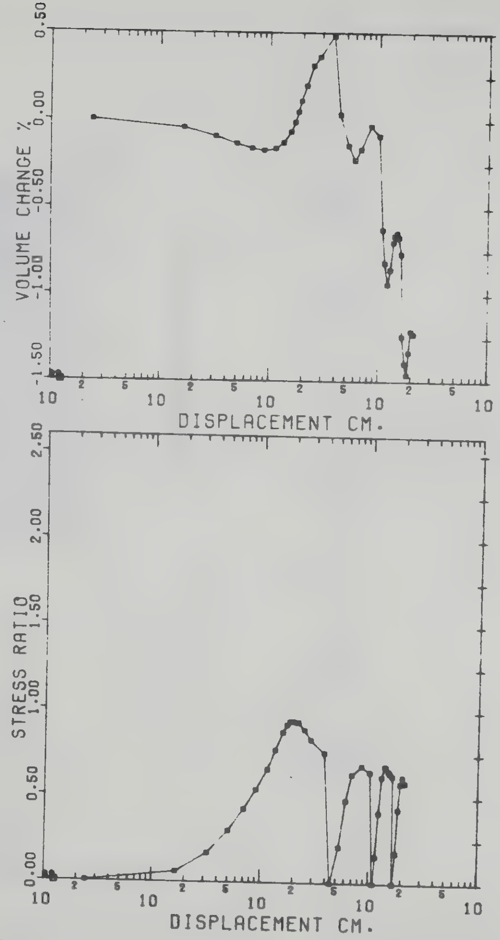

SWAN RIVER SHEAR SERIES A 8.0 KG./SQ.CM.

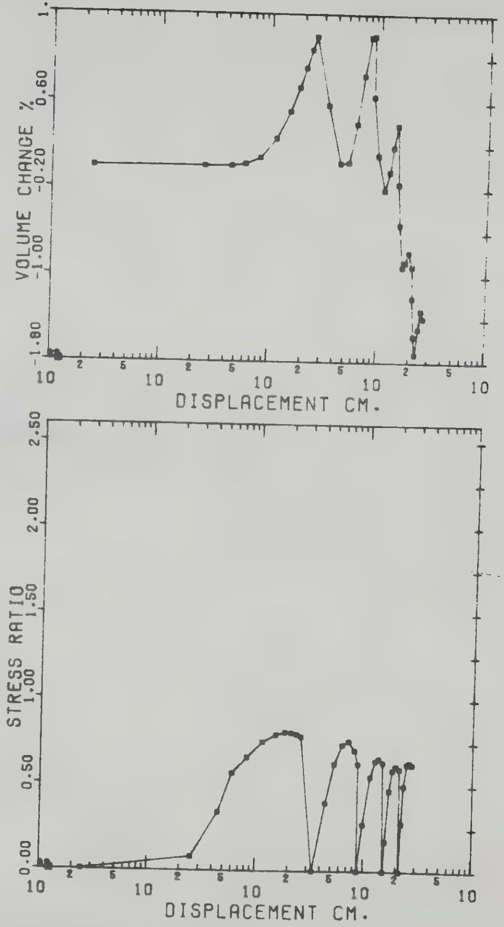

DISAGG. DENSIFIED SWAN RIVER SAND 4.0 KG./SQ.CM.

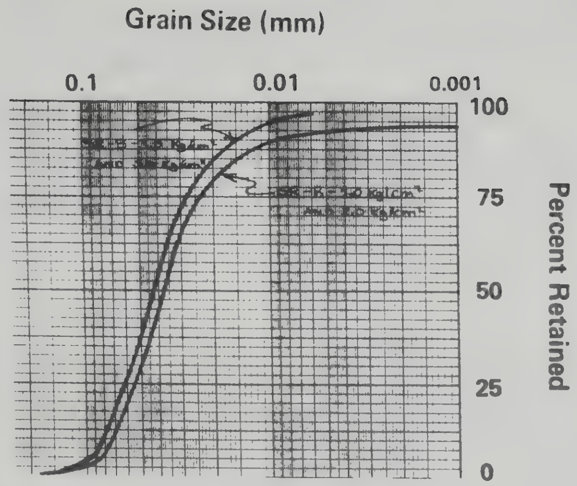

SAMPLE DESCRIPTIONS: ALL SPECIMENS CONSIST OF REDDISH SILT; THE RED COLOUR IS DUE TO IRON OXIDE. BEDDING IS HORIZONTAL AND SHEAR TOOK PLACE WITHIN SEVERAL DEGREES OF BEDDING. SPECIMENS DISPLAYED SATURATIONS OF 95.1% TO 100% (DUE TO THE EXTREME FINE-GRAINED CAPILLARY TENSION). MOISTURE CONTENT AVERAGED 17.2% (TOTAL WT BASIS) AND PARTICLE S.G. WAS 2.68.

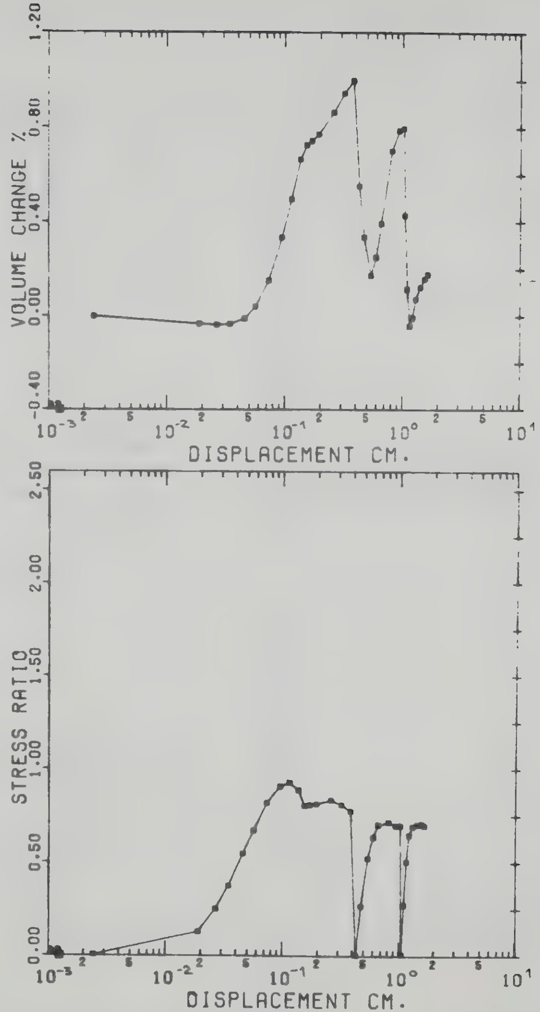

SWAN RIVER SHEAR SERIES 6 1.0 KG./SQ.CM.

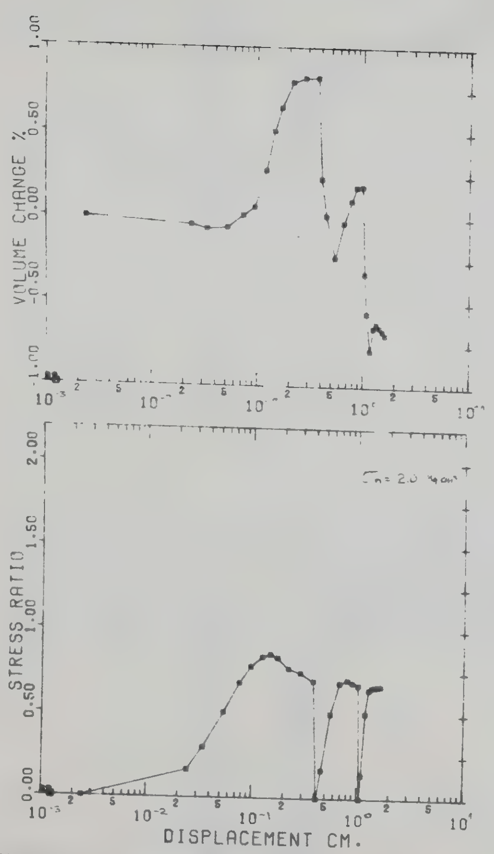

SWAN RIVER SHEAR SERIES B 2.0 KG./SQ.CM.

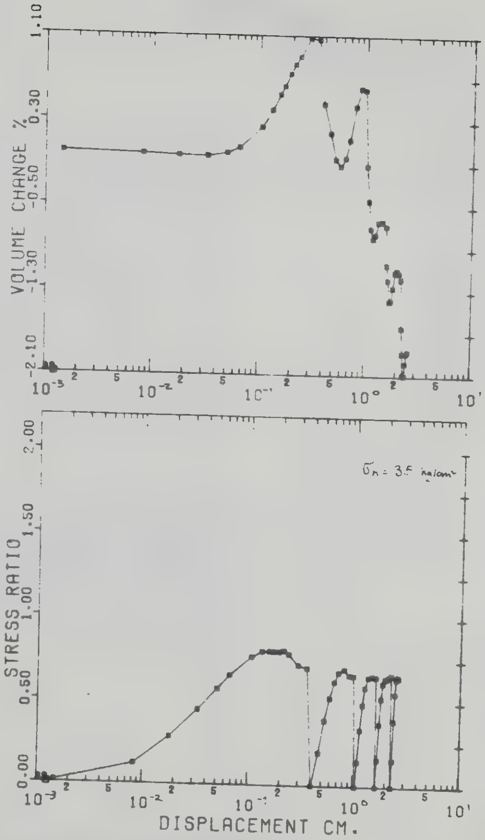

SWAN RIVER SHEAR SERIES B 3.5 KG./SQ.CM.

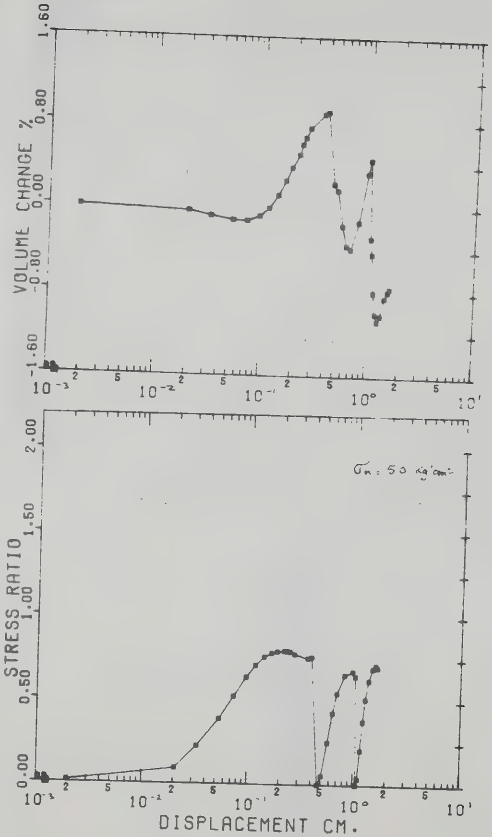

SWAN RIVER SHEAR SERIES B 5.0 KG./SQ.CM.

Medium-grained Ottawa Sand
(C-109) was used for all tests.

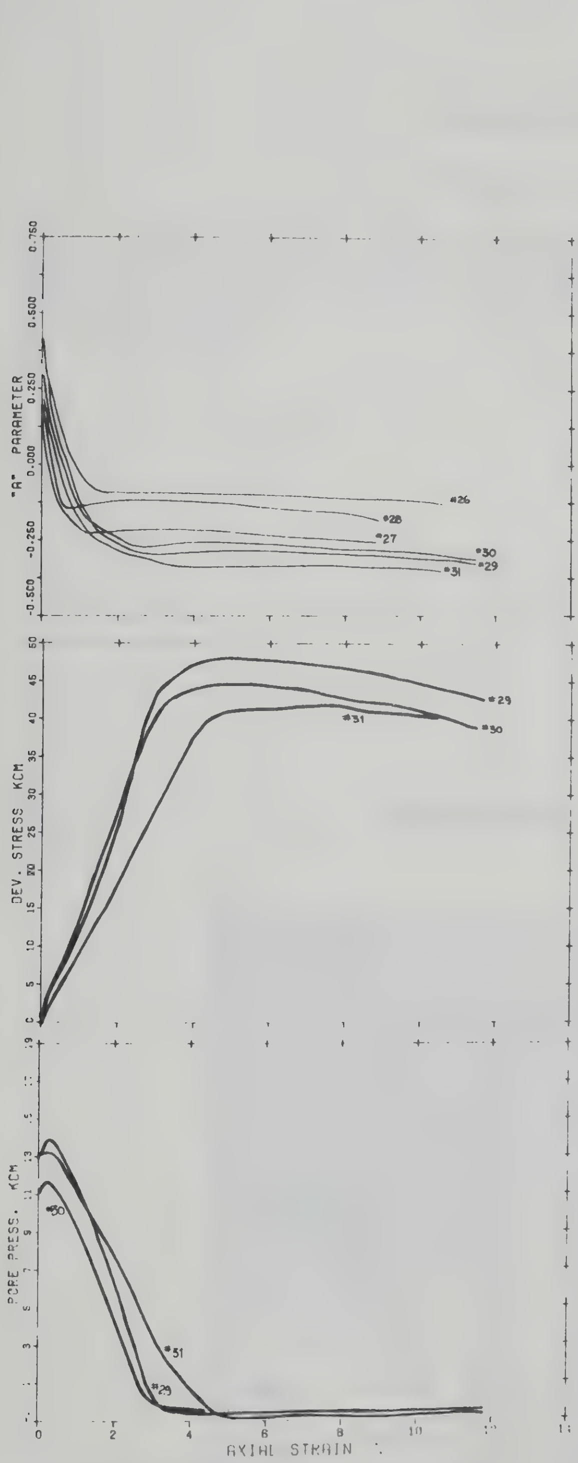

UNDRAINED OTTAWA SAND TRIAXIAL TESTS

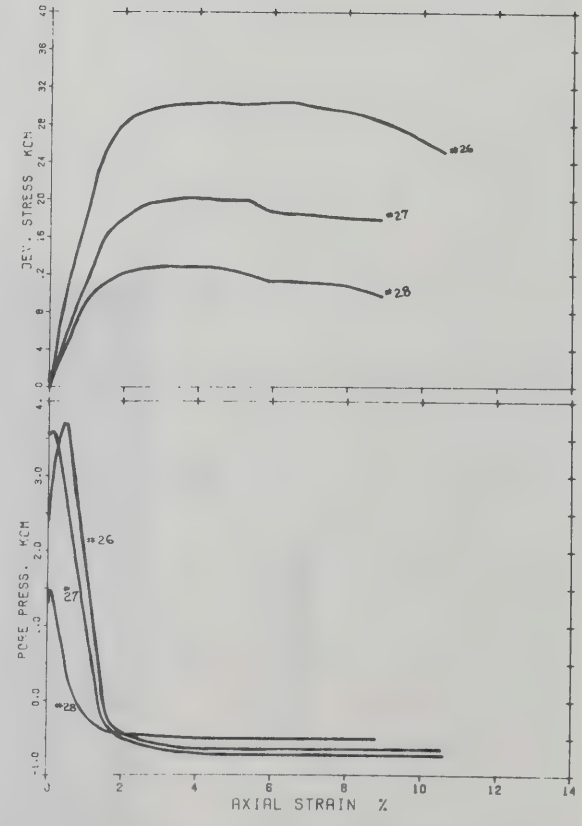

UNDRAINED OTTAWA SAND TRIAXIAL TESTS

Appendix E.2.2

Densified Tailings Sand Triaxial Tests

The grain size curve in the figure below represents the mean of several grain size analyses of triaxial tests from Appendix E.2.2. A distinctive feature of this material is a persistent muscovite content of about 0.5%.

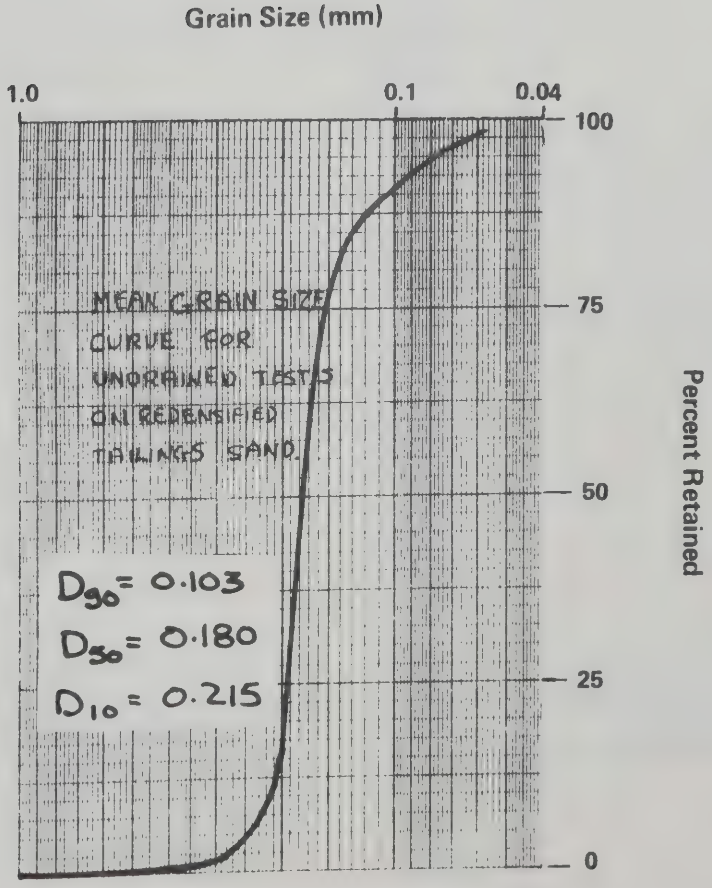

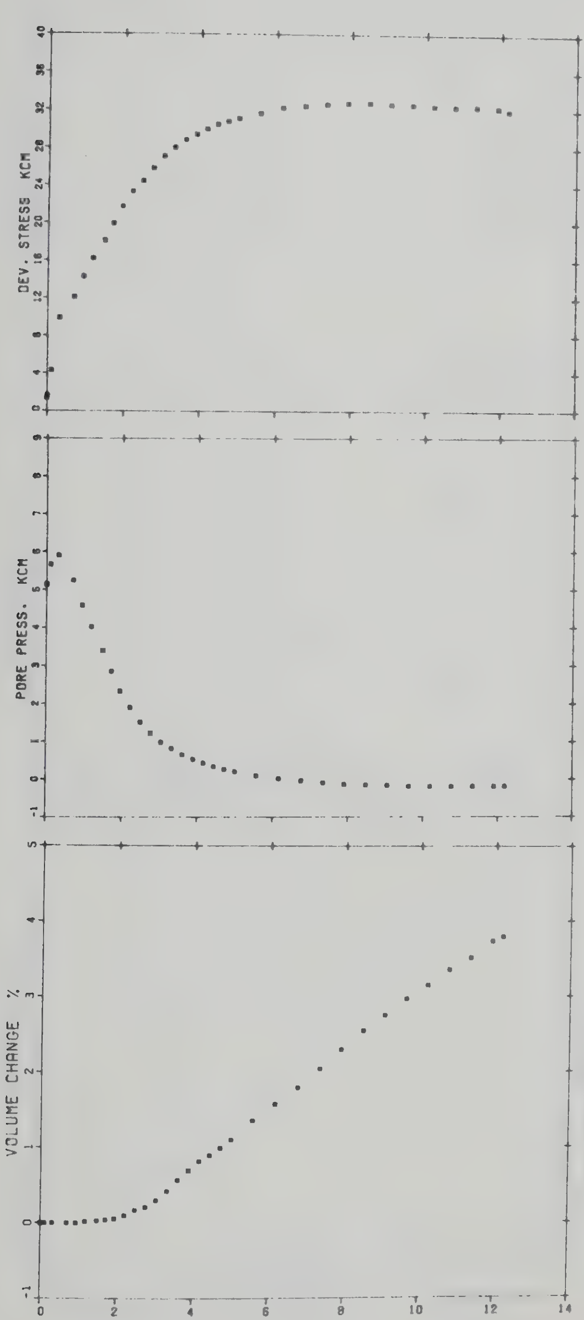

DENSIFIED TAILINGS SAND --T1-- 150/75

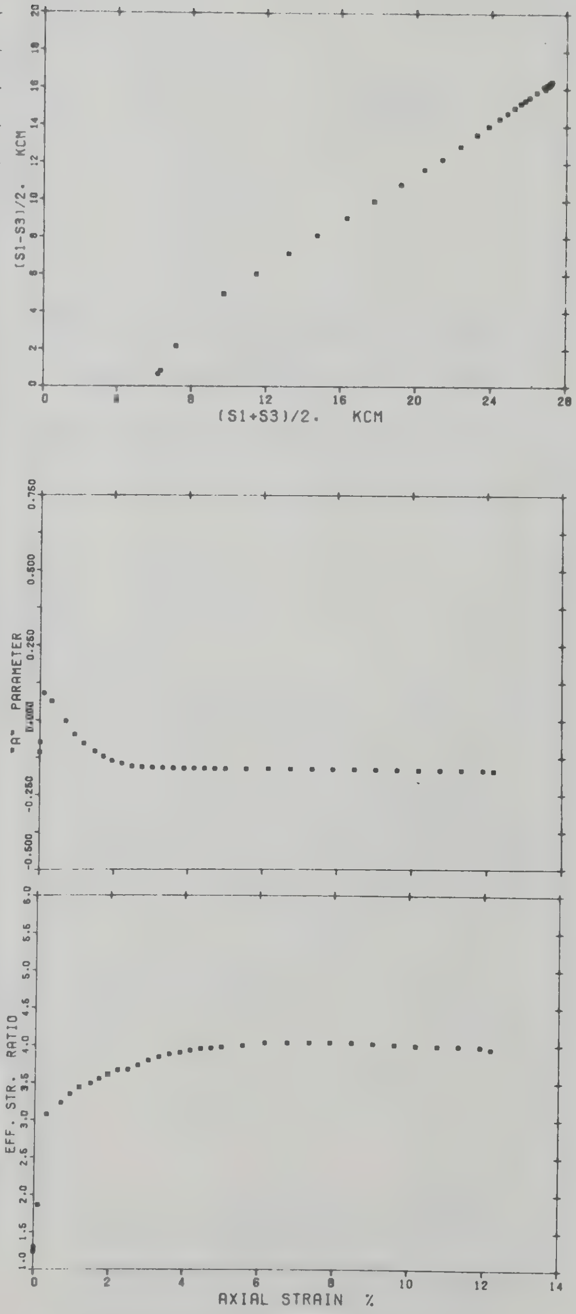

DENSIFIED TAILINGS SAND --T1-- 150/75

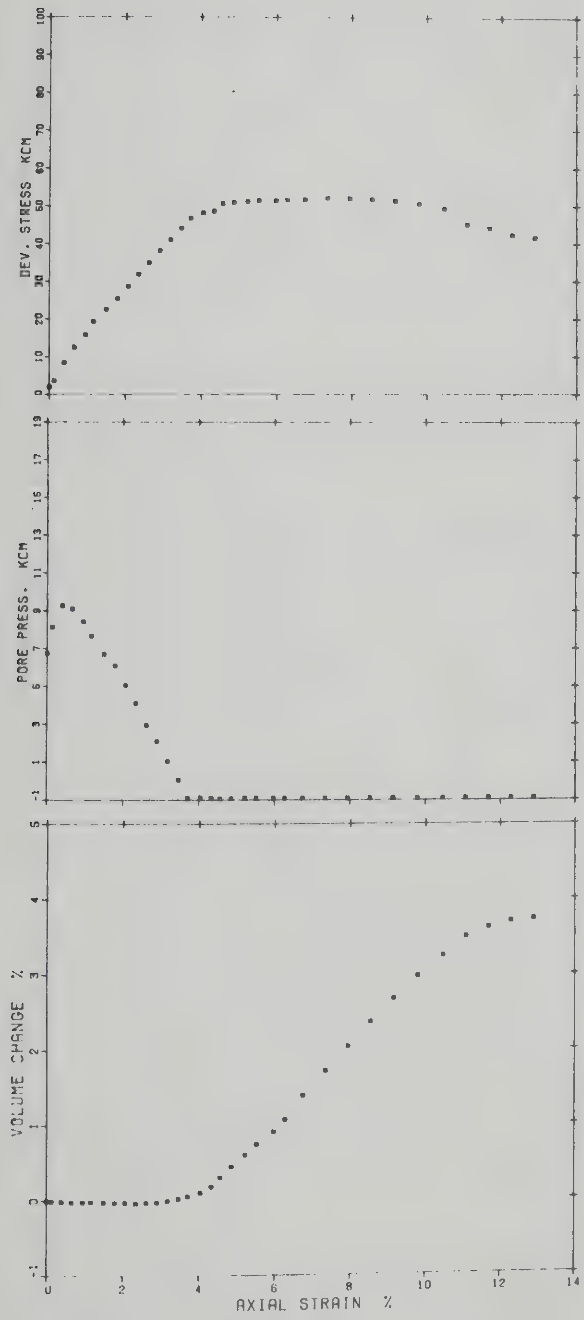

DENSIFIED TAILINGS SAND --T3-- 200/100

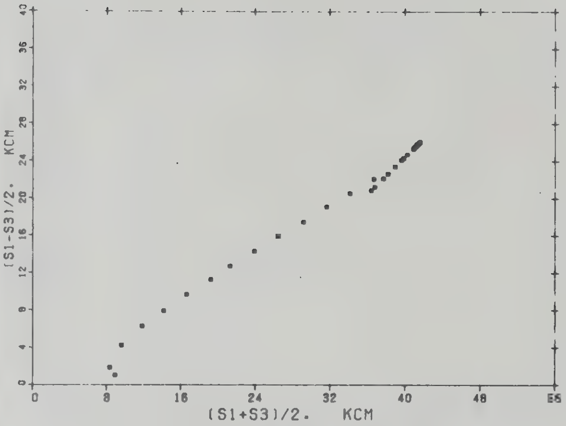

DENSIFIED TAILINGS SAND --T3-- 200/100

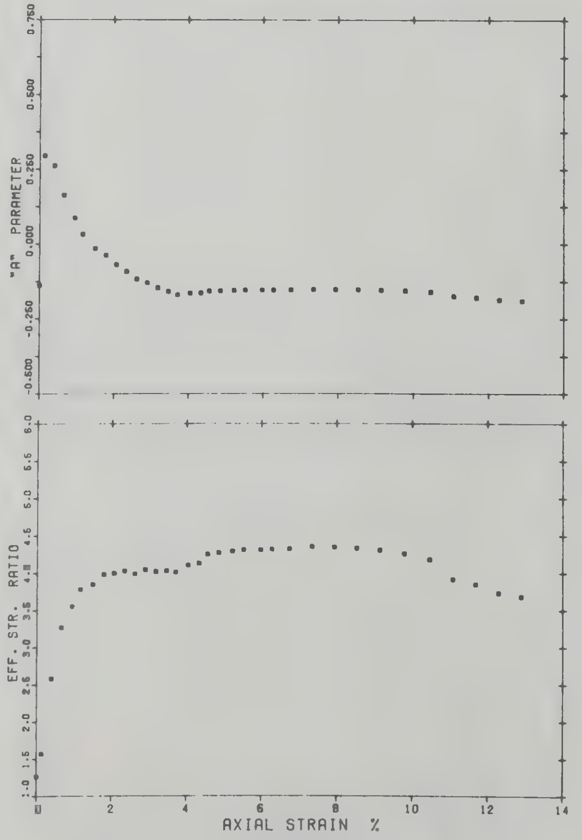

DENSIFIED TAILINGS SAND --T3-- 200/100

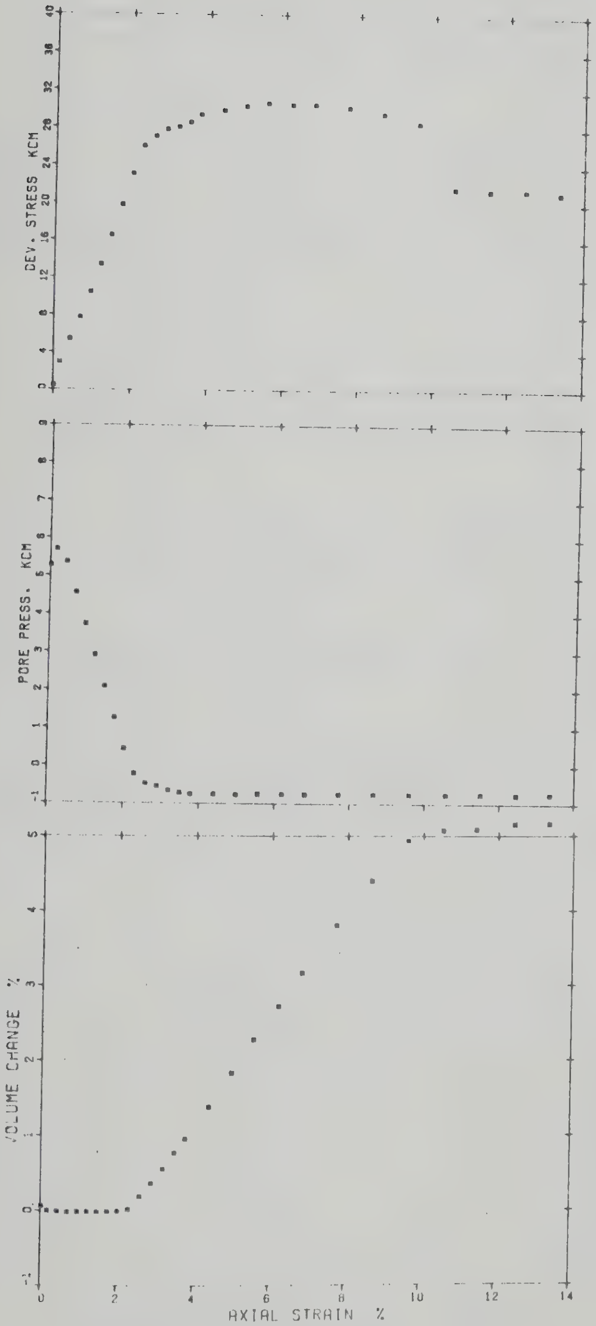

DENSIFIED TAILINGS SAND --T4-- 100/75

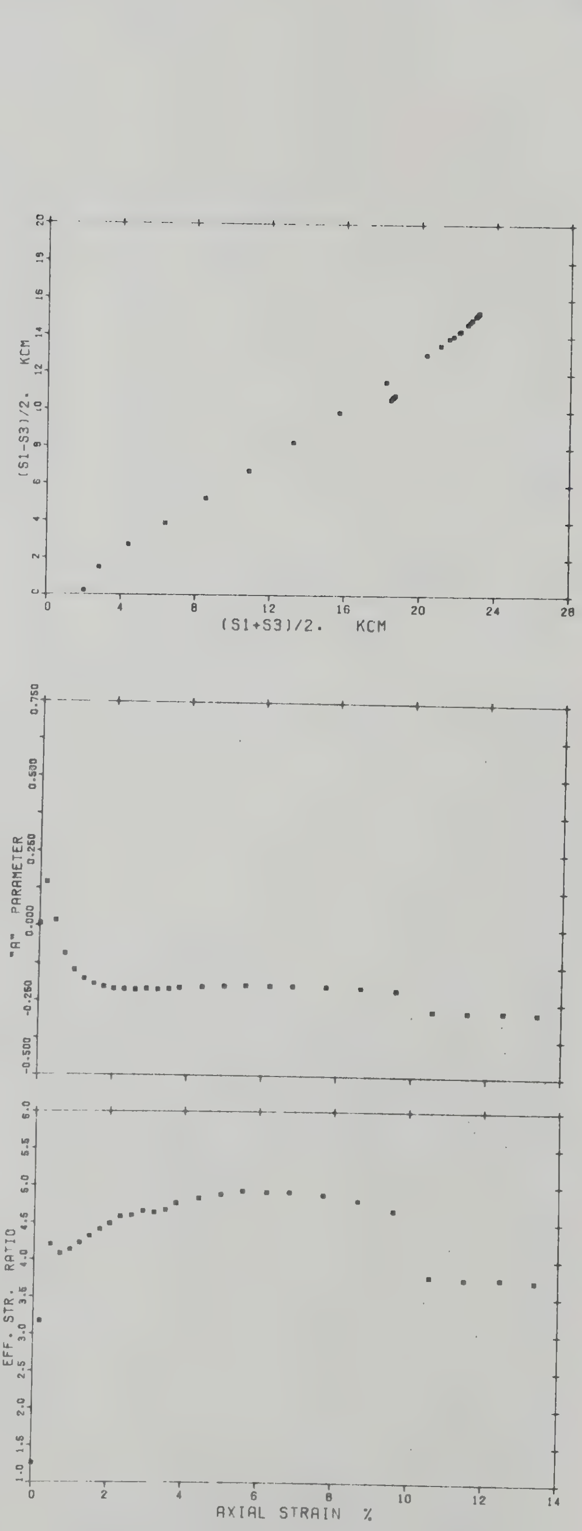

DENSIFIED TAILINGS SAND --T4-- 100/75

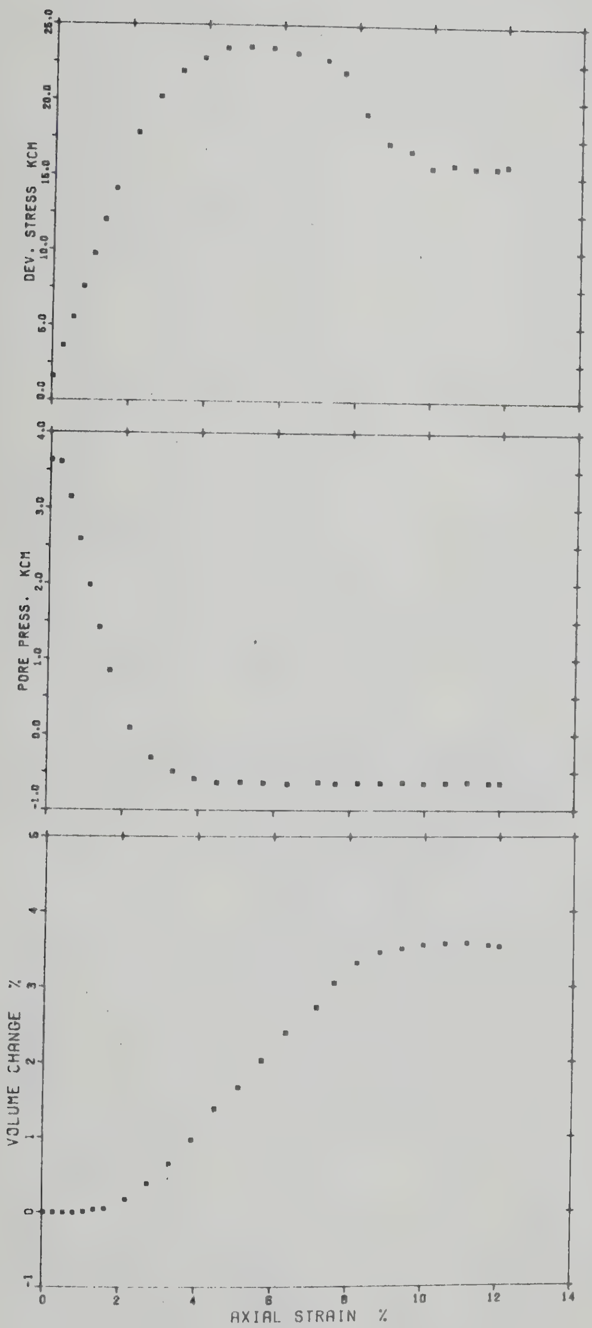

DENSIFIED TAILINGS SAND --T5-- 75/50

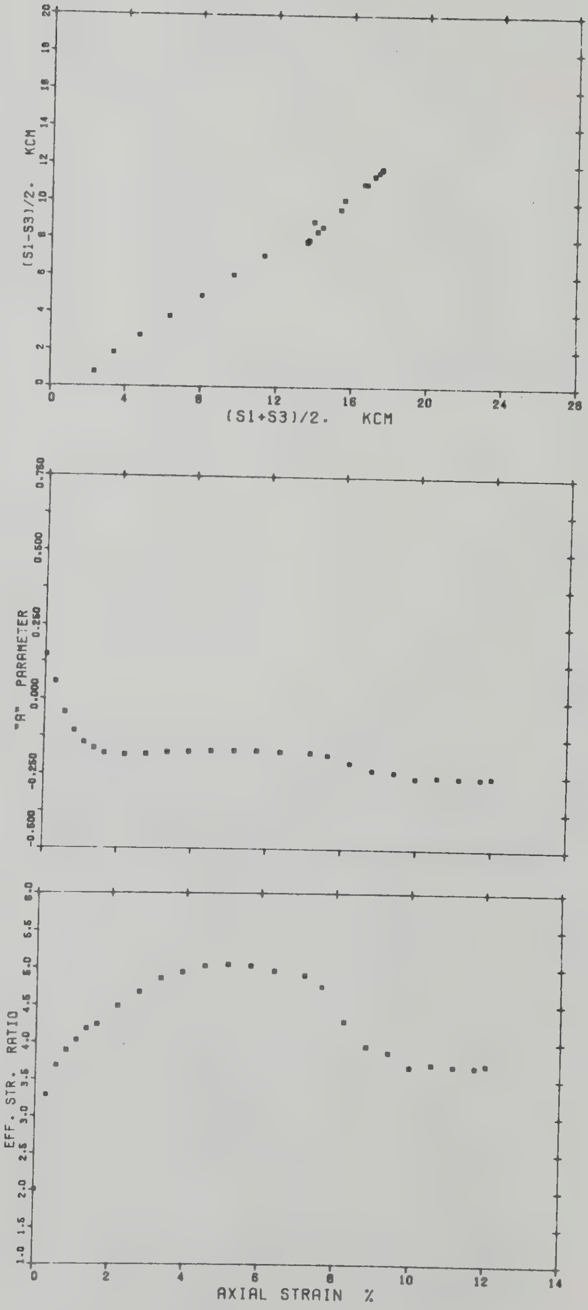

DENSIFIED TAILINGS SAND --T5-- 75/50

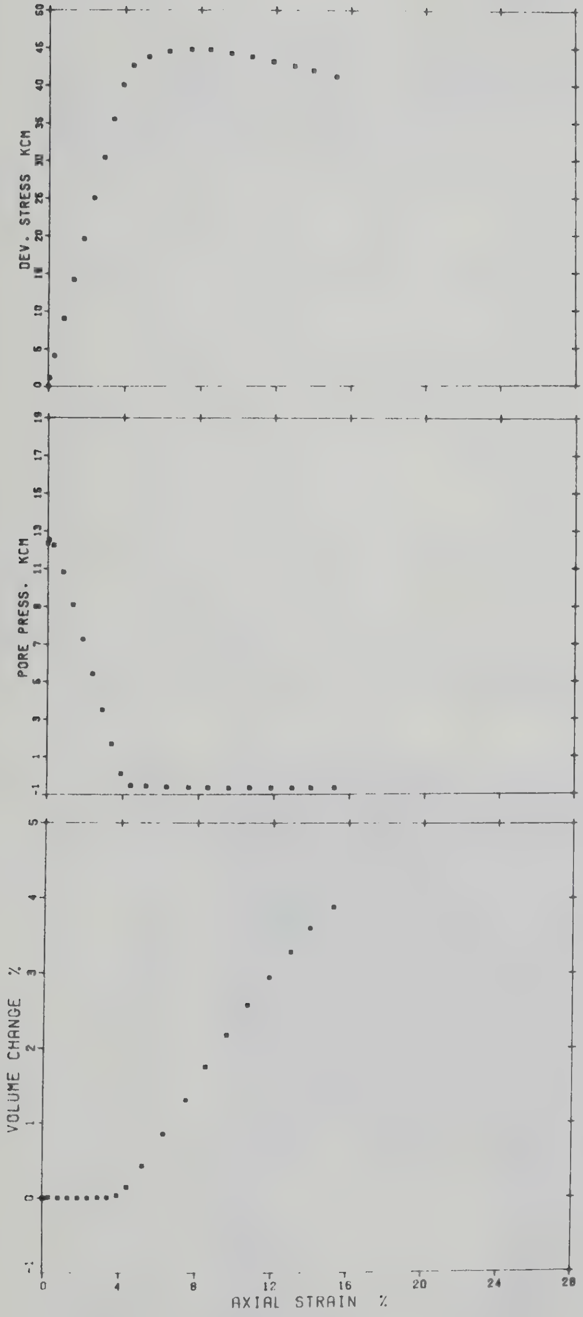

DENSIFIED TAILINGS SAND --T6-- 200/180

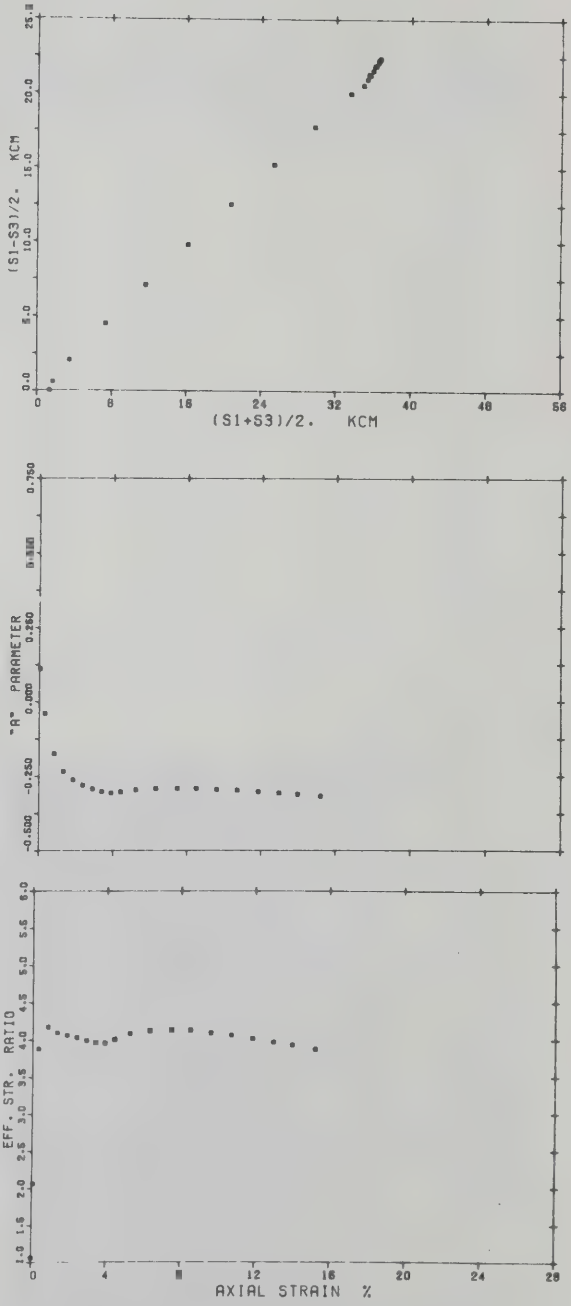

DENSIFIED TAILINGS SAND --T6-- 200/180

Appendix E.2.3

A representative grain size analysis may be found in the figure below. This curve is the mean of several determinations and is quite representative as the pit run oil sand was totally disaggregated and blended before compaction.

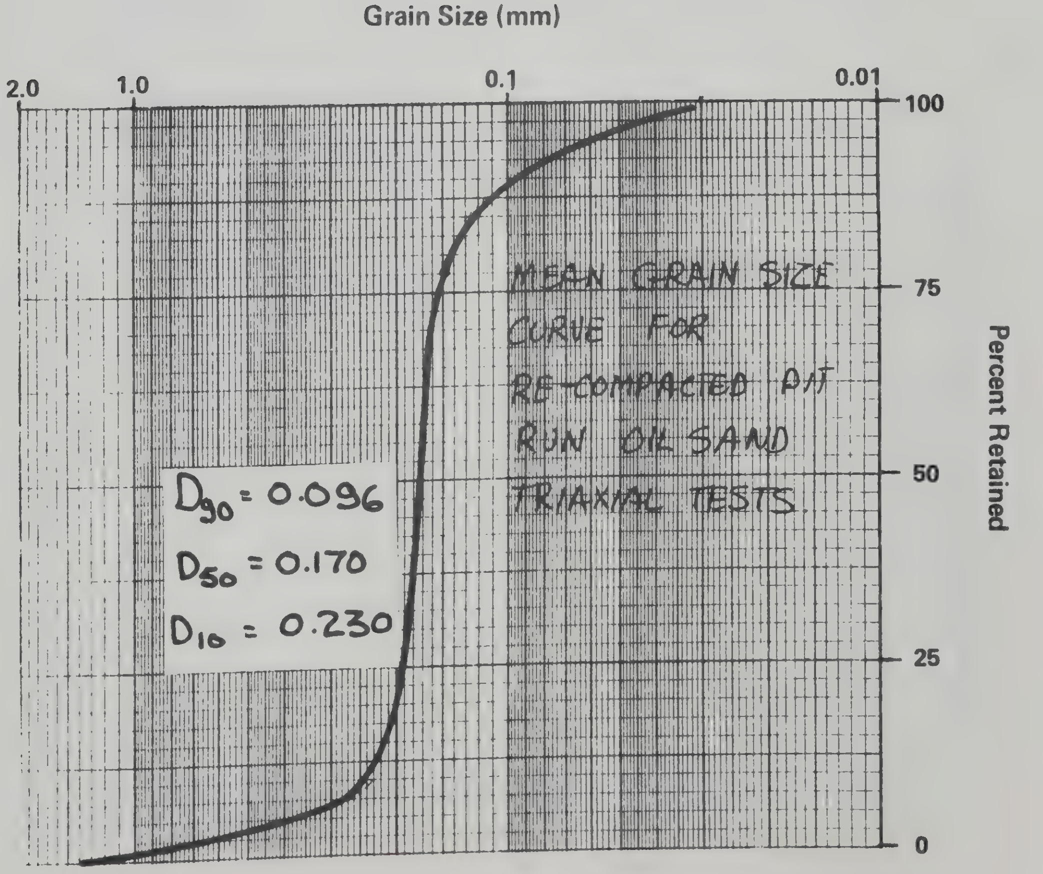

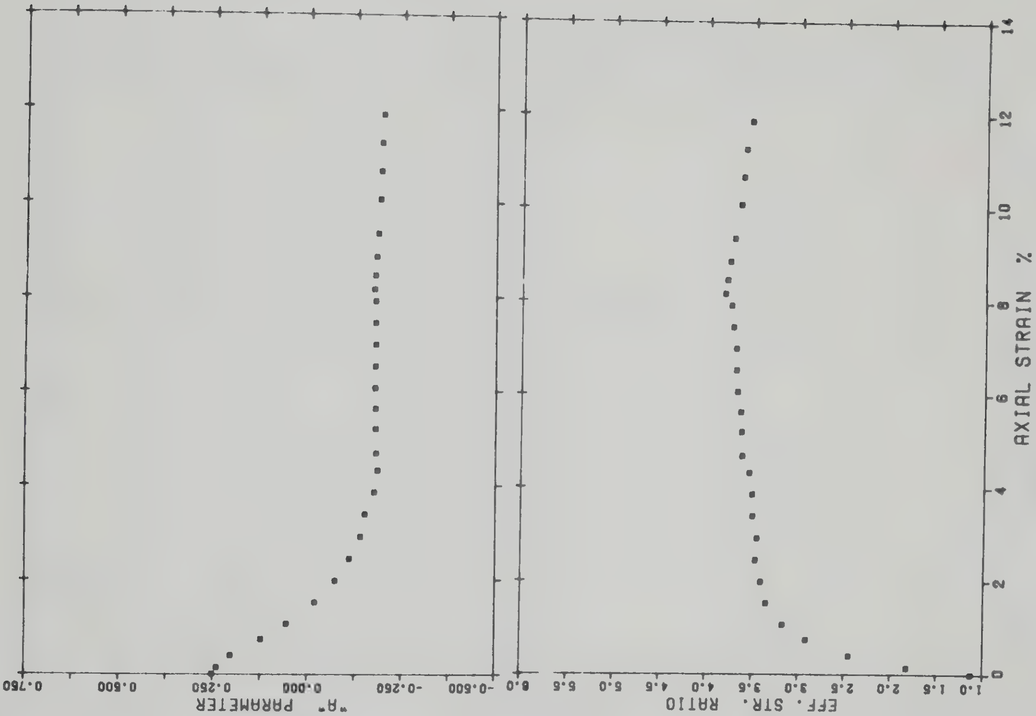

RECOMPACTED PIT RUN OIL SAND -T50- 200/100

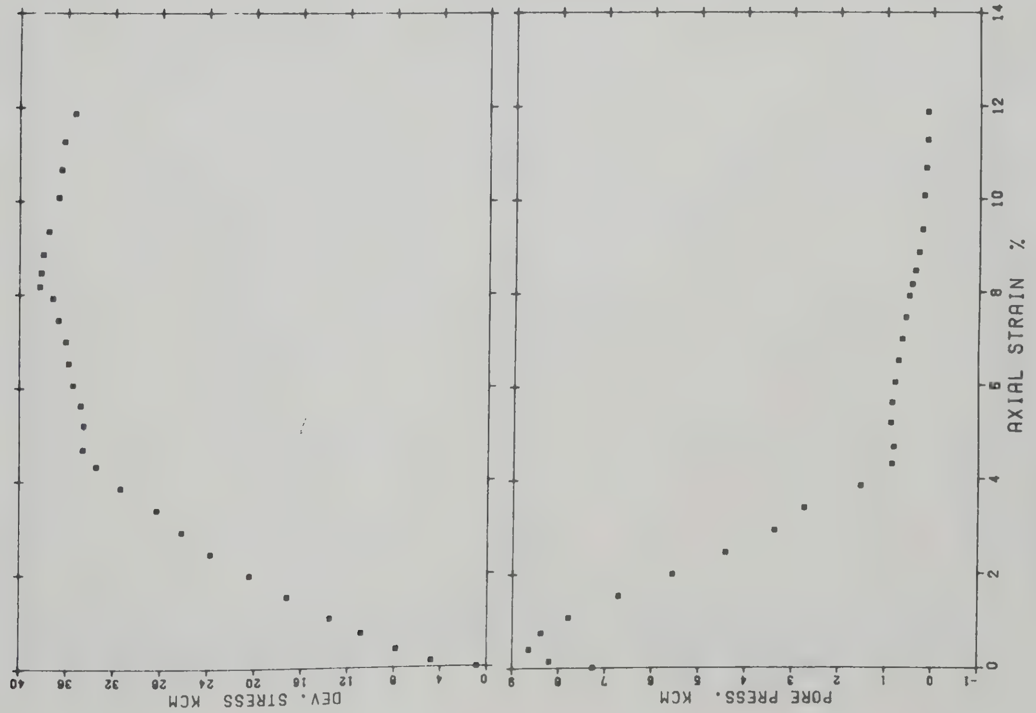

RECOMPACTED PIT RUN OIL SAND -T50- 200/100

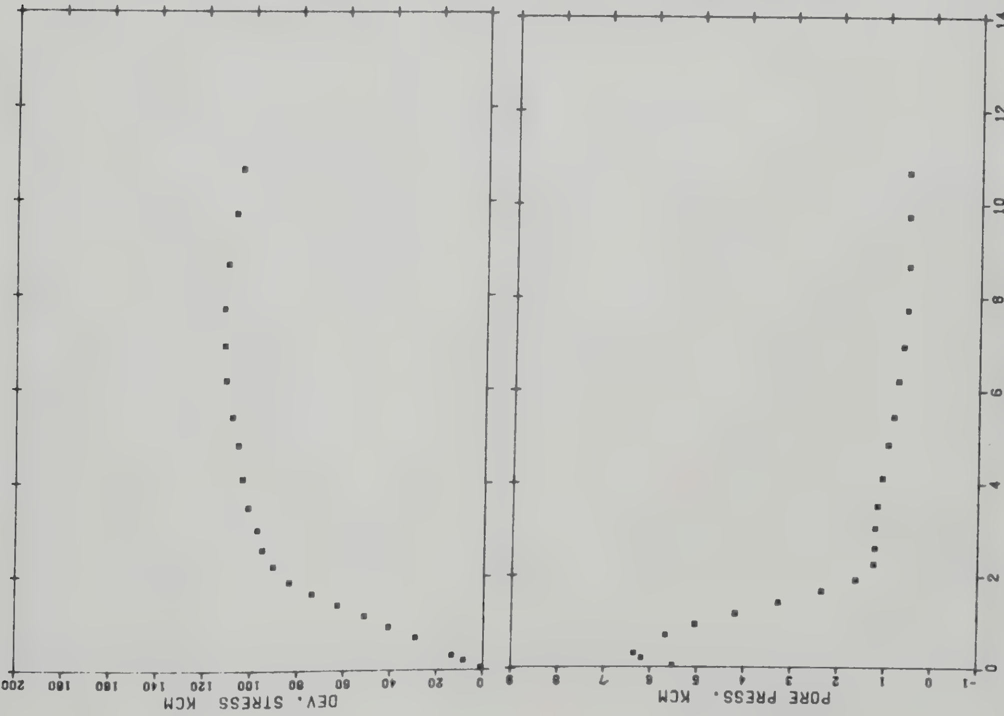

RECOMPACTED PIT RUN OIL SAND -T51- 150/75

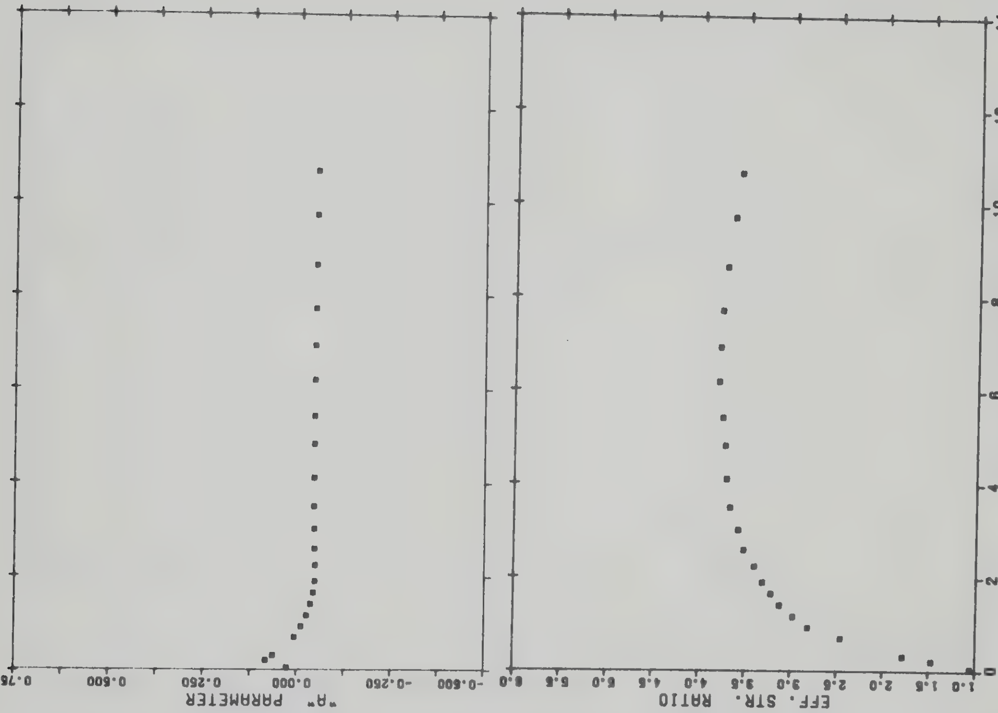

RECOMPACTED PIT RUN OIL SAND -T51- 150/75

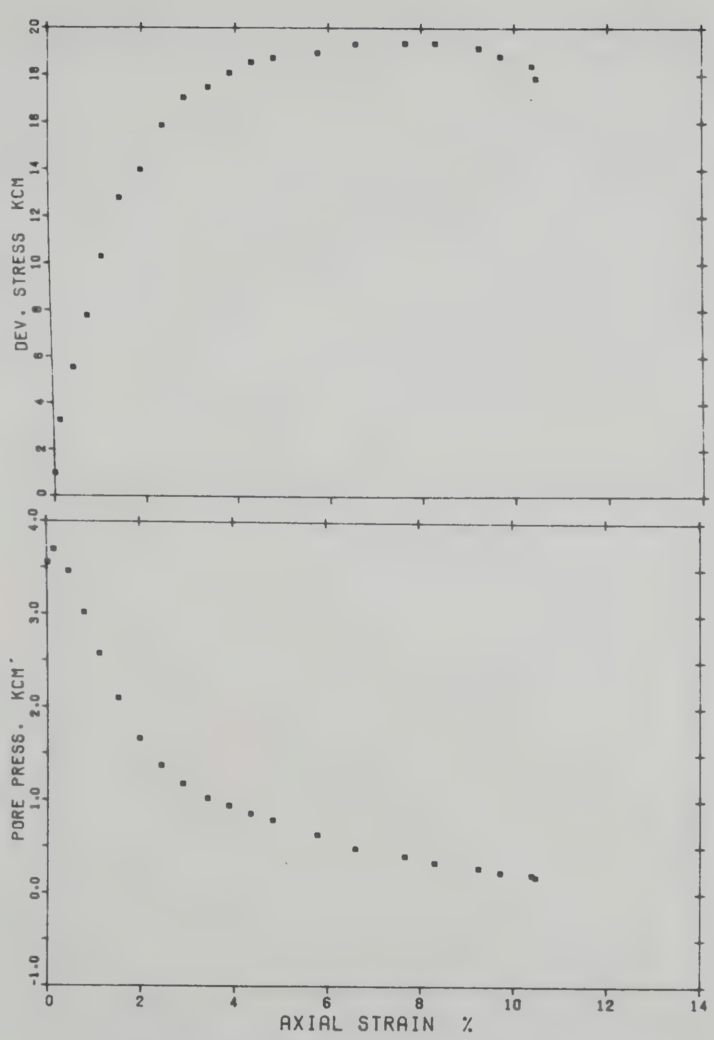

RECOMPACTED PIT RUN OIL SAND -T53- 100/50

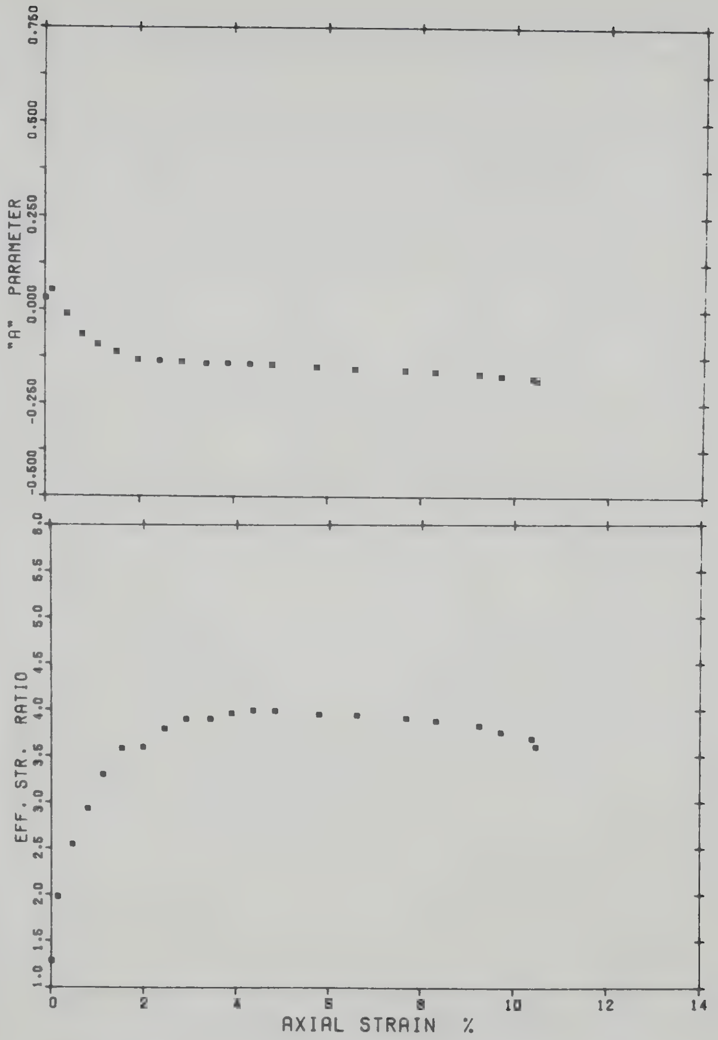

RECOMPACTED PIT RUN OIL SAND -T53- 100/50

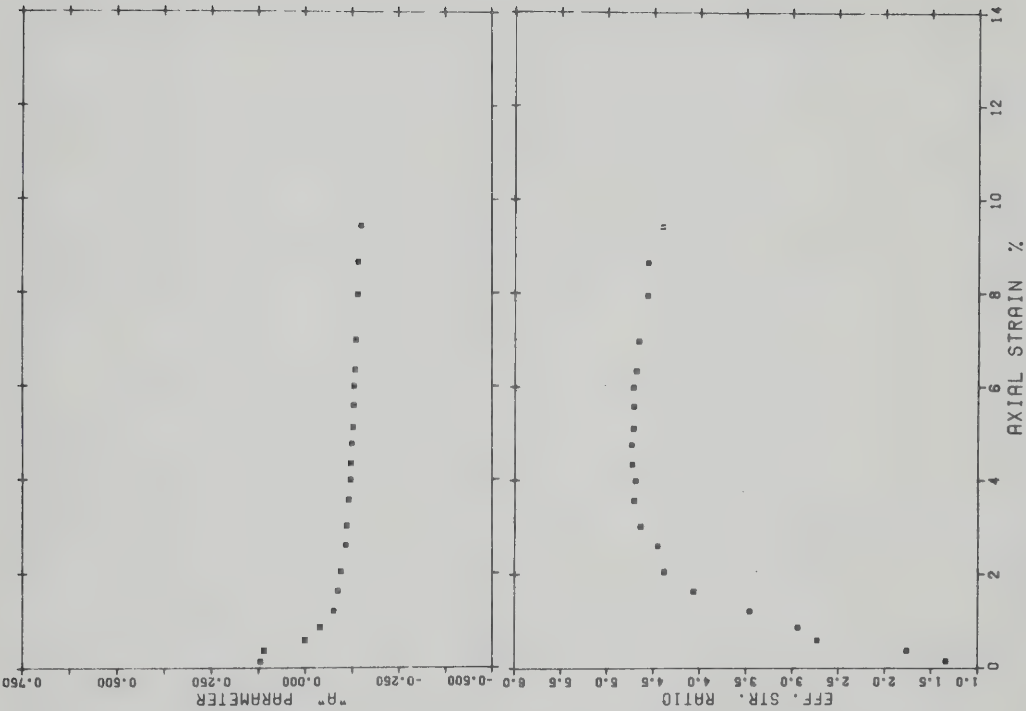

RECOMPACTED PIT RUN OIL SAND -T54- 50/25

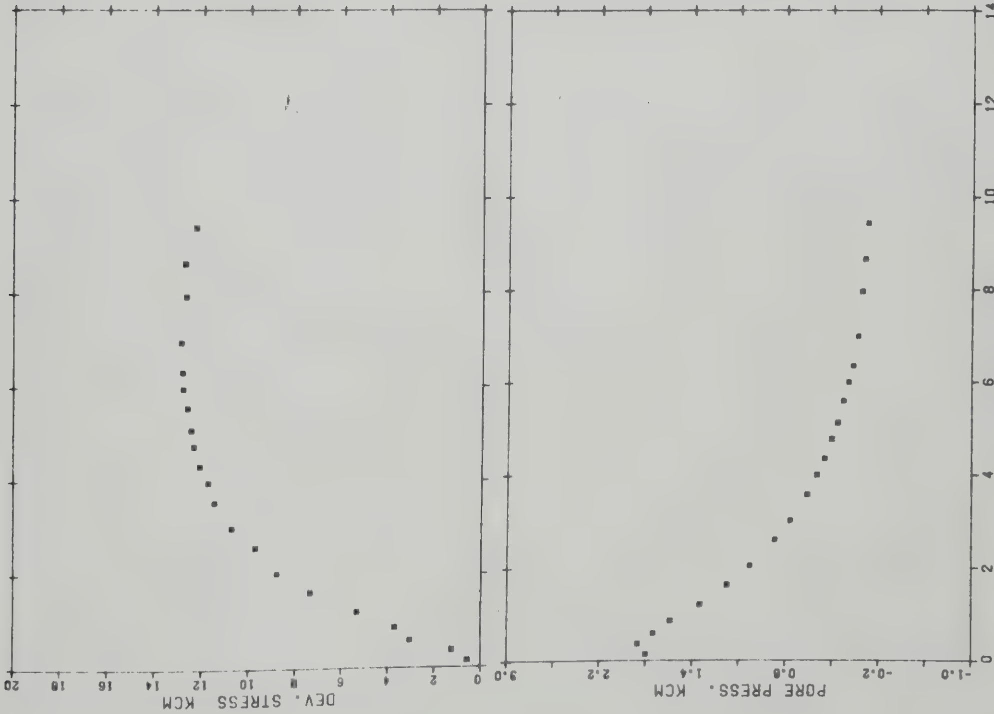

RECOMPACTED PIT RUN OIL SAND -T54- 50/25

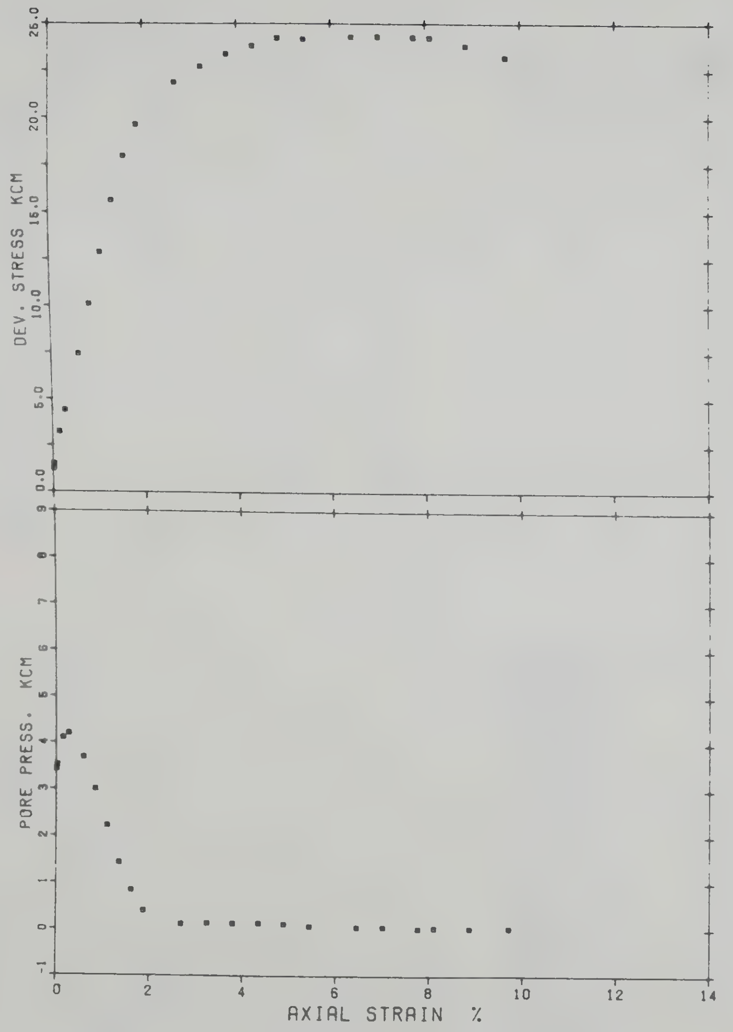

RECOMPACTED PIT RUN OIL SAND -T55- 100/50

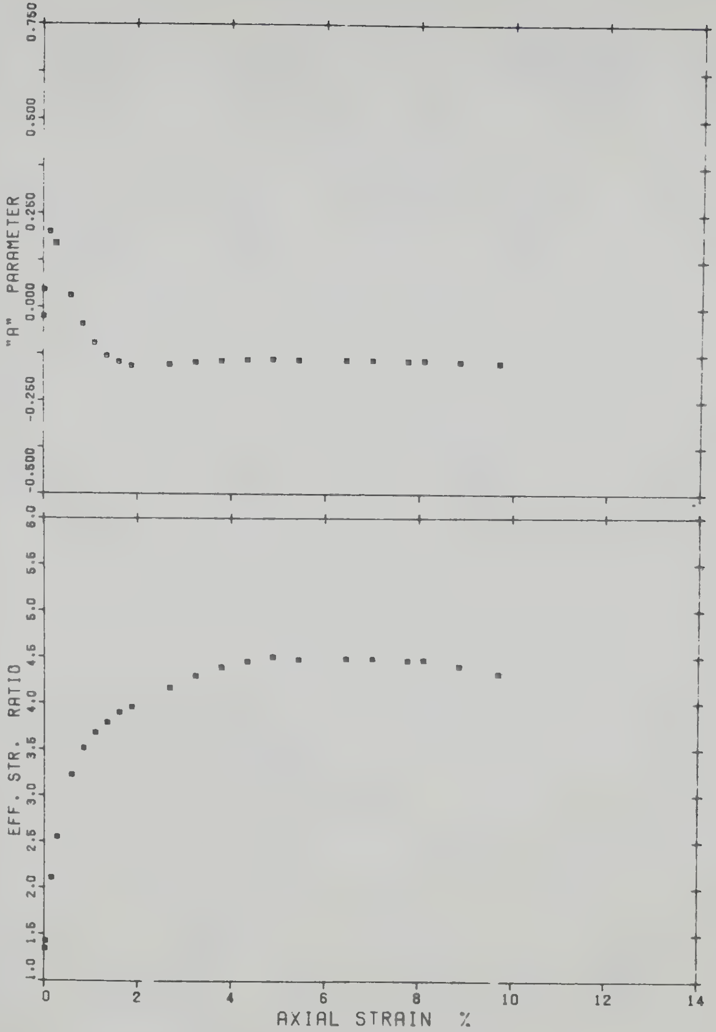

RECOMPACTED PIT RUN OIL SAND -T55- 100/50

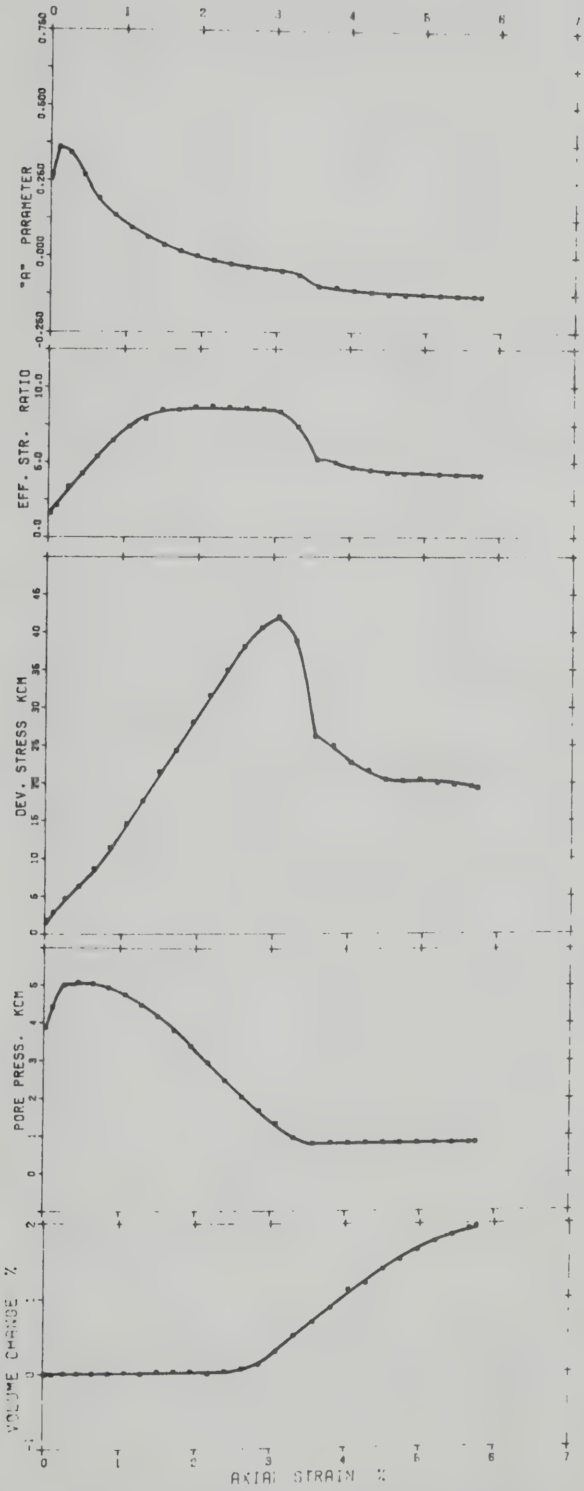

OILSAND TRIAXIAL TEST 109' [illegible].03 KG/CM2

L/D ratio = 2.054
n = 34.5%
Bulk density = 2.032
Mean oil content = 5.5%

Description: Oil-poor fine-grained sand, 7° to 12° cross-bedded with 45% zones of oil-free silt.

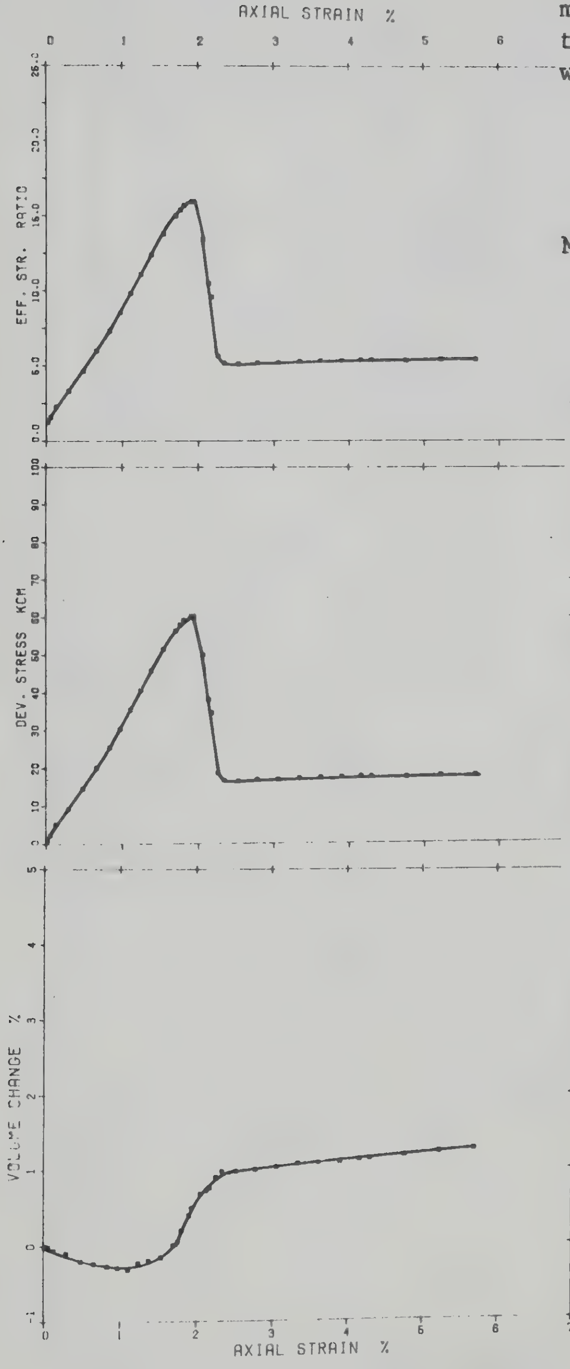

OILSAND TRIAXIAL 117.05-117.65 4.0 KCM

Post-failure moisture contents: (total weight basis)

1: 8.84%
2: 7.95%
3: 7.56%
4: 7.11%
Mean = 7.86%

5: 3.42%
6: 3.90%
7: 3.30%
8: 3.55%
Mean = 3.54%

Mean oil content = 12.07%

B.D. = 2.053 gm/cc

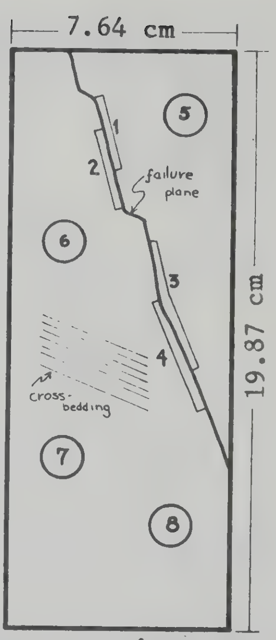

Mean moisture content (before test) = 3.5%
K = 7.0 x 10^{-8} cm/sec
m_v = 0.0006

Description: fine-grained, oil-rich sand, cross-bedded at 15° to 20°, with minor oil-free silty seams.

L/D ratio = 2.054
n = 34.5%
Bulk density = 2.032
Mean oil content = 5.5%

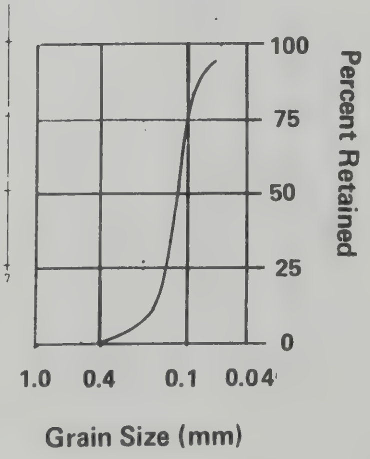

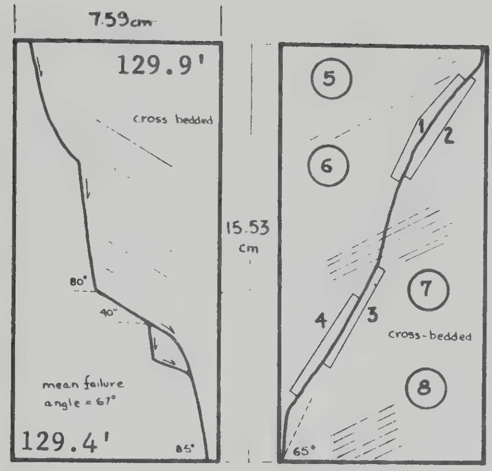

Post-failure moisture contents (total weight basis):
1 = 8.62% 5 = 5.83%
2 = 8.34% 6 = 5.09%
3 = 7.74% 7 = 4.78%
4 = 7.71% 8 = 4.49%
Means = 8.10% 5.05%

Mean total post-failure moisture content = 5.58%

Mean oil content = 11%

Bulk density = 2.068 gm/cc
K = 3.1 x 10^{-8} cm/sec
L/D ratio = 2.046
Time to failure = 41.5 hours
ΔV at 2.5% strain = +1.65%

<u>Description</u>: medium to richly saturated fine-grained sand, cross-bedded at 25° to 35° with zones of lenticular contortions.

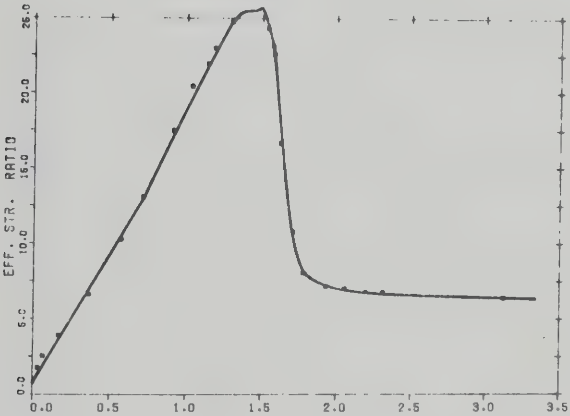

OILSAND TRIAXIAL 129.4-129.9 1.0 KCM

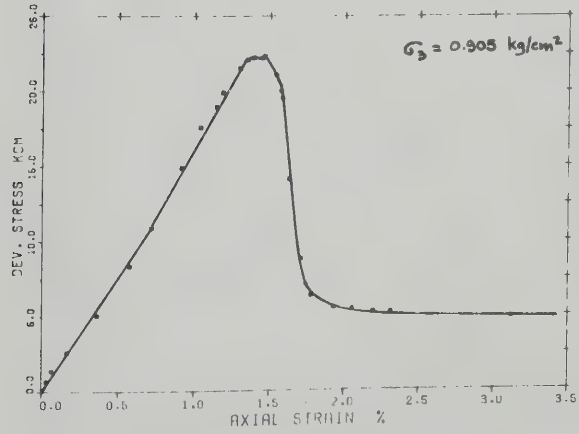

OILSAND TRIAXIAL 129.4-129.9 1.0 KCM

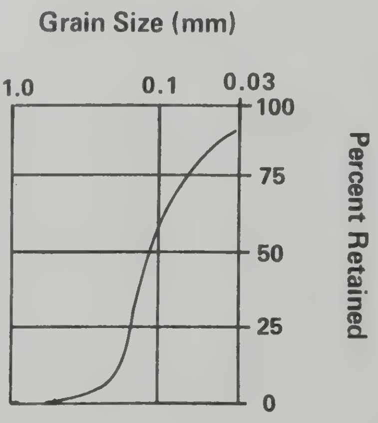

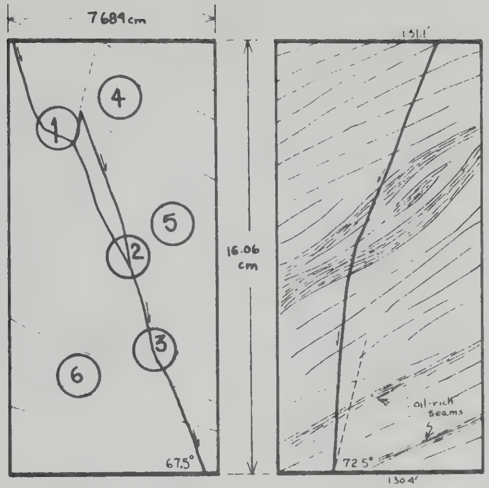

Post-failure moisture contents (total weight basis):
1 = 9.95% 4 = 8.43%
2 = 8.58% 5 = 6.27%
3 = 9.85% 6 = 7.92%
Means = 9.46% 7.54%

Mean total pre-failure moisture content = 7.7%

Mean oil content = 2.6%

Bulk density = 2.1905
$K = 1.2 \times 10^{-8}$ cm^2/sec
L/D ratio = 2.09

<u>Description</u>: largely oil-free silt with minor seams of fine-grained oil-containing sand. Bedding dips from 15° to 20°.

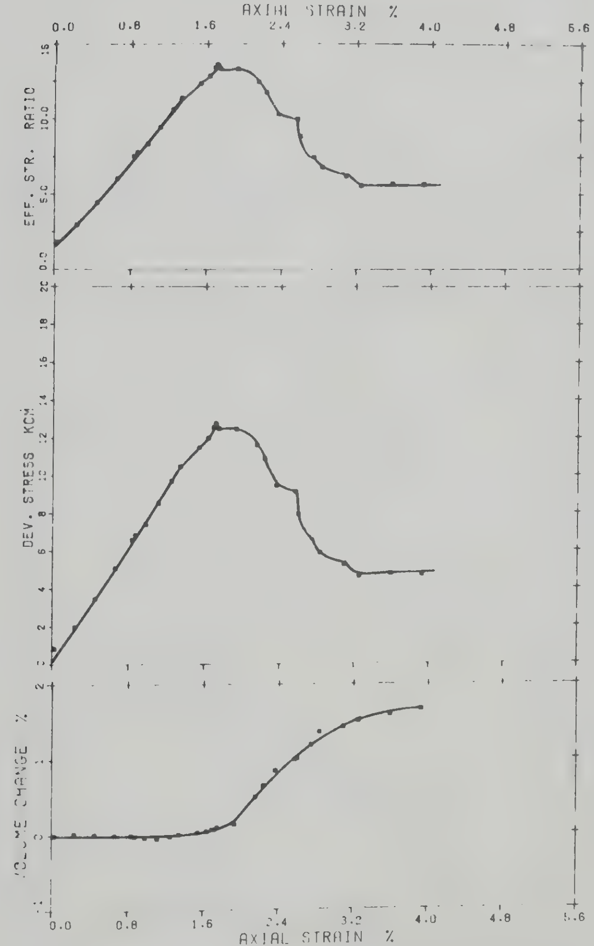

OILSAND TRIAXIAL "B" 130.5-131.05 1.0 KCM

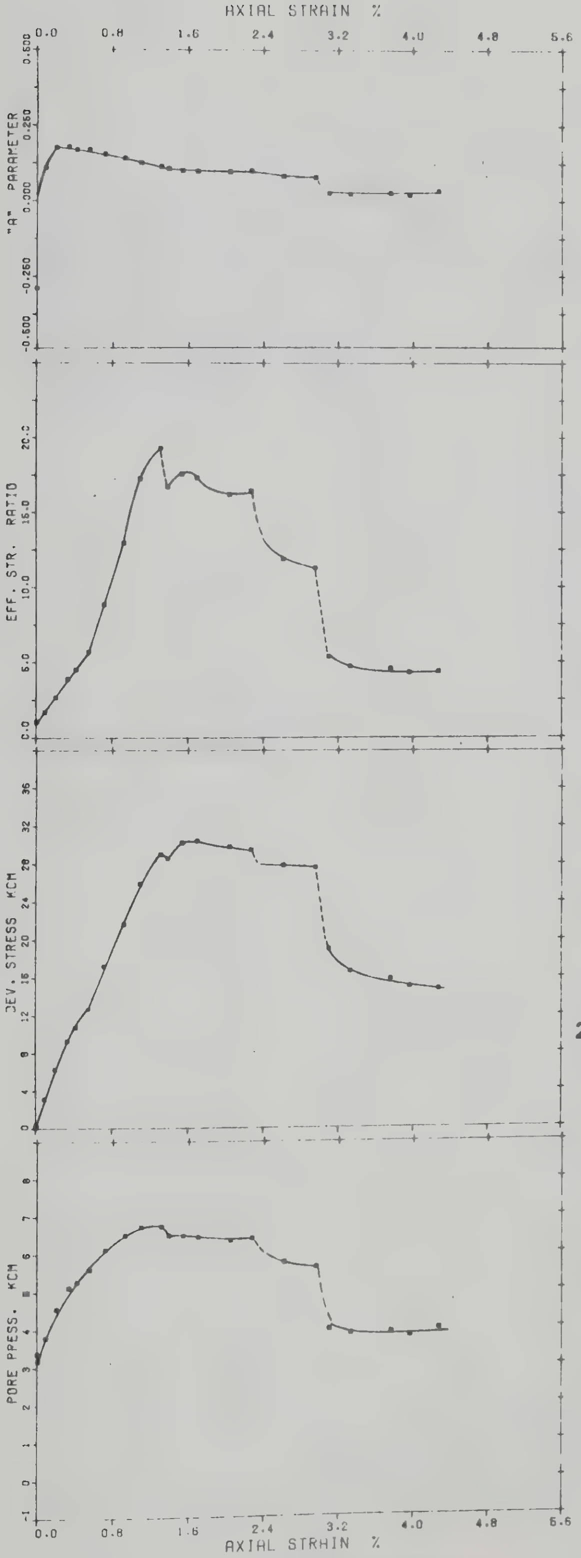

OILSAND TRIAXIAL "ATS-133'" (LEAN)

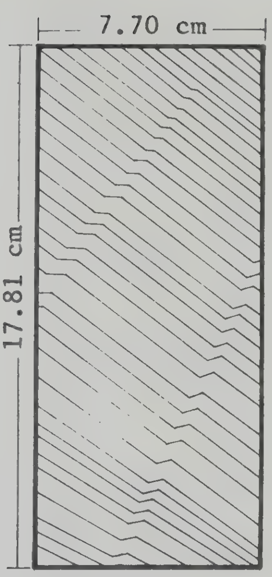

≃1% oil
Bulk density = 2.238 gm/cc
K = 6 x 10^{-9} cm/sec
L/D ratio = 2.31

Description: Oil-poor fine-grained silty sand, high-angle kink bands common, cross-bedded from 34° to 42°, well-laminated with 6 to 12 varves/cm, mica flecks on bedding planes.

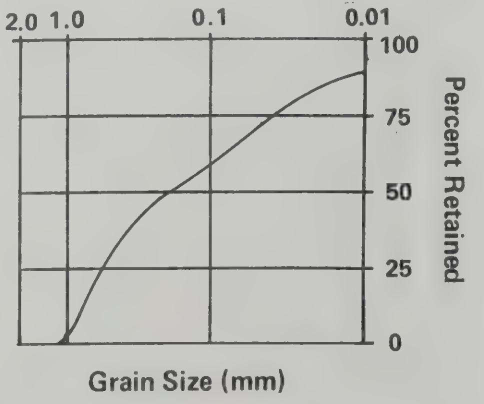

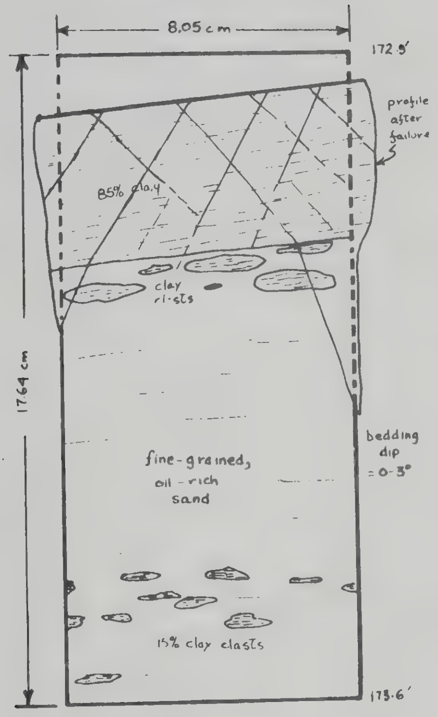

TRIAXIAL 173

Oil content of fine-grained sand = 15.1%

Oil content of clay zone = 2.3%

Bulk density = 1.92 gm/cc

Description: Lower two-thirds of specimen is fine-grained, oil-rich sand, approximately horizontally bedded with one band of clay clasts. Upper third of the specimen is clay, laminated horizontally, grading into clay clasts.

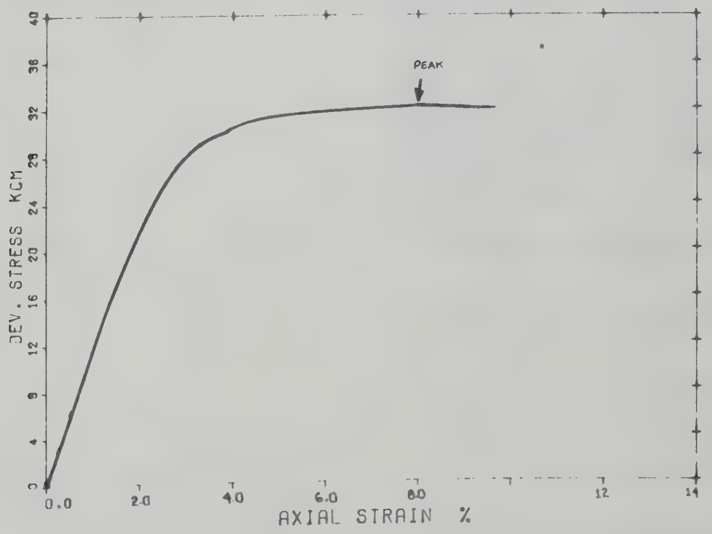

OILSAND TRIAXIAL "ATS-173"

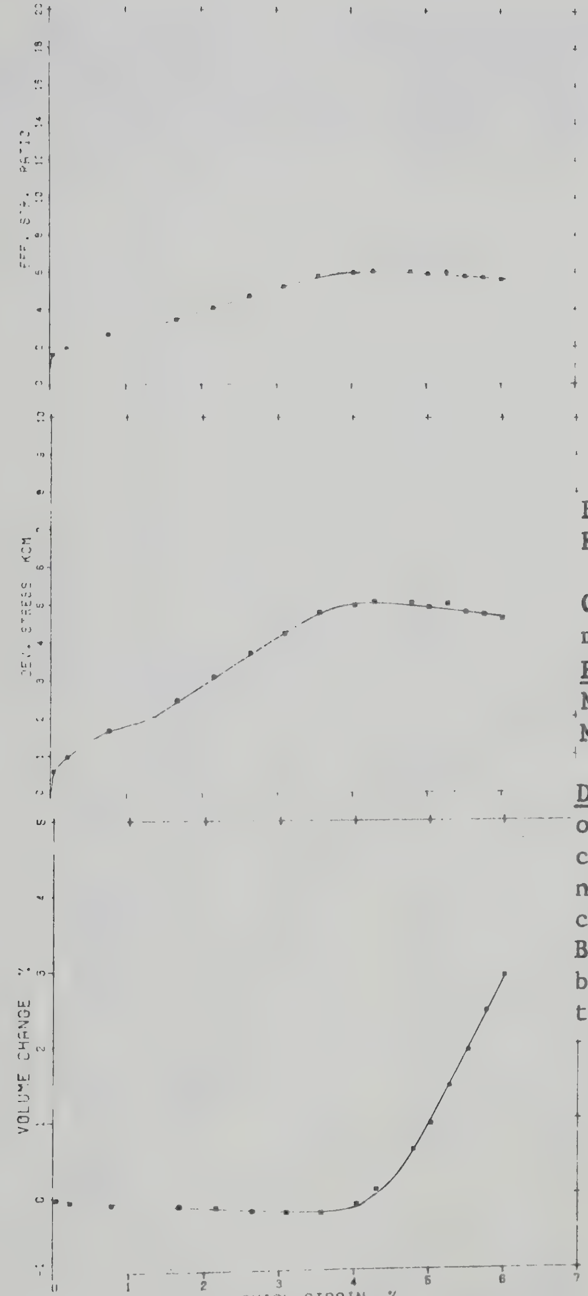

OILSAND TRIAXIAL 209.2-209.8 1.0 KCM

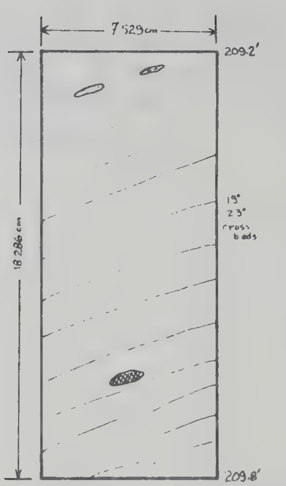

Bulk density = 1.885 gm/cc
K (permeability) = 5.25 x 10^{-6} cm/sec
C_v = 0.273 cm^2/sec
m_v = 0.0192 cm^2/kg

<u>Failure by bulging</u>

Mean oil content = 15.2%
Mean water content (pre-failure) = 1.4%

<u>Description</u>: coarse-grained oil-rich sand with a few minor clay clasts, one concretionary node (pyritic), all displaying cross-beds from 19^o to 23^o. Bedding is difficult to pick out because of the oil-richness of the material.

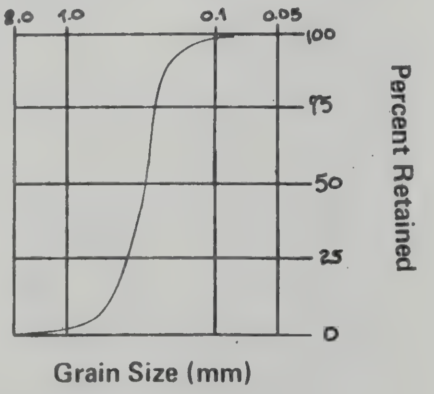

Appendix E.2.5

Grain size curves representative of all St. Peter Sandstone tests may be found on page 400. The diagram below is a typical volume change curve for a triaxial test: there is no detectable volume change before failure, and a leveling-off of volume change occurs once quasi-residual conditions are reached.

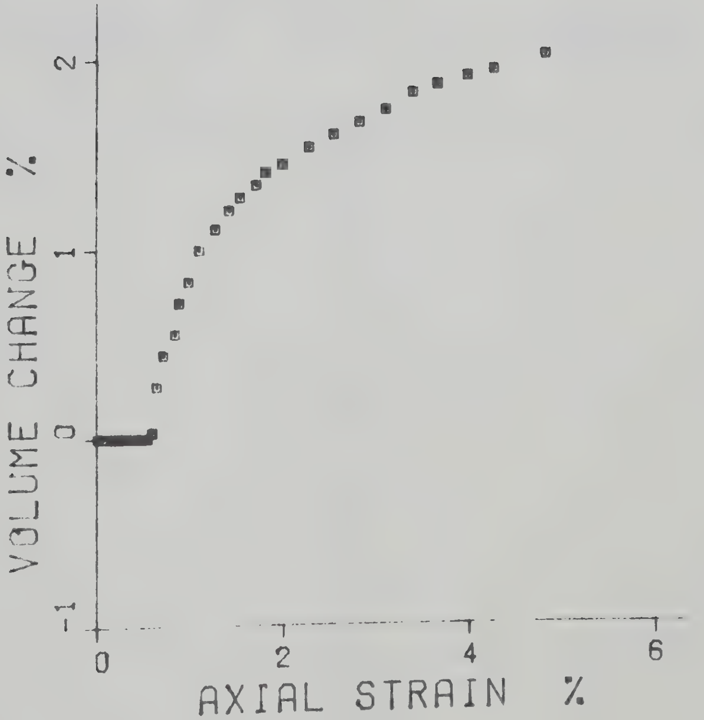

TEST 0.526

ST. PETER TRIAXIAL

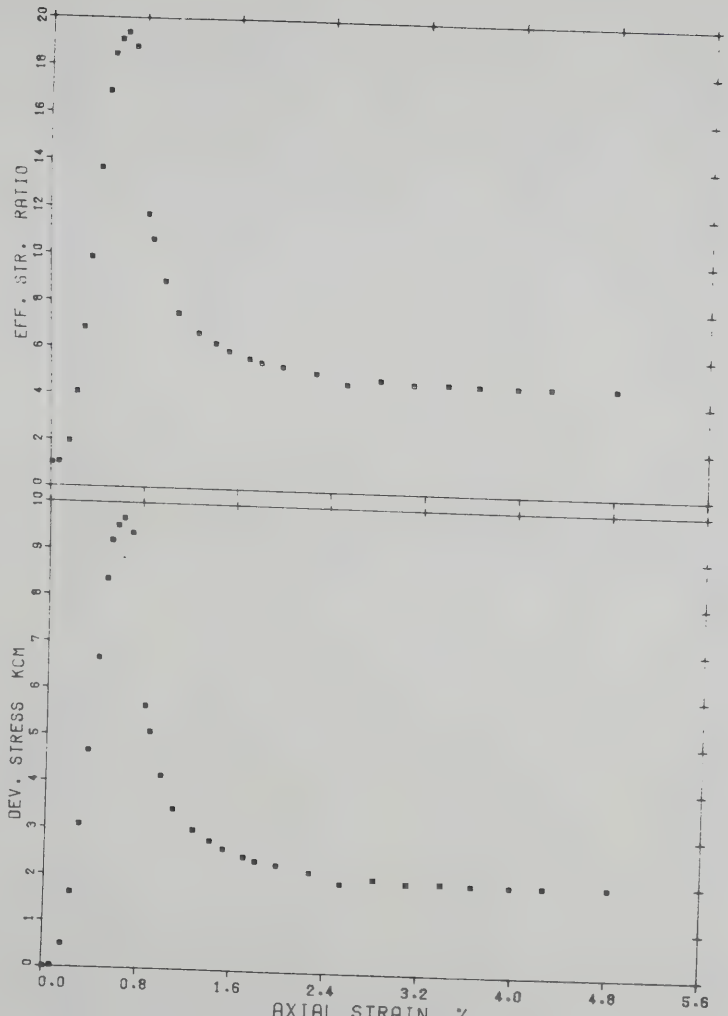

ST. PETER TRIAXIAL TEST 0.526 KG./SQ.CM.

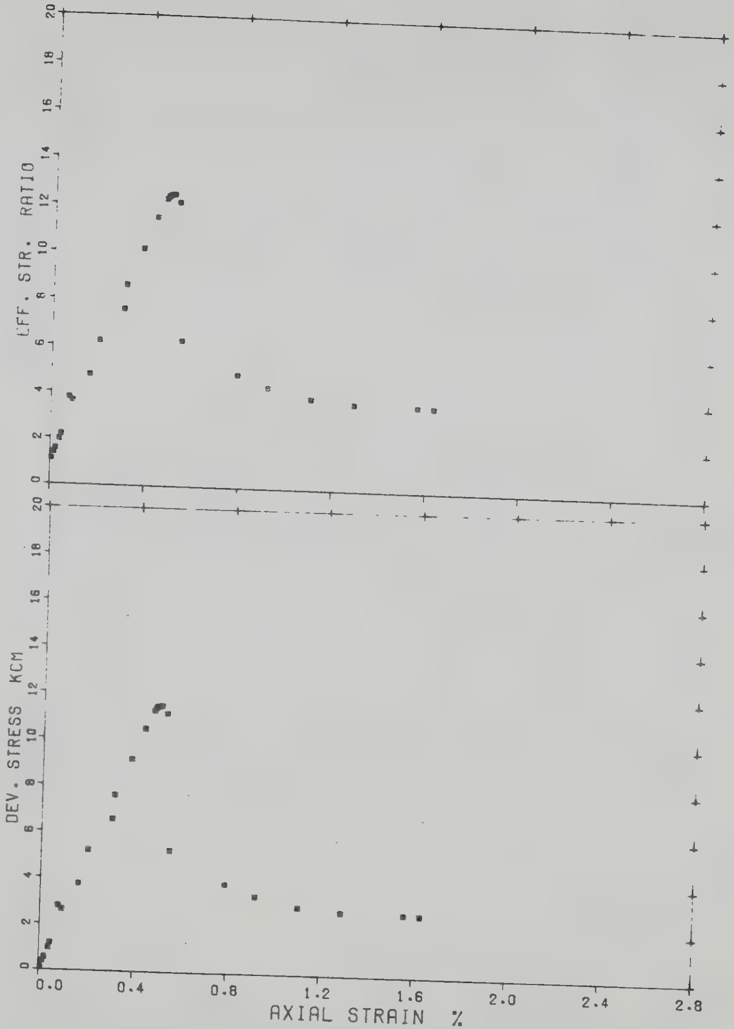

ST. PETER TRIAXIAL TEST 1.0 KG./SQ.CM.

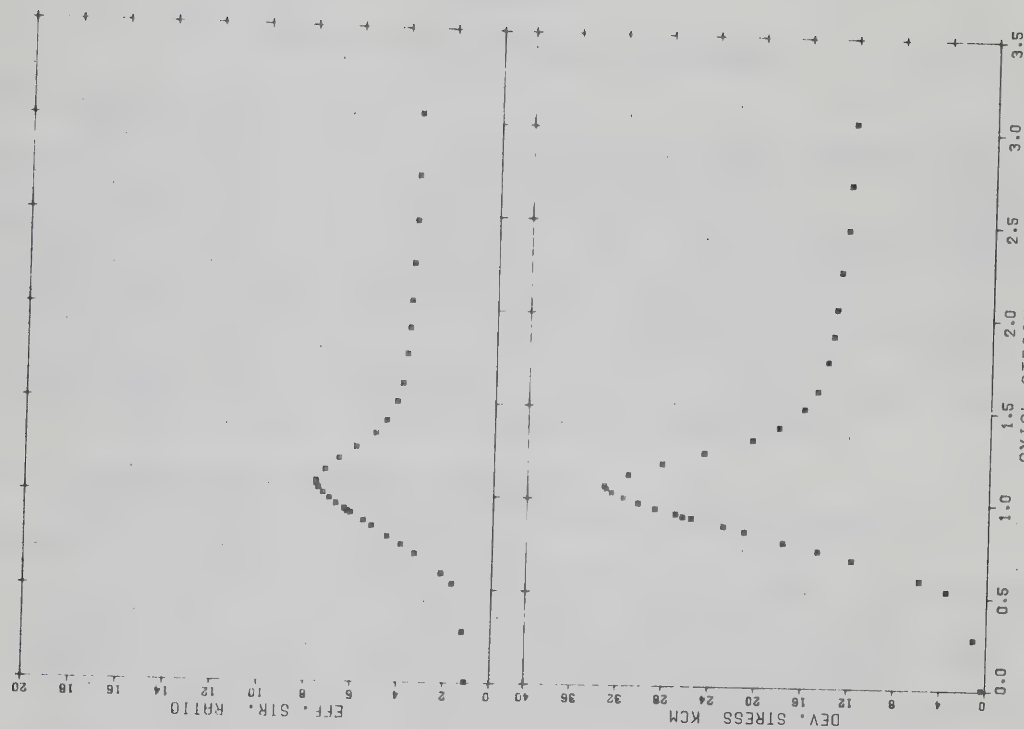

ST. PETER TRIAXIAL 5 KG./SQ.CM.

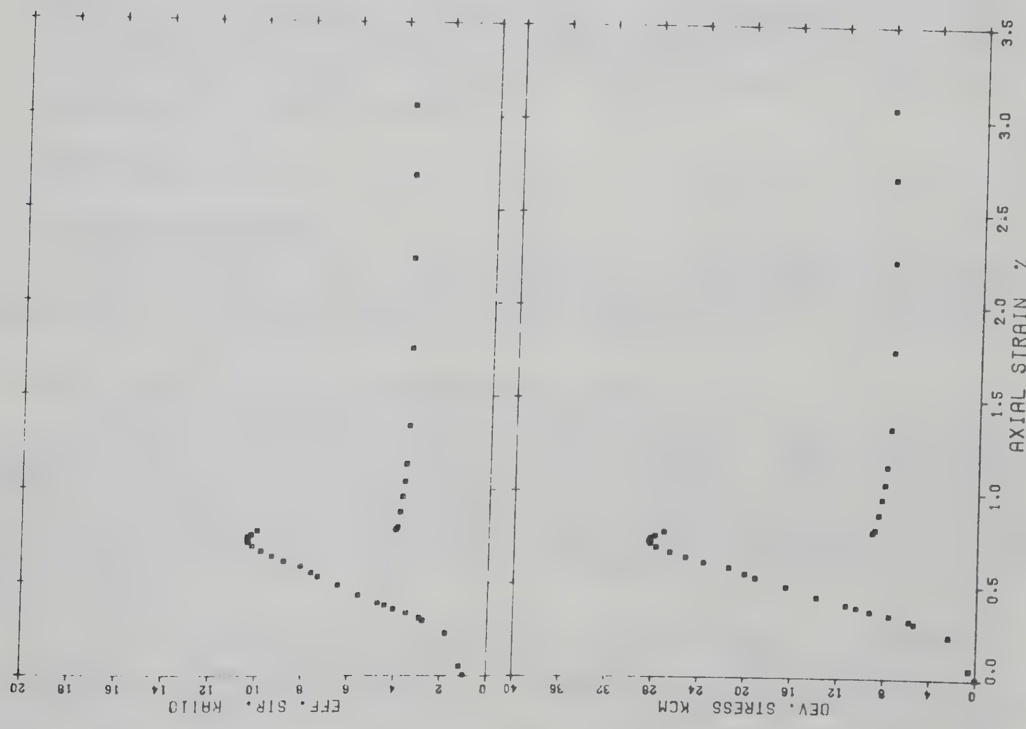

ST PETER TRIAXIAL TEST 3.0 KG./SQ.CM.

APPENDIX F

SAMPLING THE ATHABASCA OIL SANDS

F.1 Introduction

Poor quality borehole samples have generally resulted in inadequate research and engineering data (Chapter IV). To obtain samples of higher quality, borehole refrigeration techniques (permafrost sampling techniques) were employed during a coring program undertaken in January, 1974. Chilled cored oil sand sections (at -15°C) were placed in pressurized vessels as quickly as possible, stored in a chilled state, and transported in insulated and refrigerated boxes to the testing laboratories at the University of Alberta. Although samples showed obvious alteration, the methods employed have resulted in the highest quality oil sand samples obtained to date.

F.2 Rationale of the Sampling Program

The sampling operation included two steps for which an explanation is considered appropriate:

1. Down-hole refrigeration was employed to freeze interstitial water and to increase bitumen viscosities. These factors were expected to reduce core expansion through gas exsolution upon pressure release as the core was brought to the surface.
2. The core was stored and transported in pressurized and refrigerated vessels. The pressure was set to be approximately equal to the *in situ* hydrostatic pressure in order to keep gas in solution, and to permit a gradual release of gas pressures at a later time. Gradual gas exsolution was expected to be less damaging than rapid exsolution.

F.3 Equipment

F.3.1 Drilling Equipment

A rotary rig with a depth capacity of approximately 750 m was used. The rig used 3.5 in. (88.9 mm) drill pipe, and was equipped with a fluid circulation pump to flush cuttings from the borehole.

F.3.2 Drilling Fluid and Refrigeration Fluid

The hole was cored using a bentonite-water slurry to increase hole stability and to facilitate cuttings removal. Bentonite (sodium montmorillonite) forms a filter cake over permeable zones, and therefore is valuable as well in reducing infiltration, which could result in alteration of formation characteristics before geophysical logging. The drilling fluid was circulated in an open pit excavated in the frozen ground.

The refrigerant used was standard diesel fuel in a shallow, open-air pit. The large surface area of the pit took advantage of low ambient temperatures (-14°C to -22°C) as an aid in chilling the diesel fuel, and blocks of solid carbon dioxide (dry ice) were used to lower further the diesel fuel temperature before and during refrigeration. Flow of the bentonite-water slurry or the diesel fuel was controlled by moving the pump suction intake from pit to pit.

Fluid temperatures were monitored at the hole exit and the pump intake.

F.3.3 Coring Apparatus

A Christensen diamond core barrel with a nonrotating inner barrel (standard equipment for oil sands exploration) was used during this operation (Figure F.1). The advantages of this equipment are:

1. The nonrotating inner barrel prevents rotational shearing of cored specimens.
2. The inner barrel is designed to accomodate a 6.1 m segment of polyvinylchloride (PVC) pipe, which accepts and protects the continuous core during the drilling operations. The PVC liner also provides a convenient method of transporting and storing the core after it is removed from the core barrel.
3. A one-way fluid valve at the top of the inner barrel prevents fluid flushing of the core during drilling.

The major disadvantages of the equipment are:

1. The inner diameter of the diamond bit is 88.9 mm, and the inner diameter of the PVC liner is 95 mm. Although this is necessary to prevent core "jamming" during the drilling of a 6.1 m length of core, it permits significant expansion of the oil sand.
2. The PVC liner is flexible, permitting some flexure of the core length during removal from the core barrel.
3. The bottom of the inner core barrel is above the base of the diamond bit, allowing some contact of drilling fluid and core at the entry to the core barrel. The time of exposure of core may be minimized by using the maximum allowable penetration rate and minimum fluid flow.

F.3.4 Pressure Vessels

Rigid PVC or steel pipes, 1.52 m in length and 15.2 cm in outer diameter, were equipped with removable ends, Bourdon pressure gauges, and gas entry valves. This permitted storage of core and pressurization with nitrogen (Figure F.2). The rubber gaskets proved to be inadequate: many lost pressure at low temperatures as a result of excessive shrinkage and loss of flexibility.

F.4 Methodology

The borehole was cored continuously in 6.1 m sections from a depth of 30 m to a depth of 70 m. After the first 6.1 m section was cored, the core barrel was lifted off the bottom of the drill hole, the drilling fluid was displaced with diesel fuel cooled to -25^{o}C (ambient temperature was -22^{o}C), and circulation was continued for several hours until the differential between entry and exit temperatures stabilized at 4^{o}C (Figure F.3). The circulation of the diesel fuel resulted in some sloughing in the hole, because of dilution of the bitumen by the diesel fuel, and a ring of ice and sand prevented the removal of the core barrel from the hole. Circulation was restored with bentonite-water slurry, and the hole was gradually warmed until the core could be removed. For all subsequent sections of frozen core obtained, the core barrel was lifted to a level 35 m below ground surface before chilling. Constant rotation of the drill string and

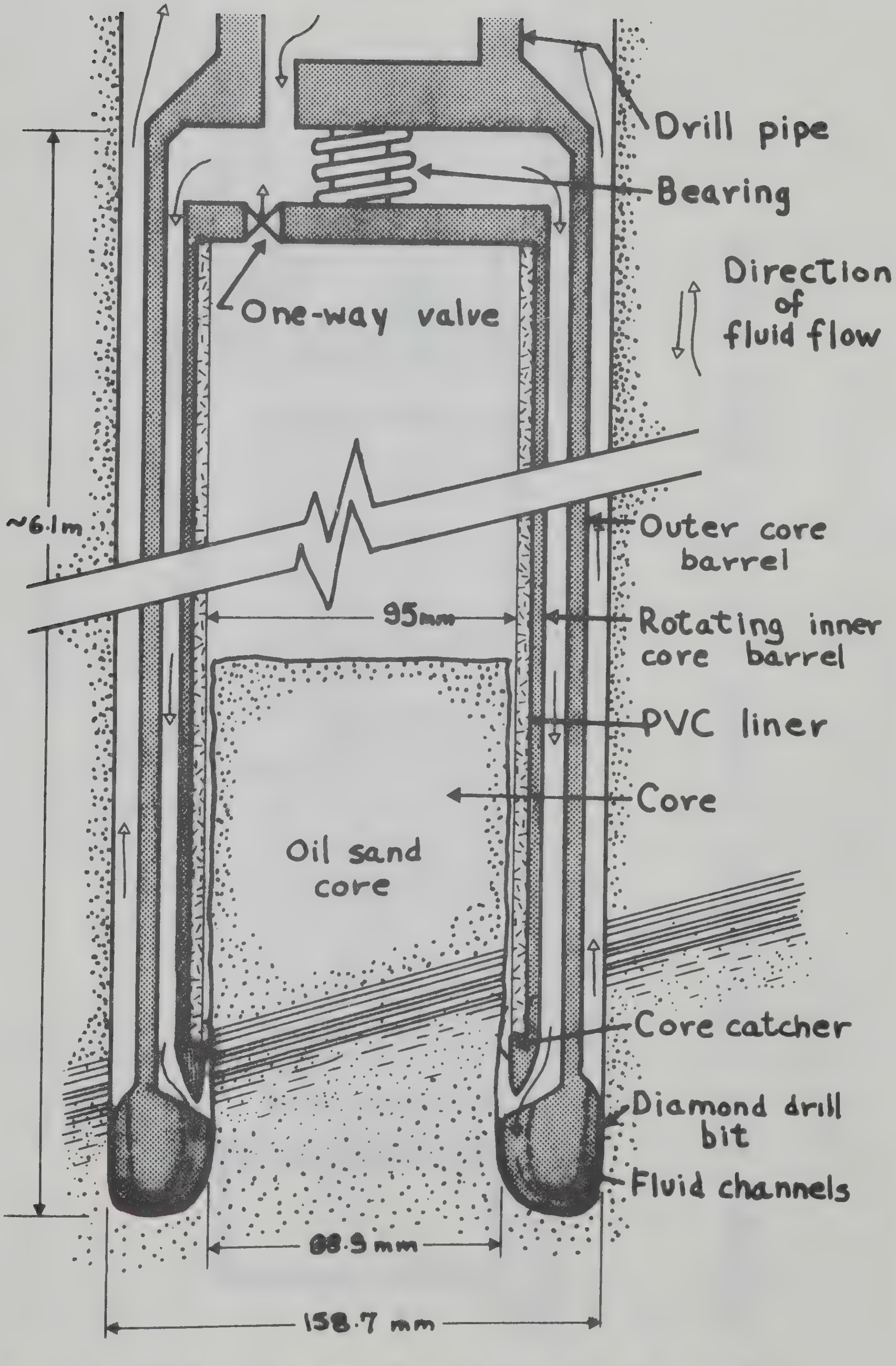

Figure F.1 Core Barrel, Schematic Representation

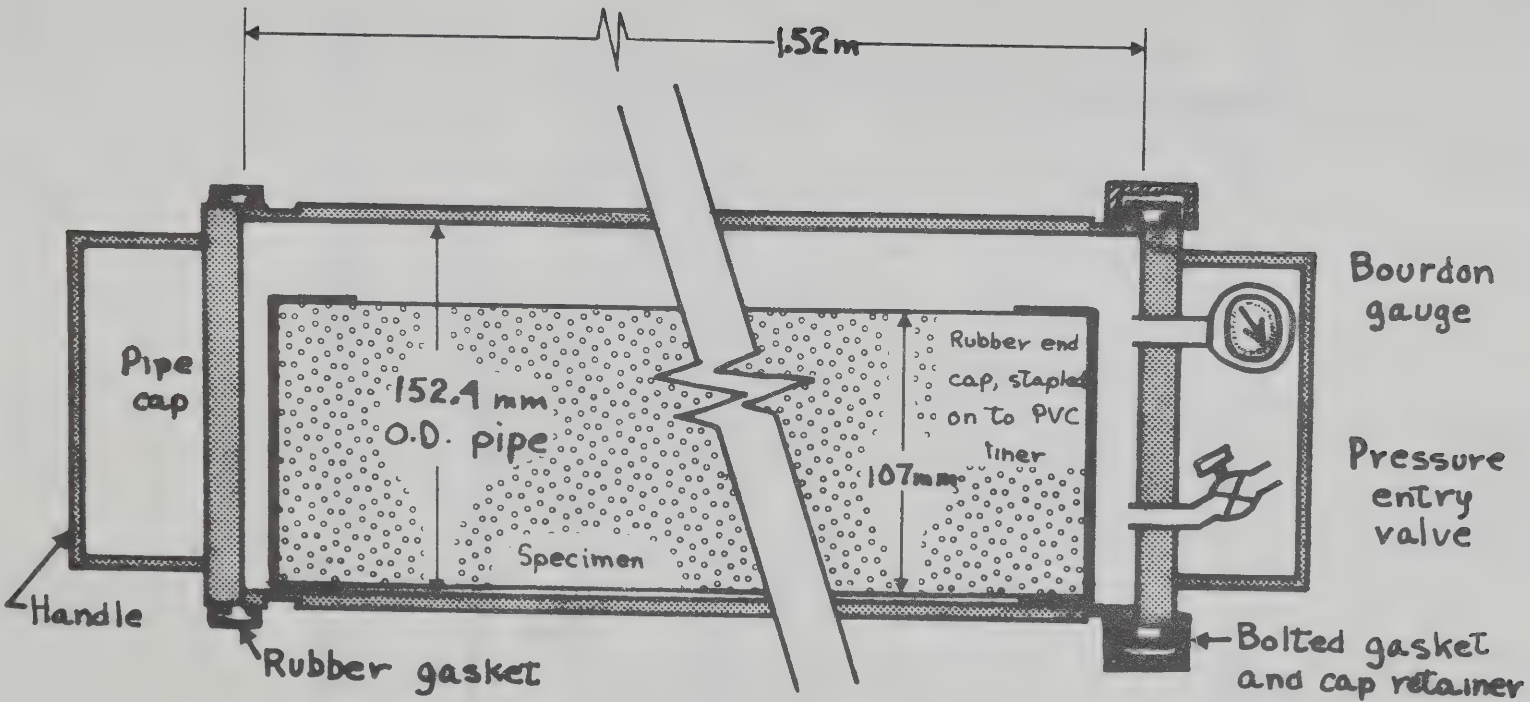

Figure F.2 Pressure Vessel for Oil Sand Core

[illegible]

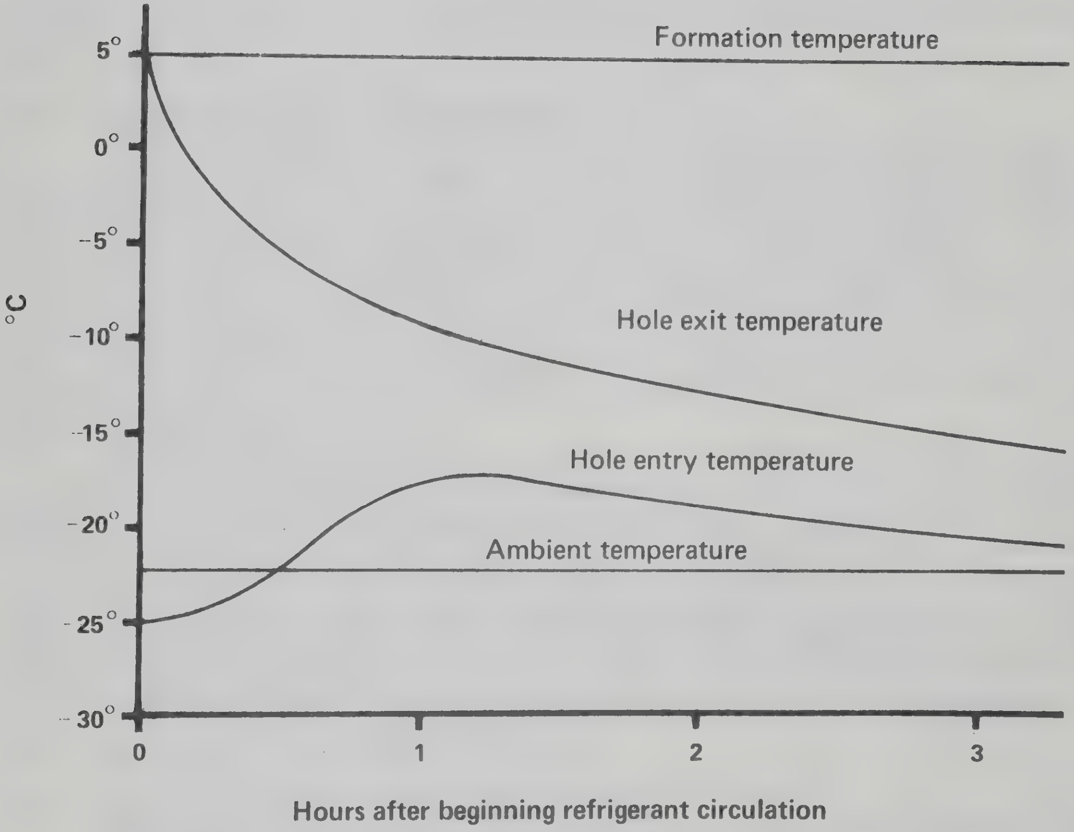

Figure F.3 Borehole Refrigeration Using a Diesel Fuel Refrigerant

occasional "spudding" (vertical movement of the drill string) during subsequent chilling operations prevented recurrence of the problem. After a chilled section of core was brought to the surface, the core in the PVC liner was removed, cut into 1.52 m lengths, and labelled. Extrusion of oil sand from the ends was noted, rubber end caps were stapled on, and the section was placed in a pressure vessel. The vessel was sealed, pressured, placed in an insulated box, and surrounded with solid carbon dioxide. Table F.1 presents typical data recorded for two 6.1 core sections. Plate F.1 shows examples of axial extrusion of core.

F.5 Evaluation of the Coring Method

After examination of field data and laboratory investigations of cored sections of oil sands, it was concluded that the core displayed considerable expansion despite the coring methods used. Coarse-grained oil-rich oil sands had expanded a minimum of 12% and a maximum of 20%. Oil-poor sands and oil-rich fine-grained sands had undergone bulk density reductions of 5% to 14%, and barren sands or oil-poor silty sands displayed the least alteration: from 1% to 6% reduction in bulk density. Nevertheless, the core was of sufficiently high quality to provide adequate experimental results in fine-grained oil-rich sands (e.g. Oil Sand Shearbox Series "C").

Visual estimates of the quality of the refrigerated core as compared to core obtained by normal methods were consistent with laboratory data: the chilled core displayed less extrusion from the liner and less overall expansion than unchilled core. The expansion of oil sands can not be eliminated by this method, since the tendency of oil sands to jam the core barrel shows that some of the expansion takes place almost immediately upon removal of lateral stress. The pressurization of the core to permit gradual gas pressure release was not wholly successful because of poor gasket seals, but it was judged that the technique has value and was partially effective.

F.6 Recommendations for Coring Oil Sands

A methodology may be outlined to obtain even higher quality core than that obtained during the course of this research. Before implementation of such a program, storage and laboratory facilities would have to be prepared in order to prevent post-sampling damage. The high cost of obtaining the core would have to be justified by the value of the results desired.

The following techniques are suggested to obtain higher quality oil sand specimens:

1. The use of a heavier chilling oil (e.g. Bunker "C" fuel oil) would diminish the dilution of bitumen in the borehole walls. Ideally, a fluid which does not dissolve bitumen or water is desirable.
2. Continuous slow rotation and gentle spudding of the drill stem may permit refrigeration to take place at the hole bottom; therefore, pore fluid stresses would not be altered greatly.
3. Rapid coring of short (1 to 2 m) sections of core is preferable to obtaining a large section. Less difficulty is encountered in removing the liner from the core barrel, no sectioning is required, and the core section is exposed for a shorter time.

TABLE F.1

EXAMPLES OF OBSERVATIONS ON CORE SPECIMENS

Depth (in feet)	Approximate Lithology	Comments
91-96	- Low oil content; silty	- Core chilled down-hole; no extrusion from either end
96-101	- Low oil content at top; rich oil sand at bottom	- Core chilled down-hole; 1 cm extrusion from bottom; 0.5 cm extrusion from top; gas bubbling slight
101-106	- Rich oil sand at top; lean oil sand at bottom	- Core chilled down-hole; 0.5 cm extrusion from top; no extrusion from bottom
166-171	- Variably saturated	- Core not chilled; 7 cm extrusion from top; 5 cm extrusion from bottom
181-186	- Oil-rich coarse-grained sand	- Core not chilled; 8 cm extrusion from both ends
193-203	- Oil-rich coarse-grained sand	- Core chilled down-hole; 0.2 cm extrusion from top; 0.5 cm extrusion from bottom

Plate F.1. Extrusion of core: The oil-rich specimen has expanded to fill the core liner, and has extruded 1 cm despite chilling to $-15^{\circ}C$. The oil-poor specimen is loose in the liner and has not extruded.

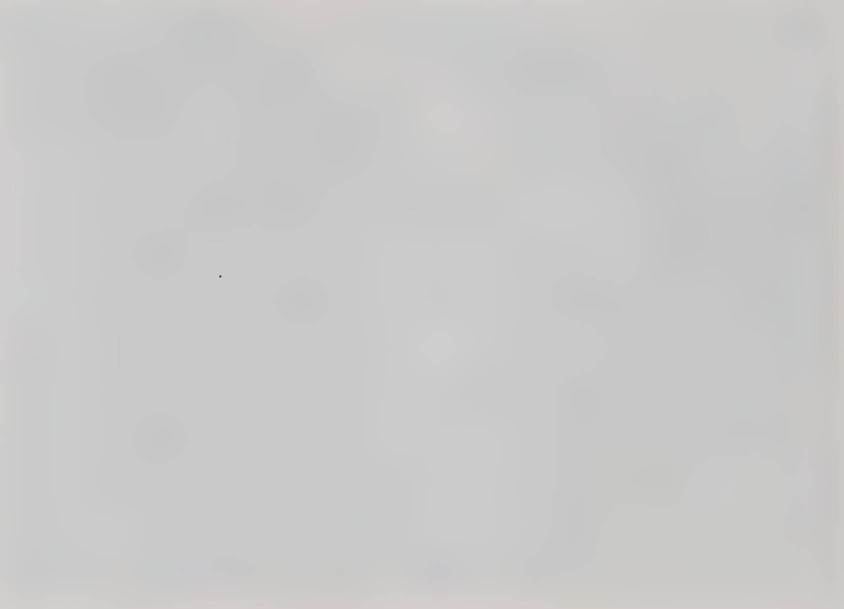

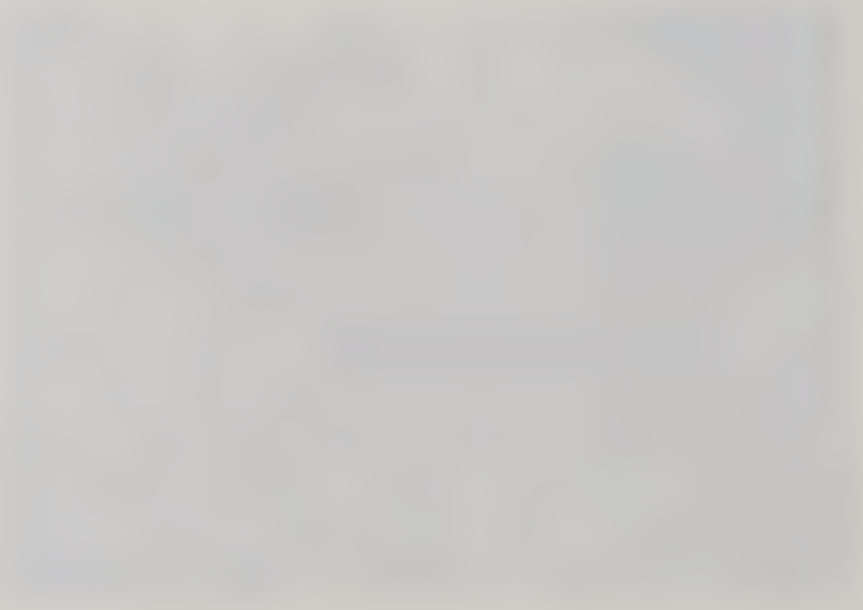

[illegible]

Furthermore, short sections could be cored without jamming the core barrel.

4. A rigid PVC liner with only one or two millimeters clearance should be used. The rigid diameter and the increased wall thickness would reduce expansion further, and eliminate possible flexural disturbance at surface.
5. Drilling should take place only under coldest winter conditions, and alternate methods of chilling the diesel fuel should be considered (e.g. radiators on refrigeration units).
6. Initial vessel pressure should be approximately equal to the hydrostatic pressure at sample depth. Only steel pressure vessels should be used, since PVC vessels become brittle at low temperatures and may explode during pressurization.
7. Vessels should be packed (externally) in dry ice, stored in very cold (-25°C) conditions, and pressure should be released gradually over a period of at least one month before specimens are prepared and tested.
8. All preparation of specimens should take place in a laboratory cold room at temperatures of -25°C to -30°C. This is the minimum temperature at which a technician can work efficiently for a one hour period.

F.7 An Ideal Coring Program

During the planning of the coring operation, several alternate methods of obtaining and preserving high quality specimens were considered; all were rejected because of cost. One method, which has particular value if "perfect" specimens are important, would entail freezing an entire column of oil sands. A hole would be drilled and cased, and a refrigerant, such as methanol (used with dry ice), would be circulated for several weeks or until a large cylinder of sand at low temperature existed. An offset hole, about one meter from the refrigerating hole, could then be cored using close-fitting liners and compressed air as the drilling fluid. The air could be cooled by refrigerating coils, or liquid air could be the source of the compressed air. The core could be preserved by methods similar to the methods described in the preceding section. A sampling program of this type is justifiable only if "perfect" samples are considered essential, since the expenditure would be very high.

APPENDIX G

GEOPHYSICAL LOGGING DATA IN THE ATHABASCA OIL SANDS

G.1 Introduction

Significant discrepancies between geophysical and laboratory data have resulted in questioning of the reliability of geophysical devices in the Athabasca Oil Sands. Chapter IV, however, presented evidence to show that the laboratory data are generally in error as a result of sample disturbance. Accordingly, it may be assumed that the geophysical data are correct. In this appendix, a series of geophysical logs are presented (Figures G.1 and G.2). Interpretation of the data and correlation with various types of geophysical data are undertaken.

G.2 Gamma Ray Log (Figure G.1)

The gamma ray log is a measure of natural radioactivity. Medium- to coarse-grained sands in the Athabasca Oil Sands are generally extremely quartzose (greater than 95% quartz) and display low natural radioactivities. Fine-grained sands and sandy silts contain appreciable quantities of clay minerals and display intermediate values of natural radioactivity. Argillaceous strata, such as intraformational clay beds or basal clays, have high natural radioactivities, with values above 60 API (American Petroleum Institute) units. Typical values drawn from Figure G.1 are:

1. Medium- to coarse-grained, oil-rich quartzose sands from 177 to 210 ft below ground surface have a mean natural radioactivity of 21 API units.
2. The fine-grained sands from 90 to 137 ft below ground surface contain appreciable quantities of clay minerals, display variable oil saturation, and have a mean natural radioactivity of about 42 API units.
3. The basal clays from 212 to 225 ft below ground surface have natural radioactivities above 60 API units.

G.3 Density Log

Bulk densities of *in situ* materials are determined by the measurement of gamma ray intensity at a fixed distance from a strong, constant, activating gamma ray source. Radiation is converted to bulk density by direct comparison to calibration on materials of known bulk density, and all raw data are automatically compensated within the recording apparatus. Log data may therefore be used directly with little error (Dresser Atlas, 1971).

Density values may be converted directly to porosity values if mineral specific gravity and pore fluid density are known. The bitumen in oil sands has a mean specific gravity of 1.01, most clay minerals have specific gravities similar to that of quartz, and the clay mineral proportion of the oil sands is low enough to permit direct conversion of bulk density to porosity.

In the Athabasca Oil Sands, a high correlation exists among lithology, sorting, and bulk density; therefore the density log correlates well with the gamma ray log, which measures lithology. Examples

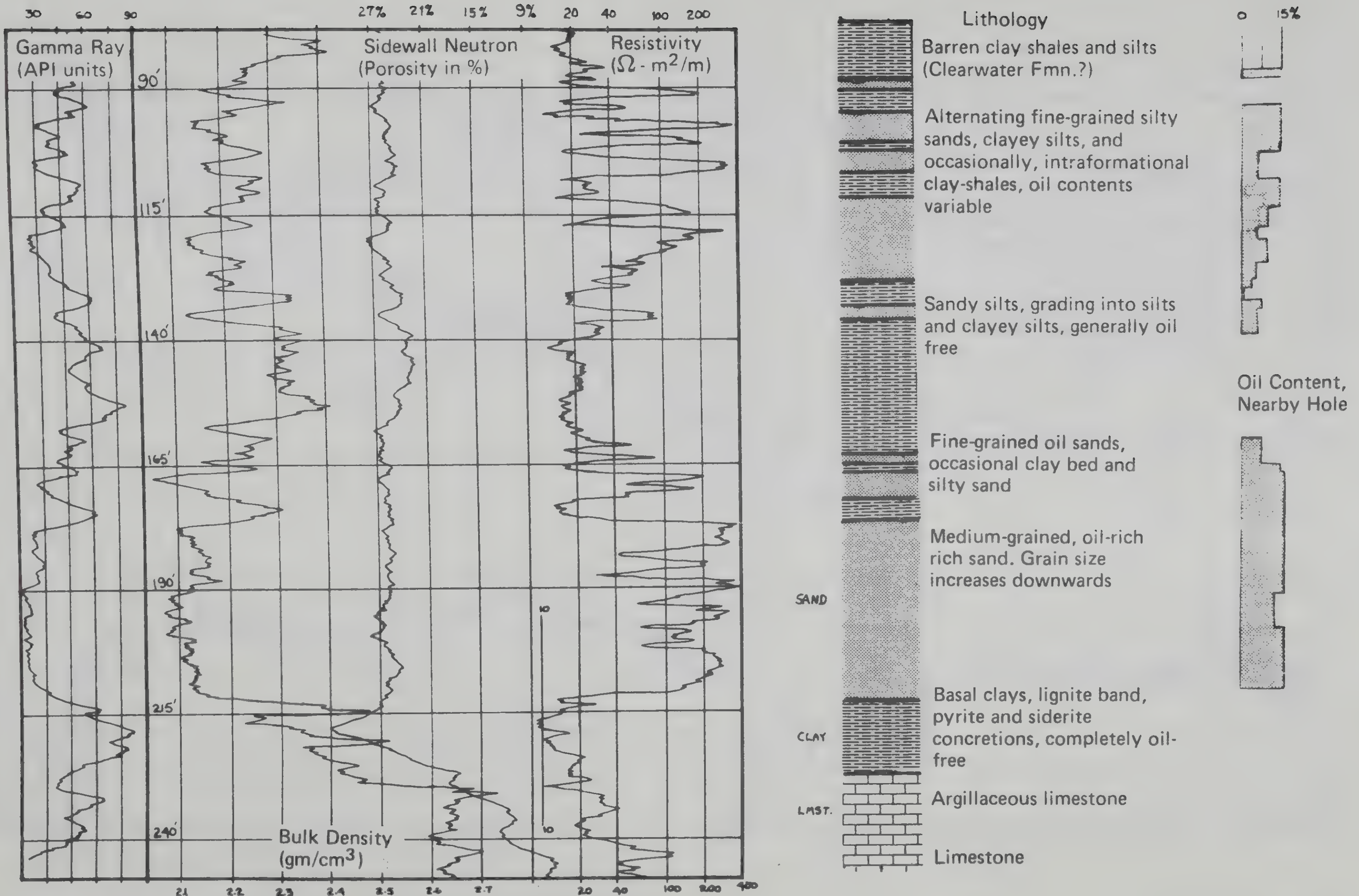

Figure G.1 Geophysical Logs in the Athabasca Oil Sands

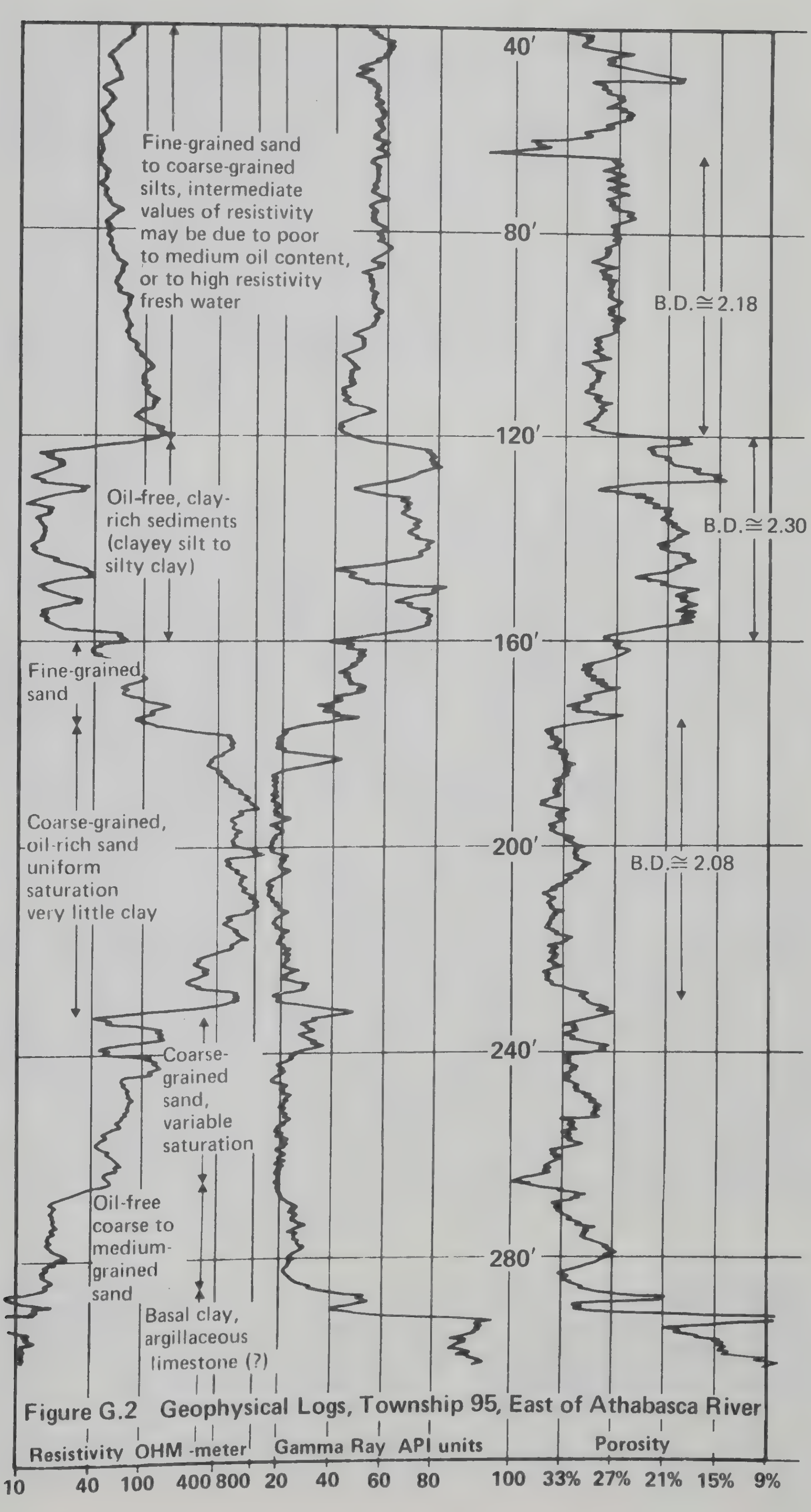

Figure G.2 Geophysical Logs, Township 95, East of Athabasca River

of this relationship drawn from Figure G.1 are presented:

1. The poorly-sorted, coarse-grained silts with little or no oil (from 137 to 155 ft below ground surface) have a mean bulk density of 2.34 gm/cc. Gamma ray data average 62 API units.
2. The medium- to coarse-grained, oil-rich sands from 177 to 210 ft below ground surface have a mean bulk density of 2.13 gm/cc (with a range of 2.06 to 2.18 gm/cc). Natural radioactivity is very low: about 21 API units.
3. Two anomalies in bulk density at 214 ft and 222 ft result from concretionary zones containing siderite and pyrite. The presence of these minerals causes high bulk density values, but the porosity values are largely unaffected, and the natural radioactivity is the same as that of the basal clays above and below the location of the anomalies.

G.4 Porosity Log

Porosity is determined by measuring the slow neutron flux or gamma ray emission resulting from activation of strata by a medium-energy neutron source. The flux is a function of the number of hydrogen atoms in the formation. The hydrogen ratio of bituminous hydrocarbons is similar to that of water, so little error arises as a result of the presence of the differing pore fluids. In strata containing considerable quantities of clay minerals, the presence of (OH^-) groups results in error because of a surfeit of hydrogen atoms. Liquid saturations of less than 100% also may result in error because of a deficit of hydrogen atoms. Detailed information may be found in publications by Stick (1960), Lynch (1962), and Youmans *et al*. (1965).

Examples of porosity values taken from Figure G.1 are:

1. The porosity value at 218 ft below ground surface is 33% ($n = 0.33$), probably because of the presence of a lignite band.
2. The mean porosity of the medium-grained, oil-rich sands from 177 to 210 ft below ground surface is 26%: this corresponds to a bulk density value of 2.22 gm/cc. The density log indicates a mean bulk density of 2.12 to 2.14 gm/cc within the same interval.
3. The porosity of the oil-free interval between 137 and 155 ft averages 23%, corresponding to a bulk density of 2.27 gm/cc. The bulk density log indicates a bulk density of about 2.33 gm/cc.

Assuming that bulk density data are reliable in the relatively uniform lithology of the Athabasca Oil Sands, the porosity log is probably not as good a measure of true porosity as the converted value of bulk density, assuming 100% saturation and a mineral specific gravity of 2.65. The differences between porosity and bulk density traces at depths of 214 and 222 ft are caused by concretionary layers containing siderite (S.G. = 3.96) and pyrite (S.G. = 5.01).

G.5 Resistivity Log

The resistivity log (or electric log, or E-log) is a horizontally focussed device, which measures the specific resistivity of a 39 cm (18 in.) thick sequence. Recording is continuous, and the trace is expressed in ohm-m^2/m (or ohm-meters). The resistivity is a function of bitumen content, salinity of pore fluid, and porosity. It is an extremely useful measure of oil content.

Resistivity values below 20 ohm-meters probably indicate no oil

whatsoever; the low values of resistivity are usually associated with low porosity values, high bulk densities, and high natural radioactivities. These data indicate high clay contents, which are in turn responsible for the lack of bitumen. Conversely, resistivity values greater than 40 ohm-meters are associated with zones of high porosity values, low density values, and low natural radioactivities (as a result of the quartzose mineralogy). Strata with resistivity values between 20 and 40 ohm-meters have variable oil contents (between values of 0% and 10%). In the zone near ground surface, the pore fluid may be fresh water, and the resultant high resistivities may be confused with the high resistivities associated with high oil contents.

Referring to Figure G.4, it may be seen that:

1. Extremely low resistivities from 218 to 240 ft below ground surface are caused by high porosities or saline pore fluid.
2. Values of resistivity in the zone from 179 to 210 ft below ground surface are high (above 40 ohm-meters) because of high oil content and associated low water content.
3. Extreme variations in resistivity in the upper zone can be attributed to the variations in oil content in the Upper Member of the McMurray Formation.
4. Low resistivity values in the zone from 136 to 160 ft below ground surface are the result of low bitumen contents in clayey zones. Density log, porosity log, and gamma ray log data all support this interpretation, and laboratory analysis confirms it.

G.6 Other Logging Devices

Sonic logs have been used in the Athabasca Oil Sands to determine *in situ* values of the elastic parameters. The value of such tools as petroleum exploration devices is questionable, and the elastic parameters are not suitable for use in civil engineering design problems. Severe attenuation of the shear wave arrival in the noncemented oil sand strata makes interpretation unreliable. Nevertheless, values of the Young's Modulus and Poisson's Ratio of approximately 75,000 kg/cm^2, and 0.30 to 0.33 respectively are obtained using this device. The Young's Modulus, however, is probably dependent on stress level and disturbance, and may prove to be useful to delineate zones of glacial disturbance in near-surface oil sands.

The measure of the membrane potential effect, or the SP (spontaneous potential) log, is not particularly useful in oil sands exploration: little differentiation between zones is apparent. The SP equipment usually is included on the same sonde as other geophysical logging devices; therefore an SP trace is usually provided routinely.

G.7 Lithological Interpretation

The remaining columns in Figure G.1 represent a lithological interpretation based on the gamma ray log only, a qualitative oil content assessment based on resistivity data only; and a more detailed lithological interpretation based on all logs. This latter interpretation has been confirmed by comparison with borehole cores. The final column is oil contents as determined on a borehole core taken some distance from the logged hole.

G.8 Borehole Data in the Athabasca Oil Sands

Figure G.2 presents logging device data from another borehole in the Athabasca Oil Sands deposit for comparison. These logging data came from a borehole approximately 70 km south of the borehole which provided the data of Figure G.1.

Analysis of logs and comparison to numerous bitumen content determinations, mineralogical determinations, and mechanical analyses enables reserve estimates to be made, and mine development may be planned on the basis of the correlative lithological interpretations.

APPENDIX H

THE BASAL CLAYS OF THE McMURRAY FORMATION

H.1 Introduction

The development of the Athabasca Oil Sands by open pit mining or by in situ methods requires knowledge of the properties of all the earth materials to be encountered. A major gap in this knowledge is the engineering index properties and mineralogy of the basal clays which underlie about 45% of the mining area (according to the writer's estimate). No engineering data have been published, and mineralogical data are confined to one study of a few specimens from three closely spaced boreholes (Halferdahl, 1969).

The aims of the basal clay study were:

1. To assess the values and ranges of the common engineering index properties.
2. To study the mineralogy of the clays.
3. To explore the local and regional variability of the basal clay deposits.

H.2 Sampling the Basal Clays

H.2.1 Borehole Samples

Fifty-eight borehole samples were obtained from core specimens stored at the Alberta Research Council. The core was the product of an oil sands exploration project undertaken during the years 1952 to 1954 by the Calvan Consolidated Oil and Gas Company. Representative samples of each 1.52 m (five foot) interval were stored in sealed tin cans; those cans containing bitumen sands had been used for analysis; most of those containing basal clays had not been opened. The report is unpublished, but the manuscript was made available to the writer. It contains driller's reports (Table H.1), cross sections, and bitumen extraction data (Scotland and Benthin, 1954). The locations of those boreholes from which samples of basal clay were obtained are plotted on Figure H.1. The map location numbers for individual samples are found in Table H.2.

The driller's logs in the manuscript were examined to determine which boreholes contained more than 1.52 m (five feet) of basal clay, and samples of those intervals were obtained from the stored core. All borehole samples were assigned code numbers: the letters "AOP" (Athabasca Oil Project) refer to the project name, the number directly following refers to the manuscript borehole number, and the last two numbers indicate the footage interval from ground surface (ground surface elevations are reported in the manuscript).

Borehole AOP-58, containing about 24 m of clay, was sampled in its entirety to provide an assessment of vertical variation. The driller's log of this borehole is presented in Table H.1. Most boreholes contained a much thinner basal clay sequence, and generally samples were chosen to represent differences in colour and lithology. Two intraformational clays from the Mildred Lake region (AOP-2 155-160 and MD-75-174.8), both 20 m above the base of the oil sands, and one

TABLE H.1

DRILLER'S LOG OF AOP-58

ATHABASCA OIL SANDS PROJECT

Area: Eymundson Creek

Hole No.: A.O.P. - 58

Location: 2420'S, 4690'E, N.W. Cor. 1-98-11w4

Elev.- 908.9 Depth-286 Recovery-98.0% Date-May 3-8/53

FROM	TO	FIELD LOG	FOOTAGE
o'0"	13'0"	Sand and gravel	
	16'0"	Clay	
	60'0"	Sand	
	70'0"	Sandy clay	
	74'0"	Clay and boulders	4'0"
	76'0"	Low o.s.	2'0"
	126'0"	Fair o.s. and clay interbeds	50'0"
	147'0"	Gray clay and fair o.s.	20'0"
	162'0"	Excellent o.s.	14'0"
	165'0"	Gray clay and some o.s. interbeds	3'0"
	177'0"	Black clay and lignite	11'0"
	186'0"	Gray sandy clay and lignite	9'0"
	196'0"	Dark clay and lignite	10'0"
	202'0"	Excellent o.s.	5'0"
	217'0"	Dark clay and lignite	15'0"
	218'0"	Sand and some bitumen	1'0"
	246'0"	Gray clay, sandy	28'0"
	256'0"	Dark clay and lignite	10'0"
	267'0"	Gray clay	11'0"
	277'0"	Dark clay	10'0"
	284'0"	Dark clay and sandy	7'0"
	285'0"	Limy clay, F. Brachiopods	1'0"
	286'0"	Limestone, hard, white, massive	1'0"

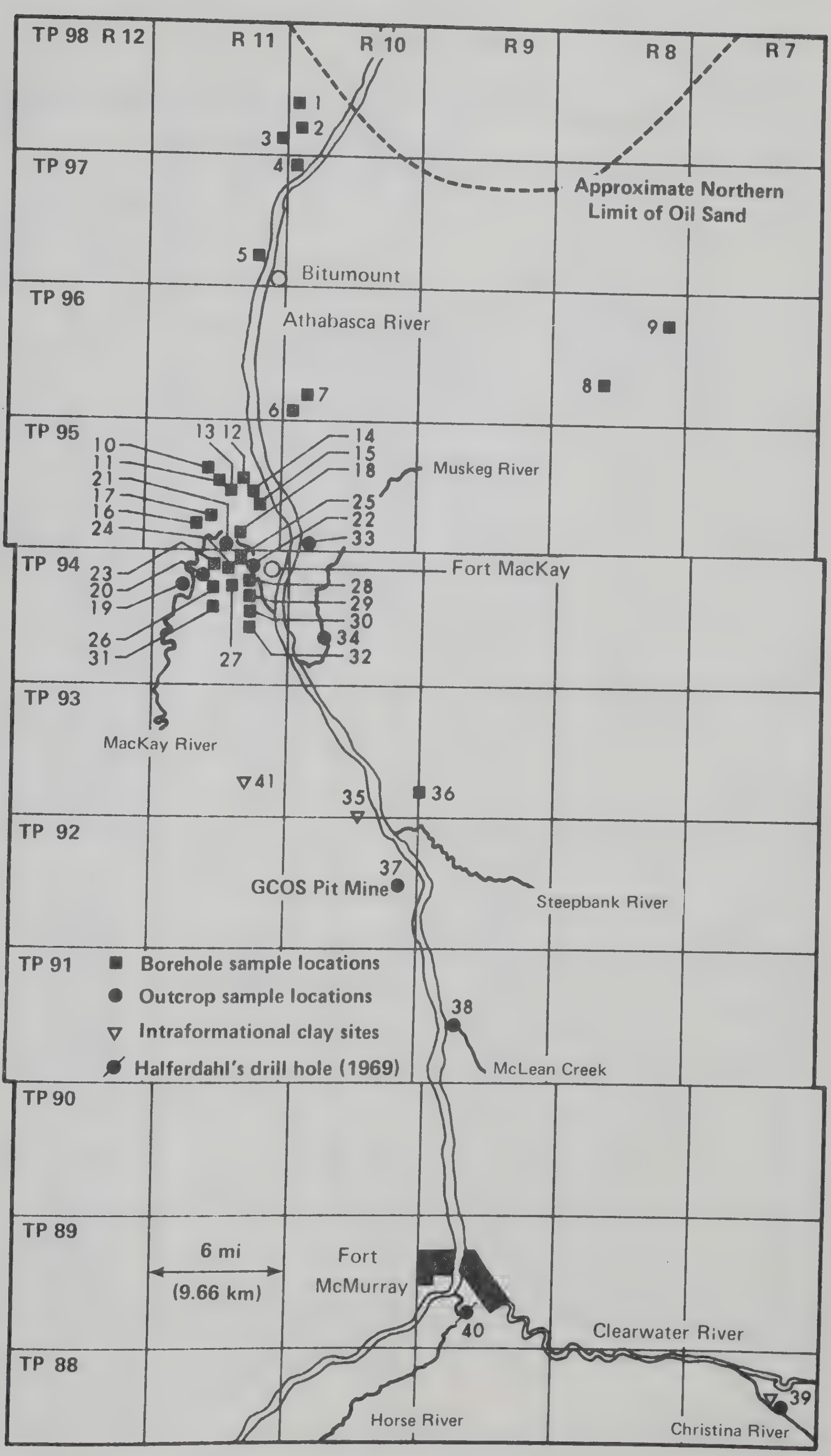

Figure H.1 Sample Locations: Basal Clay Study

TABLE H.2

BASAL CLAY STUDY

SAMPLE NUMBER BOREHOLE BASAL CLAYS		MAP NUM. -FIG. H.1	ENGINEERING INDEX PROPERTIES					MINERALOGY					PCE °C
			Lw LIQUID LIMIT	Pw PLASTIC LIMIT	Iw INDEX OF PLASTICITY	P PERCENT CLAY SIZES	A ACTIVITY	I ILLITE (10Å)	K KAOLINITE (7.2Å)	V VERMICULITE (14.8Å)	I-V ILLITE - VERMICULITE MIXED LAYER	OTHER **	PYROMETRIC CONE EQUIVALENT
MD-SYN-213		41	-	-	-	-	-	-	-	-	-		1465
AOP-12	190-195	31	51	22	29	53	0.55	4	2	0	0		1335
"	195-200	31	52	22	30	49	0.61	4	2	0	1		1335
AOP-16	135-140	28	58	23	35	49	0.72	4	2	0	1		1260
AOP-17	110-115	25	59	29	30	64	0.46	2	3	2	1		1465
AOP-18	130-135	23	24	15	9	19	0.47	4	2	2	1	Ca	1305
AOP-19	145-150	24	39	17	22	50	0.44	4	2	0	0		1190
AOP-20	140-145	18	51	20	31	55	0.56	3	3	0	1		1490
"	155-160	18	54	23	31	42	0.74	4	2	0	1		1260
AOP-23	150-155	17	50	22	28	61	0.46	4	2	2	2		1260
"	155-160	17	42	19	23	48	0.48	3	3	3	1		1335
AOP-25	165-170	13	48	20	28	57	0.49	4	2	0	1		1260
"	180-185	13	55	21	34	52	0.66	4	2	0	1		1335
AOP-26	140-145	14	24	12	12	27	0.44	3	3	0	1		1465
AOP-28	130-135	10	53	20	33	67	0.49	4	3	1	1		1335
AOP-40	223-230	5	51	21	30	59	0.51	4	3	2	1		1435
"	230-240	5	67	24	43	75	0.57	2	3	2	1	K/V(1)	1465
AOP-45	155-160	4	33	18	15	35	0.43	4	2	0	0	Ca	1165
AOP-55	200-210	2	30	16	14	29	0.48	3	3	0	0		1465
AOP-56	215-220	1	22	15	7	21	0.33	3	4	0	0		1490
AOP-58	220-225	3	28	15	13	43	0.30	3	3	1	1		1490
"	225-230	3	32	17	15	51	0.29	3	3	1	0		1490
"	230-235	3	42	23	19	73	0.26	-	-	-	-		1475
"	235-240	3	37	19	18	61	0.30	3	3	1	0		1475
"	240-245	3	44	22	22	70	0.31	3	3	0	0		1465
"	245-250	3	59	21	38	70	0.54	3	3	2	0		1465
"	250-255	3	63	26	37	66	0.56	0	4	2	0	K/V(1)	1465
"	255-260	3	53	19	34	65	0.52	3	3	0	0		1435
"	260-265	3	37	16	21	38	0.55	3	3	0	0		1475
"	265-270	3	44	17	27	47	0.57	3	3	0	0		1475
"	270-275	3	40	17	23	40	0.58	3	3	0	0		1475
"	275-280	3	27	14	13	27	0.48	3	3	1	0		1490
AOP-64	168-175	15	51	22	29	58	0.50	3	3	2	1		1465
AOP-67	240-245	12	44	17	27	56	0.48	3	3	0	1		
"	255-260	12	33	19	14	38	0.37	3	3	0	0		1490
"	260-265	12	31	15	16	36	0.44	3	3	0	0		1490
AOP-72	165-170	11	38	17	21	49	0.43	3	3	1	1		1465
"	180-185	11	50	20	30	58	0.52	3	2	2	1		1400
"	205-210	11	54	22	32	62	0.51	4	2	0	1	Ca	1230
AOP-74	185-190	16	43	19	24	53	0.45	4	2	0	0		1335

** K/V - Kaolinite-Vermiculite mixed-layer clays present.
Ca - Calcium Carbonate present.
S - Smectite present.

TABLE H.2
BASAL CLAY STUDY

SAMPLE	MAP NO.	Lw	Pw	Iw	P	A	I	K	V	I-V	OTHER	PCE
AOP-80 145-150	26	47	18	29	55	0.53	4	2	0	1		1335
AOP-84 180-185	29	44	18	26	52	0.50	3	3	0	0		1350
185-190	29	39	19	20	52	0.38	4	2	0	0		1260
190-195	29	42	21	21	58	0.36	4	2	0	0		1305
AOP-85 170-175	27	51	21	30	59	0.51	4	2	0	1		1305
180-185	27	23	12	11	28	0.39	4	2	1	1		1165
AOP-87 190-195	30	42	20	22	49	0.45	4	2	1	1		1190
AOP-90 220-225	32	34	24	10	ORGANIC		3	3	1	1		1490
AOP-92 195-200	36	23	15	8	18	0.44	4	2	1	1		1465
AOP-94 300-305	6	45	20	25	47	0.53	4	2	0	0		1165
305-310	6	37	16	21	43	0.49	4	2	0	0		1165
310-315	6	37	18	19	35	0.54	4	2	0	0	MINOR Ca	1170
AOP-95 290-295	7	43	20	23	52	0.44	4	2	0	0		1190
AOP-96 205-210	8	74	27	47	75	0.63	3	3	2	1	K/V(1)	1465
215-220	8	59	27	32	66	0.48	2	4	2	1	K/V(1)	1260
240-245	8	35	17	18	35	0.51	4	2	2	0	Minor Ca	1170
AOP-97 205-210	9	63	28	35	62	0.56	2	3	2	0	K/V(1)	1465
215-220	9	37	20	17	30	0.57	3	3	1	1		1465
240-245	9	52	18	34	53	0.64	3	3	2	1		1405
OUTCROP BASAL CLAYS												
	37	29	17	12	31	0.39	3	3	0	0		1435
	37	29	15	14	29	0.48	3	3	0	0		1435
	37	24	14	10	29	0.42	3	3	0	0		1435
MD-63-1	38	49	19	30	55	0.54	3	3	2	2	K/V(3)	1475
MD-63-2	38	86	29	57	83	0.69	2	3	3	1	K/V(3)	1475
MD-63-3	38	25	17	8	25	0.32	2	3	3	1	K/V(2)	1520
MD-63-4	38	20	16	4	20	0.20	2	3	2	0	K/V(1)	1580
MD-63-5	38	34	17	17	41	0.41	3	2	2	2	K/V(1)	1400
MD-63-6	38	90	28	62	91	0.68	3	2	2	2	K/V(2)	1530
MD-63-7	38	97	27	70	93	0.75	3	2	2	2	K/V(2)	1580
MD-7-1	22	35	15	20	39	0.51	3	3	0	1		1475
MD-7-2	22	41	18	23	57	0.40	3	3	0	2		
MD-7-3	22	56	17	39	59	0.66	3	3	0	1		
MD-7-4	22	42	16	26	48	0.54	3	3	0	1		1465
MD-7-5	22	39	18	21	49	0.43	3	4	0	0		1465
MD-74-MUSK-1	34	58	24	34	44	0.77	4	3	0	1		1250
DS-74-C-16-1	34	73	28	45	59	0.76	4	2	1	1		
MD-74-INGS-1	33	60	23	37	52	0.71	4	3	0	1		1190
DS-74-C-17-1	33	62	23	39	54	0.72	4	2	1	1		
MD-75-4-4	39	53	26	27	39	0.69	4	2	0	1		
MD-75-4-5	39	41	17	24	34	0.70	4	3	0	1		1490
MD-75-5-1	21	50	17	33	51	0.65	3	4	0	0		1510
MD-75-5-2	21	52	16	36	33	1.09	2	4	2	0	K/V(4)	1520
MD-75-6-1	19	48	29	19	71	0.27	3	4	3	1		ORGANIC
MD-75-6-3	19	55	27	28	59	0.47	4	3	1	1		1490
MD-75-7-1	20	54	22	32	60	0.53	4	3	1	0		1490

SAMPLE	MAP	Lw	Pw	Iw	P	A	I	K	V	I-V	OTHER	PCE
INTRAFORMATIONAL CLAYS												
AOP-2 155-160 (Middle Member)	35	30	18	12	25	0.48	3	3	0	0		1335
MD-NOV-1-1 (Lower Member)	T95 R9W4	30	15	15	26	0.57	3	3	0	0		
MD-75-1-3 (Middle Member)	T89 R4W4	41	25	16	41	0.38	4	4	1	0		
MD-75-4-3 (Upper Member)	39	36	22	14	23	0.61	4	3	0	0	S(1)	1400
MD-75-174.8" (Middle Member)	41	28	20	8	37	0.22	-	-	-	-	-	----
MANITOBA BASAL CLAYS	(See Figure 6.3 for locations)											
MD-75-10-1	M1	45	23	22	56	0.39	2	4	0	0		1605
MD-75-10-2	M1	35	TOO SILTY		14	--	0	4	0	0		1605
MD-75-11-1	M2	40	22	18	48	0.38	2	4	0	0		1605
MD-75-13-1	M3	28	18	10	38	0.26	2	4	2	0	K/V(1)	1490
MD-75-13-2	M3	39	22	17	47	0.36	2	4	1	1	K/V(1)	1460
*MD-75-14-1	M4	57	30	27	50	0.54	3	4	0	0	S(3) S/I(3)	1350
MIXTURE OF GEORGIA KAOLINITE AND ILLINOIS GRUNDITE	(THE NUMBERS AFTER 75 REFER TO THE RATIO OF COMPONENTS e.g. MD-75-2-8 is 20% GRUNDITE, 80% GEORGIA KAOLINITE)											
MD-75-0-10		60	30	30	61	.49	2	4	0	0		1745
MD-75-2-8		55	28	27	57	.47	2	4	0	0		1700
MD-75-4-6		52	28	24	47	.51	2	4	0	0		1615
MD-75-5-5		55	26	29	45	.64	2	4	0	0		1595
MD-75-6-4		49	26	23	41	.56	3	4	0	0		1475
MD-75-8-2		45	25	20	37	.54	3	3	0	0		1260
MD-75-10-0		44	22	22	28	.78	4	1	0	0		1190

* This specimen is probably not a basal clay, but a Pleistocene clay of mixed origin.

intraformational silty clay (Nov-1-1) from an undetermined location (in Township 95, Range, 10W4) also were sampled.

H.2.2 Outcrop Samples

Outcrop samples were gathered by shovel directly from field exposures and placed in plastic bags for storage until testing. Three specimens of basal clay were gathered at different locations from the GCOS pit floor (GCOS-1,2,3). The remaining Alberta basal clay samples were collected from outcrops where basal clays could be detected. Two outcrops, the Viewpoint outcrop one kilometer west of Fort MacKay and the McLean Creek outcrop 20 km north of Fort McMurray, were sampled extensively to assess variability in an outcrop (Samples MD-7-1 to MD-7-5 and MD-63-1 to MD-63-7). Six specimens of the basal clays overlying the Paleozoic unconformity in Manitoba (MD-75-10-1 to MD-75-14-1) were obtained during the field trip to obtain specimens of Swan River Sandstone (Chapter VI). Two intraformational clays were sampled from outcrops: MD-75-1-3 was obtained from a five centimeter thick bed on the High Hill River outcrop (60 km east of Fort McMurray) about six meters above the outcrop base; MD-75-4-3 was obtained from a 45 cm thick bed five meters below the top of the McMurray Formation on the Christina River outcrop. All outcrop sample locations in Alberta (except the High Hill River sample) are shown on Figure H.1. Manitoba sample locations are included on Figure 6.3.

H.3 Occurrence and Geology of the Basal Clays

H.3.1 Regional Variation

North of Township 92, where river erosion has exposed the base of the McMurray Formation, basal clays are common (Ells, 1915a; Hume, 1924). No basal clays have been observed in outcrops in the vicinity of, or west of, Fort McMurray. Limestone exposure occurs where paleotopographic highs existed, and paleotopographic highs are generally sites of paleosol or paleocaliche (Figure H.2). It is to be expected that the paleotopographic lows, generally below river level, contain significant basal clay deposits. Halferdahl (1969) reported a 9.8 m layer of basal clay below the Abasand pit (Location 40 on Figure H.1). Paleotopographic highs along the Steepbank River show thick (1.6 m) paleosol deposits, and adjacent lows are occasionally basal clay sites. Carrigy (1973) stated that coarse-grained sands, usually with attendant basal clay, "occupy the deeper depressions on the pre-Cretaceous erosion surface".

Although insufficient information has been collected to make conclusive statements, it seems likely that basal clays in thicknesses greater than about one meter underlie between 30% and 50% of the central part of the McMurray Formation. The maximum thickness of basal clay in a borehole as reported in published literature is 24 m (Township 96, Range 8W4: Scotland and Benthin, 1954), but verbal communications (Mossop, 1976) indicate that thicknesses of up to 27 m exist south of Fort McMurray and in paleodrainage channels in the Mildred Lake region.

4.3.2 Geology and Stratigraphy of the Basal Clays

The basal clays are transported clays deposited in water. They

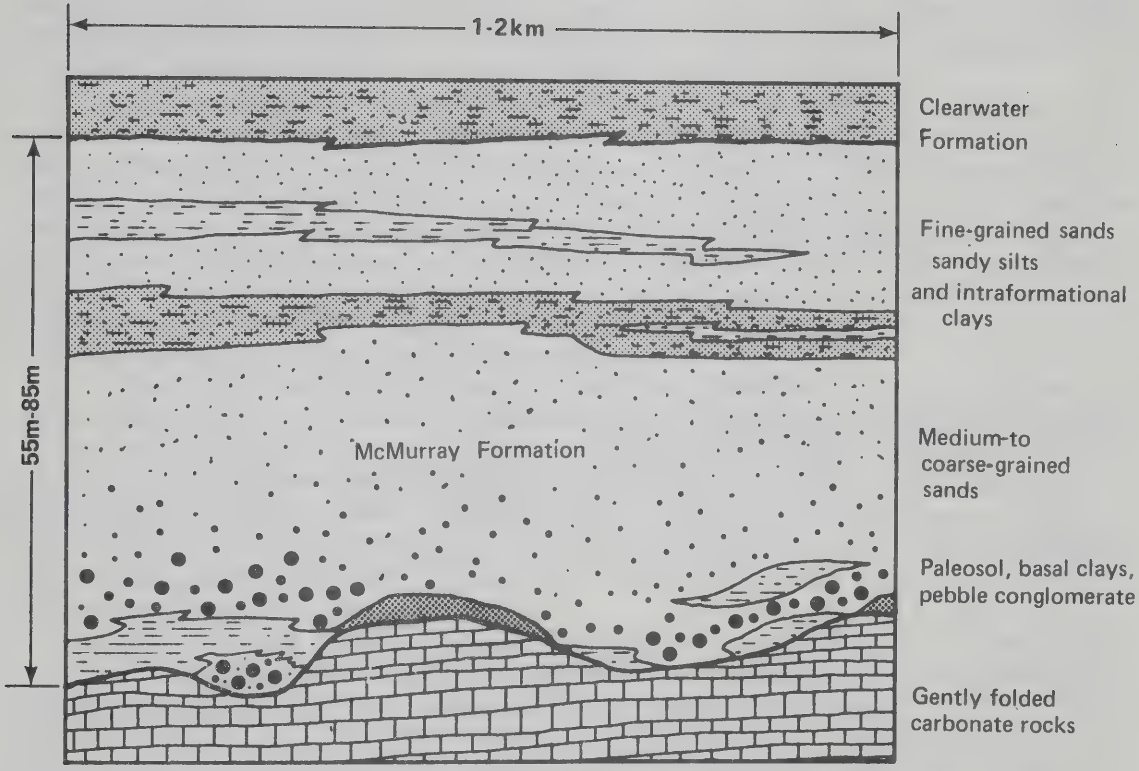

Figure H.2 Stratigraphic Position of Basal Clays, Paleosol and Intraformational Clays

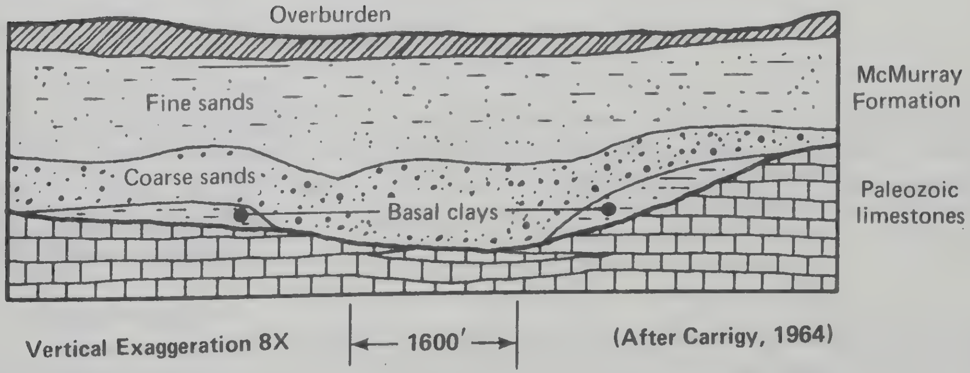

Figure H.3 Channel Overspill Deposition

are noncalcareous, display primary bedding, and contain Lower Cretaceous spores throughout their vertical sequence (Halferdahl, 1969). A simple test for carbonates serves to differentiate them from the calcareous residual paleosols, which also may have high clay contents.

The depositional regime responsible for basal clay deposits must have been quiet water, and, because the greatest thicknesses of clay correspond to paleotopographic lows, they are likely lacustrine and channel backswamp deposits. In many cases, the clays are associated laterally with sands, indicating channel overspill deposition (Figure H.3). Salinity of the depositional water has not been determined, but the adjacent paleosols suggest that large areas of dry land existed, and probably the water was fresh or slightly brackish (as in near-shore lagoons or terrestial delta marshes).

The most distinctive bed in the basal deposits, one which has been observed by the writer in boreholes and outcrops between Townships 91 and 98, and is reported in Township 89 (Halferdahl, 1969), is a bed of lignite fragments and associated black clay. Pyrite nodules are found commonly with these deposits of lignite, and marcasite has been mentioned (Carrigy, 1959). The black or dark grey clay associated with the lignite band commonly displays slickensides, even at considerable distances from river valley walls.

Significant basal clay deposits occur invariably at or near the base of the McMurray Formation, but may be separated from the underlying limestones by a layer of coarse-grained clastic material, either oil-free, oil-rich, or, in some cases, oil-stained (oil has been present, leaving a heavy bituminous residue). These clastic beds have been reported in thicknesses of several meters. Allen and Sanford (1973) mentioned a fluvial sand directly overlain by "lagoonal" deposits in units of varying thicknesses. They also mentioned a paleochannel cutting through the basal lagoonal deposits, but they did not associate the deposition of the clays with the existence of the channel.

Several diagrams of outcrops where the basal stratigraphy could be determined are presented to give some indication of the local stratigraphy (Figures H.4 and H.5).

H.4 Engineering Index Properties

H.4.1 Test Procedures

Air-dried samples of basal clay were ground, in a rubber-wheeled grinder, sufficiently fine to pass a 40 mesh sieve. Several hundred grams of each sample were mixed with distilled water for Atterberg Limit determinations, and small portions were set aside for hydrometer grain size analyses.

H.4.2 Test Results

Table H.2 is a comprehensive chart of the data obtained during the engineering index and mineralogical testing program. To ensure objectivity, extreme data points were not rejected, although some data points (e.g. MD-75-5-2) may be in error.

A grain size curve was plotted for each specimen; a few examples of typical grain size distributions are presented in Figure H.6.

Two consolidation tests were performed on remoulded slurries of basal clay: MD-63-7 with a liquid limit of 97 and an unusually high

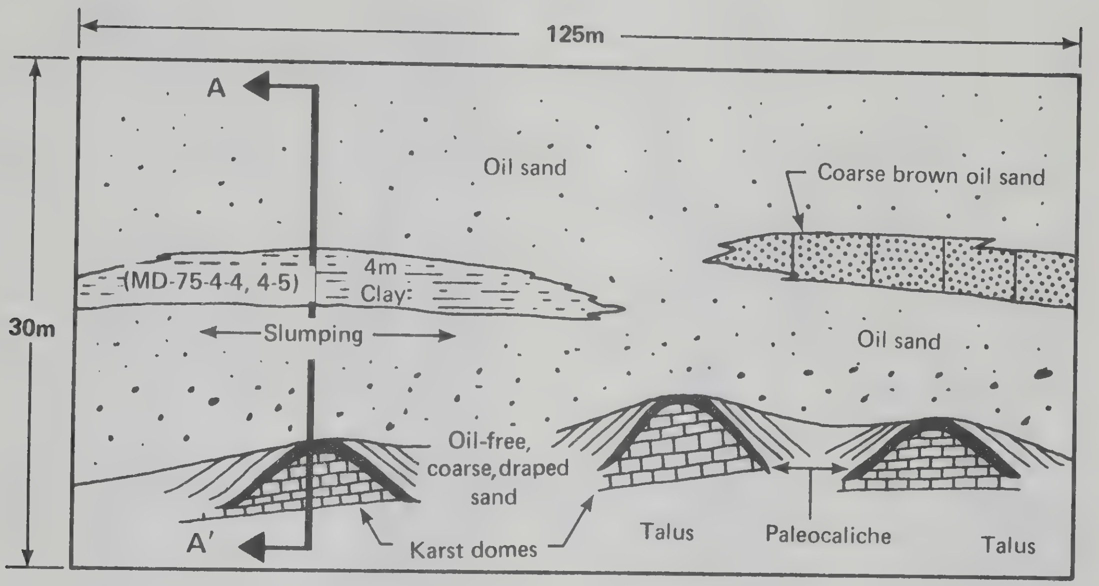

Figure H.4a Frontal Configuration of the Basal Deposits at the Christina River Outcrop

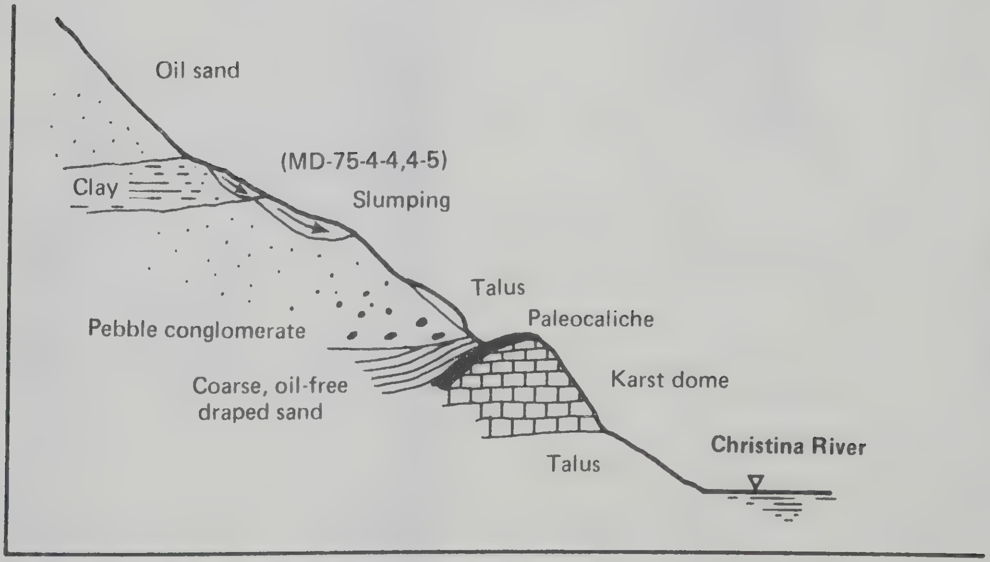

Figure H.4b Section A-A′ of the Christina River Outcrop

Figure H.4 Christina River Outcrop Stratigraphy

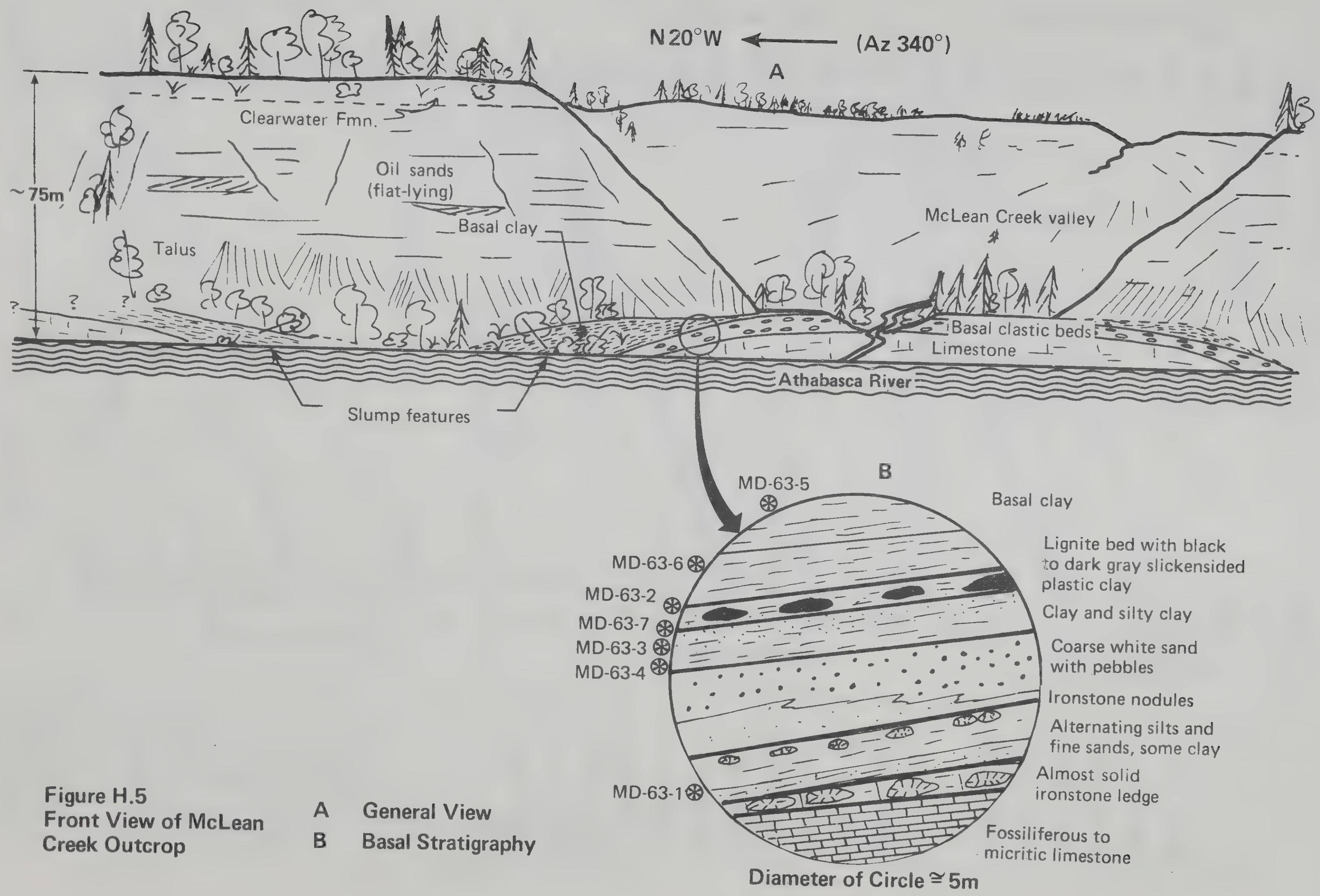

Figure H.5
Front View of McLean Creek Outcrop

A General View
B Basal Stratigraphy

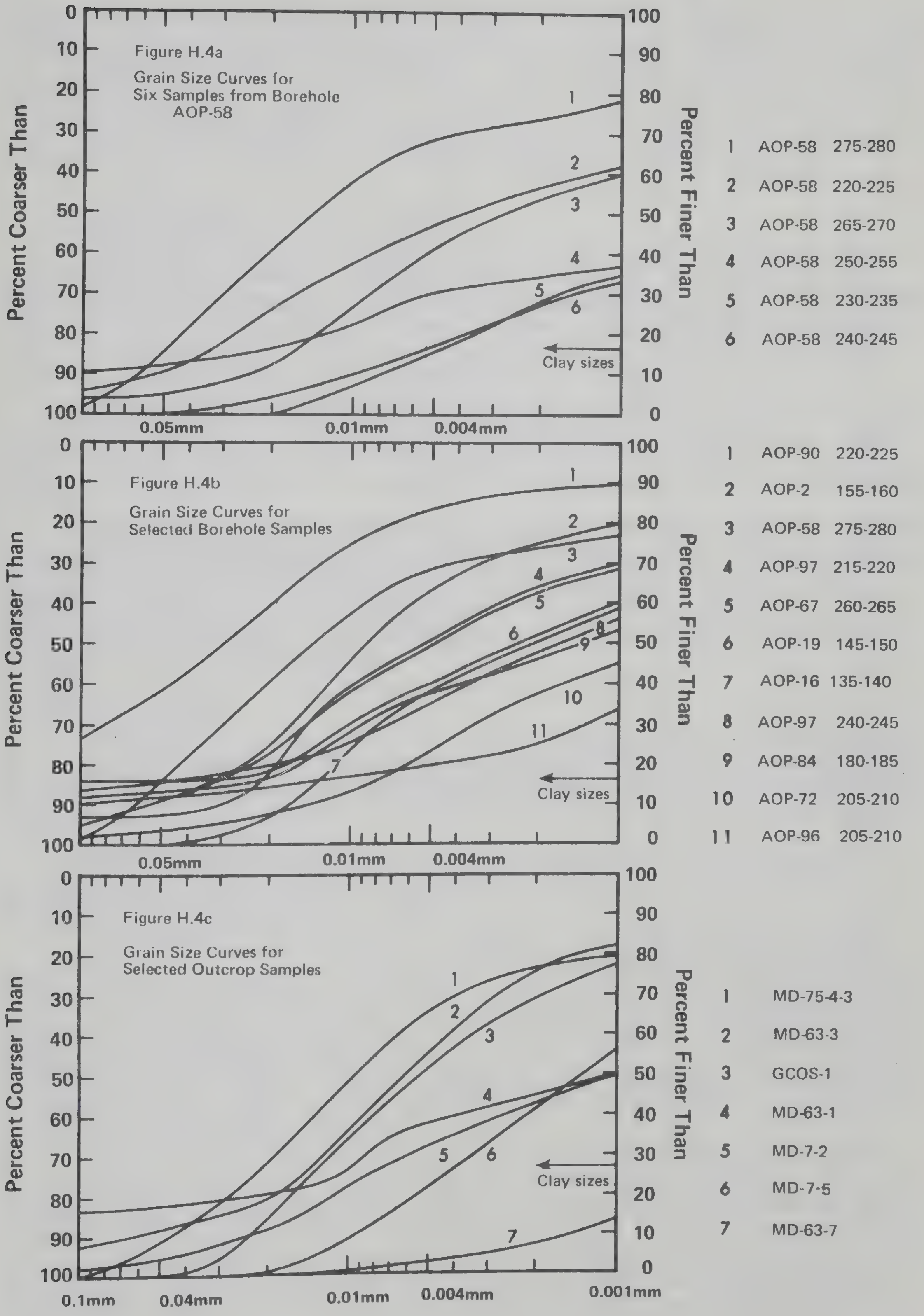

Figure H.6 Typical Grain Size Curves of Basal Clays

clay size content of 93%; and AOP-18 130-135 with a liquid limit of 24 and a clay size content of 19%. These clays were chosen to represent the range of materials investigated. The clayey silt (AOP-18) yielded a mean value for Cv of 7 x 10^{-4} cm^2/sec in the stress range 0.5 - 4.0 kg/cm^2; the fat clay, MD-63-7, a value for Cv of 8 x 10^{-6} cm^2/sec at a lower stress range of 0.125 to 2.0 kg/cm^2. The latter specimen required from 7 to 10 days to stabilize after a stress increment.

9.4.3 Interpretation of Test Results

The means and standard deviations of the index properties were determined for two sample groups: outcrop samples and borehole samples. In order to assess the effects of weathering on the index properties of basal clays, the differences between the means of the borehole and outcrop data were tested for significance at the 95% confidence level. All statistical data are reported in Table H.3.

A graph of the relationship between the index of plasticity and the liquid limit for all specimens is presented in Figure H.7. Regression lines for outcrop and borehole basal clay specimens are included along with least squares correlation coefficients and the mean standard errors.

The relationship between the percentage of each specimen smaller than two microns effective grain diameter (clay sizes) and the specimen liquid limit is plotted in Figure H.8. Regression lines were determined for several subpopulations, and the regression equations along with the coefficients of correlation and the mean standard errors are presented in the same diagram.

9.4.4 Conclusions

The general nonorganic nature of the basal clays is demonstrated by their positions on a Casagrande Plot (Figure H.7). The two specimens lying below the Casagrande "A" line are a black borehole clay associated with lignite, and a black outcrop clay with large quantities of comminuted carbonaceous matter.

The extremely fine-grained nature of several of the outcrop specimens (e.g. MD-63-7) is remarkable, and may be in part a result of weathering since exposure.

The activity of the outcrop specimens is significantly higher than that of the borehole specimens, yet no significant difference in the percentage of clay sizes, or in plastic limit, is detectable. The source of variation must therefore be attributed to mineralogical and grain size differences between the two sample bodies. This is in part confirmed by the relatively high level of significance of the difference in liquid limit means, because mineralogical changes have a significant effect on values of liquid limit.

With one minor exception, it may be assumed that all the basal clays belong to one clay population of low to medium activity. One group of fine-grained specimens from borehole AOP-58 demonstrates particularly low activity with a mean value of only 0.29. The regression line plotted through the five data points on Figure H.8 is significantly different from the population data beyond the 95% confidence level; therefore it must be assumed that these specimens represent a different clay type. These specimens differ in no way from the population other than in their unusually high clay contents for low index values.

TABLE H.3

BASAL CLAY STUDY: STATISTICAL PARAMETERS

PROPERTY		OUTCROP SAMPLES			BOREHOLE SAMPLES			SIGNIFICANCE*
		N	$\overline{X}$	$\overline{\sigma}$	N	$\overline{X}$	$\overline{\sigma}$	
	<u>INDEX PROPERTIES</u>							
Lw	Liquid Limit	26	50.1	20.0	58	43.8	11.8	93.2%
Pw	Plastic Limit	26	20.6	5.1	58	19.6	3.7	----
Iw	Index of Plasticity	26	29.5	16.2	58	24.2	9.0	94.1%
P	Percent Clay Sizes	26	50.0	19.4	57	49.8	14.3	----
A	Activity	26	0.568	0.19	57	0.488	0.10	97.6%
	<u>MINERALOGY</u>							
I	Illite	26	3.15	**	57	3.33	**	----
K	Kaolinite	26	2.92	**	57	2.61	**	----
V	Vermiculite	26	0.96	**	57	0.74	**	----
I/V	Illite-Vermiculite	26	0.88	**	57	0.54	**	----
K/V	Kaolinite-Vermiculite	26	0.69	**	57	0.09	**	----
PCE	Pyrometric Cone Equivalent	20	1460°C	94.4	58	1371°C	116.5	99.9%

* Level of significance of the difference between means.

** Mineralogy data does not closely approximate a normal distribution, therefore standard deviations and significance tests were not performed.

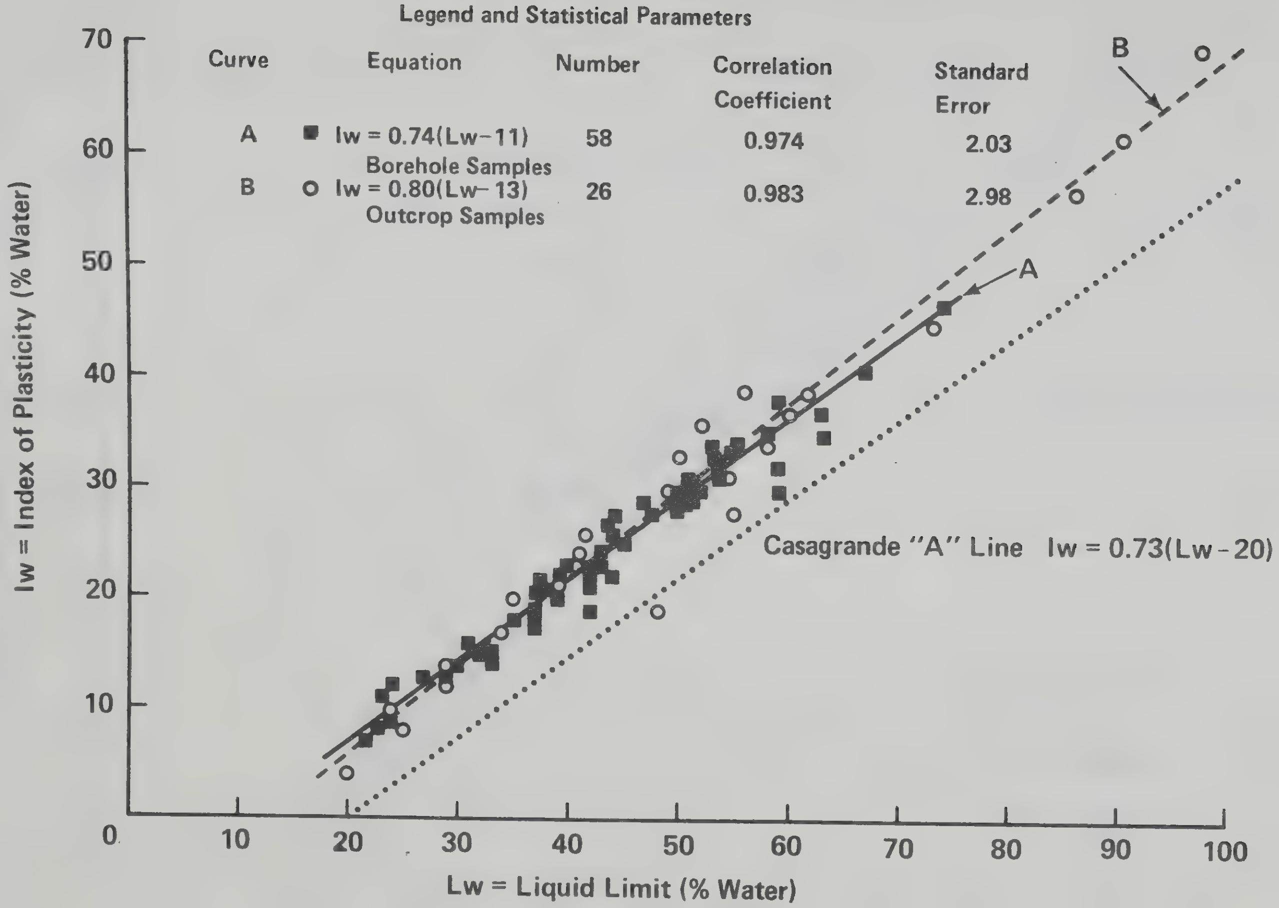

Figure H.7

Basal Clay Study: Plot of Index of Plasticity (Iw) versus Liquid Limit (Lw)

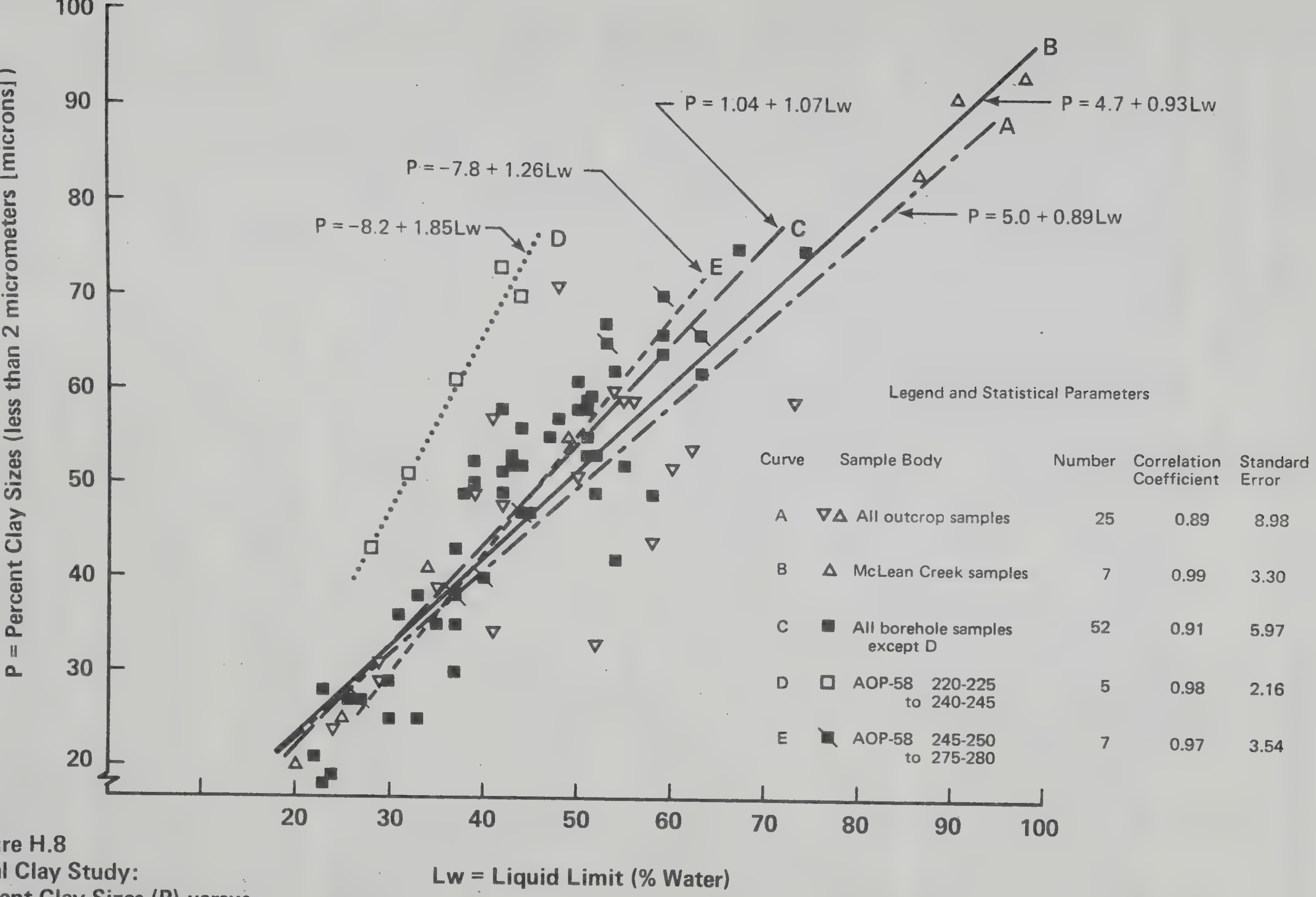

Curve	Sample Body	Number	Correlation Coefficient	Standard Error
A	▽△ All outcrop samples	25	0.89	8.98
B	△ McLean Creek samples	7	0.99	3.30
C	■ All borehole samples except D	52	0.91	5.97
D	□ AOP-58 220-225 to 240-245	5	0.98	2.16
E	■ AOP-58 245-250 to 275-280	7	0.97	3.54

Figure H.8
Basal Clay Study:
Percent Clay Sizes (P) versus
Liquid Limit (Lw)

Other regression lines in Figure H.8 display no significant differences from population data.

H.5 Mineralogy of the Basal Clays

H.5.1 Specimen Preparation for X-Ray Diffraction Analysis

X-ray diffraction analysis was performed for all samples listed in Table H.2. This included all the Alberta basal clay samples, the Manitoba clay samples, the intraformational clays, and seven artificial samples. The artificial samples were made from two commercial clays: Georgia kaolinite and Illinois Grundite. They were mixed in various proportions (10:0, 8:2, 6:4, 5:5, 4:6, 2:8, and 0:10) to assess the relationship between mineralogy and engineering index properties. The Georgia kaolinite is a refractory clay of high kaolinite content and excellent crystallinity, and the Illinois Grundite is an illitic clay of lesser crystallinity with minor amounts of kaolinite.

Fifty gram samples of clay were suspended in distilled water, allowed to sediment, and the fraction smaller than 2.0 μ in effective grain diameter was drawn off by siphoning. This process was repeated until all the clay sizes were recovered; then the clay sizes slurry was reduced in an oven (at 80°C), and ground to -100 mesh size. This procedure assured a uniform product sufficient for numerous X-ray analyses.

If a clay specimen was to be saturated with a particular cation before analysis, a one gram sample was boiled in a 1.0 N solution of the necessary salt, the excess salts were removed by centrifuge settling and several washings with distilled water, and the specimens were dried and ground.

X-ray powder slides of the untreated $< 2.0\,\mu$ fraction of all clays and cation saturated powder slides of selected clays were prepared by wetting approximately one gram of dry clay powder with distilled water to a pasty consistency (just above the plastic limit), and smearing the clay paste between two parallel strips of masking tape on a flat glass slide (Figure H.9a). The masking tape permitted a relatively thin uniform layer, and smearing the paste with a stainless steel spatula preferentially oriented the clay mineral platelets parallel to the slide. Orientation of the clay minerals enhances the peak intensity of the X-ray diffraction trace, and facilitates clay mineral specie identification.

Several specimens were fractionated into coarse (0.2 to 2.0 μ) and fine (less than 0.2 μ) fractions before X-ray analysis. The fractionating was performed in a centrifuge, and the fractions were treated and mounted by the above methods.

All untreated specimens, and all specimens which had been saturated with magnesium chloride ($MgCl_2$) before mounting, were sprayed with ethylene glycol before X-ray analysis. If heating was required, the slides which had been X-rayed in a cation-saturated or a glycolated state were used.

Selected specimens of basal clays (those with strong X-ray diffraction peaks between 7.4 Å and 7.8 Å) were prepared for photography by scanning electron microscope methods. Extremely dilute solutions of the clay sizes were prepared; a few drops were put on a mounting stub and allowed to air dry while protected from dust; and the samples were coated and photographed by the methods discussed in Chapter VII.

All of the X-ray analyses were performed and interpreted by

Figure H.9a Sample Preparation

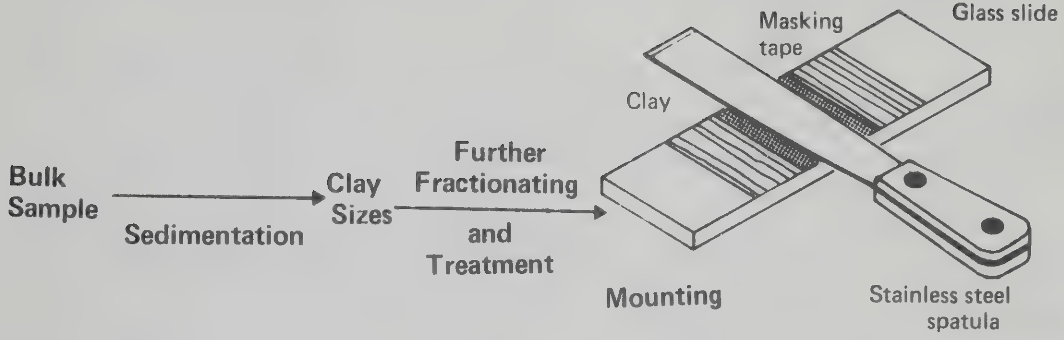

Figure H.9b Standard and Detailed Analytic Procedures

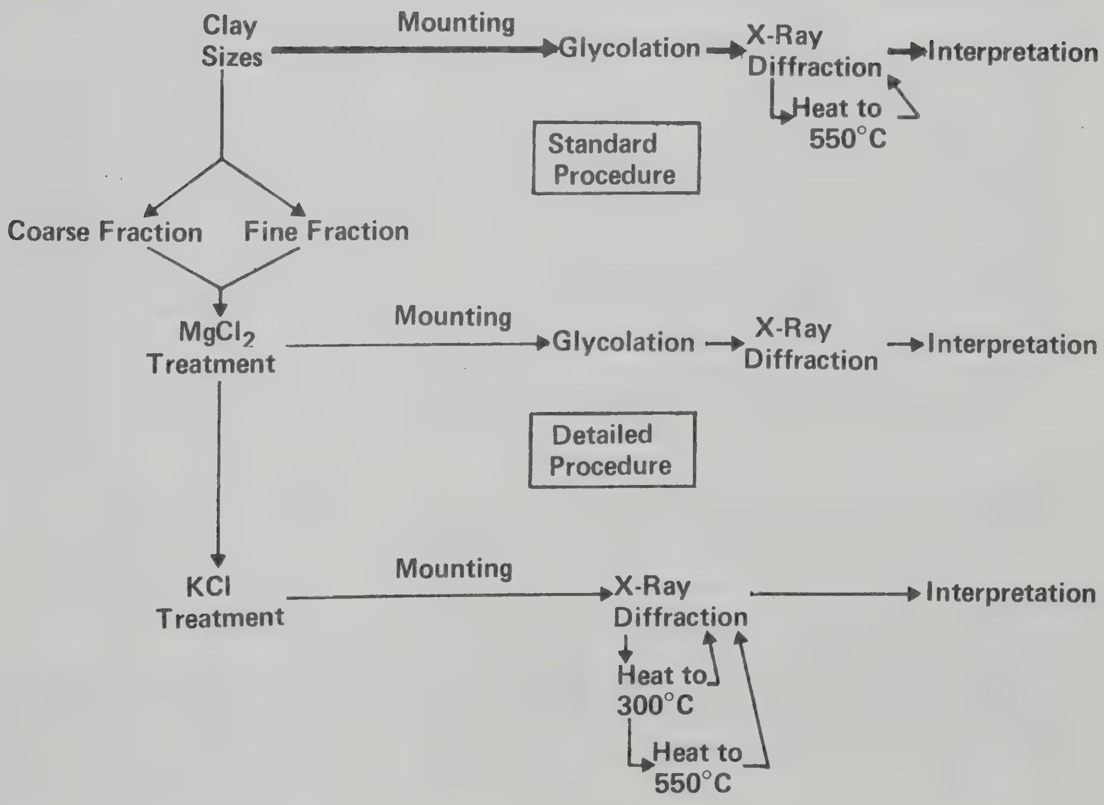

Figure H.9 X-Ray Diffraction Analysis

the staff of the Alberta Research Council under the supervision of D. Scafe, a clay mineralogist. The tests were performed as part of a larger study into the potential of the oil sands basal clays and intraformational clays for the manufacture of ceramic products.

H.5.2 Determination of Mineralogy by X-Ray Diffraction

The semiquantitative identification of clay minerals by X-ray diffraction methods has developed considerably over the last 40 years, yet there are still frequent debates concerning interpretation of results (Grim, 1968). The diffraction peaks of the (001) crystal planes of the various clay minerals are used almost exclusively for identification as they generally provide the most intense peaks in a zone where other mineral diffraction peaks are sparse. Lattice substitutions and the inherently fine-grained nature of clay minerals often result in low intensity and broad powder X-ray peaks (Grim, 1968), particularly when the clay originates in chemical weathering and neogenetic processes rather than physical attrition. Furthermore, the basal spacings of several of the clay minerals (e.g. chlorite and vermiculite) are sufficiently similar that their diffraction peaks can not be differentiated on a single standard powder X-ray trace. Therefore, many other diagnostic procedures for the semiquantitative X-ray analysis of clay minerals have been developed; for example, heating to a specific temperature to destroy a particular clay specie, or saturating the clay specimen with particular cations (Grim, 1968). All clay analyses are performed on oriented specimens to enhance peak intensity in these fine-grained minerals.

X-ray diffraction peaks often are used as a semiquantitative measure of the amounts of various clay mineral species present in a specimen. There are, however, many limitations to the determination of the quantities of clay minerals present. The procedure employs a measure of peak height ratios in one trace; therefore it is a measure only the relative proportions of clay minerals present, and does not yield total composition. The peak height ratios assume equal degrees of clay mineral crystallinity and constant specie grain size distributions between samples; this is not likely in a variable sample body of considerable size from a large geographical area. Lattice substitutions may also affect the intensity of X-ray diffraction peaks, and random mixed-layer clay minerals result in broad diffraction bands from which it is impossible to provide a truly quantitative measure.

Chemical analysis is not valuable in clay mineralogy because of the similar chemical composition of the clay minerals, and because of variable lattice substitutions which do not permit a rational allocation of cations to individual clay mineral species.

The affixing of a percentage composition to a sample of clay with a diverse mineralogy implies an accuracy that does not exist in the semiquantitative X-ray analysis methods; therefore a rank order system of compositional assessment based on relative peak intensity rather than peak ratios was employed. The measure refers to an assessment of diffraction peak strength only.

H.5.3 Methodology

The identification of clay mineral species required an extensive

X-ray diffraction analytic procedure. The total procedure was employed only for selected specimens, and when a sufficient body of data had been collected, the interpretations were applied to the remainder of the samples, each of which had been glycolated and X-rayed. The detailed methodology, with the reason for each step, is summarized as follows (Figure H.9b):

1. Fractionating: Smectite and mixed-layer clays are generally the most finely divided of the clay minerals. Analysis of the finest fraction permits more positive identification of these materials.
2. Glycolation after saturation with $MgCl_2$ results in a sharp 14.8 Å peak for vermiculite, which differentiates it from chlorite (14.0 Å).
3. Treatment with KCl collapses smectite to a basal spacing of 10 Å after heating to 300°C. Comparison with other traces determines whether significant smectite is present in the clay.
4. Ethylene glycol is used to expand any swelling clay minerals in the specimens. X-ray analysis of an untreated clay at a specific relative humidity is not useful since smectite still displays a wide range of basal spacings resulting in broad, undefinable diffraction bands between 12 and 20 Å. Ethylene glycol enforces a a uniform basal spacing of 17 Å for smectites, and a uniform basal spacing of 14.8 Å for vermiculites.
5. Heating to 300°C collapses vermiculite, but does not affect chlorite, illite, or kaolinite; therefore chlorite and vermiculite may be differentiated. Illite-vermiculite mixed-layer clay minerals are affected only partially, and a broad diffraction band on the low angle side of the illite peak still occurs, although in a subdued state.
6. Heating to 550°C destroys the 7.2 Å (001) peak of kaolinite, but does not affect the (002) chlorite peak at 7.0 Å, which facilitates examination of the (002) peak of chlorite.

All specimens prepared by the techniques discussed above were subjected to Copper Kα radiation, and the diffracted radiation was measured from 2° to at least 15° to give traces of the first basal (001) diffracted radiation peaks of each clay mineral present. The spacing and location on an X-ray diffraction trace of the common clay minerals in their normal state and in an expanded state (after treatment with ethylene glycol) are summarized in Table H.4 to aid in evaluating the X-ray diffraction traces presented.

The carbonate content of the clays was assessed by noting the reaction with dilute hydrochloric acid. Carbon content was estimated visually.

H.5.4 Test Results

Three distinct clay mineral species were identified in the basal clays of the McMurray Formation: illite is the most common, kaolinite is almost as widespread, and vermiculite is present in just under one-half of the specimens tested. All of the clays contain some kaolinite, and only one clay sample has no illite present (AOP-58 250-255). Illite-vermiculite random mixed-layer clay minerals are present in one-half of the specimens, and 12 samples display noticeable kaolinite-vermiculite mixed layering (including all seven samples from the McLean Creek

TABLE H.4

X-RAY DIFFRACTION DATA FOR COMMON CLAY MINERALS

CLAY MINERAL	LATTICE SPACING (001), ANGSTROMS (Å)		DIFFRACTED RADIATION ANGLE (DEGREES 2θ) (COPPER Kα RADIATION)	
	Natural State, Low to Medium Humidity	Expanded With Glycol	Natural State Low to Medium Humidity	Expanded with Glycol
Kaolinite	7.2(S)	7.2(S)	12.35	12.35
Halloysite	7.4(S)	7.4(S)	12.0	12.0
Chlorite	14.1(B)	14.1 (B)	6.2-6.3	6.2-6.3
Illite	10.0(S)	10.0(S)	8.9	8.9
Vermiculite	14-14.5(B)	14.8(S)	6.3	6.0
Smectite (Montmorillonite)	Variable 11 - 20 (B)	17 (B)	----	5.0

(B) = Broad diffraction peak
(S) = Sharp diffraction peak

Adapted from Grim (1968).

outcrop).

All the mineralogical data are reported in Table H.2. Reference to the series of X-ray diffraction traces demonstrates the relative assessment method using peak heights to obtain the semiquantitative mineralogical data found in Table H.2. The means of the assessments of clay mineral specie peak heights for outcrop and borehole samples are reported in Table H.3.

The occurrence of $CaCO_3$ is noted in Table H.2. Five specimens display a noticeable reaction with hydrochloric acid.

Representative X-ray diffraction traces of outcrop and borehole samples are reproduced (Figures H.10 to H.16). Figure H.10 is the trace of a glycolated sample from hole AOP-58. This specimen was the only basal clay which contained no detectable illite. The kaolinite and vermiculite peaks occur at 7.2 Å and 14.8 Å respectively, and the lack of a broad diffraction band between 10 Å and 14 Å indicates that no illite-vermiculite mixed layering is present. The shoulder on the low angle side of the kaolinite peak (from 7.3 to 7.9 Å) is indicative of kaolinite-vermiculite mixed layering. The sample contained no smectite or chlorite. The (002) peak of vermiculite, which would be expected to occur at 7.4 Å, is obscured by the strong kaolinite peak, but the vermiculite (003) peak is present at 4.84 Å.

Figures H.11, H.12, and H.13 show the results of the detailed analytic procedure employed on selected specimens to delineate mineralogy accurately. The upper trace in Figure H.11 is of a glycolated whole clay fraction (MD-63-6), and the lower trace is of the same specimen heated to 550°C. Heating has totally destroyed both the 14.8 Å peak of vermiculite and the broad peak between 7.2 Å and 7.8 Å Only illite remains as a distinct specie, but the broad shoulder on the low angle side of the 10 Å illite peak indicates that some illite-vermiculite mixed-layer clay has survived the heating process. If chlorite had been present in the original sample, a peak at 14.8 Å would show in the lower trace. Figures H.12 and H.13 each illustrate four identical X-ray analyses performed on two different size fractions of the same sample (MD-63-6). The coarse-grained fraction has a greater incidence of unmixed clays, and the X-ray traces of the fine-grained fraction indicate a much greater proportion of vermiculite and mixed-layer clays. Even in the fine-grained fraction, there is no evidence of smectite.

Figure H.14 presents a group of X-ray diffraction traces selected to demonstrate the variation in incidence of kaolinite and illite. The uppermost trace indicates that the great majority of clay minerals present are illitic. Lower traces show progressively higher proportions of kaolinite.

Figure H.15 shows selected X-ray diffraction traces on basal clays that demonstrate variations in vermiculite and mixed-layer occurrence. The occurrence of vermiculite is usually accompanied by an increased amount of mixed layering as shown by the broad diffraction band between 10 and 14 Å.

Figure H.16 is a random selection of four basal clay X-ray diffraction traces. The heights of diffraction peaks in Figure H.10 are not directly comparable because the specimens were analyzed at different recorder sensitivities to emphasize peak locations.

The last data column in Table H.2 is the Pyrometric Cone

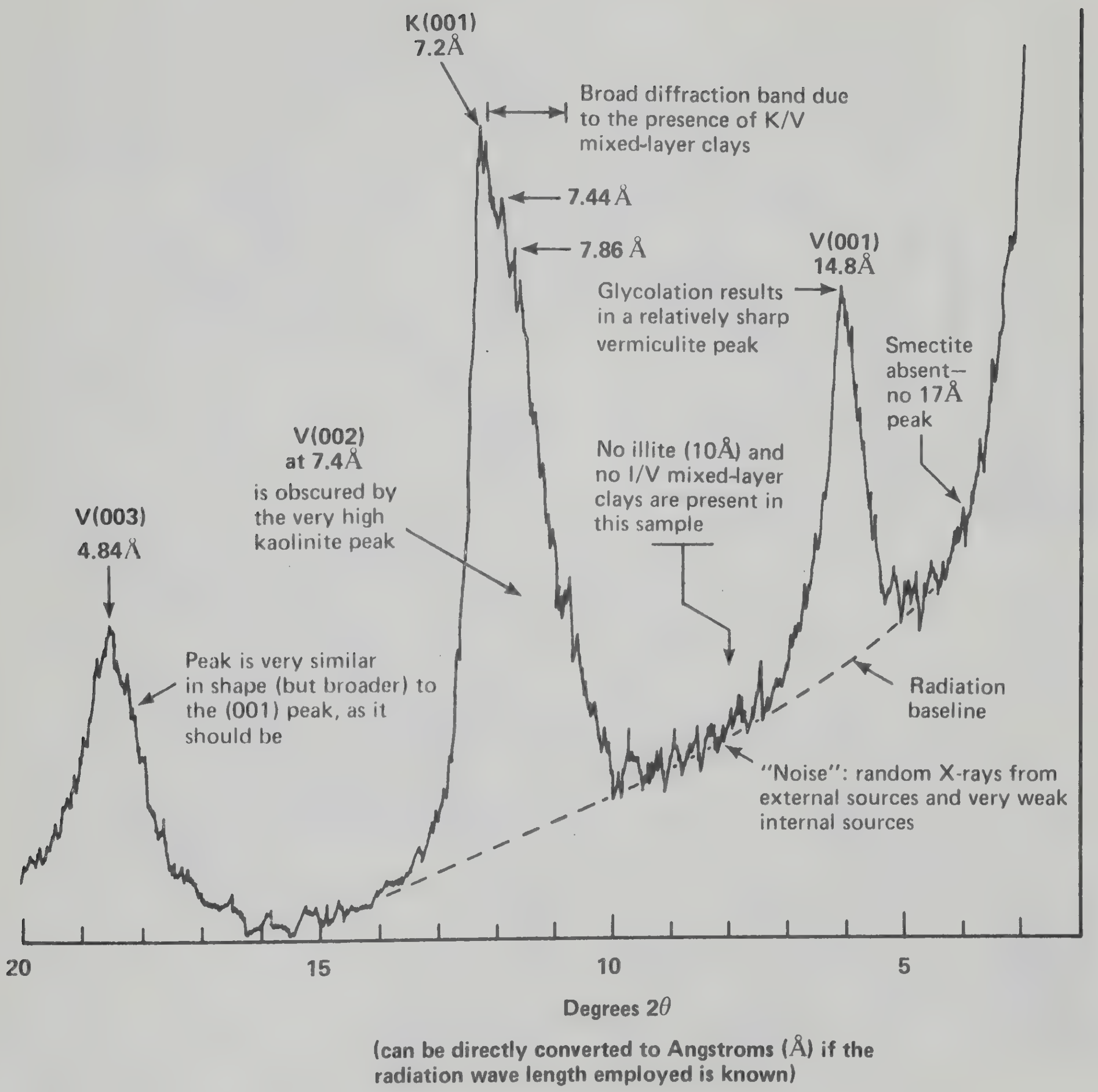

Legend

K(001): First basal plane (C-axis) refraction of kaolinite clay mineral
V(003): Third basal refraction of vermiculite
K : Kaolinite
V : Vermiculite
I : Illite
I/V : Illite-vermiculite mixed-layer clay
K/V : Kaolinite-vermiculite mixed-layer clay
Q : Quartz

Figure H.10 Identification and Interpretation of X-Ray Diffraction Peaks

(Sample # AOP-58 250′-255′, Glycolated)

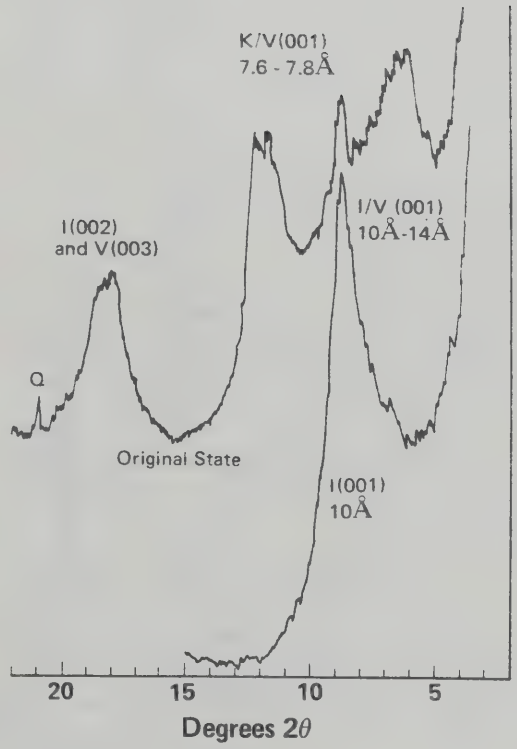

Figure H.11
MD-63-6
Whole Clay Fraction,
Heated and Unheated

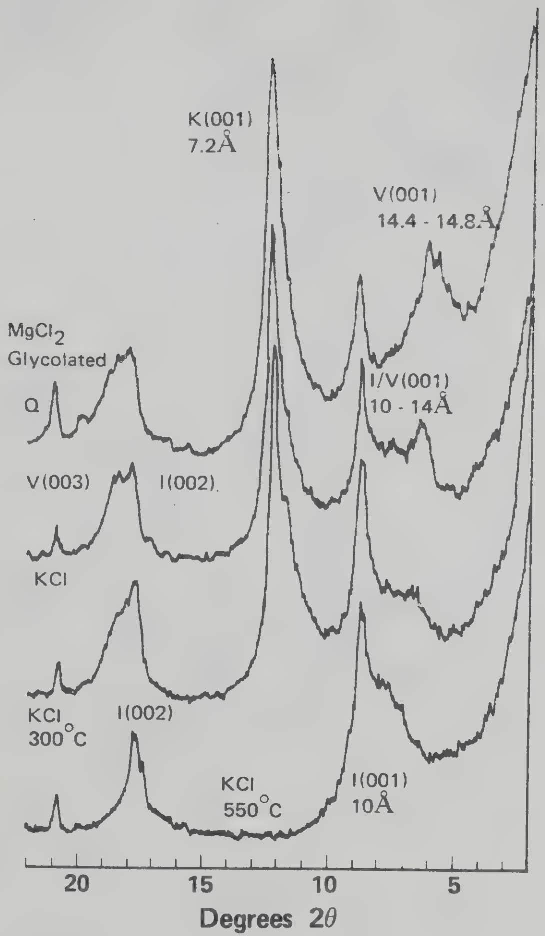

Figure H.12
MD-63-6
2.0μ - 0.2μ
Clay Fraction

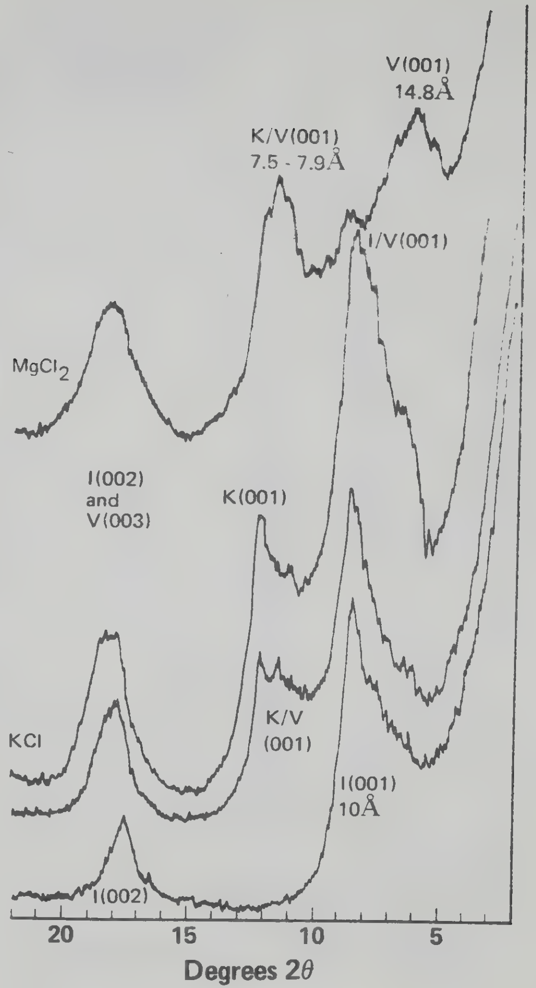

Figure H.13
MD-63-6
0.2μ - 0μ
Clay Fraction

Figure H.14
Kaolinite and Illite Incidence in Basal Clay Samples

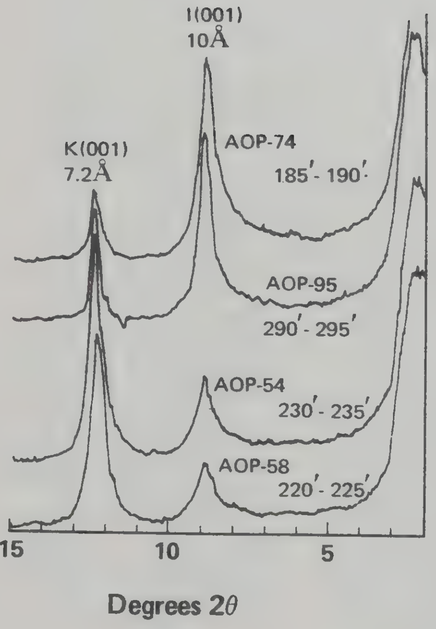

Figure H.15
Vermiculite and Kaolinite Incidence in Basal Clay Samples

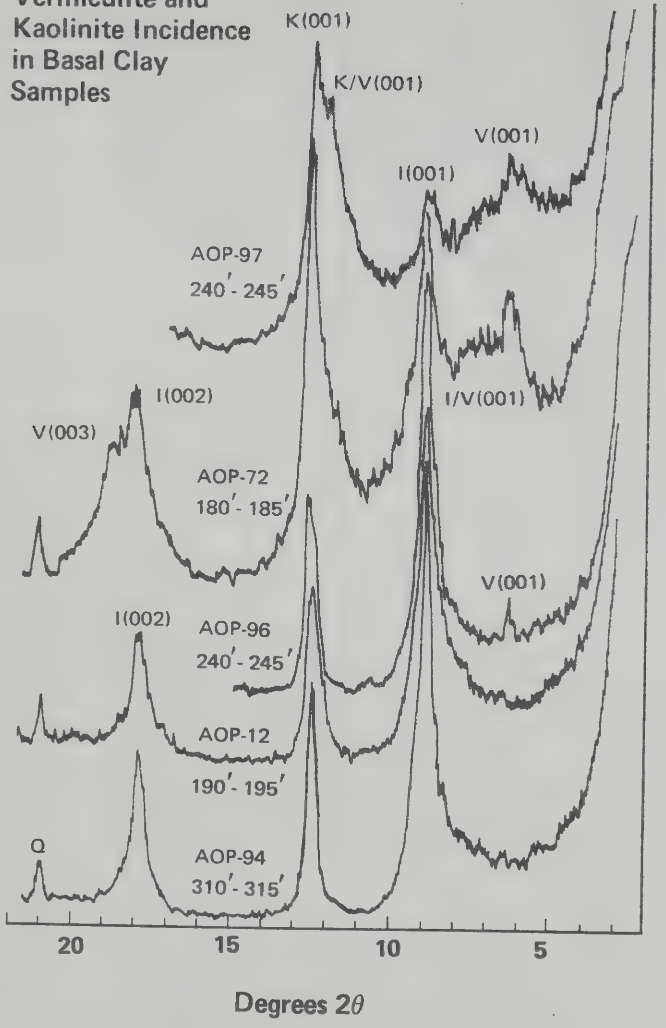

Figure H.16
X-Ray Diffraction Traces, Basal Clay Samples

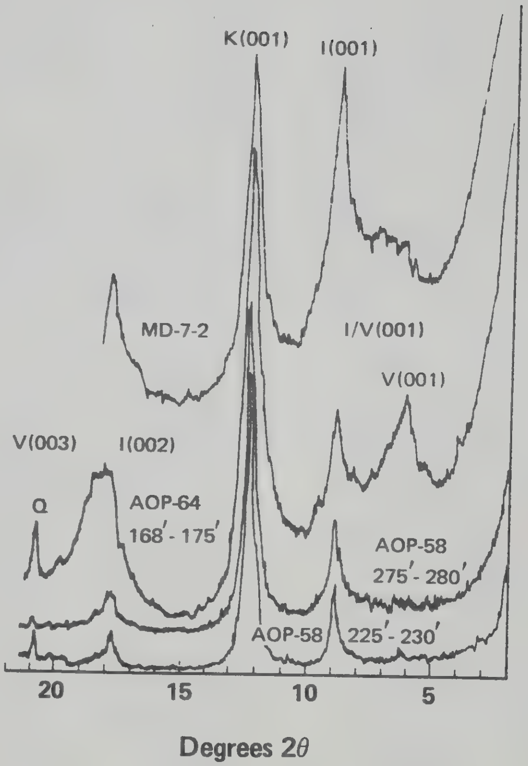

Equivalent (PCE). The PCE is defined as that temperature at which a preshaped cone of clay material will fuse and slump. It is obtained in a furnace employing a standard, constant rate of temperature increase, and by comparison to standard, calibrated ceramic cones. The mean PCE for all the basal clay samples is 1394°C with a standard deviation of 117°C. By comparison, the illitic Illinois Grundite yielded a PCE of 1190°C. The highest PCE value of basal clays is 1580°C; this was obtained from the McLean Creek outcrop samples.

H.5.5 Conclusions

The only swelling clay mineral in the basal deposit is vermiculite; its maximum swell is six percent, that is, from 14 to 14.8 Å. Because much of the vermiculite <u>in situ</u> may be in a partially hydrated state, and because vermiculite never constitutes more than one-quarter of the clay mineral present in the clay size fraction, the tendency for swelling of basal clay is negligible.

The clay minerals in the basal clay had their origin in weathering processes acting on the paleosurface before the transgression of the Lower Cretaceous sea. The illite and vermiculite in the clays are very fine grained, and are therefore not the product of intense physical attrition. In all probability, chlorite and smectite were absent at the time of deposition, and their continued absence indicates a lack of significant neogenesis of clay minerals. It is considered that the clays present today are similar mineralogically to the clays at deposition. Recent weathering is responsible for the mineralogical and size differences between outcrop samples and borehole samples.

The mineralogy of the basal clays is somewhat unusual for the Western Canadian Plains: smectite and chlorite are totally absent, whereas most clay shales of Lower and Upper Cretaceous age contain smectite, and if they are in the Rocky Mountain tectonic belt, chlorite as well. Furthermore, kaolinite-vermiculite mixed-layer clays are, in general, uncommon, but are frequently observed in the basal clays. Since the great majority of smectite is a result of alteration of volcanic ash, and since the Lower Clearwater Formation and Upper McMurray Formation (Sample MD-75-4-3) contain smectite, the basal clays were deposited before significant volcanic activity in Lower Cretaceous times.

The low activity indices of the sample body are a function of overall mineralogy: smectite is absent; the major clay species are illite and kaolinite. The difference in activity between outcrop and borehole specimens may be explained by the greater incidence of vermiculite and mixed-layer clays in outcrop specimens; this results in greater retention of interplatelet water, higher liquid limits, and hence higher activities. Further relationships may eventually be identified through detailed factor analysis.

The mean Pyrometric Cone Equivalent of outcrop specimens is significantly higher than that of the borehole specimens, and this difference is explicable in terms of the higher ratios of kaolinite to illite in outcrop specimens. The artificial specimens of Georgia kaolinite and Illinois Grundite clearly display the dependence of PCE upon the ratios of kaolinite to illite.

No detailed engineering strength testing of the basal clays has yet been published, but on the basis of the engineering index

properties and the mineralogy, residual ϕ values of 8° to 14° may be expected in the most clay-rich specimens (Kenney, 1968; Chattopadhyay, 1972). This value range should be compared to the residual ϕ of 18° obtained from the intraformational clay tests (Chapter V). The intraformational clays are actually clayey silts, since they invariably contain less than 50% clay sizes. No mixed-layer clays or vermiculite have been detected in these clayey silts. It is known that the uppermost intraformational clays may contain significant quantities of smectite (montmorillonite: Carrigy, 1966), and residual ϕ values therefore will be lower than 18°.

All specimens of basal clay which displayed a noticeable reaction with hydrochloric acid were obtained from the base of the basal strata, where the clays sit directly upon limestones (e.g. AOP-96 240-245). The absence of carbonates in the great majority of the clays attests to their relative impermeability to formation fluids: the study area has been a region of groundwater discharge (Hitchon, 1963), probably for many millions of years, yet carbonate ions are confined to the lower portions of the clays. The paleosols, however, in addition to their almost arenaceous character, invariably demonstrate high carbonate content. This is evidence of their residual nature: they are physically distinct from the basal clays, and their presence seems to preclude significant basal clay occurrence for paleogeomorphological reasons.

9.6 Summary

The basal clay study has delineated the ranges of the mineralogy and engineering index properties. The mineralogy of the clays is somewhat unusual: smectite and chlorite are absent; and illite, kaolinite, and vermiculite, in descending frequency of occurrence, are the clay species present. Mixed-layer assemblages constitute a common but minor proportion of the clays.

The nonswelling nature of the clays is reassuring for open pit mine development, but slickensided clays are common, and residual strength data should be obtained for pit wall analysis. The grain size and mineralogy suggest that an ultimate angle of residual friction of 8° to 14° may be appropriate.

SPECIAL COLLECTIONS

UNIVERSITY OF ALBERTA LIBRARY

REQUEST FOR DUPLICATION

I wish a photocopy of the thesis by

Dusseault, M.B (author)

entitled Geotechnical Characteristics of the Athabasca Oil Sands

The copy is for the sole purpose of private scholarly or scientific study and research. I will not reproduce, sell or distribute the copy I reques and I will not copy any substantial part of it in my own work without permission of the copyright owner. I understand that the Library performs the service of copying at my request, and I assume all copyright responsibility for the item requested.

Date	Name and address	Pages copied	Signature
Aug 25/77	H. Csanyi	All	x
	Alta. Research		
	Council		
Nov. 16/77	B. Jordan		
	Syncrude Canada	All	B. Jordan
10/30/79	SA JAMES CARLETON U.	P2,3 22 23	SA James

F 226

September 19